Lecture Notes in Civil Engineering

P. V. Timbadiya
P. L. Patel
Vijay P. Singh
Priyank J. Sharma *Editors*

Hydrology and Hydrologic Modelling

Proceedings of 26th International Conference on Hydraulics, Water Resources and Coastal Engineering (HYDRO 2021)

Springer

Lecture Notes in Civil Engineering

Volume 312

Lecture Notes in Civil Engineering (LNCE) publishes the latest developments in Civil Engineering—quickly, informally and in top quality. Though original research reported in proceedings and post-proceedings represents the core of LNCE, edited volumes of exceptionally high quality and interest may also be considered for publication. Volumes published in LNCE embrace all aspects and subfields of, as well as new challenges in, Civil Engineering. Topics in the series include:

- Construction and Structural Mechanics
- Building Materials
- Concrete, Steel and Timber Structures
- Geotechnical Engineering
- Earthquake Engineering
- Coastal Engineering
- Ocean and Offshore Engineering; Ships and Floating Structures
- Hydraulics, Hydrology and Water Resources Engineering
- Environmental Engineering and Sustainability
- Structural Health and Monitoring
- Surveying and Geographical Information Systems
- Indoor Environments
- Transportation and Traffic
- Risk Analysis
- Safety and Security

To submit a proposal or request further information, please contact the appropriate Springer Editor:

– Pierpaolo Riva at pierpaolo.riva@springer.com (Europe and Americas);
– Swati Meherishi at swati.meherishi@springer.com (Asia—except China, Australia, and New Zealand);
– Wayne Hu at wayne.hu@springer.com (China).

All books in the series now indexed by Scopus and EI Compendex database!

P. V. Timbadiya · P. L. Patel · Vijay P. Singh ·
Priyank J. Sharma
Editors

Hydrology and Hydrologic Modelling

Proceedings of 26th International Conference on Hydraulics, Water Resources and Coastal Engineering (HYDRO 2021)

Springer

Editors
P. V. Timbadiya
Department of Civil Engineering
Sardar Vallabhbhai National Institute
of Technology
Surat, India

P. L. Patel
Department of Civil Engineering
Sardar Vallabhbhai National Institute
of Technology
Surat, India

Vijay P. Singh
Department of Biological and Agricultural
Engineering, and Zachry Department
of Civil and Environmental Engineering
Texas A&M University
College Station, TX, USA

Priyank J. Sharma
Department of Civil Engineering
Indian Institute of Technology Indore
Indore, India

ISSN 2366-2557 ISSN 2366-2565 (electronic)
Lecture Notes in Civil Engineering
ISBN 978-981-19-9146-2 ISBN 978-981-19-9147-9 (eBook)
https://doi.org/10.1007/978-981-19-9147-9

Preface

Hydrological models have evolved as indispensable tools for effective planning and management of water resources. Hydrologic modelling aims to study the spatio-temporal variations in the hydrologic processes such as precipitation, snowmelt, interception, infiltration, evapotranspiration, sub-surface flow, surface flow and their interactions through empirical, physics-based or data-driven approaches. Hydrologic modelling is challenging due to the complexity, nonlinearity and higher spatio-temporal variability in the hydrologic processes over a region. However, with the recent technological advancements and availability of reliable gauged and satellite-based datasets, hydrological modelling tools and approaches have gained popularity in the hydrologic community. The satellite-based datasets are used to derive vital geospatial inputs for the hydrological models, such as the digital elevation model, land use–land cover, soil characteristics and geological information. Apart from that, the satellite-based products provide reliable and long-term measurements of precipitation, temperature, evapotranspiration, soil moisture and other fluxes to overcome the limitations due to the unavailability of gauged observations. Over the years, several books have discussed the aspects of hydrological modelling, but most of them were theoretical-oriented, with a narrow focus on real-world case studies.

This book covers the broader theme of hydrology and hydrological modelling while dealing with several sub-topics such as reservoir sedimentation, drought assessment, crop water requirements, sub-surface flow and groundwater flow modelling. The present book deals with hydrological modelling applications for climate change impact assessment, water balance assessment, streamflow prediction, land use–land cover changes, runoff estimation, assessment of snow cover variability and reservoir sedimentation studies. The hydrological modelling case studies through the application of several well-known tools such as the Soil and Water Assessment Tool (SWAT), Hydrologic Modeling System (HEC-HMS) and River Analysis System (RAS) from the Hydrologic Engineering Centre (HEC), MIKE NAM (Nedbør-Afstrømings-Model) and others are discussed. These case studies provide new hydrological insights across various geographical regions exhibiting different physiographic and climatic conditions, such as the Tapi, Godavari, Ganga, Baitarani, Brahmaputra, Mandovi, Mahi, Sabarmati, Sutlej, and Periyar River basins. Several

case studies dealing with drought assessment through various indices are included in this book. The crop evapotranspiration and irrigation water requirements for the Ukai-Kakrapar and Dharoi command areas are analysed. Several experimental and simulation studies about the estimation of porosity, permeability and modelling groundwater flows are also demonstrated. A couple of review papers dealing with the application of HEC-HMS and flood routing studies have been included in this book. This book will help the readers to gain new hydrological insights for various study domains and improve their conceptual understanding of the hydrological process through case studies and reviews.

Surat, India — P. V. Timbadiya
Surat, India — P. L. Patel
College Station, TX, USA — Vijay P. Singh
Indore, India — Priyank J. Sharma

Acknowledgements

The editors are grateful for the support provided by the technical advisory committee and local organizing committee of the 26th International Conference on Hydraulics, Water Resources and Coastal Engineering (HYDRO 2021) held at Sardar Vallabhbhai National Institute of Technology (SVNIT) Surat during 23–25 December 2021. The editors thank the Indian Society for Hydraulics (ISH), Pune, India, its office bearers and executive council members for their support in conducting the HYDRO 2021 International conference. The editors wish to thank all the authors for their support and contribution to this book. The editors duly acknowledge the timely and sincere efforts of the reviewers in providing their valuable comments and suggestions to maintain the quality of the book. The editors would like to thank the keynote speakers, the session chairs and co-chairs, participants and student volunteers for their contribution to the successful conduct of the conference. The editors are also thankful to the administrators of Sardar Vallabhbhai National Institute of Technology, Surat (SVNIT), India, for supporting the HYDRO 2021 International Conference. Lastly, the editors are sincerely thankful to the publishing team of Springer Nature for their support and cooperation at various steps since the beginning of the book project.

P. V. Timbadiya
P. L. Patel
Vijay P. Singh
Priyank J. Sharma

Contents

About the Editors

P. V. Timbadiya is an Associate Professor in the Water Resources Engineering section, Department of Civil Engineering, Sardar Vallabhbhai National Institute of Technology (SVNIT), Surat, India. He secured his doctoral degree and post-graduation in Water Resources Engineering from SVNIT Surat in 2012 and 2004, respectively. He has guided three doctoral thesis and 29 master's dissertations. He has over 110 research papers to his credit, including 30 articles in peer-reviewed journals. He served as Dean (Alumni and Resources Generation), and currently serving as Sectional Head, Water Resources Engineering Section at SVNIT. He played an instrumental role in setting up infrastructure facilities in the Centre of Excellence on 'Water Resources and Flood Management' such as the Experimental Hydraulics Lab, Computational Hydraulics Lab, Water Circulation System, and others. He is appointed as 'National Consultant' for Kalpsar Project by Narmada, Water Resources, Water Supply and Kalpsar Department of Government of Gujarat, India. He received 'Prof. R. J. Garde Research Award' for the year 2020 by the Indian Society for Hydraulics. He has awarded DST-SERB Core Research Grant for the project on 'Local Scouring around tandem and staggered bridge piers on Non-uniform mobile bed' in the year 2021. He is active in various professional bodies and organized numerous conferences, workshops, and short-term training programmes in his academic career.

P. L. Patel is a Professor of Hydraulics and Water Resources in the Department of Civil Engineering, Sardar Vallabhbhai National Institute of Technology (SVNIT), Surat, India. He served as the Deputy Director of SVNIT. He also worked as a Reader in the Civil Engineering Department at Delhi College of Engineering (now DTU) from 1999–2007. He served as an Assistant Executive Engineer in Border Roads Organization (BRO) from 1995–1999. He did his bachelor's in Civil Engineering from Government Engineering College, India and then pursued his Master's and Doctoral degrees in Civil Engineering from Indian Institute of Technology (IIT) Roorkee India. He has published more than 220 papers in peer-reviewed journals and conferences of repute. He has guided 12 doctoral thesis and 47 master's dissertation so far. He has also served in various academic positions in SVNIT Surat, such as

Dean (Academics), Head of Civil Engineering Department, Dean (Research and Consultancy), Dean (PG), etc. He was also instrumental in setting up a Centre of Excellence (CoE) on 'Water Resources and Flood Management' in the Institute through a research grant from World Bank-sponsored TEQIP-II. He is a recipient of visiting International Fellowship (VIF-2017) 2017 for attending the ASCE EWRI Congress-2017 in Sacramento, California, USA. He is active in various professional bodies and organized numerous conferences, workshops, and short-term training programmes in his academic career.

Vijay P. Singh is a University Distinguished Professor, a Regents Professor, and Caroline and William N. Lehrer Distinguished Chair in Water Engineering at Texas A&M University. He received his B.S., M.S., Ph.D., and D.Sc. in engineering. He is a registered professional engineer, a registered professional hydrologist, and an Honorary Diplomate of ASCE-AAWRE. He is a Distinguished Member of ASCE, a Distinguished Fellow of AGGS an Honorary Member of AWRA and a Fellow of EWRI-ASCE, IAH ISAE IWRS and IASWC. He has published extensively in the areas of hydrology, irrigation engineering, hydraulics, groundwater, water quality, and water resources (more than 1320 journal articles, 31 textbooks, 75 edited reference books, 110 book chapters, and 315 conference papers). He has received over 95 national and international awards, including three honorary doctorates. He is a member of 11 international science/engineering academies. He has served as President of the American Institute of Hydrology (AIH), Chair of the Watershed Council of the American Society of Civil Engineers and is currently President of the American Academy of Water Resources Engineers. He has served/serves as Editor-in-Chief of 3 journals and two book series and serves on editorial boards of more than 25 journals and three book series. His Google Scholar citations include 64073, h-index: 115, and I10-index: 903.

Priyank J. Sharma is an Assistant Professor in the Department of Civil Engineering at the Indian Institute of Technology (IIT) Indore, India. He worked as a postdoctoral scholar in Hydrosystems Research Laboratory at Florida Atlantic University, USA. He completed his Ph.D. in Civil Engineering with a specialization in Water Resources Engineering from Sardar Vallabhbhai National Institute of Technology (SVNIT) Surat in January 2020. He is a recipient of the 'INSPIRE Fellowship' by the Department of Science and Technology, Government of India and 'Institute Gold Medal' at SVNIT Surat. He also worked as an Assistant Manager at Essar Projects (India) Limited from 2010-2012. He has received several awards and accolades for his academic and research performance, the prominent being 'Prof. U. C. Kothyari Best Ph.D. Thesis Award 2020' from the Indian Society for Hydraulics. He has authored forty-seven research publications, including fifteen articles in peer-reviewed high-impact factor journals and five book chapters. His research interests are hydroclimatology and climate extremes, climate change impact assessment, streamflow prediction, and reservoir operation.

Comparison of Different Climate Models Projections for Watershed Using Soil and Water Assessment Tool: A Case Study of Middle Tapi Sub-basin

Vishal Sharma, Priyamitra Munoth, and Rohit Goyal

Abstract In the scenario of climate change, it is very important to forecast the future values of watershed constituents for the better management of water resources. For that, several general circulation models (GCM) were made in many countries. In this study, BNU-ESM, CCC-ma, CNRM, MPI-ESM-LR, MPI-ESM-MR climate models inputs were used to find surface runoff, actual evapotranspiration (AET), potential evapotranspiration (PET) and sediment yield using soil and water assessment tool (SWAT) in Middle Tapi sub-basin, India. Efforts have been made in this study to evaluate which model's inputs are reliable to find watershed constituents. The performance of all the climate models was evaluated using three indices, i.e. coefficient of determination (R^2) Nash–Sutcliffe model efficiency coefficient (NSE) and per cent bias (PBIAS), by comparing the results with base model developed using IMD data. The results show that all the models are better predicting the AET based on their PBIAS values and the best PBIAS value (−3.84) was given by the CNRM model for AET among all the models. The precipitation, surface runoff, sediment yield, lateral flow, total water yield and PET values were underestimated by all climate models. Deep aquifer recharge, total aquifer recharge, percolation out of soil were overestimated by BNU-ESM, CCC-ma, CNRM, MPI-ESM-LR models and underestimated by MPI-ESM-MR model. The present study also shows the impact of climate change on the hydrological process of watershed of Middle Tapi sub-basin in the near future (2011–2040), mid-future (2041–2070) and far future (2071–2100) using the representative concentration pathways (RCP) of 4.5 and 8.5 scenario.

Keywords Circulation models · SWAT · RCP 4.5 and RCP 8.5

V. Sharma (✉) · P. Munoth · R. Goyal
Department of Civil Engineering, Malaviya National Institute of Technology Jaipur, Jaipur 302017, India
e-mail: 2019pcw5287@mnit.ac.in

P. Munoth
e-mail: 2014rce9536@mnit.ac.in

R. Goyal
e-mail: rggoyal.ce@mnit.ac.in

P. V. Timbadiya et al. (eds.), *Hydrology and Hydrologic Modelling*,
Lecture Notes in Civil Engineering 312,
https://doi.org/10.1007/978-981-19-9147-9_1

1 Introduction

The climate of the Earth is changing significantly all the way through its history. Many independent investigations have provided the evidence that when the industrial revolution started the climate of earth has significantly altered [1, 2]. From 1850, each of the last three decades faced successively warmer earth surface than preceding decade [1]. "Trends of other global climate indicators like rate and patterns of temperature, precipitation and precipitation extremes, continental ice melt, atmospheric water vapour concentration, sea-level rise, ocean heat content, ocean acidification and the rate of recurrence of powerful cyclones were consistent with the feedback expected from a warming planet" [1]. The global average near-surface air temperature has been increased by 1 °C since pre-industrial times. At this trend of increasing temperature, it is obvious that the "global warming would reach 1.5 °C between 2030 and 2050 (high confidence)" [2]. In this varying atmosphere, the rainfall and runoff were varying in space and time. The changing amount of greenhouse gases (GHGs) in the atmosphere changes the precipitation and temperature. These changes in climate affect the water resources of the earth very much, so for the better management of water resources, it is required to understand the effect of climate change on the water resources and the watershed is the most basic natural hydrologic unit for the study of hydrology and water resources of any region [3]. The water balance exploration of any watershed gives the information of how much water is gained and lost in quantitative terms from any area. Therefore, an enormous number of hydrological models was developed, e.g. "MIKE System Hydrologic European (MIKE SHE)" [4], "Topographic Hydrologic Model (TOPMODEL)" [5], "Hydrologiska Byrans Vattenavdelning model (HBV)" [6], "Variable Infiltration Capacity model (VIC)", "Soil and Water Assessment Tool (SWAT)" [7], etc., to quantify the water resources of a watershed. Similarly, many GCM like "BNU-ESM (Beijing Normal University Earth System Model), CCC-ma (Canadian Centre for Climate Modelling and Analysis), CNRM (National Centre for Meteorological Research-Climate Model), MPI-LR (Max Plank Institute Low Resolution Earth System Model), MPI-MR (Max Plank Institute Mix Resolution Earth System Model)" are also developed to predict the precipitation and temperature values under different climate scenarios. For the assessment of climate change effect on the watershed of any area, it is necessary to find suitable GCM for that area. In IPCC (Intergovernmental Panel on Climate Change) [1] report, the Coupled Model Intercomparison Project - Phase 5 (CMIP5) models were used to assess the climate change. It was found that the mean rates of GHGs ("carbon dioxide, methane and nitrous oxide") were increased over the past centuries, with high confidence, "unprecedented in the last 22,000 years" [1]. The ocean warming was seen largest nearby the surface with upper 75 m warmed by 0.11 °C per decade over the period of 1971–2010. Molla et al. [8] used SWAT model for investigating climate change impact on stream flow of BARO-AKOBO river basin in Ethiopia for thirty-one years from 1986 to 2016. The RCP 8.5 scenarios based on the "IPCC 5th assessment report" set for African countries are used in the study. Krishnan et al. [9] used the projections of CMIP5 and CORDEX South Asia

datasets for examining regional climate change. The CMIP5 models used in this study were interpolated to the resolution of 1° × 1°. It uses the RCPs of 4.5 and 8.5 scenarios. In this study, the surface runoff and other parameters were identified in changing climate conditions by using CMIP5, CMIP6 and IIT-ESM (Indian Institute of Technology Earth System Model).

Therefore, the objective of present study is to evaluate the water resources in a watershed of Middle Tapi basin in terms of surface runoff, AET, PET, sediment yield and finding the suitable GCM for the study area by using water balance approach and then to predict the future hydrological component. The water budget components are estimated using the SWAT. The impact of climate change on the watershed parameters under the forcing of "RCP 4.5 and RCP 8.5" was analysed, and the outputs of all GCMs were compared.

2 Study Area and Data Source

2.1 Tapi River Basin

The Tapi River is also known as Tapti. It flows East to West direction and goes through Madhya Pradesh, Maharashtra and Gujarat and drains into Arabian Sea. "It is the second largest west flowing river of India" [10]. The surrounding mountain ranges of Tapi basin are the Satpura mountain range at North, the Ajanta and Satmala mountain range at South, the Mahadeva mountain range at East. Maximum area of Tapi river basin lies in Maharashtra which is about 80% of the total area (http://india-wris.nrsc.gov.in).

The whole Tapi river basin has "three sub-basins: first Upper Tapi basin, from Multai to Hathnur dam at meeting of Purna river with the Tapi River (29,430 km^2); second Middle Tapi basin starting Hathnur dam to Ukai dam (31,767 km^2); and third Lower Tapi basin starting from Ukai dam to Arabian Sea in the Gulf of Khambhat (3948 km^2) (Fig. 1). Tapi River originates near Multai in Betul district of Madhya Pradesh at an elevation of 752 m and travelled a total distance of 724 km before meets to the Arabian Sea (Fig. 1)" [11–14]. "The major water resources projects in the Tapi basin are Ukai, Hathnur and Girna having gross storage capacities of 7414.3 Mm^3, 388.0 Mm^3 and 608.5 Mm^3, respectively" [15].

In this study, a watershed located in Middle Tapi basin was selected which lies between 75°26′07″ E and 76°10′09″ E longitude and 20°22′12″ N to 21°09′49″ N latitude covering a geographical area of 2473.52 km^2 and perimeter of 416.6 km in plain region of Maharashtra (Fig. 1). The reason of choosing this watershed is because Tapi River is the main river of Maharashtra state for the agriculture and domestic purpose and every year Maharashtra state faces the drought situation, so it is important to study the Tapi basin so that the management of water resources could be better.

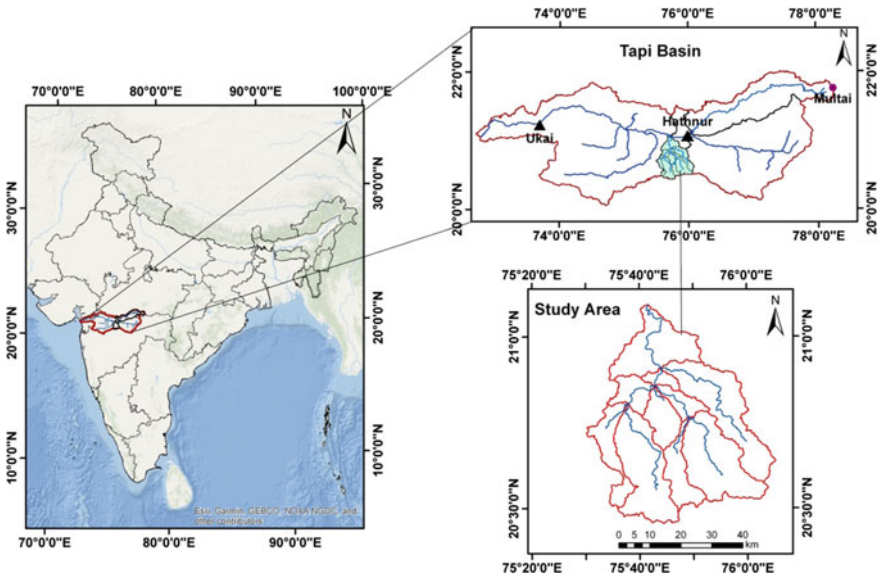

Fig. 1 Location map of study area

2.2 Data Used

The raster datasets such as "Digital Elevation Model (DEM), land use–land cover (LULC), hydrological soil group map and datasets such as precipitation, temperature and outlet" are required for the generation of water balance parameters. The digital elevation model is made with the help of Shuttle Radar Topography Mission (SRTM) void filled data of resolution 1 arc-second (30 m) (Table 1). This high-resolution global data is downloaded from USGS Earth explorer Website in the form of tiles. The elevation of study area ranges from 154 to 808 m above the mean sea level. Average elevation of study area is 344.75 m (Fig. 2).

The land use–land cover dataset was procured by "National Remote Sensing Centre (NRSC) India" of 56 m resolution for the year 2005 (Table 1). The LULC datasets were divided into six classes, i.e. "agriculture, barren land, built-up, forest, range land and water". The majority of land is agricultural land with about 64% area and least area for the residential area with 1.45% area, which is shown in Fig. 3.

The soil analogue maps (1:2,500,000 scale) of study area was obtained from National Bureau of Soil Survey and Land Use Planning (NBSS & LUP), Nagpur, and for further classification into various soil groups, this was converted in digital form in GIS platform (Table 1). The main soil groups of the study area are clayey and clay loam to gravely clay loam varying from light brown to reddish brown, black cotton, medium soil, dark yellowish brown to dark reddish brown (Fig. 4).

Table 1 Description of input data

Data type	Resolution	Source
Digital elevation model (DEM)	30 m	Shuttle Radar Topography Mission (SRTM) http://www.earthexplorer.usgs.gov/
LULC Map	56 m	NRSC https://www.nrsc.gov.in/
Soil map	1:2,500,000 scale	NBSS & LUP https://www.nbsslup.in/
Climate data	Stations	India Meteorological Department (IMD) https://mausam.imd.gov.in/
GCM data	0.5° × 0.5°	Regional climate projections in India with statistical downscaling http://www.regclimindia.in/

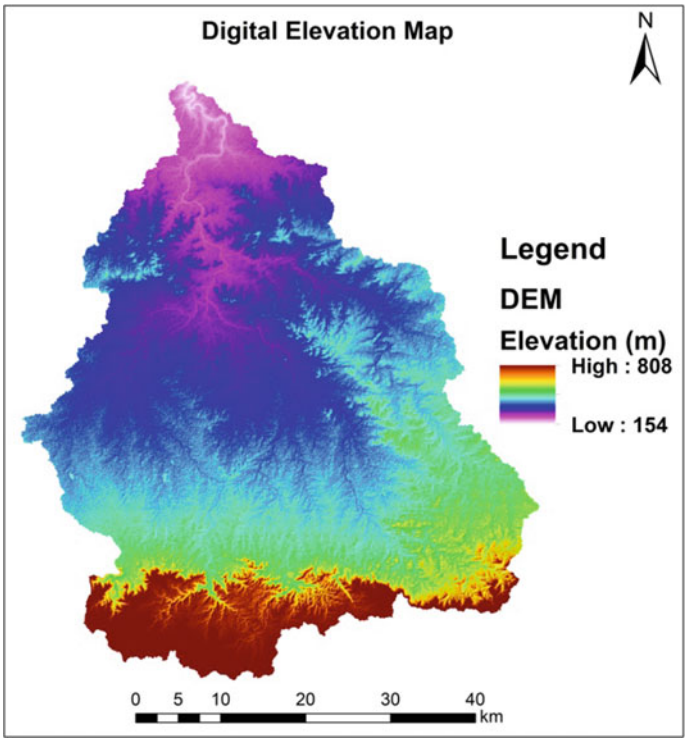

Fig. 2 DEM of study area

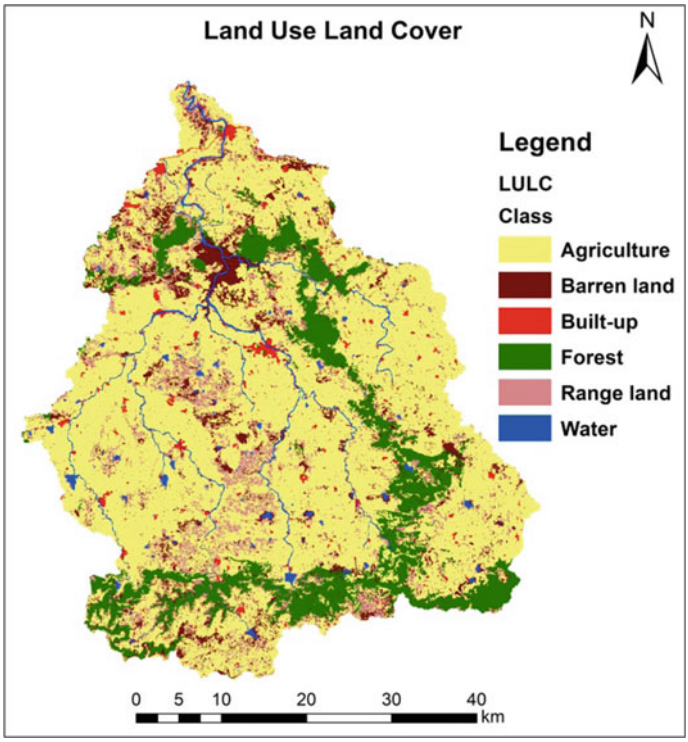

Fig.3 Land use-land cover of study area

The climate of the study area is characterized by a hot summer and general dryness throughout the year excluding during the season of south-west monsoon. The study area receives 90% of rainfall from June to November with average rainfall of about 739 mm. Major parts of the study area lie in western plateau and hilly agro-climatic zone. Daily climatic data of rainfall, maximum/minimum temperature, relative humidity and wind speed data were taken from India Meteorological Department (IMD) for the years 1970–2013 (Fig. 5; Table 1).

The projections of precipitation and temperature data of RCP 4.5 and 8.5 scenarios from 2011 to 2040, 2041 to 2070, 2071 to 2100 are used to forecast the water balance parameters of the study area. All the projections of climate models were downscaled for the study area using Kernal regression [16, 17] (Table 1; Fig. 5).

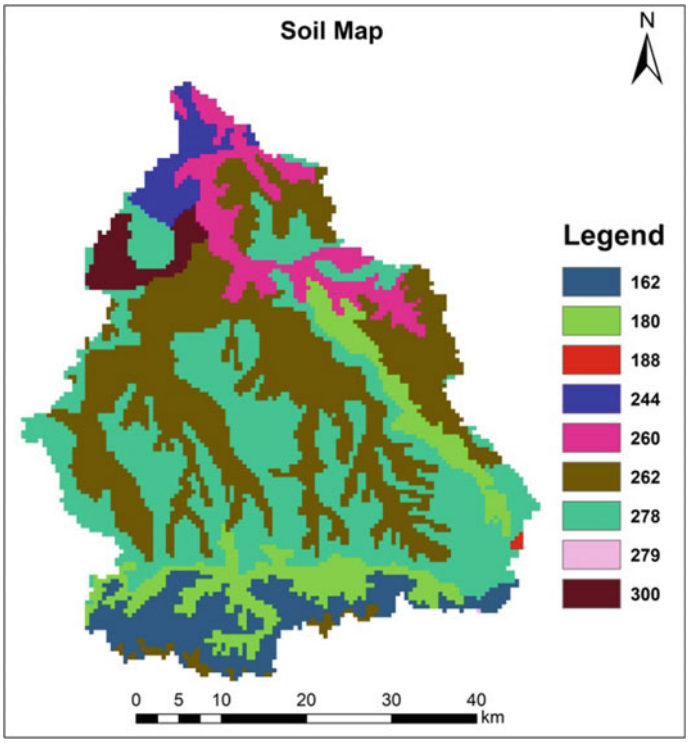

Fig. 4 Soil map of study area

3 Methodology

3.1 Hydrological Modelling Using SWAT

The SWAT model was used for the hydrological modelling of the study area and for comparison of projections of general circulation models for future scenarios. The SWAT model is computationally efficient, requires minimum data and does not require much calibration [18]. The SWAT model operates on a daily time step and designed to predict the impact of land use management on water, sediment and agricultural chemical yields in un-gauged watersheds [7]. It is developed by Agriculture Research Service of the United States Department of Agriculture. It is an all-embracing, semi-distributed and temporally uninterrupted simulations model. "Surface runoff, return flow, percolation, evapotranspiration, transmission losses, pond and reservoir storage, crop growth and irrigation, groundwater flow, reach routing; nutrient and pesticide loading, and water transfer" are the main constituents of SWAT. The Hydrological Response Units (HRUs) are the smallest simulation

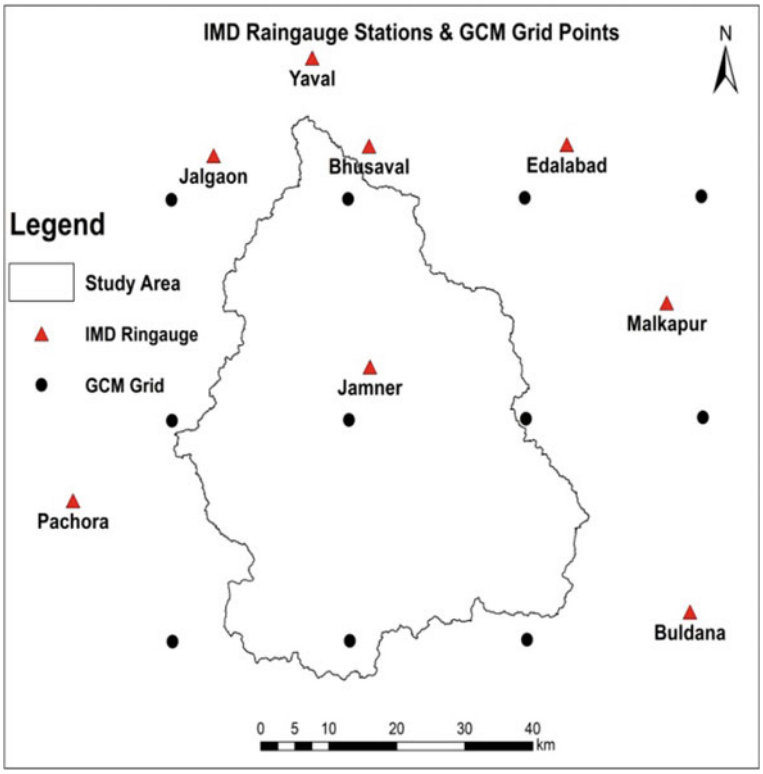

Fig. 5 Location of rain gauge stations and GCM data

units of SWAT model. The areas with a specific LULC and soil characteristics, which are scattered throughout the sub-watershed, are lumped together in one HRU. In SWAT model, "firstly the water balance parameters are calculated for HRUs, then summed together to find the total hydrologic process of sub-watershed and at last routing to the sub-watershed outlets through a river reach in the channel network to find the overall runoff and sediment yield for the watershed". SWAT model required particular data "about weather, soil properties, topography, plants and ground management practices" taking place in the watershed. The model used the following water balance Eq. (1) in the catchment, which is illustrated in Fig. 6.

$$\mathrm{SW_t} = \mathrm{SW_0} + \sum_{t=1}^{t} \left(R_{\mathrm{day}} - Q_{\mathrm{surf}} - E_{\mathrm{a}} - W_{\mathrm{seep}} - Q_{\mathrm{gw}}\right) \tag{1}$$

"where $\mathrm{SW_t}$ is the final soil water content (mm), SW_0 is the initial soil water content on day i (mm), R_{day} is the amount of precipitation on day i (mm), Q_{surf} is the amount of surface runoff on day i (mm), E_{a} is the amount of evapotranspiration

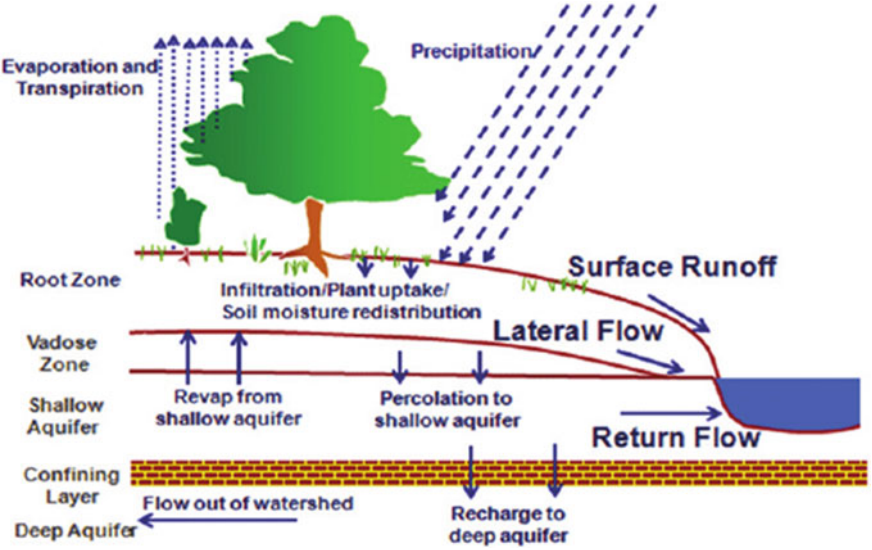

Fig. 6 Illustration of simulated hydrological cycle in SWAT source: [7]

on day i (mm), W_{seep} is the amount of water entering the vadose zone from the soil profile on day i (mm), Q_{gw} is the amount of groundwater infiltration on day i (mm) and t is time (days)".

3.2 Simulation from SWAT

Primarily, all the essential spatial data that is the LULC map, soil map and the DEM has been organized for the studied watershed area and projected to the UTM zone 43N datum. After this, the SWAT model has been set up to start hydrological simulation for the watershed. Model setup can be easily understood by the following flowchart in Fig. 7.

The first step is watershed delineation, and in this process, streams are generated by selecting projected DEM data, and 100 km^2 area threshold value was defined. This threshold is used to describe the minimum size of the sub-watershed. After it, the outlet definition, selection and snap threshold process are followed. Then, SWAT calculates the sub-basin parameters and delineates the watershed. The study area is divided into 11 sub-watersheds (Fig. 7). The second step is HRUs creation, which is done by the slope class accumulation to land use and soil. Multiple slopes bands were defined in SWAT for HRU creation. The slope bands were 0–5%, 5–10% and above 10%. The HRUs were filtered by area of 2% of total area. There were 138 HRUs which were created within the study area (Fig. 7). The third step is Edit Inputs and Run SWAT, for which the available daily observed climate data (precipitation,

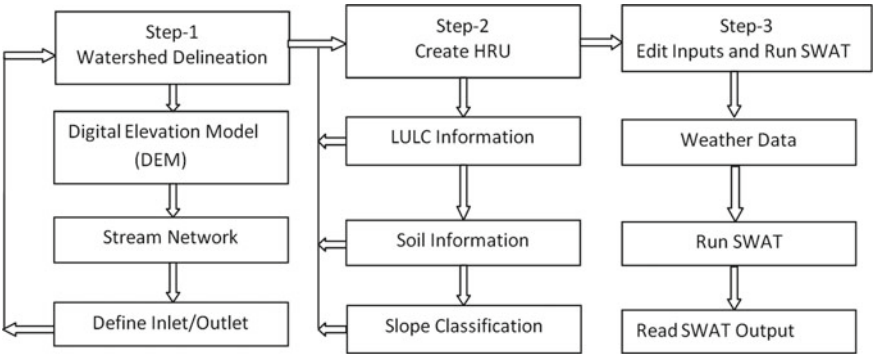

Fig. 7 Flowchart of model process

maximum/minimum temperature, wind speed and relative humidity) were selected from 1970 to 2005, and for all the climate models input data of only "precipitation and maximum/minimum temperature" were inputted for historical period (1970–2005). For the RCP 4.5 scenario and 8.5 scenario, future data from 2006 to 2100 was inputted. All the rest representative weather variables are generated by the automatic weather data generator tool. The SWAT model was simulated at monthly time step using 3 years of warm up period with default parameters. As the observed runoff data were unavailable for the study area, the outputs obtained by IMD data run were considered best and assumed as the observed data of watershed for the comparison of GCMs outputs. The performance of the SWAT model simulations of the study area was evaluated using the statistical criteria "R^2, NSE and PBIAS" suggested by Moriasi et al. [19].

4 Results and Discussion

4.1 Comparison of Climate Model with Base Model

SWAT model was simulated for a baseline period from 1970 to 2005 using the IMD rain gauge data, and the future scenarios were simulated using the five GCMs projected data. Table 2 shows the average annual basin values of different components of hydrological cycle of the watershed for the base model and GCMs.

For finding the suitable climate model for the study area, the outputs of different climate models were compared with the observed data (IMD output). All the climate models were underestimated the precipitation, lateral soil, revap from shallow aquifer to soil/plants and total water yield (Table 2). Ground water to shallow aquifer quantity, ground water to deep aquifer quantity, deep aquifer recharge, total aquifer recharge,

Table 2 Average annual basin values for base model and different GCMs

S. No.	Basin values	Base model	BNU-ESM	CCC-ma	MPI-LR	MPI-MR	CNRM
1	Precipitation (mm)	787.20	704.70	725.40	781.70	752.10	618.70
2	Surface runoff (mm)	205.84	82.7	104.75	125.35	114.35	77.51
3	Lateral soil (mm)	7.95	6.99	7.77	7.78	7.57	5.87
4	Groundwater (shallow aquifer) (mm)	193.72	225.95	268.39	251.74	249.33	170.60
5	Groundwater (deep aquifer) (mm)	13.02	13.44	15.78	14.90	14.75	10.56
6	Revaporation (shallow aquifer to soil/plants) (mm)	54.11	29.73	29.63	29.97	30.13	29.91
7	Deep aquifer recharge (mm)	13.07	13.46	15.68	14.83	14.71	10.55
8	Total aquifer recharge (mm)	261.35	269.14	313.62	296.50	294.17	211.06
9	Total water yield (mm)	420.52	329.08	396.69	399.77	386.00	264.54
10	Percolation out of soil (mm)	261.39	269.18	313.51	296.33	294.11	211.13
11	Actual evapotranspiration (mm)	312.60	346.10	326.70	353.00	336.50	324.60
12	Potential evapotranspiration (mm)	2719.10	1487.80	1482.90	1499.80	1507.60	1496.80
13	Total sediment loading (t/ha)	43.74	6.45	8.82	11.18	9.84	6.72

percolation out of soil were overestimated by BNU-ESM, CCC-ma, CNRM, MPI-LR models and underestimated by MPI-MR model (Table 2). All the climate models were underestimated the surface runoff, sediment yield and PET (Table 2).

Table 3 shows the performance indices for the surface runoff, AET and sediment load. According to the values of R^2 and NSE values, all the models fail to predict the outputs for the study area by using the outputs of IMD run as the observed data. According to PBIAS value for AET, all the models show satisfactory performance. Figures 8, 9 and 10 show the line graph and scatter plot of surface runoff, AET and sediment yield.

Table 3 Performance indices for surface runoff, AET and sediment

GCM model	Surface runoff			AET			Sediment		
	R^2	PBIAS	NSE	R^2	PBIAS	NSE	R^2	PBIAS	NSE
BNU-ESM	0.01	59.82	-1.93	0.01	**−10.7**	−1.03	0.01	85.38	−2.56
CCC-ma	0	49.11	-1.45	0.03	**−4.51**	−0.38	0.01	80.87	−2.28
CNRM	0	62.34	-2.42	0.06	**−3.84**	−0.1	0	83.89	−2.53
MPI-LR	0.01	39.1	-1.33	0.02	**−12.91**	−1.33	0.02	75.73	−2.12
MPI-MR	0.02	44.44	-1.07	0	**−7.63**	−0.73	0	77.66	−2.02

4.2 Prediction of Hydrological Components for Future RCP Scenarios

4.2.1 Precipitation

By comparing with the historical data of different climate models with the future data simulated by RCP 4.5 scenario, it was observed that in all the models the precipitation is decreased in near future (2011–2040) (Fig. 11). In mid-future (2041–2070), CCC-ma, MPI-LR and MPI-MR models show higher values of precipitation from near future, while BNU-ESM model shows lower values (Fig. 11). For far future (2071–2100), BNU-ESM and CNRM show higher precipitation, while MPI-LR and MPI-MR show lower surface runoff from mid-future (Fig. 11).

The CCC-ma model shows slight increment from historical period (725 mm, Table 2) in precipitation in near future for RCP 8.5 scenario (Fig. 12). BNU-ESM, CNRM and MPI-LR models show increment in precipitation in mid-future. Only the CNRM model shows the increase in precipitation for far future while all other models show decrease in precipitation values in far future for RCP 8.5 scenario (Fig. 12).

4.2.2 Surface Runoff

The surface runoff values show increase for CCC-ma model in all the future period for RCP 4.5 scenario (Fig. 13). The CNRM model shows decrease from near future to far future. The MPI-LR and MPI-MR models show higher values in mid-future (Fig. 13).

Figure 14 shows the results of surface runoff simulated from RCP 8.5 scenario. It is observed that BNU-ENM, CCC-ma, MPI-LR and MPI-MR show higher values for surface runoff in mid-future (2041–2070) from near future and lower values in far future (2071–2100) from mid-future (Fig. 14).

4.2.3 Actual Evapotranspiration (AET)

Figure 15 shows the simulated AET values by RCP 4.5 scenario, and it is seen that the AET values are increasing from near future to far future for all the climate models, while in RCP 8.5 scenario, the CNRM, MPI-LR and MPI-MR show the increased

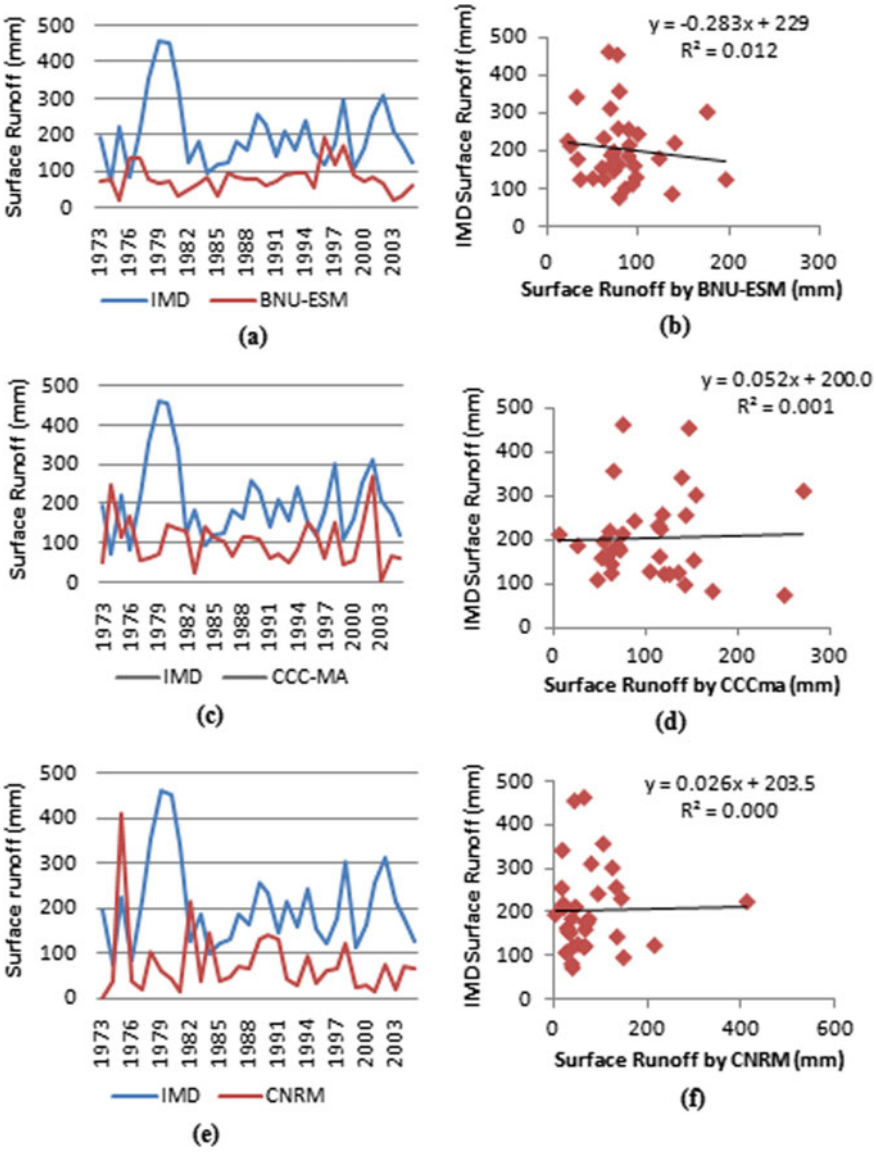

Fig. 8 Line graph and scatter plot between IMD and GCMs simulated surface runoff (**a**–**j**)

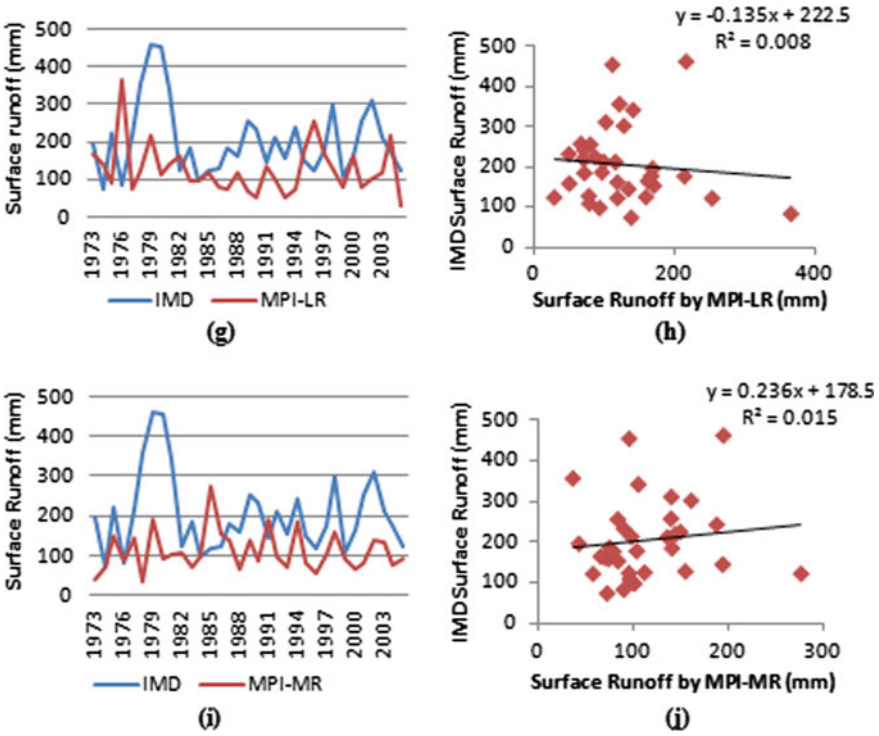

Fig. 8 (continued)

value of AET from near future to far future. The BNU-ESM and CCC-ma models show increased value of AET from near future to mid-future and decreased values from mid-future to far future (Fig. 16).

4.2.4 Sediment Load

Figure 17 shows the simulated sediment loads for RCP 4.5 scenario, and it shows that only CCC-ma model shows increase in sediment load values from near future to far future. The BNU-ESM and CNRM models show the decreased value in mid-future, while MPI-LR and MPI-MR show increased values in mid-future (Fig. 17).

Figure 18 shows the simulated sediment loads from RCP 8.5 scenario, and it was observed that BNU-ESM, CCC-ma, MPI-LR and MPI-MR models show the higher sediment in mid-future and then near future and lower values in far future, while the CNRM model shows lower sediment load in mid-future and higher in far future.

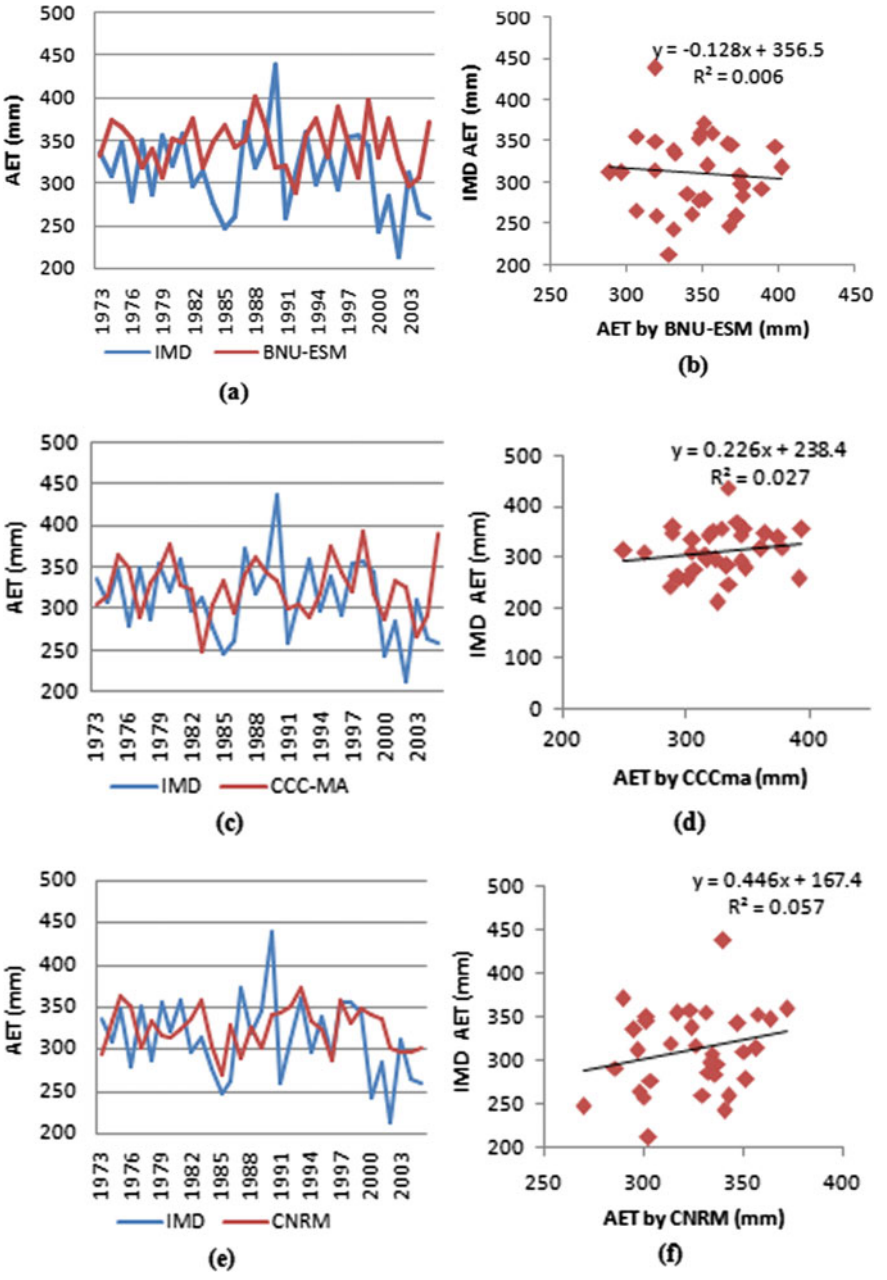

Fig. 9 Line graph and scatter plot between IMD and GCMs simulated AET (**a**–**j**)

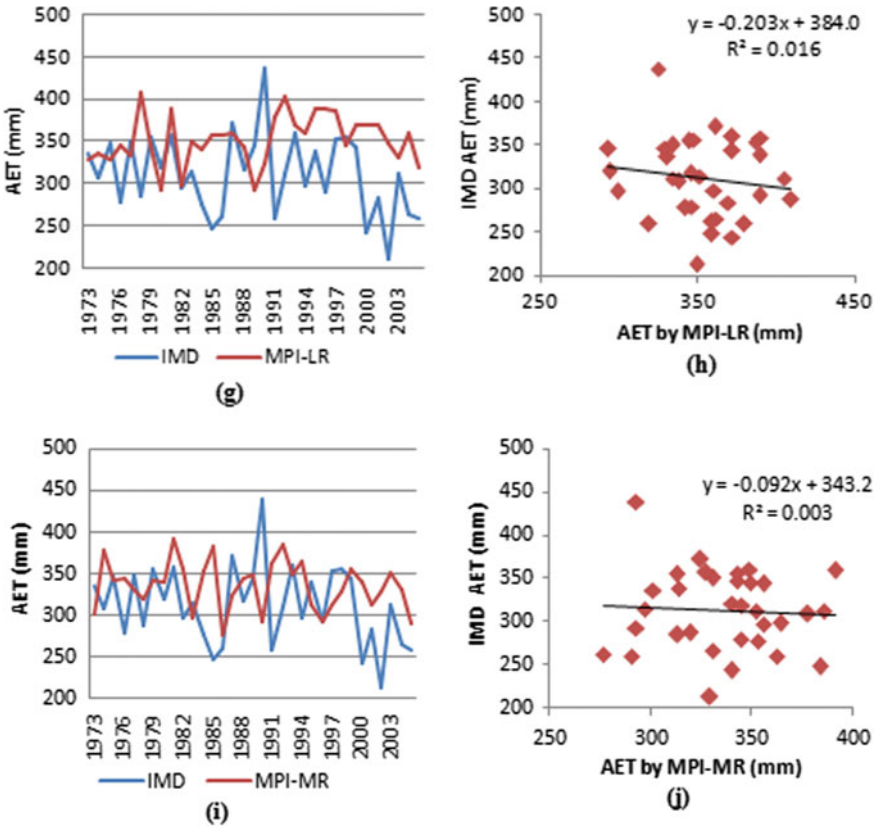

Fig. 9 (continued)

5 Limitations of the Study

Observed runoff data was unavailable for the study area. Therefore, results obtained from IMD model run were considered best and comparison was done. The comparison could be better if observed runoff data was available. All the inputs of precipitation and temperature produced by all the climate models were downscaled by kernel regression for the study area. So, the present study has the limitations of kernel regression.

6 Conclusions

SWAT model is applicable for the hydrological modelling of study area and for the prediction of future values of watershed in SWAT hydrological model. The

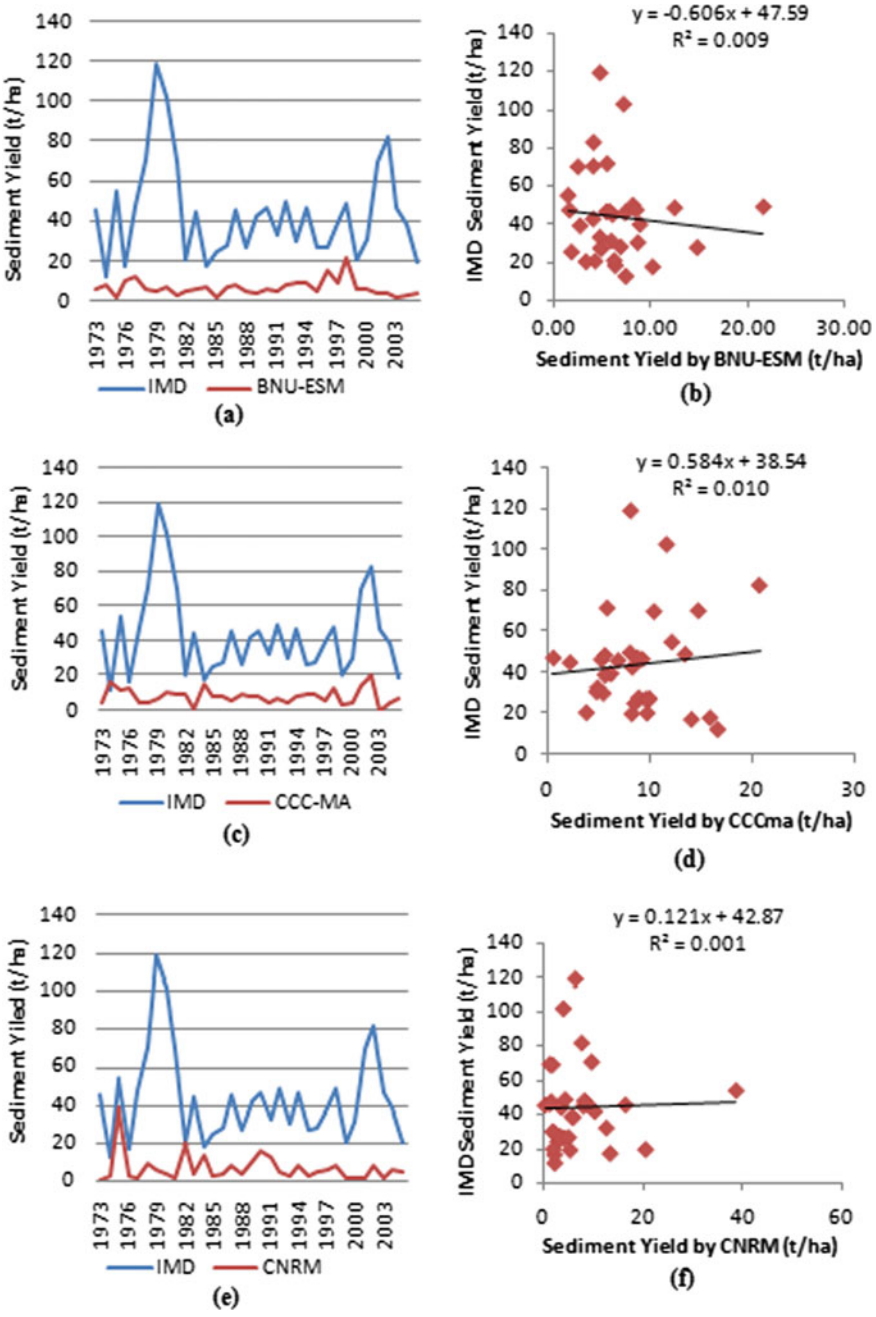

Fig. 10 Line graph and scatter plot between IMD and GCMs simulated sediment yield (**a**–**j**)

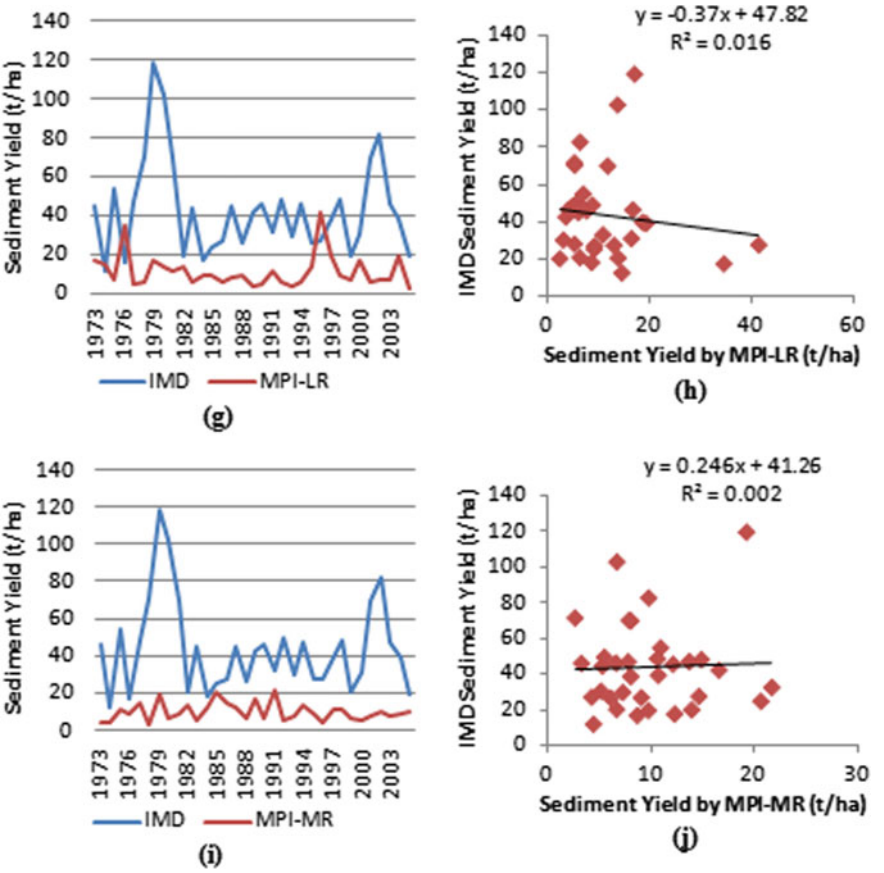

Fig. 10 (continued)

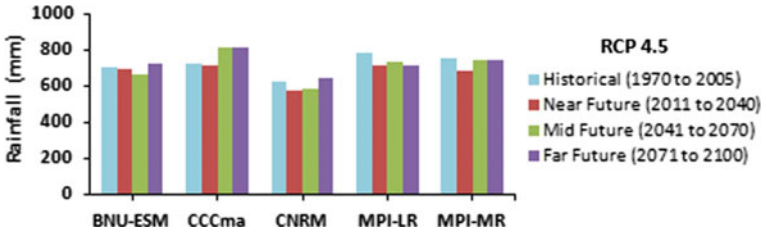

Fig. 11 Precipitation (mm) values of climate models for "near future, mid-future and far future for RCP 4.5 scenario"

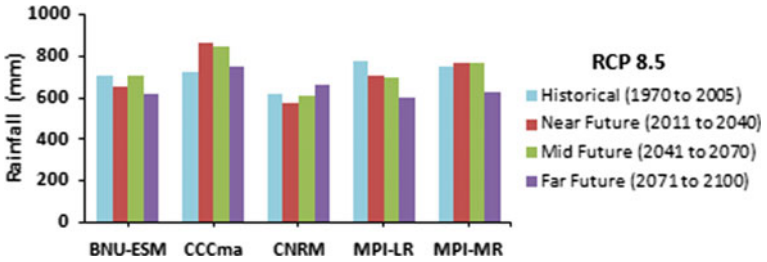

Fig. 12 Precipitation (mm) values of climate models for "near future, mid-future and far future for RCP 8.5 scenario"

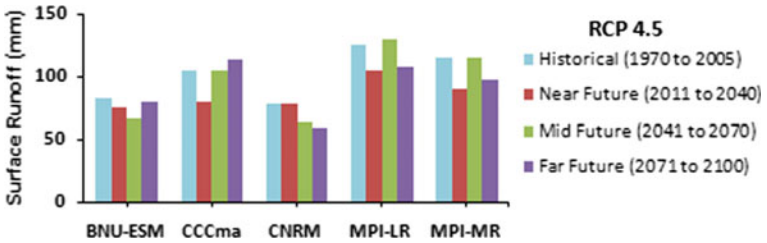

Fig. 13 Surface runoff (mm) values of climate models for "near future, mid-future and far future for RCP 4.5 scenario"

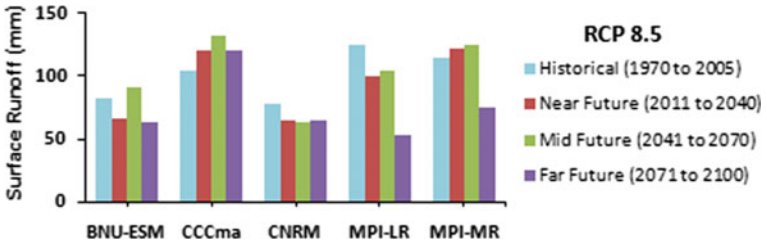

Fig. 14 Surface runoff (mm) values of climate models for "near future, mid-future and far future for RCP 8.5 scenario"

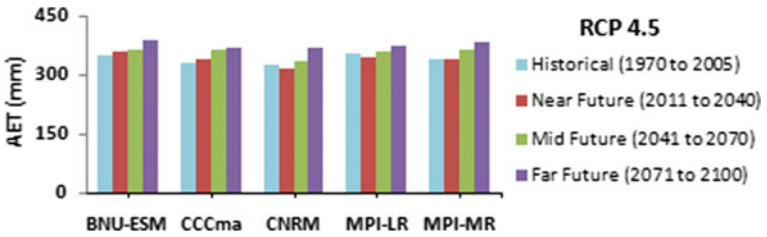

Fig. 15 AET (mm) values of climate models for "near future, mid-future and far future for RCP 4.5 scenario"

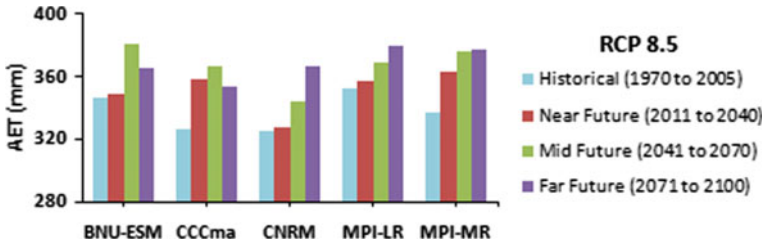

Fig. 16 AET (mm) values of climate models for "near future, mid-future and far future for RCP 8.5 scenario"

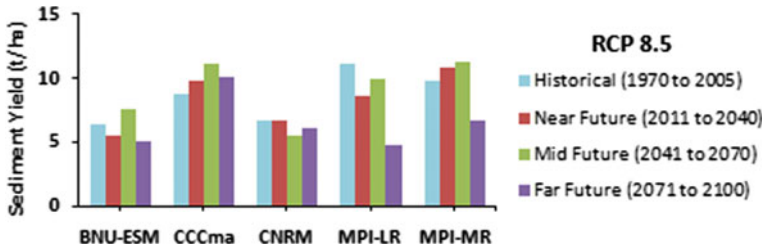

Fig. 17 Sediment yield (t/ha) values of climate models for "near future, mid-future and far future for RCP 4.5 scenario"

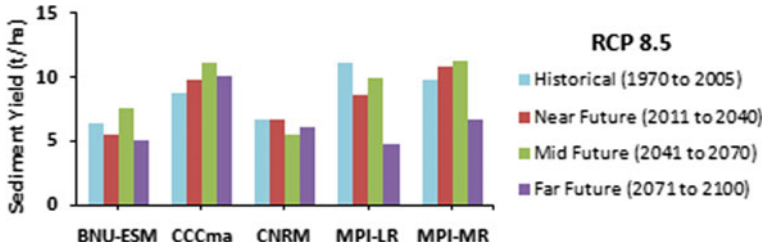

Fig. 18 Sediment yield (t/ha) values of climate models for "near future, mid-future and far future for RCP 8.5 scenario"

surface runoff, sediment yield, precipitation, lateral soil, revap from shallow aquifer to soil/plants, total water yield and PET values were underestimated by all the climate models. Deep aquifer recharge, total aquifer recharge, percolation out of soil were overestimated by BNU-ESM, CCC-ma, CNRM, MPI-LR models and underestimated by MPI-MR model. According to NSE, R^2, all the climate models were failed to predict the watershed parameters. Although all the climate models produced low per cent bias for the AET value for the study area, the CNRM model has −3.84 value of PBIAS which is best among all climate models. Almost in all climate models precipitation, surface runoff, sediment yield would decrease and actual evapotranspiration would increase in near future and mid-future for both the scenarios of RCP

4.5 and RCP 8.5; In far future precipitation, AET, sediment loading would increase and surface runoff would decrease for RCP 4.5 and precipitation, surface runoff, sediment loading would decrease and AET would increase for the scenario RCP 8.5. This type of study is helpful for the management of water resources for the study area as well as for the ungauged watersheds to take appropriate decisions under the impact of climate change.

Acknowledgements Authors are thankful to "Indian National Committee on Climate Change (INCCC), Department of Water Resources, River Development and Ganga Rejuvenation (DoWR, RD&GR), Ministry of Jal Shakti (MoJS), Government of India (GoI)", for providing the financial support for this work. Authors are also thankful to "India Meteorological Department, Prof. P.L. Patel, and Dr. P.V. Timbadiya, from the Department of Civil Engineering, SVNIT Surat", for providing the required data for Middle Tapi Basin. Authors are also thankful to Prof. Subimal Ghosh, IIT Bombay, and Statistical Downscaling Team under INCCC project. Authors are also thankful to "MNIT Jaipur" for providing all the working facilities.

References

1. IPCC (2013) Technical summary, climate change 2013: The physical science basis. Contribution of working group I to the fifth assessment report of IPCC. Cambridge University Press, Cambridge
2. IPCC (2018) Global warming of 1.5 °C. An IPCC special report on the impacts of global warming of 1.5 °C above pre-industrial levels and related global greenhouse gas emission pathways, in the context of strengthening the global response to the threat of climate change, sustainable development and efforts to eradicate poverty
3. Woo M (2012). Basin Hydrol. https://doi.org/10.1007/978-3-642-23462-0_10
4. Refsgaard JC, Storm B (1995) MIKE SHE. In: Singh VP (ed) Computer models of watershed hydrology. Water Resources Publications, Highlands Ranch, Colo, pp 809–846
5. Beven KJ, Kirkby MJ (1979) A physically based, variable contributing area model of basin hydrology. Hydrol Sci Bull 24(1):43–69
6. Bergstrom S (1976) Development and application of a conceptual runoff model for Scandinavian catchments. SMHI, Reports RHO, p 7
7. Arnold JG, Srinivasan R, Muttiah RS, Williams JR (1998) Large-area hydrologic modelling and assessment: Part 1. Model development. J American Water Resour Assoc 34(1):73–89
8. Molla S et al (2018) Investigating climate change impact on stream flow of Baro-Akobo river basin case study of Baro catchment, vol 6, Issue 5. GSJ. Online: ISSN 2320-9186
9. Krishnan R et al (2020) Introduction to climate change over the Indian region. In: Krishnan R, Sanjay J, Gnanaseelan C, Mujumdar M, Kulkarni A, Chakraborty S (eds) Assessment of climate change over the Indian region. Springer, Singapore. https://doi.org/10.1007/978-981-15-4327-2_1
10. Chandra P et al (2014) Estimation of sediment yield using SWAT model for Upper Tapi basin. ISH J Hydraul Eng 20(3):291–300
11. Munoth P, Goyal R (2019) Effects of DEM source, spatial resolution and drainage area threshold values on hydrological modelling. Water Resources Manag 33:3303–3319. https://doi.org/10.1007/s11269-019-02303-x
12. Munoth P, Goyal R (2019) Impacts of land use land cover change on runoff and sediment yield of Upper Tapi River Sub-Basin, India. Int J River Basin Manag 18(2):177–189. https://doi.org/10.1080/15715124.2019.1613413

13. Munoth P, Goyal R (2019) Effects of area threshold values and stream burn-in process on runoff and sediment yield using QSWAT model. ISH J Hydraulic Eng. https://doi.org/10.1080/09715010.2019.1670107
14. Munoth P, Goyal R (2020). Hydro morphological analysis of Upper Tapi River Sub-basin, India, using QSWAT model. Modeling earth systems and environment, vol 6, issue 4. Springer, pp 2111–2127. https://doi.org/10.1007/s40808-020-00821-x
15. Sharma P, Patel PL, Jothiprakash V (2019) Impact assessment of Hathnur reservoir on hydrological regimes of Tapi River, India. ISH J Hydraulic Eng 1–13. https://doi.org/10.1080/09715010.2019.1574616
16. Salvi K, Kannan S, Ghosh S (2013) High-resolution multisite daily rainfall projections in India with statistical downscaling for climate change impact assessment. J Geophys Res Atmos 118:3557–3558. https://doi.org/10.1002/jgrd.50280
17. Kannan S, Ghosh S (2013) A nonparametric Kernel regression model for downscaling multisite daily precipitation in the Mahanadi basin. Water Resour. Res. 49:1360–1385. https://doi.org/10.1002/wrcr.20118
18. Wagner P, Kumar S, Fiener P, Schneider K (2011) Technical note: hydrological modelling with SWAT in a monsoon-driven environment: experience from the Western Ghats, India. Trans ASABE 54:1783–1790. https://doi.org/10.13031/2013.39846.
19. Moriasi DN, Arnold JG, Van Liew MW, Bingner RL, Harmel RD, Veith TL (2007) Model evaluation guidelines for systematic quantification of accuracy in watershed simulations. Trans ASABE 50(3):885–900

Model Performance Evaluation using Streamflow and Potential Evapotranspiration over Middle Tapi Basin, India

Prabhat Dwivedi, Lalit Kumar Gehlot, and P. L. Patel

Abstract Integrated watershed planning, management and decision-making are important for the efficient utilization of available water resources. The physics-based hydrological models enable quantitative and qualitative evaluation of water at different spatial and temporal scales. The current study aims to ascertain the reliability of hydrologic simulations using the SWAT hydrologic model. The model was developed for a climate-sensitive and agriculturally dominated catchment, i.e., the Middle Tapi basin (MTB), between Hatnur and Ukai reservoirs. The monthly inflows of the Ukai reservoir were utilized to calibrate and validate the SWAT model for 1998–2007 and 2008–2013, respectively. The simulated potential evapotranspiration (PET) at the basin scale was compared with CRU-PET data to ascertain the reliability of the simulated variable. The global sensitivity analysis shows that *GWQMN.gw, REVAPMN.gw, GW_REVAP.gw, SOL_K.sol, CNCOEF.bsn, SOL_AWC.sol* are the most sensitive parameters at 5% significance level. The model performance metrics, namely *KGE, NSE,* R^2 and *PBIAS* with respect to observed streamflow during calibration (validation) period are 0.98 (0.98), 0.98 (0.97), 0.98 (0.97) and 0.6% (−1.2%), respectively. The similar statistics for PET during simulation period (1998–2013) are 0.73, 0.84, 0.94 and −4.36%, respectively. The model performance metrics show that the hydrologic model reliably simulates monthly inflows into the Ukai reservoir and PET in MTB. Thus, the developed model can accurately forecast hydrologic changes in response to climate instability in the study area, allowing for better water management practices.

Keywords Potential evapotranspiration (PET) · Soil and water assessment tool (SWAT) · Sequential uncertainty fitting version-2 (SUFI-2) · SWAT-calibration and uncertainty prediction (SWAT-CUP) · Middle Tapi basin

P. Dwivedi (✉) · L. K. Gehlot · P. L. Patel
Department of Civil Engineering, Sardar Vallabhbhai National Institute of Technology Surat, Surat 395007, India
e-mail: prabhat20011996@gmail.com

P. L. Patel
e-mail: plpatel@ced.svnit.ac.in

P. V. Timbadiya et al. (eds.), *Hydrology and Hydrologic Modelling*,
Lecture Notes in Civil Engineering 312,
https://doi.org/10.1007/978-981-19-9147-9_2

1 Introduction

The physics-based spatially distributed watershed models can predict the integrated response of the changing climatic conditions and anthropogenic activities in the watershed. These models/tools can effectively address the potential environmental and water management threats pertaining to climate variability, land-use change, reservoir operation, water yield, soil erosion, etc. The degree of accuracy and uncertainty of hydrologic model simulations is primarily a function of model inputs, model structure, calibrating variables, etc., affecting the decision-making. The researchers utilize remote sensing (RS) and geographic information systems (GIS) products, available at various spatiotemporal scales, for modeling uncertainty due to different data sources [1]. The quantification of uncertainties in hydrological simulations helps hydrologists and government authorities make decisions for long-term water resource planning and management.

The Soil Water Assessment Tool (SWAT), a hydrologic response unit (HRU)-based watershed model, evaluates the effects of topography, land development activities, climate variability and alternative watershed management strategies on water, sediment and nutrient yields from the basin [2, 3]. The SWAT model is globally accepted to simulate various water balance components and processes in the watershed. The Sequential Uncertainty Fitting (SUFI-2) in SWAT-CUP (calibration and uncertainty program) is widely used to account for parametric sensitivity and uncertainty in hydrologic simulations [4, 5]. However, calibration of the hydrologic model using a single variable, particularly in heterogeneous catchments, may lead to unrealistic hydrologic model predictions due to the non-uniqueness of the model parameters and uncertainty associated with parameters range [5–8]. This requires a thorough evaluation of the model's goodness using multivariable/multisite calibration techniques [9–13].

Due to its unique geographical setting, the Tapi river basin (TRB) is climatically heterogeneous in Peninsular India. The TRB is subdivided into Upper (UTB), Middle (MTB) and Lower (LTB) Tapi basins based on the geographic location of major hydraulic structures/dams. The MTB, an agriculture-dominated landmass, gets frequently affected due to scarce rainfall, and prolonged dry spell durations over the year [14] may lead to over-dependency on groundwater resources. The anthropogenic changes, hydro-climatic variability and streamflow regulation from major hydraulic structures (Hatnur and Girna dams) have severely impacted aquatic life and water demand for socio-economic growth in the region [15–17]. Thus, understanding the hydro-climatic variability and hydrological modeling can help derive better regional water management practices. The key objective is to develop a SWAT hydrologic model for MTB, calibrate and validate using streamflow data and ascertain the reliability of the developed model by comparing the simulated PET form hydrologic model with PET data of Climate Research Unit; https://crudata.uea.ac.uk/cru/data/hrg(CRU)).

2 Study Area and Data Sources

2.1 Middle Tapi Basin

The TRB is India's sixth largest river basin with total flow length of 724 km and drainage area of 65,145 km^2. At an elevation of 752 m, the Tapi River rises from Multai in the Betul Plateau and flows into the Arabian Sea, where it joins the Gulf of Khambhat. The MTB lies between Hatnur and Ukai dam/reservoir, having total watershed area of 32,925 km^2 (see Fig. 1). The study region has basaltic hills in peripheral part and alluvial plains in central region. The Middle Tapi River has five major tributaries on its left side, i.e., Girna, Waghur, Bori, Panjhra and Buray, while three are on its right side, i.e., Aner, Arunavati and Gomai. The Hatnur dam, an earthen dam in Maharashtra with gross (live) storage capacity of 388.0 (255.0) MCM (10^6 m^3), forms the upstream boundary for MTB, while Ukai dam, Gujarat's second largest earth-cum masonry dam with gross (live) storage capacity of 7414.29 (6730.00) MCM and located 300 km downstream of the Hatnur dam, serves the downstream boundary for MTB. The watershed elevation varies from 63 to 1563 m above mean sea level as shown in Fig. 1.

The climatology of MTB can be characterized by a hot summer and persistent dryness throughout the year with low monsoon rainfall. The daily minimum (maximum) temperature ranges from 8 °C (34 °C) in January month to 22 °C (44 °C) in May month. The average annual rainfall and PET (period 1990–2013) in the basin

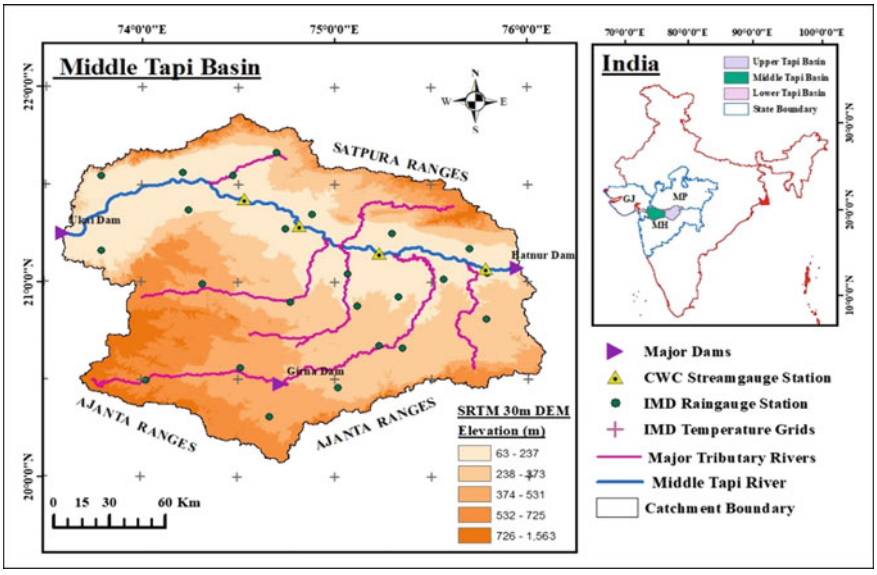

Fig. 1 Index map of study area

are 791 mm and 2248 mm, respectively. The aridity index (ratio of rainfall to PET) in the research area is 0.35, indicating that the climate is semi-arid. Agricultural land is the most frequent land use in the region, followed by deciduous forest and fallow land. The dominant soil classes in the region vary from very gentle sloping to moderate and level surface. The soil texture ranges from loamy to clayey and deep black soil. The major historical floods were observed in the years 1998 and 2006 in the MTB, after the construction of Hatnur dam [15].

2.2 Data Sources

The SWAT model requires topography, land use and land cover, soil, slope and weather data. For delineation of watershed features, the open-source Shuttle Radar Topographic Mission (SRTM, https://earthexplorer.usgs.gov) Digital Elevation Model (DEM) of 30 m grid size was used. The LULC data from NRSC, Hyderabad, with a spatial resolution of 56 m and soil map of NBSS&LUP, Nagpur (at a scale of 1:2,50,000) have been used for the development of the model. The daily rainfall data of 24 stations and daily maximum and minimum temperature data, interpolated to 0.5° × 0.5° from 1.0° × 1.0° using bilinear interpolation, have been obtained from India Meteorological Department (IMD), Pune. The daily streamflow data and releases from the Hatnur dam were obtained from Central Water Commission, Surat Division, and Tapi Irrigation Development Corporation, Jalgaon. The monthly PET data of CRU, at 0.5° × 0.5°, is used as a reference dataset for assessing simulated PET from the model.

3 SWAT Model

The SWAT model demarcates the watershed and sub-watersheds depending upon user-specified outlet points and the drainage area threshold. Each sub-watershed/subbasin is further subdivided into multiple hydrological response units (HRUs), representing a unique combination of land use, soil and slope class in the watershed. The SWAT uses land phase hydrology to control the amount of water, sediments and nutrients entering the main channel while the routing phase controls the flow of water, sediments and nutrients from the watershed drainage network to the outlet. The mathematical representation of the hydrologic cycle adopted by the SWAT model is based on the water balance equation (see Eq. (1), all having unit as mm H_2O).

$$S_{\text{final}} = S_{\text{initial}} + \sum_{i=1}^{t} \left(P_{\text{day}} - Q_{\text{overflow}} - E_{\text{actual}} - W_{\text{sepage}} - Q_{\text{ground}} \right) \tag{1}$$

where S_{initial}, S_{final}, P_{day}, Q_{overflow}, E_{actual}, W_{sepage}, Q_{ground} represents the initial soil moisture content, final soil moisture content, precipitation, surface runoff, evapotranspiration, percolation and return flow, respectively, on day i; and t is time in days. The hydrological response is anticipated separately for each HRU and subsequently routed through each subbasin in the watershed [2, 3]. In this study, the SCS-CN method with slope adjustment in CN2, plant ET method and Hargreaves method are employed to estimate land phase water balance parameters in the catchment, whereas the variable storage method is used to develop a hydrograph at the outlet of each basin in the main channel.

In the watershed delineation process, 48 subbasins were delineated in the MTB between the Hatnur dam, at the upstream boundary and Ukai dam, at the downstream boundary, wherein releases from the Hatnur dam act as inlet points to the MTB. The SWAT model resamples the spatial inputs, i.e., soil and land use, to match the input DEM grid size. The LULC map (see Fig. 2) obtained from NRSC is reclassified into six major classes, namely agriculture (AGRC- 49.88%), wasteland (BARR-10.58%), built-up (URML -1.79%), current fallow land (AGRR-16.26%), deciduous forest (FRSD-17.80%) and water body (WATR-3.70%). The primary soil texture, particularly hydrologic soil groups C and D, ranges from silty clay to clays and clay loam. The soil database comprising soil properties including hydrological soil group, texture, soil water content, soil depth, saturated hydraulic conductivity, bulk density, organic carbon content and percentage of soil texture was given as an input database to the SWAT model. In addition, the basin is divided into three major slope classes, 0–2%, 2–5% and more than 5%, fairly representing flat, moderately sloping and steep sloping land features, respectively. The area under smaller HRUs was restructured/redefined using HRU thresholds of 2, 5 and 10% for land use, soil and slope, thereby reducing total HRUs from 5186 to 2144. The CN values for each HRU are corrected for the slope class greater than 5% in the subbasin. The current study used a freely available weather generator database derived from IMD daily gridded data of 85 years with a spatial resolution of $1° \times 1°$. The station-based (24 nos.) rainfall data and grid-based minimum and maximum temperature data are used, remaining weather parameters, i.e., solar radiation, wind velocity, and relative humidity, are simulated by a weather generator. The Hatnur dam outflow from the spillway crest was given as inlet discharge into the MTB hydrological model.

The SWAT model's parameters are process-based and should be adjusted within an acceptable uncertainty range. The most frequent causes of model uncertainty are anomalies in the spatial inputs, meteorological data, calibration variables and model assumptions. The calibration process involves the identification and regionalization, if permissible, of sensitive parameters and minimizing the uncertainty for a particular set of local conditions in the watershed or sub-watershed. The approach of calculating the average rate of change of the output variable/objective function of the model in relation to changes in model parameters is known as sensitivity analysis. The key parameters with specific range must be identified in the calibration process, followed by independent validation to determine whether the model will precisely replicate the watershed process-based on objectives [6]. The model is calibrated and validated for observed streamflow data for the period of 1998–2007 and 2008–2013, respectively.

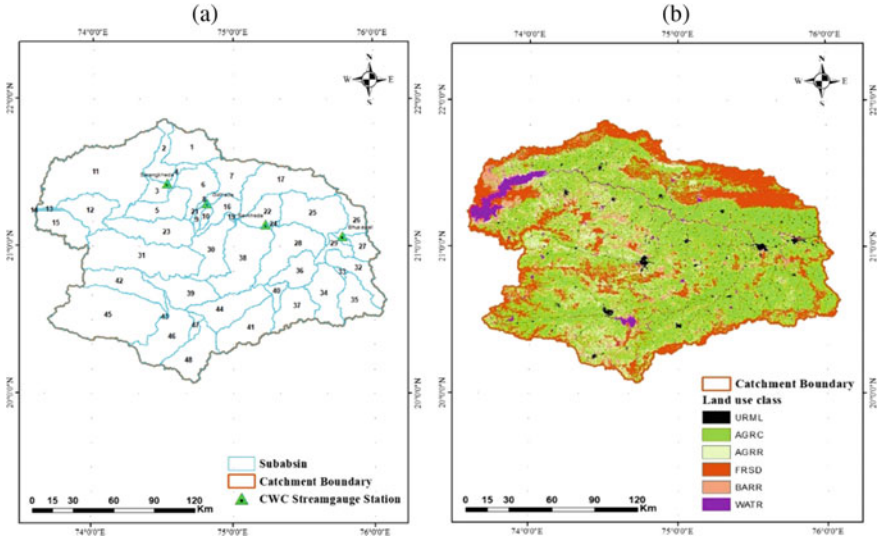

Fig. 2 **a** Sub-watersheds during watershed delineation, **b** LULC map of MTB

The four-year warm-up period (1994–1997) has been used for the stabilization of the initial model parameters. The model performance is regarded as acceptable if NSE ≥ 0.5, $R^2 \geq 0.5$, and PBIAS $< \pm 25\%$ [18]. Furthermore, the reliability of the simulation of the watershed process was ascertained by independent validation of the simulated PET with the PET data obtained from CRU due to the non-availability of the measured meteorological variables in the study region.

4 Results and Discussion

The calibration being an inverse modeling process invites parametric uncertainties; thus, parameter selection plays a crucial role for a model to represent the watershed hydrology. The parameters selected for calibration of the model comprise parameters related to water in various phases of hydrological processes, i.e., groundwater (*.gw*), land management (*.mgt*), soil (*.sol*), main channel (*.rte*), hydrological response units (*.hru*) and basin parameters (*.bsn*) (see Table 1). The uncertainty in simulated streamflow is determined statistically based on the *p-factor*, the percentage of observations encapsulated by the 95PPU (percentage prediction uncertainty) band, and *r-factor*, relative thickness of the 95PPU band with respect to the standard deviation of observed flow [5]. The objective function adopted for selecting the best parameters is *Kling–Gupta Efficiency* (*KGE*). The model calibration, validation, sensitivity ranks of the parameter during the final calibration range and uncertainty in the model simulation are assessed by SUFI-2 in SWAT-CUP. Table 1 lists the model

calibration parameters and their original and calibrated ranges, fitted values and sensitivity ranks. At a 5% level of significance, the global sensitivity analysis ranks demonstrate that groundwater (*GW_REVAP.gw, GWQMN.gw, REVAPMN.gw*), soil moisture (*SOL_AWC.sol*), and plant ET CN coefficient (*CNCOEF.bsn*) are the most dominating water balancing components affecting the streamflow, corresponding to *KGE* objective function.

The internal consistency of fit for observed and simulated inflows in the Ukai reservoir is assessed using the model performance indicators, i.e., *KGE*, *Nash–Sutcliffe* (*NSE*), *coefficient of determination* (R^2) and *percentage bias* (*PBAIS*). The respective values of model performance statistics through calibration (validation) period are 0.99 (0.97), 0.98 (0.97), 0.98 (0.97) and 0.0 (−1.7), respectively (see Table 2). The uncertainty estimators, i.e., *p-factor* (*r-factor*), through the calibration and validation are 0.48 (0.65) and 0.52 (0.59), respectively. The model performance statistics and the flow hydrograph (see Fig. 3) infer that the developed SWAT model is capable of simulating monthly inflow into the Ukai reservoir with fair confidence and accuracy. The annual water balance during calibration and validation is obtained from the *output.std* file. The average evapotranspiration and water yield from the MTB are 55% and 19%, respectively. Out of the 19% of the water yield, on average, the contributions from overland flow and groundwater flow/baseflow are 80% and 20%, respectively. The average curve number (CN) of the MTB during the simulation period was found to be 79.

The reliability of the simulated hydrological variables has been ascertained by using a variable that is not used as calibrating variable. Due to the lack of field observations, readily available PET data from CRU was used as a reference dataset in this work, and the assessment was done at the basin level, i.e., MTB. The simulated PET for MTB has been extracted from the *output.std* file of SWAT, and the average basin PET from CRU gridded dataset has been derived using Thiessen weights. The performance evaluation indicators, namely *KGE, NSE,* R^2, and *PBIAS* through the simulation period (1998–2013), are found to be 0.73, 0.84, 0.94 and −4.36%, respectively (see Table 2). The average monthly estimates of PET during the same period are shown in Fig. 4. The model performance indicator demonstrates high agreement between CRU-PET and simulated PET values on a monthly scale. The average monthly PET values have shown deviations ranging from −12.6% (in May) to 21.5% (in December), while the average annual estimates have shown a variation of 7%. Considering the various statistical indicators for calibrating variable (streamflow) and independent variable (PET), the SWAT model developed in the present study has shown reliable estimates for the watershed hydrological process from the period 1998- to 2013. Thus, a developed model can be utilized to accurately simulate the hydrologic alteration to the climate instability in the research area, and better water management practices can be employed. The model can also be used to assess the impact of LULC change, climate change, land management practices, etc., in individuals and in combination.

Table 1 Model calibration parameters, initial and calibrated range, fitted value and their sensitivity ranks

Parameter name	Initial range	Calibrated range	Fitted value	Sensitivity rank
V__ALPHA_BF.gw	0.1–0.7	0.228–0.738	0.592	24
V__GW_DELAY.gw	7–90	7.579–83.812	55.256	7
V__GWQMN.gw	110–2838	112.303–3238.197	2728.937	2
V__GW_REVAP.gw	0.1–0.2	0.02–0.2	0.169	1
V__REVAPMN.gw	85–410	132.651–430.016	317.389	3
V__RCHRG_DP.gw	0.01–0.17	0.001–0.017	0.013	28
R__CN2.mgt	−0.18 to −0.05	−0.18 to −0.012	−0.028	8
R__SOL_AWC().sol	0.14–0.48	−0.014 to 0.478	0.33	4
R__SOL_K().sol	−0.75 to −0.12	−0.357 to −0.048	−0.198	29
R__SOL_BD().sol	−0.46 to −0.1	−0.464 to −0.114	−0.213	26
V__SOL_ZMX.sol	320–2800	344.092–2781.408	2571.19	22
R__SOL_ALB().sol	0.08–0.24	0.073–0.24	0.142	18
V__CH_N2.rte	0.03–0.09	0.02–0.069	0.026	13
V__CH_K2.rte	5–85	3.601–87.135	51.111	11
R__CH_S2.rte	−0.07 to 0.01	−0.074 to 0.005	−0.021	10
V__ALPHA_BNK.rte	0.4–0.93	0.281–0.843	0.758	25
V__ESCO.hru	0.15–0.6	0.228–0.46	0.265	27
V__EPCO.hru	0.7–0.96	0.44–0.99	0.465	19
V__CANMX.hru	12–45	12.089–42.248	21.074	6
V__OV_N.hru (URML)	0.02–0.05	0.012–0.046	0.029	16
V__OV_N.hru (FRSD)	0.26–0.58	0.261–0.684	0.327	15
V__OV_N.hru (WATR)	0.01–0.04	0.017–0.036	0.031	9
V__OV_N.hru(AGRR, BARR)	0.02–0.05	0.018–0.042	0.032	30
V__OV_N.hru (AGRC)	0.02–0.05	0.023–0.046	0.034	20
R__HRU_SLP.hru	0.01–0.23	0.011–0.187	0.067	12
V__CH_N1.sub	0.02–0.06	0.019–0.047	0.024	31
V__CH_K1.sub	4–85	4.111–78.298	41.05	23
R__CH_S1.sub	0.03–0.2	0.035–0.184	0.163	14
V__SURLAG.bsn	2.5–17	2.358–16.274	4.938	17
V__EVRCH.bsn	0.6–0.98	0.646–0.985	0.832	21
V__CNCOEF.bsn	1.14–2.0	1.142–2.0	1.991	5

Table 2 Summary of model performance statistics

Performance indices	Observed streamflow		Potential evapotranspiration
	Calibration (1998–2007)	Validation (2008–13)	Simulation period (1998–2013)
KGE	0.99	0.97	0.73
NSE	0.98	0.97	0.84
R^2	0.98	0.97	0.94
PBIAS	0.00	−1.70	−4.36
p-factor	0.48	0.65	–
r-factor	0.52	0.59	–

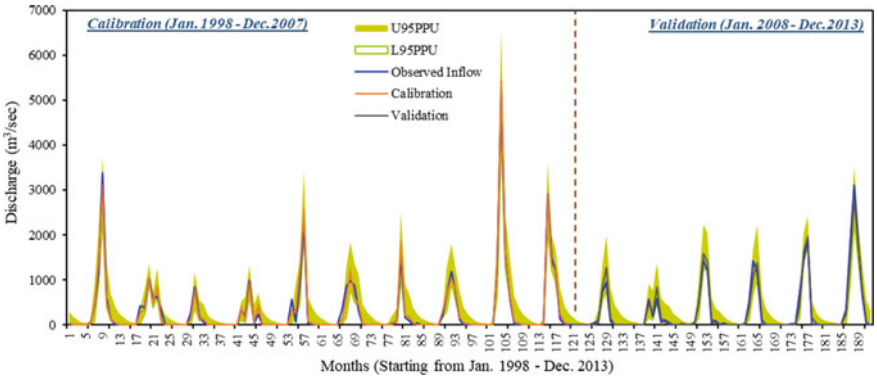

Fig. 3 Observed and simulated inflow in Ukai reservoir

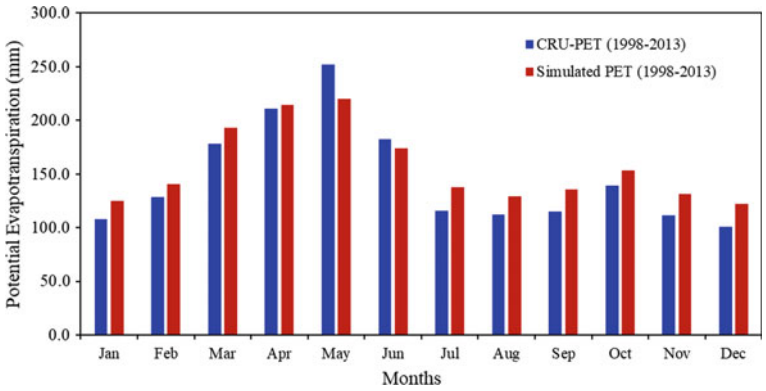

Fig. 4 Average monthly PET values

5 Conclusions

The present study has developed a SWAT hydrologic model for a semi-arid Middle Tapi basin (MTB) with releases from the Hatnur dam as an upstream boundary. The model has been successfully calibrated and validated on a monthly time scale to estimate inflows into the Ukai reservoir, which serves as the downstream boundary. The model reliability is also ascertained using PET as an independent variable, and the simulated PET has been compared with CRU-PET data at the basin scale. Since ET holds a significant portion of total water available in the global/regional hydrological cycle, the present study emphasizes reliable simulation of non-calibrating variables, i.e., PET. The main findings of the current investigation are as follows:

- The model performance metrics, namely *KGE, NSE,* R^2, and *PBIAS* concerning observed monthly streamflow through the calibration (validation) period, are 0.99 (0.97), 0.98 (0.97), 0.98 (0.97) and 0.0 (−1.7), respectively, signifying good competence of the hydrologic model to simulate monthly inflows through extensive drainage network of MTB into the Ukai reservoir.
- The respective values of the performance statistics for PET are 0.73, 0.84, 0.94 and −4.36%, respectively, indicating model capability to simulate the other hydrologic variables with fair accuracy and a high degree of confidence. Thus, the present model can give a reliable forecast of monthly inflows in the Ukai reservoir for future climate data.
- The present study used a single-site single variable approach, i.e., inflows into the Ukai reservoir, which may be considered a limitation. Based on the data's availability, the model's functioning can be further improved by incorporating a multi-metric calibration approach, i.e., multiple variables under calibration at multiple gauging sites.

Acknowledgements The authors would like to acknowledge the Indian National Committee on Climate Change, Ministry of Jal Shakti, Department of Water Resources, River Development & Ganga Rejuvenation, Government of India (GoI), and Centre of Excellence on 'Water Resources and Flood Management,' TEQIP-II, Ministry of Education, GoI, respectively, for providing funding and infrastructure facilities for this research. All data disseminating agencies, i.e., IMD Pune, TIDC Jalgaon, Ukai Civil Circle, NBSS&LUP Nagpur, and NRSC, Hyderabad, are duly acknowledged for providing necessary data to conduct the present study.

References

1. Ghoraba SM (2015) Hydrological modeling of the Simly Dam watershed (Pakistan) using GIS and SWAT model. Alex Eng J 54(3):583–594
2. Arnold JG, Srinivasan R, Muttiah RS, Williams JR (1998) Large area hydro-logic modeling and assessment part I: model development 1. JAWRA J Am Water Resour Assoc 34(1):73–89
3. Arnold JG, Allen PM, Volk M, Williams JR, Bosch DD (2010) Assessment of different representations of spatial variability on SWAT model performance. Trans ASABE 53(5):1433–1443

4. Abbaspour KC (2015) SWAT Calibration and uncertainty programs—A user manual. Swiss Federal Institute of Aquatic Science and Technology, Eawag, Switzerland
5. Abbaspour KC, Vaghefi SA, Srinivasan R (2018) A guideline for successful calibration and uncertainty analysis for soil and water assessment: a review of papers from the 2016 international SWAT conference.
6. Kouchi DH, Esmaili K, Faridhosseini A, Sanaeinejad SH, Khalili D, Abbaspour KC (2017) Sensitivity of calibrated parameters and water resource estimates on different objective functions and optimization algorithms. Water 9(6):384
7. Leta OT, Van Griensven A, Bauwens W (2017) Effect of single and multisite calibration techniques on the parameter estimation, performance, and output of a SWAT model of a spatially heterogeneous catchment. J Hydrol Eng 22(3):05016036
8. Nkiaka E, Nawaz NR, Lovett JC (2018) Effect of single and multisite calibration techniques on hydrological model performance, parameter estimation and predictive uncertainty: a case study in the Logone catchment, Lake Chad basin. Stoch Environ Res Risk Assess 32(6):1665–1682
9. White KL, Chaubey I (2005) Sensitivity analysis, calibration, and validations for a multisite and multivariable SWAT model 1. JAWRA J Am Water Resour Assoc 41(5):1077–1089
10. Cao W, Bowden WB, Davie T, Fenemor A (2006) Multivariable and multisite calibration and validation of SWAT in a large mountainous catchment with high spatial variability. Hydrol Process: Int J 20(5):1057–1073
11. Chiang LC, Yuan Y, Mehaffey M, Jackson M, Chaubey I (2014) Assessing SWAT's performance in the Kaskaskia River watershed as influenced by the number of calibration stations used. Hydrol Process 28(3):676–687
12. Franco ACL, Bonumá NB (2017) Multivariable SWAT model calibration with remotely sensed evapotranspiration and observed flow. RBRH 22
13. Zhang J, Li Q, Guo B, Gong H (2015) The comparative study of multisite uncertainty evaluation method based on SWAT model. Hydrol Process 29(13):2994–3009
14. Gehlot LK, Jibhakate SM, Sharma PJ, Patel PL, Timbadiya PV (2021) Spatio-temporal variability of rainfall indices and their teleconnections with El Niño-Southern Oscillation for Tapi Basin, India. Asia-Pacific J Atmos Sci 57:99–118
15. Sharma PJ, Patel PL, Jothiprakash V (2019) Impact assessment of Hathnur reservoir on hydrological regimes of Tapi River, India. ISH J Hydraulic Engin 1–13
16. Ramkar P, Yadav SM (2019) Identification of critical watershed using hydrolog-ical model and drought indices: a case study of upper Girna, Maharashtra, India. ISH J Hydraul Eng 1–12
17. Sahana V, Timbadiya PV (2020) Spatiotemporal variation of water availability under changing climate: case study of the Upper Girna Basin, India. J Hydro-l Eng 25(5):05020004
18. Moriasi DN, Gitau MW, Pai N, Daggupati P (2015) Hydrologic and water quality models: performance measures and evaluation criteria. Trans ASA-BE 58(6):1763–1785

Integrated Modeling of the Lower Tapi Basin Using SWAT

Aditi K. Rathod and Sanskriti Mujumdar

Abstract The Soil and Water Assessment Tool (SWAT) is a globally used integrated watershed model for studying sediment, hydrology, land use, climate change, in-stream water quality, and other water management actions on water quality and quantity. The present research aims to hydrological modeling of Lower Tapi basin using SWAT from Ukai dam to Surat city. Surat is one of India's most densely populated cities, located at the tail portion of the Tapi River. One of the biggest flood occurred in the year of 1998 and 2006. The Soil and Water Assessment Tool (SWAT) was used to establish rainfall–runoff relationship for the Lower Tapi basin. The Lower Tapi basin runoff is estimated using the SWAT model, which combines GIS data with an attribute database. SWAT a physical-based semi-distributed parameter designed to predict runoff, effect of soil and anticipate the effect of land management approaches. SWAT model is developed for the base line scenario for 1998–2017. SWAT-cup is used to calibrate and validate the SWAT model. Then, using 19 years of daily precipitation as well as daily maximum and lowest temperature data, a SWAT simulation is run for each day to determine future runoff for the associated rainfall. On a daily time scale, the model was calibrated at the Mandvi gauging site. The observed flow data was used to identify sensitivity values, which were then calibrated. For auto-calibration and validation, the SWAT-CUP SUFI-2 software was employed. The calibrated model can be utilized for further in-depth study, such as water resource management and climate and land use change impact assessments.

Keywords Integrated modeling · Hydrology · SWAT model · SWAT-CUP SUFI-2

A. K. Rathod (✉) · S. Mujumdar
Civil Engineering Department, Faculty of Technology and Engineering, The M.S. University of Baroda, Vadodara, Gujarat 390001, India
e-mail: aditirathod.a@gmail.com

S. Mujumdar
e-mail: ssmujumdar-ced@msubaroda.ac.in

P. V. Timbadiya et al. (eds.), *Hydrology and Hydrologic Modelling*,
Lecture Notes in Civil Engineering 312,
https://doi.org/10.1007/978-981-19-9147-9_3

1 Introduction

The most significant intrinsic of water resources development and administration programmers is understanding a basin's water balance [1]. Water balance equations can be used to quantify major hydrological processes. Any effort to develop water resources requires a full understanding of how these physical elements interact with hydrological component. Because hydrologic processes are so complex, it is critical to have a thorough understanding of them, which is why watershed models are so popular [1]. The majority of watershed models essentially simulate precipitation transformation into runoff, sediment discharge and nutrient losses.

Integrated watershed models are models that provide a holistic picture of the numerous hydrologic processes [2]. There are a variety of physically based semi-distributed models that are integrated. SWAT has been regarded as the most promising and computationally efficient among them by academics (Neitsch et al. [3]). As a result, an attempt has been made in this work to identify the most sensitive SWAT model parameters and to evaluate the significant hydrologic components of a river basin with an emphasis on water conservation and management.

The main goals of this study are to use the SWAT model to analyze the rainfall–runoff conduct of the Lower Tapi basin, to simulate the discharge using SWAT-CUPs with the sequential uncertainty fitting (SUFI-2) algorithm and to undertake sensitivity testing of the model parameters in terms of improving the model's actual prospects in simulating runoff.

2 Description of Model

The USDA Agricultural Research Service (USDA-ARS) and Texas a&MAgriLite Research collaborated to create the Soil and Water Assessment Tool (SWAT), a public domain model. The SWAT model is a watershed model with a long-term, continuous simulation. It is made to predict how management affects water, sediments and agricultural chemical yields on a regular basis. This model was created in the early 1990s. With the passage of time, the SWAT model's development process continues to address many emergent difficulties in hydrological modeling. Various tools, such as different hydrological response units, auto-irrigation and fertilization options, nutrition cycling routine, bacteria transfer routine and so on, were introduced to the model during its development. Water and sediment circulation can be examined and projected with the help of this model. Runoff in urban catchments can be estimated using this model. The entire catchment region has been separated into sub-catchments in order to use the model in a real-world setting. The sub-catchments are further separated into minor Hydrological Response Units (HRU) based on land use and land cover similarities, as well as soil management techniques [2]. The basin's hydrology can be separated into two phases: routing phase and land phase. Simulation of the hydrological cycle integrating whole water circulation in the basin is necessary for better estimation and forecasting of water, sediment circulation and other parameters from the basin.

3 Study Area

The Tapi basin is the Deccan plateau's northernmost basin, located approximately between 72 33′ and 78 17′ east longitudes and 20 N to 22 N latitude. The Tapi River is the Peninsula's second greatest westward draining interstate river. It begins at an elevation of 752 m near the Multai reserve forest in the Betul district of Madhya Pradesh. The river's total length is 724 km, with the first 282 km flowing through Madhya Pradesh and 54 km defining the state's common boundary with Maharashtra. It flows across Maharashtra for 228 km before entering Gujarat. The Tapi River flows across Gujarat for 214 km before joining the Arabian Sea at the Gulf of Cambay after passing through Surat.

The Tapi basin is divided into sub-basins: the Upper basin (29,430 km^2) up to the Hatnur intersection of the Purna with the major Tapi, the Middle Tapi basin (25,320 km^2) from Hatnur to the Gidhade gauging site, and the Lower Tapi basin (25,320 km^2) again from the Gidhade gauging site up to the sea (10,395 km^2) [4].

The Lower Tapi basin, which includes Surat, is located between the Ukai Dam and the Arabian Sea. One of the worst floods in Surat's history occurred in the years 1998 and 2006. The flood of 2006 is recognized as a sever calamity that resulted in the widespread destruction of structures worth INR 20 billion and impacted people's lives, with roughly 300 people dying as a result of the devastating floods [4]. Figure 1 depicts a map of the Lower Tapi basin's location.

4 Methodology and Data Collection

4.1 Methodology

SWAT necessitates a large number of spatial and temporal inputs. SWAT, being a semi-model, must process, aggregate and analyzes the data geographically utilizing GIS technologies. As a result, the model has been integrated with GIS software as a downloadable ArcSWAT for ArcGIS supplementary extension to make it easier to use. In flowchart Fig. 2, the methodology for runoff modeling at the basin outlet using SWAT is depicted.

4.2 Data Collection

4.2.1 Rainfall Data

The daily rainfall data is required as input for SWAT analysis. For this study, daily rainfall data from 8 rain gauge stations in the Lower Tapi basin was chosen from a total of 13 rain gauge stations with at least 20 years of data, and these rain gauge

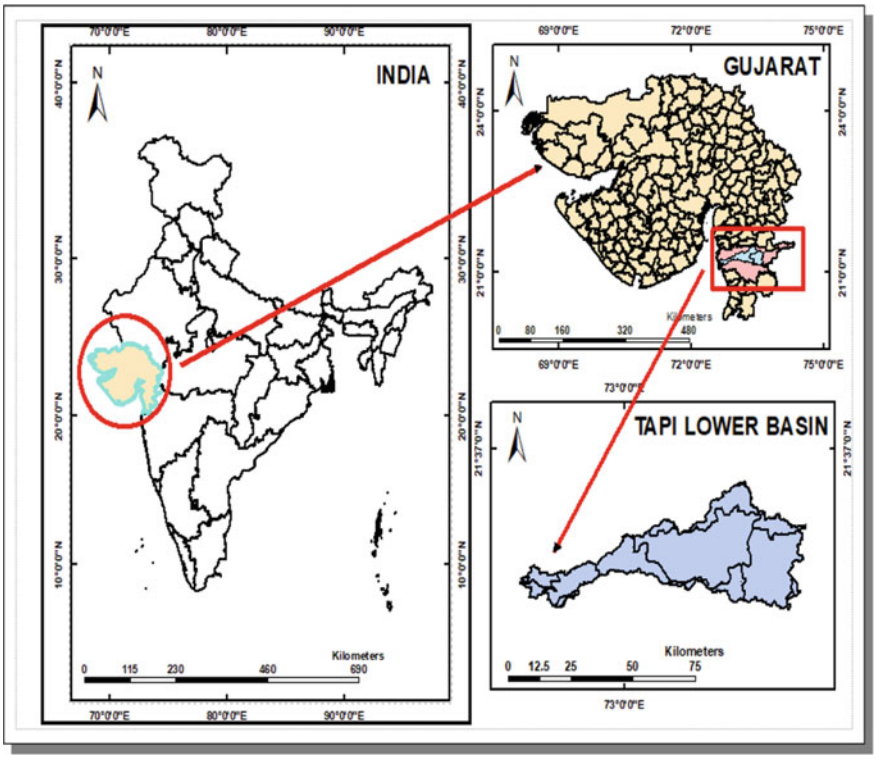

Fig. 1 Location map of Lower Tapi basin

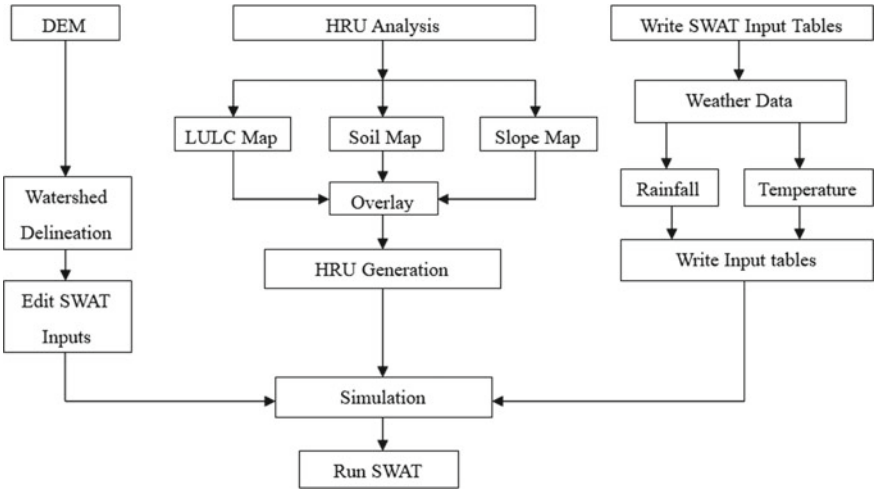

Fig. 2 Methodology of rainfall–runoff modeling

Table 1 Rain gauge station selected for study in Lower Tapi basin

Station name	District	Latitude	Longitude
Amli	Surat	21.400	73.408
Godsamba	Surat	21.279	73.231
Kadod	Surat	21.217	73.216
Kholvad	Surat	21.275	72.948
Rander	Surat	21.223	72.792
Ukai	Surat	21.256	73.580
Uteva	Surat	21.350	73.215
Zankhvav	Surat	21.443	73.319

stations were gathered through the Gujarat State Water Data Centre (SWDC). The location and name of each SWDC rain gauge station are listed in Table 1. The position of the raingauge station is depicted in Fig. 3.

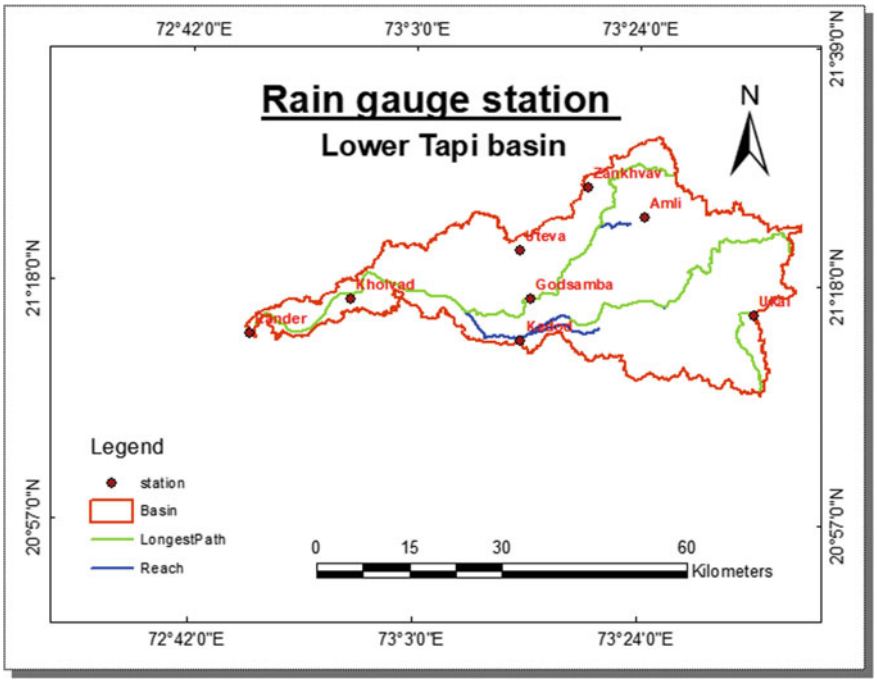

Fig. 3 Location of raingauge station

4.2.2 Runoff Data

The river flow data for the Lower Tapi basin was also acquired from the State Water Data Centre (SWDC) in Gujarat. Daily streamflow data are used to calibrate and validate the SWAT model. Runoff data from one river gauge station in the study area, i.e., the Lower Tapi basin, namely, Mandvi, is available.

4.2.3 Digital Elevation Model (DEM)

A digital elevation model (DEM) is a three-dimensional depiction of a terrain created from elevation data. DEM was retrieved from the Bhuvan ISRO Website. DEM (Cartisat-1, CartoDEM Version-3 R1) with a resolution of 30 m × 30 m was downloaded from Bhuvan (https://bhuvan.nrsc.gov.in/home/index.php). Using ArcGIS10.5, the data sets are masked and projected in UTM projection. The DEM is used to define the longest reaches, drainage surfaces and stream network of the watershed and sub-basins. Figure 4 shows the digital elevation model of Lower Tapi basin.

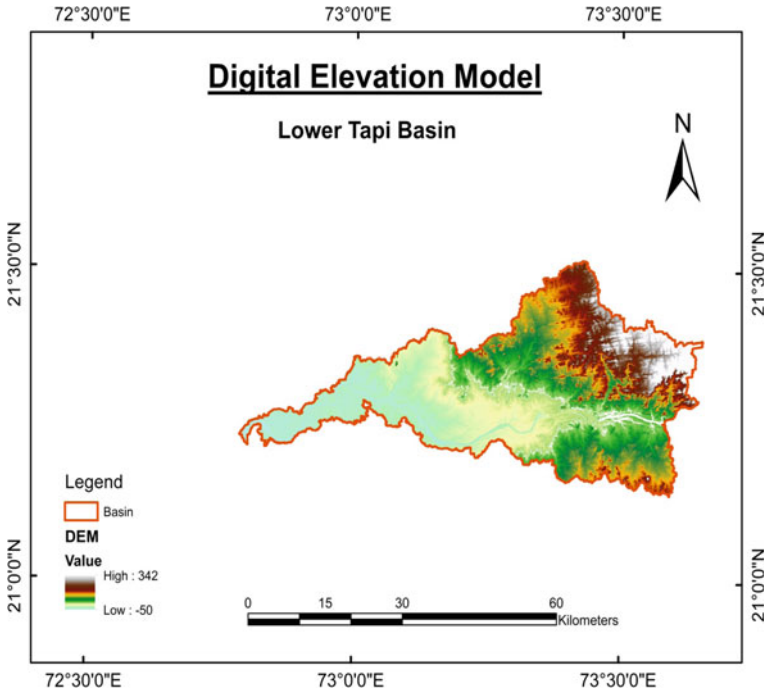

Fig. 4 Digital elevation model

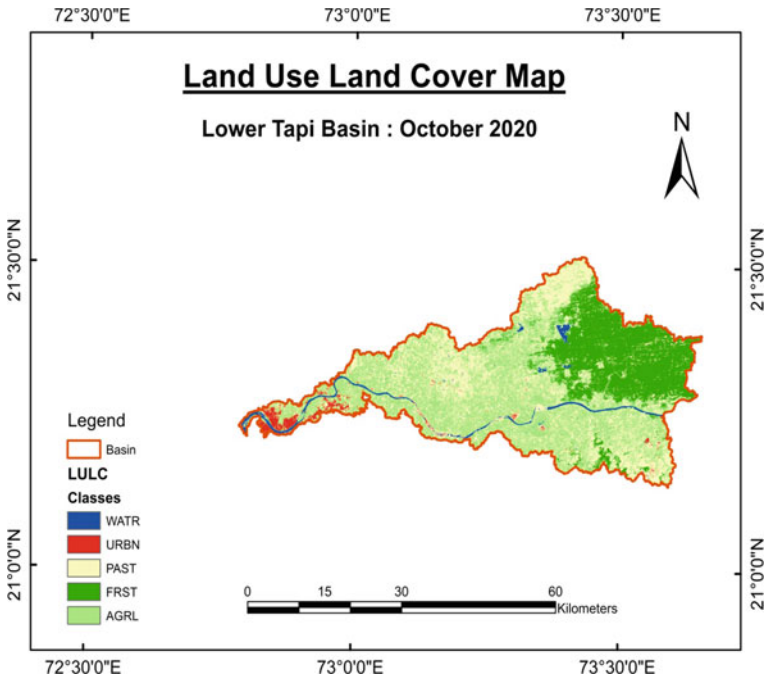

Fig. 5 Map of land use

4.2.4 Landuse Landcover Classification

The land use data was created from the LANDSAT 8 image (acquired on October 2020). The information was taken from the USGS archive. The downloaded file contains seven bands. The picture is then converted into the correct projection using ArcGIS, just as the Digital Elevation Model with about the same dataset. The supervised classification technique was used for picture classification by distinguishing unique signatures present in the Tapi Lower basin, and the image was then translated to systematic form in ArcGIS to make it acceptable with ArcSWAT. Water, pasture, Agricultural Land-Generic, Mixed Forest and Residential are among the major classifications. Figure 5 depicts the land use map of the Tapi Lower basin, while Table 2 shows the area covered by various land use types.

4.2.5 Soil Map

The Food and Agriculture Organization of the United Nations (FAO/UNESCO) provided a soil map with a geographical resolution of 1:5,000,000. The soil data from the Tapi Lower basin has been separated into three groups. The texture of the soils is clay loam, loam and clay. Figure 6 shows the soil map of study area (Lower Tapi basin).

Table 2 Tapi basin LULC classes

S. No.	Category	Area (km^2)	Area of the watershed (%)
1	Water	710.8409594	38
2	Pasture	386.9089199	21
3	Agricultural land-generic	614.9602592	33
4	Mixed forest	86.63310304	5
5	Residential	53.88316237	3
Total		1853.226404	100

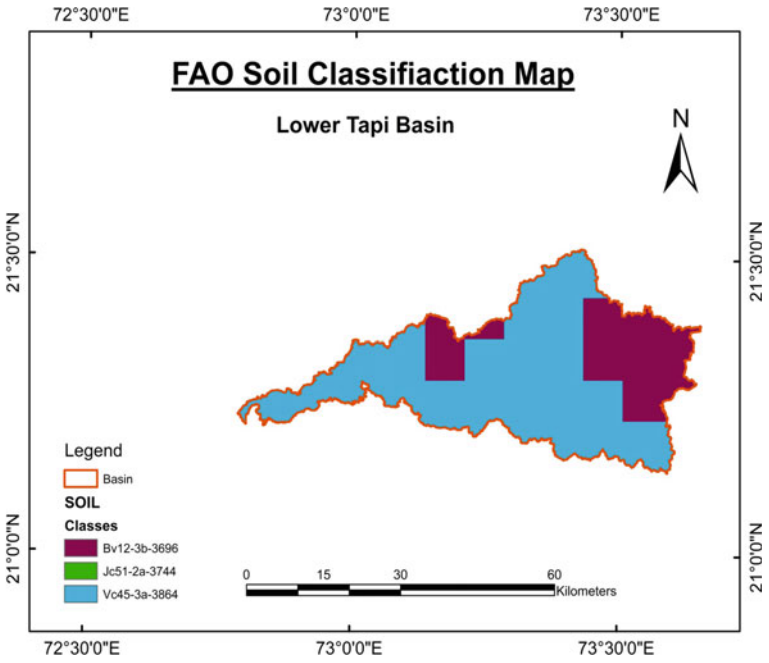

Fig. 6 Soil map of study area

5 Uncertainty Analysis and Calibration

SUFI-2 can be used for uncertainty analysis and calibration, and it can simultaneously analyze a high degree of complexity and observed values from a significant number of sampling locations. It also requires the least number of simulation experiments to generate accurate uncertainty data and calibration and that can be connected directly with SWAT-CUP by an interaction. By comparing observed stream flows at the Mandvi gauge station with daily simulated stream flows, the SWAT model has indeed been optimized for daily modeled stream flows. The model was run for a 20-year

period (1998–2017). Model sensitivities, uncertainty analysis and calibration were performed using the SWAT-CUP (uncertainty programs and calibration) interface. For the most sensitive parameters, the model has been calibrated. Many origins of errors, including generating parameters (e.g., precipitation), conceptual model, variables and observed values, are taken into consideration in SUFI-2 (Abbaspour et al. [5]). The *d*- and *p*-factor (Abbaspour et al. [6]) were used to quantify the accuracy of calibration and uncertainty measures with combination to the Nash-Sutcliff (NSE) and coefficient of correlation (R^2). In contrast to these criteria, (Moriasi et al. [7]) used the NSE and coefficient of correlation between observations and final best simulations to determine goodness of fit. NSE is a standardized statistic that determines the magnitude of remaining variables compared to actual variation in the data (Nash and Sutcliffe [8]). The NSE could be computed using Eq. 1

$$\mathrm{NSE} = 1.0 - \frac{\sum_{i=1}^{n} \left(o_i^{\mathrm{obs}} - P_i^{\mathrm{sim}}\right)^2}{\sum_{i=1}^{n} (o_i^{\mathrm{obs}} - o_i^{\mathrm{mean}})^2} \tag{1}$$

6 Calibration of a SWAT Model

6.1 SWAT Model Predictions Evaluation and Performance

For a period of time, the SWAT model, which was calibrated and verified, was used to simulate hydrological elements of the Lower Tapi basin (1998–2017). Reduce the disparity between measured and expected daily stream flows and correlate estimated daily amounts to measured stream flow values that were used to calibrated the model.

The SUFI-2 algorithm of SWAT-CUP was used to perform auto-validation and calibration in this investigation. Using the SWAT model text input file as a main source of information, the next step is to denote the observed stream flow. Another step is to set number of parameter that would be more sensitive to Tapi Lower basin. The iterative procedure used by SUFI-2 reduces the attribute values after every repetition. The number of simulations in each iterative procedure has been set to 500. After the number of iterations had been set, all of the statistical factors could be computed every time, and the best simulation could be seen in the output results as the suitable statistical value outcome.

6.2 Analysis of Results

The SWAT hydrological model for the lower Tapi basin is used, as well as model runs using SWDC observed climate data to validate and calibrate this model using

Table 3 Values of sensitive parameters

Name of the parameter	Fitted value	Minimum value	Maximum value
V_CH_N2.rte	0.0943	0.0829	0.2488
R_OV_N.hru	0.2526	−0.0547	0.3357
V_GW_DELAY.gw	22.5551	−130.2715	256.6315
R_SOL_AWC (.).sol	−0.0891	−0.3477	0.0507
V_EPCO.hru	0.8068	0.2873	0.8626
V_SLSUBBSN.hru	144.6588	61.575	164.7847
R_CN2.mgt	−0.1647	−0.3166	0.0278

actual flows. A sensitivity analysis on twelve factors was undertaken in order to determine the significant factors controlling the hydrologic processes for river discharge computing given by the SWAT model. Variable sensitivity was calculated using global sensitivity analysis in the SWAT-CUP SUFI-2 software. The values of sensitive parameters are shown in Table 3.

6.2.1 Results of Calibration and Validation

The SWAT model in the Lower Tapi basin was calibrated using the SUFI-2 approach. Plots of daily observed and simulated stream flow were generated to evaluate the model performance based on visual comparison. For some of the more intense storm events, the peak steam flow is over or under predicted (Fig. 7). Figure 7 shows that all high peaks are underestimated, and in many cases, a significant difference between observed and simulated flow can be noticed. Figure 7 depicts each day calibration of observed and simulated flow for the Lower Tapi basin.

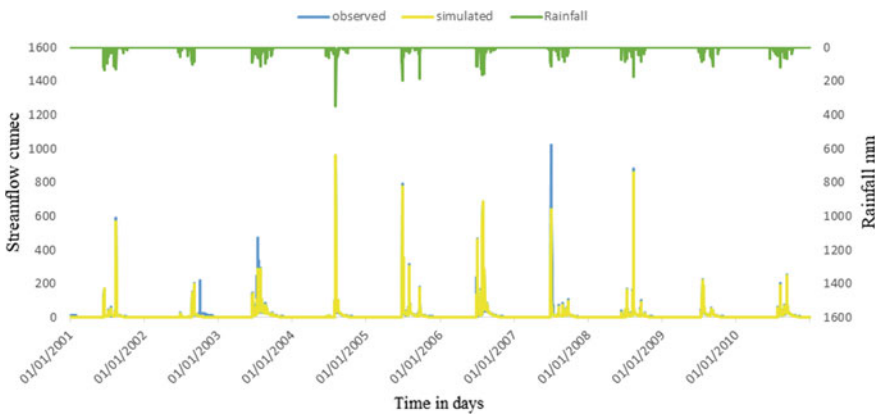

Fig. 7 Calibration of observed and simulated flows for the Lower Tapi basin on a daily basis

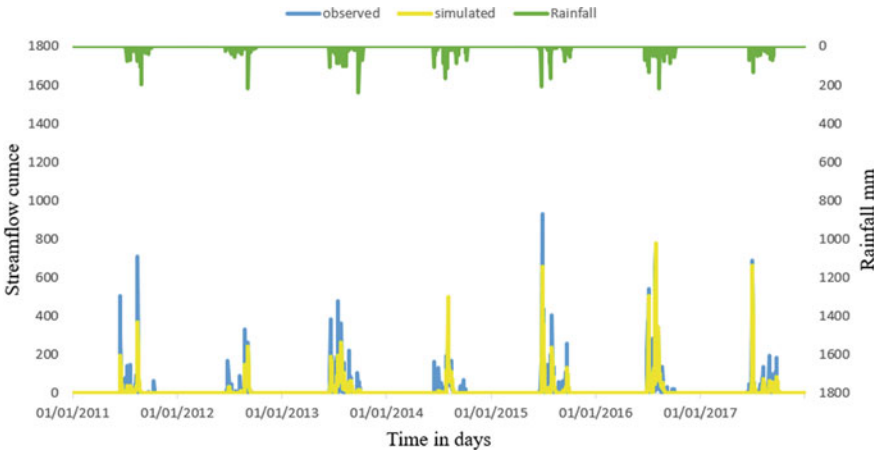

Fig. 8 Validation of observed and simulated flow for the Lower Tapi basin on a daily basis

Validation was carried out with the same parameter value ranges and 500 simulations. A seven-year validation period was used (2011–2017). The daily validation plot between observed and simulated flow is shown in Fig. 8.

7 Results and Discussion

By referring relevant literature (Gorgij et al. [9]; Geethu et al. [10]; Moriasi et al. [11]; Van Griensven et al. [12]) and SWAT documentation (Neitsch et al. [3]) [8], a set of model parameters for sensitivity analysis was chosen. To validate and calibrate the model, the parameters with the highest sensitivity were used. The most vulnerable criteria are those indicating surface response, sub-surface runoff and basin response, according to the findings. The SWAT hydrological parameters SCS runoff curve number CN2, CH N2, SOL AWC, OV N, EPCO, ESCO, ALPHA BF, GW DELAY, GWQMN, REVAPMN, SURLAG and SLSUBBSN are crucial for the model's success. SCS runoff curve number (CN2), average slope length (SLSUBBSN), ground delay (GW DELAY), Manning's "*n*" value for the main channel (CH N2), Plant uptake compensation factor (EPCO), Manning's "*n*" value for overland flow (OV N) and available water capacity of the soil layer (SOL AWC) are the most sensitive parameters for the USRB, according to the sensitivity analysis. Table 4 for daily periods gives the results of statistical evaluation criteria used to check model performance.

Table 4 Performance evaluation of a statistical model for the Lower Tapi basin on a daily basis

Statistical parameter	R^2	NSE
Calibration (2001–2010)	0.87	0.86
Validation (2011–2017)	0.83	0.82

8 Conclusions

Observed stream flow data was used to calibrate and validate the SWAT model. During the Lower Tapi basin's calibration and validation periods, the SWAT model worked admirably. For calibration and validation, twenty-year discharge data is separated into two equal halves. To determine the important parameters affecting the flow, a sensitivity analysis is carried out. The flow was auto-calibrated from 2000 to 2010 using daily observed and simulated flows. Validation of flows between 2011 and 2017 has been completed. The R2 coefficients of determination for daily calibration and validation were 0.87 and 0.83, correspondingly, showing that the calibrated and observed daily flows are in good agreement. Overall, the model responded well to the simulation of streamflow for the Lower Tapi basin. The model is therefore suitable to simulate runoff behavior of Lower Tapi basin.

Acknowledgements The author is grateful to the State Water Data Center (SWDC) for supplying the required data for this research.

References

1. Patel Dhruvesh P, Naresh N (2016) Runoff potential estimation of Anjana Khadi Watershed using SWAT model in the part of lower Tapi Basin, West India. Sustain Water Resour Manage 2:103–118 Springer
2. Venkatesh B, Chandramohan T, Purandara B, Jose M, Nayak P (2018) Modeling of river basin using SWAT model. Springer, Singapore, pp 707–7014
3. Neitsch SL, Arnold JG, Kiniry JR, Williams JR (2005) Soil and water assessment tool theoretical documentation version 2005. Grassland, Soil and Water Research Laboratory, Agricultural Research Service 808 East Blackland Road, Temple, Taxes 76502; Blackland Research Center, Texas Agricultural Experiment Station 720 East Blackland Road, Temple, Texas 76502, USA
4. Timbadiya PV, Patel PL, Porey PD (2011) Calibration of HEC-RAS model on prediction of flood for Lower Tapi River, India. J Water Resour Protect
5. Abbaspour KC, Johnson A, van Genuchten MT (2004) Estimating uncertain flow and transport parameters using a sequential uncertainty fitting procedure. Vadose Zone J 3(4):1340–1352
6. Abbaspour KC, Yang J, Maximov I, Siber R, Bogner K, Mieleitner J, Zobrist J, Srinivasan R (2007) Modelling hydrology and water quality in the pre-alpine/alpine Thur watershed using SWAT. J Hydrol 333:413–430
7. Moriasi DN, Arnold JG, Van Liew MW, Binger RL, Harmel RD, Veith T (2007) Model evaluation guidelines for systematic quantification of accuracy in watershed simulations. Trans ASABE 50(3):885–900
8. Nash JE, Sutcliffe JE (1970) River flow forecasting through conceptual models: Part I. A discussion of principles. J Hydrol 10(3):282–290

9. Gorgij Kh, Dehvari A, Ghaleno D (2020) Uncertainty analysis of hydrological parameters in the Sarbaz watershed using the SWAT model and the SUFI-2 algorithm. J Hydrosci Environ. ISSN 2345-5608
10. Geethu K, Kuduluru SK, Rejani R (2020) Application of SWAT model for estimating runoff of Nethravathi River Basin using sequential uncertainty fitting technique. Int J Sci Res (IJSR) 9(3). ISSN 2319-7064
11. Moriasi DN, Rossi CG, Arnold JG, Tomer MD (2012) Evaluating hydrology of SWAT with new tile drain equations. J Soil Water Cons
12. Griensven V, Mexiner T, Grunwald S, Bishop T, Diluzio M, Srinivasan R (2005) A global sensitivity analysis tool for the parameters of multi-variable catchment models. J Hydrol

Effect of Drainage Area Threshold on Stream Flow Modelling Using Arcswat

Shivansh and P. L. Patel

Abstract The present study explores the effect of varying threshold values of drainage area on the stream flow and water balance characteristics of the Burhanpur sub-catchment in the Upper Tapi River basin, India. Stream network and flow characteristics were derived by threshold-based stream definition in ArcSWAT 2012.10_5.24 using Shuttle Radar Topographic Mission (SRTM) Digital Elevation Model (DEM) of 30 m resolution. The SWAT models with drainage area threshold values of 50, 100, 200, 300, 400, 500, 600 and 700 km^2 were calibrated and validated on a monthly time scale. The performance of each model was evaluated in terms of statistical performance indices, i.e. Nash Sutcliffe Efficiency (NSE) and Coefficient of Determination (R^2). All the models were found to perform efficiently in estimating the stream flow from the sub-catchment. The respective NSE and R^2 values ranged between 0.8–0.85 and 0.84–0.89 during the calibration and 0.91–0.93 and 0.90–0.93 during the validation periods. The simulated stream flow and water balance were found to be optimum at 200 km^2 drainage area threshold, both during calibration (NSE = 0.85 and R^2 = 0.89) and validation (NSE = 0.93 and R^2 = 0.93) period. The results imply that an appropriate drainage area threshold value has to be used to generate optimum stream flows and water balance to enhance the performance of hydrological models.

Keywords ArcSWAT · Hydrological model · Drainage area threshold · Stream flow · Water balance

Shivansh (✉)
Department of Civil Engineering, Indian Institute of Technology Bombay, Mumbai 400076, India
e-mail: shivanshtiwary55@gmail.com; 21404004@iitb.ac.in

P. L. Patel
Department of Civil Engineering, Sardar Vallabhbhai National Institute of Technology Surat, Surat 395007, India
e-mail: plpatel@ced.svnit.ac.in

P. V. Timbadiya et al. (eds.), *Hydrology and Hydrologic Modelling*,
Lecture Notes in Civil Engineering 312,
https://doi.org/10.1007/978-981-19-9147-9_4

1 Introduction

Water is the most important element related to human existence, and it plays a very crucial role in the economic and social development of a nation. The hydrological cycle is the foundation of hydrology, and hydrological models are the simple and comprehensive characterization of a hydrologic system. Mathematical combinations of components of hydrologic cycle are termed as a watershed hydrologic model [1]. Hydrological models are a complex combination of input, model structure, parameters, and uncertainty involved and that makes calibration a challenging task [2]. In recent years, the use of remote sensing data and Geographic Information System (GIS) along with hydrological models has become very important for watershed management. Hydrological models are further classified into lumped, semi-distributed, and distributed models [3]. Distributed models are considered to be more accurate, but they have not shown significantly better results than their lumped counterparts [4–7].

Soil Water Assessment Tool (SWAT) is a comprehensive, continuous-time, semi-distributed, process-based river basin model which is computationally efficient for continuous simulation over a long period of time [8]. In this study, ArcSWAT version 2012.10_5.24 has been used with the ArcGIS platform. Watershed delineation is the first step towards developing a SWAT model. Drainage Area Threshold (DAT) is the minimum area required to form the origin of a stream [9]. DATs are very important for the detailing and accuracy of stream network generated as well as the number and size of sub-watersheds delineated. Thus, it is very important to select an optimal value of DAT for accurate stream network generation which in turn leads to better model performance. SWAT-CUP which takes into account five algorithms for calibration and uncertainty techniques, i.e. General Likelihood Uncertainty Estimation (GLUE) [10], Markov Chain Monte Carlo (MCMC) [11], Parameter Solution (Parasol) [12], Sequential Uncertainty Fitting (SUFI-2) [13, 14]. *p*-factor (percentage of uncertainty bracketed by the model) and *r*-factor (thickness of uncertainty prediction band) are two statistical performance indicators used to evaluate the model uncertainty performance. *p*-factor >0.7 and *r*-factor <1.5 are acceptable [15]. In this study, effect of DAT on streamflow output and water balance and subsequent selection of optimal DAT value has been carried out. Eight different SWAT models with DAT values 50, 100, 200, 300, 400, 500, 600, and 700 km^2 have been calibrated and validated on a monthly time scale at the Burhanpur stream gauging station in the Upper Tapi River basin, India. Eight different models were calibrated for the period of 1998–2007 using SWAT-CUP [14]. In this study, SUFI-2 algorithm has been used to calibrate the model as the same accounts for all sources of uncertainties by expressing them in ranges using Latin Hypercube Sampling.

2 Study Area and Data Source

2.1 Burhanpur Sub-catchment

Tapi River originates from Tapi Kund in Betul district in Madhya Pradesh and reaches the Arabian Sea after travelling through three sub-basins and covering around 784 km. The Upper Tapi basin, Middle Tapi basin, and the Lower Tapi basin drains areas of 29,430 km^2, 32,097 km^2, and 3618 km^2, respectively. The present study focuses on Burhanpur sub-catchment which is the northern sub-division of Upper Tapi basin which has subtropical to temperate climatic conditions.

Burhanpur sub-catchment drains an area of 10,613 km^2 till its terminal station, i.e. Hatnur dam, and is bounded by Satpura hills in the north, Gwaligarh hills in the south, and Betul plateau in the east. Tapi River travels approximately 350 km west to join Hatnur reservoir. The river is perennial in nature and has two stream gauging stations, i.e. Dedtalai and Burhanpur, with drainage areas 6770 km^2 and 8487 km^2, respectively.

Based on Thiessen polygon eight rain gauge stations (Multai, Atner, Bhainsdehi, Chikhalda, Akot, Dharni, Burhanpur, and Raver) affect the rainfall distribution in the Burhanpur sub-catchment but only five rain gauge stations (Multai, Atner, Dharni, Burhanpur, and Raver) lie within the catchment boundary. Dharni rain gauge station covers most of the Thiessen area (28.01%) followed by Bhainsdehi (21.30%) and Burhanpur (20.69%). The index map for Burhanpur sub-catchment is shown in Fig. 1.

2.2 Data Used

The datasets used in the present study along with their source and resolution has been presented in Table 1.

3 Preparation of Input Data

3.1 Digital Elevation Model (DEM)

In the present study, Shuttle Radar Topography Mission (SRTM) DEM of 30 m resolution was obtained from USGS website. Figure 1 shows the DEM for the study area where elevation varies from 211 to 1171 m. The projection system WGS_1984_UTM Zone 43 N was used for the present study.

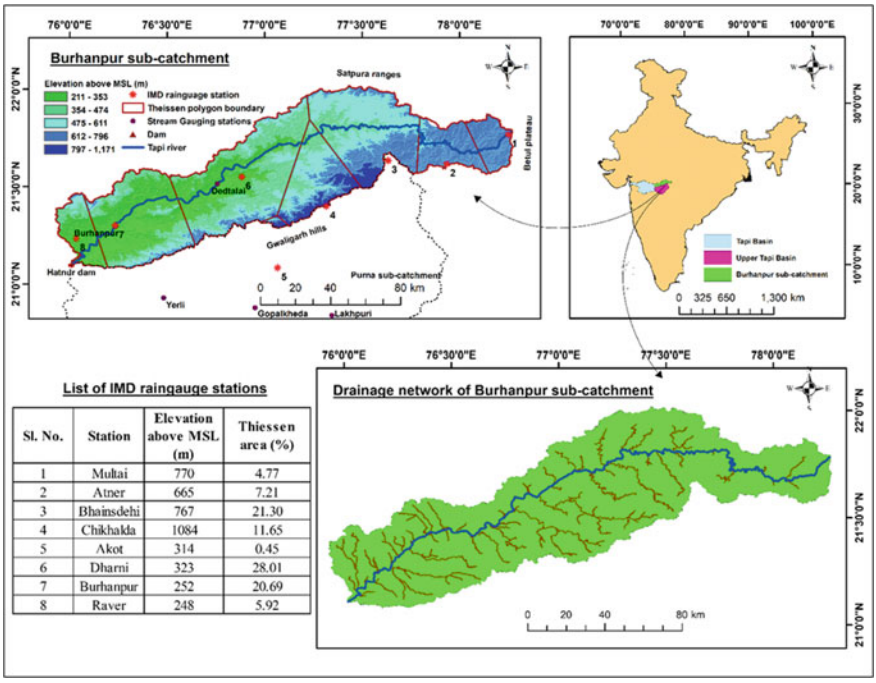

Sl. No.	Station	Elevation above MSL (m)	Thiessen area (%)
1	Multai	770	4.77
2	Atner	665	7.21
3	Bhainsdehi	767	21.30
4	Chikhakla	1084	11.65
5	Akot	314	0.45
6	Dharni	323	28.01
7	Burhanpur	252	20.69
8	Raver	248	5.92

Fig. 1 Burhanpur sub-catchment of Upper Tapi basin along with drainage networks

3.2 Land-Use Land-Cover Map

LULC map was prepared using cloud free LANDSAT Enhanced Thematic Mapper (ETM) satellite imagery of 30 m resolution of the year 2006 obtained from USGS website. The LANDSAT imagery obtained from USGS was processed, and supervised classification using maximum likelihood was employed to generate LULC Maps using ERDAS Imagine 2015 software. Six LULC classes were identified, i.e. deciduous forest (FRSD), fallow land (RNGB), scrub land (BARR), agricultural land (AGRL), built-up area (URML), and water bodies (WATR), where the bracketed codes are SWAT reference codes defined in database for various land-use type.

Figure 2 shows the LULC map for Burhanpur sub-catchment. More than 50% of the Burhanpur sub-catchment area is covered by deciduous forest, mostly as a part of Satpura Hill ranges which divides Tapi basin and Narmada basin. Agricultural land is the second most dominant land use class (33.74%) in the Burhanpur sub-catchment. Other land use classes, namely barren land (5.97%), range land (3.13%), built-up (1.34), and water bodies (0.57%), cover a relatively lesser area in the Burhanpur sub-catchment.

Table 1 Data used in present study along with the sources

S. No.	Type of data	Resolution/Scale/Unit	Period of coverage	Source/Agency
1	Satellite imagery: LANDSAT 7 ETM	30 m	2006	United States Geological Survey (USGS) Earth Explorer website
2	Shuttle Radar Topography Mission (SRTM) Digital Elevation Model (DEM)	30 m		United States Geological Survey (USGS) Earth Explorer website
3	Daily discharge data	m^3/s	Burhanpur: 1998–2013	India WRIS Portal
4	Soil data	Distributed map (scale 1:250,000)		National Bureau of Soil Survey and Land Use Planning, Nagpur (NBSS&LUP)
5	Rainfall data	Station data of 54 rain gauge stations in Tapi basin	1977–2013	India Meteorological Department (IMD): Station Data
6	Temperature data	Station data of 91 weather stations in Tapi basin	1951–2017	India Meteorological Department (IMD): Station Data

3.3 Soil Map

Soil categories for Burhanpur sub-catchment were assessed using the National Bureau of Soil Survey and Land Use Planning (NBSS&LUP) Nagpur Soil Map. The georeferenced and projected soil maps of the study area were digitized, and the polygons were allocated attributes in a GIS platform based on soil properties. The polygons were classified into hydrological soil groups, namely A, B, C, and D. The study area is characterized by the presence of four textures of soil, under the taxonomy clay loam, sandy clay loam, sandy clay, and sandy loam (Fig. 3).

3.4 Climate Input Data

SWAT model requires daily precipitation, maximum and minimum air temperature, relative humidity, wind speed, and solar radiation. These parameter values can be given as input or SWAT may generate them.

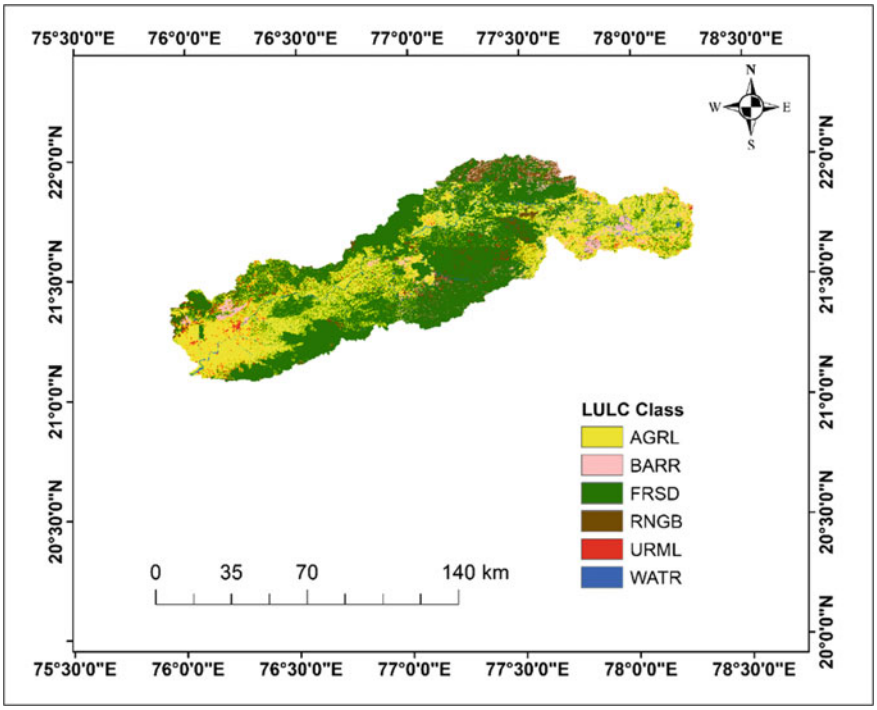

Fig. 2 Land-use land-cover map of Burhanpur sub-catchment

3.5 ArcSWAT Model Development

In this study, the geographic information system (GIS) interface used for the present study is ArcGIS 10.5© and SWAT 2012 for development of hydrological model for Burhanpur sub-catchment. Figure 4 shows the general methodology adopted to develop ArcSWAT models.

The first step towards model development is the watershed delineation using DEM. Threshold-based stream definition to generate sub-basins and nine different SWAT models were developed based on drainage area threshold values 50, 100, 200, 300, 400, 500, 600, and 700, 800 km^2. Figure 5 shows the number of sub-basins generated for each SWAT model with different DAT values. The number of watersheds delineated decreased with an increase in drainage area threshold (km^2). The number of sub-basins delineated did not change after 700 km^2 DAT values, and the any further increase in drainage area threshold had no effect on the number of sub-basins generated after watershed delineation in ArcSWAT (Fig. 5).

For all nine SWAT models, land slope was divided into three classes 0–5%, 5–12%, and >12%. HRUs were generated by overlaying LULC map, soil map, and slope map. The threshold values for land use %, soil class %, and slope class were set as 2%, 5%, and 10%, respectively [16]. Location of daily rainfall data, daily

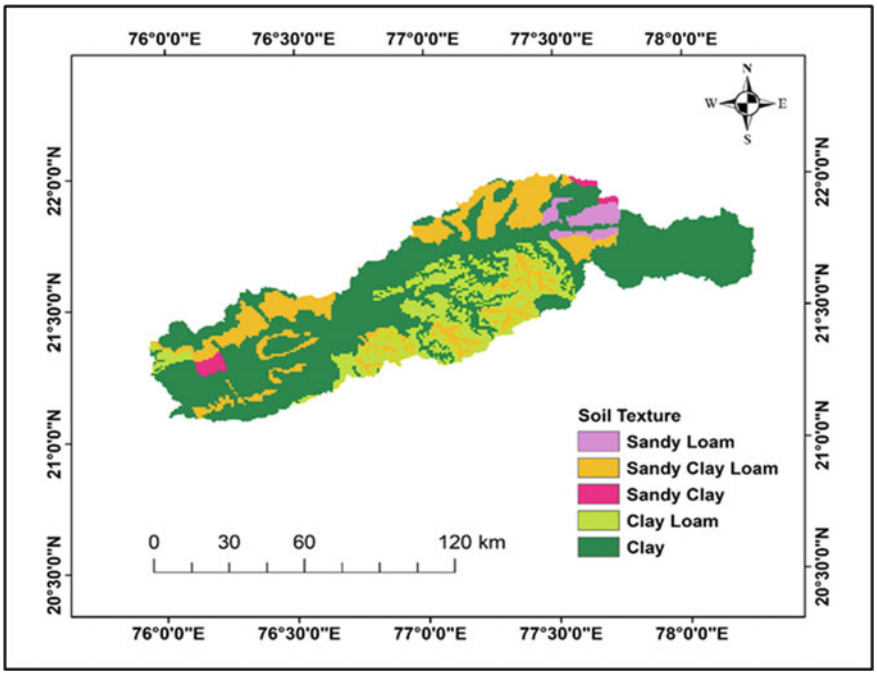

Fig. 3 Soil map of Burhanpur sub-catchment

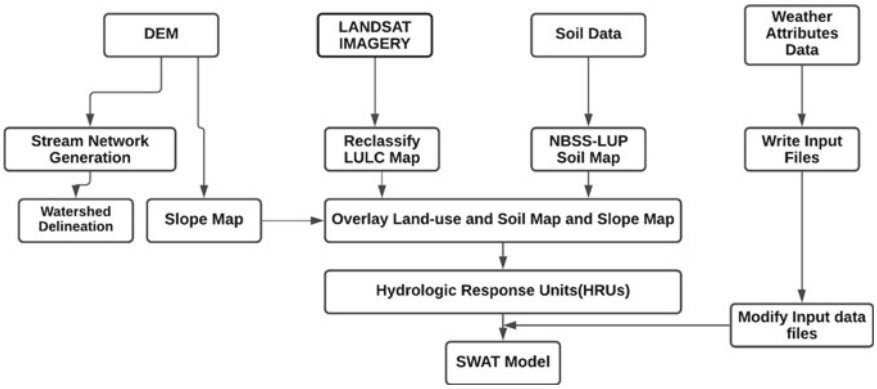

Fig. 4 General methodology adopted for developing ArcSWAT models

maximum and minimum temperature data were written and linked with the model, whereas wind speed, relative humidity, and solar radiation data were generated using the WGEN file. All nine SWAT models were run on monthly time steps for the period of 14 years (1994–2007) with 4 years as warm-up period.

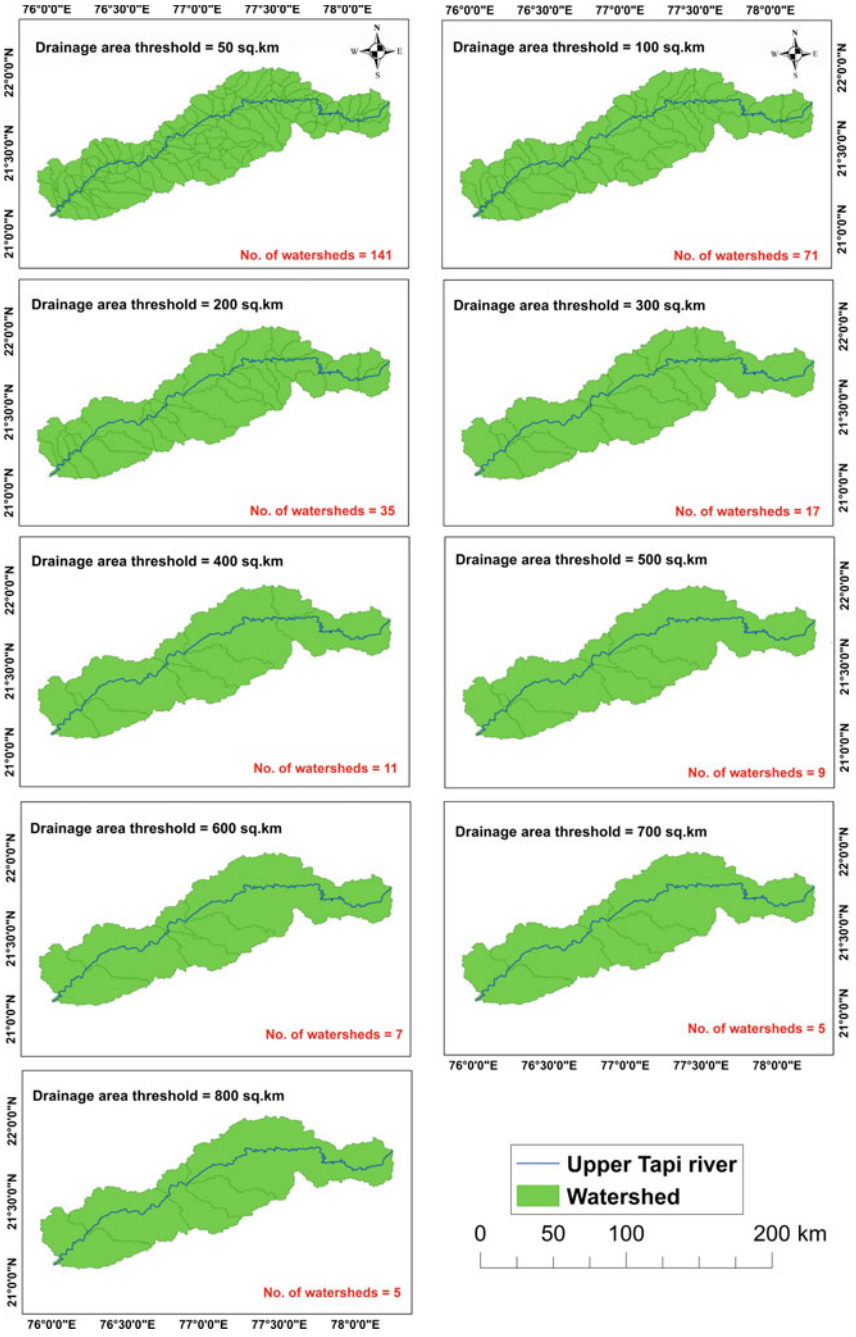

Fig. 5 Sub-basins generated for Burhanpur sub-catchment with HRU values

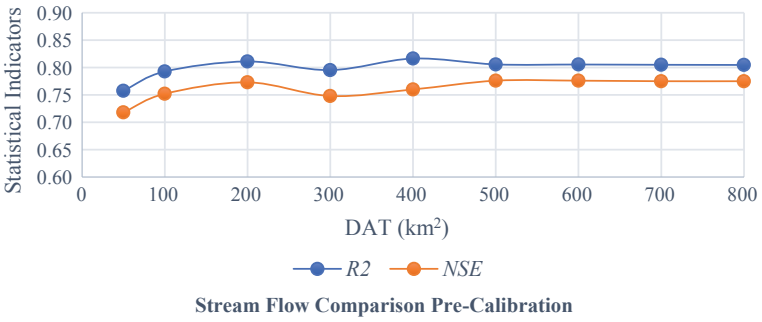

Fig. 6 Variation of statistical indicators (R^2 and NSE) with drainage area threshold (km^2)

4 Results and Discussion

4.1 Comparison of ArcSWAT Streamflow Output Pre-calibration

SWAT simulation was run for nine different SWAT models, and the stream flow at Burhanpur outlet was compared to the observed streamflow at Burhanpur stream gauging station. Figure 6 shows the variation of statistical indicators (R^2 and NSE) and drainage area threshold (km^2) before calibration. It was observed that the R^2 and NSE values increased from 0.76 and 0.72 for 50 km^2 DAT to 0.81 and 0.77 for 200 km^2 DAT. The value of R^2 and NSE decreases at 300 km^2 DAT (R^2 and NSE values 0.80 and 0.75, respectively) and then increases again and becomes constant thereafter. It was observed that increasing the DAT value beyond 700 km^2 had no effect on statistical indicators (R^2 and NSE). Based on the statistical parameters, the number of sub-basins delineated and the number of HRUs generated 8 out of 9 SWAT Models were selected for calibration and validation. SWAT model with 800 km^2 drainage threshold value was not selected for calibration and validation since the number of sub-basins delineated, number of HRUs generated, and statistical parameters like R^2 and NSE after 700 km^2 drainage threshold value did not change (Fig. 6).

4.2 Calibration of SWAT Models

Based on the literature available on SWAT modelling, the global sensitivity analysis was performed on 33 parameters shown in Table 2. Sufi-2 being iterative can handle large number of input parameters and generally does not require too many runs in each iteration [17]. Parameter sensitivity was carried out using the global sensitivity analysis which requires each iteration to have a large number of simulations. Since

the performance of model pre-calibration was not poor (Fig. 6), a lot of runs were not required to attain good model performance.

With global sensitivity analysis performed on all eight SWAT models, groundwater revap coefficient (GW_REVAP), the curve number (CN2), groundwater delay (days) (GW_DELAY), threshold depth of water in the shallow aquifer for return flow to occur (mm) (GWQMN), soil evaporation compensation factor (ESCO), available water capacity in the soil layer (mm) (SOL_AWC), and saturated hydraulic conductivity (mm/hr) (SOL_K) were highly sensitive with p-values <0.05. GW_REVAP was fitted between 0.12 and 0.14, revap coefficient close to 0 implies restricted movement of water to the rootzone, whereas revap coefficient close to 1 implies rate of transfer of water is equal to the rate of potential evapotranspiration. Curve number varied from 59–95 indicated mixed land-use conditions in the basin (Fig. 2). ESCO varied from 0.69 to 0.72, ESCO value of 0.6 indicates desert conditions. The absolute range and fitted values of all 33 parameters for all the 8 SWAT models are shown in Table 2. The models were calibrated for a period from 1998 to 2007.

The values of the performance indicators like p-factor, r-factor, R^2, and NSE for all the calibrated models are listed in Table 3. The value of the p-factor varied from 0.73 to 0.81 whereas the r-factor varied from 0.28 to 0.36. All the calibrated models were further validated using the same 33 parameters for the period of 2008–2013. The performance of the validated models is listed in Table 4. The performance of the model was found to be very good during both calibration and validation as per the criteria given by Moriasi et al. [18].

4.3 Water Balance Analysis

Annual average water balance analysis was carried out for calibration, and validation period for all eight SWAT models to check the valid division of water in the hydrologic system [19]. (Table 5). SWAT uses nearest station statistics to assign precipitation to a sub-basin, i.e. as the DAT value changes, the centroid of each sub-basin shifts leading to a change in the nearest rain gauge station from its centroid which in turn leads to a change in annual average rainfall over the sub-basin and eventually over the entire watershed. For the calibration period, the annual average rainfall in the Upper Tapi River Basin varied between 880.2 and 932.3 mm. The average SCS-curve number value varied from 82.37 to 85.93 which in turn leads to a surface runoff contributing around 66% of the total annual average flow. The annual average of potential evapotranspiration in the Burhanpur sub-catchment is 1841.24 mm for the calibration period (1998–2007), which is around 38% of the annual average rainfall.

Table 2 Fitted values of parameters for different drainage area thresholds (km^2)

Parameters	Absolute range	Fitted values for different drainage area thresholds (km^2)							
		50	100	200	300	400	500	600	700
r__CN2.mgt	[35, 98]	−0.01	−0.012	−0.0022	−0.0022	0.0281	−0.0022	−0.0 022	−0.0022
v__ALPHA_BF.gw	[0, 1]	0.84	0.7	0.7	0.7	0.69	0.7	0.7	0.7
v__GW_DELAY.gw	[0, 500]	23.83	20.92	20.92	20.92	26.1	20.92	20.92	20.92
v__GWQMN.gw	[0, 5000]	2066.92	1782.94	1782.94	1782.94	1578.28	1782.94	1782.94	1782.94
v__GW_REVAP.gw	[0.02, 0.40]	0.13	0.14	0.14	0.14	0.12	0.14	0.14	0.14
v__REVAPMN.gw	[0, 500]	135.15	140.68	140.68	140.676	236.7	140.676	140.676	140.676
v__RCHRG_DP.gw	[0, 1]	0.0016	0.0048	0.0048	0.0048	0.0008	0.0048	0.0048	0.0048
r__SOL_AWC().sol	[0, 1]	−0.57	−0.05	−0.05	−0.05	−0.998	−0.05	−0.05	−0.05
r__SOL_K().sol	[0, 2000]	0.11	0.12	0.12	0.116	0.265	0.116	0.116	0.116
r__SOL_BD().sol	[0.90, 2.50]	−0.2	−0.62	−0.622	−0.622	−0.805	−0.622	−0.622	−0.622
v__SOL_ZMX.sol	[0, 3500]	1290.02	1168.9	1168.9	1168.9	1381	1168.9	1168.9	1168.9
r__SOL_ALB().sol	[0, 0.25]	−0.53	−0.52	−0.519	−0.52	−0.51	−0.52	−0.52	−0.52
v__CH_N2.rte	[0.01, 0.30]	0.02	0.02	0.023	0.023	0.022	0.023	0.023	0.023
r__CH_S2.rte	[−0.001, 10]	0.15	0.09	0.091	0.091	0.059	0.091	0.091	0.091
v__CH_K2.rte	[−0.01, 500]	9.65	17.27	17.27	17.27	23.995	17.27	17.27	17.27
r__ALPHA_BNK.rte	[0, 1]	−0.09	−0.51	−0.51	−0.51	−0.5582	−0.51	−0.51	−0.51

(continued)

Table 2 (continued)

Parameters	Absolute range	Fitted values for different drainage area thresholds (km^2)							
		50	100	200	300	400	500	600	700
v__ESCO.hru	[0, 1]	0.72	0.69	0.69	0.69	0.6801	0.69	0.69	0.69
v__EPCO.hru	[0, 1]	0.9976	0.9	0.9	0.9	0.965	0.9	0.9	0.9
v__CANMX.hru	[0, 100]	58.46	31.57	31.57	31.57	28.5464	31.57	31.57	31.57
v__OV__N.hru__URML	[0.01, 30]	0.24	0.22	0.223	0.223	0.1923	0.223	0.223	0.223
v__OV__N.hru_FRSD	[0.01, 30]	0.17	0.19	0.186	0.186	0.1695	0.186	0.186	0.186
v__OV__N.hru_AGRL	[0.01,30]	0.04	0.05	0.047	0.047	0.0371	0.047	0.047	0.047
v__OV__N.hru_BARR	[0.01,30]	0.04	0.04	0.043	0.043	0.0444	0.043	0.043	0.043
v__OV__N.hru_RNGB	[0.01, 30]	0.05	0.05	0.05	0.05	0.0537	0.05	0.05	0.05
v__OV__N.hru_WATR	[0.01, 30]	0.03	0.03	0.027	0.027	0.0278	0.027	0.027	0.027
v__HRU_SLP.hru	[0, 1]	−0.21	0.06	0.063	0.063	−0.1714	0.063	0.063	0.063
v__BLAI{1}.plant.dat	[0.50, 10]	6.63	5.69	5.69	5.69	5.95	5.69	5.69	5.69
v__BLAI{7}.plant.dat	[0.50, 10]	7.97	8.08	8.08	8.08	8.74	8.08	8.08	8.08
v__BLAI{16}.plant.dat	[0.50, 10]	2.9	2.74	2.74	2.74	3.31	2.74	2.74	2.74
v__CH_N1.sub	[0.01, 30]	0.0271	0.03	0.0295	0.0295	0.028	0.0295	0.0295	0.0295
v__CH_K1.sub	[0, 300]	18.61	14.21	14.21	14.21	8.27	14.21	14.21	14.21
v__CH_S1.sub	[0.0001, 10]	−0.13	−0.17	−0.174	−0.174	0.12	−0.174	−0.174	−0.174
v__SURLAG.bsn	[0.05, 24]	14.28	17.95	17.95	17.95	12.13	17.95	17.95	17.95

Table 3 Performance of the models during calibration (1998–2007)

Drainage area threshold (km^2)	*p*-factor	*r*-factor	R^2	NSE
50	0.73	0.28	0.88	0.85
100	0.79	0.35	0.88	0.84
200	0.81	0.36	0.89	0.85
300	0.8	0.34	0.84	0.8
400	0.78	0.33	0.87	0.84
500	0.79	0.36	0.88	0.85
600	0.79	0.36	0.88	0.85
700	0.8	0.36	0.87	0.85

Table 4 Performance of the models during validation (2008–2013)

Drainage area threshold (km^2)	*p*-factor	*r*-factor	R^2	NSE
50	0.65	0.38	0.93	0.93
100	0.67	0.47	0.93	0.93
200	0.68	0.49	0.93	0.93
300	0.68	0.47	0.93	0.93
400	0.65	0.47	0.92	0.92
500	0.65	0.49	0.91	0.91
600	0.65	0.49	0.91	0.91
700	0.64	0.5	0.91	0.91

4.4 Selection of Optimal Value of Drainage Area Threshold (km^2)

Based on the statistical performance indicators like *p-factor*, *r-factor*, R^2, NSE, and water balance analysis, 200 km^2 was selected as the optimal value of the drainage area threshold. 200 km^2 model was able to capture 81% of uncertainties (*p*-factor = 0.81) with thickness of the uncertainty band (*r*-factor = 0.36) with $R^2 = 0.89$, NSE = 0.85. Also, the water balance analysis for 200 km^2 showed more acceptable results with ET accounting for 39.3% of annual average rainfall which is justified considering humid climatic setting in the region. Curve number 83.52 is acceptable considering dominance of HSG D and HSG C covering 58.2% and 40% area, respectively. High curve number is also aided by the presence of high slope (6.17°) in the region. Surface runoff contributes around 70% of the total annual average flow for the same reason stated above.

Table 5 Water balance components during calibration (cali) and validation (vali)

	Drainage area threshold (km^2)							
	50		100		200		300	
Hydrological components	Cali	Vali	Cali	Vali	Cali	Vali	Cali	Vali
Precipitation (mm)	918.4	1081.9	923.3	1079.8	931.6	1094.3	880.2	1045.8
Evapotranspiration (mm)	331.7	417.1	376.5	410.3	366.9	407.8	356.3	397.5
Surface runoff (mm)	276.31	295.01	287.51	282.41	320.05	300.42	291	286.49
Return flow (mm)	190.89	237.93	138.77	214.81	132.51	246.87	123.53	228.1
Lateral flow (mm)	3.85	5.03	3.75	6.5	3.41	6.17	3.25	5.9
	400		500		600		700	
	Cali	Vali	Cali	Vali	Cali	Vali	Cali	Vali
Precipitation (mm)	862	1044.7	925.1	1075.7	932.3	1106	932.3	1106
Evapotranspiration (mm)	268.9	383.6	356.3	325.7	357.6	403.9	364.8	408.9
Surface runoff (mm)	265.14	303.96	328.99	447.42	334.36	245.49	306.76	296.12
Return flow (mm)	203.12	182.61	124.83	59.15	127.21	319.59	138.71	252.52
Lateral flow (mm)	2.98	4.55	2.98	34.03	2.98	5.44	3.36	5.84

5 Conclusions

In this study, the effect of drainage area threshold (DAT) values on streamflow output and water balance analysis were carried out. The following are the key conclusions derived from this study:

1. The sensitivity analysis of hydrological input parameters was carried out using the observed data at Burhanpur stream gauging station for the period (1998–2007). Parameters like GW_REVAP.gw, CN2.mgt, GW_DELAY.gw, GWQMN.gw, ESCO.hru, SOL_AWC.sol, SOL_K.gw were found to be sensitive for all eight different drainage area threshold value-based models.
2. After going through the rigorous process of calibration and validation of eight different SWAT models with different drainage area thresholds on a monthly time scale, based on the performance evaluation parameters and annual water balance analyses, 200 km^2 drainage area threshold was found as an optimal value to develop SWAT model in the Burhanpur sub-catchment of Upper Tapi River basin, India.
3. For 200 km^2 DAT model, the value of statistical performance indicators was NSE = 0.85 and $R^2 = 0.89$ for calibration (1998–2007) and NSE = 0.93 AND $R^2 = 0.93$ for validation (2008–2013) periods. Model performance has been

found to be very good [18]. The value for *p*-factor and *r*-factor for calibrated model was acceptable according to criteria given by Abbaspour et al. [15].

4. For the 200 km^2 DAT model, surface flow contribution was 70% of total flow which is justified considering high slope and clayey soil being the most dominant soil type in the region whereas ET accounted for 39% of total annual rainfall which is relatively less even though there is humid climatic setting in the Burhanpur sub-catchment.

Acknowledgements The authors are thankful to Centre of Excellence (CoE) on "Water Resources and Flood Management" under TEQIP-II, Sardar Vallabhbhai National Institute of Technology (SVNIT), for financial support and computational facilities. The authors are grateful to Central Water Commission (CWC), India Meteorological Department (IMD), United States Geological Survey (USGS), National Bureau of Soil Survey and Land Use Planning (NBSSLUP) for providing input data for the present study.

References

1. Singh VP, Woolhiser DA (2002) Mathematical modeling of watershed hydrology. J Hydrol Eng 7(4):270–292
2. Yang J, Reichert P, Abbaspour KC, Xia J, Yang H (2008) Comparing uncertainty analysis techniques for a SWAT application to the Chaohe Basin in China. J Hydrol 358(1–2):1–23
3. Jajarmizadeh M, Harun S, Salarpour M (2012) A review on theoretical consideration and types of models in hydrology. J Environ Sci Technol 5(5):249–261
4. Beven K (1989) Changing ideas in hydrology—The case of physically-based models. J Hydrol 105(1–2):157–172
5. Grayson RB, Moore ID, Mcmahon TA (1992) Physically based hydrologic modeling: 1. A terrain-based model for investigative purposes. Water Resour Res 28(10):2639–2658
6. Khakbaz B, Imam B, Hsu K, Sorooshian S (2012) From lumped to distributed via semi-distributed: calibration strategies for semi-distributed hydrologic models. J Hydrol 418:61–77
7. Reed S, Koren V, Smith M, Zhang Z, Moreda F, Seo DJ, Participants DM (2004) Overall distributed model intercomparison project results. J Hydrol 298(1–4):27–60
8. Arnold JG, Moriasi DN, Gassman PW, Abbaspour KC, White MJ, Srinivasan R, Santhi C, Harmel RD, Van Griensven A, Van Liew MW, Kannan N (2012) SWAT: model use, calibration, and validation. Trans ASABE 55(4):1491–1508
9. Winchell M, Srinivasan R, Di Luzio M, Arnold J (2013) ArcSWAT interface for SWAT2012: user's guide. Blackland Research Center, Texas AgriLife Research, College Station, pp 1–464
10. Beven K, Binley A (1992) The future of distributed models: model calibration and uncertainty prediction. Hydrol Process 6(3):279–298
11. Vrugt JA, Ter Braak CJ, Clark MP, Hyman JM, Robinson BA (2008) Treatment of input uncertainty in hydrologic modeling: doing hydrology backward with Markov chain Monte Carlo simulation. Water Resour Res 44(12)
12. van Griensven AV, Meixner T, Grunwald S, Bishop T, Diluzio M, Srinivasan R (2006) A global sensitivity analysis tool for the parameters of multi-variable catchment models. J Hydrol 324(1–4):10–23
13. Abbaspour KC, Johnson CA, Van Genuchten MT (2004) Estimating uncertain flow and transport parameters using a sequential uncertainty fitting procedure. Vadose Zone J 3(4):1340–1352
14. Abbaspour KC, Yang J, Maximov I, Siber R, Bogner K, Mieleitner J, Zobrist J, Srinivasan R (2007) Modelling hydrology and water quality in the pre-alpine/alpine Thur watershed using SWAT. J Hydrol 333(2–4):413–430

15. Abbaspour KC, Rouholahnejad E, Vaghefi SR, Srinivasan R, Yang H, Kløve B (2015) A continental-scale hydrology and water quality model for Europe: calibration and uncertainty of a high-resolution large-scale SWAT model. J Hydrol 524:733–752
16. Her Y, Frankenberger J, Chaubey I, Srinivasan R (2015) Threshold effects in HRU definition of the soil and water assessment tool. Trans ASABE 58(2):367–378
17. Abbaspour KC, Vaghefi SA, Srinivasan R (2017) A guideline for successful calibration and uncertainty analysis for soil and water assessment: a review of papers from the 2016 international SWAT conference. Water 10(1):6
18. Moriasi DN, Arnold JG, Van Liew MW, Bingner RL, Harmel RD, Veith TL (2007) Model evaluation guidelines for systematic quantification of accuracy in watershed simulations. Trans ASABE 50(3):885–900
19. Dooge JC (1992) Hydrologic models and climate change. J Geophys Res Atmos 97(D3):2677–2686

Hydrologic Impact Evaluation of Land Use and Land Cover Change in Subbasins of Tapi River Using SWAT Model

Ankur Sharma, Ruchi Khare, Mahendra Kumar Choudhary, and Vishnu Prasad

Abstract The current research is based on the comparative analysis conducted using land-use maps of 2005 and 2015. SWAT simulations are undertaken on a monthly time scale to estimate runoff for associated rainfall. The coefficient of correlation (R^2) and Nash–Sutcliffe efficiency (NSE) for rainfall and the accompanying runoff for the calibration period of 10 years (1988–97) are determined to be 0.99 and 0.99 respectively at Gidhade station and 0.95 and 0.9 for Sarangkheda station. And for the next 7 years (1998–2004) of the validation period, values of R^2 and NSE are 0.99 and 0.99 and 0.99 and 0.98 for Sarangkheda and Gidhade stream gauge stations. The above-mentioned results are comparatively similar for both land-use maps for 2005 and 2015. Based on model predictions, it is found that the annual surface runoff reduced marginally while the evapotranspiration increased, while baseflow and deep aquifer recharging remain unchanged. The surface runoff has decreased by 3.23% in the ten years, water in shallow aquifer returning to root zone has lowered by 0.34%, and evapotranspiration has increased by 1.07%. In terms of land-use classes, there has been a significant increase in rangeland and a decline in agricultural land.

Keywords Watershed modeling · SWAT model · Landuse/landcover (LULC) change · Rainfall–runoff

A. Sharma (✉) · R. Khare · M. K. Choudhary · V. Prasad
Department of Civil Engineering, Maulana Azad National Institute of Technology, Bhopal 462003, India
e-mail: ankursharma1912@gmail.com

R. Khare
e-mail: ruchikhare@manit.ac.in

M. K. Choudhary
e-mail: mkchoudhary@manit.ac.in

P. V. Timbadiya et al. (eds.), *Hydrology and Hydrologic Modelling*,
Lecture Notes in Civil Engineering 312,
https://doi.org/10.1007/978-981-19-9147-9_5

1 Introduction

In recent years, research has focused on the hydrological impact of land-use change, significantly regarding rainfall–runoff response [3]. This is because the dynamics of the rainfall–runoff process are driven by LULC change in combination with rainfall, properties of soil and terrain. LULC impacts on the processes of hydrology occur quickly as compared to soil and elevation, allowing researchers to investigate their direct impact [7]. Drought, flooding, landslides, and extreme soil erosion are becoming more common worldwide, particularly in the tropics and are influenced by climate change, and anthropogenic activities mainly LULC modification are also an important factor [6]. Due to the effects of this change on watershed, it is crucial to study this interaction between environment and human beings.

Several studies have already been conducted worldwide to examine the effect of LULC change on water balance parameters at the sub basin scale [10]. In past years, the assessment of LULC alterations has gained importance in providing options for land developments and forecasting environmental consequences at small scales [2]. Previous and current LULC change scenarios were used in hydrological models to find out the response of water balance in the catchments [13]. The impact of changes in land-use on runoff characteristics varies by location.

Land use management has changed streamflow patterns, deep and shallow aquifer recharge, surface and sub-surface runoff, and return flow, among other factors, with various environmental consequences [8]. As a result, it is essential to look into the impact of LULC changes on runoff characteristics in the area of interest, especially if the area has any unique features. This paper uses a Tapi river sub-basins case study to examine the effects of LULC alterations on streamflow. Sub-watershed runoff and water yield were computed and compared for a similar period.

2 Study Area and Data Source

2.1 Sub Basins of Middle Tapi River Basin

The Tapi basin covers 65,145 km^2 or approximately 2% of the country's entire geographic area. It originates in the Madhya Pradesh district of Multai and ends in the Arabian Sea near Surat. Apart from supporting various residential water supply schemes, industry, and hydropower in its watershed, the Tapi River is a crucial source of irrigation and acts as a significant part in the agricultural economies of Maharashtra and Gujarat. However, the river basin used in this study has an area of 17,684.99 km^2, starting Savkheda Station till Ukai Dam, as shown in Fig. 1. Since the basin is at the middle part of the basin, observed discharge data at savkheda has been used as the inlet discharge data for the study.

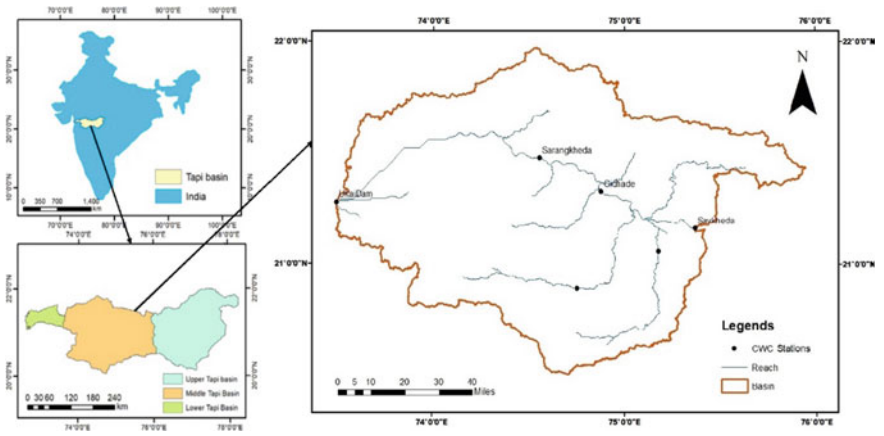

Fig. 1 Index map of the study area

3 Data Collection

3.1 Digital Elevation Model (DEM)

The watershed was delineated and additional topographic processing was done using a digital elevation model (DEM) SRTM DEM with 30 m resolution obtained from the USGS.

3.2 Land Cover/Land Use (LULC)

The bare surface was obtained using two land-use maps created by India's National Remote Sensing Centre (NRSC) in 2005 and 2015 (1:250,000). Unless their location agreed with the location of the bare surface generated from NRSC LULC data, all fallow land found from satellite images was classed as agricultural land. The final land-use data is divided into six categories, included in the SWAT2012 database. Water (or WATR in SWAT), general agricultural (AGRL), shrub grassland (RNGB), barren surface (BARR), forest (FRSD), and urban (URMD) settlements were the six types of settlements.

3.3 Soil Data

Meteorological data resolution substantially impacts streamflow and sediment load modeling, and a fine spatial resolution soil map will improve the model's prediction

accuracy. The National Bureau of Soil Survey and Land Use Planning provided the soil map for this investigation (NBSS&LUP). Initially, the complete area was digitized manually in ArcGIS using state-wise soil maps in JPG format. Then, a separate excel file was prepared for the corresponding soil series properties according to the required format. And finally, both were imported to ArcSWAT. According to the Middle Tapi Basin, the soil map (30 arc-second raster resolution) was projected to WGS1984 UTM Zone 43 N using the raster re-projection tool in ArcGIS.

3.4 Weather Data

Meteorological data is one of the most crucial information required by the SWAT model. The SWAT model typically requires at least two observed metrological data to acquire proper runoff, namely daily rainfall data and temperature data. In contrast, the other metrological parameters can be simulated by the SWAT model utilizing a weather generator. Rainfall data for 24 different stations in the basin was received from the Indian Meteorological Department (Pune) for this study. IMD also provided temperature data (maximum and minimum) in a grid format ($01^\circ \times 01^\circ$). Other climatic characteristics, such as solar radiation, relative humidity, and wind speed, were simulated using the SWAT model and weather generator.

3.5 Streamflow Data

SWAT is a model that simulates the effects of land use and management on water, agricultural chemical yields, and sediments of watersheds that are not gauged [11]. Even with the lack of data for calibration and validation, the model is run and implemented. However, calibration and validation are still required in hydrologic modeling investigations. The Central Water Commission (Surat) provided the rainfall data needed for this investigation. The most powerful instrument for calibrating and validating the model's performance is discharge data. In the present work, daily discharge data for the period from 1988 to 2004 including three separate stations, namely Gidhade, Sarangkheda, and Savkheda, were used.

4 Materials and Methods

4.1 SWAT Model

The Soil and Water Assessment Tool was developed by the USDA's Agricultural Research Service in Texas. There are mainly two ways to categorize SWAT:

1. It can be classed as a deterministic model based on input and uncertainty.
2. It can also be classed as a semi-distributed model based on spatial representation of the watershed.

SWAT considers a variety of physical processes to represent surface runoff and sediment in a watershed. Examples of physical processes include evapotranspiration, evaporation, infiltration, prospective and actual evapotranspiration, lateral flow, and groundwater contribution. Because sediment, pesticides, and nutrients are delivered through streamflow from upland watersheds, the accuracy of sediment, pesticide, and nutrient prediction is dependent on the precision of hydrologic cycle prediction [5]. The hydrology simulation in the SWAT model can be divided into two essential parts: (1) land and (2) routing phases of the hydrological cycle. This model allows its user to estimate the relative influence of climate, soil, management, and vegetation changes (Arnold and Allen 1998).

4.2 Selection of Input Parameters

The SWAT model was parameterized with land-use inputs for two time periods using parameter ranges which were assigned during calibration of the model (Table 1). With the NSE results in hand, there is a solid case to be made for employing the discovered parameters as an input to model study for the complete watershed over a more extended period to analyze the basin's response to land-use change [4, 12].

Table 1 SWAT parameters were used in model calibration

Parameter	Description	Initial range	Calibrated value
r__CN2.mgt	SCS runoff curve number	−0.3 to 0.3	−0.285
v__REVAPMN.gw	Threshold depth of water in the shallow aquifer for "revap" to occur (mm)	50–150	52.5
v__ESCO.bsn	Soil evaporation compensation factor	0.6–0.9	0.7875
r__SOL_K().sol	Saturated hydraulic conductivity	−0.6 to 0.3	−0.5325
r__SOL_AWC().sol	Available water capacity of the soil layer	0–0.6	0.405
v__GW_REVAP.gw	Groundwater "revap" coefficient	0.1–0.25	0.20125
v__ALPHA_BF.gw	Baseflow alpha-factor (days)	0–0.4	0.39
v__SURLAG.bsn	Surface runoff lag time	0.1–1.5	1.255
v__HRU_SLP.hru	Average slope steepness	0.001–0.01	0.004325
v__RCHRG_DP.gw	Deep aquifer percolation fraction	0.003–0.01	0.008775

5 Results and Discussions

5.1 Calibration and Validation

SWAT simulation covered 20 years from 1985 to 2004 using SWAT-CUP. This software (Calibration and Uncertainty Procedures) has been prepared in order to calibrate the data outputs from SWAT simulations [1]. The process of calibration was carried out using 1988 to 1997 streamflow data, and it was validated using the remaining data from 1998 to 2004. Calibration of the model using identified set of parameters and their corresponding values has improved the model prediction capability. Firstly, the procedure was implemented for the model prepared using land-use data of the year 2005, which improved the precalibrated model at Sarangkheda station, *NSE* right from 0.91 to 0.99 and R^2 from 0.97 to 0.99. The procedure also enhanced the performance of uncalibrated model at Gidhade station, *NSE* from 0.89 to 0.95 and R^2 from 0.94 to 0.95.

Compared to prior SWAT modeling studies, these calibrated values are relatively high. Secondly, the same calibration and validation process was implemented for the model prepared using land-use data of the year 2015. And, hence again same results were drawn, i.e., at Sarangkheda station, *NSE* is 0.99, and R^2 is 0.99, and at Gidhade station, *NSE* is 0.95 and R^2 is 0.95. Furthermore, based on the criterion, NSE greater than 0.5 and values R^2 of above 0.5 are regarded as "acceptable and satisfactory" [9].

The improvement can be seen in the calibration plot shown in Fig. 2 where it can be seen that there is a marked improvement in line fitting, especially for baseflow. Validation also yields good simulation results, both using land-use data of 2005 and 2015, at Sarangkheda station, *NSE* is 0.99, R^2 is 0.99, and at Gidhade station, *NSE* is 0.99, and R^2 is 0.98. Several factors can influence the model's performance. In this case, we are using observed discharge data at Savkheda station as an inlet point, tremendously increasing the model performance. Due to which similar calibration and validation results have been observed both for LULC of 2005 and 2015.

5.2 Land Use/Land Cover (LULC) Change

The SWAT model was parameterized with few more land-use inputs for the two time period using parameter settings identified during calibration of the model (Table 1). With the NSE results in place, there is a solid case to be made for employing the discovered parameters as input to the model for the complete watershed over a more extended period to analyze watershed balance components to the change in land use. From 2005 to 2015, the LULC change in the Tapi River's Middle watershed indicated an increase in grassland and water but a decline in the forest, barren, and available agricultural land, which can be observed in Fig. 3.

The LULC alteration resulted in a 2.4 mm reduction in annual surface runoff (Table 3) not only decrease in the runoff but also in revaporization from shallow

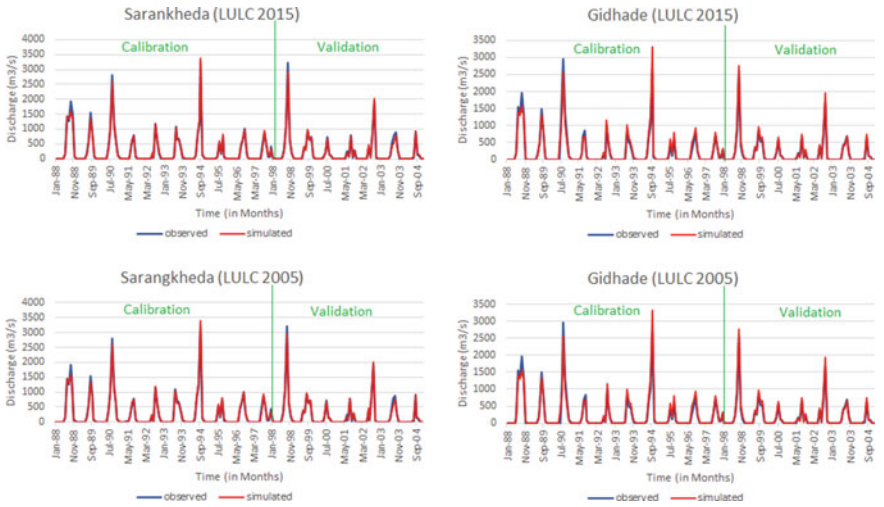

Fig. 2 Discharge versus time series plot of at Sarangkheda and Gidhade stations both using land cover maps of 2005 and 2015

aquifer cab noted by an annual value of 1.05 mm. Moreover, evapotranspiration has increased by 3.7 mm per year, whereas percolation and deep aquifer recharge have remained constant. In addition, the base is also unaltered. While the percentage cover of urban land remained unchanged for both periods, the percentage cover of agricultural land decreased by 3.9% (Table 2). There was also a major increase in the percent cover of grasslands, while the percent cover of barren land declined by 1.1%. There is a slight rise in the water-covered area and a decrease in the forest area.

Increased evapotranspiration and decreased shallow aquifer revaporization are direct results of grasslands, while barren lands decreased. In addition, in 10 years, the reduction in surface runoff results from a combination of land-use changes, including changes in evapotranspiration, percolation, and agricultural cover. These reactions are ruled by the same hydrologic principles that influence LULC's linkages with surface runoff, infiltration, evapotranspiration, percolation, and deep aquifer recharge.

6 Conclusions

The following conclusions can be drawn from the preceding research:

1. This study found that LULC change impacts the hydrologic responses of Middle Tapi Basin watersheds regarding water quantity and hydrologic occurrence timing. According to model simulations, annual surface runoff declined as evapotranspiration increased, also base flow and deep aquifer recharge remained steady.

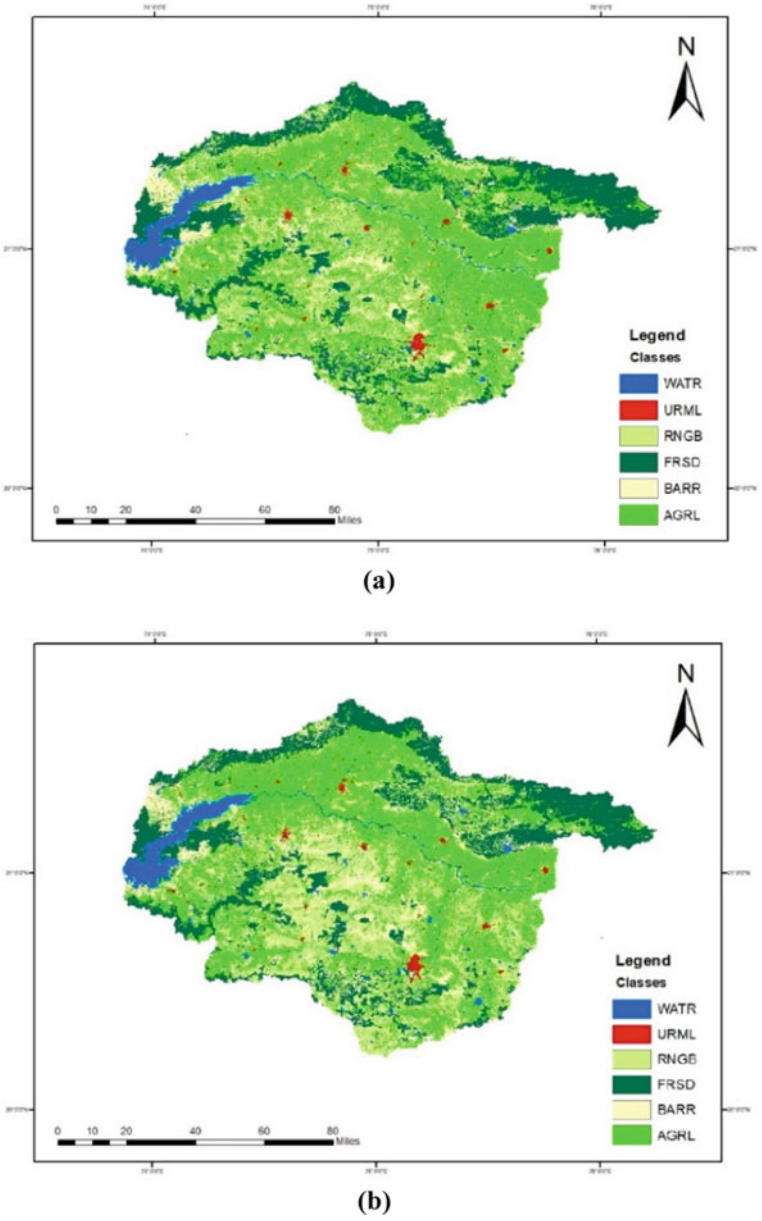

Fig. 3 Land use/land cover (LULC) maps **a** 2005 and **b** 2015 for the watersheds of Middle Tapi

Table 2 Percent area of LULC classes for 2005 and 2015 with its relative changes

LULC classes	LULC code	2005 Percent cover (%)	2015 percent cover (%)	The difference in percent cover (2015–2005)
Urban	URML	1.54	1.54	0
Agricultural	AGRL	42.12	38.19	−3.92
Grassland	RNGB	18.69	23.93	5.23
Forest	FRSD	21.01	20.93	−0.07
Barren	BARR	11.98	10.91	−1.07
Water	WATR	4.66	4.91	0.25
Total	-	100	100	0

Table 3 Water balance for the 2005 and 2015 LULCs

Hydrologic variables	LULC 2005		LULC 2015	
	mm	%	mm	%
Surface runoff	4.95	7.0815	47.9	6.8526
Baseflow	0.37	0.053	0.37	0.053
Revap shallow aquifer	302.1	43.219	301.0	43.069
Deep aquifer recharge	2.88	0.412	2.88	0.412
Evapotranspiration	344	49.213	347.7	49.742
Precipitation	699	100	699	100

As per land-use classes, there is a modest decline in agricultural land and a high increase in grassland.

2. Below-mentioned three hydrological variables show the following changes in terms of percentage. Surface runoff has decreased by 3.23% in the ten years from 2005 to 2015, water in shallow aquifer which were returning to root zone has lowered by 0.34%, and evapotranspiration has increased by 1.07%.
3. It was discovered that the model's performance in terms of NSE and R^2 does not change significantly for both LULCs. One of the critical reasons for strong model performance for both LULCs could be the use of observed discharge data at Savkheda as an inlet.
4. tWater sustainability involves research based on a hydrological change in response to changes in land-use patterns, and hence, efforts must be made to bridge information gaps and provide a decision-making support system for this critical ecosystem.

Acknowledgements The authors acknowledge the financial support received from under the INCCC sponsored R&D Project, Ministry of Water Resources, Government of India, to carry out the present work. The authors are also thankful to India Meteorological Department (IMD), Central Water Commission (CWC), National Remote Sensing Centre (NRSC), and National Bureau of Soil

Survey and Land Use Planning (NBSS & LUP) for providing the necessary data to conduct the present study.

References

1. Abbaspour KC, Rouholahnejad E, Vaghefi S, Srinivasan R, Yang H, Klove B (2015) A continental-scale hydrology and water quality model for europe: calibration and uncertainty of a high-resolution large-scale SWAT model. J Hydrol 524:733–752
2. Aghsaei H, Mobarghaee Dinan N, Moridi A, Asadolahi Z, Delavar M, Fohrer N, Wagner PD (2020) Effects of dynamic land use/land cover change on water resources and sediment yield in the Anzali wetland catchment, Gilan, Iran. Sci Total Environ 712 Article 136449
3. Amini A, Ali T, Ghazli A, Akib S (2011) Impacts of land-use change on streamflows in the Damansara Watershed, Malaysia. Arab J Sci Eng 36(5):713–720
4. Arnold JG, Allen PM (1998) Estimating hydrologic budgets for three Illinois watersheds. J Hydrol 176:57–77
5. Briones RU, Ella VB, Bantayan NC (2016) Hydrologic impact evaluation of land use and land cover change in Palico Watershed, Batangas, Philippines using the SWAT model. J Environ Sci Manag 19(1):96–107
6. Hurkmans R, Terink W, Uijlenhoet R, Moors EJ, Troch PA, Verburg PH (2009) Effects of land use changes on streamflow generation in the Rhine basin. Water Resour Res 45(6):W06405
7. Miller SN, Kepner WG, Mehaffey MH, Hernandez M, Miller RC, Goodrich DC, Kim DK, Heggem DT, Miller WP (2002) Integrating landscape assessment and hydrologic modeling for land cover change analysis. J Am Water Resour Assoc 38:915–929
8. Ni X, Parajuli PB, Ouyang Y, Dash P (2021) Assessing land-use change impact on stream discharge and stream water quality in an agricultural watershed. J Catena 198 Article 105055. https://doi.org/10.1016/j.catena.2020.105055
9. Santhi C, Arnold JG, Williams JR, Dugas WA, Srinivasan R, Hauck LM (2001) Validation of the SWAT model on a large river basin with point and nonpoint sources. J Am Water Resour Assoc 37(5):1169–1188
10. Sanyal J, Densmore L, Carbonneau P (2014) Analysing the effect of land-use/cover changes at sub-catchment levels on downstream flood peaks: a semi-distributed modeling approach with sparse data. CATENA 118:28–40
11. Srinivasan R, Xiaoming Z, Jeffrey GA (2010) SWAT Ungauged: hydrological budget and crop yield predictions in the Upper Mississippi River Basin. Am Soc Agric Biol Eng 53(5):1533–1546
12. Zhang X, Xinxiao Y, Sihong W, Wenhong C (2008) Effects of changes in land use and land cover on sediment discharge of runoff in a typical watershed in the Hill and Gully Loess Region of Northwest China. Front For China 3(3):334–341. https://doi.org/10.1007/s11461-008-0056-1
13. Zhu C, Li Y (2014) Long-Term hydrological impacts of land use/land cover change from 1984 to 2010 in the Little River Watershed, Tennessee. Int Soil Water Conserv Res 2(2):11–21. https://doi.org/10.1016/S2095-6339(15)30002-2

Temporal Variation of Percolation and Evapotranspiration Components in the Water Cycle for the Ropar District, Punjab, India, Using SWAT

Thallam Prashanth and Sayantan Ganguly

Abstract Hydrological modeling is the mathematical representation of hydrological processes. Hydrological models analyze a basin's yield and response over time. Solving the continuity equation can quantify the amount of water available as direct surface runoff, groundwater recharge, evapotranspiration, etc., over time. It is observed that both annual/monthly precipitation and temperature vary with respect to time and space in the Ropar. The main objectives of this study are to validate the monthly average streamflow using the SWAT model at the Ropar headwork and determine the variation in groundwater recharge and evapotranspiration with respect to time at Ropar district in Punjab. The study also aims to analyze annual rainfall trends, evapotranspiration, and percolation obtained from SWAT from 2008 to 2019 at Ropar. The model was calibrated for the period from 2008 to 2015, and NSE of 0.55 was obtained in the study. The results are validated for the simulated flow for a period of 2016–2019 where R^2 value of 0.722 and NSE value of 0.6 are achieved.

Keywords Hydrologic modeling · Water-balance equation · SWAT modeling · Land-phase · Routing-phase · Modified SCS-CN

1 Introduction

The quantification of hydrologic variables is essential in water resources development and management. A proper water management plan must be developed to meet the water demand among the population residing in arid and semi-arid regions [1]. Currently, rainfall–runoff models are increasingly used to analyze the yield and response of any basin due to changes in land use, weather parameters, etc. [2]. Hydrologists must select a simple model that utilizes fewer parameters and consumes less

T. Prashanth (✉) · S. Ganguly
Department of Civil Engineering, Indian Institute of Technology Ropar, Rupnagar, Punjab 140001, India
e-mail: thallam.21cez0007@iitrpr.ac.in

S. Ganguly
e-mail: sayantan.ganguly@iitrpr.ac.in

P. V. Timbadiya et al. (eds.), *Hydrology and Hydrologic Modelling*,
Lecture Notes in Civil Engineering 312,
https://doi.org/10.1007/978-981-19-9147-9_6

time [3]. A model is a mathematical representation of the physical processes, here, the physical process is a water cycle, and therefore, the model is said to be a hydrological model. Based on their mathematical structure, hydrological models are divided into three categories: spatial, temporal representation and simulation [4]. Spatial representation tells how the weather parameters vary with respect to location. Based on spatial representation, it is further sub-divided into three types, namely lumped (low resolution), semi-distributed (medium resolution), and distributed models (higher resolution). Temporal representation tells how the weather parameters vary with respect to time. It is further sub-divided on temporal representation into two types: event-based (simulates individual event) and continuous based (simulates long-term event). Simulation basis tells about different methods to determine hydrological parameters mathematically. Based on the simulation basis of the hydrological processes, it is further divided into three types, namely empirical models (fitted regression equations), conceptual models (partial representation of hydrological process), physical models (hydrological process is represented in detailed manner) [4].

The Variable Infiltration Capacity (VIC), Hydrologic Engineering Center-Hydrological Modeling Software (HEC-HMS), and Soil and Water Assessment Tools (SWAT) models help to quantify hydrological parameters and prepare a proper water management plan for a basin. These models also help to analyze the change in the basin response in terms of quality and quantity when there is a change in land use, land cover, and soil type [1]. We can also determine the runoff at any location on the stream by digitizing the outlet. When there is a change in rainfall, temperature, and the magnitude of changes in land use, hydrological modeling plays a significant role in it.

The SWAT model has been used for several basins to determine climate change impact on water availability [5]. Kiprotich et al. [6] studied assessing the effects of land use and climate change on direct surface runoff response using SWAT+ on the upper Athi basin. They obtained that Nash–Sutcliffe *efficiency* (NSE) of about 0.89 for calibration and validation. Similarly, Park et al. [7] used the SWAT model to evaluate mixed forest evapotranspiration and soil moisture for the Seolma-cheon basin. Chandra et al. [8] validated SWAT for determining sediment yield for the Upper Tapi basin. Their results show that SWAT is a suitable modeling tool for determining the hydrological parameters and analyzing the sediment yield for a watershed.

In Ropar, the annual/monthly precipitation and temperature vary with time and space. For proper water management in Ropar, streamflow, evapotranspiration, and percolation are to be quantified. The primary objectives of this study are to calibrate and validate the monthly average streamflow by using the SWAT model at the Ropar headwork to predict the variation in groundwater recharge and evapotranspiration with respect to time in the Ropar district in Punjab. The study also computes the annual trends of rainfall, percolation, and evapotranspiration with respect to time obtained from SWAT.

2 Materials and Methods

2.1 Study Area and Data Source

The present study encompasses the Sutlej basin, which originates from the Manasarover lake (Elevation = 4570 m) at Mount Kailash in China (Tibetian Plateau) and extends toward the Shipkila at Himachal Pradesh (Greater and lesser Himalayan Ranges), Punjab (Siwalik Hills or Outer Himalayas) in India. The Sutlej basin covers 3% area of the Xizang state in China, 62% area of the Himachal Pradesh state, and 35% area of the Punjab state in India. The Sutlej basin extends at latitudes of 30°N to 33°N and longitudes of 74°E to 82°E. As per the digital world soil map provided by Food and Agricultural Organization (FAO), the basin is covered maximum by loam, clay, and sandy loam at 0–30 cm depth from ground level. As per the data available from the NASA power data access viewer during the period from 1998 to 2020, the average annual rainfall of the Sutlej basin is 582 mm, the temperature ranges from 0.96 to 48 °C, the wind ranges from 0.22 to 10.62 m/s, and the solar radiation ranges from 0.65 to 30.89 MJ/m^2/day. The basin receives most rainfall from June to September (South-West Monsoon). Figure 1 shows the index map of the Sutlej basin.

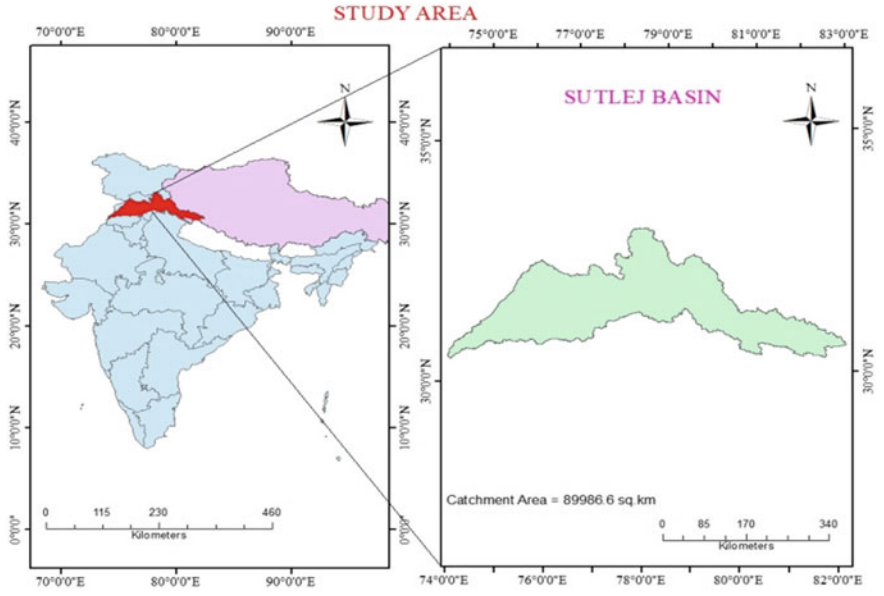

Fig. 1 Index map of the study area

2.1.1 Data Collection

The ASTER (Advanced Spaceborne Thermal Emission and Reflection Radiometer) digital elevation models (DEM) required for the study area is available on the USGS Earth Explorer website (Fig. 2). The DEM is of 30m resolution and is used to generate the stream network (Figs. 3 and 4), hill shade, delineate watershed, etc. Land use and land cover (LULC) is developed by performing supervised classification for Sentinel 2 satellite images. In Fig. 5, we observed five significant classes, waterbody, agriculture, forest, buildup, and barren land. The soil map (Fig. 6) is available on the Food and Agricultural Organization (FAO) Website on a scale of 1:5000000. Harmonized World Soil Database (HWSD) viewer provides information about soil type. SWAT generates Hydrological Response Units (HRUs) using slope, LULC, and soil map. HRUs are a unique combination of slope, LULC, and soil. Weather parameters like precipitation, maximum and minimum temperature, wind, humidity, and solar radiation data are available in the NASA portal at 0.5° * 0.5° resolutions (Fig. 7).

2.2 Methodology

Soil and Water Assessment Tool (SWAT) is a physical-based, semi-distributed, and continuous representation of hydrological processes in an area [9]. SWAT computes runoff using modified soil conservation service, curve number method (SCS-CN) and Green-Ampt infiltration equation. When using daily data, the modified SCS-CN method is used to calculate runoff, whereas the Green-Ampt infiltration equation is preferred when using hourly data [10]. SWAT calculates evapotranspiration by using the Penman–Monteith equation. The SCS-CN method cannot calculate runoff in Himalayan ranges due to a lack of slope steepness factor, and it has been modified to calculate runoff in Himalayan ranges. Penman–Monteith differs from penman's method by incorporating the aerodynamic parameters and the bulk surface resistance. SWAT computes snow runoff by utilizing the average daily temperature.

$$\mathrm{SW}_t = \mathrm{SW}_0 + \sum_{i=1}^{t} \left(R_{\mathrm{day}} - Q_{\mathrm{surf}} - E_a - w_{\mathrm{seep}} - Q_{\mathrm{gw}} \right) \tag{1}$$

SW_t final soil water content (mm)
t Time (days)
SW_0 initial soil water content
R_{day} Amount of precipitation on day 'i'
Q_{gw} amount of return flow on day 'i'
E_{a} Amount of Evaporation on day 'i'
w_{seep} amount of water entering the vadose zone from the ground surface on day 'i'
Q_{surf} amount of surface runoff on day 'i'

Fig. 2 Sutlej basin DEM

SWAT has two major components:

- The land phase of the hydrological cycle determines the volume of water, amount of sediment, nutrients, etc., along with the higher-order stream network.
- The routing phase of the hydrological process tells about the water, sediment, nutrients, etc., movements from the source to the sink.

Figure 8 tells SWAT to create a stream network, hill shade, and watershed delineation using DEM. LULC is developed by performing supervised classification on the sentinel-2 image using the google earth engine. The soil map is acquired from the

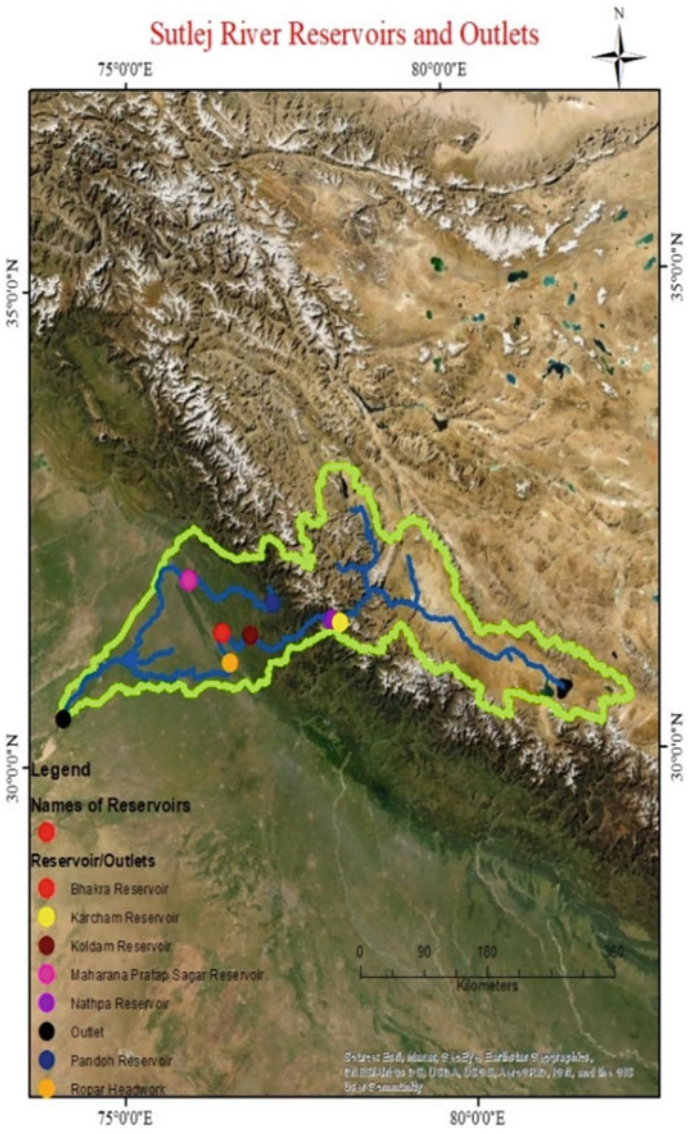

Fig. 3 Sutlej river sub-basins and reaches

FAO Website and clipped to my study using Arc-GIS. The user gives slope ranges in SWAT. It creates Hydrological Response Units by overlaying slope, land use, and soil data for the whole Sutlej basin. It requires various datasets spatially and temporally. The weather generator database prepares input files for SWAT and then writes all input tables in the SWAT editor. The SWAT model simulates the land and routing phases by considering the physical effect of hydrological processes. We can finally

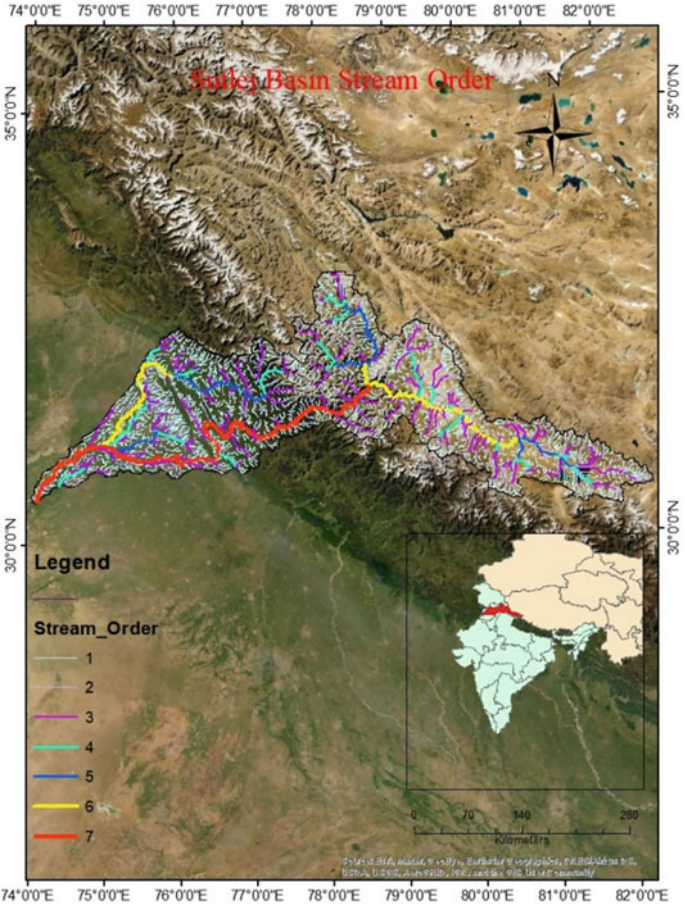

Fig. 4 Sutlej basin stream order

read and visualize all the hydrologic elements like runoff at various outlets, groundwater recharge, and evapotranspiration at different basins for a given weather data when it completes the simulation. The simulated flow is compared with the observed flow to analyze various hydrological elements over time.

Nonparametric Trend Analysis

Mann–Kendall test: It is used as the data set when the time series does not follow any continuous distribution. In this test, the null hypothesis (H_0) tends to have no trend, while the alternate hypothesis (H_a) is said to be in decreasing or increasing trend. The Mann–Kendall test statistic 'S' is determined by:

$$S = \sum_{k=1}^{n-1} \sum_{j=k+1}^{n} \operatorname{sgn}\left(X_j - X_k\right) \tag{2}$$

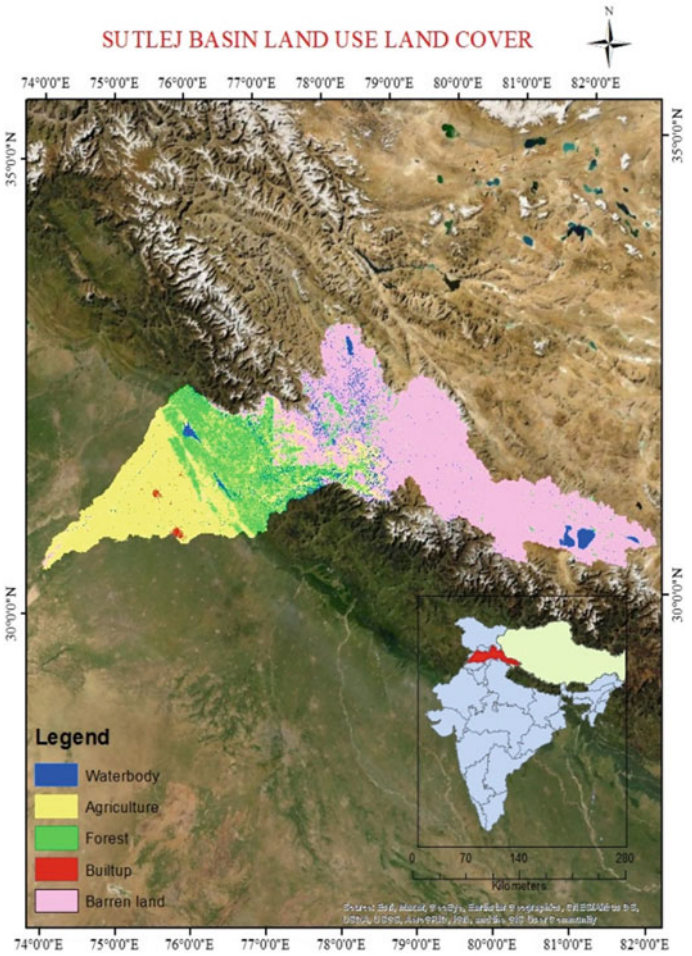

Fig. 5 Sutlej basin LULC

X_j, X_k the annual values for the year's j and k and n is the number of data values.

The Signum function sgn $(X_j – X_k)$ is calculated by:

$$\operatorname{sgn}\left(\mathrm{X_j} - X_k\right) = \begin{cases} 1 & \text{if}\left(X_j - X_k\right) > 0 \\ 0 & \text{if}\left(X_j - X_k\right) = 0 \\ -1 & \text{if}\left(X_j - X_k\right) < 0 \end{cases} \tag{3}$$

$$\operatorname{Var}(S) = \frac{n(n-1)(2n+5) - \sum_{p=1}^{q} t_p\left(t_p - 1\right)\left(2t_p + 5\right)}{18} \tag{4}$$

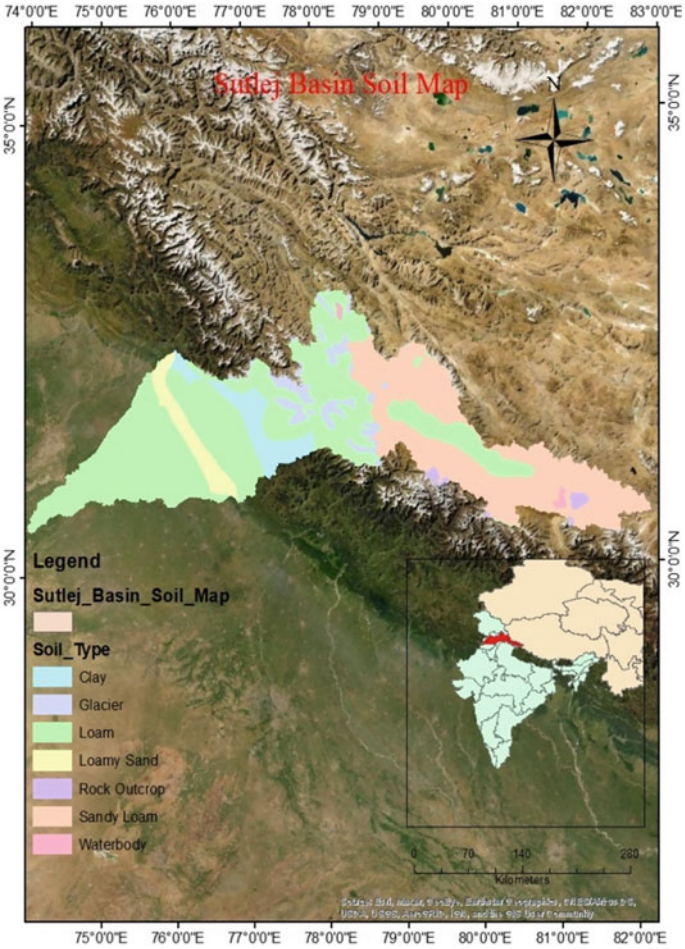

Fig. 6 Sutlej basin soil map

where 'q' is the number of tied groups and 't_p' is the number of data values of the pth group.

$$Z_c = \begin{cases} \frac{S-1}{\sqrt{\text{var}(S)}} & \text{if } S > 0 \\ 0 & \text{if } s = 0 \\ \frac{S+1}{\sqrt{\text{var}(S)}} & \text{if } S < 0 \end{cases} \tag{5}$$

Significance level 'α' is used for testing either decreasing or increasing monotone trend (a two-tailed test). At significance level 'α' ($\alpha = 95\%$), if the condition-$Z_c \geq Z_{\alpha/2}$ is satisfied, then the trend is considered significant.

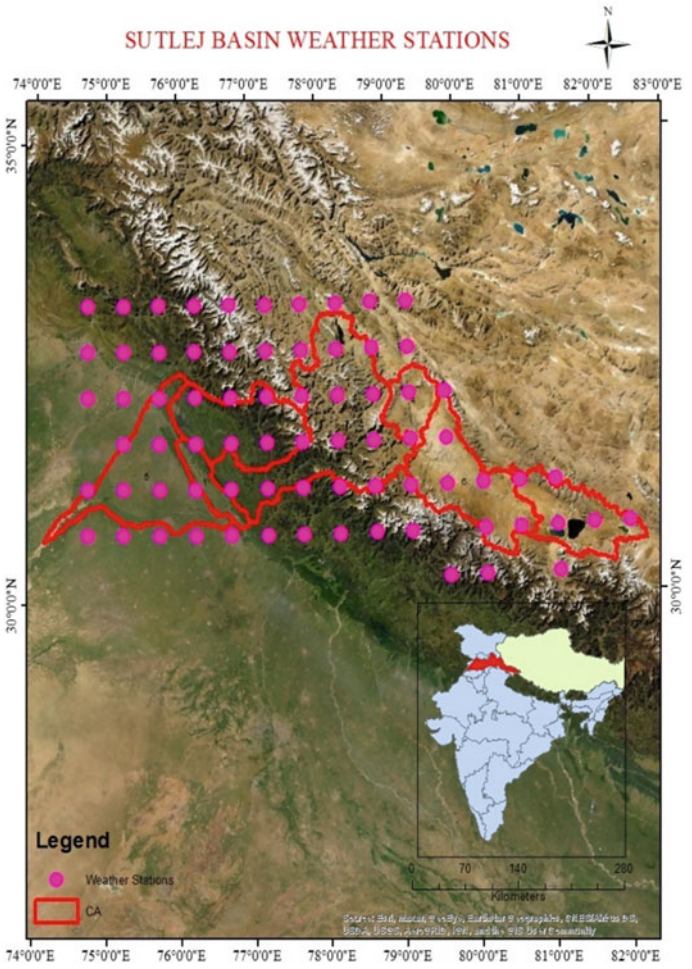

Fig. 7 Sutlej basin weather stations

Sen's Slope Estimator

Sen developed the nonparametric test for measuring the slope of a trend in the sample of 'N' pairs of data. The slope of the simple least square regression line in form $Y(t) = Q * t + B$ determines the rate of increase/decrease trend in the variable, where Q is the trend given by slope in unit time 't,' making an intercept of B.

The slope 'Q_i' is calculated using the formula-$Q_i = \frac{X_j - X_k}{j-k}$ where X_j, X_k are the annual values in years j and k, respectively, and n is the number of data values. The 'n' values of Q_i are ranked from smallest to largest, and the Sen's estimator is calculated by:

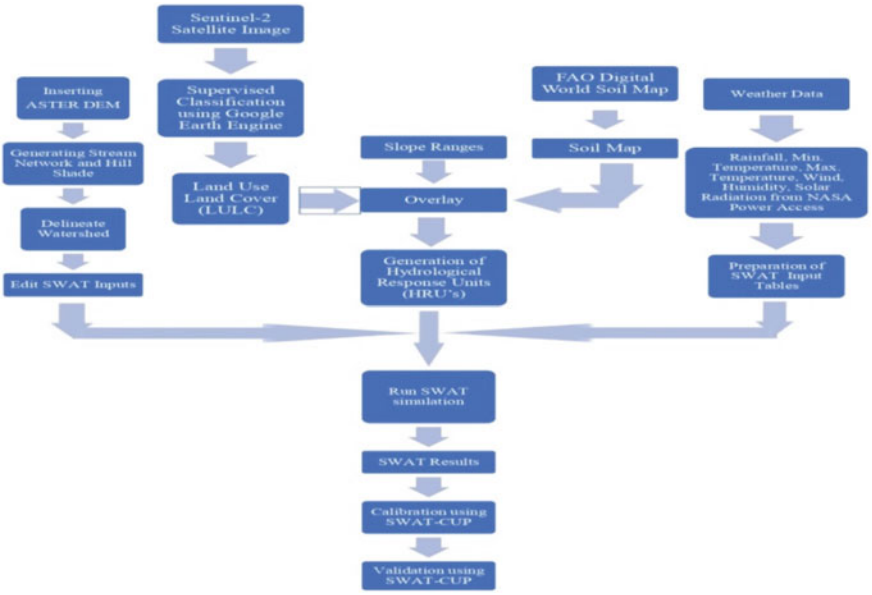

Fig. 8 Workflow of hydrological modeling using SWAT

$$Q_{\text{median}} = \begin{cases} Q_{\frac{n+1}{2}} \text{ if '}n\text{' is odd} \\ \frac{\left(Q_{\frac{n}{2}} + Q_{\frac{n+1}{2}}\right)}{2} \text{ if '}n\text{' is even} \end{cases} \quad (6)$$

The median of these values indicates the steepness of the trend, and its sign indicates the reflection of the data trend. Confidence interval about time slope is $C_\alpha = Z_{1-\alpha/2} * \text{var(S)}$. $M_1 = \frac{n-C_\alpha}{2}$, $M_2 = \frac{n+C_\alpha}{2}$. The lower and upper limits of the confidence interval are $Q_{\min}$ and $Q_{\max}$ for M_1th and $(M_2 + 1)$th of n ordered slope estimates. If the same sign demarcates $Q_{\min}$ and $Q_{\max}$, then they are significant.

3 Results and Discussion

The simulated streamflow obtained from SWAT is compared with the observed streamflow provided by Ropar Headwork Division (30°59′10″N, 76°31′14″E) by using SWAT-CUP. Figure 9 indicates the water availability (stream flow) with respect to time (months) near Ropar headwork, and it gives information about peak flows observed between July to October. Figure 10 shows the variation of annual rainfall (mm), evapotranspiration (mm), and percolation (mm) with respect to time in the Ropar district. In 2009, 2012, and 2016, evapotranspiration was more than rainfall, and there was no recharge in those years. When rainfall increases, percolation and evapotranspiration increase. Figure 11 shows the variation of water percolation with

annual rainfall. The water table rises when there is a minimum rainfall of 500 mm. Figure 12 shows that as rainfall increases evapotranspiration also increases. Annual percolation, evapotranspiration from SWAT, and annual rainfall data (2008–2019) are not following a normal distribution. Therefore, a nonparametric test like Mann–Kendall, Sen's slope estimator is suitable. Table 1 shows Z_c values obtained from the Mann–Kendall test and is compared with $Z_{\alpha/2}$ at a 5% significance level. At a 5% significance level, it is observed that evapotranspiration has a significantly increasing trend while percolation and rainfall have no trend from 2008 to 2019. Table 2 shows Q_i values from Sen's slope estimator test at a 5% significance level. Here, we should compare signs of $Q_{\max}$ and $Q_{\min}$. It is observed that evapotranspiration has the same sign, i.e., significantly increasing; percolation and rainfall have opposite signs, i.e., no significant trend.

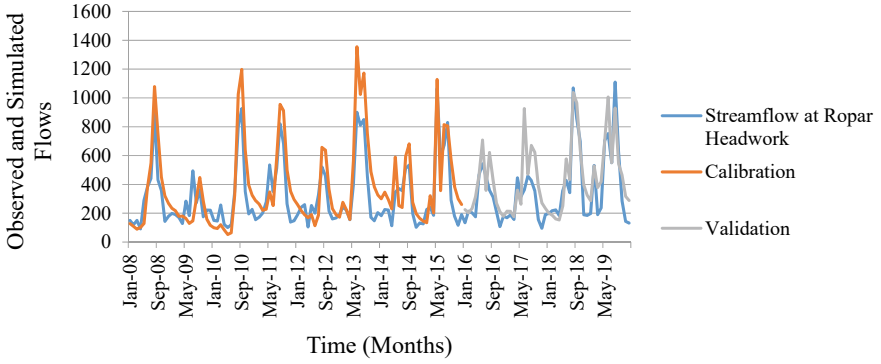

Fig. 9 Streamflow (cumecs) versus time (months) at Ropar headwork

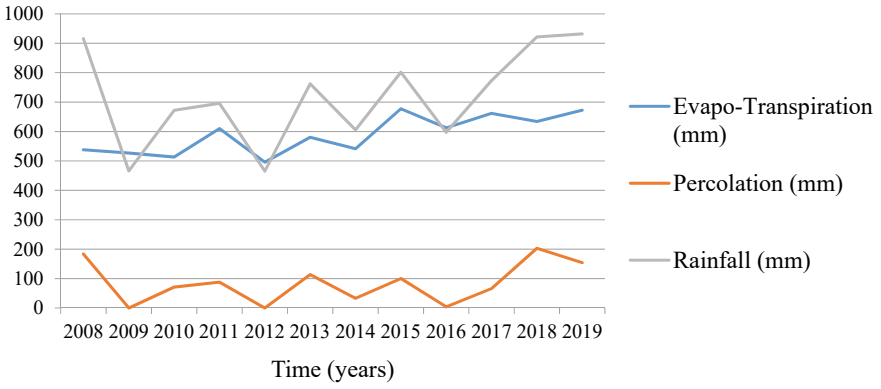

Fig. 10 Variation of annual rainfall, percolation, evapotranspiration with repsect to time in Ropar

Table 1 Z_c obtained from the Mann–Kendall test at 5% significance level

Parameters	Z_c	$Z_{0.05/2}$	Type of trend
Evapotranspiration	2.4	1.96	Significantly increasing
Percolation	0.82	1.96	No trend
Rainfall	1.57	1.96	No trend

Table 2 Q_i obtained from Sen's slope estimator test at 5% significance level

Parameters	Q_{median}	Q_{min}	Q_{max}	Sign	Type of trend
Evapotranspiration	13.53	3.15624	23.1729	same	Significant
Percolation	6.62	4.42958	− 24.245	not same	Not significant
Rainfall	28.08	28.5911	− 26.113	not same	Not significant

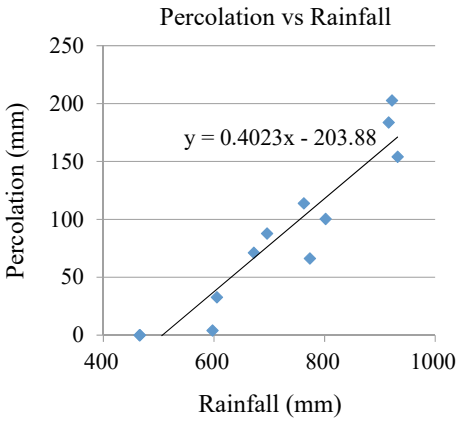

Fig. 11 Percolation versus rainfall

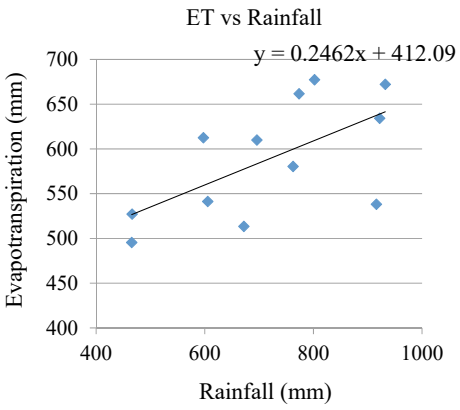

Fig. 12 Evapotranspiration versus rainfall

3.1 Calibration and Validation

For a watershed, it is essential to determine the key parameters which will help calibrate the model. SWAT-CUP is a user-friendly tool that helps understand how hydrologic variables respond within the basin. Sequential uncertainty fitting algorithm (SUFI-2) is one of the algorithms used in SWAT-CUP, which provides better-optimized results and gives broad knowledge on how parameters are responding within the basin so that users can perform sensitivity analysis to achieve goodness of fit. In this study, the model was calibrated for the period from 2008 to 2015 and validated for 2016 to 2019. In calibration, an R^2 value of 0.8 and an NSE value of 0.55 were obtained (Fig. 13), while in validation, an R^2 value of 0.722 and an NSE value of 0.6 were obtained (Fig. 14). Table 3 shows the parameters used for calibration and validation in the SWAT-CUP.

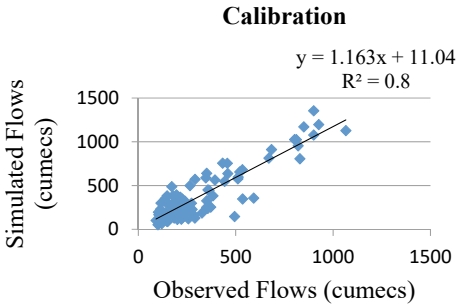

Fig. 13 Scattered plot between simulated and observed flows from 2008 to 2015

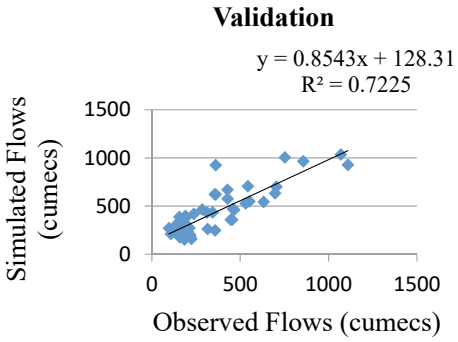

Fig. 14 Scattered plot between simulated and observed flows from 2016 to 2019

Table 3 Parameters used for calibration and validation

S. No.	Parameter	Fitted parameter	Minimum value	Maximum value
1	V__CN2.mgt	67.894806	41.336697	69.590004
2	V__ALPHA_BF.gw	0.430663	0.357901	0.877631
3	V__GW_DELAY.gw	140.487167	101.554291	317.848022
4	V__GWQMN.gw	2.555232	1.504731	2.924327
5	V__GW_REVAP.gw	0.036951	0.02881	0.110216
6	V__ESCO.hru	0.871015	0.848365	0.935479
7	V__CH_N2.rte	0.316455	0.131072	0.320238
8	V__CH_K2.rte	98.222443	38.499077	119.206322
9	V__ALPHA_BNK.rte	0.547293	0.334021	0.797655
10	V__SOL_AWC(..).sol	0.542261	0.187152	0.620212
11	V__SOL_K(..).sol	4.596707	0	32.833622
12	V__SOL_BD(..).sol	1.625816	1.227363	1.965239
13	V__SFTMP.bsn	1.090274	0.546916	5.980496
14	V__SURLAG.bsn	14.516365	5.881654	18.216955
15	V__RCHRG_DP.gw	0.522412	0.183072	0.697224

4 Conclusions

The following conclusions are derived from the preceding study:

1. The SWAT model quantifies all hydrological parameters for a Sutlej Basin. The model simulated the variation of hydrological parameters with time (monthly scale). This quantification of all hydrological parameters can be used in the future for proper water management.
2. Global sensitivity analysis in SWAT-CUP tells us which parameters are more sensitive. In this study, CN2, GW_DELAY.gw, ALPHA_BF.gw, SURLAG.bsn, RCHRG_DP.gw, etc., are the most dependent parameters in the model.
3. It had been observed that R^2 values obtained 0.8 for calibration and 0.722 for validation respectively at Ropar headwork which accesses goodness of fit.
4. We found no trend for rainfall or percolation at 5% significance in Mann–Kendall and Sen's slope estimator, but there is an increase in the significant trend for evapotranspiration. When there is a water shortage in Ropar and evapotranspiration losses must be reduced, artificial recharge structures based on water availability near higher-order streams and lithology in the Ropar district must be built.
5. These results can be helpful for stakeholders or government officials for better water management in the Ropar district and also beneficial in locating areas suitable for artificial recharge structures.

Acknowledgements The authors of the paper gratefully acknowledge the financial help received from SERB for the project titled 'A feasibility study on aquifer storage and recovery of water by artificial recharge in and around Punjab region, India' (grant no.: SRG/2019/000738) under the Start-up Research Grant (SRG) scheme.

References

1. Patil NS, Raikar RV, Manoj S (2014) Runoff modelling for Bhima river using SWAT hydrological model. Int J Eng Res Technol (IJERT) 3. ISSN 2278-0181
2. Tasdighi A, Arabi M, Harmel D (2018) A probabilistic appraisal of rainfall-runoff modeling approaches within SWAT in mixed land use watersheds. J Hydrol. ISSN 2278-0181
3. Devi GK, Ganasri BP, Dwarakish GS (2015) A review on hydrological models. Aquat Procedia 4(2015):1001–1007
4. Jajarmizadeh M, Harun S, Salarpour M (2012) A review on theoretical consideration and types of models in hydrology. J Environ Sci Technol 5(5):249–261
5. Saade J, Atieh M, Ghanimeh S, Golmohammadi G (2021) Modeling impact of climate change on surface water availability using SWAT model in a Semi-Arid Basin: case of El Kalb River, Lebanon. Hydrology 8:134
6. Kiprotich P, Wei X, Zhang Z, Ngigi T, Qiu F, Wang L (2021) Assessing the impact of land use and climate change on surface runoff response using gridded observations and SWAT+. Hydrology 8:48
7. Park GA, Park JY, Joh HK, Lee JW, Ahn SR, Kim SJ (2014) Evaluation of mixed forest evapotranspiration and soil moisture using measured and SWAT simulated results in a hillslope watershed. KSCE J Civ Eng 18(1):315—322
8. Chandra P, Patel PL, Porey PD, Gupta ID (2014) Estimation of sediment yield using SWAT model for Upper Tapi basin. ISH J Hydraul Eng 20(3):291–300
9. Kangsabanik S, Murmu S (2017) Rainfall-runoff modelling of Ajay river catchment using SWAT model. In: IOP conference on series: earth and environmental science, vol 67, p 012033
10. Arnold JG, Srinivasan R, Muttiah RS, Allen PM (2000) Regional estimation of base flow and groundwater recharge in the Upper Mississippi river basin. J Hydrol 227(1–4):21–40

The Role of Objective Functions in Assessment of Water Balance Components Using SUFI-2 Algorithm in Semi-arid Basin

Alka Sharma, P. L. Patel, and Priyank J. Sharma

Abstract The Soil and Water Assessment Tool calibration and uncertainty program (SWAT-CUP) is equipped with many algorithms. The sequential uncertainty fitting 2 (SUFI-2) algorithm is one of the algorithms which is used in the Dharoi catchment of Sabarmati basin, India, for calibrating and validating the SWAT hydrologic model by considering seven objective functions. The different objective functions are examined to understand their influence on the results obtained during calibration, the best-fitted parameter values, and water balance components estimation. During calibration and validation processes, statistical performance indices of all the objective functions are found to give satisfactory results. The best-fitted parameter values using different objective function are different, except in case of Nash–Sutcliffe efficiency (NSE) and ratio of root mean square error and the standard deviation of observations (RSR). Due to same-fitted value generated by using NSE and RSR, the obtained water balance components, i.e., surface runoff (Q_s), lateral flow (Lat), evapotranspiration (E_a), and percolation (Perc) are also found to be the same. The range of 45–59% (20–30%) (11–14%) evapotranspiration (surface runoff) (percolation) using different objective functions is estimated for the present area. It is concluded that the water balance estimated given by NSE and KGE is relatively reasonable than other objective functions. This analysis would help in selecting the objective functions used to produce predictive hydrological model during calibration in SWAT-CUP using SUFI-2 algorithm.

Keywords Rainfall · Water balance · Runoff · Objective function

A. Sharma (✉) · P. L. Patel
Department of Civil Engineering, Sardar Vallabhbhai National Institute of Technology Surat, Surat 395007, India
e-mail: alkagsits@gmail.com

P. J. Sharma
Department of Civil Engineering, Indian Institute Technology Indore, Indore 453552, India

P. V. Timbadiya et al. (eds.), *Hydrology and Hydrologic Modelling*,
Lecture Notes in Civil Engineering 312,
https://doi.org/10.1007/978-981-19-9147-9_7

1 Introduction

Hydrological models are the caricature of the hydrological behavior of the basin. They help to understand the impact studies related to climate and land-use change, to manage water resources, to study water quality and sedimentation, and to predict future water availability of a basin. The Soil and Water Assessment Tool (SWAT) is physically based, semi-distributed, continuous, and watershed-scale simulation model that simulates the large number of physical processes such as evapotranspiration loss, surface and subsurface runoff, groundwater flow, sedimentation, and snow contribution [1]. Hydrological modeling includes (i) calibration and validation from observed streamflow and climatic data and (ii) generation of streamflow series using the weather data of global climatic models (GCM) or regional climate models (RCM). Therefore, a properly calibrated and validated model and its uncertainty analysis are necessary for the reliable hydrological model and to analyze the basin to ensure proper water management.

The process of calibration and uncertainty analysis is always inter-related, and the results obtained during calibration always be investigated with the quantified degree of uncertainty in predicting the model [2]. Various parameters need to be calibrated in a physically based, semi-distributed hydrological model like SWAT. Calibration process is executed by selecting the parameter values within respective uncertainty ranges and then comparing the simulated and observed measured data [1]. SWAT includes several calibration techniques which include manual as well as automatic calibration using the shuffled complex evolution method. The SWAT calibration and uncertainty program (SWAT-CUP) connect SWAT model to algorithms, viz., sequential uncertainty fitting 2 (SUFI-2), generalized likelihood uncertainty estimation (GLUE), parameter solution (ParaSol), Markov chain Monte Carlo (MCMC), and particle swarm optimization (PSO) algorithms [2] which are frequently and widely used by researchers to perform uncertainty analysis and calibrating [3, 4].

Among these algorithms, SUFI-2 is one of the most popular algorithms to carry out calibration/validation and uncertainty analysis [5]. Many objective functions are incorporated in the SUFI-2 algorithm for performing the calibration and uncertainty analysis. To simplify the burden of calibrating a model, many researchers [6, 7] have contributed to verify the reliability and accuracy of hydrological model based on the statistical performance and graphical representation. Moriasi et al. [7] suggested model performance as "satisfactory" if Nash–Sutcliffe efficiency (NSE) > 0.50, ratio of root mean square error to the standard deviation of observed values (RSR) < 0.70, and percent bias (PBIAS) $\pm$ 25% for model simulation. Ritter and Munoz-Carpena [8] gave the threshold of > 0.65 to consider a model as a satisfactory one. Legates and McCabe [9] reported over sensitive nature of NSE to extreme values which is considered inappropriate for model evaluation and proposed modified coefficient of efficiency that replaced square differences by absolute values. Gupta et al. [10] proposed Kling-Gupta efficiency (KGE) to improve the bias and variability of the model. Kouchi et al. [11] compared eight objective functions (NSE, MNS, RSR, R^2 (coefficient of determination), KGE, bR^2 (modified coefficient of determination),

PBIAS) with different algorithms (SUFI-2, GLUE, and PSO) of SWAT-CUP and calibrated the SWAT model at monthly time scale in the two watersheds in Iran. They obtained different parameter ranges by using the three algorithms with the same objective function during the calibration process. Similarly, different objective functions gave different parameter ranges with the different algorithms. Hence, the resulting parameter range leads to different estimation of water balance for the watershed, and it can be said that the calibrated models are "conditioned" and based on the choice of objective function and algorithm utilized during the calibration process.

A valid question is whether the choice of the objective function can influence the water balance component of hydrologic model which is the representation of the hydrologic behavior of a multi-faceted natural system? In the present work, an attempt is made to answer this question and to represent the hydrologic phenomenon for semi-arid Dharoi catchment of Sabarmati basin, India, by using SUFI-2 algorithm with different objective functions, viz., NSE, MNS, RSR, R^2, KGE, bR^2, and PBIAS. The current work also aims to identify objective function for water resources estimate of the basin.

2 Material and Methods

2.1 Study Area

One of the major west-flowing rivers of India is the Sabarmati River which originates at an elevation of 762 m from the Aravalli Hills of Rajasthan in village Tejpur in Udaipur and after traveling 370 km meets the Gulf of Cambay in the Arabian Sea. The total catchment area of the basin is 30,674 km^2 that is shared by Rajasthan (19%) and Gujarat states (81%) [12]. The basin lies between 70° 58′ E and 73° 51′ E and 22° 15′ N to 24° 47′ N. Sabarmati basin covers Udaipur, Sirohi, Pali, and Dungarpur districts of Rajasthan and Sabarkantha, Kheda, Ahmedabad, Mahesana, Gandhinagar, and Banaskantha districts of Gujarat in the east of the Sabarmati River basin. There are several dams and reservoirs on Sabarmati and its tributaries. Dharoi dam is in the northern part of the Sabarmati River basin. The catchment area of the Dharoi catchment is 5540 km^2, out of which about 2640 km^2 lies in Gujarat state and the rest of the part lies in Rajasthan. The terrain of the Sabarmati basin is hilly in the early reaches up to Dharoi after which the river flows mostly in plains. The mean annual rainfall of the Dharoi catchment is 633 mm [12]. The monsoon season starts from June to September months in the basin. The catchment is mainly covered by agricultural and forest lands. The index map of presented study area is shown in Fig. 1.

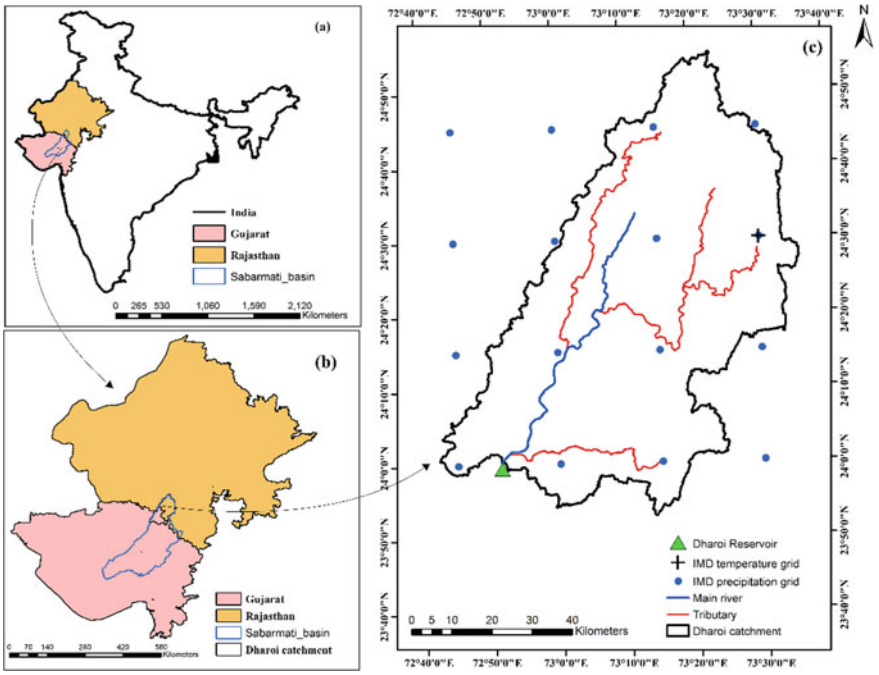

Fig. 1 Dharoi catchment location

2.2 SWAT Input Data

Quality of input data is the most important and critical part of any modeling. Results obtained from hydrologic models are purely based on given input data. Table 1 shows the data source used in this study. The digital elevation model (DEM) (30 m resolution) is downloaded from the United States Geological Survey [13] (Fig. 2a). SWAT uses DEM for the delineation of stream network and watershed boundary and then computes the slope of the catchment. Land-use/land-cover imagery of year 2005 is obtained from National Remote Sensing Centre (NRSC), Hyderabad, India, and reclassified into six classes which are forest (48.51%), water/stream (4.13%), agricultural land (27.39%), built-up area, fallow land (5.6%), and scrub land (14.08%). Soil map is collected from NBSS and LUP, Nagpur, and then digitized for the present study area. The soil type present in study is hydrologic soil group B (68%), C (19%), and D (13%) (Fig. 2c) which have low, moderate, and high runoff potential, respectively. The daily gridded rainfall (temperature) dataset of 0.25° × 0.25° (1° × 1°) spatial resolution of Dharoi basin is taken for the analysis in the present study for the period from 1995 to 2015. The Köppen-Geiger climate classification the study area consists of two major climate types. Out of these, the dominant climate type is arid BSh (82%), followed by tropical AW and temperate Cwa (18%) [14] (Fig. 2c).

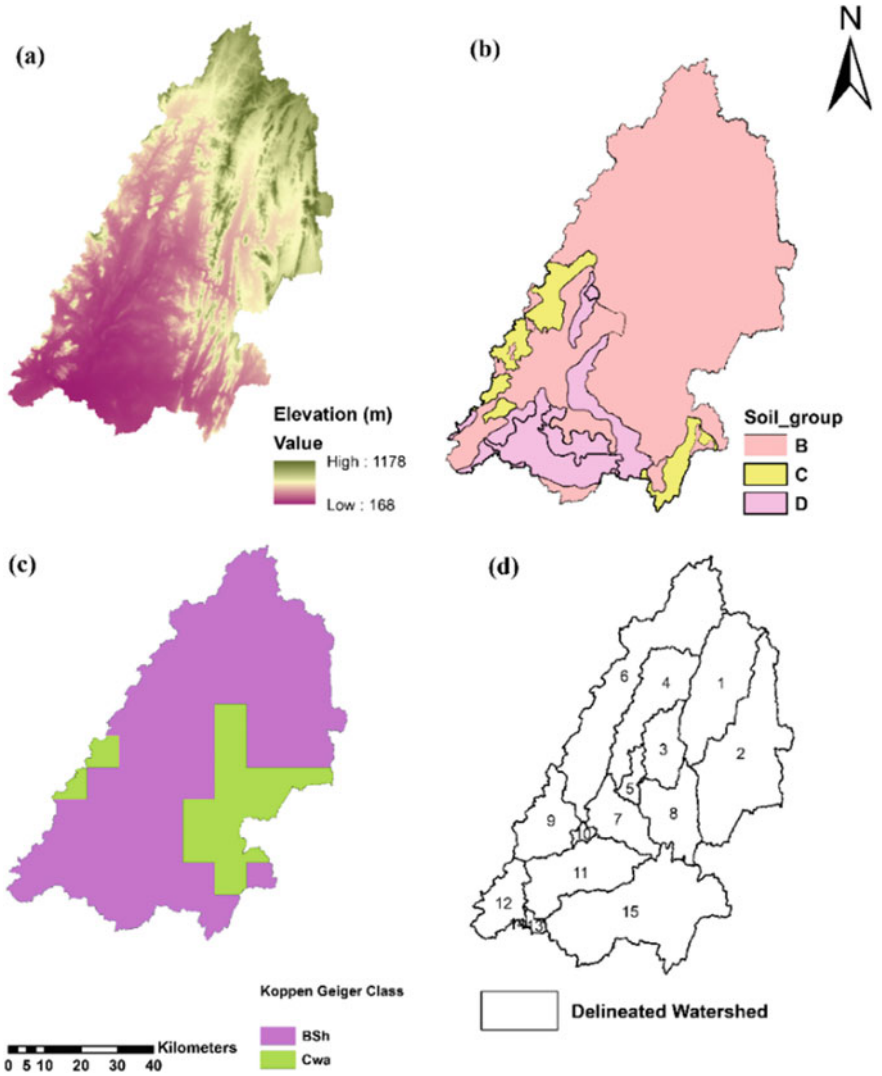

Fig. 2 **a** Digital elevation model, **b** Soil map **c** Köppen-Geigger climate classification, and **d** Delineated watersheds

Table 1 Data and data source

Input data	Data source
SRTM DEM	https://earthexplorer.usgs.gov/
Meteorological data	India Meteorological Department, Pune, India
Land use/land cover	NRSC, Hyderabad, India
Soil types	National Bureau of Soil Survey and Land Use Planning (NBSS and LUP), Nagpur, India

Weather generator is used to simulate relative humidity, wind speed, and solar radiation due to non-availability of these climatic data. The time series of inflow into Dharoi is collected from reservoir Narmada, Water Resources, Water Supply and Kalpsar Department, Government of Gujarat, India.

2.3 Model Setup

Input data presented in Table 1 is used to set up the Soil Water Assessment Tool (SWAT) model. The SWAT model predicts watershed hydrological processes at hydrological response units (HRUs) based on soil types, land-use types, and slope classes using Eq. 1.

$$\mathrm{SW}_t = \mathrm{SW}_o + \sum_{i=1}^{t} \left(R_{\mathrm{day}} - Q_{\mathrm{surf}} - E_a - W_{\mathrm{seep}} - Q_{\mathrm{gw}} \right) \tag{1}$$

where SW_t is the final water content (mm H_2O), SW_o is the initial soil water content on day i (mm H_2O), t is time (days), R_{day} is the amount of precipitation on day i (mm H_2O), Q_{surf} is the amount of surface runoff on day i (mm H_2O), E_a is the amount of evapotranspiration on day i (mm H_2O), W_{seep} is the amount of water entering the vadose zone from the soil profile on day i, and Q_{gw} is the amount of groundwater flow on day i (mm H_2O). Curve number (CN) method is utilized in this study to obtain runoff, and to route the flood, variable storage method is utilized. The ArcGIS 10.5 and Arc-SWAT 2012 are used in this study. The calibration and uncertainty analysis are performed using sequential uncertainty fitting 2 (SUFI-2) [15] algorithm.

The threshold drainage area of 20,000 ha is used to divide the catchment into 15 subbasins (Fig. 2d) and then into 667 Hydrologic Response Units (HRUs). Calibration is performed at monthly scale for the years 1993–2009 which includes two years (1993–1994) of warm-up period. The built-in semi-automated SUFI-2 algorithm [2, 16] of the SWAT-CUP software was used to identify the best-fitting parameter set. Detailed information about uncertainty analysis techniques using SUFI-2 is given in the SWAT-CUP 2012 user manual [16]. The SUFI-2 technique used *p*-factor and *r*-factor to calculate the uncertainty of the measurements. The *r*-factor is the average thickness of the 95PPU divided by the standard deviation of the measurements, and the *p*-factor is the percentage of measured data surrounded by the 95% prediction uncertainty (95PPU), calculated as 2.5 and 97.5% of the cumulative distribution of an output variable obtained via Latin hypercube sampling [16]. As a result, the goal of the SUFI-2 method is to maximize the *p*-factor while minimizing the *r*-factor in order to reach the ideal parameter range. Flowchart of methodology is given in Fig. 3.

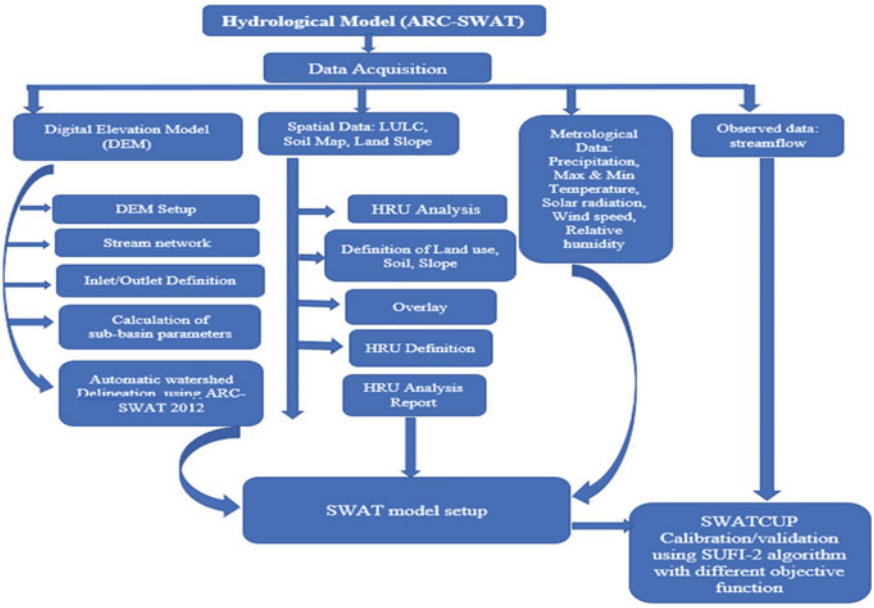

Fig. 3 Methodology of present work

2.4 Parameterization

Calibration process starts with the selection of parameters and defining the acceptable initial parameter ranges. The selected parameters range can be changed by two methods, i.e., replace and relative. The absolute range of parameters taken in present work is presented in Table 2.

2.5 Objective Functions

SUFI-2 algorithm is linked with eleven objective functions, out of which seven (NSE, MNS, RSR, R^2, KGE, bR^2, PBIAS) are used in present work to evaluate their influence on the predicted flow, calibrated parameter range, and water balance components (Table 3).

Here, Q is any variable (discharge), a is observed time series value, s is for the computed time series value, i stands for the ith observed or computed time series value, Q is the average observed time series value of variable Q, $\overline{Q}_s$ is the average computed time series value of variable Q, h is the coefficient of the regression line between the observed and computed time series value, v is the modified Nash–Sutcliffe efficiency factor, num is the total number of observed or simulated time series value, j represents the rank, and d is the linear regression coefficient between

Table 2 Parameters taken in present study

Parameters	Method	Description	Absolute ranges
CN2.mgt	Relative	SCS runoff curve number for moisture condition II	35–98
SOL_AWC.sol	Relative	Available water capacity of the soil layer (mm H_2O/mm soil)	0–1
SOL_BD.sol	Relative	Moist bulk density mm layer (g/cm^3)	0.9–2.5
SOL_K.sol	Relative	Saturated hydraulic conductivity (mm/hr)	0–2000
Alpha_Bnk	Replace	Base flow alpha factor for bank storage (days)	0–1
GWQMN.gw	Replace	Threshold depth of water in the shallow aquifer required for return flow to occur (mm)	0–5000
GW_DELAY.gw	Replace	Groundwater delay (days)	0–500
GW_REVAP.gw	Replace	Groundwater recap coefficient	0.02–0.2
ALPHA_BF.gw	Replace	Base flow alpha factor (days)	0–1
EPCO.hru	Replace	Plant uptake compensation factor	0–1
ESCO.hru	Replace	Soil evaporation compensation factor	0–1
CH_N2.rte	Replace	Manning's n value for the main channel	− 0.01 to 0.3
CH_K2.rte	Replace	Effective hydraulic conductivity in main channel alluvium (mm/hr)	− 0.01 to 500
SURLAG.bsn	Replace	Surface runoff lag coefficient	0.05–24

Table 3 Objective functions considered in the present work

Nash–Sutcliffe efficiency	$\mathbf{NSE} = 1 - \frac{\sum_i (Q_a - Q_s)_i^2}{\sum_i (Q_{a,i} - \overline{Q}_a)^2}$
Modified nash–sutcliffe efficiency	$\mathbf{MNS} = 1 - \frac{\sum_i \lvert Q_a - Q_s \rvert_i^v}{\sum_i \lvert (Q_{a,i} - \overline{Q}_a) \rvert^v}$
Ratio of the standard deviation of observations to root mean square error	$\mathbf{RSR} = \frac{\sqrt{\sum_{i=1}^{\text{num}} (Q_a - Q_s)_i^2}}{\sqrt{\sum_{i=1}^{\text{num}} ((Q_{a,i} - \overline{Q}_a))_i^2}}$
Coefficient of determination	$\boldsymbol{R}^2 = \frac{\{\sum_i (Q_{a,i} - \overline{Q}_a)(Q_{s,i} - \overline{Q}_s)\}^2}{\sum_i (Q_{a,i} - \overline{Q}_a)^2 \sum_i (Q_{s,i} - \overline{Q}_s)^2}$
Kling-Gupta efficiency	$\mathbf{KGE} = 1 - \sqrt{(\mathrm{d} - 1)^2 + (\propto - 1)^2 + (\beta - 1)^2}$
Modified coefficient of determination	$\boldsymbol{bR}^2 = \begin{cases} \lvert h \rvert R^2 (if \lvert h \rvert \leq 1) \\ \lvert h \rvert^{-1} R^2 (if \lvert h \rvert > 1) \end{cases}$
Percent bias	$\mathbf{PBIAS} = 100 \frac{\sum_{i=1}^{n} (Q_a - Q_s)_i}{\sum_{i=1}^{n} (Q_{a,i})}$

Table 4 Good-of-fit criteria of considered objective function

Indices	NSE	MNS	RSR	R^2	KGE	bR^2	PBIAS
Range	$-\infty$ to 1	$-\infty$ to 1	0–∞	0–1	$-\infty$ to 1	0–1	$-\infty$ to ∞
Optimal value	1	1	0	1	1	1	0
Satisfactory value	> 0.5	≥ 0.4	≤ 0.7	> 0.5	≥ 0.5	≥ 0.4	$< \pm 25$

computed and observed variables, and $\propto = \frac{\sigma_s}{\sigma_m}$ and $\beta = \frac{\mu_s}{\mu_m}$, where σ_s and σ_m are the standard deviations of the computed and observed time series value, respectively. μ_s and μ_m stand for means of the computed and observed time series value, respectively.

3 Results and Discussions

3.1 Model Calibration and Validation

Calibration is a process to compare observed and computed variables with the fitted parameter values [17], while in other hand, a good validation result shows the reliability of the calibrated results and fitted parameters range. This study involves the hydrological modeling for the calibration period of 1995–2009 and validation period of 2010–2014 at monthly time step for Dharoi catchment (Fig. 1). Detailed description of utilized seven objective functions and their optimal and acceptable ranges are given in Table 4. The satisfactory threshold for other statistical indices except for bR^2 and MNS is given by Moriasi et al. [7].

3.2 Calibration and Validation

The simulated and observed discharges at monthly scale (calibration period—1995–2009 and validation period—2010–2014) using different objective functions are shown from Fig. 4a–f. The computed discharges show good agreement with rainfall.

The calibrated model overestimated peak flows while using R^2 and bR^2 as these objective functions are used to minimize the total errors between the computed and observed values. The R^2 and bR^2 objective functions are oversensitive in nature to high extreme values due to the presence of squared difference [9]. The obtained calibrated results are similar using NSE, MNS, and RSR objective functions, especially the RSR and NSE objective functions (Fig. 4a). These objective functions fit the simulated and observed base flows recession curves resulting significant reduction of simulated peak flows. The same results using the taken objective function are reported by Sao et al. [18] for Pursat River basin, Cambodia.

The objective function KGE performed well and shows good agreement between simulated and observed flows, with little overestimation of peak flows (Fig. 4d). The

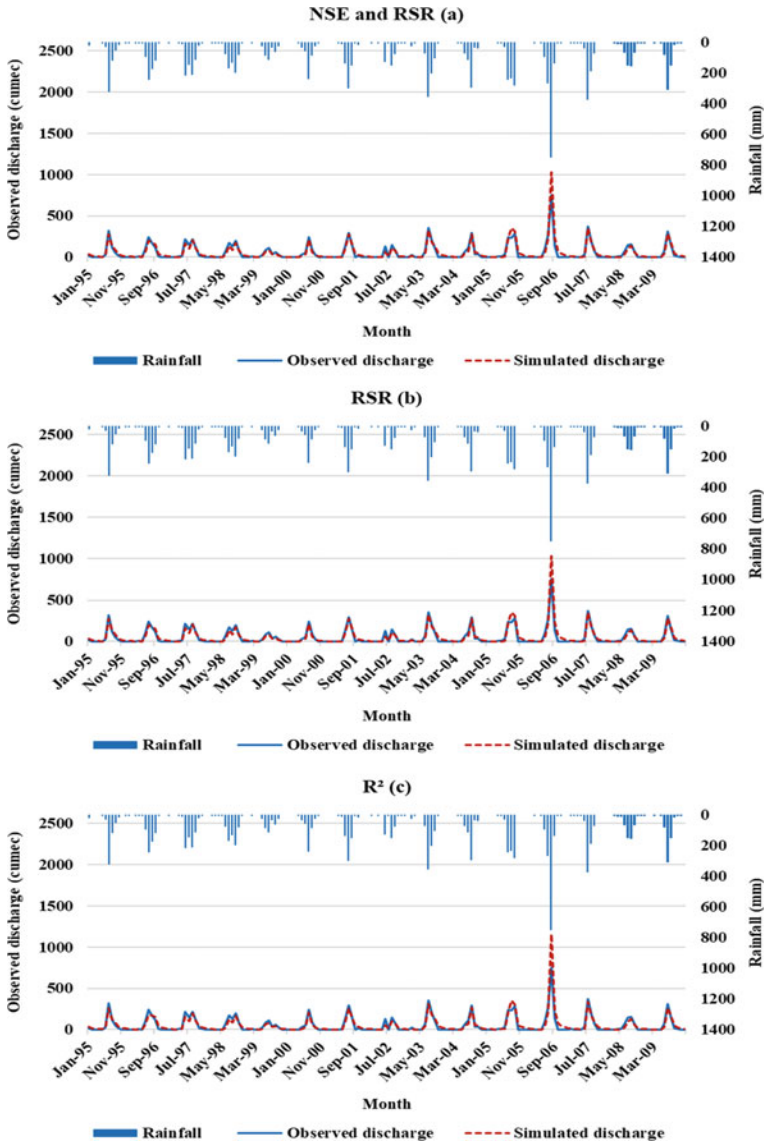

Fig. 4 Simulated discharges at monthly scale using different objective functions

KGE objective function highlights the error between the measured and simulated data and then reduces the errors.

The peak flows are sometimes overestimated, and simulated base flows are sometimes underestimated in case of PBIAS (Fig. 4g) objective function. The limitation of this objective function is that it either overpredicts or underpredicts [19, 20].

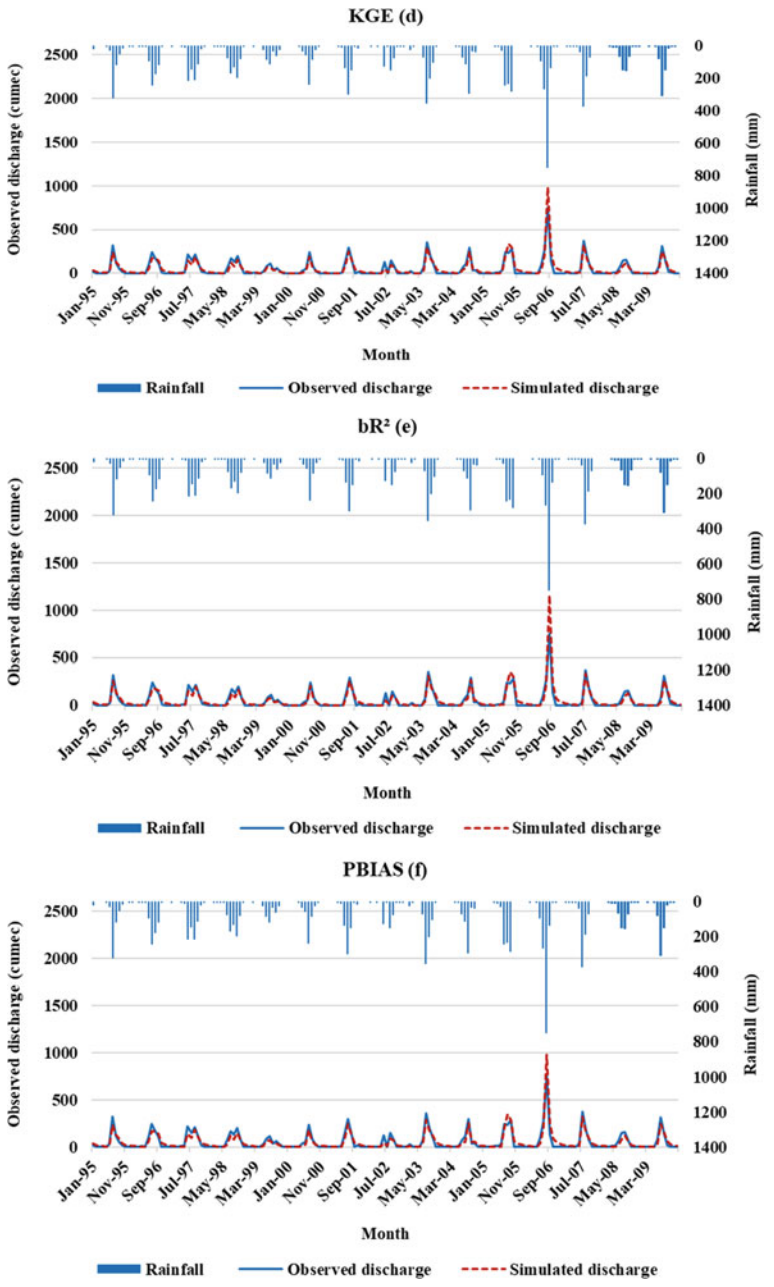

Fig. 4 (continued)

3.3 Statistical Performance of Model

The obtained calibrated parameter sets using seven different objective functions are analyzed and influenced considered objective function on other statistical indices (Fig. 5a–g). For the assessment of performance of the model, the *p*-factor, and *r*-factor are calculated by comparing observed flow to simulated monthly flow. The *p*-factor and *r*-factor are independent of objective function, and the values of 0.45 (0.35), 0.30 (0.25) respectively are obtained during the calibration (validation) period for all seven objective functions. All objective functions gave satisfactory performance as criteria given in Fig. 5. The objective functions (NSE, MNS, RSR, bR^2, and KGE) (Fig. 5a–c, e–f) satisfied all statistical indices, during the calibration/validation process, whereas R^2 did not perform well during the validation period with the objective function PBIAS (−30.1) (Fig. 5d), while calibration and validation, parameter set obtained using PBIAS (Fig. 5g), satisfy all other statistical indices (MNS, NSE, RSR). Calibration period of 1995–2009 is selected as it covers dry, wet, and normal years [21]. The validation period (2010–2015) covers wet and normal years, and hence, the performance of the statistical indices using objective functions gave relatively better results than calibration.

3.4 Water Balance Estimation

Figure 6 shows average annual water balance components (rainfall *P*, surface flow or runoff Q_s, lateral flow Q_{lat}, actual evapotranspiration E_a, and percolation Perc) of the calibrated model using different objective functions based on the obtained best-fitted parameters. The estimated water balance components and water yields are different for different objective function. The annual average E_a using different objective functions ranges from 296.5 to 358.9 mm (49–59% of total rainfall). On the other hand, Q_s varies from 159.6 to 203.5 mm (20–33% of the total rainfall). The estimated annual average Q_{lat} generated by considered objective functions ranged from 53.6 to 67.6 mm (10–11%). It is worthy to note that RSR and NSE provide same water yield in the calibrated model. Due to semi-arid climate zone in Dharoi catchment, obtained E_a loss varies in the range of 50–60%. The E_a loss estimated by NSE and RSR provided more close results as compared to other objection functions. The type of soil present in the study area allows Perc loss ranges from 11 to 14%. The reasonable estimation is given by almost all objective functions (MNS, NSE, RSR, PBIAS, and KGE) (Fig. 6).

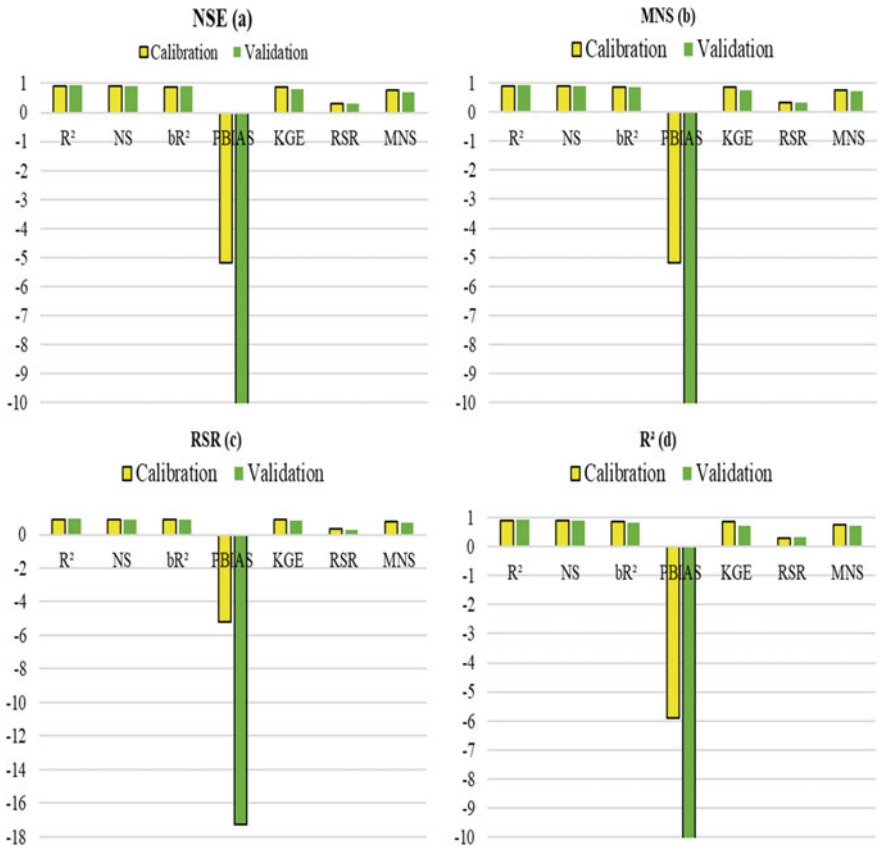

Fig. 5 Model performance evaluated using different objective functions

3.5 Best-Fitted Parameters

The results discussed in previous sections are dependent upon the values of best-fitted parameter using the considered objection function during calibration (Table 5). During the calibration process, the most sensitive parameters noticed are CN2, GWQMN, GW_REVAP, ESCO, SOL_AWC, and SOL_K. The best-fitted parameter values NSE and RSR are same and reflect reasonable water balance components based on the land use, soil type, and climatic condition. The average curve number of the catchment is 70, and one can expect change from 10 to 14% increase or decrease during the calibration process. All objective functions gave relative change ranges from 10 to 14% except bR^2 and R^2 (Table 5). The bR^2 (R^2) objective function gave relative change of 20% (20%) which will produce surface runoff up to 33% which may not be possible due to type of land use, soil type, and antecedent moisture condition. The smaller thresholds (Table 5) of the parameter GWQMN 402.60 (428.18) are produced for bR^2 (R^2), which is responsible for relative more groundwater flow and

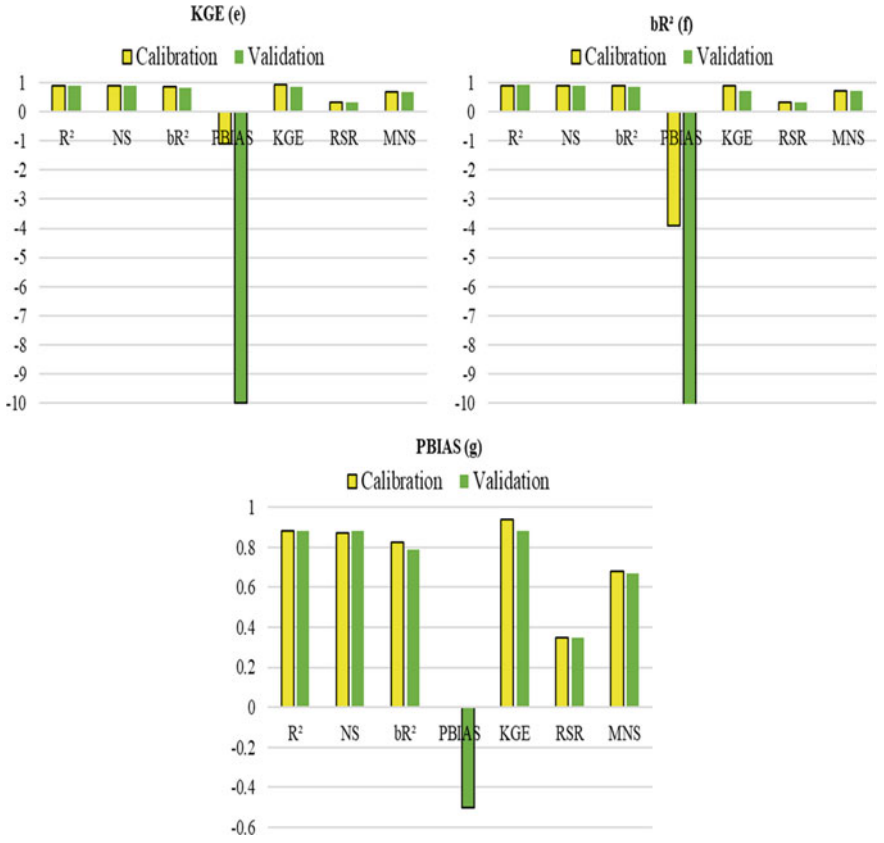

Fig. 5 (continued)

lower estimation of E_a loss with smaller value of GW_REVAP of 0.12. Low ESCO value indicates more water extraction from deep soil layers to meet the evaporative demand resulting in high evapotranspiration loss, lower water yield, streamflow, and base flow. The lowest value of ESCO is noticed using NSE and RSR objective functions. The best-fitted parameter value of SOL_AWC (SOL_K) is noticed in the accepted range from −8 to −18% (−2 to 4%) for all objective functions (Table 5).

4 Conclusions

The SWAT is applied to Dharoi catchment of Sabarmati basin, India. The model is calibrated (validated) for a period from 1995–2009 (2010–2015) using SUFI-2 algorithm with linked objective functions. Total 14 parameters are considered during analysis, out of which the most sensitive parameters are CN2, GWQMN,

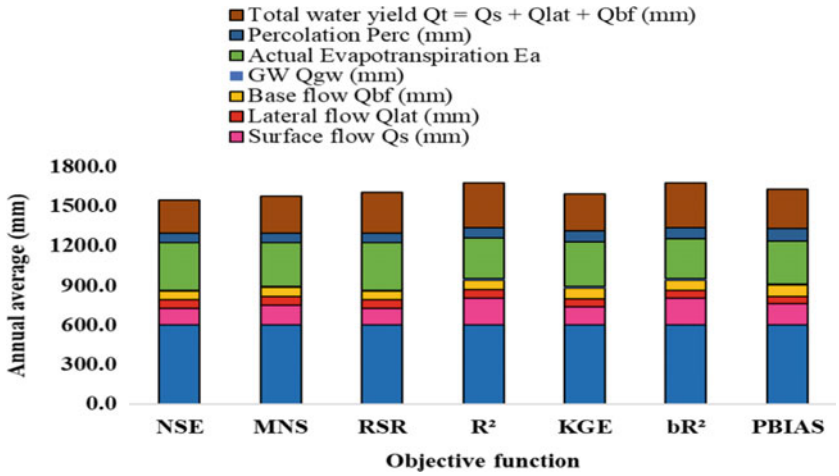

Hydrological Components	Notations	NSE	MNS	RSR	R^2	KGE	bR^2	PBIAS
Precipitation	P (mm)	604.7	604.7	604.7	604.7	604.7	604.7	604.7
Surface flow	Q_s (mm)	124.9	144.5	124.9	203.5	135.5	202.5	159.7
Lateral flow	Q_{lat} (mm)	62.2	65.9	62.2	65.2	61.1	59.6	53.6
Base flow	c (mm)	65.2	71.5	65.2	71.6	83.7	78.4	87.9
GW	Q_{gw} (mm)	8.2	7.9	8.2	10.5	8.9	12.6	6.2
Actual Evapotranspiration	E_a (mm)	359.0	326.5	359.0	302.3	333.9	296.5	325.5
Percolation	$Perc$ (mm)	68.9	75.4	68.9	80.4	86.7	81.3	91.1
Total water yield	$Q_t = Q_s + Q_{lat} + Q_{lat}$ (mm)	252.2	281.9	314.4	340.3	280.2	340.5	301.1

Fig. 6 Water balance components analysis using different objective functions

GW_REVAP, ESCO, SOL_AWC, and SOL_K. The present work investigated the influence of objective functions on the parameter optimizations, calibration results, and water resources estimation. The performance of considered objective functions showed satisfactory results while calibrating the SWAT model. However, the best-fitted parameters obtained using different objective functions are different which led to different estimations of water balance components. The NSE and RSR generated same simulated flows and best-fitted parameter values, and as a result, the same estimated water balance components among all objective functions are investigated in the current work [18]. It can be suggested that the use of KGE, NSE, RSR, MNS, and PBIAS objective functions yields reasonable water balance component estimation of any watershed.

Table 5 Best-fitted parameter value based on objective function

S. No.	Parameter name	NSE	MNS	RSR	R^2	KGE	bR^2	PBIAS
1	SURLAG.hru	2.5	2.1	2.5	2.5	2.1	2.5	2.2
2	CN2.mgt	0.1	0.1	0.1	0.2	0.1	0.2	0.1
3	ALPHA_BF.gw	0.2	0.2	0.2	0.2	0.1	0.1	0.1
4	GW_DELAY.gw	65.4	46.7	65.4	51.0	65.1	63.7	63.9
5	GWQMN.gw	557.8	600.1	557.8	402.6	520.3	421.2	560.3
6	GW_REVAP.gw	0.2	0.2	0.2	0.1	0.2	0.1	0.2
7	ESCO.hru	0.4	0.3	0.4	0.5	0.4	0.5	0.4
8	EPCO.hru	0.5	0.7	0.5	0.7	0.7	0.6	0.5
9	SOL_BD.sol	0.0	0.0	0.0	0.0	−0.1	0.0	−0.1
10	SOL_K.sol	−0.1	−0.1	−0.1	−0.1	−0.1	−0.1	−0.2
11	SOL_AWC.sol	0.0	0.0	0.0	0.0	0.0	0.0	0.0
12	CH_N2.rte	0.5	0.7	0.5	0.8	0.8	1.0	0.9
13	CH_K2.rte	1.2	3.2	1.2	6.0	6.9	25.6	31.2
14	ALPHA_BNK.rte	0.9	0.9	0.9	1.0	1.0	0.9	1.0

Acknowledgements The authors would like to acknowledge the Indian National Committee on Climate Change, Ministry of Jal Shakti, Department of Water Resources, River Development and Ganga Rejuvenation, Government of India, for providing funding for this research. India Meteorological Department, Pune, for rainfall data, Central Water Commission for Meteorological data, and Dharoi dam office for inflow data are duly acknowledged. The authors are also thankful to India Meteorological Department (IMD), Pune, for providing necessary data to conduct the present study. The authors gratefully acknowledge the infrastructure support provided by Centre of Excellence (CoE) on Water Resources and Flood Management, TEQIP-II, for performing the current study. The authors acknowledge the Water Resources Department, SVNIT, Surat, to carry out the present work.

References

1. Arnold JG, Srinivasan R, Muttiah RS, Williams JR (1998) Large area hydrologic modeling and assessment part I: model development 1. JAWRA J Am Water Resour Assoc 34(1):73–89
2. Abbaspour KC (2015) SWAT calibration and uncertainty programs. A User manual 17–66
3. Ha LT, Bastiaanssen WG, Van Griensven A, Van Dijk AI, Senay GB (2018) Calibration of spatially distributed hydrological processes and model parameters in SWAT using remote sensing data and an auto-calibration procedure: a case study in a Vietnamese river basin. Water 10(2):212
4. Roth V, Nigussie TK, Lemann T (2016) Model parameter transfer for streamflow and sediment loss prediction with SWAT in a tropical watershed. Environ Earth Sci 75(19):1–3
5. Abbaspour KC, Vejdani M, Haghighat S, Yang J (2007) SWAT-CUP calibration and uncertainty programs for SWAT. InMODSIM 2007 international congress on modelling and simulation, modelling and simulation society of Australia and New Zealand 2007 Dec (pp 1596–1602). Swiss Federal Institute of Aquatic Science and Technology, Dübendorf, Switzerland

6. Daggupati P, Yen H, White MJ, Srinivasan R, Arnold JG, Keitzer CS, Sowa SP (2015) Impact of model development, calibration and validation decisions on hydrological simulations in West Lake Erie Basin. Hydrol Process 29(26):5307–5320
7. Moriasi DN, Arnold JG, Van Liew MW, Bingner RL, Harmel RD, Veith TL (2007) Model evaluation guidelines for systematic quantification of accuracy in watershed simulations. Trans ASABE 50(3):885–900
8. Ritter A, Munoz-Carpena R (2013) Performance evaluation of hydrological models: statistical significance for reducing subjectivity in goodness-of-fit assessments. J Hydrol 14(480):33–45
9. Legates DR, McCabe GJ Jr (1999) Evaluating the use of "goodness-of-fit" measures in hydrologic and hydroclimatic model validation. Water Resour Res 35(1):233–241
10. Gupta HV, Wagener T, Kling LYH, Yilmaz KK, Martinez GF (2009) Decomposition of the mean squared error and NSE performance criteria: Implications for improving hydrological modelling. J Hydrol 377:80–91
11. Houshmand Kouchi D, Esmaili K, Faridhosseini A, Sanaeinejad SH, Khalili D, Abbaspour KC (2017) Sensitivity of calibrated parameters and water resource estimates on different objective functions and optimization algorithms. Water 9(6):384
12. CWC (2014) Sabarmati Basin Watershed Atlas. Central Water Commission, New Delhi
13. https://earthexplorer.usgs.gov/.
14. Rubel F, Kottek M (2010) Observed and projected climate shifts 1901–2100 depicted by world maps of the Köppen-Geiger climate classification. Meteorol Z 19(2):135
15. Arnold JG, Moriasi DN, Gassman PW, Abbaspour KC, White MJ, Srinivasan R, Santhi C, Harmel RD, Van Griensven A, Van Liew MW, Kannan N (2012) SWAT: Model use, calibration, and validation. Trans ASABE 55(4):1491–1508
16. Abbaspour KC, Johnson CA, Van Genuchten MT (2004) Estimating uncertain flow and transport parameters using a sequential uncertainty fitting procedure. Vadose Zone J 3(4):1340–1352
17. James LD (1982) Selection, calibration, and testing of hydrologic models. Hydrol Model Small Watersheds 437–472
18. Sao D, Kato T, Tu LH, Thouk P, Fitriyah A, Oeurng C (2020) Evaluation of different objective functions used in the sufi-2 calibration process of swat-cup on water balance analysis: a case study of the Pursat river basin, Cambodia. Water 12(10):2901
19. Yapo PO, Gupta HV, Sorooshian S (1996) Automatic calibration of conceptual rainfall-runoff models: sensitivity to calibration data. J Hydrol 181(1–4):23–48
20. Harmel RD, Smith PK, Migliaccio KW (2010) Modifying goodness-of-fit indicators to incorporate both measurement and model uncertainty in model calibration and validation. Trans ASABE 53(1):55–63
21. Yoo C (2006) Long term analysis of wet and dry years in Seoul Korea. J Hydrol 318(1–4):24–36

Assessment of Future Land Use Land Cover Change Impacts on Hydrologic Regime of a River Basin

Kashish Sadhwani, T. I. Eldho, and Subhankar Karmakar

Abstract Land use and land cover change (LULC) has significant impact on hydrologic response at the river basin/watershed level. Quantitative assessment of LULC impacts on runoff generations on river basin scale is important for water resources development and impact assessment of extreme events. Based on the historical LULC changes, the future LULC can be projected, and its impacts can be assessed using a hydrologic model. In this study, the future LULC of Periyar river basin in Western Ghats in South India is projected using multi-layer perceptron–artificial neural network (MLP-ANN) technique in land change modeler (LCM) of TerrSet model. The soil and water assessment tool (SWAT) model was used to study the effect of LULC change on streamflow. The model was calibrated for the period 1984–2004 and then validated for 2006–2012. The results show good co-relation for streamflow with R^2, NSE, and PBIAS, 0.92, 0.84, and 6.5% for calibration period, and 0.85, 0.67, and 11.8% for validation period, respectively. The impact of LULC change for far future is analyzed, and change was compared at monthly, seasonal, and annual scale. The results suggested an increase in streamflow annually. Also it suggests an increase in streamflow in winter and monsoon season whereas a slight decrease in summer season. This information will be useful for planners and researchers to understand the impacts of future LULC changes on river basin hydrology. Further, it will be helpful in decision-making for preparing future development strategies.

Keywords Land cover change · SWAT · Future LULC · Land change modeler

K. Sadhwani (✉) · T. I. Eldho
Department of Civil Engineering, Indian Institute of Technology Bombay, Mumbai 400076, India
e-mail: kashishksh@gmail.com

T. I. Eldho
e-mail: eldho@civil.iitb.ac.in

S. Karmakar
Environment Science and Engineering Department, Indian Institute of Technology Bombay, Mumbai 400076, India
e-mail: skarmakar@iitb.ac.in

P. V. Timbadiya et al. (eds.), *Hydrology and Hydrologic Modelling*,
Lecture Notes in Civil Engineering 312,
https://doi.org/10.1007/978-981-19-9147-9_8

1 Introduction

Flooding is the most common ecological and natural disaster in India for the last two decades such as 2005 Mumbai, 2015 Chennai, 2016 Assam, 2017 Gujrat, and 2018 Kerala. It is important to understand the impacts of future LULC change on hydrological responses as past studies have shown that LULC change has showed a significant impact over change in the streamflow, which results in flooding [16, 22, 25–27, 29]. The rapid LULC change, such as extensive agriculture expansion, deforestation, unplanned urbanization, and population growth, particularly in a developed country like India, has been a major challenge for water resource management. LULC change alters basin hydrology by affecting surface runoff, evapotranspiration, soil erosion, soil infiltration capacity, and water quality of the basin. The IPCC AR5 report stated that extreme rainfall events during the Indian summer monsoon are expected to increase, and floods are likely to increase in future. In this regard, it becomes important to study the role of LULC change in flooding as it will improve our understanding of the hydrological dynamics involved in the flooding. For future LULC change assessment, several modeling techniques are available including land change modeler (LCM), Markov chain, cellular automata (CA), CA_Markov, GeoMod, and stochastic choice (STCHOICE) [7, 10, 12, 23, 28]. All these techniques are embedded in TerrSet (formerly IDRISI) environment and help in developing specific realizations. Among these, LCM has been highly recognized tool in LULC change analysis and incorporated in various studies [24, 26]; Ananad et al. (2018). Modeling the effects of past and future LULC and climate change on hydrology in the river basin can be useful for management of water resource and extreme events (floods and droughts) in the area which may help to the management of same at a sub-basin level.

Within the above framework, the main objectives of this study are to assess and compare the historical (1988) and projected future LULC (2050) change impact on streamflow and other hydrological parameters for Periyar river basin, Western Ghats India. The Periyar river basin situated in the Western Ghats of India which is one of the highly affected river basins during the 2018 flood of Kerala. In addition, Western Ghats is global hotspots region due to the biodiversity and presence of a variety of species [21]. In this study, the open source and semi-distributed hydrological model SWAT is used for computing the impacts of LULC and climate change on streamflow, and SWAT-CUP with sequential uncertainty fitting algorithm (SUFI-2) is used for calibration, validation, and sensitivity analysis on a river sub-basin scale.

2 Study Area and Data Source

2.1 Periyar River Basin (PRB)

Periyar river is the second-longest river of Kerala with a length of approximately 244 km. It originates at Sivagiri peak at an elevation of 2438 m above mean sea level (MSL) and joins the Arabian Sea toward the west. The watershed area ranges from longitude 76° E to 77° 30′ E and latitude 9° 16′ N to 10° 20′ N (Fig. 1). The soil texture over the region varies slightly from clayey to loamy with significant proportions of loam as per the National Bureau of Soil Survey and Land Use Planning (NBSS & LUP) (Fig. 2c). The elevation details and slope map of the region are shown in Fig. 2a and Fig. 2b, respectively. The elevation varies from the highest point of 2695 m above mean sea level at Anamudi Peak (https://www.keralatourism.org/munnar/anamudi-peak-kerala.php) to the lowest point near the sea.

The slope of the watershed has been categorized into four classes 0–2%, 2–8%, 8–16%, and above 16%. The average annual rainfall of PRB is approximately 3200 mm [6]. There are two hydrological observation stations managed by CWC at Neeleshwaran (10° 12′ N 76° 5′ E) and Vandiperiyar (9° 32′ N 77° 4′ E) in the watershed. There are three major dams with significant storage in PRB, namely Mullaperiyar (443.23 million cubic meters (MCM)), Idukki (1460 MCM), and Idalmalayar (1018 MCM) [18]. Details of the reservoirs are mentioned in Table 1.

2.2 Data Collection

For simulation of the SWAT model, digital elevation model (DEM) from Cartosat (30 m resolution), LULC from Landsat (30 m resolution), soil data from National Bureau of Soil Survey and Land Use Planning (NBSS & LUP), India and climatic data, including precipitation and temperature, from India Meteorological Department (IMD, 0.25° resolution) are used. The solar radiation and wind velocity data collected from Climate Forecast System Reanalysis and interpolated at 0.25° as the same grid points to precipitation data for this study. The hydrological data such as observed runoff is collected from a gaging location at Neeleshwaram for the years 1980–2019 at a daily time scale from the Central Water Commission of India.

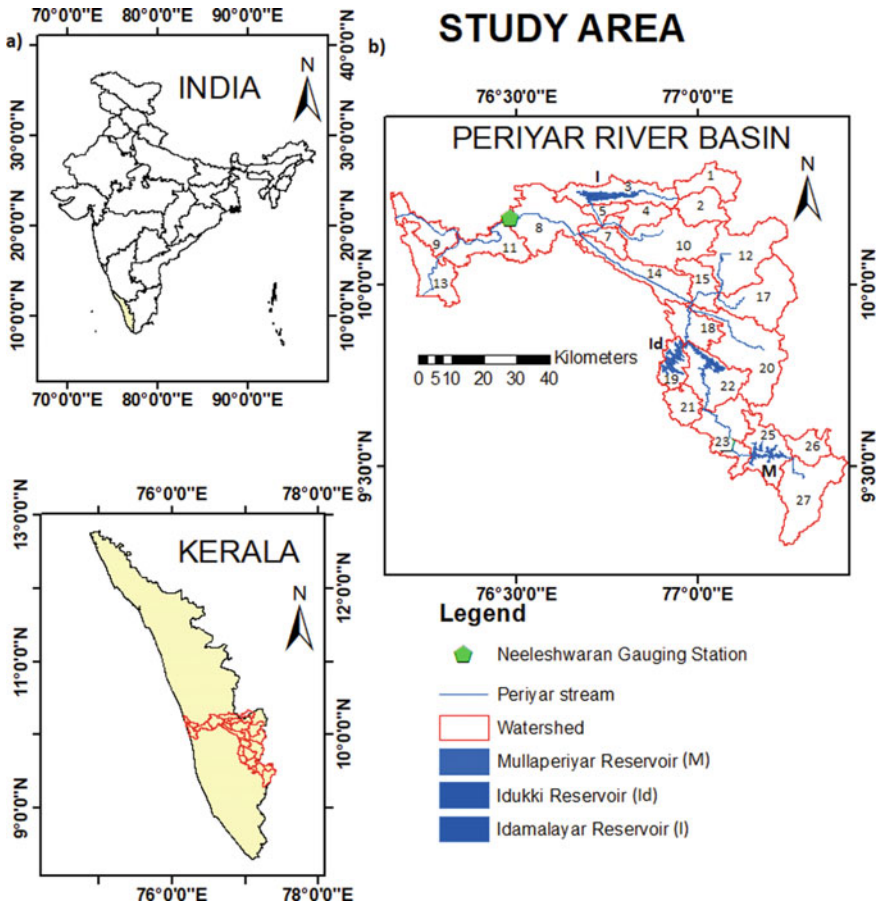

Fig. 1 **a** Location; **b** watershed and sub-basins details of Periyar river basin

3 Methodology

3.1 SWAT Model

A physically based and open-source SWAT hydrological model which is coupled with ArcGIS is used for simulating the streamflow at sub-basin scale in this study. The SWAT model is developed for simulating ungaged and particularly has limited data in the river basin scale [4]. It is also used for assessing the impact of LULC and climate change for streamflow and sediment yields, pesticides, nitrate, and phosphate load in the channel by different researchers [30]. The SWAT model includes large uncertainty in calibration from inputs and observed data. SWAT-Calibration and Uncertainty Program with sequential and uncertainty fitting (SUFI-2) algorithm is

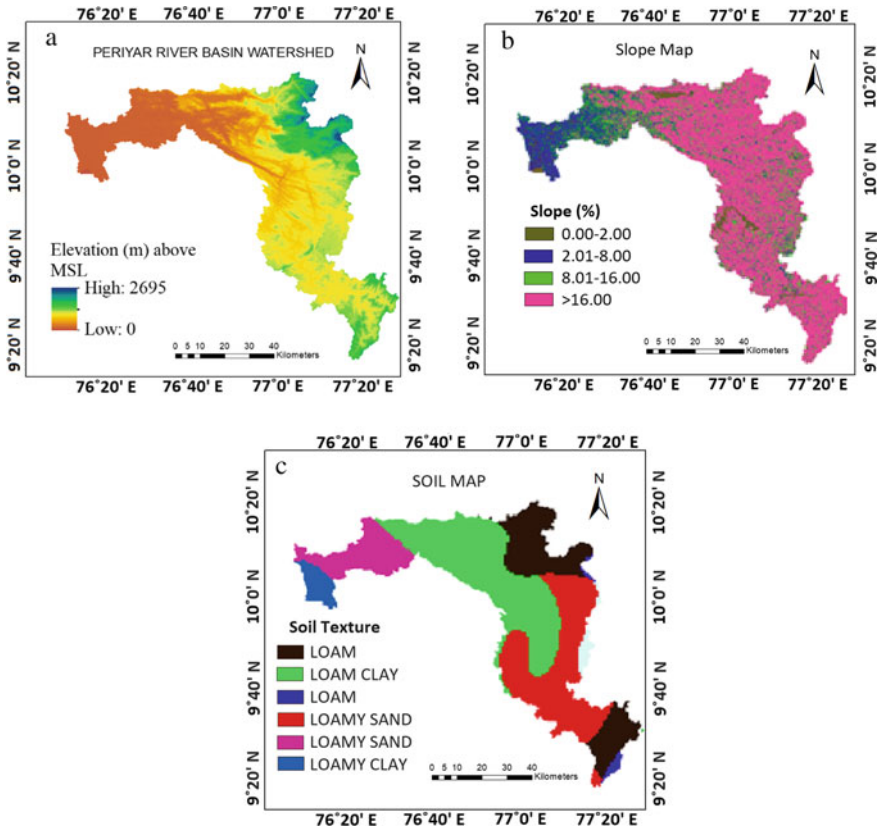

Fig. 2 **a** DEM, **b** slope map, **c** soil map of PRB

Table 1 Details of reservoirs [18] (*Source*: Kerala State Electricity Board; Mohankrishnan and Verma,

Name of reservoir	Built in year	Full reservoir level (m)	Full reservoir capacity (MCM)	Effective volume (MCM)	Surface area at FRL (km^2)
Idamalayar	1985	169	1089	1017.80	28.3
Idduki	1973	168.91	1996	1460	60.03
Mullaperiyar	1895	53.64	443.23	324	20.55

used for calibration because of its simplicity and effectiveness [4]. The SWAT model divides the watershed into sub-basins and hydrological response units (HRUs) on the basis of uniqueness of terrain, LULC, and soil types. The soil conservation service (SCS) curve number (CN) method is used for computing surface runoff [5] on the basis of the soil hydrological groups, antecedent soil moisture, and LULC

characteristics. The details of theoretical documentation of SWAT model is given in Website (https://swat.tamu.edu/documentation/).

3.2 Classification and Future LULC Projection

The historical LULC for 1988 is prepared from Level 2 Landsat images. These images are collected during post monsoon season (October to January) as they were cloud free. The supervised image classification with maximum likelihood technique is used because of its suitability due to availability of several ground truth points [15]. Six major land use classes are identified, namely forest, cropland, plantation, barren, built-up, and water body, in the river basin, and LULC maps are classified using 100 reference points for each class. For validation of the processed LULC data, randomly selected ground truth points were compared with the LULC map. The overall accuracy of classification and kappa coefficient, which is a standard measure for agreement of classified raster, is used to measure the performance of processed raster [8, 9, 11, 14]. Overall accuracy is computed by dividing the total correctly classified pixels by the total number of pixels in the error matrix [11]. Kappa coefficient is the measure of probability of correct classification [8]. The overall accuracy and kappa coefficient (κ) are 84% and 0.82, respectively, which are considered substantial [3]. For the assessment of future streamflow due to future LULC change, 2050 LULC is projected. Land change modeler (LCM) is used for projection of LULC which is incorporated within TerrSET (formerly IDRISI) software developed by Clark labs. LCM compares two maps to identify the trend of transition from one class to another and then uses a multi-layer perceptron (MLP) neural system to develop an empirical relation between the transition and influencing elements (driver variables) responsible for land cover change. The results develop a series of transition potential maps for land use change, and these are used with Markov chain transition matrix technique [20] to generate future LULC maps. LULC maps of 1998 and 2002 are used to project 2016 LULC map with elevation, slope, distance from road, water, forest, and plantation as driver variables. The projected and classified LULC map of 2016 was compared to calibrate and validate the parameters of LCM. The same parameters are used to project LULC map of 2050 with 2016 and 2030 as input. Since long-term (62 years) LULC change impact is assessed in this study, so only LULC of 1988 and 2050 has been represented (Fig. 3).

3.3 Calibration and Validation of the SWAT Model

The sensitivity parameters are evaluated for streamflow before calibration of SWAT model at monthly time-step for the period of 1998–2004 (7 years) at river gage station which is located Neeleshwaram (Fig. 1). The same simulation setup is used in the validation of streamflow for another 7 years (2006–2012) after calibration.

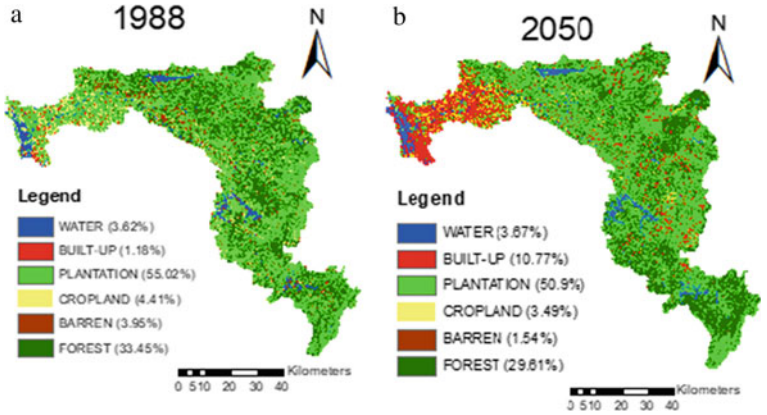

Fig. 3 Classified map for 1988 (**a**) and projected map of 2050 (**b**) of the Periyar river basin

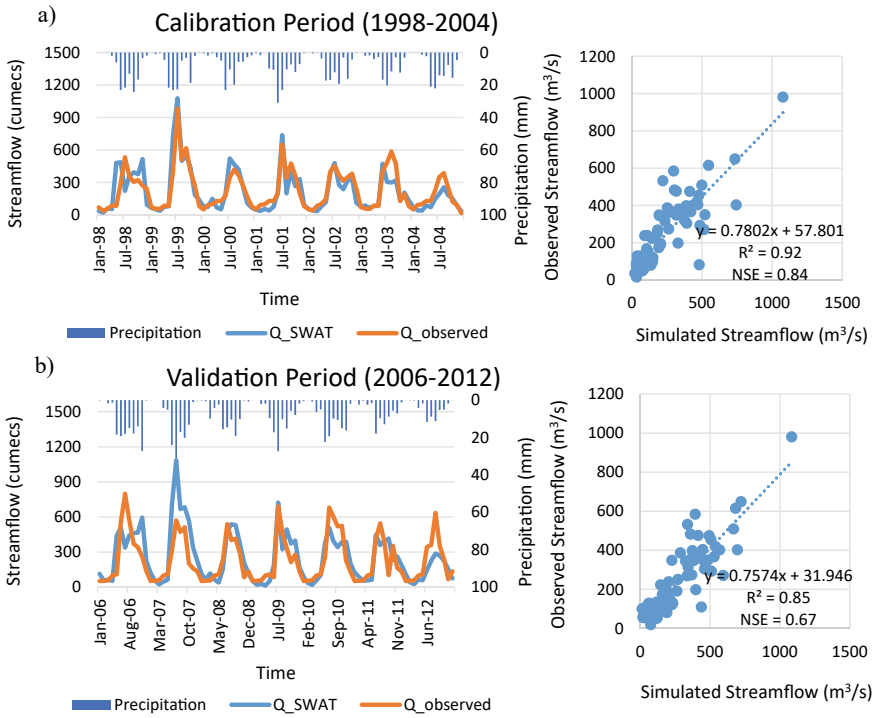

Fig. 4 Comparison of observed and simulated monthly streamflow values for the calibration (**a**) and validation (**b**) period

Latin hypercube (LH) one factor at a time approach, which is incorporated within SUFI-2 algorithm, is used to identify the sensitivity parameters [1, 17]. The LH sampling is based on considering p parameter combinations, where p is the number of simulations. These sampled parameter sets are used as input in SWAT, and the simulation results are compared with gaged data. The performance of the model for simulating streamflow is evaluated by the Nash–Sutcliffe coefficient (NSE), the coefficient of determination (R^2), and percent bias (PBIAS) [13]. The process is repeated to reduce the uncertainty bands and fix suitable parameter ranges.

After fixing the model parameters, the impact of long term LULC change on streamflow will be assessed. For this, the simulations of SWAT model will be compared by changing the LULC between 1988 and 2050, keeping the climatic variables same for the period 1981–2014.

4 Results and Discussion

4.1 LULC Change from 1988 and 2050

The spatial distribution of different LULC classes for 1988 and 2050 maps is presented in Fig. 3, and their corresponding area and percentage growth are listed in Table 2. Forest, plantation, cropland, and barren land areas are expected to decrease, and built-up area will increase from 1988 to 2050. Water bodies remain nearly same with marginal decrease of 0.05%. Built-up areas will increase from 1.81 to 14.21%, whereas forest, plantation, cropland, and barren land will decrease from 33.45% to 29.61%, 55.02% to 50.9%, 4.41% to 3.49%, and 3.95% to 0.71%, respectively, from 1988 to 2050. Major reason for such change can be understood from the historical transition pattern, i.e., plantation and cropland transition into built-up area in conjunction with forest areas into cropland and plantation. Thus, the sequence of conversion of land use was identified as forest to plantation and cropland, which further changes to built up. The maximum percentage change in growth was observed in the built-up area (+812.7%), i.e., it increased by 9.59% of total basin area. Water bodies remain fairly same with a marginal positive growth of 1.38%. Whereas, the maximum negative growth occurred in barren (− 61.01%) followed by cropland (− 20.81%), forest (− 11.47%), plantation (− 7.48%), respectively. The results indicate that the expansion of urbanization in the PRB will lead to land degradation, potentially affecting streamflow in future. In addition, reduction in forest and plantation is alarming as it will also affect the streamflow and alter the natural balance of the watershed ecosystem.

Table 2 Area (km^2) and overall amount of change (%) in LULC of study area over the period of 1988–2050

LULC type	1988 (Km^2)	Percent of study area	2050 (Km^2)	Percent of study area	Amount of change (Km^2)	Percentage growth
Water	173.5	3.62	175.89	3.67	2.39	1.38
Built-up	56.55	1.18	516.18	10.77	459.63	812.7
Plantation	2637.01	55.02	2439.55	50.9	− 197.46	− 7.48
Cropland	211.36	4.41	167.26	3.49	− 44.09	− 20.81
Barren	189.31	3.95	73.80	1.54	− 115.5	− 61.01
Forest	1603.2	33.45	1419.15	29.61	− 184.04	− 11.47
Total	4792.83	100	4792.83	100		

4.2 Calibration and Validation of the SWAT Model

The most sensitive parameters adjusted during calibration of the SWAT model for streamflow were water use in reach (WURCH) followed by threshold depth of water in the shallow aquifer (GWQMN), SCS-CN, and other parameters as shown in Table 3. For streamflow, the parameters related to base flow and surface runoff have almost equal sensitivity. The SWAT model is calibrated spatially at Neeleshwaram gaging station in sub-basin 8 for streamflow. The comparisons between observed and simulated scattered plot for monthly streamflow during the period of calibration (01/01/1998 − 12/31/2004) and validation 01/01/2006 − 12/31/2012) are presented in Fig. 3. The results show good co-relation for streamflow with R^2, NSE, and PBIAS, 0.92, 0.84, and 6.5% for calibration period, and 0.85, 0.67, and 11.8% for validation period, respectively. Overall, the reliability between the results simulated by the model and the observed values as well as their R^2, NSE, and PBIAS values indicated that the model performed well for a monthly time scale [19].

4.3 Impacts of Historical and Projected LULC Change

Figure 5c illustrates the spatial distribution of the mean monthly change in the evapotranspiration under the LULC change. The results show that ET is expected to increase in downstream end and decrease in upstream part of PRB. The major reason for this could be the reduction in forest and plantation cover in upper region. This reduced ET in upper region will result in increased streamflow in these regions. Figure 6c illustrates the spatial distribution of the mean monthly change in the surface runoff under the LULC change. The results showed that the surface runoff would increase by 2.64%. Figure 7 shows the monthly and seasonal change in streamflow due to LULC change. It is observed that streamflow increases in all seasons with annual increase of 2.5%, and in monsoon, the increase is up to 2.73%. The spatial

Table 3 Sensitivity parameters for streamflow calibration

Rank	Parameter	Description	Min value	Max value	Fitted value
1	WURCH.hru	Water use in reach ($\times 10^4$ m^3)	0	5005.677	2.502839 (v)
2	GWQMN.gw	Threshold depth of water in the shallow aquifer required for return flow to occur (mm)	− 1124.862	3375.138	2390.642 (v)
3	CN2.mgt	initial SCS-CN II value	− 0.01945	0.00685	− 0.010442 (r)
4	ALPHA_BNK.rte	Baseflow alpha factor for bank storage	0	0.304392	0.066205 (v)
5	SOL_AWC.sol	Available water capacity of the soil layer	0.043715	0.681285	0.274834 (v)
6	ESCO.hru	Soil evaporation compensation factors	− 0.13739	0.020885	− 0.062602 (r)
7	ALPHA_BF.gw	Base flow alpha factor (day)	0	0.054575	0.004994 (v)
8	GW_DELAY.gw	Groundwater delay (days)	20.88599	280.314	125.0463 (v)
9	SURLAG.bsn	Surface runoff lag time (days)	8.138288	24.31816	19.06779 (v)
10	USLE_K.sol	USLE soil erodibility factor	− 0.65783	0.047428	− 0.574255 (r)
11	GW_REVAP.gw	Groundwater revap coefficient	0.02	0.118601	0.029416 (v)

v: absolute change; r: relative change

distribution of the change in surface runoff (Fig. 6a and b) under LULC change from 1988 to 2050 indicated that the streamflow would mainly increase throughout the basin. This may be because of increase in urbanization and reduction in plantation/forests. Figure 6c indicates that most of the basins near the river channel are showing maximum increase in surface runoff as these are the areas where maximum changes in LULC are observed. Thus, it can be understood that LULC change shows significant impact on surface runoff. At a sub-basin scale, the proportions of changes for urban land use is positively correlated, whereas those for forests, plantation, and barren land were negatively correlated. Similar results have been reported in past studies that an increase in the agriculture area and a decrease in the forest area may increase the surface runoff [2, 7, 26, 27]. This increase in streamflow due to LULC change suggests that there are high possibilities of flood occurrence in future. Thus,

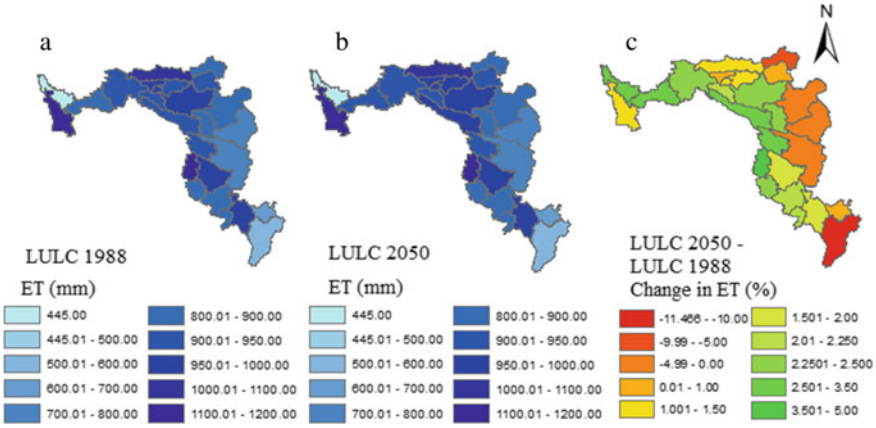

Fig. 5 Spatial distribution of actual evapotranspiration in mm **a** for LULC 1988, **b** for LULC 2050, and **c** change in ET (%)

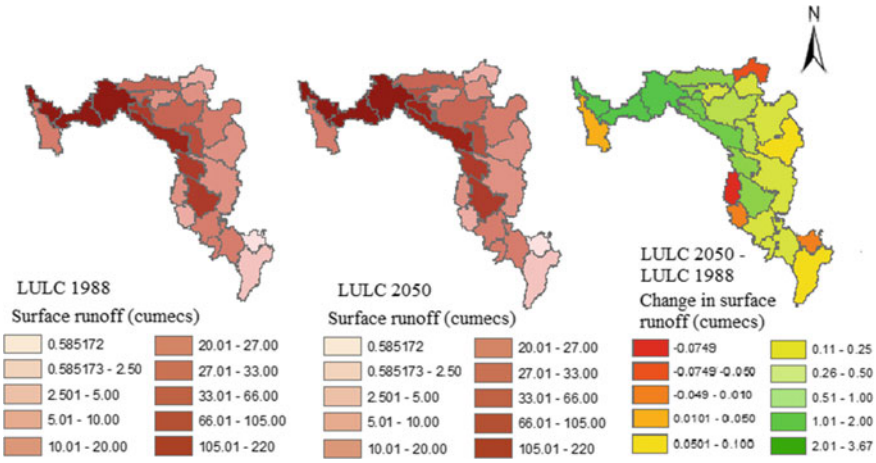

Fig. 6 Spatial distribution of actual streamflow in m^3/s **a** for LULC 1988, **b** for LULC 2050, and **c** change in streamflow

planners should consider LULC change impact on the streamflow as an important parameter when planning water resource management.

5 Conclusions

In this study, the impact of long-term LULC change is investigated on streamflow of Periyar river basin using SWAT hydrological model. The results indicated that

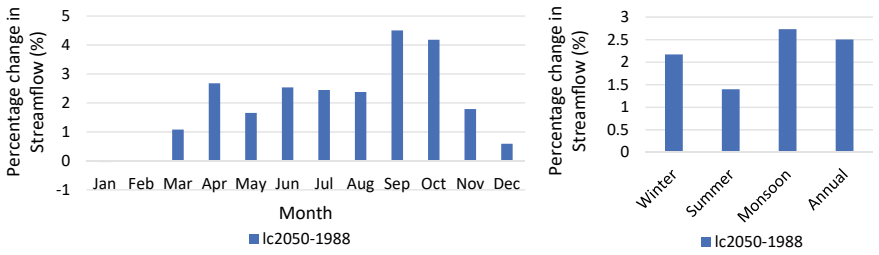

Fig. 7 Monthly and seasonal change in streamflow with LULC change from 1988 to 2050 for PRB

the major changes in LULC that affected surface runoff were an expansion of urban area and decline of forest and plantation area from 1988 to 2050. From the analysis, it can be concluded that forest and plantation have an inverse relation with surface runoff and directly in relation with ET. On contrary, this relations reverse with urban area with increased urbanization leading to increased surface runoff and a decrease in ET. LULC change shows significant variation in streamflow, and thus, it is an essential component for water resource management and planning. The variation of streamflow is estimated to become more severe in future due to component of LULC change. This will lead to amplified streamflow during flooding condition in the Periyar river basin. In such situations, damage caused by floods will be higher. Since both the prevalence and size of extreme weather events in India are on the rise, it logical to assume that agricultural and urban growth will also contribute to an increase in the severity of such occurrences (drought and floods). Long-term water resource planning, therefore, needs to be flexible in light of these considerations. To lessen the impact of urban and agricultural sprawl, policymakers and planners should design a comprehensive land use strategy.

Acknowledgements The authors wish to acknowledge the sponsors of the project entitled "Impact of Climate Change on Water Resources in River basins from Tadri to Kanyakumari" by INCCC, Ministry of Water Resources, Government of India. We wish to express our sincere gratitude to Central Water Commission and India Meteorological Department, India, for providing us hydrological and meteorological data. The authors also acknowledge the National Bureau of Soil Survey and Land Use Planning, India, for giving soil data.

References

1. Abbaspour KC, Johnson CA, Van Genuchten MT (2004) Estimating uncertain flow and transport parameters using a sequential uncertainty fitting procedure. Vadose Zone J 3(4):1340–1352
2. Anand J, Gosain AK, Khosa R (2018) Prediction of land use changes based on land change modeler and attribution of changes in the water balance of Ganga basin to land use change using the SWAT model. Sci Total Environ 644:503–519
3. Anderson JR (1976) A land use and land cover classification system for use with remote sensor data, vol. 964, US Government Printing OfficeArnold, J.G., Srinivasan, R., Muttiah,

R.S. and Williams, J.R. (1998) Large area hydrologic modeling and assessment part I: model development. JAWRA J Am Water Resour Assoc 34(1):73–89
4. Arnold JG, Moriasi DN, Gassman PW, Abbaspour KC, White MJ, Srinivasan R, Santhi C, Harmel RD, Van Griensven A, Van Liew MW, Kannan N (2012) SWAT: model use, calibration, and validation. Trans ASABE 55(4):1491–1508
5. Arnold JG, Srinivasan R, Muttiah RS, Williams JR (1998) Large area hydrologic modeling and assessment part I: model development 1. JAWRA J Am Water Res Assoc 34(1):73–89
6. CWC (2018) Kerala Floods of August 2018, Central Water Commission, New Delhi, 2018. https://sdma.kerala.gov.in/wp-content/uploads/2020/08/CWC-Report-on-Kerala-Floods.pdf
7. Chanapathi T, Thatikonda S (2020) Investigating the impact of climate and land-use land cover changes on hydrological predictions over the Krishna river basin under present and future scenarios. Sci Total Environ 721:137736
8. Cohen J (1960) A coefficient of agreement for nominal scales. Educ Psychol Measur 20(1):37–46
9. Congalton RG (1991) A review of assessing the accuracy of classifications of remotely sensed data. Remote Sens Environ 37:35–46
10. Eastman JR, Van Fossen ME, Solarzano LA (2005) Transition potential modeling for land cover change. GIS, Spat Anal Model 17:357–386
11. Jensen JR (2005) Thematic map accuracy assessment. In: Keith CC (ed) Introductory digital image processing–a remote sensing perspective, 3rd edn. Prentice Hall Series in Geographic Information Science: Saddle River, NJ, USA; Sect. C, pp 495–515
12. Kamusoko C, Aniya M, Adi B, Manjoro M (2009) Rural sustainability under threat in Zimbabwe–simulation of future land use/cover changes in the Bindura district based on the Markov-cellular automata model. Appl Geogr 29(3):435–447
13. Legates DR, McCabe GJ (1999) Evaluating the use of "goodness-of-fit" measures in hydrologic and hydroclimatic model validation. Water Resour Res 35(1):233–241
14. Liu C, Frazier P, Kumar L (2007) Comparative assessment of the measures of thematic classification accuracy. Remote Sens Environ 107(4):606–616
15. Lu D, Weng Q (2007) A survey of image classification methods and techniques for improving classification performance. Int J Remote Sens 28(5):823–870
16. Marhaento H, Booij MJ, Hoekstra AY (2018) Hydrological response to future land-use change and climate change in a tropical catchment. Hydrol Sci J 63(9):1368–1385
17. McKay MD, Beckman RJ, Conover WJ (1979) A Comparison of three methods for selecting values of input variables in the analysis of output from a computer code. Technometrics 21(2):239. https://doi.org/10.2307/1268522
18. Mohanakrishnan A, Verma CVJ (1997) History of the Periyar Dam with century long performance. Central Board of Irrigation & Power
19. Moriasi DN, Arnold JG, Van Liew MW, Bingner RL, Harmel RD, Veith TL (2007) Model evaluation guidelines for systematic quantification of accuracy in watershed simulations. Trans ASABE 50(3):885–900
20. Muller MR, Middleton J (1994) A Markov model of land-use change dynamics in the Niagara Region, Ontario, Canada. Landscape Ecol 9(2):151–157
21. Myers N, Mittermeier RA, Mittermeier CG, Da Fonseca GA, Kent J (2000) Biodiversity hotspots for conservation priorities. Nature 403(6772):853
22. Petelet-Giraud E, Cary L, Cary P, Bertrand G, Giglio-Jacquemot A, Hirata R, Aquilina L, Alves LM, Martins V, Melo AM, Montenegro S, Aurouet A (2018) Multi-layered water resources, management, and uses under the impacts of global changes in a southern coastal metropolis: When will it be already too late? Crossed analysis in Recife, NE Brazil. Sci Total Environ 618:645–657
23. Pontius GR, Malanson J (2005) Comparison of the structure and accuracy of two land change models. Int J Geogr Inf Sci 19(2):243–265
24. Rahman K, da Silva AG, Tejeda EM, Gobiet A, Beniston M, Lehmann A (2015) An independent and combined effect analysis of land use and climate change in the upper Rhone River watershed, Switzerland. Appl Geogr 63:264–272

25. Shi P, Ma X, Hou Y, Li Q, Zhang Z, Qu S, Chen C, Cai T, Fang X (2013) Effects of land-use and climate change on hydrological processes in the upstream of Huai River, China. Water Resour Manag 27(5):1263–1278
26. Sinha RK, Eldho TI (2018) Effects of historical and projected land use/cover change on runoff and sediment yield in the Netravati river basin, Western Ghats, India. Environ Earth Sci 77(3):1–19
27. Sinha RK, Eldho TI, Subimal G (2020) Assessing the impacts of land use/land cover and climate change on streamflow of a humid tropical river basin in Western Ghats, India. Int J River Basin Manag 1–12
28. Wu F, Webster CJ (2000) Simulating artificial cities in a GIS environment: urban growth under alternative regulation regimes. Int J Geog Inf Sci 14(7):625–648
29. Zhang X, Liu Y, Fang Y, Liu B, Xia D (2012) Modeling and assessing hydrologic processes for historical and potential land-cover change in the Duoyingping watershed, southwest China. Phys Chem Earth, Parts A/B/C 53:19–29
30. Zuo D, Xu Z, Yao W, Jin S, Xiao P, Ran D (2016) Assessing the effects of changes in land use and climate on runoff and sediment yields from a watershed in the Loess Plateau of China. Sci Total Environ 544:238–250

Impact Assessment of Climate Change on Hydrological Parameters: Evaluation of Water Balance Components of a River Basin

Raju Narwade and S. K. Ukarande

Abstract In recent years, climate change has become a big concern over the world. Global warming and climate change have made the problem terrible. It has attracted the attention of researchers all over the world. Due to climate change, unusual changes are happening in the atmosphere, so accurate modeling will help us address the issue by modeling in terms of parameter finding, assessment, and estimation. Hydrological models are extensively used for different water projects to understand catchment water balance, prediction of streamline flow, rainfall, runoff, flood forecasting, and other water resource management projects. Two watersheds of the Manjra River basin, the tributary of the Godavari River basin, namely MNJR012 and MNJR013, were selected. The Soil and Water Assessment Tool (SWAT) hydrological model is used for impact assessment on those watersheds. Remote sensing data like digital elevation model (DEM), soil map, land use/land cover (LULC), and weather data are used. The simulated and observed data were then compared, and regression analysis was performed which gave values of R^2 0.933 and 0.971 for Watersheds MNJR012 and MNJR013, respectively, which is closer to 1; hence, the simulated values obtained are validated. It has been observed that simulated data and observed data were in very close agreement with each other, which validated the results.

Keywords Climate change · Hydrological parameter · Soil Water Assessment Tool (SWAT) · River basin · Watershed delineation

R. Narwade (✉)
Department of Civil Engineering, Pillai HOC College of Engineering and Technology, Via Panvel, Rasayani 410207, India
e-mail: narwaderajp@mes.ac.in

S. K. Ukarande
K. J. Somaiya Institute Engineering, and Information Technology, Mumbai 400022, India
e-mail: principal@tech.somaiya.edu

P. V. Timbadiya et al. (eds.), *Hydrology and Hydrologic Modelling*,
Lecture Notes in Civil Engineering 312,
https://doi.org/10.1007/978-981-19-9147-9_9

1 Introduction

Water is the fundamental element for the sustenance of life. Due to the increase in population, majority of the river basins are considered as overstressed. Water on the earth is available in several forms in the environment, such as surface bodies like a lake, moisture in the air, snow, and groundwater. These water bodies are interconnected through the hydrological cycle. The hydrological cycle starts when water evaporates from surface water bodies due to solar insolation. When these vapors get condensed, they form clouds and precipitate to fall on earth.

Out of this, only 22% of water seep underground, and only less than half reach the actual groundwater reservoir; the remaining water gets received by oceans, evaporation, and surface water bodies like rivers and lakes. The major components of the hydrological cycle are precipitation, i.e., rainfall, snowfall, hail, sleet, fog, and other components like runoff, evapotranspiration, percolation, etc. These components of the hydrological cycle play a vital role in water resource management and water budgeting projects. Climate change highly affects water resources by altering several water balance components; land use/land cover affects the water quality of streams and water bodies due to pollutants and soil erosion. Water shortage is a main reason of the degradation of the eco-environment in most river basins, and also it is a serious problem for society. To manage effective water resources, attention should be given on the proper distribution of water resources. Based on different scales models, the water balance components have been evaluated during the past few years. To overcome the issue of water shortage, the appropriate water resource management and water budgeting are compulsory.

After the Ganga River basin, the Godavari River is the second largest in India. This basin comes under six different states: Maharashtra, Madhya Pradesh, Orissa, Chhattisgarh, Telangana, and Andhra Pradesh. The water flows in the Godavari basin are shared among these states. The majority of the population in the state depends upon agriculture. In recent years, farmers have been forced to depend upon groundwater for these agricultural needs due to the dwindling nature of rainfall and surface water flows—the overexploitation of groundwater results in depletion of the shallow aquifer. For sustainable water resource management and agricultural development, it is necessary to understand available water resources, their characteristics, and their variation over time [2].

Every year in Maharashtra state, the Marathwada region faces water scarcity problems due to the depletion of water levels. In such cases, proper water budgeting is necessary for further water management and distribution. Two watersheds of the Manjra River MNJR012 and MNJR013 are selected. The Manjra River is a tributary river of the Godavari River and flows through the Marathwada region. Also, it is a major source of water in the Marathwada and surrounding region. Hence, the smaller watersheds of the Manjra River basin are selected to study the characteristics of watersheds and components in detail.

2 Data Used and Methodology

2.1 Methodology

The SWAT, a hydrological model, is used. In this model, watersheds in Manjra River basin are divided into sub-watersheds, which are further subdivided into (HRUs) Hydrologic Response Units. The HRU includes attributes of land use/land cover, slope, and soil [20]. The HRUs are generally used to simplify the simulation because all land use and soil areas unite into a single response unit. The ArcSWAT requires spatially distributed data which are DEM, soil map and land-use/land-cover data, shape file, grid data, and also weather data and streamflow data are required as input for calibration and future prediction in SWAT. Flowchart of methodology is shown in Fig. 1.

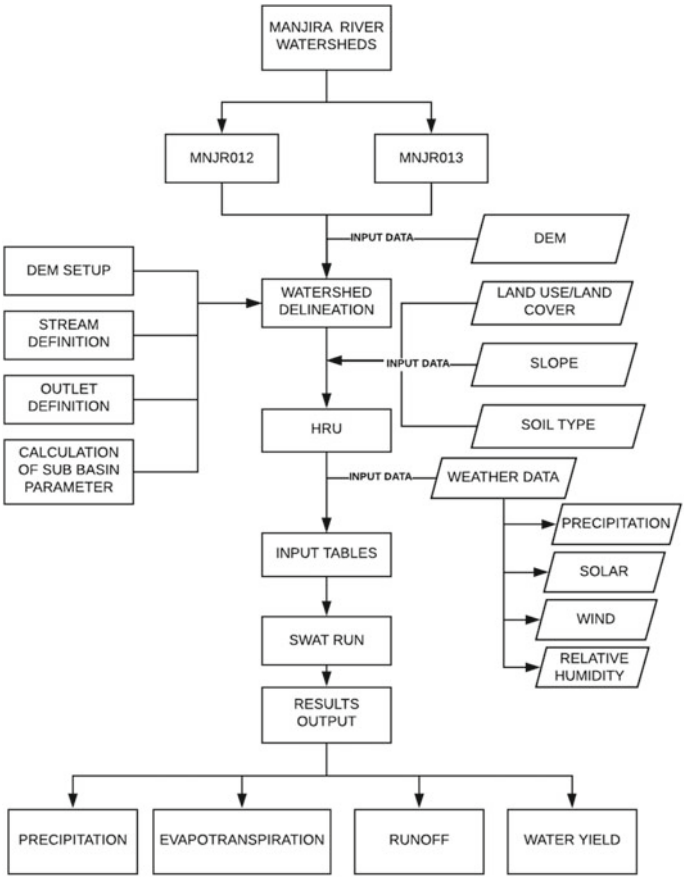

Fig. 1 Flowchart of methodology

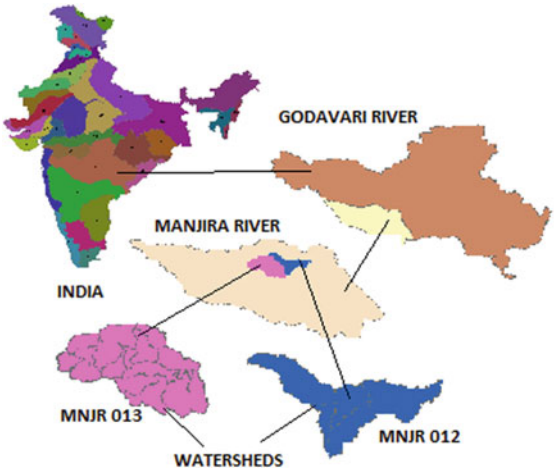

Fig. 2 Study area (Watersheds MNJR012 and MNJR013)

Study Area and Data Collection

2.1.1 The Manjra River Basin

The Manjra River is a tributary of the second largest river of India, which is the Godavari. It flows through Maharashtra, Telangana, and Karnataka states. The river is 724 km long which starts from the Beed district and ends in Telangana state. This basin has a catchment area of about 30,844 km^2. Lendi, Terna, Tawarja, Gharni, Manyad, and Teru are the six tributaries of the Manjra River. Singur dam and Nizam Sagar are two major projects in the Manjra River and play a vital role in fulfilling the water requirement of the surrounding region in Maharashtra and Telangana states.

The Manjra River consists of a total of 28 watersheds, among them two watersheds selected. The Central Ground Water Board has given codes to these watersheds. The study area consists of two watersheds having codes MNJR012 and MNJR013 in the Manjra River basin as shown in Fig. 2. Watershed MNJR012 has an area of 756 km^2 and comes under the Lendi River stream. It covers some areas of Andhra Pradesh and some areas of the Maharashtra district. Watershed MNJR013 has an area of about 1249 km^2 and comes under the Terna stream, and it covers some part of Karnataka and Maharashtra states.

2.1.2 Data Collection

For any hydrologic model, the data required are rainfall, discharge data, DEM, LULC, type of soil. Daily rainfall data can be obtained from Indian Meteorological Department (IMD), Pune. Metrological datasets can also be obtained from India Water

Portal (IWP), Ministry of Earth Science (data.gov.in), Central Water Commission (CWC) processing system (nasa.pps.eosdis.nasa.gov), etc. Free satellite images and GIS data can be downloaded from various websites available based on the type of data, such as IndiaRemotSensing.com http://glovis.usgs.gov, www.divagis.org/gData, www.gadm.org/cou-ntry, www.mappinghack-s.com.

2.2 Selection of Input Parameters

- Digital Elevation Model: Shuttle Radar Topography Mission project is led by the National Geospatial-Intelligence Agency (NGA) and NASA. (SRTM 90) meter (3 arc-second) resolution.
- Soil Map: National Bureau of Soil Survey and Land Use Planning (NBSSLUP), Nagpur
- LULC Map: Indian Space Research Organisation (ISRO), International Geo-Sphere Biosphere Program (IGBP) was used.

2.3 SWAT Hydrological Model Overview

This is a river basin-scale hydrological model which is designed to simulate the hydrological process, nutrient cycle, and sediment transport throughout the watershed. The area ranges from 00,015 to 491,700 km^2. The SWAT modeling is initialized by some input data like soil map, land-use/land-cover data, weather data, elevation data, sub-basin routing, etc. The smallest unit in the SWAT model is the HRU unit, i.e., Hydrological Response Unit, which is used to simulate runoff, erosion, nutrient cycle, infiltration, etc. These units are defined by soil data and land-use data. The simulation also requires meteorological data as input data, which includes rainfall data, temperature, wind, humidity, and solar data, which is provided by ArcSWAT 2012. The simulation gets routed through the internal network. For the selected study area, land use, soil map, and slope data were obtained from the Indian dataset. The development of the entire database required for the model is the initial step for model setup. ArcSWAT 2012 delineates sub-watersheds by using DEM. All the parameters for the selected catchment area were calculated for each basin. SWAT allows importing land use and soil map in the model. The land use gives brief specifications about the land-use layers, and the soil map reclassifies the type of soil into the hydrological soil group based on infiltration rate. A threshold percentage of 10% was adopted to eliminate minor land use, soil, slope. The model requires daily data of precipitation and temperature. This model allows loading weather stations into the project and assigning the weather data to sub-watersheds. Using this data, SWAT model prepares input tables for SWT run, which furthers produces simulated values of water balance components.

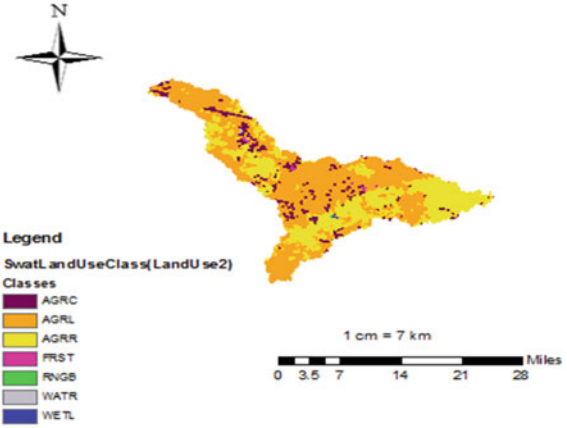

Fig. 3 LULC map of MNJR012

2.4 Thematic Maps

The thematic map of LULC, Soil and digital elevation model were prepared as follows.

2.5 Land Use/Land Cover (LULC)

Land-use documents are used to show how people are using land, whereas land-cover documents specify the physical land type such as open water, forest, bare land. The distribution of land in Watersheds MNJR012 and MNJR013 and land-use/land-cover map of the Manjra River basin are shown in Figs. 3 and 5, respectively. The figures show land-use classes such as Water (WATR), Rangeland Brush (RNGB), Agricultural Land-Generic (AGRL), Agricultural Land-Row Crops (AGRR), Agricultural Land-Close Grown (AGRC), and Forest (FRST).

2.6 Soil Map

The soil map of Watersheds MNJR012 and MNJR013 of the Manjra River basin are shown in Figs. 4 and 6, respectively. In Watersheds MNJR012 and MNJR013, clay loam and clay soils are shown in Table 1.

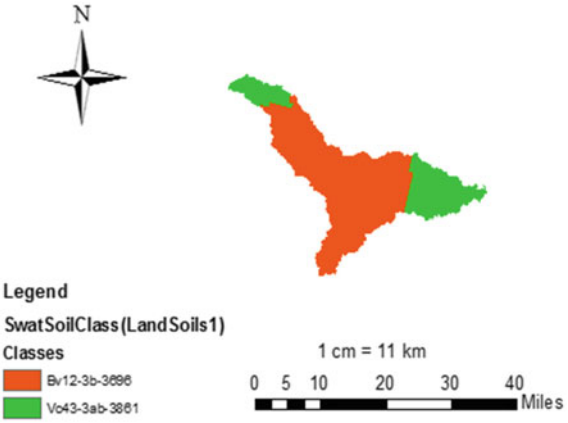

Fig. 4 Soil map of MNJR012

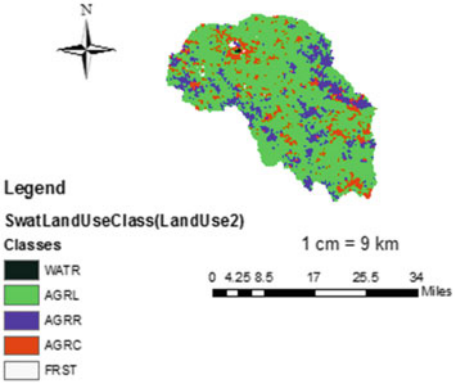

Fig. 5 LULC map of MNJR12

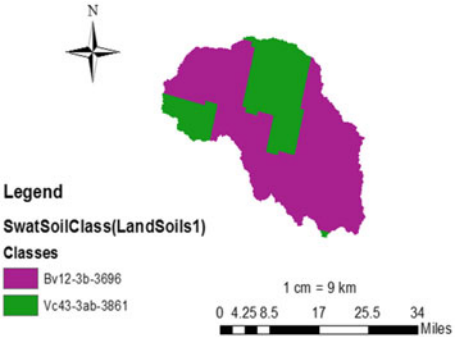

Fig. 6 Soil map of MNJR013

Table 1 Soil classification

Class	Type
Bv12-3b-3696	Clay loam
Vc43-3ab-3861	Clay
Vo43-3ab-3861	Clay

2.7 Digital Elevation Model Map

Figures 7 and 8 show the DEM of Watersheds MNJR012 and MNJR013 in the Manjra River. The data required for DEM are collected from hydrosheds.

3 Results and Discussions

The four different water balancing components of watersheds are generated using the SWAT model and GIS. The water balancing components rainfall, runoff, evapotranspiration, and groundwater recharge are evaluated. The SWAT model also gave the land-use/land-cover distribution in the study area. It has also prepared land use/land cover and soil maps.

For each watershed, a separate SWAT simulation was used.

Precipitation (P)−Runoff (Q)−Evapotranspiration (ET)−Base flow

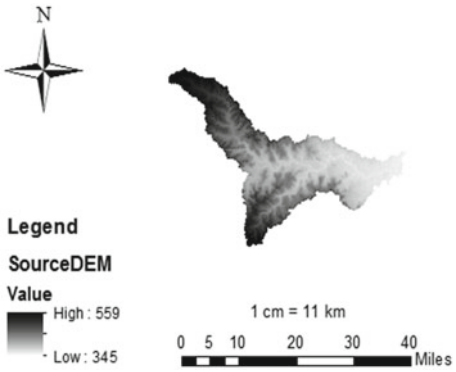

Fig. 7 DEM of Watershed MNJR012

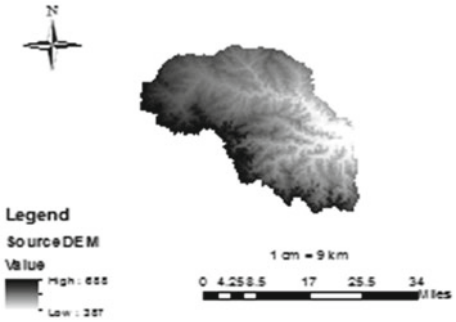

Fig. 8 DEM of Watershed MNJR013

$$\pm \Delta \text{TWS} - (\text{other components}) = 0 \ldots\ldots\ldots\ldots (\text{Water Balancing Equation}) \quad (1)$$

ΔTWS is change in terrestrial water storage and other components which include groundwater storage (shallow and deep) and soil moisture.

3.1 Watershed MNJR012

Figure 9 gives water balancing components in the MNJ012. All parameters indicate the average values.

Precipitation (P) = 979.2 mm, Total runoff (Q) = 420.17 mm, Groundwater recharge = 7.71 mm and Evapotranspiration (ET) = 515.1 mm. So, from (Eq. 1);

$$979.2 - 420.17 - 515.1 - 7.71 = 36.1$$

Therefore, $979.2 - 420.17 - 515.1 - 7.71 - 36.1 = 0$.

As the summation of water balance components is equal to zero, this means the incoming and outgoing of water in Watershed MNJR013 are equal. Table 2 shows the value of incoming and outgoing of water in Watershed MNJR012 region, which are equal, which justifies the water balance equation.

Using the SWAT simulation, monthly basin values of important parameters for Watershed MNJR012 of the Manjra River were derived which are shown in Table 3. It includes precipitation values, runoff, water yield, evapotranspiration of selected watershed. These components are shown in Figs. 10, 11, 12, and 13 in the graphical form.

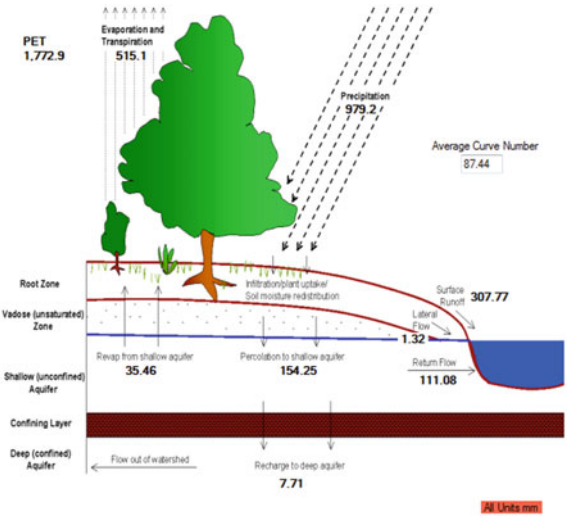

Fig. 9 Water balance components of Manjra Watershed MNJR012

Table 2 Water balance components of Watershed MNJR012

Components	Incoming (mm)	Outgoing (mm)
P	979.2	
ET	–	515.1
Q	–	420.17
ΔTWS	–	36.1
Groundwater recharge	–	7.71
Total	**979.2**	**979.2**

Bold values in the columns indicate the total precipitation i.e. total water entering in the watershed in the form of precipitation and total water leaving in the form of runoff, groundwater recharge, evapotranspiration and other components

Table 3 Monthly basin value of Manjra Watershed MNJR01

Month	Rain (mm)	Runoff (mm)	Water yield (mm)	E.T. (mm)
1	0.1	0.11	1.57	11.91
2	0.17	0.1	0.71	7.21
3	12.83	2.13	2.63	41.2
4	9.26	0.18	0.54	52.51
5	20.17	0.3	0.57	20.19
6	157.66	14.98	14.14	60.76
7	224.25	68.54	68.76	71.19
8	228.08	92.12	105.2	74.22
9	165.9	62.2	91.64	69.11
10	125.38	55.45	91.68	54.96
11	31.82	10.69	37.33	32.19
12	3.74	2.36	13.25	19.88

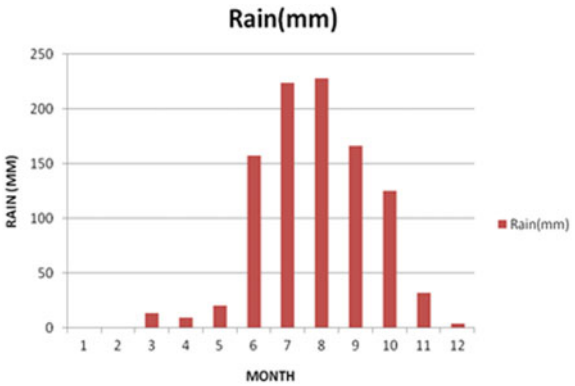

Fig. 10 Monthly rainfall (average) MNJR012

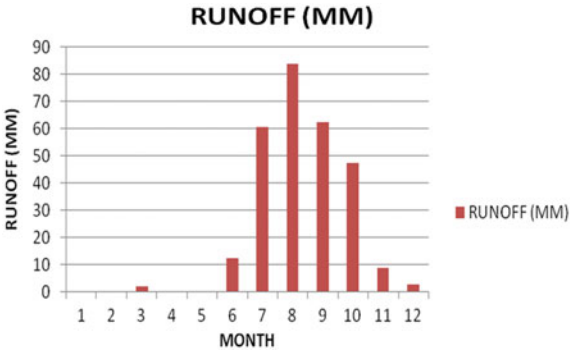

Fig. 11 Monthly runoff (average) MNJR012

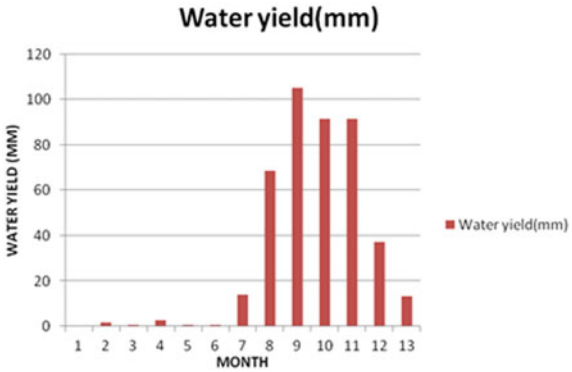

Fig. 12 Monthly water yield (average) MNJR012

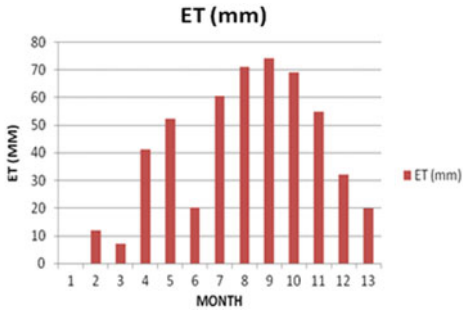

Fig. 13 Monthly evapotranspiration (average) MNJR012

3.2 Watershed MNJR013

Figure 14 gives water balancing components in the watershed.

Precipitation (P) average = 959.8 mm, Total runoff (Q) average = 396.38 mm, Groundwater recharge (average) = 7.97 mm, Evapotranspiration (ET) average = 519.2 mm.

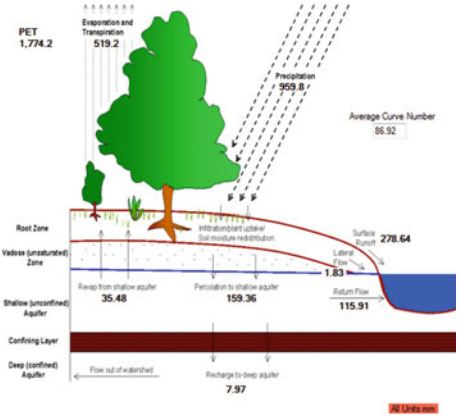

Fig. 14 Water balance components of MNJR012

Table 4 Water balance components of MNJR01

Water balance component	Incoming (mm)	Outgoing (mm)
P	959.8	
ET	–	519.2
Q	–	396.38
ΔTWS	–	36.25
Groundwater recharge	–	7.97
Total	**959.8**	**959.8**

$959.8 - 396.38 - 519.2 - 7.97 = 36.25\ldots$. from Eq. (1);

The value 36.25 mm including other components as mentioned for MNJ012.

Therefore, $959.8 - 396.38 - 519.2 - 7.97 - 36.25 = 0$.

As the summation of water balance is equal to zero, this means the incoming and outgoing of water in Watershed MNJR013 are equal. Table 4 shows the values of incoming and outgoing of MNJR013 watershed.

The basin values (monthly) of important parameters for Watershed MNJR013 of Manjra River were derived by SWAT simulation and are as follows: Table 5 gives average monthly values of P, Q, E.T, and water yield for MNJR013 in the Manjra River. Figures 15, 16, 17, and 18 show the graphs of the components.

Modeling has given the water balance components of Manjra River watersheds.

So we can get the information about availability of water for all purposes use. This will help in real water resource management and distribution of water for different purposes in that region.

Table 5 Monthly basin value of Manjra Watershed MNJR013

Month	Rain (mm)	Runoff (mm)	Water yield (mm)	E.T. (mm)
1	0.1	0.16	1.83	12.2
2	0.62	0.22	0.86	7.52
3	12.29	1.84	2.36	40.45
4	9.24	0.17	0.55	52.83
5	21.9	0.29	0.57	21.8
6	154.15	12.25	11.72	61.89
7	216.69	60.67	61.18	71.01
8	218.87	83.74	96.88	73.76
9	170.87	62.31	91.71	69.14
10	120.48	47.4	85.12	56.4
11	29.74	8.88	37.16	32.38
12	5	2.61	14.54	20.04

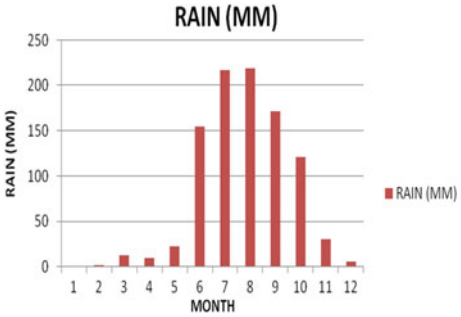

Fig. 15 Monthly rainfall (P) average MNJR013

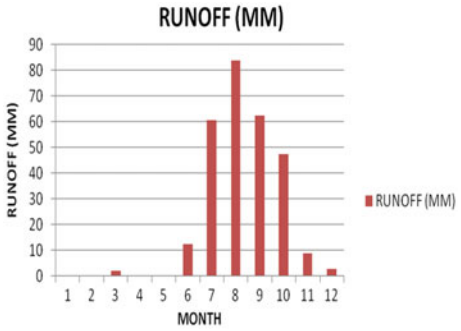

Fig. 16 Monthly runoff (Q) average MNJR013

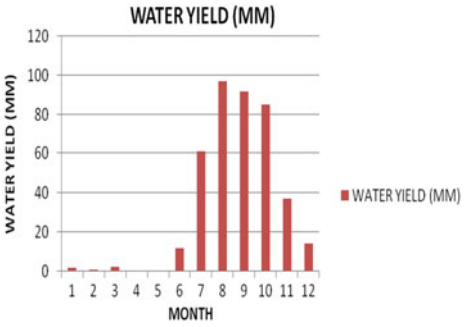

Fig. 17 Average monthly water yield for MNJR013

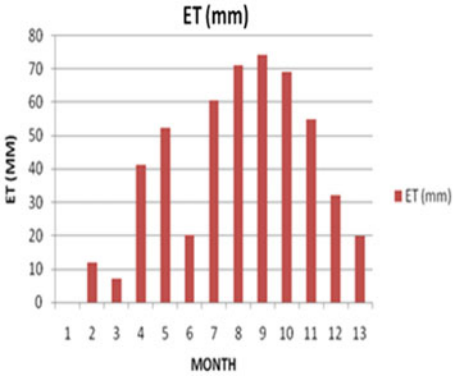

Fig. 18 Average monthly evapotranspiration MNJR013

3.3 Validation

The different water balancing components of Manjra River watersheds are evaluated by SWAT simulation. The regression analysis was performed to validate these simulated results; these simulated values have been compared with observed values. The coefficient of determination, i.e., R^2 was found for each watershed. The range of coefficient of determination R^2 is between 0 and 1. It is considered that if the value of R^2 is closer to 1, then the similarity between the two datasets is more.

(a) ***Watershed MNJR012:***

To validate the simulated results, regression analysis was carried out between simulated and observed precipitation values. The observed precipitation data were derived from global weather data. Table 6 shows simulated and observed rainfall values for Watershed MNJR012.

Figure 19 shows a graphical representation of the simulated and observed precipitation values of the Manjra Watershed MNJR012. The regression analysis gave value of R^2 as 0.933, which is closer to 1; hence, the simulated values obtained from SWAT simulation are validated. Table 7 shows a summary of regression analysis for rainfall values of Watersheds MNJR012 and MNJ013 of the Manjra River.

Table 6 Monthly observed and simulated values of rainfall MNJR012

Rainfall (mm)		
Month	Simulated values	Observed values
Jan	0.11	5.57
Feb	0.18	3.36
Mar	12.82	13.16
Apr	9.27	8.4
May	20.17	16.06
June	157.67	152.56
July	224.25	204.39
Aug	228.08	262.66
Sept	165.9	232.72
Oct	125.38	84.61
Nov	31.82	33.07
Dec	3.74	2.42

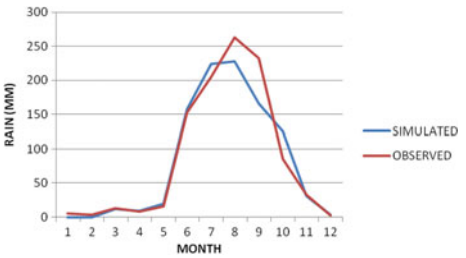

Fig. 19 Graphical representation of simulated and observed rainfall MNJR012

Table 7 Regression analysis for MNJR012 and MNJ013 watersheds

Sr. No.	Summary (MNJ012)	Summary (MNJ013)
Regression statistics		
R (multiple)	0.966083663	0.971735413
R (square)	0.933317643	0.944269713
R square (adjusted)	0.926649407	0.938696684
Standard error	24.79042288	21.74800299
Observations	12	12

(b) ***Watershed MNJR013:***

For validation of the simulated result, regression analysis was carried out for simulated and observed precipitation values. The observed precipitation data were derived from global weather data. Table 8 shows simulated and observed rainfall data for Watershed MNJR013.

Table 8 Monthly simulated and observed values of rainfall for MNJR013

Rainfall (mm)		
Month	Simulated values	Observed values
Jan	0.1	5.33
Feb	0.62	3.07
Mar	12.29	13.08
Apr	9.24	7.94
May	21.9	18.54
June	154.15	161.98
July	216.69	209.62
Aug	218.87	275.82
Sept	170.87	242.7
Oct	120.48	91.74
Nov	29.74	38.5
Dec	5	2.77

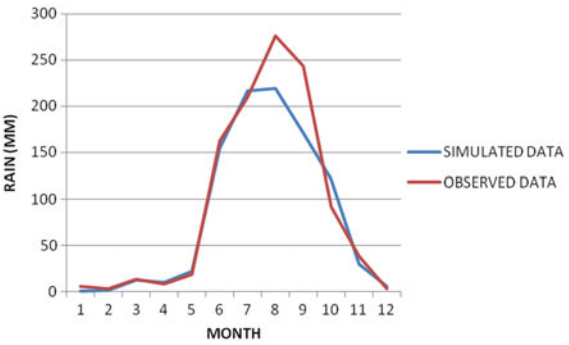

Fig. 20 Graphical representation of simulated and observed rainfall data for MNJR013 watershed

Figure 20 shows a graph between the simulated and observed precipitation values of the Manjra River Watershed MNJR013. The regression analysis gave the value of R^2 as 0.971, which is closer to 1; hence, the simulated values obtained from SWAT simulation are validated. Table 7 shows the summary of regression analysis for rainfall values of Watershed MNJR013 of the Manjra River.

4 Conclusions

In this study, the water balance components for the Manjra River Watersheds MNJR012 and MNJR013 were evaluated through SWAT simulation, which are precipitation, runoff, water yield, and evapotranspiration. Also, land use/land cover and soil classification were obtained. The necessary thematic maps and databases

were prepared. To validate the obtained data, simulated data were compared with observed data, and regression analysis was performed, which gave values of R^2 0.933 and 0.971 for Watersheds MNJR012 and MNJR013, respectively, which is closer to 1; hence, the simulated values obtained are validated. This study can be further used for different effective water resource management projects.

References

1. Nilawar AP, Waikar ML (2019) Impacts of climate change on streamflow and sediment concentration under RCP 4.5 and 8.5: a case study in Purna River basin, India. Sci Total Environ 650(2):2685–2696
2. Mistry A, Narwade R, Nagarajan K (2020) Estimation of water balance components of watersheds in the Manjira River Basin using SWAT model and GIS. Int J Eng Adv Technol 9(3):3898–3907
3. Jasrotia AS, Majhi A, Singh S (2009) Water balance approach for rainwater harvesting using remote sensing and GIS techniques, Jammu Himalaya, India. Water Resour Manag 23:3035–3055
4. Perez-Valdiviaa C, Cade-Menumb B, McMartin DW (2017) Hydrological modeling of pipestone creek watershed using soil and water assessment tool (SWAT): assessing impacts of wetland drainage on hydrology. J Hydrol Reg Stud 14:109–129
5. Cheng GD, Li X, Zhao WZ, Xu ZM, Feng Q, Xiao SC, Xiao H (2014) Integrated study of the water-ecosystem-economy in the Heihe River Basin. Nat Sci Rev 1(3):413–428
6. Rivas-Tabaresa D, Tarquisa AM, Willaarts B, De Miguel A (2019) An accurate evaluation of water availability in sub–arid Mediterranean Watershed through SWAT-Cega-Eresma-Adaja. Agric Water Manag 212:211–225
7. Deus D, Gloaguen R, Krause P (2013) Water balance modelling in a semi-arid environment with limited in situ data using remote sensing in lake Manyara, East Afr Rift Tanzania. Remote Sens 5(4):1651–1680
8. Fang GH, Yang J, Chen YN, Xu CC, Maeyer PD (2015) Contribution of meteorological in calibrating a distributed hydrologic model in the watershed in the Tianshan Mountains, China. Environ Earth Sci 74:2413–2424
9. Ayivi F, Jha MK (2018) Estimation of water balance and water yield in Reedy Fork-Buffalo Creek Watershed in North Carolina using SWAT. Int Soil Water Conserv Res 6:203–213
10. McCabe GJ, Wolock DM (2015) Temporal and spatial variability of the global water balance. Clim Change 120(1–20):375–387
11. Desta H, Lemma B (2017) SWAT based hydrological assessment and characterization of lake ziway, Sub-watersheds Ethiopia. J Hydrol 13:122–137
12. Haseena S, Surinaidu L, Giridhar M (2015) Assessment of groundwater and surface water resources in the Godavari Basin. In: 2nd National Conference on Water Environment and Society Science and Research Technology
13. Ma J, Sun W, Yang G, Zhang D (2018) Hydrological analysis using satellite remote sensing big data and CREST model. IEEE Access 6:9006–-9016
14. Trenberth KE, Smith L, Qian T, Dai A, Fasullo J (2006) Estimates of global water budget and its annual cycle using observational and model data. J Hydrometeorology (Special Section, National Centre for Atmospheric Research) 8(4):758–-769
15. Yuan L, Forshay KJ (2019) Using SWAT to evaluate streamflow and lake sediment loading in Xinjiang River basin with limited data. Water 12(1):39
16. Hui L, Xiaoling X, Lim KJ, Xiaobin X, Sagong M (2010) Assessment of soil erosion and sediment yield in Liao watershed, Jiangxi province, China, using GIS and R.S. J Earth Sci 21:941–953

17. Coffey ME, Workman SR, Taraba JL, Fogle AW (2014) Statistical procedures for evaluating daily and monthly hydrologic model predictions. Trans ASAE 47(1):59–68
18. Adnan M, Kang S, Zhang G, Saifullah M, Anjum MN, Ali AF (2019) Simulation and analysis of the water balance of the Nam Co Lake using SWAT model. Water 11(7):1383
19. Cerkasova N, Umgiesser G, Erturc A (2018) Development of a hydrology and water quality model for transboundary river watershed to investigate the impact of climate change—A SWAT application. Ecol Eng 124:99–115
20. Neitsch SL, Amold JC, Kiniry JR, Williams JR, King KW (2002) Soil and water assessment tool manual, Version 2000
21. Ngongondo C, Xu CY, Tallaksen LM, Alemaw B (2015) Observed and simulated changes in the water balance components over Malawi, during 1971–2000. Quatern Int 369:7–16
22. Abdelwahaba OMM, Riccib GF, De Girolamoc AM, Gentile F (2018) Modelling soil erosion in a Mediterranean watershed: comparison between SWAT and AnnAGNPS models. Environ Res 166:363–376
23. Can T, Xiaoling C, Lu J, Gassman PW, Sabine S, Jose-Miguel SP (2015) Assessing impact of different land use scenarios on water budget of Fuhe River, China using SWAT model. Int J Agri Biol Eng 8(3):95–109
24. Wang JF, Gao YC, Wang S (2016) Land use/cover change impacts on water table change over 25 years in a desert-oasis transition zone of the Heihe River basin, China. Water 8(1):11
25. White ED, Easton ZM, Fuka DR, Collick AS, Adgo E, McCartney M, Awulachew SB, Selassie YG, Steenhuis TS (2011) Development and application of a physically based landscape water balance in the SWAT model. Hydrol Processes 25(6):915–925
26. Worqlul, AW, Ayana EK, Yen H, Jeong J, MacAlister C, Taylor R, Gerik TJ, Steenhuis TS (2018) Evaluating hydrologic responses to soil characteristics using SWAT model in a paired-watersheds in the Upper Blue Nile Basin. CATENA 163:332–341
27. Yang DW, Gao B, Jiao Y, Lei HM, Zhang YL, Yang HB, Cong ZT (2015) A distributed scheme developed for eco-hydrological modeling in the upper Heihe River. Sci China Earth Sci 58:36–45
28. Yin Z, Qi F, Zou S, Yang L (2016) Assessing variation in water balance components in mountainous inland river basin experiencing climate change. Water 8:472

Websites

29. Global Weather Data for SWAT. https://globalweather.tamu.edu
30. Central Ground Water Board. http://cgwb.gov.in/watershed/cdgodavari.html
31. India-WRIS. http://tamcnhp.com/wris/#/waterData
32. Earth explorer-USGS. https://www.usgs.gov/earthexplorer-0
33. Hydro SHEDS. https://hydrosheds.org

Anthropogenic Influence on Streamflow in the Mahi Bajaj Sagar Basin, India

Mithun Choudhary, Mahesh Kumar Jat, and Mahender Choudhary

Abstract Climate change and its impact on associated natural and manufactured systems have stressed water resources. Since the last decade, the flow of most rivers in Rajasthan has been showing a decrease in water. Mahi Sagar reservoir, one of the largest water reservoirs, is also experiencing a decline in river runoff due to climate change impact and human activities. The effect of climate change (CC) on regional hydrology imposes challenges because of the connection between the climate system and the hydrological cycles and the basin's characteristics. Using daily climate data, this research was conducted using hydrological semi-distributed model, and a Soil Water Assessment Tool (SWAT) is verified to a baseline from 1990 to 2005. Subsequently, we reconstructed natural runoff for 2006–2018 without considering the local human impact. We observed short-term variation in streamflow throughout the impact period based on reconstructed streamflow and observed streamflow data. Trend analysis and the SWAT model were taken in the experiment to analyze the relative contribution of CC and human activities on streamflow. The outcome of the study showed that total relative change in the assessment period 2006–2011, 2012–2018, and 2006–2018 is 29%, 48%, and 46%, respectively, and for the same periods, impact by climate change 48%, − 4%, and 26.51%, respectively, and impact by human activities 51%, 104%, and 73.49% on streamflow.

Keywords Climate change · SWAT · Streamflow · Trend analysis · Mahi Bajaj Sagar basin

M. Choudhary (✉) · M. K. Jat · M. Choudhary
Department of Civil Engineering, Malaviya National Institute of Technology, Jaipur 302017, India
e-mail: 2018rce9506@mnit.acin

M. K. Jat
e-mail: mkjat.ce@mnit.ac.in

M. Choudhary
e-mail: mahender@mnit.ac.in

P. V. Timbadiya et al. (eds.), *Hydrology and Hydrologic Modelling*,
Lecture Notes in Civil Engineering 312,
https://doi.org/10.1007/978-981-19-9147-9_10

1 Introduction

According to previous scientific research, climate change (CC) is one of the primary factors affecting availability of water and its spatial distribution across the globe. In a developing country such as India, CC and human activities significantly influence regional water resources [1]. Streamflow is an important component of the hydrological cycle in a river catchment. Streamflow unpredictability has an impact on water consumption trends in diverse sectors like agriculture, domestic industry, generation of hydropower, wastewater management units, and navigation [2]. Previously, scientists examined streamflow data to evaluate variability over very long time period and attribute total streamflow fluctuation through time to changes in CC and human activities. Precipitation, evaporation, and soil moisture availability are all affected by climate change [2–4]. Over the last decade, CC studies have been done to assess the impact of CC on water resources at the basin level [5–9] using distributed hydrological, for example, SWAT, VIC, and MIKE-SHE. These models utilize fine resolution data for better accuracy in outcome [10–13]. The distributed hydrological models are the most efficient and reliable modeling tool for (climate change impact assessment) studies [14–16] to understand the hydrological phenomenon at a basin scale because they can easily relate most of the physically observed parameters directly in to the model parameters.

Researchers in the last decade preferred various methodologies to quantify the relative impact of CC and human activities on surface runoff. These methodologies come under certain categories, first category hydrological modeling [17–19], second category climate elasticity [20] and method of decomposition [21], third category hydrological sensitivity method [22], and fourth category experimental approach [23]. The hydrological modeling method is based on the hydrological model because it is technically sound and can physically depict hydrological processes in the watershed. Lumped model as SIMHYD is a version of HYDROLOG model, and the Xinanjiang model [24], etc., lacks in representing underlying surface properties or input parameters of the model in the watershed. Despite the use of lumped models, a semi-distributed model such as SWAT, VIC, GBHM (geomorphological-based model of hydrology) is applied for very long time so that results might be trustable for quantifying the impact of CC and human activities in regional surface runoff. Climate elasticity and decomposition method come under the Budyco framework [25] and also have certain drawbacks as these two methods have functions in the form of equations that impose problems for analyzing variation in runoff in the given scenarios. The hydrological sensitivity method is based on the single factor at a time approach analysis where only one component was changed, while the others remained constant. This method is very time-consuming as it does not provide flexibility in projecting climate change scenario. The most efficient strategy is the experimental approach, which has typically been employed for small catchments; however, it is cost-effective, but it is difficult to apply to a large-sized watershed. Many studies provide access for quantifying the effect of climate change or land use/land cover change on streamflow. These approaches are limited to regional impact assessment.

It is often necessary to determine how much streamflow is influenced by human activity relative to climate change, particularly long-term streamflow observed in the Mahi Bajaj Sagar basin. In the last decade, as the author knows, less attention has been given to the Mahi Bajaj Sagar basin. Therefore, present study investigates the relative impact of CC and human activities on streamflow at the Mahi Bajaj Sagar basin.

2 Study Area and Data Source

2.1 Mahi Bajaj Sagar Basin

Mahi Bajaj Sagar basin is a part of Mahi River catchment of India, which is situated in the vicinity of 23°37′37 N and 74°32′39E as shown in Fig. 1. Mahi Bajaj Sagar basin covered 6149 sq.km. Most of the part of the basin is covered with fine loamy-textured soil. The research area receives between 850 and 1000 mm of rain per year. The climate of Mahi Bajaj Sagar basin is semi-arid. It is known for hot summer and general dryness except during the southwest monsoon, which experiences heavy rainfall. The monsoon season is a short period; nearly 85% of the total rainfall comes from this southwest monsoon. Mean monthly air temperature ranges from 12 to 15 °C in winter season and 35–47 °C in summer season. Dominant land use/land cover in the region of Mahi Bajaj Sagar basin is agriculture. Karif and Rabi season are the crop season which required water for irrigation from the Mahi Sagar reservoir. The reservoir's current discharge capacity is 383m^3/sec and has the potential of maximum discharge 10,887 m^3/sec from the Mahi Bajaj Sagar basin. Stormwater drainage for the Mahi Bajaj Sagar basin has been disrupted due to the influence of anthropogenic factors such as encroachment of hutments in large numbers, particularly in the surrounding Mahi River in both urban and rural areas.

2.2 Data Collection

The long-term available meteorology data from 1975 to 2018 at the daily temporal scale has been used in the present study to arrive at statistical inference. Land use/land cover (LULU) information was extracted from the classification of satellite images for the years 1990 and 2010 from October to November of the Karif season. All of the images used in this study were taken during the post-monsoon season and were cloud-free. The supervised maximum likelihood classification techniques were used to classify LULC images for respective years. Soil information was obtained from food organizations and subset to the study area. DEM data from the United States Geological Survey was obtained and used to delineate the basin at a threshold value of 100 km^2. Table 1 contains information about the data used in this study.

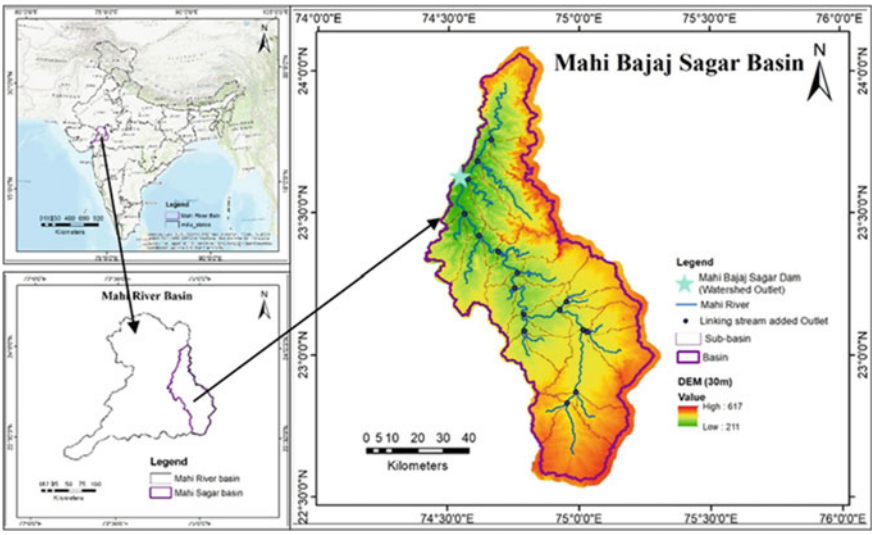

Fig. 1 Study area location map of Mahi Bajaj Sagar basin

Table 1 Data used in the present study

Variable	Period	Temporal resolution	Spatial agency
Precipitation	1975–2018	Daily (25°*25°)	Indian Meteorology Department (IMD)
Temperature (max. and min.)	1975–2018	Daily (05°*05°)	Indian Meteorology Department (IMD)
Observed streamflow	1984–2018	Daily	Rajasthan Government
LULC data	1990, 2010 (Kharif season)	30 m	Landsat Data Satellite Imageries USGS (http://earthexplorer.usgs.gov/)
Soil data	1971–1981	1 km	Harmonized World Soil Database v1.2, FAO UNESCO soil map of the world (https://www.fao.org/soils-portal/)
DEM	–	30 m	ASTER Data USGS

3 Method

3.1 Quantifying Impacts on Streamflow

Individual impacts of CC and human activities (anthropogenic) in terms of LULC change on basin hydrology are challenging to investigate. This present study estimates the relative impact of CC and human activity on runoff and method adopted from [19]. In the present study, meteorological data for 35 years (1984–2018) has been used as a baseline case to determine the effect of CC on runoff regime of the study area. A semi-distributed hydrological model (SWAT) was used. SWAT simulates watershed hydrological response as a function of meteorological and LULC characteristics over a period in Mahi Bajaj Sagar basin. SWAT model was conceptualized for the study area, and calibrated and validated periods are provided in Table 2. Calibrated SWAT model was applied to simulate rainfall-runoff for the study area considering constant LULC conditions from 1990 to 2005. The constant change in hydrological response of watershed with constant LULC reflects the influence of the effect of CC alone that is the change produced by precipitation and temperature. The second simulation hydrology of the basin was simulated from 2006 to 2018 using a calibrated model with the same setting for generating natural streamflow without considering local human activities, such as no LULC change. The difference between streamflow during the impact period and streamflow during the baseline period is made up of two parts. One part is the possible changes due to human activities as ΔR_h and the second part from climate change as ΔR_c, observed streamflow denoted as R_i, and the streamflow corresponding to the baseline period is R_b. As a result, the major difference between observed streamflow for the period of assessment and the period of baseline reflects the streamflow response as shown in Eqs. (1–2) sum of ΔR_h and ΔR_c

$$\Delta R_h + \Delta R_c = R_i - R_b \tag{1}$$

$$\Delta R_h = R_i - R_m \tag{2}$$

$$\Delta R_c = R_m - R_b \tag{3}$$

Table 2 Calibration and validation monthly simulation at Mahi Bajaj Sagar basin

Variable	Calibration (1990–2005)	Validation (2006–2010)
R^2	0.74	0.70
NSE	0.73	0.72
PBIAS	− 0.20	− 12.20

* *NSE* Nash–Sutcliff;
* *PBIAS* Percentage BIAS

where ΔR_h (m^3/s) is change in runoff due to human-induced activities, ΔR_c (m^3/s) is change in runoff due to effect of CC, R_b is the observed runoff for yearly basis in the period of assessment in m^3/s, and R_m is the generated or reconstructed streamflow monthly basis (latter converted to yearly basis) for the period of assessment by the use state of art hydrological model.

$$PR = \frac{R_i}{R_b} - 1 \times 100\% \tag{4}$$

where the percentage of change in the observed annual runoff in the baseline period is denoted by PR (relative change).

The percentage change from human activities and CC is estimated in respective time frames by Eqs. (5) and Eq. (6) and denoted by (PH, PC)

$$\mathrm{PH} = \frac{\Delta \mathrm{R_c}}{\Delta \mathrm{R_h} + \Delta \mathrm{R_c}} \times 100\% \tag{5}$$

$$\mathrm{PH} = \frac{\Delta R_c}{\Delta R_h + \Delta R_c} \times 100\% \tag{6}$$

3.2 SWAT Model Setup

The USDA Agriculture Research Service's Soil Water Assessment Tool (SWAT Model) [26] is the outcome of nearly 40 years of modeling work [27]. SWAT model is a basin-scale model classified as semi-distributed. It follows the continuous-time model and operates in daily time steps. The SWAT model is intended to simulate various hydrological components of the water cycle as well as various water, agriculture, and sediment yield management processes. SWAT is physically based and can simulate for long periods of time. It takes less time to simulate the process. The SWAT model required climate data input as well as observed data for model validation.

3.3 Mann-Kendall's Test

The M-K method is used to analyze climate and environmental time series data. It was proposed by [28] and is frequently used with time series [29] of climate data. This test has two benefits. First, it is a nonparametric measure that does not require the data to be distributed on a regular basis. Second, because time series are inhomogeneous, it is impervious to abrupt breaks. The null hypothesis H0 states that no trend exists (data is independent and randomly ordered) [30]. This test was performed against the

alternative hypothesis H1, which supposes that the data exhibits the trend depicted in Eq. 4.

$$S = \sum_{k=1}^{n-1} \sum_{k+1}^{n} sgn\left(x_j - x_k\right) \tag{7}$$

The trend test is applied to time series x_k, which is ranked $k = 1, 2, 3 \ldots n-1$, which is ranked for $j = i, i+1, i+2, i+3 \ldots..$each data point x_j is used as a reference point, as shown in Eq. 5 [30].

$$\begin{aligned} sgn\left(x_j - x_k\right) &= 1 \text{ if } x_j - x_k > 0 \\ &= 0 \text{ if } x_j - x_k = 0 \\ &= -1 \text{ if } x_j - x_k < 0 \end{aligned} \tag{8}$$

3.4 Sen's Slope Test

The magnitude of the trend can be calculated using Sen's slope estimator in time series [30, 31]. To measure the real slope of an existing trend, such as the quantity of change per year, Sen's nonparametric approach [30] was applied, and the test was conducted using the MAKESENS micro excel [32].

4 Results and Discussions

4.1 Precipitation and Temperature Trend Analysis at the Mahi Bajaj Sagar Basin

Figure 2 depicts the precipitation trend in the Mahi Bajaj Sagar basin. In the selected period, the observed precipitation shows a decreasing trend, and observed air temperature shows an increasing trend. Precipitation and temperature had regression slopes of − 1.52 and 0.011, respectively. The observed precipitation reached a maximum of 1564.22 mm in 1994 and a minimum of 442.16 mm in 2000. The decadal variability in precipitation at the Mahi Bajaj Sagar basin depicted was uneven distribution. The temperature varies greatly during the summer season. As a result, there is variation from north to south in the Mahi Bajaj Sagar basin. The maximum air temperature was 44.84 °C shown in the year 1991. In the winter season, less variation forms south to north but high variation in the east to the west section of Mahi Bajaj Sagar basin during the period 1984–2018. The lowest air temperature is observed in the year 1990 which is 4.29 °C. The results of the applied test (Mann-Kendall) showed the

decreasing trend for annual precipitation during the period 1984–2018 at the Mahi Bajaj Sagar basin. However, the predicted trend is insignificant (Fig. 2). Similarly, for air temperature, the trend increases for both maximum and minimum air temperatures (Figs. 3 and 4). Furthermore, for this period, step-change precipitation and temperature were not taken into account. The Mahi Bajaj Sagar basin's climate has warmed over the last 35 years (Fig. 4). Year 1990 was the coldest year, followed by 1977. Temperature increased from 1984 to 2018, according to the Mann-Kendall test results (Fig. 3). During the years 1984–2018, there was a statistically significant trend. The overall analysis of precipitation and temperature shows climate change in the region of Mahi Bajaj Sagar basin.

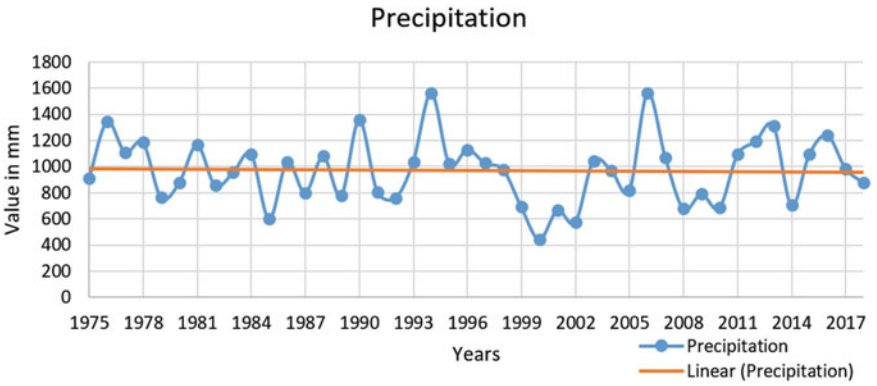

Fig. 2 Trend in observed annual precipitation using Mann-Kendall test percentage error

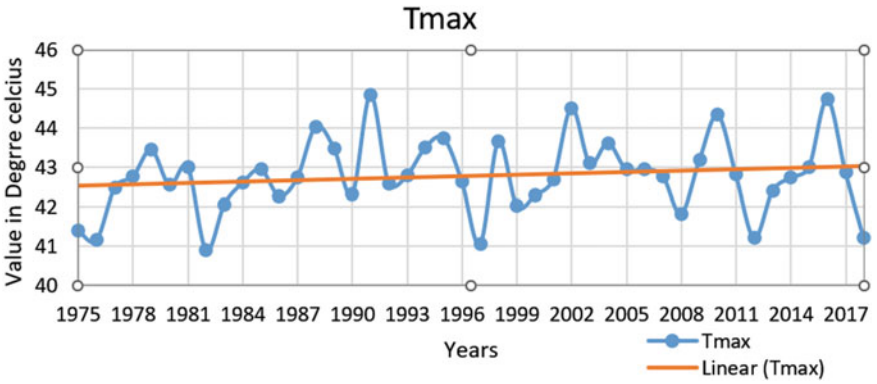

Fig. 3 Annual maximum temperature using Mann-Kendall trend

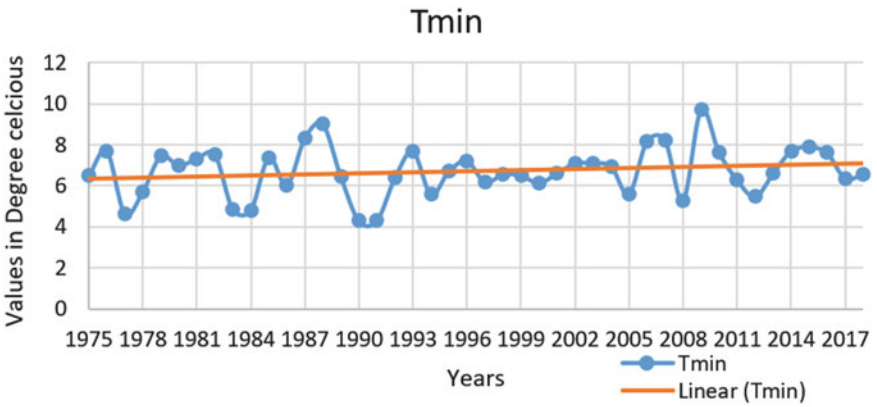

Fig. 4 Annual minimum temperature using Mann-Kendall trend

4.2 Streamflow Trend Analysis at the Mahi Bajaj Sagar Basin

Figure 5 depicts the observed annual streamflow at the Mahi Bajaj Sagar basin outlet from 1984 to 2018. The findings of the Mann-Kendall test revealed a statistically significant decrease in yearly streamflow for the Mahi Bajaj Sagar basin. The regression slope was − 0.54, detected by Sen's slope estimator. Significant step-change point is not observed. But outliers were present in the streamflow in the years 1984, 2011, and 2017. The minimum flow in the year 2000 was 10 m^3/sec, and the maximum flow in the year 2011 was 269.89 m^3/sec.

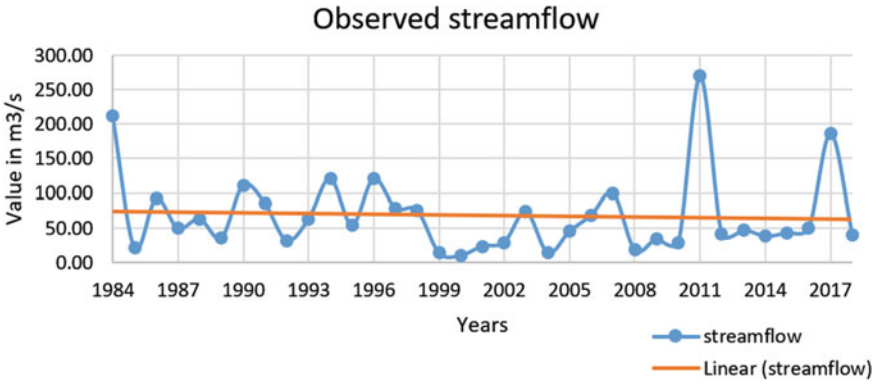

Fig. 5 Annual observed streamflow at the outlet of Mahi Bajaj Sagar basin

4.3 Performance of SWAT Model

The calibration process was applied to the SWAT model using the SWAT-Cup [33] uncertainty program. The sensitive parameters for runoff were determined during the calibration of the SWAT model [2]. Table 3 lists their statistical data and rankings. The most responsive surface runoff parameter was 11 parameters, i.e., compensation factor for soil evaporation (ESCO), followed by the saturated hydraulic conductivity of the soil (Sol_K), initial SCS-CN II value in runoff process (CN2), alpha factor for base flow in groundwater simulation (Alpha_BF), groundwater delay which has units in days (GW_Delay), water capacity available in the soil layer (SOL_AWC), shallow aquifer threshold depth required for groundwater (GWQMN), plant uptake compensation factors in evaporation process (EPCO), hydraulic conductivity in the main channel alluvium (CH_K2), Manning's "n" value in channel process (CH_N2), and average slope steepness in the geomorphological process (HRU_SLP). These parameters were found to be best for the simulated model after sensitivity analysis throughout the calibration process. In this study, ESCO.hru, Sol_K.sol, and CN2.mgt are the most sensitive parameters, followed by other parameters as shown in Table 3. In SWAT-CUP, sensitivity estimation t-stat and p-value factor are taken [34]. Most sensitive parameters, according to their rank, directly reflect an understanding of the basin's hydrology. All the parameters have rank depending on the sensitivity statistics such as maximum and minimum values and fitted value of the parameters. Calibration statistics illustrated in Table 2 for the Mahi Bajaj Sagar basin were verified as per the criteria followed by researchers [35–37]. To use the hydrological model to simulate streamflow for the baseline period and impact period, SWAT model calibrates for baseline period and natural streamflow which is generated for impact period. Figure 6 depicts graph for model-simulated streamflow compared to observed streamflow for the Mahi Bajaj Sagar basin outlet.

Table 3 Parameters selected for the calibration of the SWAT model

Parameters	Parameter initial max. range	Parameter initial min. range	Fitted value	Rank
V_ESCO.hru	0.34	1.02	0.39	1
R_SOL_K.sol	0.00	1077.36	3.05	2
R_CN2.mgt	− 0.25	0.04	− 0.01	3
V_ALPHA_BF.gw	0.39	1.18	0.96	4
V_GW_DELAY	0.00	296.11	84.39	5
R_SOL_AWC.sol	0.00	0.518	0.09	6
A_GWQMN.gw	2032.10	6117.89	3833.93	7
R_EPCO.hru	0.09	0.07	0.82	8
V_CH_K2	− 0.66.93	311.78	− 41.56	9
V_CH_N2	0.0	0.29	0.14	10
R_HRU_SLP.hru	0.41	1.24	0.49	11

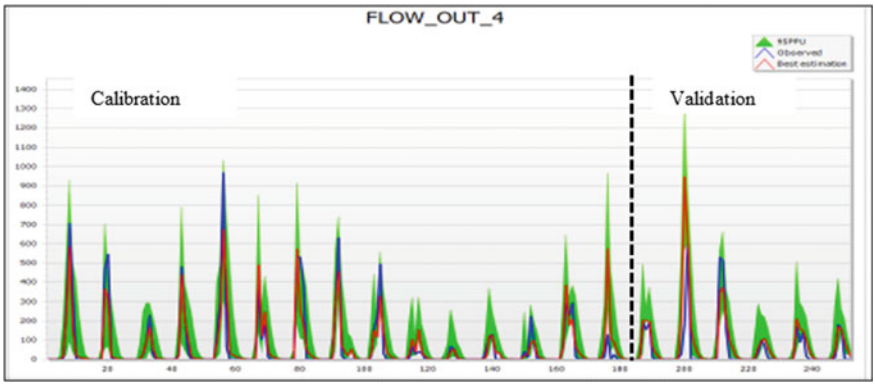

Fig. 6 Plot for observed and simulated runoff at Mahi Bajaj Sagar basin

4.4 Streamflow Reconstruction for Impact Period

After the SWAT model calibration process, use the same hydrometeorological condition for the baseline. Calibrated SWAT model was used to reconstruct the natural streamflow data for the impact period from 2006 to 2018 with no local human activity. (No changes in land use/land cover in the basin). Figure 7 shows reconstructed streamflow from calibrated SWAT model for Mahi Sagar basin.

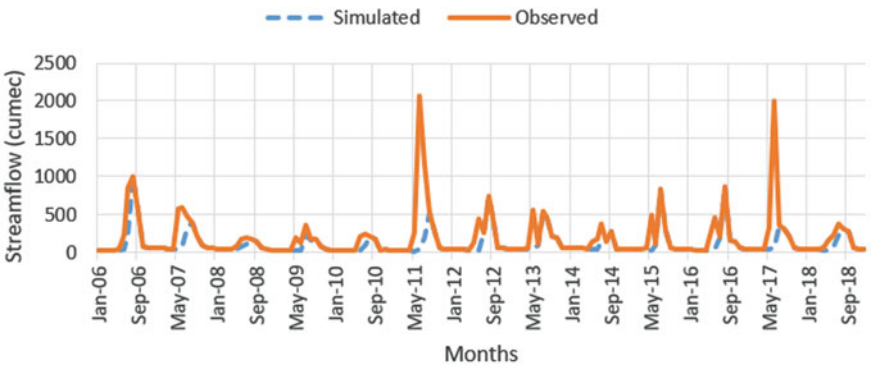

Fig. 7 Monthly time series of streamflow and simulated streamflow for period 2006–2018 at the outlet of Mahi Bajaj Sagar basin

4.5 *Quantification of Impacts on Streamflow at Mahi Bajaj Sagar Basin*

In this study, the observed runoff and reconstructed streamflow by hydrological model and the impact of CC and human activities on runoff were calculated using Eqs. (1)–(6) for impact period and summarized in Table 4. The observed and reconstructed average annual streamflow at the Mahi Bajaj Sagar basin accounted 1474.92 m^3/sec and 935.29 m^3/sec in the baseline period. Three observations are shown in Table 4. First, the average yearly streamflow for 2006–2018 was smaller than the baseline case, which implies that the observed runoff at the Mahi Bajaj Sagar basin falls under the selected period. The absolute and relative combined impacts of CC and human activities on streamflow accounted 680.35 cumecs and 46.13%, respectively. The most significant impact observed is 709.25 cumecs and 48.09%, respectively, appearing in the 2012 impact period (2012–2018). Second, the difference between the natural streamflow (reconstructed streamflow) and the streamflow of the baseline case shows the deficient streamflow because of CC. Figure 8 depicts human activities responsible for streamflow changes, especially downstream in the different periods. The changes in streamflow because of climate change (PC) were 48.64% and − 4.70% in the years 2006 to 2011 and 2012 to 2018, respectively. For the same years, changes caused by human activities (PH) were 51.36% and 104%, respectively, on streamflow. Third, in the impact period 2006 to 2018, human activities and CC contributed for 73.49 and 26.51% of the overall decline in the runoff. Human activities are the primary cause of the recently identified decreased runoff in the Mahi River in the Mahi Bajaj Sagar basin.

Table 4 Impact of CC and human activity on runoff at Mahi Bajaj Sagar basin

Period	Observed streamflow (m^3/sec)	Reconstructed streamflow (m^3/sec)	Total change [PR (%)]	Impact of climate change [PC (%)]	Impact of human activities [PH (%)]
Baseline Period (1990–2005)	1474.92	935.29			
Impact Period (2006–2011)	1039.41	1263.09	29.58	48.64	51.36
Impact Period (2012–2018)	765.67	1508.16	**48.09**	− 4.69	104.69
Impact Period (2006–2018)	794.57	1294.58	**46.13**	**26.51**	**73.50**

PR Percentage of relative change
PC Percentage of climate change
PH Percentage of human activities

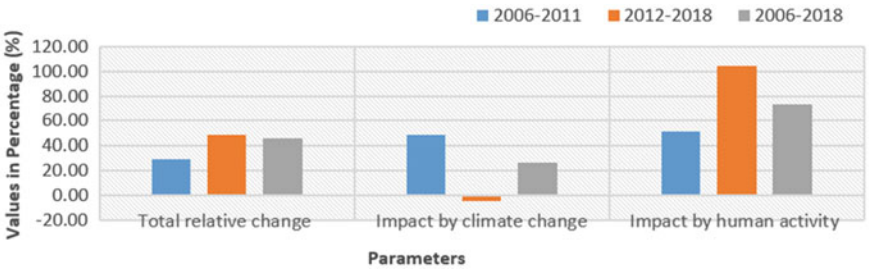

Fig. 8 CC and human activities at Mahi Bajaj Sagar basin

4.6 Discussion and Conclusion

Previous studies are conducted for quantification of climate influence in the basin. Basin characteristics and local activities in terms of LULC affect the streamflow. Streamflow is the resultant of various catchment hydrological processes and is impacted by so many factors. Changes in streamflow can be caused by any factor, including climate and LULC. However, quantifying the individual impact is quite difficult as major changes are linked with climate and human activities. The result from this study shows the percentage of changes from both phenomena in the hydrological system. From this study's conclusion, human activities impact streamflow is significantly higher than climate change impact. Similar results found in studies done over last 10 years. Thier studies reported that climate change might be factor for the variation in runoff [17, 38, 39]. On the other side some researchers [15, 20, 40, 41] found human activities are primary factors for variation in runoff. In addition to this, urban expansion [42] is also responsible for variation of surface runoff in diverse catchment like Mahi Bajaj Sagar basin. Large-scale human activities, including excessive irrigation and soil conservation practices and change in land use/land cover, are the direct factors for reducing the streamflow in the Mahi Bajaj Sagar basin.

Acknowledgements The authors express their thanks to the Malaviya National Institute of Technology Jaipur for providing the platform to conduct this research. The authors also would like to acknowledge the sponsorship of the project entitled "Climate change impacts studies for Rajasthan (Area of Inland and Mahi Basin)" by INCCC, Ministry of Jal Shakti, Department of Water Resource River Development and Ganga rejuvenation, Government of India.

References

1. Mondal A, Narasimhan B, Sekhar M, Mujumdar PP (2016) Hydrologic modelling. Proc Indian Natl Sci Acad 82:817–832. https://doi.org/10.16943/ptinsa/2016/48487
2. Dey P, Mishra A (2017) Separating the impacts of climate change and human activities on streamflow: a review of methodologies and critical assumptions. J Hydrol 548:278–290. https://doi.org/10.1016/j.jhydrol.2017.03.014
3. Gleick PH (1989) Climate change. Hydrology 329–344
4. Dooge JCI (1992) Sensitivity of runoff to climate change: a Hortonian approach. Bull Am Meteorol Soc 73:2013–2024
5. Chawla I, Mujumdar PP (2015) Isolating the impacts of land use and climate change on streamflow. Hydrol Earth Syst Sci 19:3633–3651. https://doi.org/10.5194/hess-19-3633-2015
6. Deshpande NR KB (2014) Assessing hydrological response to changing climate in the Krishna Basin of India. J Earth Sci Clim Change 5. https://doi.org/10.4172/2157-7617.1000211
7. Wijesekara G (2013) An integrated modeling system to simulate the impact of land-use changes on hydrological processes in the Elbow River watershed in Southern Alberta, vol 167. https://doi.org/10.11575/PRISM/24908
8. Omer A, Elagib NA, Zhuguo M et al (2020) Water scarcity in the Yellow River Basin under future climate change and human activities. Sci Total Environ 749:141446. https://doi.org/10.1016/j.scitotenv.2020.141446
9. Oeurng C, Cochrane TA, Chung S et al (2019) Assessing climate change impacts on river flows in the Tonle Sap Lake Basin, Cambodia. Water (Switz) 11. https://doi.org/10.3390/w11030618
10. Devatha CP, Deshpande V, Renukaprasad MS (2015) Estimation of soil loss using USLE model for Kulhan Watershed, Chattisgarh—a case study. Aquat Procedia 4:1429–1436. https://doi.org/10.1016/j.aqpro.2015.02.185
11. Singh G, Kumar E (2017) Input data scale impacts on modeling output results: a review. J Spat Hydrol 13
12. Sahana V, Timbadiya PV (2020) Spatiotemporal variation of water availability under changing climate: case study of the Upper Girna Basin, India. J Hydrol Eng 25:05020004. https://doi.org/10.1061/(asce)he.1943-5584.0001890
13. Shivhare N, Dikshit PKS, Dwivedi SB (2018) A comparison of SWAT Model calibration techniques for hydrological modeling in the Ganga River watershed. Engineering 4:643–652. https://doi.org/10.1016/j.eng.2018.08.012
14. Mango LM, Melesse AM, McClain ME et al (2011) Land use and climate change impacts on the hydrology of the upper Mara River Basin, Kenya: results of a modeling study to support better resource management. Hydrol Earth Syst Sci 15:2245–2258. https://doi.org/10.5194/hess-15-2245-2011
15. Wang GQ, Zhang JY, Pagano TC et al (2013) Identifying contributions of climate change and human activity to changes in runoff using epoch detection and hydrologic simulation. J Hydrol Eng 18:1385–1392. https://doi.org/10.1061/(asce)he.1943-5584.0000559
16. Sinha RK, Eldho TI, Subimal G (2020) Assessing the impacts of land use/land cover and climate change on surface runoff of a humid tropical river basin in Western Ghats, India. Int J River Basin Manag 1–38. https://doi.org/10.1080/15715124.2020.1809434
17. Ma Z, Kang S, Zhang L et al (2008) Analysis of impacts of climate variability and human activity on streamflow for a river basin in arid region of northwest China. J Hydrol 352:239–249. https://doi.org/10.1016/j.jhydrol.2007.12.022
18. Li Z, Liu W, Zhang XC, Zheng FL (2009) Impacts of land use change and climate variability on hydrology in an agricultural catchment on the Loess Plateau of China. J Hydrol 377:35–42. https://doi.org/10.1016/j.jhydrol.2009.08.007
19. Chang J, Wang Y, Istanbulluoglu E et al (2015) Impact of climate change and human activities on runoff in the Weihe River Basin, China. Quat Int 380–381:169–179. https://doi.org/10.1016/j.quaint.2014.03.048

20. Zheng H, Zhang L, Zhu R et al (2009) Responses of streamflow to climate and land surface change in the headwaters of the Yellow River Basin. Water Resour Res 45:1–9. https://doi.org/10.1029/2007WR006665
21. Wang D, Cai X (2010) Comparative study of climate and human impacts on seasonal baseflow in urban and agricultural watersheds. Geophys Res Lett 37:1–6. https://doi.org/10.1029/2009GL041879
22. Zuo D, Xu Z, Wu W et al (2014) Identification of streamflow response to climate change and human activities in the Wei River Basin, China. Water Resour Manag 28:833–851. https://doi.org/10.1007/s11269-014-0519-0
23. Brown AE, Zhang L, McMahon TA et al (2005) A review of paired catchment studies for determining changes in water yield resulting from alterations in vegetation. J Hydrol 310:28–61. https://doi.org/10.1016/j.jhydrol.2004.12.010
24. Xu CY (1999) Climate change and hydrologic models: a review of existing gaps and recent research developments. Water Resour Manag 13:369–382. https://doi.org/10.1023/A:1008190900459
25. Lee C-H, Yeh H-F (2019) Impact of climate change and human activities on streamflow variations based on the Budyko Framework. Water 11
26. Kumar N (2014) Impacts of climate change and land-use change on the water resources of the Upper Kharun Catchment, Chhattisgarh, India, pp 16–17
27. Williams JR, Arnold JG, Kiniry JR et al (2008) History of model development at Temple, Texas. Hydrol Sci J 53:948–960. https://doi.org/10.1623/hysj.53.5.948
28. Mann HB (1945) Nonparametric tests against trend. The Econometric Society Stable. https://www.jstor.org/stable/1907187. References Linked references are available on JSTOR for this article: You may need to log in to JSTOR. Econometrica 13:245–259
29. Prajapat DK, Lodha J, Choudhary M (2020) A spatiotemporal analysis of Indian warming target using CORDEX-SA experiment data. Theor Appl Climatol 139:447–459. https://doi.org/10.1007/s00704-019-02978-7
30. Panda A, Sahu N (2019) Trend analysis of seasonal rainfall and temperature pattern in Kalahandi, Bolangir and Koraput districts of Odisha, India. Atmos Sci Lett 20:1–10. https://doi.org/10.1002/asl.932
31. Sen PK (1968) Estimates of the regression coefficient based on Kendall's Tau. J Am Stat Assoc 63:1379–1389. https://doi.org/10.1080/01621459.1968.10480934
32. Salmi T (2002) Detecting trends of annual values of atmospheric pollutants by the Mann-Kendall test and Sen's slope estimates-the Excel template application MAKESENS. Ilmatieteen laitos
33. Abbaspour KC (2012) Swat-cup 2012. SWAT Calibration uncertain program—a user man, vol 106
34. Abbaspour KC, Vaghefi SA, Srinivasan R (2017) A guideline for successful calibration and uncertainty analysis for soil and water assessment: a review of papers from the 2016 international SWAT conference. Water (Switz) 10. https://doi.org/10.3390/w10010006
35. Narsimlu B, Gosain AK, Chahar BR et al (2015) SWAT model calibration and uncertainty analysis for streamflow prediction in the Kunwari River Basin, India, using sequential uncertainty fitting. Environ Process 2:79–95. https://doi.org/10.1007/s40710-015-0064-8
36. Gassman PW, Arnold JG, White M et al (2010) The worldwide use of the SWAT model: networking impacts, simulation trends, and future developments. In: Proceedings of watershed technological conference, February 21–24 Costa Rica American Society of Agricultural Biological Engineering Earth University
37. Tankpa V, Wang L, Awotwi A et al (2021) Modeling the effects of historical and future land use/land cover change dynamics on the hydrological response of Ashi watershed, northeastern China. Environ Dev Sustain 23:7883–7912. https://doi.org/10.1007/s10668-020-00952-2
38. Kazemi H, Sarukkalige R, Badrzadeh H (2019) Evaluation of streamflow changes due to climate variation and human activities using the Budyko approach. Environ Earth Sci 78:1–17. https://doi.org/10.1007/s12665-019-8735-9

39. Wu J, Miao C, Zhang X et al (2017) Detecting the quantitative hydrological response to changes in climate and human activities. Sci Total Environ 586:328–337. https://doi.org/10.1016/j.scitotenv.2017.02.010
40. Jiang S, Ren L, Yong B et al (2011) Quantifying the effects of climate variability and human activities on runoff from the Laohahe basin in northern China using three different methods. Hydrol Process 25:2492–2505. https://doi.org/10.1002/hyp.8002
41. Dong W, Cui B, Liu Z, Zhang K (2014) Relative effects of human activities and climate change on the river runoff in an arid basin in northwest China. Hydrol Process 28:4854–4864. https://doi.org/10.1002/hyp.9982
42. Jat MK, Choudhary M, Saxena A (2017) Urban growth assessment and prediction using RS, GIS and SLEUTH model for a heterogeneous urban fringe. Egypt J Remote Sens Sp Sci 20:223–241

Estimation of River Discharge in Mandovi Basin, Goa

Raghavendra Talawar and Jayakumar Seelam

Abstract Rivers are an important aspect of terrestrial hydrology. In fact, they are the reason for the interaction processes between land, ocean, and atmosphere. Most river discharge estimates are available at the gauging location, and scarce information is available on the discharge at the confluences. In this paper, studies are carried out to estimate discharge values for Mandovi River in Goa state. Ganjem watershed (599 km^2 area) was modelled using the soil and water assessment tool) programme by USDA- ARS (Department of Agricultural-Agricultural Research sciences). Cartosat-1 DEM—Version-3R1 (Resolution 32 m), soil, land use/land cover, precipitation, and temperature data are used in this study. The model was simulated for five years (2010–2014), and discharge for each year is estimated. The model was calibrated using three years of data and validated for two years. SWAT analysis reveals that the model parameters CN2, GWDELAY, GWQMIN, SURLAG, and ALPHA_BF are sensitive for the Mandovi basin. The simulated and observed values are in good agreement. Statistical analysis showed that co-relation coefficient R^2 and Nash–Sutcliffe efficiency (NSE) were 0.88 and 0.80, which indicate model results that are in good agreement with measurements.

Keywords DEM · SWAT · Sensitive parameters · Watershed · Hydrological modelling

1 Introduction

Rivers are the sources where freshwater is easily available to the mankind. As we can see that all civilizations are based on the river banks. Rivers are the important part of global hydrological cycle as they carry freshwater from land to sea or their

R. Talawar (✉) · J. Seelam
Ocean Engineering Division, CSIR—National Institute of Oceanography, Dona Paula, Panaji, Goa 403004, India
e-mail: raghu.talawar123@gmail.com

J. Seelam
e-mail: jay@nio.org

P. V. Timbadiya et al. (eds.), *Hydrology and Hydrologic Modelling*,
Lecture Notes in Civil Engineering 312,
https://doi.org/10.1007/978-981-19-9147-9_11

destination [1]. From the various components of water cycle, river discharge is the only component that can be estimated precisely [2, 3].

In India, major river basins are gauged, but medium and small rivers are ungauged. In India, there are several catchments where the existing gauges are discontinued due to economic constraints that do not provide required hydrological data [4]. Available methods for river discharge prediction include regional model parameters, synthetic unit hydrographs, utilizing relationships between model parameters and basin physical properties, calibrated model parameters for similar gauged basins to ungauged basins, remote sensing observations, hydrological model simulations, and integrated meteorological and hydrological models. Numerous hydrological models are available for river discharge estimation. The SWAT programme is widely used in the literature. It has proved to be an effective tool for runoff and sediment estimation, land use land cover changes, water resources, and non-point source pollution problems. Hence in this study, SWAT is used for river discharge estimation.

2 Study Area

The watershed considered for study is the Mandovi River situated in Goa, described as the lifeline of Goa. Out of 11 main rivers in Goa, Mandovi is considered to be the major one. Mandovi is gauged at Ganjem, and the discharge values for daily estimates are available. Rainfall occurs in monsoon months from June to September similarly discharges which are also high during these periods. The details of the basin, map, and location are shown in Fig. 1 and Table 1.

3 Methodology

Figure 2 shows the methodology adopted for the work in the form of a flow chart.

Arc-SWAT, a plug-in of Arc-GIS, was used to make essential files to execute the SWAT model. Arc-SWAT programme delineates the digital elevation model (DEM) and produces watershed and sub-watershed automatically. Outlets, stream network, and monitoring points are generated automatically based on given threshold value. Hydrologic response units (HRUs) are extracted from basic modelling. Rainfall/precipitation and temperature data from Global dataset are used as user defined data for weather parameters. After all these procedures, the SWAT model was run for five years with the default parameters. The model did not perform well; therefore, we modified parameters till a better comparison was obtained. With calibrated parameters, the model performed well.

The discharge data at the Ganjem station were available, but no discharge data were available at Panaji (Mandovi watershed), where the river drains into the Arabian Sea. To obtain discharge data at this location, area ratio method was used, which can be done if watersheds are in hydro meteorologically similar basins [5]. The discharge

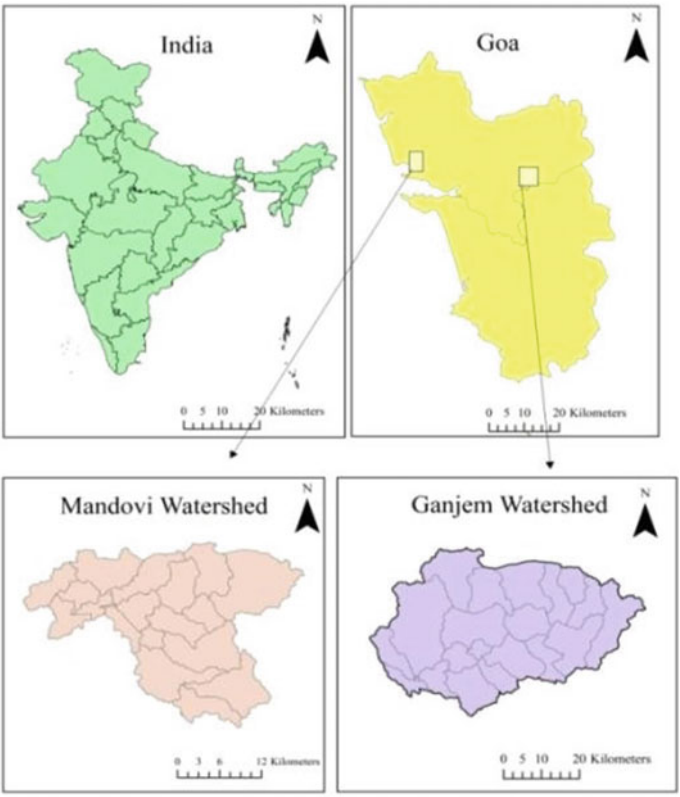

Fig. 1 Basin location/map of study area

Table 1 Description of catchments

Catchment characteristics	Ganjem	Panaji
Latitude	15°30′10″ N	15°30′12″ N
Longitude	74°08′16″ E	73°49′54″ E
Watershed area	599 km^2	1981 km^2
Land use/Land cover	Forest-100%	Range brush-7.9%; forest-92.1%
Soil texture	Sandy_Clay_Loam	Sandy_Clay_Loam

values of the Ganjem station are multiplied with an area ratio as shown below equation no. 1. The area ratio obtained was 3.30. Hence, discharge data at Panaji were obtained for comparison with the model results.

$$\text{Qungauged} = \text{Qgauged} * \left(\frac{\text{Aungauged}}{\text{Agauged}}\right) \quad (1)$$

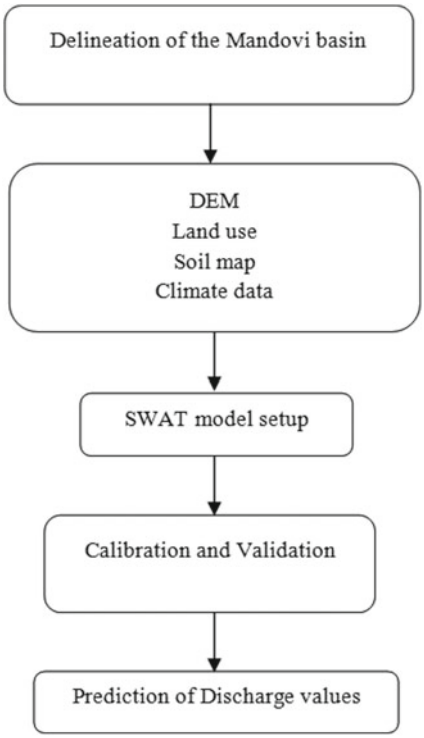

Fig. 2 Methodology of work

3.1 Description of SWAT Model

SWAT model was programmed/developed by the United States Department of Agricultural-Agricultural Research sciences to help the water experts assess the impact of management and climate on water distribution in watersheds and river basins. This model is semi-distributed, physically based, that emphasizes surface processes. It takes into account one watershed and breaks them into number of sub-basins. The sub-basins are divided into combinations of soil, slope, and land use called hydrologic response units (HRUs). The SWAT runs by segregating all similar land use and soil areas into a single response unit. Various models have been developed to fit the conditions favourable to a particular region that may not adequately perform when tested on other regions. Hence, the question arises as to which watershed scale model to use amongst various available models. Climate change impacts on surface runoff, hydrology, groundwater, crop development, etc., are assessed using the SWAT model. The outputs of the SWAT model include runoff, sediment, redistribution, phosphate, sulphate, climate change assessment. The model gives daily, monthly, and yearly time series results. The water balance equation for the model is shown below.

Table 2 Details of data collection

Sl. No.	Data type	Source and description
1	DEM	Bhuvan Website Product-Cartosat-1: DEM—Version-3R1 Resolution 32 m
2	Soil	Arc-SWAT Website, Soil HWSD FAO (Indian dataset for SWAT 2012)
3	LULC	Arc-SWAT Website, Land use water base (Indian dataset for SWAT 2012)
4	Weather data	Arc-SWAT Website, Global weather data include precipitation and temperature. (Global dataset for SWAT 2012)

$$S_{\mathrm{Wt}} = S_{\mathrm{Wo}} + \sum^{t} \left(R_{\mathrm{day}} - Q_{\mathrm{surf}} - E_{\mathrm{a}} - W_{\mathrm{seep}} - Q_{\mathrm{gw}}\right) \tag{2}$$

S_{Wt} Water content in soil at time t
S_{Wo} Water content in soil initially
t Time in days
R_{day} Rainfall/precipitation (mm)
Q_{surf} Surface runoff (mm)
E_{o} Evapotranspiration (mm)
W_{seep} Percolation to the bottom of soil profile on day i (mm)
Q_{gw} Amount of water returning to the groundwater on day i (mm).

3.2 Data Collection

The various types of data vital for the study are digital elevation model, soil map, land use/land cover, and weather data like precipitation and temperature. The sources of the data are shown in Table 2. The discharge data were obtained from the India WRIS Website for five years (2010–2014). The observed data from Ganjem showed that the peak discharge values in 2010, 2011, 2012, 2013, and 2014 were 153, 276, 266, 452, 313 cumecs, respectively, and the discharge values for five years (2010–2014) range between 0 and 452 cumecs.

3.3 Evaluation of Model Performance

To assess the accurateness of the SWAT programme, R^2 and NSE statistical index were used. The R^2 value ranges from 0 to1, where 1 demonstrates the best match between observed/recorded and predicted/simulated values. NSE ranges between $-\infty$ and 1, wherein 1 indicates an excellent correlation between predicted and observed values. If the NSE values are zero or negative, then the model cannot predict discharge

values. After repeated simulation trials, the R^2 and NSE for calibration were found to be 0.91 and 0.87 and for validation 0.86 and 0.84. The correlation coefficient values greater than 0.5 are acceptable and in good relation as per [6, 7]

4 Results and Discussion

For the Ganjem watershed, after the setup of the SWAT model, the output was obtained from 2010 to 2014. Initially, the value of R^2 obtained was 0.59, which indicated that calibration is necessary. Hence, the calibration process was done manually. Calibration was worked for three years starting from 2010 to 2012 to match simulated with observed data values. The parameters are identified and adjusted with respect to their standard ranges to obtain better R^2 and NSE values within the allowable limits. Table 3 shows the adjusted parameters during the calibration of the model, and Fig. 3 shows the comparison of discharges.

Validation is carried out after the completion of calibration. Validation is done for a period from 2013 to 2014. Validation is done to determine the accuracy of the model after calibration. The values of R^2 and NSE after validation are 0.86 and 0.84. The R^2 and NSE values obtained for calibration are 0.91 and 0.87 as shown in Fig. 4. Figure 5 shows the scatter plot of simulated versus observed flow after validation.

Table 3 Identified sensitivity parameters for the study

Sl. No	Identified sensitive parameter	Original value	Calibrated value
1	CN2	72	80
2	ALPHA__BF	0.048	1
3	ESCO	0.95	1
4	EPCO	1	0.5
5	GW_DELAY	31	5
6	SURLAG	24	0.2

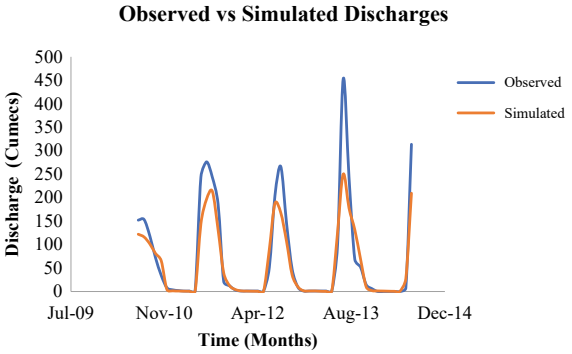

Fig. 3 Comparison graph of observed and simulated flow after calibration (Ganjem)

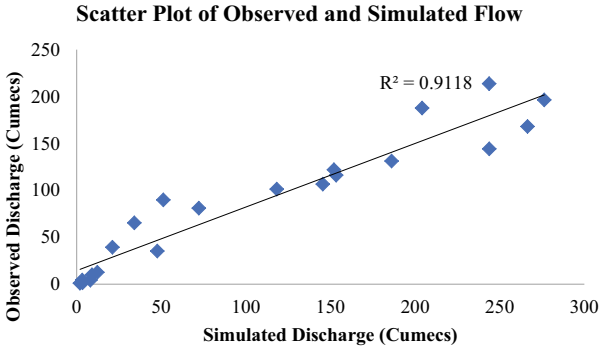

Fig. 4 Scatter plot of observed and simulated flow after calibration (Ganjem)

Fig. 5 Scatter plot of observed and simulated flow after validation (Ganjem)

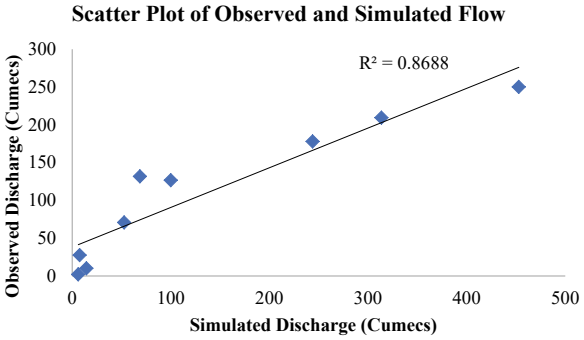

The calibrated SWAT model was used to obtain the river discharge at Panaji. R^2 and NSE values obtained were 0.85 and 0.8, which correlate well with measurements. The scatter plot of discharge by area ratio method and simulated flow for Panaji are shown in Fig. 6.

Fig. 6 Scatter plot of discharge area ratio method and simulated flow (Panaji)

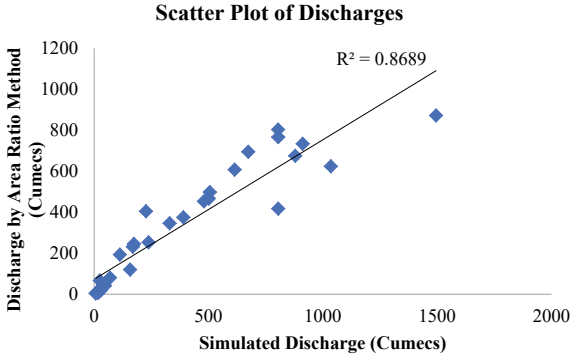

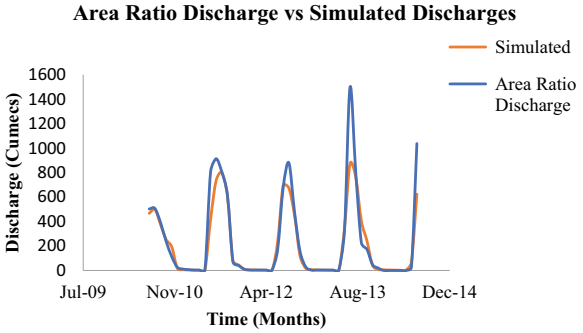

Fig. 7 Comparison of discharge by area ratio method and simulated flow (Panaji)

The discharge data at panaji were obtained using area ratio method where the peak values during 2010, 2011, 2012, 2013, 2014 were 507, 913, 881, 1497, 1037 cumecs. Whereas for the simulated discharge, the peaks were 498, 734, 675, 871, 624 cumecs, respectively. Comparison of discharges is shown in Fig. 7. It is observed that the SWAT model simulates the average discharges well but misses out predicting the peak discharges. The peak discharges from SWAT model under predicted the 2013 peak discharge by 58% and for 2014 by 60%, whereas for other periods, the under prediction is between 76 and 98%. This wide variation in the prediction of peak discharge by SWAT model needs further investigations.

5 Conclusions

SWAT programme/model was used to analyze the river discharge for Mandovi Basin in Goa, India. The model was calibrated and validated. The calibration and validation were done with reference to observed data from the India WRIS Website. During the calibration, CN_2, GW_DELAY, GWQMN, ALPHA_BF, and SURLAG were the most sensitive parameters for the study area. The model performance with default values was reasonable; however, they improved after parameter calibration.

In this study, parameter regionalization was attempted, where the calibration parameters of the Ganjem watershed were used in the simulation of the Mandovi watershed. The runoff for the Mandovi watershed was predicted and was compared with the runoff values obtained using the area ratio method. The comparison showed that the model performance was good. The discharge values for Mandovi watershed range from 0 to 1497 cumecs obtained by area ratio method, whereas the discharge values obtained from SWAT model simulation range from 0 to 871 cumecs.

The simulation results are good; R^2 and NSE values for calibration were 0.91 and 0.87; for validation, it was 0.86 and 0.84. The statistical coefficients (R^2 and NSE) were proved effective, which exhibits that the SWAT model can reasonably simulate the runoff in the study area. The correlation between observed and simulated discharges is good; however, the SWAT model is observed to underestimate the peak discharges during some periods like in August 2013.

References

1. Dai A, Trenberth KE (2002) Estimates of freshwater discharge from continents: Latitudinal and seasonal variations. J Hydrometeorol 3(6):660–687
2. Hagemann S, Dumenil L (1997) A parametrization of the lateral water flow for the global scale. Clim Dyn 14(1):17–31
3. Fekete BM, Vörösmarty CJ, Grabs W (1999) Global, composite runoff fields based on observed river discharge and simulated water balances
4. Prabhanjan A, Rao EP, Eldho TI (2014) Application of SWAT model and geospatial techniques for sediment-yield modeling in ungauged watersheds. J Hydrol Eng 20(6):C6014005
5. Sisay E, Halefom A, Khare D, Singh L, Worku T (2017) Hydrological modelling of an ungauged urban watershed using SWAT model
6. Moriasi DN, Arnold JG, Van Liew MW, Bingner RL, Harmel RD, Veith TL (2007) Model evaluation guidelines for systematic quantification of accuracy in watershed simulations. Trans ASABE 50(3):885–900
7. Jimeno-Sáez P, Senent-Aparicio J, Pérez-Sánchez J, Pulido-Velazquez D (2018) A Comparison of SWAT and ANN models for daily runoff simulation in different climatic zones of peninsular Spain. Water 10(2):192

Reservoir Sedimentation Analysis Using SWAT Model

R. S. Sabale, S. Londhe, and M. K. Jose

Abstract Many water resource projects require sediment yield analysis, which is useful for estimating reservoir life, locating vulnerable areas prone to erosion, and ensuring that natural resources are conserved. The conventional methods available for sediment analysis are more complex and time-consuming and require more data to process. The soil and water assessment tool (SWAT) which is a semi-distributed, continuous, physical-based model and has better accuracy requires fewer efforts than conventional models which was employed in this study to predict sediment load. The Koyna basin is the largest and important basin in the state of Maharashtra, India. Due to topographical, geological, and meteorological features basin suffers from frequent floods, landslides and as a result Koyna basin has large soil erosion. These critical situations seek an attention to alleviate these issues. Therefore, in this work, the agro-hydrological model SWAT was formulated for the Koyna dam basin in Maharashtra, India for 308 Km^2 basin area. The SWAT model was processed by using the meteorological data obtained from India Meteorological Department (IMD) for the period (2010–2020). The SWAT model was calibrated for (2013–2017) and validated for the period (2018–2020) with the help of the SUFI-2 algorithm in the SWAT-CUP tool. The sensitivity of work was assessed by statistical parameters like R^2, NSE, and Pbias. The values of statistical parameters in calibration and validation periods indicate the acceptance of the model. The results showed that the spatial distribution of erosion in the different sub-basins revealed a maximum sediment yield value of 145 t/ha/year for sub-basin 17 and minimal sediment transport in sub-basins 1, 9, 12, and 16. This would suggest that these sub-basins require immediate water

R. S. Sabale (✉)
Department of Civil Engineering, Visvesvaraya Technological University, Belagavi, Karnataka 590018, India
e-mail: ranjeetsabale123@gmail.com

S. Londhe
Department of Civil Engineering, Vishwakarma Institute of Information Technology Pune, Pune 411037, India
e-mail: shreenivas.londhe@viit.ac.in

M. K. Jose
National Institute of Hydrology, Belagavi, Karnataka 590019, India

P. V. Timbadiya et al. (eds.), *Hydrology and Hydrologic Modelling*,
Lecture Notes in Civil Engineering 312,
https://doi.org/10.1007/978-981-19-9147-9_12

and soil conservation efforts in order to decrease erosion and sediment transfer. The study concludes that the SWAT model is a very efficient tool for sediment analysis and can be used for the same basins in other regions. The outcomes of work may be useful for water managers for sustainable water resource management.

Keywords Sediment yield · SWAT · SWAT-CUP · Calibration–validation · Koyna

1 Introduction

In the catchment basin, runoff and sediment yield modeling is critical. Sediment yield refers to the volume of sediment that is transported with surface runoff and deposited in reservoirs. Despite having just one outflow point, the watershed is characterized by a variety of socioeconomic activities, as well as geographical, hydrological, and climatic heterogeneity. In addition to the size and shape of the watershed, spatial and temporal variability have the visible change in the quantity of runoff [1]. The sedimentation is thought to be responsible for around 0.5–1.0% of global water storage loss on a yearly basis [2]. Moreover, the cost of replacing the lost storage has been estimated to be in excess of US$13 billion, excluding other environmental and socioeconomic consequences [2]. Therefore, modeling the hydrological processes of the watershed, such as runoff and sediment output, is helpful in managing and protecting natural resources [3]. Ultimately, this approach will lead to aid sustainable soil and water resource management and hence help to strengthen nation's economy.

The Koyna dam, which is built on the Koyna River and has a capacity of 105 TMC, is the largest dam in Maharashtra, India. The dam has total catchment area of 891.78 km^2. The basin is a part of Sahyadri hill ranges and falls into Western Ghat. The basin characterized by undulating topography, steep slopes, loose and fragile soil, and excessive rainfall resulting in frequent floods, and consequently, considerable soil erosion has been observed in the study area. The sediment deposition in the dam reduces its capacity, causing concerns such as flooding, waterlogging, and the submergence of valuable agricultural land in nearby area. The downstream portion of the Koyna dam, which includes parts of Sangli and Kolhapur districts, saw significant flooding for more than 15 days in year 2019. As a result, research into runoff and sediment yield in dam basins is required. The outcomes of present study could be used as a decision-making tool in the long-term development of soil and water resources. A very sparse and few research on the Koyna basin exist, at least to the authors' knowledge, mostly concerned with discharge measurement, and flood foresting downstream of the dam [4, 5]. The sediment yield analysis for the Koyna dam basin is not supported by these researchers.

Hydrological models that deal with hydrological simulations of drainage basins, such as MIKE-SHE, HEC-RAS, SWAT, GSFLOW, SWAT-MODFLOW, and MODFLOW, among others, also have the capacities to work with changing climatic conditions [6–10]. Sabale and Jose [11] integrated the SWAT and MODFLOW model

to study the impact of conjunctive use of surface and groundwater on the groundwater levels in command area. The soil and water assessment tool (SWAT) model was developed by the United States, Department of Agriculture's research and is widely used in surface water modeling to simulate runoff and sediment load in basins [12]. Researchers in India have used and validated the SWAT model to simulate runoff and sediment yield in various river basins [1, 13–15]. Kumar et al. [16] used the SWAT model to identify the Damodar river basin's critical erosive watershed in a data scare catchment. The model was calibrated and validated for two watersheds totaling 174.49 km^2 watershed areas. The authors found that the SWAT model is useful in data-scarce situations to prioritize water management methods, and that the methodology is particularly beneficial to developing countries with limited resources, such as India. The sediment load for Ujjani Dam in Maharashtra was calculated using the SWAT model by Shendge et al. [17]. The study area was divided into 27 subbasins, and the average annual sediment load was 888,010 tons per year, according to the authors. Jain and Sharma [18] investigated the runoff and sediment generation from the 7820 km^2 Vamsadhara river basin using the SWAT model. The authors conducted a sensitivity analysis using SWAT-CUP and found that the SWAT model is an effective tool for runoff and sediment simulation. The SWAT model was used to simulate the flow of the Manimala River in Kerala [19]. The authors concluded that curve numbers and the SOL_AWC were influencing parameters for runoff.

In the current work, by keeping the objective as to determine reservoir sedimentation, the SWAT model is used for Koyna basin. The SWAT model was processed for (the years 2010 to 2020). SWAT model utilizes some starting period to overcome its initial losses in terms of evaporation and percolation; hence, the first three years (2010–2012) were skipped for the warm-up period. The model was calibrated and validated in SWAT-CUP using the SUFI-2 algorithm for the periods (2013–2017) and (2018–2020), respectively, using observed stream flows data. The calibration and validation were carried on monthly time steps basis. Statistical metrics such as the coefficient of determination (R^2), Nash–Sutcliffe efficiency (NSE), and percentage bias (Pbias) were used to assess the work's sensitivity.

2 Materials and Method

2.1 Description of Study Area

The Koyna dam basin (Fig. 1) is located between longitudes 17°54″ and 17°16″ N and latitudes 73°42″ and 74°06″ E in the Satara district of Maharashtra, India. The Koyna River originates at Mahabaleshwar, the Satara district's highest relief. The Koyna River, which flows north–south for 65 km and occupies an area of 2036 km^2, is the principal source of the Koyna dam. The current study has been carried out over the 308 km^2 area. The average elevation in the research region is between 248 and 1435 m.

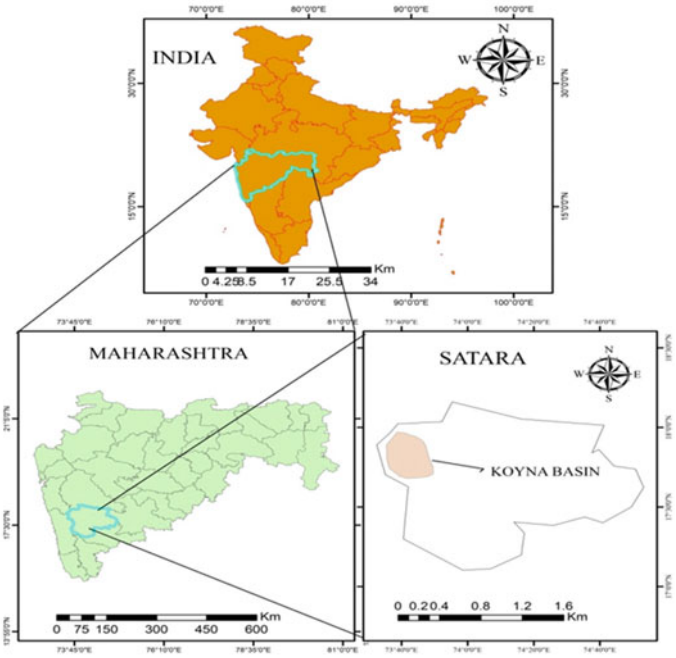

Fig. 1 Location map

The study basin is farmed with fruits trees, paddy, and maize. The land cover of study area is comprised with 31.50% agricultural area; 42.94% barren, 6.13% water bodies, and 19.32 mixed forest. The loam soil (Nd51-2b-3820) is a major soil present in the study area. The basin is located in Satara district and gathers water from the Western Ghat's east side. The Koyna dam basin has a subtropical climate with an annual average rainfall of 5000 mm. The temperature in the basin ranges from 50 to 400 degrees Celsius, with an average wind speed of 8.7 km per hour.

2.2 SWAT Model

The SWAT version used in this study was ArcSWAT 2012. The SWAT model is a physical-based and semi-distributed hydrological model that is mostly used for surface water modeling. It was developed by the United Nations' agricultural research center [20, 21]. It can forecast the effects of land use/land cover on hydrology and agricultural output. It can anticipate the impact of land use on runoff, sediment, water quality, and nutrient production at the basin size throughout time [22]. In the present work, after processing of the model, the study area has been divided into 17 sub-basins (Fig. 2) and 69 hydrologic response units (HRUs).

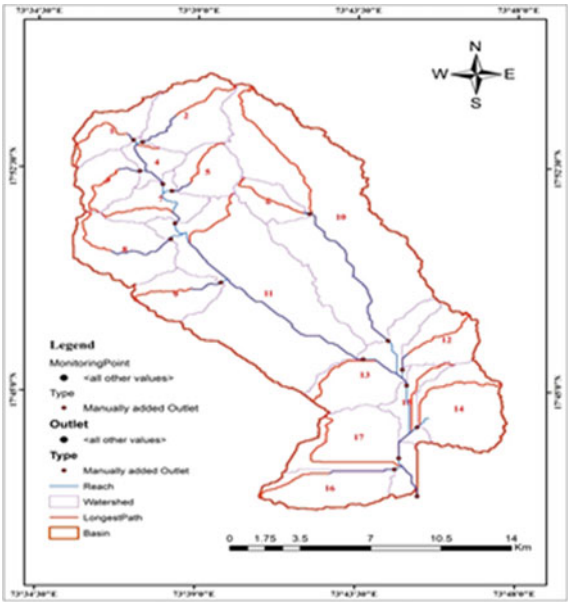

Fig. 2 Sub-basins map

2.3 Data Used

2.3.1 DEM Map

For current study, the digital elevation model (DEM) was obtained from (search.earthdata.nasa.gov) Website with 30 m resolution. The DEM is used to calculate the length of the channel, the channel slope, and the overland slope. The DEM of the research region is shown in Fig. 3, with a minimum elevation of 248 m and a relief of 1435 m. The flowchart of SWAT model and the methodology adopted in this study is shown in Fig. 4.

2.3.2 Soil Map

The soil map for the current research region was obtained from the National Bureau of Soil Survey and Land Use Planning, Department of India, at a scale of 1:250,000. The data was accessible in a detailed format, revealing the soil texture profile, and it was then digitized for model use. Figure 5 depicts the soil types found in the research region. The Loam soil (Nd51-2b-3820, 100%) was the most abundant soil in the study basin.

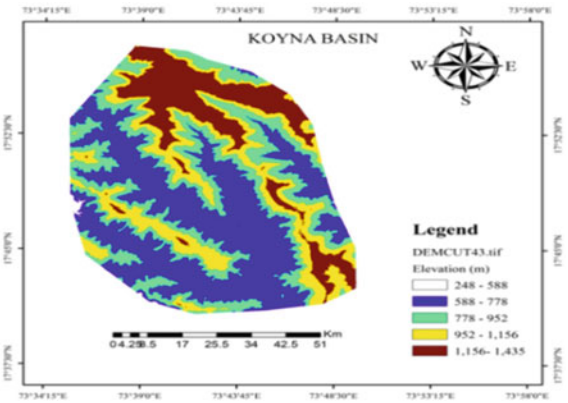

Fig. 3 DEM map

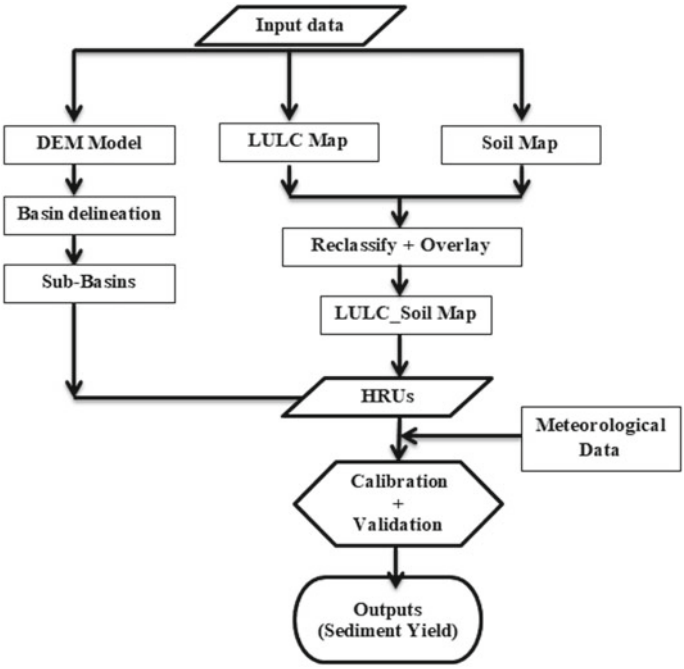

Fig. 4 Flowchart of SWAT model

2.3.3 LULC Details of Study Area

The study area's land use and land cover map (LULC) depicts the physical use of the area, such as forest, urban, and bare land, and reports on how the area is used (Fig. 6). In present work, the LULC data for the timeframe (2018–2019) was collected from earth-explorer; data without clouds was chosen for work. Moreover, the land use

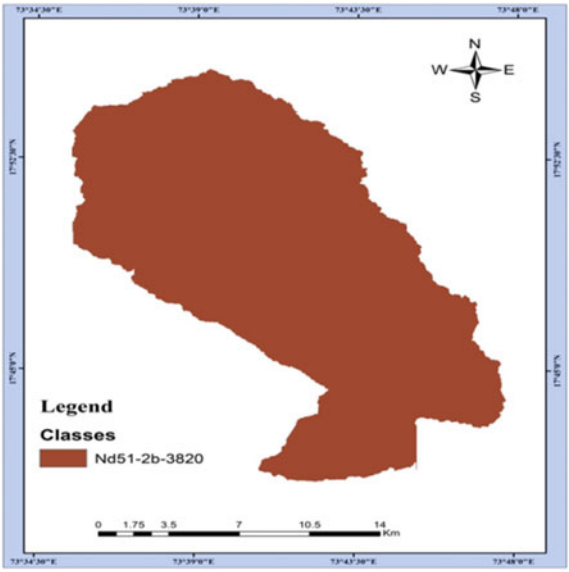

Fig. 5 Soil map

map for the study area was created by using maximum likelihood classification in ArcSWAT-2012 and using Landsat-8 imagery.

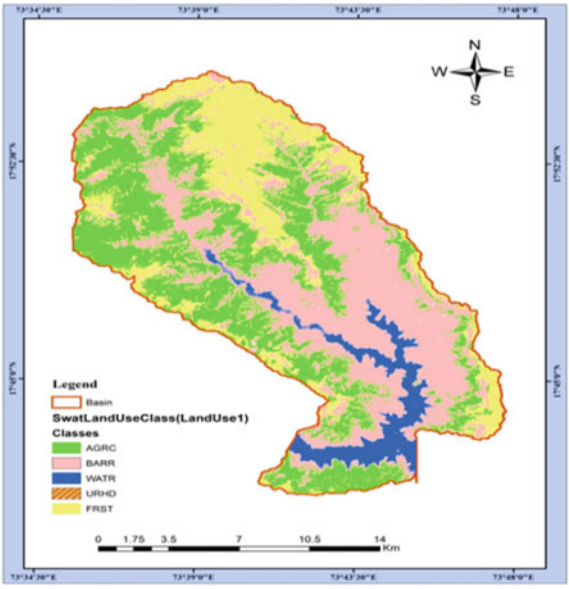

Fig. 6 LULC map

Table 1 Statistical parameters for sensitivity analysis

Statistical parameter	Formula	Authors
Coefficient of determination (R^2)	$R^2 = \left[\frac{\sum_{i=1}^{n}(O_i-\overline{O})(P_i-\overline{P})}{\sqrt{\sum_{i=1}^{n}(O_i-\overline{O})^2}\sqrt{\sum_{i=1}^{n}(P_i-\overline{P})^2}}\right]$	[23]
Nash–Sutcliffe efficiency (NSE)	$\mathrm{NSE} = 1 - \left[\frac{\sum_{i=1}^{n}(Y_i^{\mathrm{Obs}}-Y_i^{\mathrm{Sim}})^2}{\sum_{i=1}^{n}(Y_i^{\mathrm{Obs}}-\overline{Y^{\mathrm{Obs}}})^2}\right]$	[24]
Percentage bias (Pbias)	$\mathrm{Pbias} = \left[\frac{\sum_{i=1}^{n}(Y_i^{\mathrm{Obs}}-Y_i^{\mathrm{Sim}})*100}{\sum_{i=1}^{n}Y_i^{\mathrm{obs}}}\right]$	[23]

2.3.4 Meteorological Data

Precipitation, sun radiation, temperature (max and min), relative humidity, and wind velocity were collected from the India Meteorological Department (IMD) weather data center on a daily and monthly basis for the time (2010–2020). In the 'C' drive, the SWAT database was updated with IMD gridded data and climate forecast system reanalysis (CFSR) global data. The errors in meteorological data such as missing rainfall data presented as (-999.00) were removed before the SWAT model was processed.

3 Results and Discussion

3.1 Model Performance

For calibration and validation, the observed stream flow data from Mahabaleshwar station for monthly time steps was used. The sensitivity of the work is assessed by statistical parameters like R^2, Pbias [23], and NSE [24] (Table 1).

The range of statistical parameters is shown in Table 2. The determination coefficient (R^2) is a number between 0 and 1, with 1 being the best result, indicating that estimated values match measured real values. The best value for PBIAS is zero. A pattern of underestimation bias is indicated by positive numbers, whereas an overestimation bias model is indicated by negative values [25].

3.2 Model Calibration

The model's calibration is critical since it displays the degree of fitness and shows how well simulated and observed data match. To overcome its initial losses and produce the best simulation results, the model was given a three-year warm-up period for

Table 2 Values/range of statistical parameters [23, 24]

Performance ratings	NSE	R^2	Percentage bias (%)	
			Sediment	Flow
Very good	0.75–1	0.75–1.00	< ± 15	< ± 10
Good	0.65–0.75	0.65–0.75	± 15 to ± 30	± 10 to ± 15
Satisfactory	0.50–0.65	0.50–0.65	± 30 to ± 55	± 15 to ± 25
Unsatisfactory	< 0.50	< 0.50	> ± 55	> ± 25

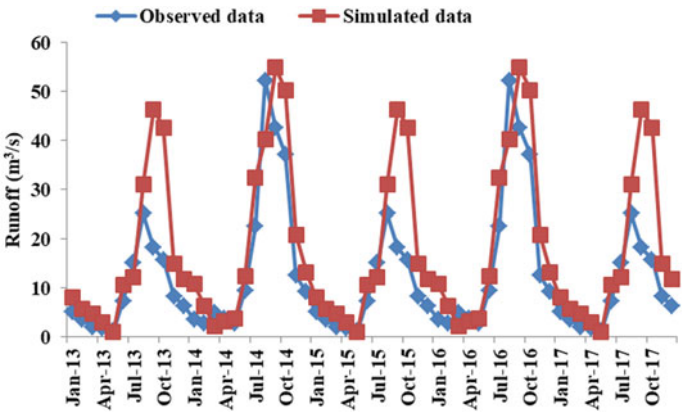

Fig. 7 Monthly basis data for calibration

the current investigation. SWAT-CUP tool was used to complete the calibration for the period (2013–2017) (Fig. 7). Initially, self-calibration was utilized in SWAT, and afterward, SWAT-CUP was used to change sensitive parameters (Table 3). The R^2 value during calibration was 0.74 which indicates the acceptance of model (Fig. 8).

3.3 Model Validation

Model validation was done for monthly time steps during a three-year period (2018–2020) (Fig. 9). From the Fig. 10, results showed that R^2 value during validation is 0.70 indicating good agreement between simulated data and observed data.

3.4 Sediment Yield

During the calibration (2013–2017) and validation (2018–2020) periods, the average annual soil loss values were 10.15 and 19.37 t/ha/year, respectively. These values

Table 3 Values of sensitive parameters used in calibration

Parameter	Process	Details of parameter	Range
CN2	.mgt	Curve number 2 for wetting conditions	−50%; + 50%
ALPHA_BF	.gw	Base flow factor (days)	0–1
SURLAG	.bsn	Coefficient of surface runoff lag	0–10
ESCO	.hru	Soil evaporation factor	0–1
SLSUBBSN	.hru	Slope length	−50%; + 50%
SLOPE	.hru	Average steepness	−15%; + 15%
SOL_AWC	.sol	Soil available water capacity	−20%; + 20%
SOL_K	.sol	Hydraulic conductivity (Saturated)	−50%; + 50%
SOL_Z	.sol	Soil depth	0–3000
SOL_BD	.sol	Moist bulk density	−15%; + 15%

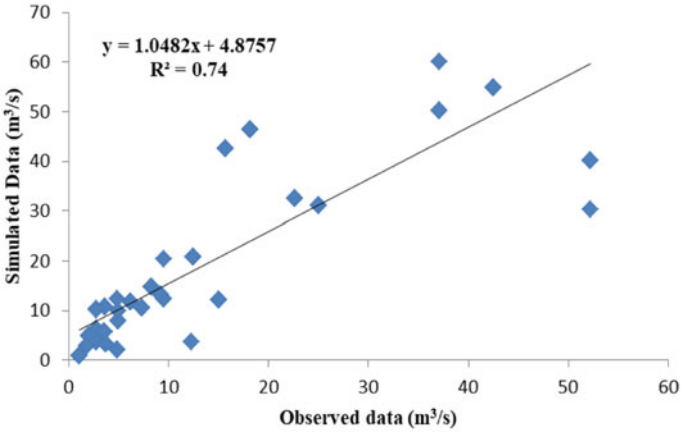

Fig. 8 Scattergrams for calibration

fluctuate spatio-temporally; moreover, the erosion rate is governed by rainfall, land use/land cover, soil texture, and by topography.

For both the calibration and validation periods, Figs. 11 and 12 depict the variation in sediment yield between the various sub-watersheds. For the calibration period, the spatial distribution of erosion in the different sub-basins revealed a maximum sediment yield value of 145 t/ha/year for sub-basin 17 and minimal sediment transport in sub-basins 1, 9, 12, and 16. This would suggest that these sub-basins require immediate water and soil conservation efforts in order to decrease erosion and sediment transfer.

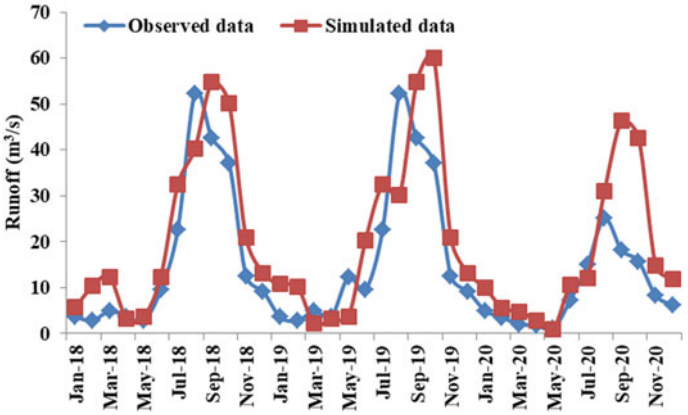

Fig. 9 Monthly basis data for validation

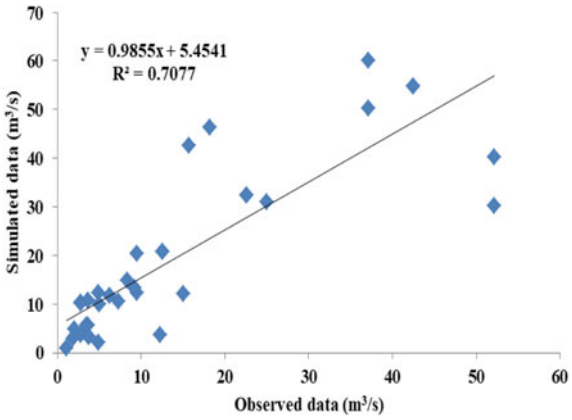

Fig. 10 Scattergrams for validation

4 Results and Discussion

The hydrological models are quite good at modeling runoff and sediment yield on a basin scale; therefore, they can be utilized as a tool for soil and water resource management planning. The SWAT model was used in this study for the Koyna dam basin in Maharashtra, India to estimate sediment yield. The SWAT model was run over a period of time (2010–2020), and the data obtained from HDUG Nasik, i.e., observed flows were used for calibration and validation. The model was calibrated and validated with the help of the SUFI-2 algorithm in SWAT-CUP for monthly time steps, statistical measures such as NSE (0.68), R^2 (0.74), and Pbias (11%) were obtained at the time of calibration, and NSE (0.72), R^2 (0.70), and Pbias (14 %) were found at the validation phase. From this study, it is observed that sub-basin numbers

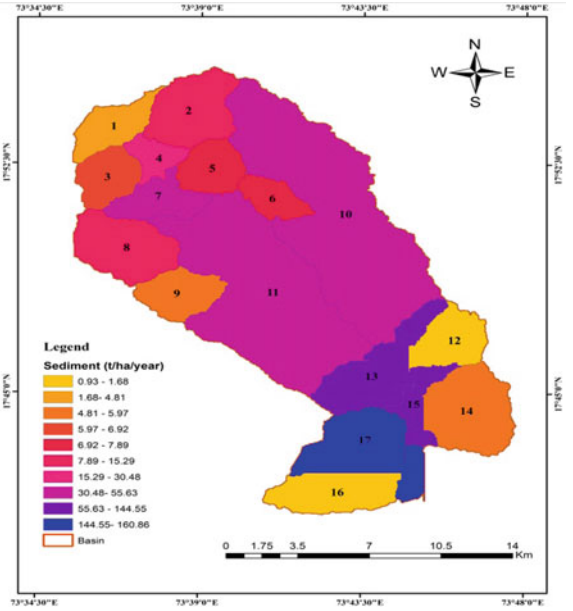

Fig. 11 Spatial distribution of sediment yield during calibration period (2013–2017)

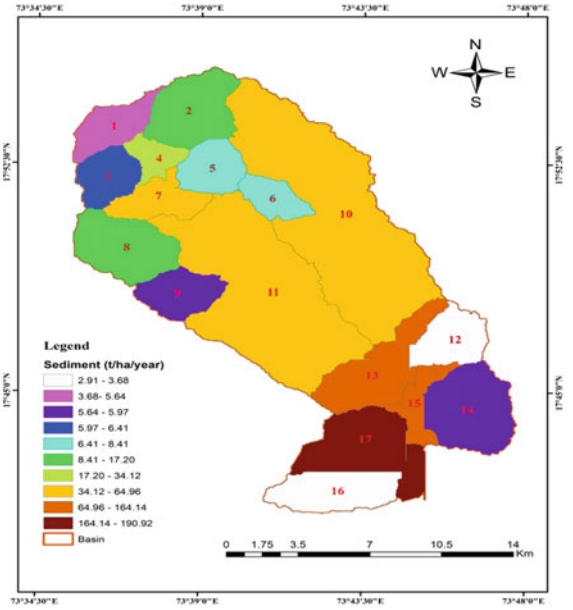

Fig. 12 Spatial distribution of sediment yield during validation period (2018–2020)

13, 15, and 17 are more vulnerable for erosion and hence to be maintained to alleviate the soil losses.

5 Conclusion

The study concludes that the results are satisfactory; indicating that the model is capable of accurately reproducing reported sediment yields. The SWAT model has been proved to be a reliable method for simulating sediment transport in the Koyna basin. The outcomes of work will be useful to researchers and policymaker to conserve the soil and water resources in Koyna basin.

References

1. Dutta S (2016) Soil erosion, sediment yield and sedimentation of reservoir: A review. Model Earth Syst Environ 2(3):1–18
2. CENTRAL WATER COMMISSION (2020) Compendium on sedimentation of reservoirs in India. http://www.cwc.gov.in/sites/default/files/compendium1122020.pdf
3. Abebe T, Gebremariam B (2019) Modeling runoff and sediment yield of Kesem Dam Watershed, Awash Basin, Ethiopia. SN Appl Sci 1(5):1–13. https://doi.org/10.1007/s42452-019-0347-1
4. Shinde S, Aher S, Pawar A, Kantamaneni K (2020) Spatio-temporal variability of discharge over the past 40 years in Krishna and Koyna Rivers, India. Iran J Sci Technol Trans Civil Eng 44(0123456789):395–407. https://doi.org/10.1007/s40996-020-00375-z
5. Time, Real, and Streamflow Forecasting (2018) DMP Report
6. Che D, Mays LW (2015) Development of an optimization/simulation model for real-time flood-control operation of river-reservoirs systems. Water Resour Manage 29(11):3987–4005
7. Dowlatabadi S, Ali Zomorodian SM (2016) Conjunctive simulation of surface water and groundwater using SWAT and MODFLOW in firoozabad watershed. KSCE J Civ Eng 20(1):485–496
8. Kaleris V, Langousis A (2017) Comparison of two rainfall-runoff models: effects of conceptualization on water budget components. Hydrol Sci J 62(5):729–748. https://doi.org/10.1080/02626667.2016.1250899
9. Liu W et al (2020) Quantifying the streamflow response to groundwater abstractions for irrigation or drinking water at catchment scale using SWAT and SWAT–MODFLOW. Environ Sci Eur 32(1). https://doi.org/10.1186/s12302-020-00395-6
10. Zhang M, Zhang J, Song Y (2019) Preliminary research and application of MIKE SHE model in Jialingjiang river basin. IOP Conf Ser Earth Environ Sci 304(2)
11. Sabale R, Jose MK (2021) Hydrological modeling to study impact of conjunctive use on groundwater levels in command area. J Indian Water Works Assoc 53(3):190–197
12. Arnold JG et al (2012) SWAT: model use, calibration, and validation. Trans ASABE 55(4):1491–1508
13. Chandra P, Patel PL, Porey PD, Gupta ID (2014) Estimation of sediment yield using SWAT model for upper Tapi basin. ISH J Hydraul Eng 20(3):291–300
14. Dutta S, Sen D (2018) Application of SWAT model for predicting soil erosion and sediment yield. Sustain Water Resour Manag 4(3):447–468
15. Prabhanjan A, Rao EP, Eldho TI (2015) Application of SWAT model and geospatial techniques for sediment-yield modeling in ungauged watersheds. J Hydrol Eng 20(6):1–6

16. Kumar S, Mishra A, Raghuwanshi NS (2015) Identification of critical erosion watersheds for control management in data scarce condition using the SWAT model. J Hydrol Eng 20(6):1–8
17. Shendge RB, Chockalingam MP, Saritha B, Ambica A (2018) Swat modelling for sediment yield: a case study of Ujjani reservoir in Maharashtra, India. Int J Civ Eng Technol 9(1):245–252
18. Jain M, Sharma D (2014) Hydrological modeling of Vamsadhara River Basin, India using SWAT. In: International conference on emerging trends in computer and image processing (ICETCIP'2014) 15–16 Dec 2014 Pattaya (Thailand), pp 82–86
19. Venkatesh B et al (2018) V6 water science and technology library modeling of a river basin using SWAT model
20. Arnold JG, Srinivasan R, Muttiah RS, Williams JR (1998) Large area hydrologic modeling and assessment part I: model development. J Am Water Resour Assoc 34(1):73–89
21. Neitsch SL, Arnold JG, Kiniry JR, Williams JR (2005) Soil and water assessment tool, theoretical documentation version 2005. Agricultural Research Service Blackland Research Center. Temple, TEXAS, USA
22. Neitsch SL et al (2002) TWRI report TR-192 soil and water assessment tool user's manual. http://swat.tamu.edu/media/1294/swatuserman.pdf
23. Moriasi DN, Arnold JG, Van Liew MW, Bingner RL (2007) Model evaluation guidelines for systematic quantification of accuracy in watershed simulations. Trans ASABE 50(3):885–900
24. Nash JE, Sutcliffe JV (1970) River flow forecasting through conceptual models: part I. a discussion of principles. J Hydrol 10(3):282–290
25. Gupta HV, Sorooshian S, Yapo PO (1999) Status of automatic calibration for hydrologic models: comparison with multilevel expert calibration. J Hydrol Eng 4(2):135–143

Assessing the Performance of SWOT Simulator in Estimating River Discharge of a Tropical Basin

Taha Aawar, M. S. Adarsh, and C. T. Dhanya

Abstract River discharge, one of the most informative hydrologic variables for different applications such as water resources management, flood forecasting, and long-term change studies in the water cycle, is measured only across a few stations, however. The measurement and maintenance of river discharge data at in situ hydrological observations (HO) stations are challenging due to the cost involved and the accessibility. Hence, studies often rely on remote sensing methods, particularly satellite data, as a complementary source for estimating river discharge. Interest in space-based observation for remote sensing of river discharge has gained momentum recently due to continuous availability and open access of multiple satellites such as optical, microwave, and altimetry at various spatial and temporal scales globally. Surface Water and Ocean Topography satellite mission (SWOT), to be launched in 2022, aims to estimate discharges in rivers wider than 100 m directly. This study aims to assess the applicability of the SWOT mission to estimate the discharge of Gopalkheda station in the Tapi river basins, a tropical basin in India, using SWOT-like data. In situ, HO station data and satellite data are used in a SWOT Simulator along with multiple river discharge estimating algorithms used by SWOT satellite to derive the discharge series. The results are compared with the in situ river discharge to assess the performance of SWOT-derived river discharge.

Keywords River discharge · Remote sensing · Satellite data · SWOT satellite mission

---

The original version of this chapter was revised: The author Taha Aawar's name has been updated. The correction to this chapter can be found at https://doi.org/10.1007/978-981-19-9147-9_45.

T. Aawar (✉) · M. S. Adarsh · C. T. Dhanya
Department of Civil Engineering, Indian Institute of Technology Delhi, Hauz Khas, New Delhi 110016, India
e-mail: taha.aawar@civil.iitd.ac.in

M. S. Adarsh
e-mail: adarsh.m.s@civil.iitd.ac.in

C. T. Dhanya
e-mail: dhanya@civil.iitd.ac.in

P. V. Timbadiya et al. (eds.), *Hydrology and Hydrologic Modelling*,
Lecture Notes in Civil Engineering 312,
https://doi.org/10.1007/978-981-19-9147-9_13

1 Introduction

River discharge has a significant role in water resources management; thus, understanding river discharge is advantageous for mitigating and controlling floods, drought, etc. Discharge estimation using satellite data is a complicated process due to numerous limitations like temporal and spatial resolution of satellites, type of satellites available, and accuracy of the satellite images [1, 2]. Based on the literature, the global discharge database information has been regularly downsizing throughout the last few years. This issue leads to understanding the importance of remote sensing techniques and applications in measuring rivers' height, width, and slope [3–6]. Recently, remote sensing and GIS techniques have been widely used to estimate river discharge through calibration in situ observation data [7–9]. Various studies have been conducted to estimate the discharge using satellite and remote sensing data products in the last few decades [2, 3, 9–18]. The river discharge through satellite products data is estimated by measuring its different hydraulic components, such as river width, depth, or velocity either solely or jointly [19–21]. The Surface Water and Ocean Topography (SWOT) satellite mission planned to be launched in 2022 can estimate discharge by simultaneously measuring water surface elevation, river width and slope, using a temporally and spatially continuous Ka-band radar interferometer [22, 23]. SWOT is the first such satellite devoted to terrestrial hydrology, which was developed by the National Aeronautics and Space Administration (NASA) and French: Centre National D'études Spatiales (CNES) with contributions from the Canadian Space Agency (CSA) and The United Kingdom Space Agency (UKSA) [24–31].

The SWOT mission satellite is designed to complete one earth cycle observation within 21 days at an altitude of 800–1000 km generating a large amount of data. This satellite carries a payload module containing a KaRIn radar interferometer to measure ocean water level, Jason class altimeter, DORIS antenna, microwave radiometer, X-band antenna, laser reflector assembly, and GPS. Likewise, the SWOT mission can observe the ocean water level, estimate inland water bodies wider than 250 × 250 m with a target of 10,000 square metres, and discharge rivers more than 100 m wide [32, 33]. One of the most remarkable points of the SWOT is that it can accurately measure soil, snow, and vegetation layers with less penetration using KaRIn. KaRIn is the first satellite instrument to completely dissolve surface water bodies with high altitude accuracy [34, 35].

In order to investigate the capabilities of SWOT, identify applications, and develop algorithms to process the large output data, studies have been carried out by generating synthetic SWOT-like observations by corrupting the observed or modelled data with SWOT error characteristics [25, 36]. Using the CNES SWOT Hydrology Simulator [34], proxy SWOT-like data are produced that account for additional measurement error sources and produce outputs that are comparable to those expected from actual SWOT products.

This paper attempts to evaluate the SWOT satellite's performance with the observation data in one of India's prominent rivers, the Tapi river basin. We use existing

satellites and in situ observations data to supply inputs for SWOT Simulator to generate SWOT-like output data and compare with in situ observation.

2 Study Area, Material, and Method

2.1 Study Area

Based on Central Water Commission (CWC), India has 20 river basins in which 12 are prominent, and rest eight rest are composite and small basins. A seasonal tropical river basin with high intensity of rainfall and flood is located in central India called Tapi River Basin. Tapi River Basin has a 724 km length and 65,145 km^2 catchment area divided into upper Tapi river (Multai to Hathnur dam), middle Tapi river (Hathnur dam to Ukai dam), and lower Tapi river (Ukai dam to the Arabian Sea). Tapi river basin has three discharge gauge stations of which two located in the upper part of the basin, and the rest is in the middle part. In this study, the Gopalkheda gauge station is selected as in situ reference data. This station belongs to the branch of the Purnais river which located in the Akoal district of Maharashtra. The total average rainfall in this area is 704.7 mm [37]. Figure 1 shows the study area map.

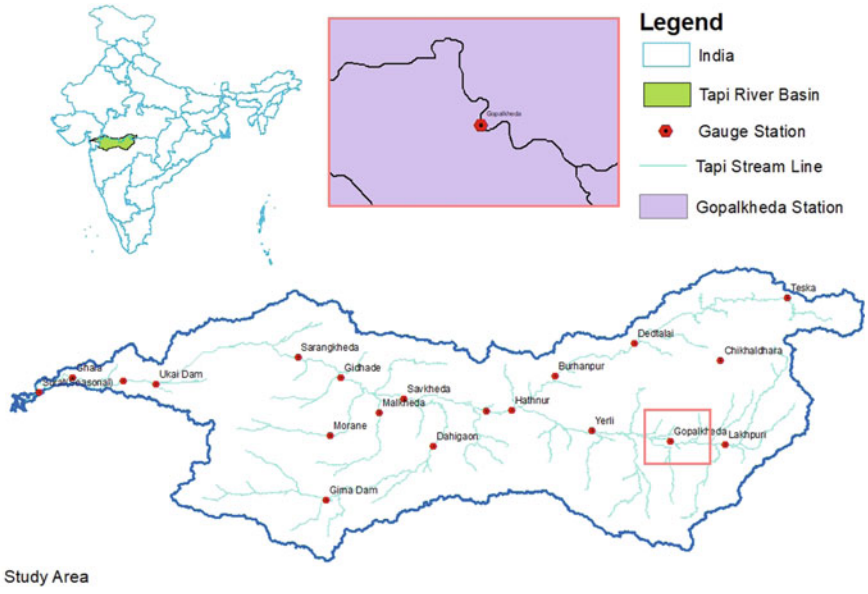

Fig. 1 Tapi River Basin—Study area

2.2 *In Situ* Data Requirement

The monsoon season in India generally peaks between July and October of every year. Our study focussed on these months and selected HO observations for each year from 2010 to 2017. Accordingly, we obtained discharge and water surface elevation data from India-WRIS (www.indiawris.gov.in) Website for the study area.

2.3 *Surface Water Extend from Satellite*

One of the inputs for the SWOT simulator is the river surface water extent at the study location. In order to obtain the water extent, we used images from multiple satellites such as the Sentinel-1 SAR satellite and Landsat-5, 7, 8 and Sentinel-2 Satellites. The images were processed to extract the surface water extent and converted to polygon shapefiles for use in SWOT Simulator.

2.4 *CNES SWOT Hydrology Simulator*

Amongst the inputs that the CNES SWOT hydrology simulator uses are radar parameters (power, bandwidth, baseline, thermal noise level, etc.), SWOT orbit, a land coverage map referred to as a water mask, and a digital elevation model (DEM).

A simulator run begins with finding all ascending and descending orbits intersecting the area of interest and selecting the ones to use. In the next step, the simulator calculates the complex interferograms by taking into account the chosen orbit, the DEM, the land cover mask, the water topography, and the instrument characteristics. A complex output image reflects the magnitude of the backscattering of the surface (corrupted by speckle), and the phase reflects the topography of land and water (with thermal noise).

It is possible to simulate various situations by changing parameters, like the backscattering model for each class (land, water, etc.), or by adding a wind field that will locally modulate water roughness and backscattering. In the next step, the simulator generates a "pixel cloud" product, a water mask associated with geolocated heights and uncertainties, in which the water pixels are demonstrated as a point cloud. Land pixels are mostly disposed of or discarded.

We create the water extent at rivers using the polygon shapefile extracted from Satellite images. These shapefiles must contain attributes with water surface elevations input as "HEIGHT", River flag (RIV_FLG) with 1 for the river and 0 for the lake [34]. Figure 2 illustrates the river network and river pixel cloud (river mask), which SWOT Simulator generated at Gopalkheda.

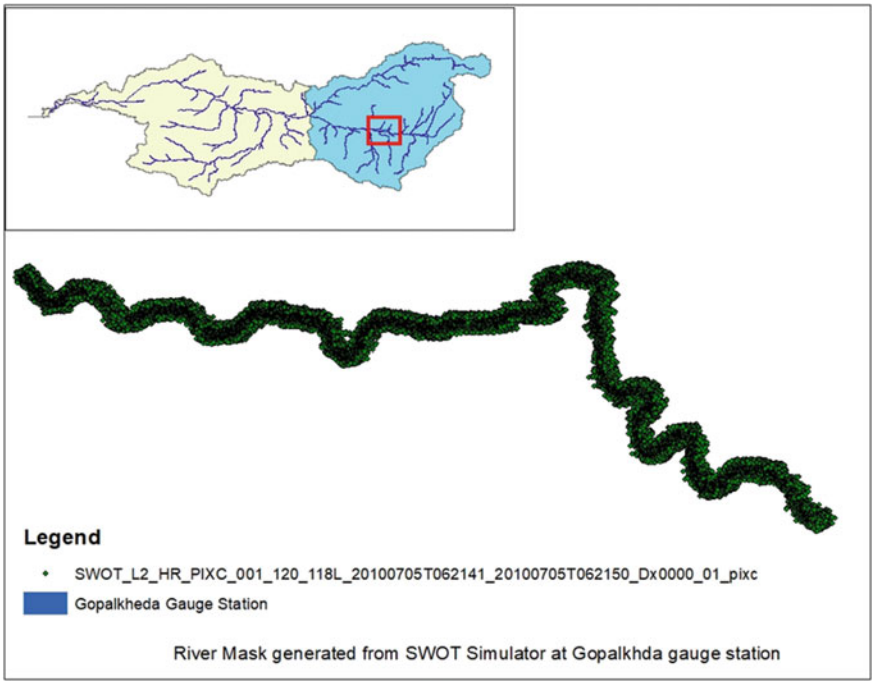

Fig. 2 Generated river mask for Gopalkheda gauge station

2.5 SWOT RiverObs Simulator

The resulting pixel cloud of water surface heights is processed with a RiverObs package in the SWOT simulator, which uses a priori information of river centerline and node database spaced at ~200 m along the river centerline and reaches database computed by aggregating nodes to ~10 km. It uses an offline SWOT River Database (SWORD), which contains the river feature in shapefiles through its global and satellite-related database [38]. Generated nodes that have average water level and river with are shown in Fig. 3 at the Gopalkheda HO station of the study area.

2.6 Empirical Equation

Discharge being a significant characteristic of the river, researchers have tried various methods to estimate discharge from satellite data products. [22, 39] used the stage-rating curve and hydraulic manning equation to estimate river discharge from satellite data products. [20, 40, 41] used an empirical method in order to carry out river discharge from satellite data. Sichangi et al. [40] developed the manning's equation form to derive discharge using satellite water level and river width with an assumption

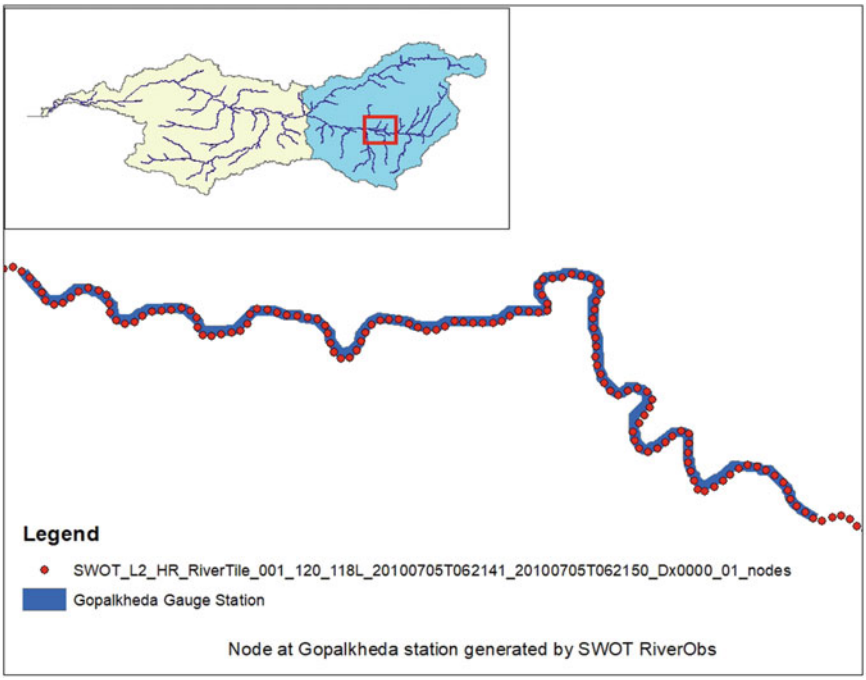

Fig. 3 Nodes generated from RiverObs at Gopalkheda gauge station

of the trapezoidal cross-section according to Eq. (1):

$$q = aWD^{\frac{5}{3}} + b \tag{1}$$

where a and b are constant, which can evaluate by calibration of in situ data, W is river width, q is the discharge, and D is water depth obtained from Eq. (2):

$$D = H - h \tag{2}$$

H is water level height, and h is the zero flow water level. Huang et al. [41] expand the Eq. 1 for various cross-section areas shapes, which result is shown in Eq. (3):

$$q = aW(H - h)^{\frac{5}{3}} \tag{3}$$

where a is the constant ratio between roughness and slope and can estimate from the least square fitting using calibrated in situ data (Huang et al., 2018).

For the present study, power-law fitting [42] as presented in Eqs. (4–6) is used in order to estimate discharge.

$$h = aQ^b \tag{4}$$

$$W = cQ^d \quad \text{m} \tag{5}$$

$$\begin{aligned} Wxh &= (a+c)Q^{(b+d)} \\ Wxh &= AQ^B \end{aligned} \tag{6}$$

where W is river width, h is water depth, and Q is discharge. A and B are constant slope roughness ratios.

3 Performance Evaluation

Nush–Sutcliffe efficiency (NSE) coefficient, root mean square error (RMSE), and relative root mean square error (RRMSE) are used according to the following formula to evaluate the discharge estimation performance.

$$\text{NSE} = 1 - \frac{(Q_{\text{Obs}} - Q_{\text{Est}})^2}{\left(Q_{\text{Obs}} - \overline{Q_{\text{Obs}}}\right)^2} \tag{7}$$

$$\text{RMSE} = \sqrt{\frac{(Q_{\text{Obs}} - Q_{\text{Est}})^2}{n}} \tag{8}$$

$$\text{RRMSE} = \frac{\text{RMSE}}{\overline{Q_{\text{Obs}}}} \times 100\% \tag{9}$$

4 Results and Discussion

SWOT satellite missions can simultaneously measure the water surface elevation (WSE) and river width (W), whilst other satellites do not have this ability. Consequently, the SWOT simulator estimated the time series of water surface elevation and river width on the Gopalkheda gauge station of the Tapi river basin plot in Fig. 4.

In the present study, Eqs. (4 and 6), as illustrated in Figs. 5 and 6, are used, respectively, to derive the discharge from joint estimation using SWOT data products and solo estimation using in situ data water level for the Gopalkheda gauge station, as shown in Table 1.

Based on Eq. 6, the SWOT river width product and in situ water level are used to calculate discharge at the Gopalkheda gauge station. The result demonstrated a comparable estimated discharge value in comparison with actual discharge. On the other hand, Eq. 4 is used to estimate discharge from in situ water level data. This process has been done in order to check the accuracy of the river width and

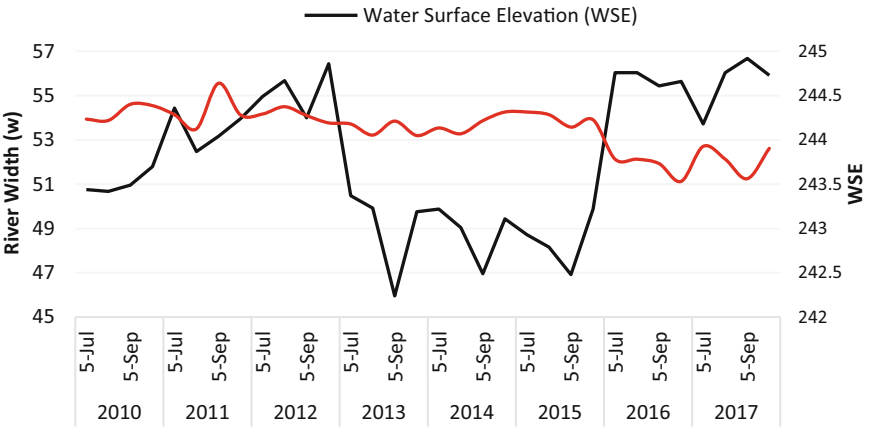

Fig. 4 River width and water surface elevation SWOT data

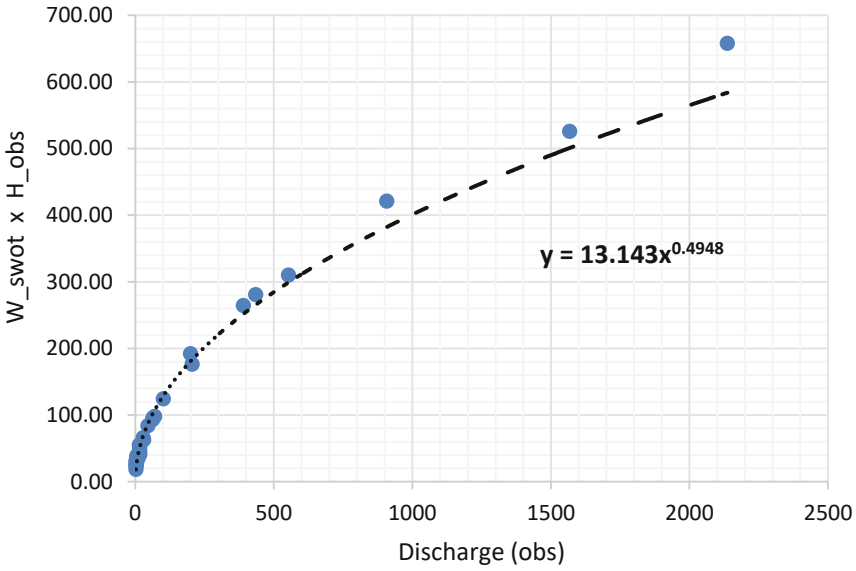

Fig. 5 Discharge via width to the height power equation

performance of SWOT satellite data. Appropriately, estimated discharge is showing consistency, as shown in Figs. 5 and 6.

Nush–Sutcliffe efficiency (NSE) coefficient, root mean square error (RMSE), and relative root mean square error (RRMSE) to calculate the performance of SWOT data products to estimate discharge using Eqs. 7, 8, and 9 are presented in Table 2.

Based on the NSE value, the result shows a consistency between the estimated discharge using SWOT data and in situ using Eq. 6. Figure 7 shows the estimated

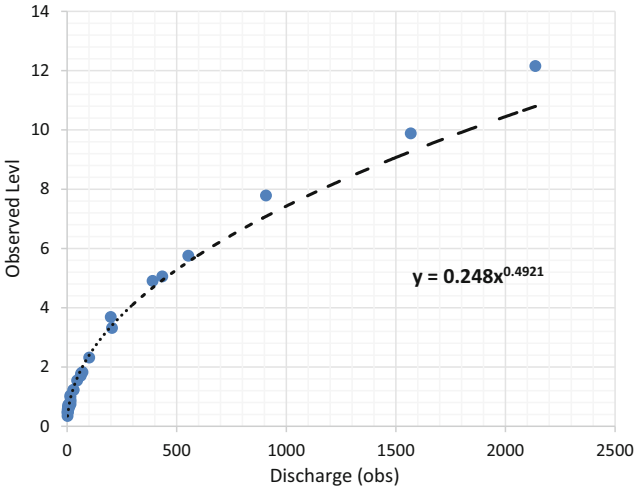

Fig. 6 Discharge via water level power equation

discharge using SWOT products and in situ observations. In addition, the RMSE in using SWOT satellite data shows improvement with respect to in situ data.

5 Conclusions

Recently, satellite data products have been widely used in order to estimate discharge amongst the researchers. This research attempted to use SWOT satellite mission synthetic data products to evaluate the performance of this satellite mission, which will be launched in 2022.

Although various methods to estimate river discharge from satellite data are used by many researchers, we used an empirical equation method to derive river discharge from the synthetic SWOT data products in the Gopalkheda gauge station in the Upper Tapi river basin. As shown in Fig. 7, the discharge is high during August, September, and October 2012, 2013, and 2015, which is the cause for the high value of RMSE by increasing the data time interval, this may decrease. NSE coefficient value for jointly used satellite river width and in situ water level express a good performance estimated value (0.94) near the ideal NSE value (1). Whilst for in situ data, NSE comes 0.94. Root mean square error indicates the improvement in the satellite data used compared with h solo in situ data. In order to obtain a temporally continuous estimate of water surface elevation using SWOT, it is recommended to input the height as a time series using Python wrapper to process the full time series through the CNES simulator quickly and efficiently [34]. The result of this study shows the applicability of SWOT satellite in Indian basin, promising to estimate river discharge reliably. The current study shall need to be scaled temporally and spatially to assess the performance of SWOT satellites data products in other basins of India.

Table 1 Estimation of discharge using SWOT data

Year	Date	Width (w) from SWOT	Water Surface Elevation (Observation)	Zero water Level	Observation Discharge (Q)	Water Depth (h)	$w*h$	Estimated discharge from SWOT data (Q')	Estimated discharge from h solo (Q'')
2010	5-Jul	53.94	240.9	236	***390.29***	4.9	264.31	***430.94***	***429.63***
	5-Aug	53.88	241.75		***553.39***	5.75	309.81	***594.08***	***594.66***
	5-Sep	54.61	237.7		***62.6***	1.7	92.84	***52.01***	***49.98***
	5-Oct	54.55	236.74		***16.39***	0.74	40.37	***9.66***	***9.22***
2011	5-Jul	54.14	236.71	236	***5.53***	0.71	38.44	***8.75***	***8.48***
	5-Aug	53.5	236.55		***3.03***	0.55	29.43	***5.10***	***5.05***
	5-Sep	55.56	241.05		***435.03***	5.05	280.58	***486.25***	***456.78***
	5-Oct	54.13	236.69		***8.67***	0.69	37.35	***8.26***	***8.00***
2012	5-Jul	54.17	236.66	236	**8.15**	0.66	35.75	**7.56**	**7.31**
	5-Aug	54.5	237.54		**46.24**	1.54	83.93	**42.42**	**40.89**
	5-Sep	54.1	243.78		**907.84**	7.78	420.9	**1103.59**	**1099.27**
	5-Oct	53.77	237.82		**70.58**	1.82	97.86	**57.86**	**57.42**
2013	5-Jul	53.72	238.31	236	**101.57**	2.31	124.09	**93.50**	**93.20**
	5-Aug	53.22	239.31		**205.28**	3.31	176.16	**189.81**	**193.59**
	5-Sep	53.85	237.22		**28.58**	1.22	65.7	**25.86**	**25.47**
	5-Oct	53.2	245.88		**1568.23**	9.88	525.62	**1729.10**	**1786.45**

(continued)

Table 1 (continued)

Year	Date	Width (w) from SWOT	Water Surface Elevation (Observation)	Zero water Level	Observation Discharge (Q)	Water Depth (h)	$w*h$	Estimated discharge from SWOT data (Q')	Estimated discharge from h solo (Q'')
2014	5-Jul	53.54	236.34	236	**2.5**	0.34	18.2	**1.93**	**1.90**
	5-Aug	53.28	237.03		**15.01**	1.03	54.88	**17.97**	**18.06**
	5-Sep	53.87	237.78		**64.55**	1.78	95.89	**55.52**	**54.88**
	5-Oct	54.26	236.73		**8.72**	0.73	39.61	**9.30**	**8.97**
2015	5-Jul	54.26	236.63	236	**5.84**	0.63	34.18	**6.91**	**6.65**
	5-Aug	54.14	248.15		**2136.8**	12.15	657.8	**2720.94**	**2719.66**
	5-Sep	53.58	236.73		**11.55**	0.73	39.11	**9.07**	**8.97**
	5-Oct	53.91	236.63		**9.85**	0.63	33.96	**6.82**	**6.65**
2016	5-Jul	52.13	236.86	236	**16.87**	0.86	44.83	**11.94**	**12.52**
	5-Aug	52.13	239.68		**199.5**	3.68	191.84	**225.50**	**240.11**
	5-Sep	51.93	236.97		**15.8**	0.97	50.37	**15.12**	**15.98**
	5-Oct	51.13	237.22		**30.63**	1.22	62.38	**23.29**	**25.47**
2017	5-Jul	52.71	236.47	236	**3.9**	0.47	24.77	**3.60**	**3.67**
	5-Aug	52.13	236.46		**1.96**	0.46	23.98	**3.37**	**3.51**
	5-Sep	51.25	236.63		**4.11**	0.63	32.29	**6.15**	**6.65**
	5-Oct	52.62	236.49		**4.39**	0.49	25.78	**3.91**	**3.99**

To highlight the key results of the model and guide the reader's attention, the numbers in the table are displayed in bold font. This emphasizes the importance of the data and encourages the reader to focus on the model's results.

Table 2 Performance evaluation metrics

Discharge estimate used	n	$\overline{\mathbf{Q}_{obs}}$	$\sum (Q_{obs} - Q_{Est})^2$	$\sum \left(\mathbf{Q}_{obs} - \overline{Q_{obs}}\right)^2$	NSE	RMSE (Cumecs)	RRMSE (%)
River width from SWOT data	32	216.98	412,882.11	7,101,500.28	0.94	113.59	52.35
Height from in situ data	32	216.98	430,183.54	7,101,500.28	0.94	115.94	53.44

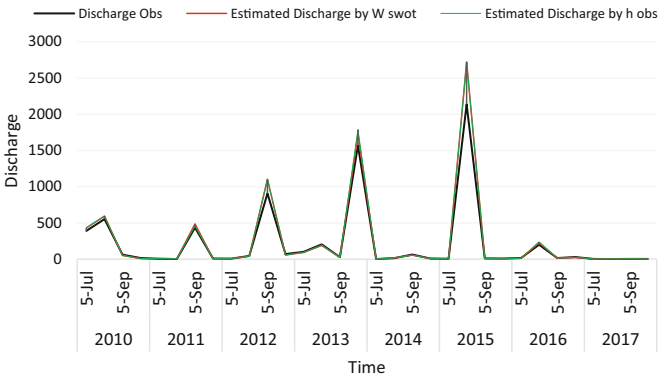

Fig. 7 Estimated discharge and in situ discharge graph

References

1. Aawar T, Khare D (2020) Assessment of climate change impacts on streamflow through hydrological model using SWAT model: a case study of Afghanistan. Model Earth Syst Environ 6(3):1427–1437. https://doi.org/10.1007/s40808-020-00759-0
2. Duvvuri S (2018) Hydrological modelling of cooum river basin using gis and swat model. Dec 306–311
3. Tourian MJ, Schwatke C, Sneeuw N (2017) River discharge estimation at daily resolution from satellite altimetry over an entire river basin. J Hydrol 546:230–247. https://doi.org/10.1016/j.jhydrol.2017.01.009
4. Maillard P, Bercher N, Calmant S (2015) New processing approaches on the retrieval of water levels in Envisat and SARAL radar altimetry over rivers: a case study of the São Francisco River, Brazil. Remote Sens Environ 156:226–241. https://doi.org/10.1016/j.rse.2014.09.027
5. Sneeuw N et al (2014) Estimating runoff using hydro-geodetic approaches. Surv Geophys 35(6):1333–1359. https://doi.org/10.1007/s10712-014-9300-4
6. Santos da Silva J, Calmant S, Seyler F, Rotunno Filho OC, Cochonneau G, Mansur WJ (2010) Water levels in the Amazon basin derived from the ERS 2 and ENVISAT radar altimetry missions. Remote Sens Environ 114(10):2160–2181. https://doi.org/10.1016/j.rse.2010.04.020

7. Smith LC, Isacks BL, Bloom AL, Murray AB (1996) Estimation of discharge from three braided rivers using synthetic aperture radar satellite imagery: potential application to ungaged basins. Water Resour Res 32(7):2021–2034. https://doi.org/10.1029/96WR00752
8. Smith LC, Pavelsky TM (2008) Estimation of river discharge, propagation speed, and hydraulic geometry from space: Lena River, Siberia. Water Resour Res 44(3):1–11. https://doi.org/10.1029/2007WR006133
9. Gleason CJ, Durand MT (2020) Remote sensing of river discharge: a review and a framing for the discipline. Remote Sens 12(7):1–28. https://doi.org/10.3390/rs12071107
10. Anh DTL, Aires F (2019) River discharge estimation based on satellite water extent and topography: an application over the Amazon. J Hydrometeorol 20(9):1851–1866. https://doi.org/10.1175/JHM-D-18-0206.1
11. Aawar T, Khare D, Singh L (2019) Identification of the trend in precipitation and temperature over the Kabul River sub-basin: a case study of Afghanistan. Model Earth Syst Environ 5(4):1377–1394. https://doi.org/10.1007/s40808-019-00597-9
12. Submitted T (2001) Hydrological modelling for micro watersheds using swat model. 1648
13. Tarpanelli A, Amarnath G, Brocca L, Massari C, Moramarco T (2017) Discharge estimation and forecasting by MODIS and altimetry data in Niger-Benue River. Remote Sens Environ 195:96–106. https://doi.org/10.1016/j.rse.2017.04.015
14. Zhu L, Suomalainen J, Liu J, Hyyppä J, Kaartinen H, Haggren H (2018) A Review: remote sensing sensors. Multi-purposeful Appl Geospatial Data. https://doi.org/10.5772/intechopen.71049
15. Kebede MG et al (2020) Discharge estimates for ungauged rivers flowing over complex high-mountainous regions based solely on remote sensing-derived datasets. Remote Sens 12(7). https://doi.org/10.3390/rs12071064
16. Sichangi AW, Wang L, Hu Z (2018) Estimation of river discharge solely from remote-sensing derived data: an initial study over the Yangtze River. Remote Sens 10(9). https://doi.org/10.3390/rs10091385
17. Junqueira AM, Mao F, Mendes TSG, Simões SJC, Balestieri JAP, Hannah DM (2021) Estimation of river flow using CubeSats remote sensing. Sci Total Environ 788:147762. https://doi.org/10.1016/j.scitotenv.2021.147762
18. Tarpanelli A et al (2013) Toward the estimation of river discharge variations using MODIS data in ungauged basins. Remote Sens Environ 136:47–55. https://doi.org/10.1016/j.rse.2013.04.010
19. Alsdorf DE, Rodríguez E, Lettenmaier DP (2007) Measuring surface water from space. Rev Geophys 45(2):1–24. https://doi.org/10.1029/2006RG000197
20. Bjerklie DM, Moller D, Smith LC, Dingman SL (2005) Estimating discharge in rivers using remotely sensed hydraulic information. J Hydrol 309(1–4):191–209. https://doi.org/10.1016/j.jhydrol.2004.11.022
21. Kouraev AV, Zakharova EA, Samain O, Mognard NM, Cazenave A (2004) Ob' river discharge from TOPEX/Poseidon satellite altimetry (1992–2002). Remote Sens Environ 93(1–2):238–245. https://doi.org/10.1016/j.rse.2004.07.007
22. Durand M, Fu LL, Lettenmaier DP, Alsdorf DE, Rodriguez E, Esteban-Fernandez D (2010) The surface water and ocean topography mission: observing terrestrial surface water and oceanic submesoscale eddies. Proc IEEE 98(5):766–779. https://doi.org/10.1109/JPROC.2010.2043031
23. Pavelsky TM, Smith LC (2008) RivWidth: a software tool for the calculation of river widths from remotely sensed imagery. IEEE Geosci Remote Sens Lett 5(1):70–73. https://doi.org/10.1109/LGRS.2007.908305
24. Yoon Y, Durand M, Merry CJ, Clark EA, Andreadis KM, Alsdorf DE (2012) Estimating river bathymetry from data assimilation of synthetic SWOT measurements. J Hydrol 464–465(2012):363–375. https://doi.org/10.1016/j.jhydrol.2012.07.028
25. Domeneghetti A et al (2018) Characterizing water surface elevation under different flow conditions for the upcoming SWOT mission. J Hydrol 561(April):848–861. https://doi.org/10.1016/j.jhydrol.2018.04.046

26. Durand PIM, Development and comprehensive validation of SWOT river discharge algorithms from AirSWOT, simulator, and field measurements
27. Yang Y et al (2019) Enhancing SWOT discharge assimilation through spatiotemporal correlations. Remote Sens Environ 234(October). https://doi.org/10.1016/j.rse.2019.111450
28. Yoon Y, Garambois PA, Paiva RCD, Durand M, Roux H, Beighley E (2016) Improved error estimates of a discharge algorithm for remotely sensed river measurements: test cases on Sacramento and Garonne Rivers. Water Resour Res 52(1):278–294. https://doi.org/10.1002/2015WR017319
29. Domeneghetti A et al (2018) Characterizing water surface elevation under different flow conditions for the upcoming SWOT mission. J Hydrol 561:848–861. https://doi.org/10.1016/j.jhydrol.2018.04.046
30. Garambois P, Roux H, Monnier J (2015) Retrieving river discharge from SWOT-like data time-series : a sample of rivers types 17(0):15838
31. Oubanas H et al (2018) Discharge estimation in ungauged basins through variational data assimilation: the potential of the SWOT mission. Water Resour Res 54(3):2405–2423. https://doi.org/10.1002/2017WR021735
32. Biancamaria S, Lettenmaier DP, Pavelsky TM (2016) The SWOT mission and its capabilities for land hydrology. Surv Geophys 37(2):307–337. https://doi.org/10.1007/s10712-015-9346-y
33. Desai S (2018) Surface water and Ocean topography mission project science requirements document. Jet Propuls Lab
34. Elmer NJ, Hain C, Hossain F, Desroches D, Pottier C (2020) Generating proxy SWOT water surface elevations using WRF-hydro and the CNES SWOT hydrology simulator. Water Resour Res 56(8):1–31. https://doi.org/10.1029/2020WR027464
35. Biancamaria S et al (2017) Satellite radar altimetry water elevations performance over a 200 m wide river: evaluation over the garonne river. Adv Sp Res 59(1):128–146. https://doi.org/10.1016/j.asr.2016.10.008
36. Bonnema M, Hossain F (2019) Assessing the potential of the surface water and ocean topography mission for reservoir monitoring in the mekong river basin. Water Resour Res 55(1):444–461. https://doi.org/10.1029/2018WR023743
37. CWC (2014) Water year book 2012—2013-Tapi Basin
38. Altenau EH, Pavelsky TM, Durand MT, Yang X, de Frasson MRP, Bendezu L (2021) The surface water and Ocean topography (SWOT) Mission river database (SWORD): a global river network for satellite data products. Water Resour Res 57(7):1–15. https://doi.org/10.1029/2021WR030054
39. Leon JG et al (2006) Rating curves and estimation of average water depth at the upper Negro River based on satellite altimeter data and modeled discharges. J Hydrol 328(3–4):481–496. https://doi.org/10.1016/j.jhydrol.2005.12.006
40. Sichangi AW et al (2016) Estimating continental river basin discharges using multiple remote sensing data sets. Remote Sens Environ 179:36–53. https://doi.org/10.1016/j.rse.2016.03.019
41. Huang Q et al (2018) Discharge estimation in high-mountain regions with improved methods using multisource remote sensing: a case study of the upper Brahmaputra river. Remote Sens Environ 219(October):115–134. https://doi.org/10.1016/j.rse.2018.10.008
42. Leopold LB, Maddock TJ (1953) The hydraulic geometry of stream channels and some physiographic implications (USGS Numbered Series No. 252). Prof Pap U.S. Gov Print Off Washington, D.C., p 57, [Online]. Available: https://doi.org/10.3133/pp252

Intercomparison of the Performance of CHIRPS Satellite Rainfall Data and Gauge Gridded IMD Data for Hydrological Modelling

K. Gupta

Abstract Precipitation is one of the primary inputs governing the hydrology of the basins. The hydrological models developed for Indian region utilize multiple sources of precipitation data with varying degrees of uncertainties. In this study, the two widely used sources of precipitation data such as Climate Hazards Group InfraRed Precipitation with station data (CHIRPS) satellite rainfall data and gauge gridded Indian Meteorological Department (IMD) data have been used for hydrological modelling, and their performance has been compared in predicting the streamflow as compared to the observed streamflow data. Daily rainfall data over Payaswani River Basin for 30 years (1989–2018) has been used for analysis. The hydrological model is developed using DHI MIKE NAM (Nedbør—Afstrømnings-Model) model. Out of 30 years data, 20 years data is used for calibration, and 10 years data is used for validation. The performance of model can be evaluated using various performance indicators such as overall volume error, peak flow root mean square error (RMSE), low flow RMSE, and aggregate objective error. The results indicated that gauge gridded IMD data performed better than CHIRPS data for all indices except overall volume error.

Keywords Precipitation · Uncertainties · Hydrological model · CHIRPS · IMD

1 Introduction

The forecasting of streamflow is key to important decisions for hydrologist for planning water resources management for the basin as well as for carrying out any hydrodynamic studies. Although there are various hydrological models to study the rainfall runoff process, but the MIKE NAM model is quite popular amongst researchers as well as industry (Aredo et al. [1]).

K. Gupta (✉)
Sanskriti University, Mathura 281401, India
e-mail: karang.civil@sanskriti.edu.in

Department of Civil Engineering, Sanskriti University, Mathura, India

P. V. Timbadiya et al. (eds.), *Hydrology and Hydrologic Modelling*,
Lecture Notes in Civil Engineering 312,
https://doi.org/10.1007/978-981-19-9147-9_14

There have been various studies around the globe by usage of MIKE 11 NAM model for rainfall runoff modelling. Makungo et al. [2] applied MIKE 11 NAM model to obtain the runoff for the ungauged catchment in Nzhelele River, South Africa using regionalization of parameters and obtained best results. Aherwar and Aherwar [3] compared the modelling results of two models MIKE NAM and SCS-CN for rainfall runoff modelling in Shipra River basin in Madhya Pradesh, India and found the MIKE NAM model outperformed SCS-CN model. Sajadi et al. [4] also investigated the rainfall runoff modelling in Gonbad Catchment in Hamedan and obtained satisfactory results. Ghosh et al. [5] applied MIKE NAM rainfall runoff model in the lower Gangetic plain, West Bengal and obtained a promising result as compared to the observed data. Kumar et al. [6] examined the performance of MIKE NAM model for the simulating the streamflow for temperate catchment such as Jhelum catchment and obtained the NSE of 0.96 and R-squared value of 0.9 when compared with the observed data.

In all hydrological modelling studies, the precipitation data is the primary input for any hydrological model to forecast streamflow. There are various sources to obtain precipitation data in India such as ground-based rain gauge station data such as Indian Meteorological Department (IMD) gridded data as well as remote sensing-based sources such as Climate Hazards Group InfraRed Precipitation with station data (CHIRPS) and Tropical Rainfall Measuring Mission (TRMM). Intercomparison of various sources of precipitation data for obtaining accurate hydrological model would enable better judgement to the hydrological modeller. In past, few hydrological modelling studies have been carried out comparing various satellite products over different basins globally [7] and [8] and only few studies over Indian basins (Sulugodu & Dekas [9]; Shrannya et al. [10]).

Shrannya et al [10] compared TRMM and CHIRPS data for streamflow modelling for Gurupura Basin, Western Ghats and showed that TRMM performs better than CHIRPS data. Sulugodu & Dekas [9] compared the IMD gridded precipitation data and CHIRPS precipitation data over Nethravati River basin and found the CHIRPS data performs better as compared to IMD data. However, the performance of the various sources of satellite data may also vary based on the catchment characteristics. Therefore, present study compares the IMD and CHIRPS precipitation data over Payaswani River basin in Kerala and Karnataka using MIKE 21 NAM (Nedbør-Afstrømnings-Model) model.

2 Materials and Method

2.1 Study Area and Data Source

2.1.1 Payaswani River Basin

The origin of Payaswani river lies in Patti Ghat reserve forest which falls in the Coorg district of Karnataka at an altitude of about 1350 m above M.S.L. Payaswani river is a tributary to the Chandragiri. The length of river is 105 km. The river's catchment area is 1538 sq km. There is one CWC Hydrological Observation Station at Erinjipuzha. The study area is a subbasin in Payaswani River basin draining the water to Erinipuzha station on this river. The study area of Payaswani River subbasin is shown below in the index map as shown in Fig. 1.

2.1.2 Data Collection

The daily rainfall data was collected from CHIRPS database using Google Earth Engine for Erinjipuzha Basin as well as using IMD gridded ($0.25^0 \times 0.25^0$) database for a period of 30 years, and the daily discharge data for stream gauging site at Erinjipuzha CWC station was obtained from India WRIS Website. The Hargreaves formula was used to derive potential evapotranspiration using IMD temperature gridded data ($1^0 \times 1^0$).

2.2 MIKE NAM Model

The MIKE NAM (NedborAfstromnings Model) model is used in this study to simulate the hydrological process of rainfall runoff. This model is a lumped conceptual rainfall runoff model which is based on the consideration that the moisture content is stored in three mutually interrelated systems such as baseflow, interflow, and overland flow [11]. It considers each sub-catchment as one unit and therefore considers the average value of the parameters of the model as well as input and output variable over the entire catchment. The schematic showing its functioning is shown in Fig. 2.

2.3 Selection of Input Parameters

There are 9 parameters which needs to be calibrated whilst running the NAM model, and these 9 parameters represent the storage at surface, root zone, and ground water. These 9 parameters are described in the Table 1.

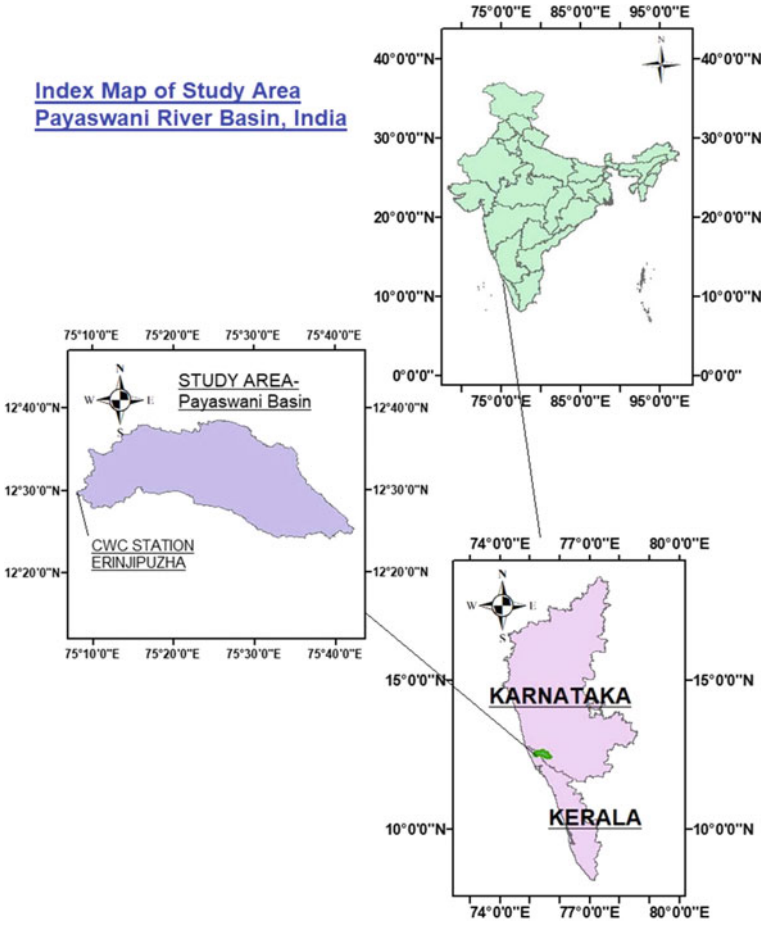

Fig. 1 Index map of study area

3 Results and Discussion

The calibration of hydrological model NAM was carried out for 20 years (1989–2008) using both CHIRPS and IMD data as shown in Fig. 3.

The calibration statistics obtained for each precipitation source is shown in Table 2. It can be observed that except overall water balance error (WBL), the IMD dataset shows lower error RMSE than CHIRPS dataset.

The calibrated model obtained using each of the dataset (IMD and CHIRPS) was used for validation for 10 years (2009–2018) with CWC station data at Erinjipuzha. The validation results are shown in Fig. 4.

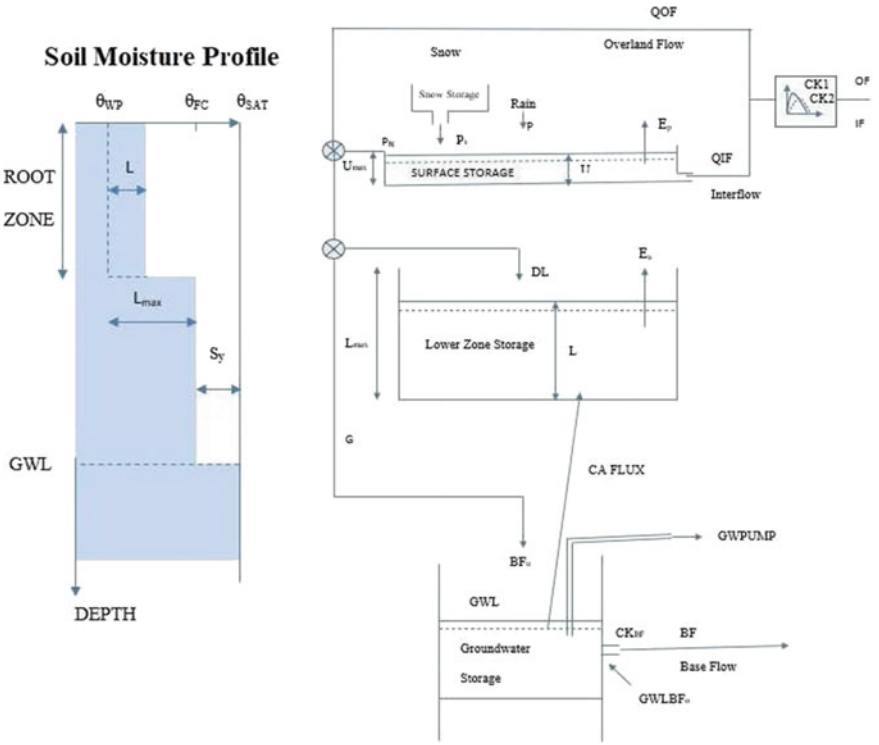

Fig. 2 Schematic of NAM model [11].

However, the Sulugodu & Dekas [9] showed that CHIRPS dataset performs better than IMD dataset in streamflow forecasting using hydrological model. The discrepancy in the behaviour of the dataset for the different river basins indicates that the performance of precipitation dataset in streamflow forecasting can be attributed to the nature of catchments.

4 Conclusions

The main conclusions derived from the present study are discussed below:

(i) The accuracy of hydrological model depends on the choice of precipitation dataset.
(ii) It has been observed that IMD gridded precipitation dataset ($0.25^0 \times 0.25^0$) yields lower RMSE error in peak flow, low flow as well as aggregate objective as compared to CHIRPS database for Payaswani River basin.
(iii) The performance of the precipitation datasets for streamflow forecasting depends on the nature of catchments.

Table 1 Different parameters of the NAM model

Parameter	Unit	Description	Effects
*U*max	mm	Maximum content of water in surface storage	1. Flow overland 2. Flow in infiltration 3. Losses in evapotranspiration 4. Flow in interflow
*L*max	mm	Maximum content of water in lower zone/root storage	1. Flow overland 2. Flow in infiltration 3. Losses in evapotranspiration 4. Flow in base flow
C_{OOF}		Coefficient for overland flow	1. Volume of flow on overland flow 2. Flow in infiltration
C_{KIF}	Hrs	Constant for interflow drainage	Surface storage drains as interflow
T_{OF}		Threshold of overland flow	Minimum soil moisture over which overland flow occurs
T_{IF}		Threshold of interflow flow	Minimum soil moisture over which interflow flow occurs
TG		Threshold of groundwater recharge	Minimum soil moisture over which groundwater recharge occurs
C_{K1}	Hrs	Overland flow's timing constant	It has effect on routing of overland flow along different slopes of catchments as well as channels
C_{K2}	Hrs	Interflow's timing constant	It is responsible to route interflow along various slopes of catchment
C_{KBF}	Hrs	Base flow's timing constant	It is responsible to route flow through linear groundwater recharge

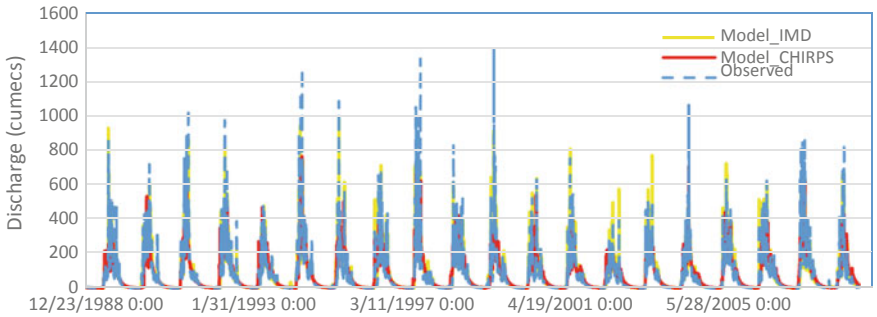

Fig. 3 Time series plot of observed and predicted discharge at Erinjipuzha CWC station (Calibration)

Table 2 Calibration statistics for IMD as well as CHIRPS datasets

Index	Rainfall_IMD	Rainfall_CHIRPS
Overall water balance error (WBL)	10.661	0.106
RMSE	46.053	80.432
Peak flow RMSE	46.053	80.432
Low flow RMSE	1.414	2.261
Aggregate objective	104.18	163.230

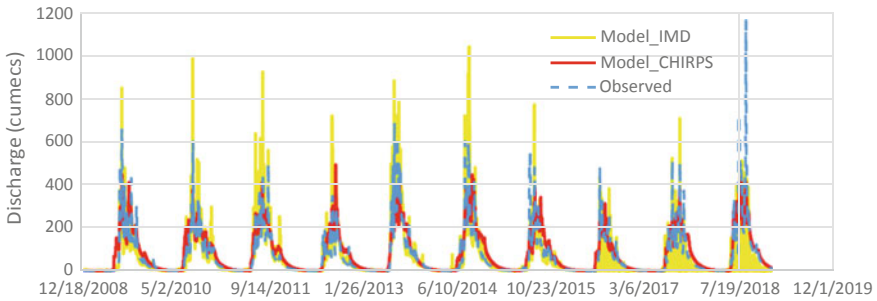

Fig. 4 Time series plot of observed and predicted discharge at Erinjipuzha CWC station (Validation)

The future studies in this direction may be carried out by considering the different types of catchments and the impact of the nature of catchment on the performance of the rainfall runoff model. Moreover, the intercomparison of more number of rainfall datasets can be carried out for the hydrological modelling.

Acknowledgements The author acknowledges Dr Ruchi Kalra, MD Hatch Marine Consultants for the guidance as well as funding support whilst preparing the manuscript.

References

1. Aredo MR, Hatiye SD, Pingale SM et al (2021) Modeling the rainfall-runoff using MIKE 11 NAM model in Shaya catchment, Ethiopia. Model Earth Syst Environ 7(4):2545–2551
2. Makungo R, Odiyo JO, Ndiritu JG, Mwaka B (2010) Rainfall–runoff modelling approach for ungauged catchments: A case study of Nzhelele River sub-quaternary catchment. Phys Chem Earth Parts A/B/C 35(13–14):596–607
3. Aherwar P, Aherwar H (2019) Comparison of rainfall runoff simulation by SCS-CN and NAM model in Shipra river basin of Madhya Pradesh India. J Pharmacogn Phytochem 8(4):3419–3427
4. Sajadi Bami Y, Porhemmat J, Sedghi H, Jalalkamali N (2020) Performance evaluation of mike nam rainfall-runoff (RR) model in daily flow simulation (Case Study: Gonbad Catchment in Hamedan). J Appl Eng Sci 10(1)

5. Ghosh A, Roy MB, Roy PK et al (2022) Evaluating the performance of MIKE NAM model on rainfall–runoff in lower Gangetic floodplain, West Bengal, India. Model Earth Syst Environ 1–17
6. Kumar R, Huda M, Maryam M, Lone MA (2022) Research Rainfall runoff modeling using MIKE 11 NAM of Jhelum river of Kashmir Valley India. Mausam 73(2):365–372
7. Tuo Y, Duan Z, Disse M, Chiogna G (2016) Evaluation of precipitation input for SWAT modeling in Alpine catchment: A case study in the Adige river basin (Italy). Sci Total Environ 573:66–82
8. Beck HE, Vergopolan N, Pan M, Levizzani V, Van Dijk AI, Weedon GP, Wood EF et al (2017) Global-scale evaluation of 22 precipitation datasets using gauge observations and hydrological modeling. Hydrol Earth Syst Sci 21(12):6201–6217
9. Sulugodu B, Deka PC (2019) Evaluating the performance of CHIRPS satellite rainfall data for streamflow forecasting. Water Resour Manage 33(11):3913–3927
10. Sharannya TM, Al-Ansari N, Deb Barma S, Mahesha A (2020) Evaluation of satellite precipitation products in simulating streamflow in a humid tropical catchment of India using a semi-distributed hydrological model. Water 12(9):2400
11. Danish Hydraulic Institute (DHI) (2003) Mike 11–A modeling system for rivers and channels, Reference manual

PMF Estimation for Extreme Events from PMP Atlas, a GIS, and Hydrologic Model-Based Case Study in Tehri Catchment

Mohit Jani, Praveen K. Thakur, Arpit Chouksey, S. P. Aggarwal, P. Chauhan, and Atul Singh

Abstract In the current generation due to climate change, many regions of the earth are facing extreme weather conditions. India also facing adverse effects like atypical floods and droughts due to climate change. Extreme floods are now a common phenomenon in lower Himalayan regions. Many cities and towns of the hills are adversely affected by these events. Central Water Commission (CWC) has published probable maximum precipitation (PMP) atlas for major river basins of India. In which, the current study is based on the PMP atlas for Ganga River Basin. CWC has provided the isohyetal maps of precipitation for various return periods and duration. It is difficult to have a specific precipitation estimation of any subbasin in this large river basin. So, the current study focuses on the precipitation value estimation of Tehri Subbasin of Ganga River. Isohyetal map of 24-h (1 day) duration and different return periods is used in this study. The hourly time distribution function is calculated from station wise rain spells. The catchment delineation is processed by taking Tehri Dam as an outlet. Each specific sub-watershed consists of a precipitation value. GIS tools are used to extract the precipitation value of each subbasin from the isohyetal map. The datasets were used to generate probable maximum flood (PMF) graphs

M. Jani (✉)
Department of Civil Engineering, Malaviya National Institute of Technology, Jaipur 302017, India
e-mail: mjani2197@gmail.com

P. K. Thakur · A. Chouksey · S. P. Aggarwal · P. Chauhan
Water Resources Department, Indian Institute of Remote Sensing, Dehradun 248001, India
e-mail: praveen@iirs.gov.in

A. Chouksey
e-mail: arpit@iirs.gov.in

S. P. Aggarwal
e-mail: spa@iirs.gov.in

P. Chauhan
e-mail: prakash@iirs.gov.in

A. Singh
Tehri Hydro Development Corporation Limited, Rishikesh 249201, India
e-mail: aksingh@thdc.co.in

P. V. Timbadiya et al. (eds.), *Hydrology and Hydrologic Modelling*,
Lecture Notes in Civil Engineering 312,
https://doi.org/10.1007/978-981-19-9147-9_15

from a calibrated hydrological model of the study area. The data validation has been done by performing hydrologic modeling of Tehri Catchment and comparing it with the designed PMF of Tehri Dam which is 15,500 cumec. The resulting hydrological model for the extreme event has generated 15,883 cumec of inflow at the Tehri Dam which showed quite similar results with the designed PMF of Tehri Dam. The results have shown that PMP atlas can be very useful to study the hydrological applications of extreme events.

Keywords Hydrologic modeling · GIS · PMP atlas · PMF · Tehri catchment

1 Introduction

Extreme precipitation is a common phenomenon in India nowdays. The Himalayan region also faces frequent and uneven amount of rain fall across the year. Town and villages in these regions face a constant threat of their lives and livestock. In the recent years, specially, the mountainous regions of Himalayas have faced extreme weather events. Durga Rao et al. [1] suggested for development of the flood forecast models to enhance the preparedness in these vulnerable regions. The main reason for the sudden catastrophe is flash flood which occurs in relatively very small time-period and wash out a significant amount of area [2].

India Meteorological Department has developed PMP atlas for various river basins for Indian subcontinent. The major aim is to get an idea of the various duration rainfalls ranging from 12-h to 72-h and return periods. Rakhecha and Clark [3] have used in situ maximization and storm transportation method to develop the PMP for one day duration for different locations in India. This duo went a step further and since rainfall data for the heaviest storms that occurred in different parts of India during the period 1880–1983, improved estimates of one-, two-, and three-day point PMP for India have been made by Clark and Rakhecha [4].

The PMP atlas have supported datasets in many research areas. One significant study by Dauji et al. [5] showed that the accuracy of rainfall time distribution curve for a costal site where they have taken Standard Projected Storm (SPS) dataset from the PMP atlas. Kavya et al. [6] also estimated the designed flood at the reservoir outlet based on the CWC-based PMP atlas. The studies like this have shown the applicability of the PMP atlas in various discipline.

2 Study Area and Methodology

2.1 Study Area

The present study is more focused in precipitation dataset generation from PMP atlas by CWC. In which, a calibrated hydrologic model is used to validate the datasets

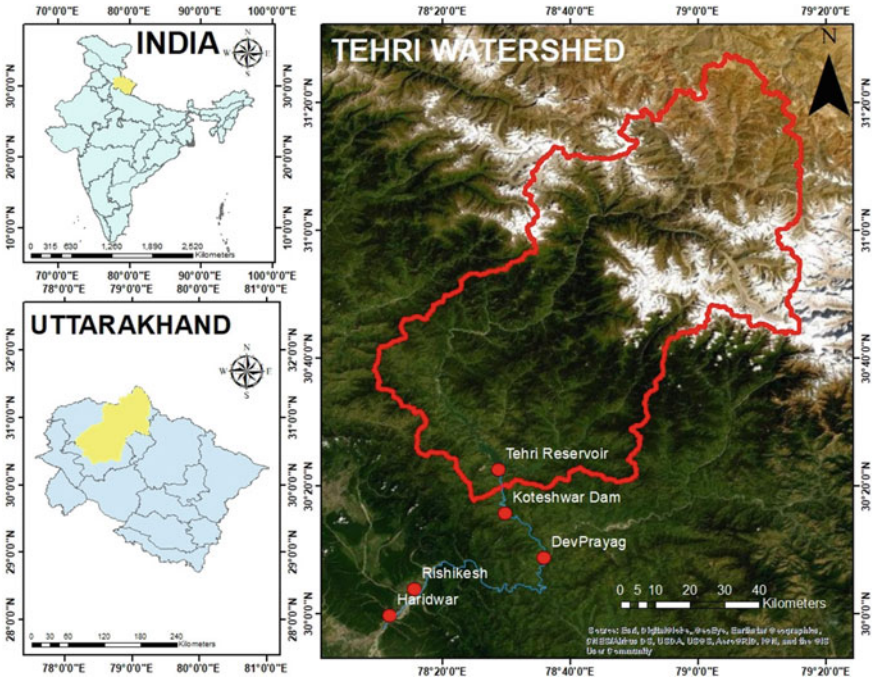

Fig. 1 Index map of study area

with the generated results. The following map shows the study area which is Tehri Basin. The basin is stretched in districts of Uttarakhand State (i) Tehri-Gharwal, (ii) Uttarkashi, and (iii) Rudraprayag. The study area consists of two rivers, named Bhagiratahi and Bhilangana, which later forms the Ganges River (Fig. 1).

2.2 Methodology

Probable maximum flood is the flood that may be expected from the severe combination of hydrological and meteorological parameters that are possible in a drainage area. Probable maximum precipitation (PMP) atlas for Ganga River Basin is used to get the PMF hydrographs for the study area. The Central Water Commission of India develops PMP atlas for Ganga Basin. There is a total of two reports which are divided into volume-I and volume-II. Volume-I, the main report, consists of the theory part of generating the PMP atlas, and the volume-II consists of the maps and tables of the PMP atlas. The study area lies in the catchment 401A (Fig. 2).

Based on the orography and location if the catchment, rainstorm, which can affect this zone, has been analyzed using the depth duration (DD). As per the report of volume-I from the records, 20 severe rainstorms were found that contribute to the

Fig. 2 Ganga river basin with catchment boundaries (PMP atlas Ganga basin Vol-II, page no. 19)

maximum average areal rainfall over this zone. Standard Projected Storm (SPS) obtained from the severe rainstorms and then adjusted with moisture maximization factors (MMF) to get PMP estimates.

Hershfield statistical method is used to generate the PMP maps for the Ganga River Basin [7] (Fig. 3).

The maximum 1-day rainfall values for every station are plotted for each return period on separate maps. Smooth isohyets of rainfall were then drawn at the appropriate interval to prepare generalized maps. The spatial distribution of the point values prepared for maximum rain of return periods of 5, 25, 100, 10,000 years. The following methodology was adopted in getting out the precipitation value from the PMP atlas (Fig. 4).

The PMP values have been calculated for the duration of 1-day. The most affecting factor to the peak discharge is the variability of the rainfall in time. The time distribution for the duration of 1-day is calculated from the station wise rain spells. This dataset is taken from PMP atlas (Fig. 5).

Based on this time distribution curve, the hourly precipitation values are derived or each watershed. There is total 52 number of watersheds present in the catchment. The total four isohyetal maps of return periods of 5, 25, 100, 10,000 years and 1-day duration are extracted and processed for the precipitation data. After the successful data extraction from the PMP atlas, the datasets then fed to the meteorologic model in the simulation software. Here, a calibrated hydrologic model is utilized to check

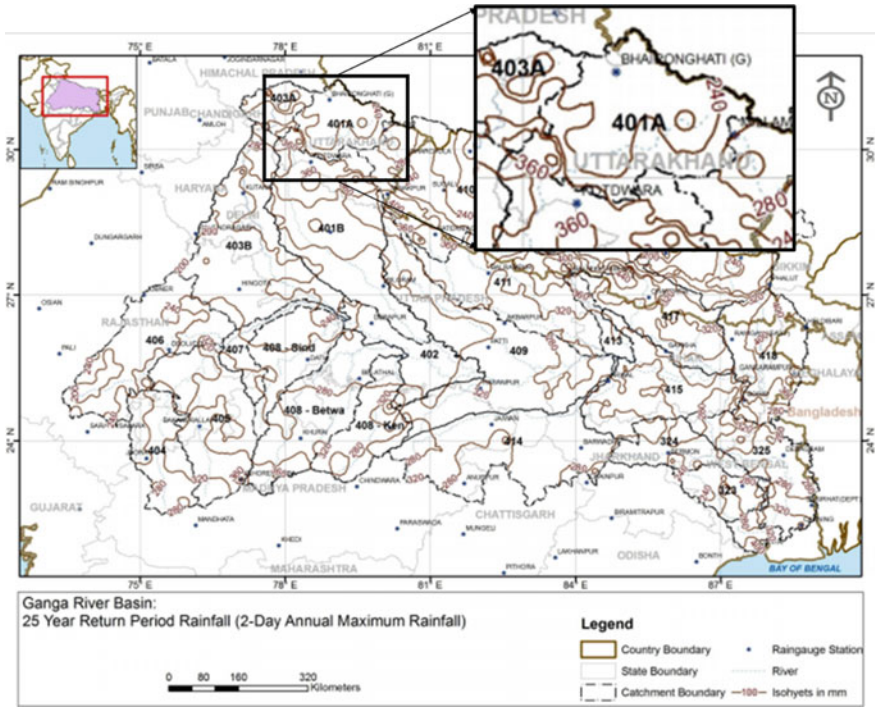

Fig. 3 1-day rainfall (mm) for a 25-year return period (PMP atlas Ganga Basin Vol-II, page no. 455)

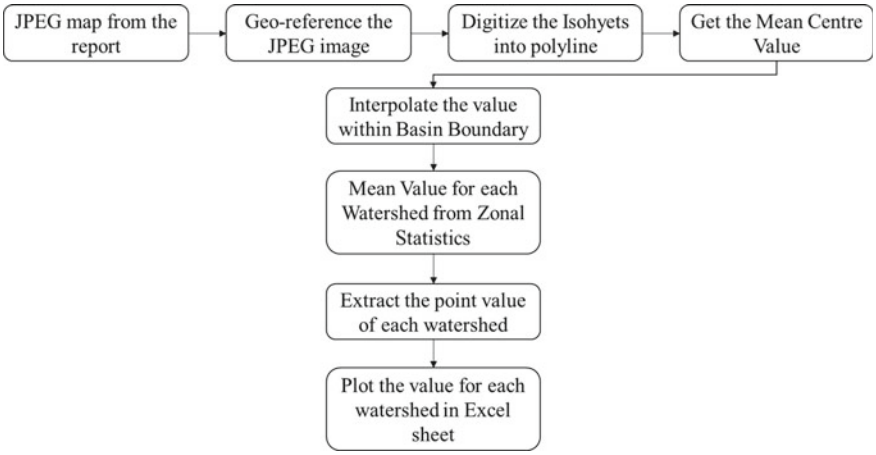

Fig. 4 Extracting the precipitation value from isohyet map

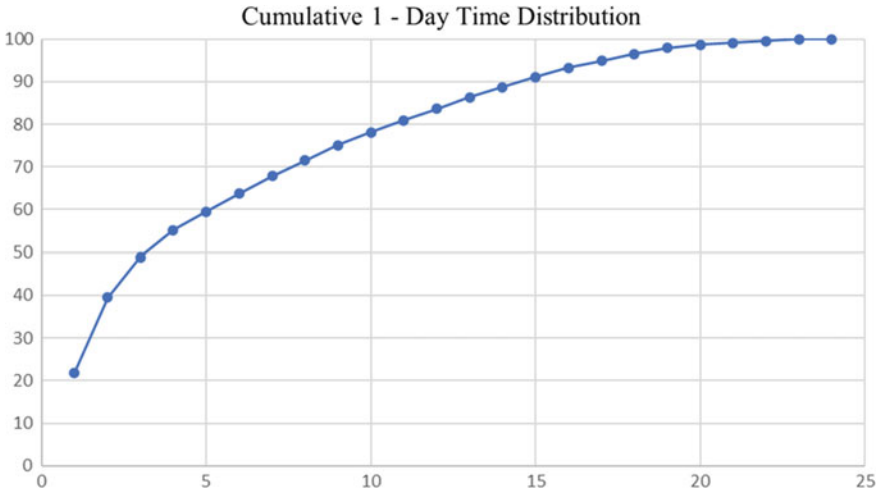

Fig. 5 1-day time duration (hours vs. %precipitation)

the scalability of the precipitation dataset. The hydrologic simulation was performed in HEC-HMS software. In which the simulation windows were taken as 48 h to get a smooth flood hydrograph (Fig. 6; Table 1).

The above table gives a brief description of the rainfall values in mm based on the time distribution graph. These values put into the meteorologic model, and the final simulation is calculated.

3 Results and Discussion

The following output was generated by performing hydrologic simulations for all four return periods (Table 2).

The following graphs represent the flood hydrographs and its peaks at various intervals. The maximum peak shown in the graph is of 10,000-year return period which is 15,883 m^3/s (Fig. 7).

Tehri Dam has designed PMF of 15,540 cumec and the maximum result we obtained for 10,000-year return period and 24-h duration also 15,833 cumec. This dataset shows the reliability of the given method for simulations on various return periods [8].

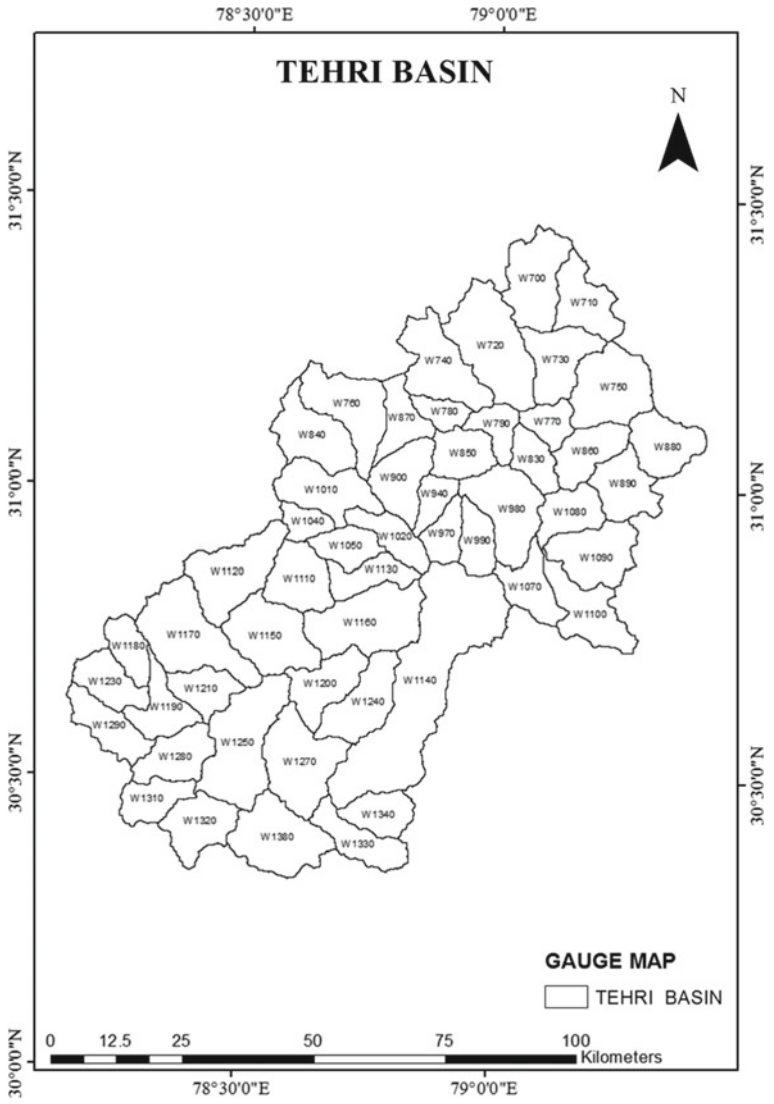

Fig. 6 Watershed in the Tehri Basin

4 Conclusions

Based on the preceding results, it shows that PMP atlas is a very convenient tool to generate precipitation datasets for event-based hydrological model and can be useful to estimate PMF hydrograph for small catchments.

Table 1 Time-series dataset for 1-day 25-year return period

Watersheds	Precipitation	Time Distribution																						
		21.9	17.6	9.4	6.3	43	42	4.1	3.7	3.6	3	2.8	2.7	Z7	2.4	2.4	Z1	1.7	16	1.4	0.8	0.4	0.4	0.4	0.1
W700	184	40.22	32.32	17.26	11.57	7.90	7.71	7.53	6.79	6.61	5.51	5.14	496	4.96	4.41	441	3.86	3.12	2.94	Z57	147	0.73	0.73	0.73	0.18
W710	180	39.51	31.75	16.96	11.37	7.76	7.58	7.40	6.68	6.50	5.41	5.05	4.87	4.87	4.33	4.33	3.79	3.07	2.89	Z53	1.44	0.72	0.72	0.72	0.18
W720	185	40.43	32.49	17.35	11.63	7.94	7.75	7.57	6.83	6.65	5.54	5.17	4.98	4.98	4.43	4.43	3.88	3.14	2.95	2.58	1.48	0.74	0.74	0.74	0.18
W730	180	39.44	31.70	16.93	11.35	7.74	7.56	7.38	6.66	6.48	5.40	5.04	4.86	4.86	4.32	432	3.78	3.06	2.88	Z52.	1.44	0.72	0.72	0.72	0.18
W740	188	4119	33.10	17.68	11.85	8.09	7.90	7.71	6.96	6.77	5.64	5.27	5.08	5.08	4.51	451	3.95	3.20	3.01	Z63	150	0.75	0.75	0.75	0.19
W750	175	38.52	30.96	16.53	11.08	7.56	7.39	7.21	6.51	6.33	5.28	4.93	4.75	4.75	4.22	4.22	3.69	2.99	2.81	Z46	141	0.70	0.70	0.70	0.18
W7G0	195	4Z72	34.33	18.34	12.29	8.39	8.19	8.00	7.22	7.02	5.85	5.46	5.27	5.27	4.68	4.68	4.10	3.32	3.12	Z73	1.56	0.78	0.78	0.78	0.20
W770	179	39.16	31.47	16.81	11.26	7.69	7.51	7.33	6.62	6.44	5.36	5.01	4.83	4.83	4.29	4.29	3.75	3.04	2.86	Z50	143	0.72	0.72	0.72	0.18
W780	188	41.10	33.03	17.64	11.82	8.07	7.88	7.69	6.94	6.76	5.63	5.25	5.07	5.07	4.50	4.50	3.94	3.19	3.00	Z63	150	0.75	0.75	0.75	0.19
W790	183	40.05	32.19	17.19	11.52	7.86	7.68	7.50	6.77	6.58	5.49	5.12	4.94	4.94	4.39	4.39	3.84	3.11	2.93	Z56	146	0.73	0.73	0.73	0.18
W830	179	39.21	31.51	16.83	11.28	7.70	7.52	7.34	6.63	6.45	5.37	5.01	4.83	4.83	4.30	4.30	3.76	3.04	2.86	Z51	143	0.72	0.72	0.72	0.18
W840	198	43.42	34.90	18.64	12.49	8.53	8.33	8,13	7.34	7.14	5.95	5.55	5.35	5.35	4.76	4.76	4.16	3.37	3.17	Z7S	1.59	0.79	0.79	0.79	0.20
W850	186	40.66	32.68	17.45	11.70	7.98	7.80	7.61	6.87	6.68	5.57	5.20	5.01	5.01	4.46	4.46	3.90	3.16	2.97	Z60	149	0.74	0.74	0.74	0.19
W860	175	38,31	30.79	16.44	11.02	7.52	7.35	7.17	6.47	6.30	5.25	4.90	4.72	4.72.	420	420	3.67	Z97	2.80	Z45	140	0.70	0.70	0.70	0.17
W870	191	41.85	33.63	17.96	12.04	8.22	8.03	7.83	7.07	6.88	5.73	5.35	5.16	5.16	4.59	4.59	4.01	3.25	3.06	Z68	153	0.76	0.76	0.76	0.19
W880	170	37.29	29.97	16.01	10.73	7.32	7.15	6.98	6.30	6.13	5.11	4.77	4.60	4.60	4.09	4.09	3.58	Z89	2.72.	2.38	1.36	0.68	0.68	0.68	0.17
W890	171	37.37	30.03	16.04	10.75	7.34	7.17	7.00	6.31	6.14	5.12	4.78	4.61	4.61	410	410	3.58	Z90	2.73	2.39	137	0.68	0.68	0.68	0.17
W900	191	4191	33.68	17.99	12.06	8.23	8.04	7.85	7.08	6.89	5.74	5.36	5.17	5.17	459	4.59	4.02	3.25	3.06	Z68	153	0.77	0.77	0.77	0.19
W940	189	41.29	33.18	17.72	11.88	8.11	7.92	7.73	6.98	6.79	5.66	5.28	5.09	5.09	4.52	4.52	3.96	3.20	3.02	Z64	1.51	0.75	0.75	0.75	0.19
W970	188	41.10	33.03	17.64	11.82	8.07	7.88	7.69	6.94	6.76	5.63	5.26	5.07	5.07	450	450	3.94	3.19	3.00	Z63	150	0.75	0.75	0.75	0.19

(continued)

Table 1 (continued)

Watersheds	Precipitation	Time Distribution																							
		21.9	17.6	9.4	6.3	43	42	4.1	3.7	3.6	3	2.8	2.7	Z7	2.4	2.4	Z1	1.7	16	1.4	0.8	0.4	0.4	0.4	0.1
W980	181	39.61	31.83	17.00	11.39	7.78	7.60	7.42	6.69	6.51	5.43	5.06	4.88	4.88	434	4.34	3.80	3.07	2.89	Z53	1.45	0.72	0.72	0.72	0.18
W990	184	40.32	32.40	17.30	11.60	7.92	7.73	7.55	6.81	6.63	5.52	5.15	4.97	4.97	4.42	442	3.87	3.13	2.95	Z5S	147	0.74	0.74	0.74	0.18
W1010	199	43.49	34.95	18.67	12.51	8.54	8.34	8,14	7.35	7.15	5.96	5.56	5.36	5.36	4.77	4.77	4.17	3.38	3.18	2.78	1.59	0.79	0.79	0.79	0.20
W1020	193	42.36	34.04	18.18	12.19	8.32	8.12	7.93	7.16	6.96	5.80	5.42	5.22	5.22	4.64	4.64	4.06	3.29	3.09	2.71	1.55	0.77	0.77	0.77	0.19
WlOW	202	4413	35.47	18.94	12.70	8.67	8.46	8,26	7.46	7.25	6.05	5.64	5.44	5.44	4.84	4.84	4.23	3.43	3.22.	Z82	161	0.81	0.81	0.81	0.20
W1050	198	43.46	34.93	18.65	12.50	8.53	8.33	8,14	7.34	7.14	5.95	5.56	5.36	5.36	4.76	4.76	4.17	3.37	3.18	Z78	159	0.79	0.79	0.79	0.20
W1070	177	38.86	31.23	16.68	11.18	7.63	7.45	7.28	6.57	6.39	5.32	4.97	4.79	4.79	4.26	4.26	3.73	3.02	2.84	2.48	1.42	0.71	0.71	0.71	0.18
W1080	174	38,21	30.71	16.40	10.99	7.50	7.33	7.15	6.46	6.28	5.23	4.89	4.71	4.71	4.19	4.19	3.66	2.97	2.79	2.44	140	0.70	0.70	0.70	0.17
W1090	171	37.39	30.05	16.05	10.76	7.34	7.17	7.00	6.32	6.15	5.12	4.78	4.61	4.61	4.10	4.10	3.59	Z90	2.73	Z39	137	0.68	0.68	0.68	0.17
WllOO	170	37.24	29.93	15.99	10.71	7.31	7.14	6.97	6.29	6.12	5.10	4.76	4.59	4.59	4.08	4.08	3.57	Z89	2.72.	2.38	1.36	0.68	0.68	0.68	0.17
W1110	205	44.80	36.00	19.23	12.89	8.80	8.59	8,39	*151*	7.36	6.14	5.73	5.52	552.	4.91	4.91	4.30	3.48	3.27	2.86	164	0.82	0.82	0.82	0.20
W1120	210	45.90	36.89	19.70	13.20	9.01	8.80	8,59	7.75	7.54	6.29	5.87	5.66	5.66	5.03	5.03	4.40	3.56	3.35	Z93	168	0.84	0.84	0.84	0.21
W1130	197	43.18	34.70	18.53	12.42	8.48	8.28	8.08	7.30	7.10	5.92	5.52	5.32	5.32	4.73	4.73	4.14	3.35	3.15	Z76	158	0.79	0.79	0.79	0.20
W1140	197	43.15	34.68	18.52	12.41	8.47	8.28	8.08	7.29	7.09	5.91	5.52	5.32	5.32.	4.73	4.73	4.14	3.35	3.15	Z76	158	0.79	0.79	0.79	0.20
W1150	211	46,12	37.07	19.80	13.27	9.06	8.85	8,63	7.79	7.58	6.32.	5.90	5.69	5.69	5.05	5.05	4.42	3.58	3.37	Z95	168	0.84	0.84	0.84	0.21
W1160	199	43.68	35.11	18.75	12.57	8.58	8.38	8.18	7.38	7.18	5.98	5.59	5.39	5.39	4.79	4.79	4.19	3.39	3.19	2.79	160	0.80	0.80	0.80	0.20
W1170	217	47.42	38.11	20.35	13.64	9.31	9.09	8.88	8.01	7.79	6.50	6.06	5.85	555	5.20	5.20	4.55	3.68	3.46	3.03	173	0.87	0.87	0.87	0.22
W1180	221	48.33	38.84	20.75	13.90	9.49	9.27	9.05	8.17	7.95	6.62	6.18	5.96	5.96	5.30	5.30	4.63	3.75	3.53	3.09	177	0.88	0.88	0.88	0.22
W1190	224	48,97	39.36	21.02	14.09	9.62	9.39	9.17	8.27	8.05	6.71	6.26	6.04	6.04	5.37	5.37	4.70	3.80	3.58	3.13	179	0.89	0.89	0.89	0.22

(continued)

Table 1 (continued)

Watersheds	Precipitation	Time Distribution																							
		21.9	17.6	9.4	6.3	43	42	4.1	3.7	3.6	3	2.8	2.7	Z7	2.4	2.4	Z1	1.7	16	1.4	0.8	0.4	0.4	0.4	0.1
W1200	209	45.73	36.75	19.63	13.16	8.98	8.77	8.56	7.73	7.52	6.26	5.85	5.64	5.64	5.01	5.01	4.39	3.55	3.34	2.92	1.67	0.84	0.84	0.84	0.21
W1210	220	48,12	38.67	20.65	13.84	9.45	9.23	9.01	8.13	7.91	6.59	6.15	5.93	5.93	5.27	5.27	4.61	3.74	3.52	3.08	1.76	0.88	0.88	0.88	0.22
W1230	224	49.00	39.38	21.03	14.10	9.62	9.40	9.17	8.28	8.05	6.71	6.26	6.04	6.04	5.37	5.37	4.70	3.80	3.58	3.13	179	0.89	0.89	0.89	0.22
W1240	206	45.07	36.22	19.35	12.97	8.85	8.64	8.44	7.61	7.41	6.17	5.76	5.56	5.56	4.94	4.94	4.32	3.50	3.29	Z88	1.65	0.82	0.82	0.82	0.21
W1250	222	48.63	39.08	20.87	13.99	9.55	9.33	9.10	8.22	7.99	6.66	6.22	6.00	6.00	5.33	5.33	4.66	3.78	3.55	3.11	1.78	0.89	0.89	0.89	0.22
W1270	219	47.99	38.56	20.60	13.80	9.42	9.20	8.98	8.11	7.89	6.57	6.14	5.92	5.92	5.26	5.26	4.60	3.72	3.51	3.07	175	0.88	0.88	0.88	0.22
W1280	227	49.74	39.97	21.35	14.31	9.77	9.54	9.31	8.40	8.18	6.81	6.36	6.13	6.13	5.45	5.45	4.77	3.86	3.63	3.18	182	0.91	0.91	0.91	0.23
W1290	227	49.74	39.98	21.35	14.31	9.77	9.54	9.31	8.40	a 18	6.81	6.36	6.13	6.13	5.45	5.45	4.77	3.86	3.63	3.18	182	0.91	0.91	0.91	0.23
W1310	232	50.82	40.84	21.81	14.62	9.98	9.75	9.51	8.59	a35	6.96	6.50	6.27	6.27	5.57	5.57	4.87	3.95	3.71	3.25	186	0.93	0.93	0.93	0.23
W1320	233	51.08	41.05	21.92	14.69	10.03	9.80	9.56	8.63	a40	7.00	6.53	6.30	6.30	5.60	5.60	4.90	3.96	3.73	3.27	1.87	0.93	0.93	0.93	0.23
W1330	222	48.60	39.05	20.86	13.98	9.54	9.32	9.10	8.21	7.99	6.66	6.21	5.99	5.99	5.33	5.33	4.66	3.77	3.55	3.11	178	0.89	0.89	0.89	0.22
W1340	215	47.16	37.90	20.24	13.57	9.26	9.04	8.83	7.97	7.75	6.46	6.03	5.81	5.81	5.17	5.17	4.52	3.66	3.45	3.01	1.72	0.86	0.86	0.86	0.22
W1380	230	50.41	40.51	21.64	14.50	9.90	9.67	9.44	8.52	8.29	6.91	6.44	6.21	6.21	5.52	5.52.	4.83	3.91	3.68	3.22.	1.84	0.92	0.92	0.92	0.23

Table 2 Flow output at various return periods

Time	Flow output (m^3/s)			
(Hrs)	5	25	100	10,000
0	520	520	520	520
1	520	520	520	520
2	520	520	520	520
3	520	520	520	557
4	520	520	520	715
5	520	520	520	1058
6	520	520	521	1950
7	520	520	524	4311
8	520	520	546	7674
9	520	520	637	10,430
10	520	521	915	12,506
11	520	524	1428	14,050
12	520	535	1993	15,020
13	520	569	2443	15,571
14	520	644	2786	15,809
15	520	773	3054	15,883
16	520	943	3272	15,822
17	520	1112	3460	15,621
18	520	1255	3616	15,240
19	520	1372	3729	14,655
20	520	1466	3782	13,885
21	520	1529	3757	12,901
22	520	1555	3646	11,696
23	521	1548	3460	10,340
24	521	1510	3211	8969
25	522	1442	2914	7667
26	523	1346	2596	6461
27	525	1238	2285	5381
28	526	1129	1998	4448
29	526	1028	1742	3664
30	526	936	1516	3021
31	525	855	1323	2504
32	524	785	1161	2093
33	523	727	1028	1770
34	522	679	920	1516

(continued)

Table 2 (continued)

Time	Flow output (m^3/s)			
(Hrs)	5	25	100	10,000
35	521	640	834	1317
36	520	611	766	1159
37	520	589	714	1033
38	520	573	675	935
39	520	563	646	864
40	520	556	624	817
41	520	550	609	793
42	520	546	598	784
43	520	543	593	785
44	520	540	593	794
45	520	541	599	796
46	520	545	607	779
47	520	552	612	757
48	520	558	613	738
Peak Flow	526	1555	3782	15,883

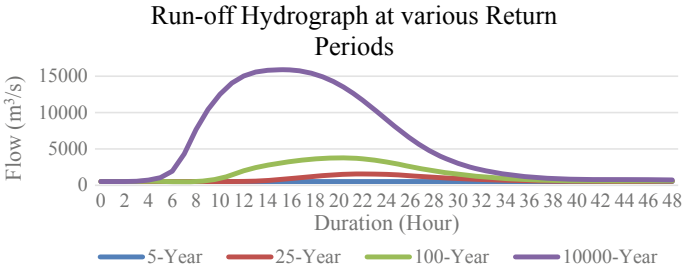

Fig. 7 Runoff hydrographs at various return periods

Acknowledgements The authors acknowledge the financial support received from Indian Institute of Remote Sensing, (IIRS-ISRO) to carry out present work. The authors are also thankful to India Meteorological Department (IMD), Central Water Commission (CWC), and Tehri Hydro Development Corporation (THDC) for providing necessary data to conduct the present study.

References

1. Durga Rao KHV, Venkateshwar Rao V, Dadhwal VK, Diwakar PG (2014) Kedarnath flash floods: a hydrological and hydraulic simulation study. Current Sci
2. Bisht S, Chaudhry S, Sharma S, Soni S (2018) Assessment of flash flood vulnerability zonation through geospatial technique in high altitude Himalayan watershed, Himachal Pradesh India. Remote Sens Appl Soc Environ 12:35–47
3. Rakhecha PR, Clark C (1999) Revised estimates of one-day probable maximum precipitation (PMP) for India. Meteorol Appl 6(4):343–350
4. Clark Rakhecha CPR (2002) Areal PMP distribution of one-day to three-day duration over India. Meteorol Appl J Forecasting Pract Appl Practical Tech Model 9(4):399–406
5. Dauji S, Srivastava PK (2021) Accuracy of rainfall time distribution curves in literature for a coastal site near Mumbai, India. Earth Sci India 14(1)
6. Kavya BM, Kishan S, Arun M, Surendra HJ, Narandra BK (2020) Estimation of design flood at a reservior (outlet) by CWC based hydrometeriological approach. In: AIP conference proceedings, vol 2204, No. 1. AIP Publishing LLC, p 020010
7. Hershfield DM (1965) Method for estimating probable maximum rainfall. J Am Water Works Ass 57(8):965–972
8. Mann PPS, Vishnoi RK, Govil R (2007) Evolution of spillway scheme for Tehri project. Water Energy Int 64(1):227–236

A Review: Contribution of HEC-HMS Model

Mukul Kumar Sahu, H. R. Shwetha, and G. S. Dwarakish

Abstract The rapid increase of population worldwide, urbanization, and industrialization significantly impact hydrologic processes locally and globally. Thus, development planning and managing various water resources are required to meet multiple water demands. However, acquiring gauge discharge data has always been difficult since measurements cannot be taken at every point along the river. Thus, HEC-HMS (Hydrologic Modeling System) is the hydrological model that can transform rainfall into a runoff by using known parameters, data, and appropriate mathematical equations to simulate flow records at the desired location. HEC-HMS was developed by the USACE and is freely accessible. It can estimate runoff from rainfall. In this paper, we review the studies carried out by researchers on the HEC-HMS model worldwide to ascertain its ability to simulate runoff with accuracy and use for making decisions. It could be seen that many researchers compared different modelling methods to obtain the best model suitable under different hydrological conditions and found HEC-HMS as a good model over others and recommended it for simulation of runoff. The reviews show that the HEC-HMS rainfall-runoff model has many flood modelling and water resource planning and management applications. In most studies, HEC-HMS rainfall-runoff modelling was found to be efficient and dependable in predicting runoff accuracy in various river basins. As a result, the model can simulate runoff in an ungauged basin for water resource planning, development, management, and decision-making.

Keywords HEC-HMS · Rainfall-Runoff Modelling · Simulation Model

M. K. Sahu (✉) · H. R. Shwetha · G. S. Dwarakish
Department of Water Resources and Ocean Engineering, National Institute of Technology Karnataka, Surathkal 575025, India
e-mail: mukulkumarsahu.207wo010@nitk.edu.in

H. R. Shwetha
e-mail: hrshwetha@nitk.edu.in

G. S. Dwarakish
e-mail: dwaraki@nitk.edu.in

P. V. Timbadiya et al. (eds.), *Hydrology and Hydrologic Modelling*,
Lecture Notes in Civil Engineering 312,
https://doi.org/10.1007/978-981-19-9147-9_16

1 Introduction

Watershed models are required for proper assessment, development, and management of water resources. Computer simulation of rainfall-runoff began in early 1960 [5]. However, calculating runoff from an ungauged or poorly gauged watershed is problematic in developing nations like India. Hydrologic models help us in better understanding hydrological phenomenon occurring in the watershed. There are several components of the hydrologic cycle like surface runoff, infiltration, evaporation, sub-surface flow, depression storage, and baseflow. Integration of various hydrological processes helps in the management of water resources and also in the design of the hydraulic structure. The hydrological processes depend on rainfall patterns and land use land cover of the basin and vary in spatial and temporal scales.

To simulate the various hydrological process of the basin, the development of the model came into existence in, 1992 [30]. In 1967, Leo R Beard and other Hydrological Engineers Circle staff members, with the US Army Corps of Engineers, developed a mathematical watershed model HEC-1 to simulate the flood hydrograph. HEC-1 was upgraded to increase its capabilities [31]. The initial release of HEC-HMS was known as version 1.0, and it included all the features of HEC-1 with minor improvements. The second release, version 2.0, introduced the Soil Moisture Accounting (SMA) approach, which expanded the programme's capabilities from event-based simulation to continuous simulation. The third major update, version 3.0, introduced a new graphical interface to develop potential and snowmelt evapotranspiration methods. In addition, some new infiltration representation approaches were introduced in the model. The fourth, version 4.0, adds sediment movement, and surface erosion to the computation is an important update. After the fourth version, 4.0 of HEC-HMS, the 4.1 series of performances started, and HEC-HMS 4.9 is the latest version of the HEC-HMS programme and had the advantage that it does not overwrite the observed stage data with observed flow data as it done in its previous version 4.8.

HEC-HMS is made up of four primary parts as follows. (a) An analytical model for calculating runoff and channel routing from overland flows, (b) an innovative graphical user interface with interactive elements for demonstrating hydrological system components, (c) massive time-variable datasets require a framework for storing and managing them, and (d) a standard for showing and reporting model output in rainfall-runoff simulations. Many alternatives are available in HEC-HMS, such as the basin model, which consists of three processes: loss, transform, and base flow. Runoff prediction and its response at the outlet are very challenging in hydrology. In any watershed modelling, its calibration and validation require many spatial and temporal data. There is a great challenge to assure modelling quality due to the non-availability of high-resolution data utilized in the model's development, calibration, and validation. So, choosing a model that requires minimum input data is structured and highly precise for the present scenario. HEC-HMS is one of those models that require less data. Rainfall-runoff modelling can be done on an event-by-event basis or on a continuous basis. It can be utilized in both lumped and distributed parameter-based modelling scenarios. It can be used to investigate urban flooding, flood frequency,

flood warning systems, reservoir spillway capacity, and stream restoration, amongst other things. This paper summarizes the literature reviews of the HEC-HMS model to depict rainfall-runoff dynamics in basins.

2 Overview of Reviewed Papers

The papers published across different journals from 1971 to 2021 were reviewed in this study. The areas of reviewed watersheds simulated using the HEC-HMS model were mainly between 100–5000 km^2. The paper reviewed was fifty.

The performance of HEC-HMS model outputs was assessed using several indices such as Nash–Sutcliffe Efficiency (NSE), Pearson's Correlation Coefficient (R), Root Mean Square Error (RMSE), and Coefficient of Determination (R^2). These were the most commonly used indices. Index of Agreement (IA), Relative Volume Error (RVE), Relative bias (r bias), Volume Ratio (VR), and Index of Volumetric Fit (IVF) were least used.

The data required for the river basin modelling is divided into three groups, (i) basin information like the channel or the river's topography, (ii) hydro-meteorological data, and (iii) data on flow rates and stages over time for model calibration and validation. These are used to establish model input and output boundary conditions. Recent advancements in remote sensing have enabled the acquisition of some of this data. Satellites and airborne remote sensing allow for the collection of spatially scattered data across broad areas and eliminate the need for expensive ground surveys. On the other hand, ground measurements are essential for validating satellite products. More and more geospatial datasets linked to hydrology such as topography, soil, and land use have become available through numerous open sources due to advancements in remote sensing in recent decades.

The review was broadly categorized into two summary sections, based on the applications of the HEC-HMS model: (i) streamflow simulation, (ii) flood modelling.

3 Application of HEC-HMS Model

3.1 Application for Streamflow Simulation

At various regional and national scales, research on water resources concentrated on extreme weather events (floods and droughts), rainfall-runoff models, streamflow modelling, and agriculture water ungauged basins. The HEC-HMS model was considered as adequately capable of simulating stream flows in ungauged basins [14] and to analyze runoff processes for the development and management of water resources [6, 16, 26, 28].

In several river basins, the HEC-HMS model was employed in this research to understand hydrological processes better. Models are categorized based on how the representation of catchment processes (deterministic or stochastic), and how the catchment is spatially detached (lumped or distributed). The continuity, momentum, and data-driven techniques have been used to build routing models that estimate wave propagation along a river channel [27].

The Hydrologic Modeling System (HEC-HMS) is intended to simulate the precipitation runoff process of the dendritic watershed system. The system incorporates traditional hydrologic processes such as unit hydrographs, infiltration, hydrologic routing, and procedures for continuous simulation such as snowmelt, evapotranspiration, and soil moisture accounting.

Before developing HEC-HMS software, the researchers used Geographic Information Systems (GIS) with HEC-1 software. GIS handles the datasets (raster or grid-based data, triangular irregular networks, vector, or contour-based line networks) used in hydrologic modelling. Grid cell or raster storage of information was used in the initial GIS applications in hydrologic modelling [24]. In other cases, infiltration, interflow, and overland flow processes in a sub-basin were regarded as discrete contributing processes. As a result, the processes in difficult terrain are physically considered as simple plane processes that happen on their own. The Soil Conservation Service Curve Numbers (SCS-CN) were created by evaluating small, reasonably uniform attribute watersheds, with the assumption of continuous rainfall [9]. After the release of HEC-HMS software, the researchers in their studies had used different methods to simulate the rainfall-runoff process using the soil conservation service curve number method and SCS-UH (Unit Hydrograph) to convert precipitation excess into direct runoff [3, 6, 18]. Hamdan et al. [16] developed a hydrological model combining HEC-HMS, the Geospatial Hydrologic modeling Extension (HEC-GeoHMS), and Geographical Information Systems to simulate the rainfall-runoff process over the Al Adaim river basin and embankment dam in Iraq (GIS). The SCS-CN method was used to calculate loss parameters, the SCS-UH for runoff transformation, and the Muskingum method for routing purposes. For the embankment dam, reservoir modelling was done. Both actual and simulated hydrographs were found to be strongly related, according to the findings. The dam's discharge was successfully simulated for the period under consideration but slightly overstated.

Combining the fine-scale event and coarse-scale continuous hydrologic modelling systems for Mona Lake watershed, West Michigan, Chu et al. [8] developed a strategy. The SCS-CN and Soil Moisture Accounting (SMA) methods were used as a loss model for the event and continuous hydrologic modelling. The Clark-UH (Unit Hydrograph) for excess precipitation into direct hydrographs and the Watershed Modelling System (WMS) model developed basin model. For continuous modelling, they had used the parameters of event modelling. Took five-minute time steps for event-based modelling, and hourly time steps were taken for continuous hourly modelling. The results of their model imply that fine-scale (5 min time step) event hydrologic modelling, aided by extensive field data, aids coarse-scale (hourly time step) continuous modelling. De Silva et al. [11] also developed an event-based and continuous hydrological model for the Kelani river basin, Sri Lanka. The

study considered the Green and Ampt loss methods in event-based modelling and a five-layer SMA method for continuous modelling. The Clark-UH and the recession base flow method simulated direct runoff. Extremely high precipitation events in November 2005 were utilized to calibrate model parameters, and extremely high rainfall events were used to test the event model in April–May 2008, May–June 2008, and May 2010. Their results also concluded that event-based hydrologic modelling supported with intensive field data helps to improve continuous modelling.

Majidi et al. [22] utilized the HEC-HMS software version 3.4 to simulate the rainfall-runoff mechanism in the Abnama watershed in southern Iran. The Green-Ampt method for loss estimation, SCS Unit Hydrograph for transforming excess rainfall into the direct runoff, and Muskingum method for routing purposes. Considered five rainstorm events for the rainfall-runoff simulation and initially found that their results were not up to the requirement. So, they had used the optimization method for calibration, and sensitivity analysis was carried out. After that, the correlation between the observed and simulated discharges indicated a good match and revealed that lag time was a susceptible component. Alhan et al. [20] developed the hydrological model to simulate an event that occurred over the Ayamama watershed, Istanbul, Turkey, on September 9, 2009. The methods used in basin modelling were the Green-Ampt method for infiltration loss, the Clark-UH method, and Kinematic wave routing. The Rational method was used to compare the outcomes (WMS). It was emphasized that the HEC-HMS model outperformed the Rational method.

3.2 Application for Flood Modelling

Flood modelling is essential to understand the possible impacts of floods of a given magnitude and initiate on the ground efforts to mitigate the effect. Progress in hydrodynamic modelling (HEC-HMS) during the last decade has led to considerable improvement to simulate flooding scenarios [27]. Changes in land use in a basin affect hydrological processes on various temporal and spatial dimensions. It can influence the frequency and intensity of floods by affecting runoff generation and flow patterns by changing hydrological parameters as interception, infiltration, and evaporation. At a watershed size, such affects on hydrological processes will have a considerable impact on the ecology, environment, and local economy. Therefore, it is critical to understand and assess the impacts of land use change on the watershed hydrologic process for anticipating flood potential and hazard reduction. These have become a crucial concern for watershed planning, management, and long-term development [7, 10, 32, 33].

The integrated GIS module, Watershed Modelling System (WMS), Hydrological Modeling System (HEC-HMS), and River Analysis System (HEC-RAS) models have been utilized in flood mapping and modelling [1, 2, 15, 21, 23, 25, 29]. GIS components handle DEM processing and morphometric analysis, as well as producing inputs for the WMS programme. The WMS is in charge of delineations and model

scenarios that are used as digital input data for the HEC-HMS. The hydrologic equations that manage the interactions between rainfall and runoff are controlled by the HEC-HMS, which generates hydrographs for various scenarios and rainfall return times. The HEC-RAS deals with hydraulic equations to calculate depth of flow and flood area and helps develop flood plains. Pistocchi and Mazzoli [25] performed their study on Romagna river basins; Knebel et al. [21] developed the San Antonio river basin framework. Gul et al. [15] introduced a combined hydrologic and hydraulic modelling approach for the Bostanli river basin in Izmir, Turkey, for testing the efficiency of structural flood control measures. Thakur et al. [29] developed the hydrologic model and flood plain for Copper Slough Watershed (CSW), Champaign. Abdelkarim et al. [1] evaluated the impact of flash flood hazards on the Tabuk City, Kingdom of Saudi Arabia (KSA). Abdessamed and Abderrazak [2] studied the inundation behaviour during extreme flood events by considering concrete retaining walls developed by local authorities and without it for the Ain Sefra watershed in the southwest of Algeria. Niyazi et al. [23] evaluated the hydrological characteristics and mapped the flood-prone areas for different return periods over the Jazan basin in Jazan Province, Saudi Arabia. The aforementioned researchers' findings demonstrated the importance of employing an integrated modelling method to assess and minimize flash flood dangers in arid regions around the world. Dukic and Eric [13] compared the Systeme Hydrologique European Transport (SHETRAN) and Hydrologic Modeling System (HEC-HMS) models to simulate flash floods and to examine whether or not using a complicated hydrological model yields more accurate results. The SHETRAN and HEC-HMS models were calibrated for the storm in September 2007 and validated the runoff results for the storm events in June 2009, May 2010, and June 2010. The St. Venant equation and SCS-CN method in the SHETRAN and HEC-HMS models were utilized, respectively. The results show that the SHETRAN model, which is more sophisticated, beats the simpler HEC-HMS model in the runoff but not for soil moisture. They came to the conclusion that more complex models do not always yield greater model performance. Depending on the hydrological variable under consideration, the dependability of hydrological model simulations can vary.

Ali et al. [4] simulated rainfall-runoff to observe the effect of land use land cover (LULC) over the Lai Nullah basin. They used the SCS-CN method to estimate losses, the SCS-UH method for transformation, and the recession method for base flow development of a model. They considered five rainstorm events for calibration and validation. They forecasted the LULC using the calibrated result obtained by HEC-HMS, based on the Islamabad master plan and growth pattern. Hejagi and Markus [17] highlighted the flood issues due to urbanization on 12 Northeastern Illunois, Chicago watershed. The percentage change of urbanization in the study area was very significant. Design peak flood was obtained with the help of the design storm method and HEC-HMS modelling. Sensitivity analyzes suggested that urbanization caused to arise in peak flow compared to that obtained due to climate variability, and discharge increased more than regular discharge. By including urbanization on annual runoff and flood events for the Quinhuai River watershed in Jiangsu Province, China, Du et al. [12] built a distributed hydrologic model and a dynamic land use change model. Future land use maps were created using a Markov chain and a

Cellular Automata model (CA–Markov model), and HEC-HMS was used to compute the runoff. Flood volume also increases due to imperviousness for all flood events. Potential changes in the peak were linearly related to flood volume. Kabeja et al. [19] investigated the effect of land cover change on flash flood peak discharge using HEC-HMS in two medium-sized mountainous watersheds in China. The first one was the Yanhe catchment, and the second one was the Guangyuan catchment. Series of Landsat images were utilized to evaluate the land use changes between 1990 and 2016. Hydrologic response of the basin and sub-basin scale was generated using Hydrologic Modeling System (HEC-HMS) under four LULC scenarios. The change in LULC occurred due to an increase in forest area resulted in a decrease in flood peak discharge. The results concluded that the LULC is vital in estimating peak discharge. As imperviousness increases, runoff increases. Developed models could evaluate the hydrological impacts and thus prove helpful in watershed management, water resources planning, and flood management.

4 Limitations

The limitations of HEC-HMS are as follows:

- Stream networks with branching or looping cannot be modelled.
- In the stream network, there is no way to model backwater.
- ArcGIS with the Spatial Analyst Extension is required for the additional tool HEC-GeoHMS.
- Other than the US Army Corps of Engineers, no support is offered.
- The model code is not available to the general public.

5 Conclusions

In general, Rainfall-runoff models are the most commonly used instruments for studying hydrological processes. The extensive review of the HEC-HMS rainfall-runoff model concluded that intended output (hydrological variable) and data availability primarily determine the modelling method and approach. Researchers analyzed various modelling methods to find the optimum model for diverse hydrological circumstances, found HEC-HMS superior to others, and recommended runoff simulation due to its automatic calibration technique. Many researchers evaluated using the HEC-GeoHMS tool for basin model construction and acquiring basin features. Some researchers used formulae to find model parameters value, while others optimized it during calibration. The majority of the researchers employed the auto-calibration technique in HEC-HMS to calibrate the model. The statistical analysis of HEC-HMS rainfall-runoff modelling indicates that the model is robust and capable of simulating accurate runoff in the best agreement with observed hydrograph in many watersheds. The HEC-GeoHMS tool may be used to construct river

basin models and find basin characteristics. The auto-calibration and manual calibration both functions better in HEC-HMS. The soil moisture accounting loss method works more accurately for continuous modelling.

Further research is going on to improve runoff predictions and face significant challenges like climate change, soil erosion, and floods. LULC is vital in calculating curve numbers, which helps calculate initial losses during precipitation. Due to urbanization, there is a significant change in land use patterns, which directly affects the peak of the hydrograph. Therefore, it is necessary to know at what rate the hydrograph peaks are changing and develop IDF curves for precipitation. Finally, import them into the model for learning peak hydrographs for different return periods. So that various measures can be taken according to peak hydrographs for safety purposes. Also, remote sensing and field data can be used in the HEC-HMS model. Each model has its strengths and weaknesses. Hence, the model should be chosen based on the research's final purpose.

References

1. Abdelkarim A, Gaber AF, Youssef AM, Pradhan B (2019) Flood Hazard assessment of the Urban area of Tabuk City, Kingdom of Saudi Arabia by integrating spatial-based hydrologic and hydrodynamic modelling. Sensors 19(5):1024
2. Abdessamed D, Abderrazak B (2019) Coupling HEC-RAS and HEC-HMS in rainfall–runoff modelling and evaluating floodplain inundation maps in arid environments: case study of Ain Sefra city, Ksour Mountain. SW of Algeria. Environ Earth Sci 78(19):1–17
3. Asadi A, Boustani F (2013) Performance evaluation of the HEC-HMS hydrologic model for lumped and semi-distributed stormflow simulation (study area: Delibajak Basin). Am J Eng Res (AJER) 2(11):115–121
4. Ali M, Khan SJ, Aslam I, Khan Z (2011) Simulation of the impacts of land-use change on surface runoff of Lai Nullah Basin in Islamabad, Pakistan. Landscape Urban Plan 102(4):271–279
5. Boughton W (2006) Calibrations of a daily rainfall-runoff model with poor quality data. Environ Model Softw 21(8):1114–1128
6. Choudhari K, Panigrahi B, Paul JC (2014) Simulation of rainfall-runoff process using HEC-HMS model for Balijore Nala watershed, Odisha, India. Int J Geomatics Geosci 5(2):253–265
7. Chen Y, Xu Y, Yin Y (2009) Impacts of land use change scenarios on storm-runoff generation in Xitiaoxi basin, China. Quat Int 208(1–2):121–128
8. Chu X, Steinman A (2009) Event and continuous hydrologic modelling with HEC-HMS. J Irrig Drain Eng 135(1):119–124
9. DeVantier BA, Feldman AD (1993) Review of GIS applications in hydrologic modelling. J Water Resour Plan Manag 119(2):246–261
10. DeFries R, Eshleman KN (2004) Land-use change and hydrologic processes: a major focus for the future. Hydrol Process 18(11):2183–2186
11. De Silva MMGT, Weerakoon SB, Herath S (2014) Modelling of event and continuous flow hydrographs with HEC–HMS: case study in the Kelani River Basin, Sri Lanka. J Hydrol Eng 19(4):800–806
12. Du J, Qian L, Rui H, Zuo T, Zheng D, Xu Y, Xu CY (2012) Assessing the effects of urbanization on annual runoff and flood events using an integrated hydrological modelling system for Qinhuai River basin, China. J Hydrol 464:127–139
13. Dukic V, Eric R (2021) SHETRAN and HEC HMS model evaluation for runoff and soil moisture simulation in the Jičinka River Catchment (Czech Republic). Water 13(6):872

14. Gumindoga W, Rwasoka DT, Nhapi I, Dube T (2017) Ungauged runoff simulation in Upper Manyame catchment, Zimbabwe: application of the HEC-HMS model. Phys Chem Earth, Parts A/B/C 100:371–382
15. Gul GO, Harmancioglu N, Gul A (2010) A combined hydrologic and hydraulic modelling approach for testing efficiency of structural flood control measures. Nat Hazards 54(2):245–260
16. Hamdan ANA, Almuktar S, Scholz M (2021) Rainfall-runoff modelling using the HEC-HMS model for the Al-Adhaim river catchment, northern Iraq. Hydrology 8(2):58
17. Hejazi MI, Markus M (2009) Impacts of urbanization and climate variability on floods in Northeastern Illinois. J Hydrol Eng 14(6):606–616
18. Ibrahim-Bathis K, Ahmed SA (2016) Rainfall-runoff modelling of Doddahalla watershed—an application of HEC-HMS and SCN-CN in ungauged agricultural watershed. Arab J Geosci 9(3):170
19. Kabeja C, Li R, Guo J, Rwatangabo DER, Manyifika M, Gao Z, Wang Y, Zhang Y (2020) The impact of reforestation induced land cover change (1990–2017) on flood peak discharge using HEC-HMS hydrological model and satellite observations: a study in two mountain basins, China. Water 12(5):1347
20. Kazezyılmaz-Alhan CM, Yalçın İ, Javanshour K, Aytekin M, Gülbaz S (2021) A hydrological model for Ayamama watershed in Istanbul, Turkey, using HEC-HMS. Water Pract Technol 16(1):154–161
21. Knebl MR, Yang ZL, Hutchison K, Maidment DR (2005) Regional scale flood modelling using NEXRAD rainfall, GIS, and HEC-HMS/RAS: a case study for the San Antonio River Basin Summer 2002 storm event. J Environ Manage 75(4):325–336
22. Majidi A, Shahedi K (2012) Simulation of rainfall-runoff process using Green-Ampt method and HEC-HMS model (case study: Abnama Watershed, Iran). Int J Hydraul Eng 1(1):5–9
23. Niyazi BA, Masoud MH, Ahmed M, Basahi JM, Rashed MA (2020) Runoff assessment and modelling in arid regions by integration of watershed and hydrologic models with GIS techniques. J Afr Earth Sc 172:103966
24. Pentland RL, Cuthbert DL (1971) Operational hydrology for ungaged streams by the grid square technique. Water Resour Res 7(2):283–291
25. Pistocchi A, Luzi L, Napolitano P (2002) The use of predictive modelling techniques for optimal exploitation of spatial databases: a case study in landslide hazard mapping with expert system-like methods. Environ Geol 41(7):765–775
26. Putty MRY, Prasad R (2000) Understanding runoff processes using a watershed model a case study in the Western Ghats in South India. J Hydrol 228(4):215–227
27. Rupa RC, Mujumdar PP (2019) Flood modelling: recent Indian contributions. In: Proc Indian Natn Sci Acad (Vol. 85, No. 4, pp. 705–722).
28. Sampath DS, Herath S, Weerakoon SB (2015) HEC-HMS model for runoff simulation in a tropical catchment with intra-basin diversions-case study of the Deduru Oya river basin, Sri Lanka
29. Thakur B, Parajuli R, Kalra A, Ahmad S, Gupta R (2017) Coupling HEC-RAS and HEC-HMS in precipitation runoff modelling and evaluating flood plain inundation map. World Environ Water Resour Congr 240–251
30. USACE (US Army Crops Engineers) (1992) HEC-HMS technical reference manual. Hydrologic Engineering Center, Davis, CA
31. USACE (US Army Crops Engineers) (2000) HEC-HMS technical reference manual. Hydrologic Engineering Center, Davis, CA
32. Vorosmarty CJ, Green P, Salisbury J, Lammers RB (2000) Global water resources: vulnerability from climate change and population growth. Science 289(5477):284–288
33. Wang G, Liu J, Kubota J, Chen L (2007) Effects of land-use changes on hydrological processes in the middle basin of the Heihe River, northwest China. Hydrol Process Int J 21(10):1370–1382

Simulation of Reservoir Inflow Using HEC-HMS

Mahesh Shelke, S. N. Londhe, P. R. Dixit, and Pravin Kolhe

Abstract Reservoir inflow plays a key role in hydrological predictions such as drought and flood predictions as well as in reservoir operations, and thus precise prediction of reservoir inflow is of utmost importance. As reservoir inflow pattern predominantly depends upon the rainfall-runoff process, land use and land cover pattern and climate change within a catchment area, accurate prediction of it, is a difficult task. Koyna dam reservoir is one of the major reservoirs in India which serves the multipurpose functions including hydroelectric power generation and thus for efficient reservoir operation; accurate inflow prediction is the need of the day. Consequently, present study aims in predicting the Koyna reservoir inflow using—a conceptual model, Hydrologic Engineering Centre's Hydrologic Modelling System (HEC-HMS; version 4.8). The Soil Conservation Service Curve Number (SCS-CN), SCS unit hydrograph, and time interval were selected for each component of the inbuilt processes of loss method, transform method, and channel routing, respectively, while developing the HEC-HMS model. To evaluate the model performance, relative error (%), root mean square error (RMSE), correlation coefficient (r), and Nash–Sutcliffe efficiency (CE-NSE) are used along with simulated and observed hydrographs and scatter plots. From all the results, it can be said that the overall performance of the HEC-HMS model is reasonable and trustworthy and can be applied in similar area of research interest.

M. Shelke (✉) · S. N. Londhe
Department of Civil Engineering, Vishwakarma Institute of Information Technology, Pune 411048, India
e-mail: mahesh.shelke78@gmail.com

S. N. Londhe
e-mail: shreenivas.londhe@viit.ac.in

P. R. Dixit
Vishwakarma Institute of Information Technology, Pune 411048, India
e-mail: Pradnya.dixit@viit.ac.in

P. Kolhe
Water Resource Department—Government of Maharashtra, Mumbai, India

P. V. Timbadiya et al. (eds.), *Hydrology and Hydrologic Modelling*,
Lecture Notes in Civil Engineering 312,
https://doi.org/10.1007/978-981-19-9147-9_17

Keywords Reservoir inflow · Conceptual model HEC-HMS · SCS-CN · Koyna reservoir

1 Introduction

The reservoir plays a key role in overriding the effect of irregularities of inflow hydrograph and regulate it based on the user's needs. Rainfall is the main cause for the streams to form in the watershed which then contribute to the reservoir inflow. The Indian subcontinent experiences monsoon every year from June to September in which most of the water is received. The mathematical model is an effective technique to predict the hydrologic parameter such as inflow into the reservoir. Since last few decades, computerized simulations are becoming very popular because of its simplicity. Since the last decade, a conceptual model, namely Hydrologic Engineering Centre-Hydrologic Modelling System (HEC-HMS), developed by US army and corps has been used by many for prediction of the reservoir inflow. Oleyiblo and Li [1] presented a universal application of HEC-HMS and its potential applicability and suitability for flood forecasting in catchments and stated the importance of hydrological parameters predictions for the effective reservoir management program. Castro and Maidment [2] mentioned that hydrological modeling is a frequently used tool to estimate the basin's hydrological response to precipitation, and the HEC-HMS computer model can be reliably used to simulate catchment flows. Gumindoga et al. [3] applied HEC-HMS to simulate runoff in ten gauged and ungauged upper Manyame sub-catchments in Zimbabwe, and noted that the HEC-HMS model adequately denotes the hydrological response of the catchment and can be used to consider the impact of other future land development scenarios. Rauf and Ghumman [4] developed the conceptual HEC-HMS model for runoff simulation in the Astore watershed of Pakistan's Upper Indus River Basin using 20 years of dataset. Tassew et al. [5] applied HEC-HMS model for the flow simulation for tropical conditions for the Gilgel Abay Catchment (1609 km^2), Upper Blue Nile Basin, Ethiopia. The model developed is based on the hydrological characteristics, topography, soil type, and land use of the study area. HEC-HMS is one of the most widely used modeling tools for simulating flood hydrology within the engineering community due to its applicability, capability, and suitability [1, 6–12]. Although the HEC-HMS model has been examined and calibrated at a global scale, little effort has been made in the context of the Western part of the state of Maharashtra in India which is home for the Koyna River catchment. It is said that since its inception in 1964 Koyna project has become the "powerhouse" of Mumbai, the largest city in India making this project and all the studies related to it very important. The Koyna River catchment covers an area of 891.78 km^2. The Koyna River catchment has extensive agricultural practices; therefore, it is economically important and as it experienced the unpredicted flood events in past which makes this catchment more vulnerable for hydrological studies.

2 Study Area

The Koyna River basin stretches between 17,054″ to 17,016″ N and 73,042″ to 74,006″ E. The river originates at Mahabaleshwar at an elevation of around 700 m from the mean sea level and meets Shivsagar reservoir formed due to Koyna dam at around 75 km from its origin. Koyna dam is ranked 17th in India considering height and live storage capacity. It has gross storage capacity of 2986.68 million cubic meter (MCM) and live storage capacity 2835.54 MCM. Figure 1 shows the study area.

2.1 Data Used

Daily rainfall, evaporation, and discharge of the catchment area under consideration was provided by from the Water Resource Department-Government of Maharashtra for the period of 1997–2015. For the present study, nine rain gauges and one discharge gauging station are considered. The rain gauges are installed at stations, namely

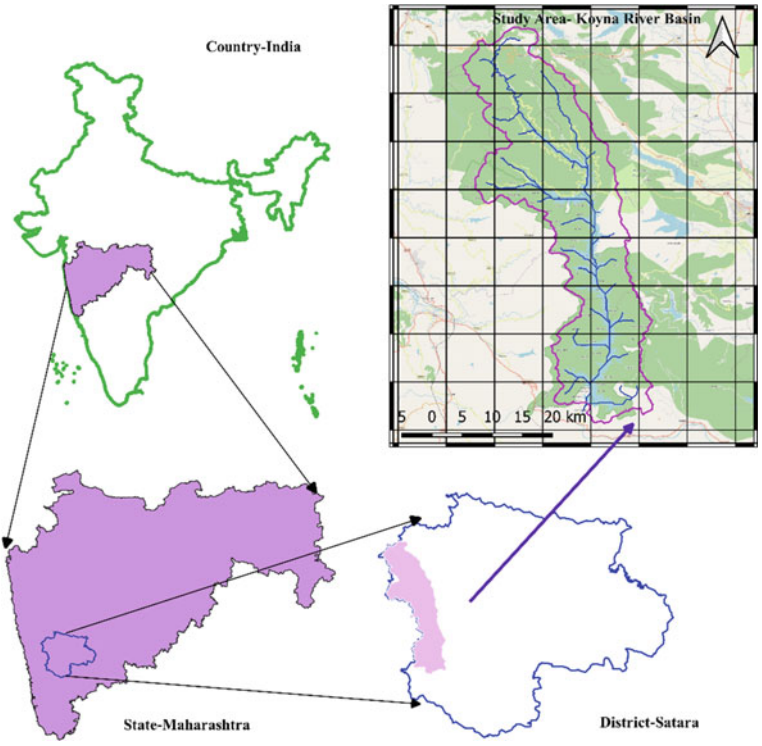

Fig. 1 Index map of study area

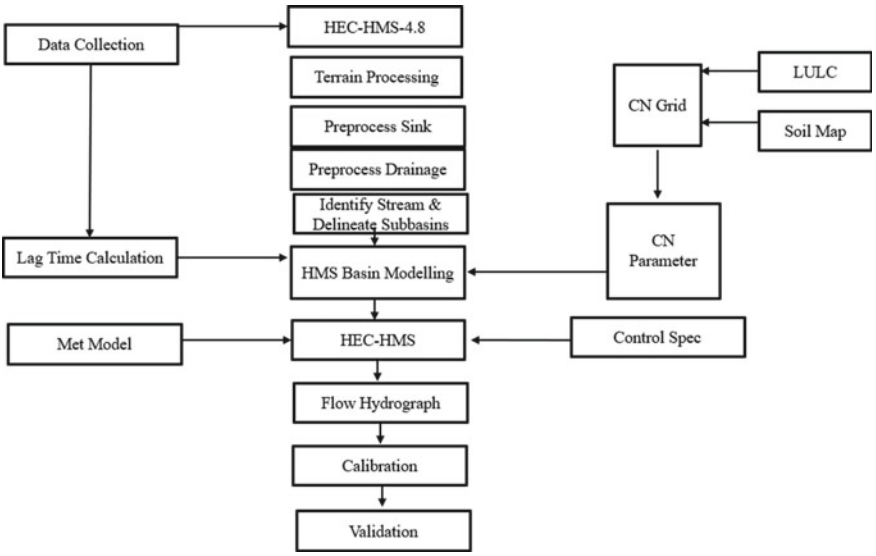

Fig. 2 Methodology chart

Koyna Dam, Navaja, Kati, Kargaon, Bamnoli, Valvan, Sonat, Pratapgad, and Mahabaleshwar. Daily discharge data of one gauging station at Koyna covers complete catchment. The details about the location of rain gauges and discharge station shown in Fig. 2.

2.2 Methodology

The inflow was simulated using the tool named Hydrologic Modelling System (HEC-HMS) for the Koyna Catchment, Western part of Maharashtra, India. The river catchment was delineated, and its properties were extracted from a 30 m × 30 m CARTOSAT Digital Elevation Model (DEM) provided by ISRO-Bhuvan (https://bhuvan-app3.nrsc.gov.in/data/download/index.php). The HEC-HMS consists of three sections of the modeling; first one named basin model consists of the catchment area details; second is meteorological section containing rainfall and discharge dataset, third control specification section for the definition of time of simulation run. To account for the loss, runoff estimation, and flow routing, Soil Conservation Service Curve Number (SCS-CN), Soil Conservation Service Unit Hydrograph (SCS-UH), and lag methods were used, respectively. Figure 2 explains the complete methodology adopted for present work.

The two raster images, land use, and soil class are overlapped on each other, and CN value is calculated. The calculation of CN number was done using GDAL Raster Calculator available within QGIS open-source application [13]. Mean of CN number was taken using Zonal Statistics Tool. The land use land cover map prepared using the LISS-3 (Linear imaging self-scanning). The QGIS plugin named semi-automatic classification was used which allows for the supervised classification of remote sensing images, providing tools for the download, the preprocessing, and post-processing of images. The soil data were gathered from earthdata.nasa.gov. Based on data, it is concluded that the study area lies within soil class 3 (moderately high runoff potential: < 50% sand and 20–40% clay) and 4 (high runoff potential: < 50% sand and > 40% clay). The precipitation values were estimated by the most used Thiessen polygon method, and weights were worked out in QGIS 3.6 version software. The method was selected because of its easy-going application; correctness depends on the sampling density. Table 1 showed the weights for each subbasin.

The Soil Conservation Service Curve Number (SCS-CN) loss method was preferred to estimate direct runoff from a specific rainfall. SCS unit hydrograph method is used to transform the precipitation into surface runoff. The lag time is calculated for each subbasin using Kirpich equation. Advantages of SCS-CN curve loss model are simple and conceptual model for the estimation of the direct runoff volume from a rainfall, sound supported by empirical data and relies only on the curve number, which is function of soil type and land use, land cover that are major runoff-creating watershed characteristics. It is commonly used on different environments and provides better results compared to initial and constant loss rate method. Prior to hydrological modeling, methodology can be separated into four main stages:

Table 1 Rain gauge weights

Subbasin	Rain gauge	Weight	Subbasin	Rain gauge	Weight
Subbasin 1	Valvan	0.04	Subbasin_5	Valvan	0.21
	Bamnoli	0.06		Bamnoli	0.78
	Sonat	0.39		Sonat	0.01
	Pratapgad	0.24	Subbasin_6	Bamnoli	1.00
	Mahabaleshwar	0.27	Subbasin_7	Kati	0.31
Subbasin 2	Bamnoli	0.13		Kargoan	0.56
	Sonat	0.74		Bamnoli	0.13
	Mahabaleshwar	0.14	Subbasin_8	Navaja	0.49
Subbasin_3	Valvan	0.91		Kati	0.51
	Sonat	0.09	Subbasin_10	Kati	0.26
Subbasin_4	Valvan	1.00		Koyna Dam	0.74
Subbasin_9	Navaja	0.39	Subbasin_11	Navaja	0.18
	Kati	0.47		Koyna Dam	0.82
	Koyna Dam	0.14			

terrain processing, preprocess sink, preprocess drainage, identify stream, and delineate the subbasin. This process was done in latest version of HEC-HMS-4.8. Daily simulation time step was used in estimating the parameters of the selected models. Each model run combines a basin model, meteorological model, and control specifications with run options to obtain results. In this study, 7-year continuous data were used (5 year for calibration and 2 for validation) recorded in the period from 1993–2014.

3 Results and Discussions

3.1 Calibration

In reservoir operations, the very critical aspect of the hydrograph is the peak flow because the peak flow relates to the maximum downstream flooding. The inbuilt automatic simplex search algorithm is used for optimization. In present study, the percent error in peak discharge is used as statistical error measure to judge the performance of optimized model where in objective goal was to minimize the percent error. (HEC-HMS User Manual 2021). The results of the hydrological model in this study showed a satisfactory fit between the model results and observations after optimization; the hydrograph shape and timing of peaks coordinated well although the model tended to overestimate the runoff before optimization. The calibration of the model improved the results greatly by decreasing and increasing the overestimated and underestimated volume of the runoff, respectively. The modeling results of peak discharge, total volume, and their relative errors with respect to the observed data, the Nash–Sutcliffe efficiency and coefficient of determination values during calibration are mentioned in Table 2. Lag time of reaches and CN curve number are most sensitive parameters in HEC-HMS modeling [5]. Hence, those are considered for the calibration process. The calibration was done for five events (1997, 2001, 2002, 2006, 2009). Results of this calibration are shown in Table 2, and Fig. 4 shows good correlation between simulated and observed inflow.

The calculated values of the percent error both in total volume and peak flow between simulated and observed flow values were very high before the optimization ($> \pm 20\%$) as well as the time of simulated peak discharge value was not matched with the observed dataset. The calibration was done on the basis of trials and error method for which the percent error both in volume and peak flow falls in the range between the value of -15.85 to 5.76% for the total volume and -5.86 to 8.48% for the peak flow, respectively. As per the statistical parameter values obtained for each event, it showed that the model performs well. The model simulation can be judged

Table 2 Simulated and observed peak flow (m^3/s) and volume (MM) for calibrated events

Description		Year				
		1997	2001	2002	2006	2009
Peak discharge (m^3/s)	BOP	2221.3	1777.9	1551	2254.7	2362.5
	AOP	2210.2	1715	1565.4	2290.7	2292.3
Observed discharge (m^3/s)		2400.7	1873.9	1478.7	2468.8	2241
Relative error (%) for peak		7.94	8.48	−5.86	7.21	−2.29
Total volume (MM)	BOP	5542	3814	4093	6916	4143
	AOP	5286	3606	3906	6922	3942
Observed volume (MM)		5525.52	3112.23	3544.45	7345.25	3481.99
Relative error (% for Volume)		4.34	−15.85	−10.2	5.76	−13.2
RMSE Std. Dev		0.3	0.4	0.4	0.3	0.4
NSE		0.925	0.851	0.850	0.936	0.862
R^2		0.9263	0.8833	0.872	0.9472	0.8881
Peak discharge simulated date		31-Jul-97	09-Jul-01	07-Aug-02	03-Jul-09	15-Jul-09
Peak discharge observed date		31-Jul-97	09-Jul-01	07-Aug-02	03-Jul-09	15-Jul-09

Note Before Optimization—BOP, After Optimization—AOP, Million Cubic Meter—MM

as satisfactory if Nash–Sutcliffe efficiency is greater than 50%, good if it is greater than 65%, and very good if it is greater than 75%. However, if the relative percent error is less than ± 20%, then it can be considered as a very good classification [5].

3.2 Validation

The validation of the simulated results of peak discharge, total volume, and their relative errors of two events (2004 and 2010) with respect to the observed dataset, along with Nash–Sutcliffe efficiency (NSE) and the coefficient of determination (R^2) values are presented in Table 3. As shown in the results Figs. 5 and 6, the model predicted peak discharge accurately based on the available historical flood data. Figure 7 shows the good correlation between observed and simulated inflow.

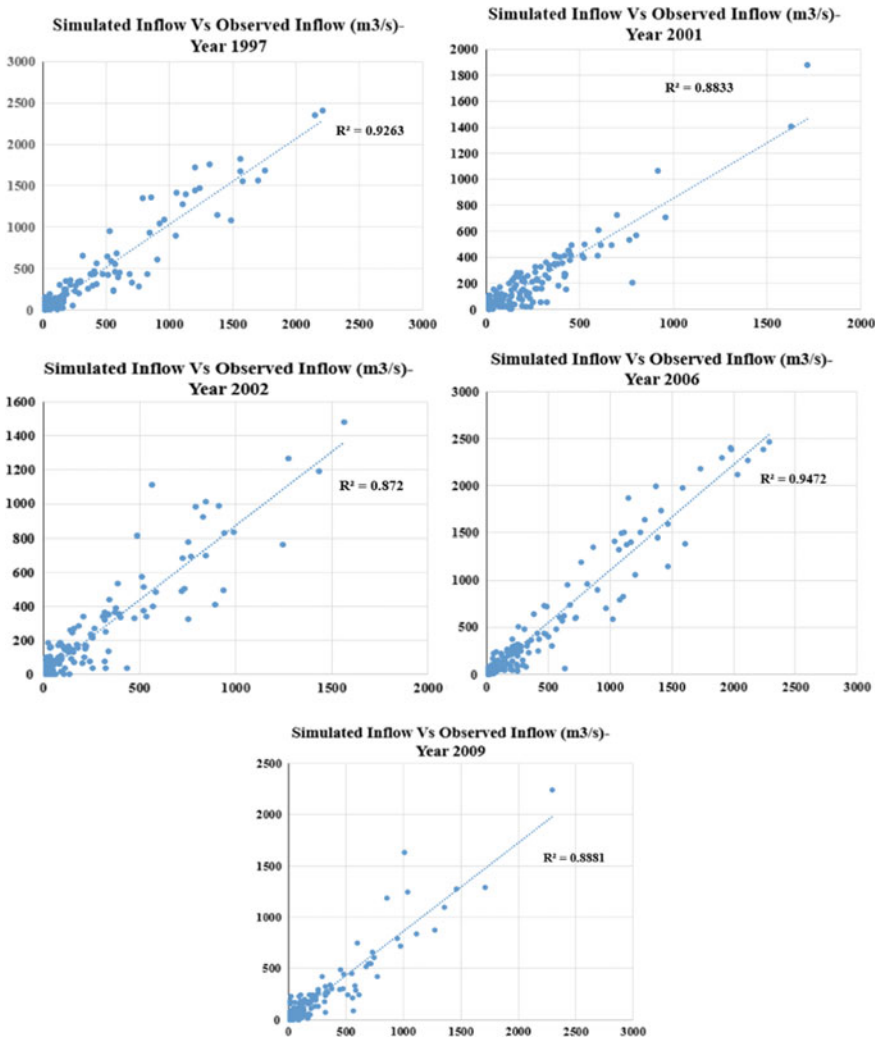

Fig. 4 Scattered plots of simulated inflow verses observed inflow for calibration

4 Conclusions

The present case study aimed to develop a hydrological model of the catchment area for River Koyna, Western Maharashtra, India, lying upstream of the Koyna Dam using HEC-HMS 4.8 version. According to performance criteria given by Rauf and

Table 3 Simulated and observed peak flow (m^3/s) and volume (MM) for validation events

Description	Year	
	2004	2010
Peak discharge (m^3/s)	2393.5	1826.6
Observed discharge (m^3/s)	2301.8	1917.8
Relative error (%) for peak	−3.98	4.6
Total volume (MM)	5181.24	4088.84
Observed volume (MM)	4661.99	3774.51
Relative error (% for Volume)	−11.14	−8.33
RMSE Std. Dev	0.3	0.4
NSE	0.8940	0.8610
R^2	0.8671	0.8660
Peak discharge simulated date	03-Aug-04	26-Jul-10
Peak discharge observed date	03-Aug-04	26-Jul-10

Note Before Optimization—BOP, After Optimization—AOP, Million Cubic Meter—MM

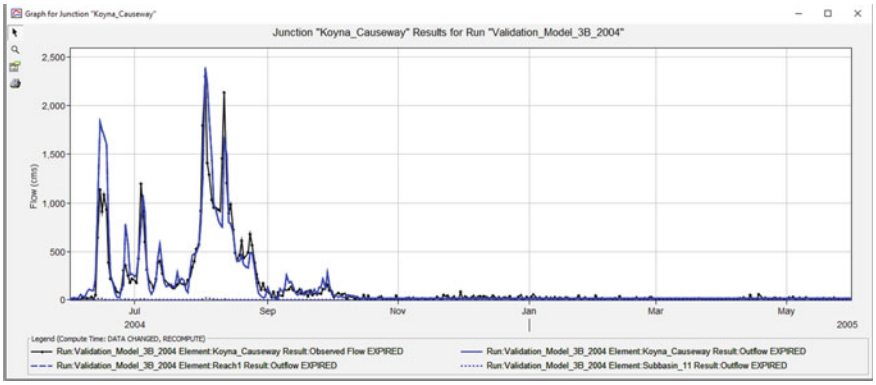

Fig. 5 Predicted inflow verses time for duration June 1, 2004 to May 31, 2005

Ghumman [4], the results of calibration and validation, suggested that model has been found to be performed reasonably well for outlet location (i.e., Koyna), as RMSE, NSE, R2 all are within an acceptable range. After calibration, the value peak flow and total runoff volume for all events are satisfactorily close to the observations with a very small-scale error in peak and volume ($< \pm 20\%$). This shows that HEC-HMS is suitable for the studied catchment. Also, it is possible to suggest that the calibrated parameters values can be further used to other nearby basins. The satisfactory values of peak discharges corresponding to precipitation are obtained. Hence, it can be concluded that the proposed methodology is suitable for prediction of inflows of the river Koyna catchment.

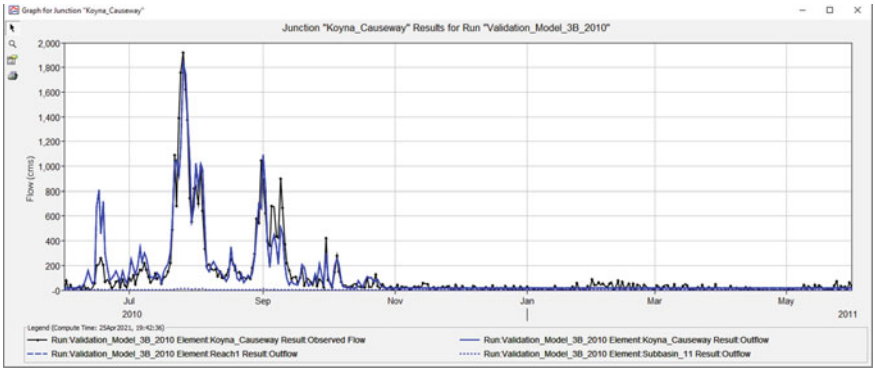

Fig. 6 Predicted inflow verses time for duration June 1, 2010 to May 31, 2011

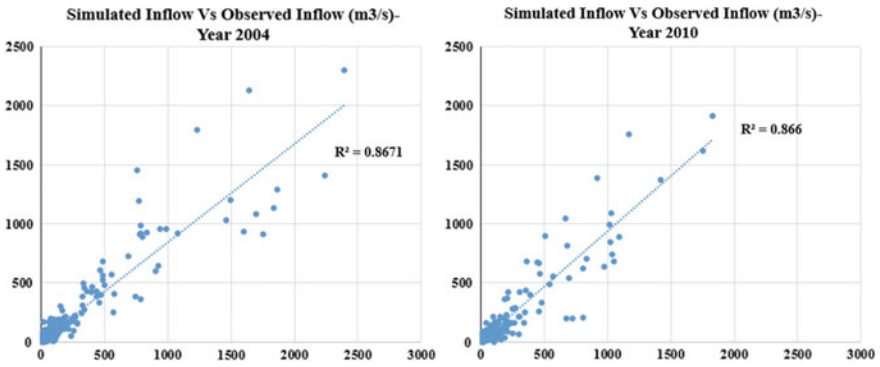

Fig. 7 Simulated inflow verses observed inflow scattered plots for validation

Acknowledgements The authors would like to acknowledge the Department of Water Resources, Government of Maharashtra for providing data for this research.

References

1. Oleyiblo JO, Li Z-J (2010) Application of HEC-HMS for flood forecasting in Misai and Wan'an catchments in China. Water Sci Eng 3(1):14–22
2. Castro CV, Maidment DR (2020) GIS preprocessing for rapid initialization of HEC-HMS hydrological basin models using web-based data services. Environ Model Softw 130:104732
3. Gumindoga W, Rwasoka DT, Nhapi I, Dube T (2017) Ungauged runoff simulation in Upper Manyame catchment, Zimbabwe. Appl HEC-HMS Model Phys Chem Earth 100:371–382
4. Rauf A-u, Ghumman AR (2018) Impact assessment of rainfall runoff simulations on the flow duration curve of the upper Indus river—a comparison of data-driven and hydrologic models. Water 10:87

5. Tassew BG, Belete MA, Miegel K (2019) Application of HEC-HMS model for flow simulation in the lake Tana Basin: the case of Gigel Abay catchment, upper Blue Nile Basin Ethiopia. Hydrology 6:21. https://doi.org/10.3390/hydrology6010021
6. Halwatura D, Najim MMM (2013) Application of the HEC-HMS model for runoff simulation in a tropical catchment. Environ Model Softw 46:155e162
7. HEC-HMS User's Manual—Version 4.8 (2021) US army corps of engineers hydrologic engineering center
8. Knebl MR, Yang Z-L, Hutchison K, Maidment DR (2005) Regional scale flood modelling using NEXRAD rainfall, GIS, and HEC-HMS/RAS: a case study for the San Antonio River Basin Summer 2002 storm event. J Environ Manage 75(2005):325–336
9. Rosas MA, Vanacker V, Viveen W, Gutierrez RR, Huggel C (2020) The potential impact of climate variability on siltation of Andean reservoirs. J Hydrol 581(2020):124396
10. Nithila Devi N, Sridharan B, Kuiry SN (2019) Impact of urban sprawl on future flooding in Chennai city, India. J Hydrol 574(2019):486–496
11. Chu X, Steinman A (2009) Event and continuous hydrologic modeling with HEC-HMS. J Irrig Drainage Eng ASCE 119
12. Chen Y, Wang Y, Zhang Y, Luan Q, Chen X (2020) Flash floods, land-use change, and risk dynamics in mountainous tourist areas: a case study of the Yesanpo Scenic Area, Beijing, China. Int J Disaster Risk Reduction 50:101873
13. QGIS Development Team (2020) QGIS Geographic information system. Open-Source Geospatial Foundation. http://qgis.org

Effect of Changes in Land Use/Land Cover on Runoff from Watershed Using CN Approach

M. Velayudha Das and S. Poongothai

Abstract Due to population explosion and economic development, the changes in land use/land cover (LULC) have an impact on storm water runoff characteristics naturally in the watershed hydrologic responses. The curve number (CN), which expresses the potential for runoff, is a function of LULC, soil type, and moisture content. Therefore, to investigate the effect of LULC changes in the rainfall-runoff simulation process, some models need CN as data input. The present study describes how to estimate the CN due to LULC changes during 1995–2019 and the runoff volume using NRCS-CN model and GIS tool in a part of the Manimuktha watershed of Tamil Nadu, India. IRS IC LISS III imagery data have been utilized for measuring the qualitative and quantitative spatial information on LULC changes and arrayed under the categories of agriculture, forests, settlements, wasteland, and water bodies. The result showed that from 1995 to 2019, the values of CN increased from 79.60 to 81.61, which indicates that the LULC changed significantly and the runoff was more. This study also recommends suitable strategies to control the negative effects like the increase of soil erosion and flood risks in the study area.

Keywords Watershed · Land use/land cover · Curve number · NRCS-CN model · GIS

1 Introduction

A watershed is a resource region that bounded vertically by topographical area influenced by human activities and horizontally by a stream system that drains into a common point. Due to unprecedented population pressure, over exploitation and the increasing demand of society of land and water resources are affecting the stability of our ecosystems. Therefore, watershed managers and stakeholders now agree that understanding and managing natural resources on a watershed basis is the best method to safeguard important resources [3, 6]. Land use and land cover

M. Velayudha Das (✉) · S. Poongothai
Department of Civil Engineering, Annamalai University, Annamalainagar 628002, India
e-mail: mvdas6979@yahoo.com

P. V. Timbadiya et al. (eds.), *Hydrology and Hydrologic Modelling*,
Lecture Notes in Civil Engineering 312,
https://doi.org/10.1007/978-981-19-9147-9_18

(LULC) has dramatically changed due to human activities and global climate change [5] and modify watershed hydrological processes and water availability [8] in a short period of recent years [14]. Different types of land use categories have been extracted by many researchers by remote sensing (RS) techniques using satellite imagery. Geographic Information System (GIS) analyzes all types of geographically spatial and temporal referenced data and gives planners a better grasp of the issues and aids in the development of a better solution for sustainable development [2, 9].

Integration of GIS with the Natural Resources Conservation Service-Curve Number (NRCS-CN) method is a powerful tool for estimating surface runoff from an ungauged watershed [1]. It is a conventional method for proper utilization and management of water [11] and primarily uses land use and soil mapping data as input factors in the estimation of precipitation runoff [15]. The curve number (CN) is a hydrologic parameter utilized to indicate the potential storm water runoff for drainage area as a function of land use, soil type, and soil moisture [4]. Therefore, it is necessary to quantify the effects of LULC changes in the runoff characteristics and the availability of water resource in recent years [7, 10]. The study's objective is to assess the change in surface runoff characteristics based on the analysis of LULC changes in the Muktha River sub-watershed between the years 1995–2019. The study's findings aid in the development of measures by watershed managers and decision-makers to deal with the harms brought on by excessive surface runoff brought on by LULC dynamics.

2 Materials and Methods

3 Study Area and Data Source

3.1 Muktha River Sub-watershed

The study region is the Muktha River sub-watershed (4CIA2e) in the Vellar basin, Kallakurichi district, Tamil Nadu, India (Fig. 1). With a total area of 251.151 km^2 in the toposheets 58 I/9 and I/13, this rural sub-watershed area spans 78°43′ 9.22″–78° 59′ 21.73″ E and 11° 46′ 12.80″–11° 53′ 42.38″ N. The sub-watershed has two major topographic regions such that the western part is covered by Kalrayan Hills (85.761 km^2), and the rest is almost plain terrain (165.390 km^2).

3.2 Data Collection

Remote sensing data-IRS IC LISS III Satellite data (year 1995 and 2019) were used to create land use/land cover maps (Source: IRS, Chennai). Daily rainfall data from the rain gauge stations of Gomukhi Dam and Manimuktha Dam during 1992–2019

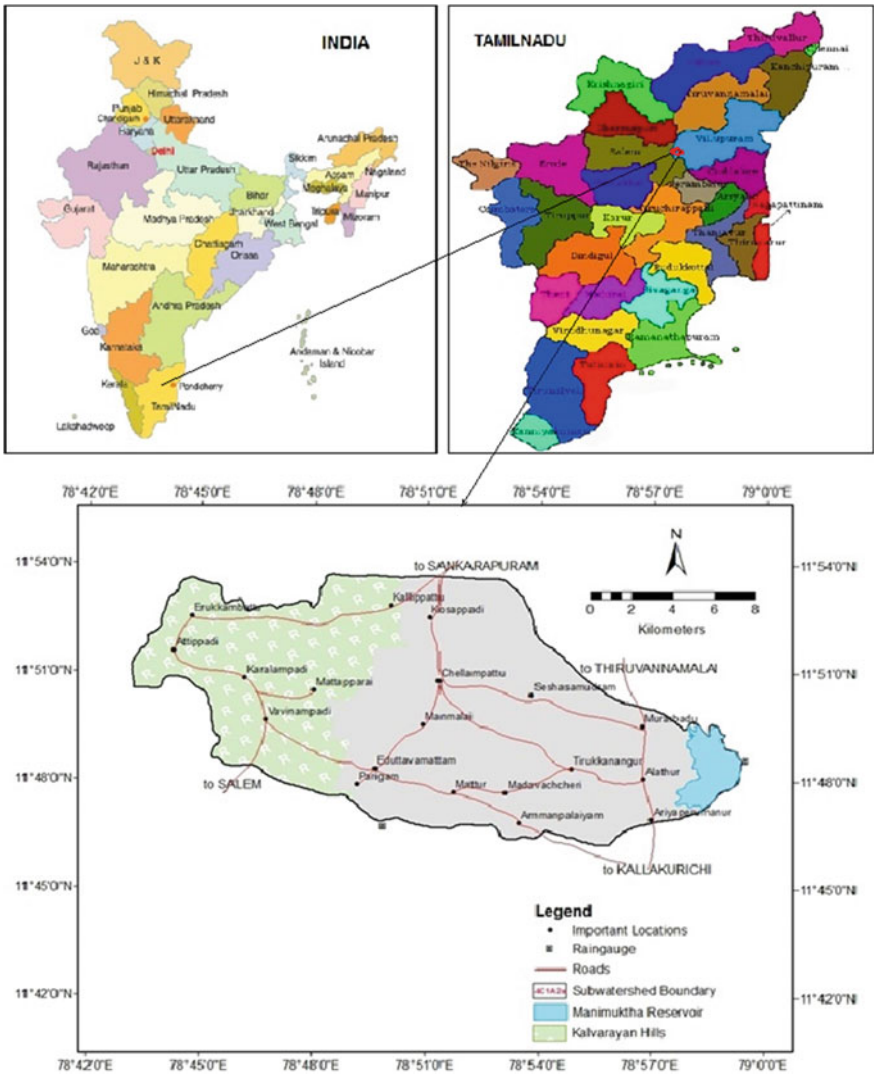

Fig. 1 Index map of the study area

were utilized to calculate the study area's daily runoff (Source: IWS, Chennai). The field survey on infiltration rates of soil was conducted using double-ring infiltration method [13].

3.2.1 LULC Data

The two years IRS IC LISS III imagery in 1995 and 2019 (Figs. 3 and 4) data have been utilized for measuring the qualitative and quantitative spatial information on LULC changes and used to know the past patterns of LULC in the study area. The digitization of the LULC maps and its changing trends were analyzed using ArcGIS 10.7 software and compared with ground truth.

3.2.2 NRCS-CN Method

Among the methods for estimating runoff from rainfall, an empirical approach, SCS-CN method (Soil Conservation Service-Curve Number (National Engineering Handbook, USA) (USDA, 1972)) renamed as Natural Resources Conservation Service-Curve Number (NRCS-CN) technique has largely been used to ungauged watersheds to establish the rainfall–runoff relations [12]. This runoff method depends on rainfall, hydrological soil groups (HSGs), LULC, and antecedent moisture conditions (AMCs). It combines the water balance equation with the relationship of infiltration losses and surface storage as

$$Q = \frac{(P - I_a)^2}{(P - I_a + S)} \quad (Q \text{ is valid for } P \geq I_a) \tag{1}$$

where Q—direct runoff in mm, P—rainfall in mm, I_a—initial abstraction in mm, and S—potential retention in mm. In practice, S is expressed in terms of the curve number (CN) as

$$S = \frac{25400}{\text{CN}} - 254 \tag{2}$$

The non-dimensional CN is derived from the tables of Chap. 7 in the SCS handbook (1972). The Indian Ministry of Agriculture (1976) adapted $I_a = 0.3S$ in Eq. (1) to fit for Indian conditions as

$$Q = \frac{(P - 0.3S)^2}{(P + 0.7S)} \tag{3}$$

The runoff from the sub-watershed is calculated using the value of CN. Figure 2 shows the methodology of GIS-based NRCS-CN runoff method (Figs. 3 and 4).

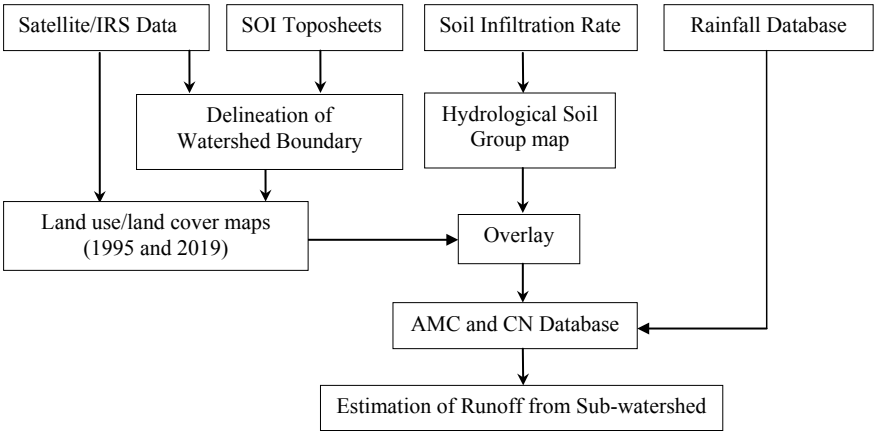

Fig. 2 Flowchart showing the methodology of NRCS-CN method

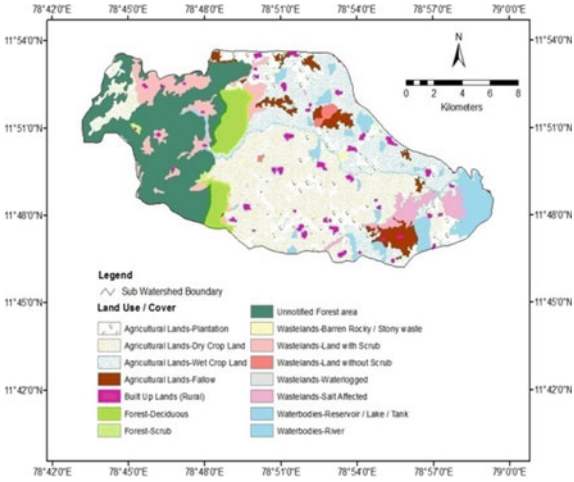

Fig. 3 LULC maps of years 1995 and 2019

3.3 Antecedent Moisture Condition

According to USCS, soil is grouped into HSG *A*, *B*, *C*, and *D* with regard to potential rate and minimum infiltration rate (Table 1). The AMC expressed in I, II, and III levels, according to 5 days antecedent precipitation limits (Table 2) and curve number for AMC-II in Indian condition (Table 3).

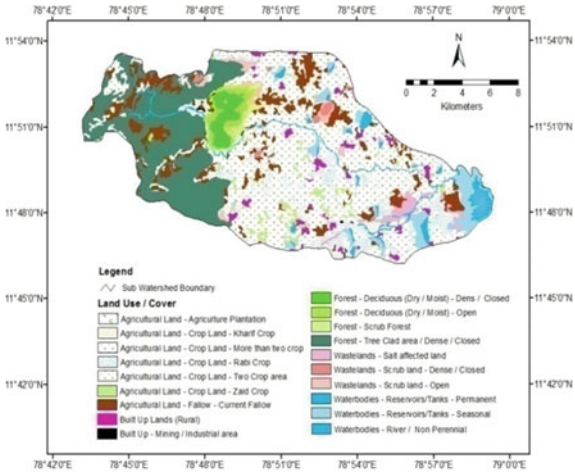

Fig. 4 LULC maps of years 1995 and 2019

Table 1 USDA-SCS soil classification

HSG	Soil type	Runoff	Infiltration rate (mm/hr)	Water transmission
A	Well drained sands and gravels	Low	More than 7.5	High
B	Moderately coarse to fine textures	Moderately low	3.8–7.5	Moderate
C	Clay loams—moderately fine	Moderately high	1.3–3.8	Slow
D	Clay soils—swell when wet, heavy plastic	High	Less than 1.3	Very slow

Table 2 Classification of AMC

AMC group	Soil characteristics	Total 5 days antecedent rainfall (mm)	
		Dormant season	Growing season
I	Dry soil but not to wilting point	Less than 13	Less than 36
II	Average conditions	13–28	36–53
III	Heavy rainfall or light rainfall—occurred within the last 5 days (Saturated soil)	More than 28	More than 53

3.4 Area Weighted CN

The area with a particular soil group type and LULC was multiplied, and its weight was found under AMC conditions for the year 1995 and 2019 as

Table 3 CN for AMC-II (Indian condition)

LULC	Practices	Conditions	HSG			
			A	*B*	*C*	*D*
Cultivation	Row		76	86	90	93
	Contoured	Poor/Good	70/65	79/75	84/82	88/86
	Terraced	Poor/Good	66/62	74/71	80/77	82/81
	Bunded	Poor/Good	67/59	75/69	81/76	83/79
	Rice		95	95	95	95
Orchards	Stony cover/Without stony		39/41	55/55	67/69	71/73
Forest	Dense/Open/Shrubs		26/28/33	40/44/47	58/60/64	61/64/67
Pasture		Poor/Fair/Good	68/49/39	79/69/61	86/79/74	89/84/80
Wasted land			71	80	85	88
Hard surface			7	86	91	93
Water bodies			100	100	100	100

$$\mathrm{CN} = \frac{\sum (\mathrm{CN}_i \times A_i)}{A} \tag{4}$$

where CN—weighted CN, CN_i—CN from the weighted area A_i, and A—total area of the watershed.

4 Results and Discussions

Change Detection of LULC

Based on the resolution of IRS data, the information available was arrayed and grouped under five land use (level-1) categories, i.e., agriculture, forests, settlement (built up), wasteland, and water bodies have been identified for the years 1995 and 2019 (Figs. 3 and 4). These level-1 classes were further converted into other land use classification systems level-2 and 3. The areas under different LULC classes of the study area were calculated in km^2 and percentage (Table 4). The study area was dominated by agricultural land in 1995 was 142.742 km^2 (56.83%) and increased to 153.162 km^2 (60.99%) in 2019 due to a trend in change in agriculture. The crop land was increased to 19.29%, but the plantation area was reduced to 97.73% from 1995 to 2019. Fallow lands were 3.86% in 1995 and increased to 8.63% in 2019. It was observed that the settlement area gradually increased from 3.471 km^2 (1.38%) in 1995 to 5.213 km^2 (2.07%) including rock-mining area of 0.137 km^2 (0.06%) in 2019. The forest area was covered 62.351 km^2 (24.83%) of the study area in 1995 and declined to 59.398 km^2 (23.65%) in 2019 due to competing land uses (agriculture and human settlements mainly), the rising unemployment problem, insufficient income from agriculture and also demand for fuel wood are the major causes of deforestation.

Table 4 Changes of LULC area in 1995 and 2019

LULC level	Area in 1995		Area in 2019		Change detection during 1995–2019	
	km^2	%	km^2	%	km^2	%
Agricultural Lands Plantation	22.886	9.11	0.520	0.21	(-)22.366	(-)97.73
Crop land	110.16	43.86	130.970	52.15	(+)21.805	(+)19.29
Fallow	9.691	3.86	21.672	8.63	(+)11.981	(+)114.89
Subtotal	142.74	56.83	153.162	60.99	(+)10.420	(+)7.30
Built-up Lands	3.471	1.38	5.213	2.07	(+)1.742	(+)50.19
Forest Lands Deciduous	10.745	4.28	7.647	3.05	(-)3.098	(-)28.83
Scrub forest	0.575	0.23	4.386	1.75	(+)3.811	(+)662.78
Tree clad area/Dense	51.031	20.32	47.365	18.85	(-)3.666	(-)7.18
Subtotal	62.351	24.83	59.398	23.65	(-)2.953	(-)4.74
Waste Lands Barren Rocky	0.721	0.29	1.650	0.66	(+)0.929	(+)128.85
Scrub	16.184	6.44	7.624	3.03	(-)8.56	(-)52.89
Salt affected	7.307	2.91	4.460	1.78	(-)2.847	(-)38.96
Subtotal	24.212	9.64	13.734	5.47	(-)10.478	(-)43.28
Water bodies Reservoir/Tank	8.908	3.55	15.624	6.22	(+)6.716	(+)75.39
River/Stream	9.467	3.77	4.020	1.60	(-)5.447	(-)57.54
Subtotal	18.375	7.32	19.644	7.82	(+)1.269	(+)6.91
Total	251.15	100	251.151	100	–	–

Waste land in 1995 was 9.64% (24.212 km^2), reduced to 5.47% in 2019. This was due to changes in forest lands and agricultural lands during that period. Water bodies covered 7.32% (18.375 km^2) of the total area in 1995 and increased to 7.82% in 2019 probably due to seasonal variation.

Rainfall and Runoff

The hydrological soil groups' spatial distribution of *A* (26.383 km^2), *B* (29.698 km^2), *C* (83.631 km^2), and *D* (111.439 km^2) in the study area was obtained using ArcGIS 10.7 software, as shown in Fig. 5. By overlaying tools of the ArcGIS 10.7 software, the HSG and LULC layers were overlaid, and the weighted CN (using Eq. (4)) of AMC-I, II, and III conditions from the LULC map of years 1995 and 2019 is presented in Table 5. From the results, it is inferred that between the years 1995 and 2019, the agricultural land area expanded by 7.30%, while the forest land area declined by 4.74%, resulting in higher CN values in the year 2019.

The computed annual runoff with respect to rainfall values for the past 27 water years (1992–2019) is presented in Fig. 6. The annual runoff was more during 2005–2006 (1134.02 mm) and less during 2016–2017 (64.28 mm). The average annual surface runoff rate of the study area was 423.08 mm, which represented 35.01% of the normal annual rainfall (1106.69 mm). The correlation of annual rainfall and

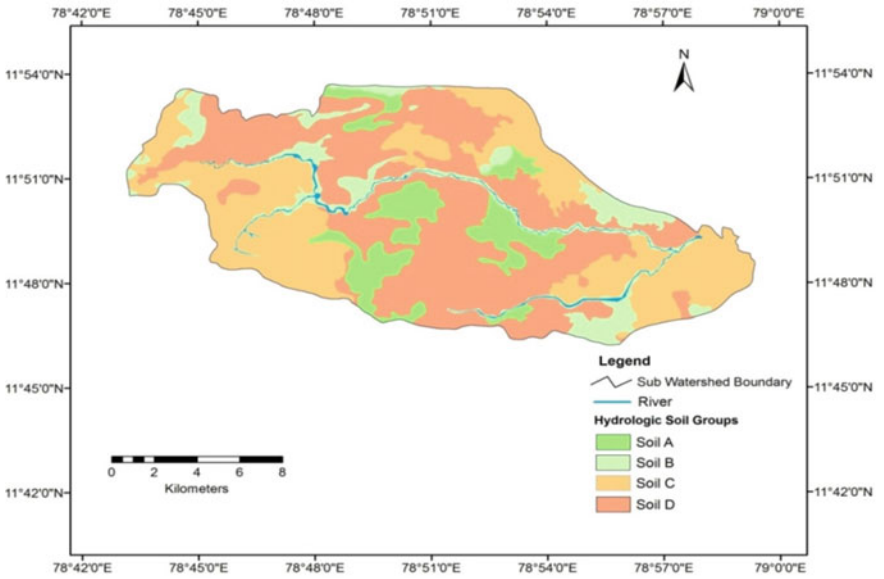

Fig. 5 Hydrological soil group map

Table 5 Weighted CN of years 1995 and 2019

Year	CN		
	AMC-I	AMC-II	AMC-III
1995	62.52	79.60	91.68
2019	65.25	81.61	92.64

estimated runoff using the NRCS-CN method is shown in Fig. 7. A straight line equation of $y = 0.592x - 292.9$, where y-runoff, x-rainfall, and the coefficient of determination (r^2) 0.89 were obtained, which was in good correlation [13].

5 Conclusions

The following conclusions are derived from the foregoing study:

- LULC study has helped in understanding the dynamic human activities on land in space and time. Land use planning needs to be done according to the land suitability classes. Forest protection and replantation is necessary to preserve the environmental resources.
- GIS-based NRCS-CN method can be used effectively to assess the runoff from the ungauged sub-watershed. The increasing value of CN indicates that the LULC changes significantly, and the runoff is more.

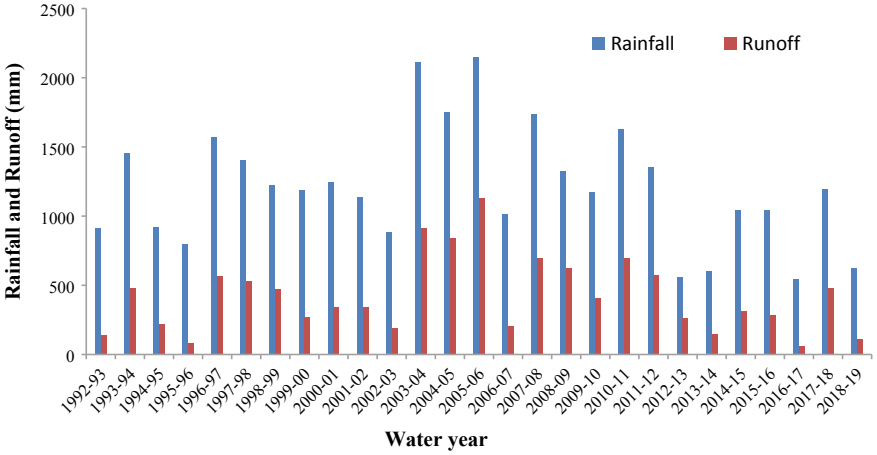

Fig. 6 Bar chart showing water year-wise annual rainfall and estimated runoff

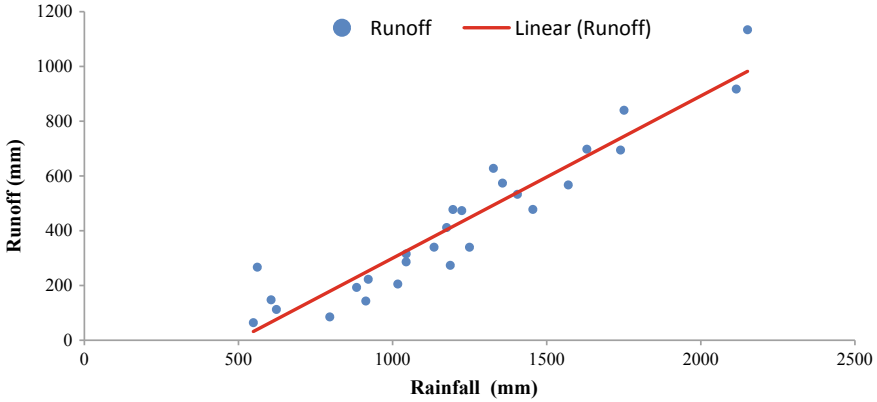

Fig. 7 Correlation of annual rainfall and estimated runoff during 1992–2019

- The result showed that the LULC changes can generate negative impacts such as increase in surface runoff, soil erosion and flood risks, and reduction of base-flow.
- Agronomic and engineering measures like contour-farming, vegetative barriers, strip-cropping, mixed-cropping, contour-bunding, and terraces are suggested to retard and reduce the overland runoff, soil erosion, and increase infiltration.

References

1. Anil Kumar P, Viswanadh GK (2017) Estimation of runoff by using SCS curve number method integrated with GIS. Int Adv Res J Sci Eng Technol 4(7):34–38
2. Anji Reddy M (2019) Remote sensing and geographical information systems. Textbook 4th edn. BSP Publications, New Delhi
3. Bhattacharyya R, Ghosh BN, Mishra PK, Mandal B, Rao CS, Sarkar D, Das K, Anil KS, Lalitha M, Hati KM, Franzluebbers AJ (2015) Soil degradation in India: challenges and potential solutions. Sustainability (Special Issue: Soil degradation) 7(4):3528–3570
4. Dubayah R, Lerrenmaier D (1997) Combing remote sensing and hydrological modeling for applied water and energy balance studies. NASA EOS Interdisciplinary Working Group Meeting, San Diego, USA
5. Dwarakish GS, Ganasri BP (2015) Impact of land-use change on hydrological systems: a review of current modeling approaches. Cogent Geosci 1(1):1–15
6. FAO (2012) The state of food and agriculture. Food and Agriculture Organization of the United Nations, Rome
7. Jaiswal MK, Amin N (2021) Impact of land-use land cover dynamics on runoff in Panchnoi River basin, North East India. GeoScape 15(1):19–29
8. Li P, Li H, Yang G, Zhang Q, Diao Y (2018) Assessing the hydrologic impacts of land use change in the Taihu Lake Basin of China from 1985 to 2010. Water 10(11):1512
9. Mondal A, Kundu S, Khare D (2017) Past, present and future land use changes and their impact on water balance. J Environ Manage 197:582–596
10. Samie M, Ghazavi R, Vali A, Pakparvar M (2019) Evaluation of the effect of land use change on runoff using supervised classified satellite data. Global NEST J 21(2):245–252
11. Shanmukha Srinivas G, Satyanarayana Moorthy DV, Yaswanth Kumar Y, Jyothi P (2018) Surface runoff estimation using RS and GIS—a case study of Swarnamukhi River, India. Int J Sci Res 9(5):780–784
12. United States Department of Agriculture (1972) Hydrology. In: National engineering handbook, soil conservation service (Section 4(10)). Soil Conservation Service, USDA, Washington
13. Velayudha Das M, Poongothai S (2018) Estimation of surface runoff using GIS-based NRCS-CN method in upper Manimuktha sub-watershed, Tamil Nadu, India. Int J Adv Eng Res Dev 5(3):68–79
14. Yin J, He F, Xiong YJ, Qiu GY (2017) Effects of land use/land cover and climate changes on surface runoff in a semi-humid and semiarid transition zone in northwest China. Hydrol Earth Syst Sci 21:183–196
15. Zhang W-Y (2018) Application of NRCS-CN method for estimation of watershed runoff and disaster risk. J Geomatics Nat Hazards Risk 1(1):2220–2238

Examining Curve Number-Based Modified Models for Runoff Estimation

Pankaj Upreti and C. S. P. Ojha

Abstract The curve number method is a universally accepted and widely explored model in the last four decades which is used to estimate event-based surface runoff. Its simplicity and versatility have made it popular, and the basic equation is used as an important part of various hydrological models. In the development of the SCS-CN model, various advanced and more data-intensive models were developed. These different versions introduced new parameters, but it cannot be applied directly in approximating real situations. To overcome these problems, this study has proposed two simple SCS-CN event-based runoff models. The two simple versions of the SCS-CN model (M_1) are presented by taking initial abstraction as a function of P ($\mathrm{Ia} = \alpha P$) instead of S (M_2) and by incorporating P_5 in the fractional form to obviate undesirable sudden jump (M_3). The performance of existing M_1 and formulated M_2 and M_3 models has been compared using root mean square error (RMSE), Nash–Sutcliffe efficiency (NSE), PBIAS statistics, and ranking and grading system. Based on their ranking score for M_2 and M_3, model scores were significantly higher than the M_1 model. Based on all statistics criteria and r^2 value, both M_2 and M_3 models performed significantly well over the existing model.

Keywords Antecedent rainfall · Event-based model · Initial abstraction · Maximum potential retention

1 Introduction

In applied hydrology, runoff estimation from any catchment is an important and major activity and useful in water resources management, assessment and planning of flooding hazards, study of reservoir sedimentation at the downstream, etc. In

P. Upreti (✉) · C. S. P. Ojha
Department of Civil Engineering, IIT Roorkee, Roorkee 247667, India
e-mail: pankaj.upreticot@gmail.com; pupreti@ce.iitr.ac.in

P. Upreti
Department of Agricultural Engineering, GMV Rampur Maniharan, Rampur Maniharan 247451, India

P. V. Timbadiya et al. (eds.), *Hydrology and Hydrologic Modelling*,
Lecture Notes in Civil Engineering 312,
https://doi.org/10.1007/978-981-19-9147-9_19

the rainfall-runoff transformation process, the runoff pattern is totally dependent on rainfall amount, its duration and intensity, antecedent conditions, land use and land cover, infiltration capacity of soil, and uncounted multiple other factors. Different variables influence the runoff amount and different variables-based models exist in the literature. Among them, the soil conservation services-curve number (SCS-CN) method is the most common and widely used method across the globe. According to Ponce and Hawkins [1], method is very simple, and fewer parameters are required while estimating event-based runoff from ungauged watersheds. Ajmal and Kim [2] revealed that the conventional SCS-CN model has some misinterpretation due to the basic empirical assumption. Since its development, hydrologists still debate the physical basis of the model and its empirical framework to validate their mathematical consistency and application significance. The success of this model depends on the reliable estimation of curve number value or S, which describes the runoff potential of watershed. The value of S is assumed as constant in the original model and taken from NEH-4 table. But, in actual, it changes due to antecedent moisture availability. Therefore, Hawkins [3] recommended the use of curve number (CN) or S value derived from the rainfall-runoff dataset over tabulated CN value. Tedela et al. [4] established that S value is not constant for a watershed but varies with rainfall and watershed characteristics. Upreti and Ojha [5] investigated the role of antecedent precipitation in runoff estimation. In the present study, we identify two more simple, accurate, and reliable SCS-CN-based hybrid model and compare these performances with the existing SCS-CN model. The basic SCS-CN model described in this study is reference as M_1 model. In model M_2, one of the assumptions of the basic model has been changed, and model M_3 incorporates 5-days previous rainfall, P_5 in fractional form to obviate undesirable sudden jump (M_3). The details of these models are presented here as:

1.1 M_1 Model

This is the most popular and widely used method to calculate runoff depth from a rainfall event in numerous hydrologic studies. The two basic assumptions of this method are as follows: (a) The ratio of actual runoff (Q, mm) and maximum possible runoff ($P-I_a$) is equal to the ratio of actual retention ($P-I_a-Q$) and maximum potential retention (S, mm), and (b) Initial abstraction (I_a) is the function of S. The combination of both assumptions leads to general form of the SCS-CN equation and is given as:

$$Q = \frac{(P - I_a)^2}{P - I_a + S} \tag{1}$$

where $I_a = \lambda S$. The value of λ (initial abstraction coefficient) was taken as 0.2 in application to both gauged and ungauged watershed, and the resulting equation becomes:

$$Q = \frac{(P - 0.2S)^2}{(P + 0.8S)} \tag{2}$$

for $P > I_a$, otherwise $Q = 0$.

This Eq. (2) is the most generally used form of SCS-CN method and the present study calibrates the parameter S instead of taking its value calculated from CN conversion to S.

1.2 M_2 Model

In the original SCS-CN method (taken as M_1 model in this study), one of the assumptions is that the initial abstraction ($I_a = \lambda S$) is the function of S, and λ (initial abstraction coefficient) is taken as 0.2. Later, Woodward et al. [6] found better results with its value as 0.05. In the formulation of model M_2, we assume that initial abstraction I_a is the function of rainfall amount P ($I_a = \alpha P$) instead of S. The rationale behind this assumption is that the generated runoff is highly dependent on rainfall event distribution, so initial abstraction (I_a), which is a part of rainfall-runoff transformation process, should be a function of rainfall amount of that individual event. We assume α value as 0.05 suggested by Woodward et al. [6], and Eq. (2) becomes:

$$Q = \frac{(P - 0.05P)^2}{P - 0.05P + S} \tag{3}$$

or

$$Q = \frac{0.9025P^2}{0.95P + S} \tag{4}$$

Equation (4) characterizes both the effect of rainfall variation on runoff and the watershed characteristic in the form of S.

1.3 M_3 Model

In the M_3 model, P_5 criterion was applied to analyze the effect of 5-days previous rainfall on runoff. Based on 5-days previous rainfall, we only know the watershed condition (AMC I or AMC II or AMC III) before runoff in the SCS-CN method. In this manner, these antecedent conditions and their corresponding S value create a sudden jump in runoff calculation. To avoid undesirable sudden jumps in runoff estimation and improve the prediction efficiency, M_3 model was developed by replacing S to $S\frac{P}{(P+P_5)}$ and substituting it in fundamental SCS-CN equation. In this way, new

expression varies storm-wise and with prior rainfall (P_5) value. This M_3 model gives the following equation as:

$$Q = \frac{\left(P - 0.2S\left\{\frac{P}{P+P_5}\right\}\right)^2}{\left(P + 0.8S\left\{\frac{P}{P+P_5}\right\}\right)} \tag{5}$$

After simplification, Eq. (5) yields

$$Q = \frac{(P + P_5 - 0.2S)^2}{(P + P_5 + 0.8S)} \cdot \frac{P}{(P + P_5)} \tag{6}$$

Replacement of S in this way changes runoff prediction for those events only for which P_5 value is greater than zero. For $P_5 > 0$ events, S value significantly changes with P_5 amount. If P_5 value tends to infinity ($S \to 0$), then $Q = P$, which indicates that all rainfall converts into runoff since soil had no storage capacity. Similarly, if S value tends to infinity (CN $\to$ 0), there will be no runoff. In order to avoid sudden jump, above expression as Eq. (6) provides variation in S value.

2 Material and Methods

2.1 Watersheds and Data

In the present study, the data used to evaluate model performance are taken from the USDA-ARS water database (http://www.ars.usda.gov/arsdb.html). This study considered a wide range of 114 USA watersheds which areas varying from 0.17 to 30,351.45 ha. The proposed models examined over 28,849 rainfall-runoff events. All three models were applied to the rainfall-runoff dataset for their comparative evaluation. The maximum and minimum average rainfall (P) and runoff depth (Q), average 5-days previous rainfall (AMC-5), and average runoff coefficient (C) of all 114 watersheds are presented in Table 1.

Table 1 Average minimum and maximum values of P, Q, AMC-5, and C

	Rainfall, P (mm)	Runoff, Q (mm)	5-days prior rainfall, AMC-5 (mm)	Runoff coefficient, C
Maximum	45.86	13.94	39.03	0.47
Minimum	8.49	1.39	8.71	0.08

2.2 Performance Evaluation

Model prediction accuracy assessment is an important aspect in hydrological modeling. For evaluating model performance RMSE, NSE as well as PBIAS criterion was used as indices of agreement between observed and computed runoff. These are given in Eqs. (7), (8), and (9), respectively, as follows:

$$\text{RMSE} = \left[\frac{1}{n}\sum_{i=1}^{n}(Q_o - Q_c)_i^2\right]^{1/2} \tag{7}$$

$$\text{NSE} = 1 - \left[\frac{\sum_{i=1}^{n}(Q_o - Q_c)_i^2}{\sum_{i=1}^{n}\left(Q_o - \overline{Qo}\right)_i^2}\right] \tag{8}$$

$$\text{PBIAS} = \left[\frac{\sum_{i=1}^{n}(Q_o - Q_c)_i}{\sum_{i=1}^{n}(Q_o)_i}\right] \tag{9}$$

where Q_O is the observed runoff in mm, Q_c is the computed or calculated runoff in mm, $\overline{Q_O}$ is the mean runoff value calculated from n number of events from that particular watershed, and i is an integer varying from 1 to n.

Senbeta et al. [7] suggested r^2 statistic to evaluate performance improvement of the modified model over the existing one and expressed as:

$$r^2 = \frac{(\text{NSE}_2 - \text{NSE}_1)}{1 - \text{NSE}_1} \tag{10}$$

where NSE_1 and NSE_2 are the efficiency of existing and modified models, respectively. It value more than 10% indicates a significant improvement in model performance.

2.3 Parameter Estimation

In order to compute the optimized value of model parameter S, the least-square fitting technique was used to minimize the sum of squared difference between computed and observed runoff (Eq. (11)), employing Microsoft Excel (Solver) [8].

$$\sum_{i}^{n}(Q_{oi} - Q_{ci})^2 = \sum\left[Q_o - \left\{\frac{(P - \lambda S)^2}{P + (1 - \lambda S)}\right\}\right]^2 \Rightarrow \text{Minimum} \tag{11}$$

All three models M_1, M_2, and M_3 allowed variation of parameter S in optimization. In model M_1 and M_3, an initial estimate of parameter S was taken as 250 mm and allowed to vary in the range of 1–2500. The parameter S ranged between 1 and 1000

Table 2 Range of value of parameter S (mm) resulting from application of M_1, M_2, and M_3 models

Model	Value				90% confidence interval	
	Mean	Median	Minimum	Maximum	Lower	Upper
M_1	67.91	56.57	21.90	315.15	61.55	74.26
M_2	133.11	99.66	31.10	909.26	115.51	150.71
M_3	89.43	77.73	29.24	252.13	82.77	96.08

with its initial estimate as 125 mm in the M_2 model. It is noted that the parameter S in all model formulation was allowed to vary within the prescribed range. The range of calibrated parameter S resulting from the application of all three models is presented in Table 2.

3 Results and Discussion

In the present study, rainfall-runoff data having 28,849 total events were selected for application of the M_1, M_2, and M_3 model to the 114 USA watersheds. The mean, median, maximum, minimum, and lower and upper bound (at 10% CI) values of RMSE, NSE, and PBIAS for all three models are presented in Table 3, and variation in these criterions is also drawn by Box and Whisker plot in Fig. 1. The RMSE value of 99 and 95 watersheds for M_2 and M_3 model was found lesser than M_1. The mean value of RMSE for M_2 and M_3 was also found lesser than M_1. The NSE value cannot be judged by their mean value since this is negative in some watersheds for all three models. There are 6, 1, and 5 watersheds in M_1, M_2, and M_3 models, respectively, which exhibit negative NSE value. The NSE value less than 0.5 was found for 30, 20, 24 watersheds for M_1, M_2, M_3 models, respectively. Similarly, its value greater than 0.8 was found 7, 7, 19 watersheds for M_1, M_2, M_3 model, respectively. There are 55, 65, and 59 watersheds for which NSE values lies in between 0.6 and 0.8. Although, the mean and median values of NSE were improved for M_2 and M_3 model over the existing M_1 model. The average value of NSE reveals that both model M_2 and M_3 performed equally well.

For PBIAS statistics, the M_1 model indicated very good performance in 30 watersheds only, and it reaches up to 74 and 79 watersheds for M_2 and M_3 models. The PBIAS value is positive in 104 and negative in only 10 watersheds for model M_1. It means the M_1 model underestimated the runoff value in these watersheds but proposed M_2 and M_3 models underestimated (positive PBIAS) runoff in 71 and 74 watersheds and overestimated (negative PBIAS) runoff in 43 and 40 watersheds. It means, from the PBIAS statistics point of view, M_2 and M_3 model performed well.

When we see the overall collective performance of PBIAS using their mean value of all 114 watersheds, it decreased from + 15.10% (M_1) to + 3.67% and + 4.12% for M_2 and M_3 model, respectively.

Table 3 Different statistical values of RMSE, NSE, and PBIAS for all three models over 114 US watersheds

	M_1			M_2			M_3		
	RMSE (mm)	NSE	PBIAS (%)	RMSE (mm)	NSE	PBIAS (%)	RMSE (mm)	NSE	PBIAS (%)
Mean	5.60	0.55 (0.60)	15.10	5.28	0.62 (0.63)	3.67	5.17	0.61 (0.64)	4.12
Median	5.00	0.62 (0.63)	14.63	4.71	0.66 (0.66)	2.76	4.48	0.68 (0.69)	1.74
Maximum	11.62	0.92	50.37	11.38	0.94	47.80	10.91	0.94	41.14
Minimum	1.14	−1.03	−27.54	1.24	−0.25	−25.22	1.68	−0.72	−24.65
Lower bound (10% C.I.)	5.27	0.51	13.17	4.96	0.59	1.89	4.87	0.57	2.22
Upper bound (10% C.I.)	5.93	0.59	17.02	5.61	0.65	5.46	5.48	0.64	6.01

In bracket, mean and median values of all 114 watersheds are given excluding negative NSE

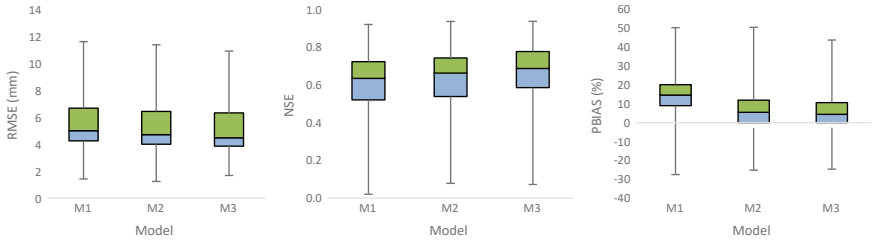

Fig. 1 Box and Whisker plot for variation of RMSE (mm), NSE, and PBIAS (%) for watersheds using different models

Based on the r^2 criterion, significant improvement was found in 56 and 71 watersheds for M_2 and M_3 models, respectively, over the existing M_1 model. A total of 99 watersheds for M_2 and 95 for the M_3 model show improvement in NSE over the M_1 model. Figure 2 shows that how much M_2 and M_3 models performed well in terms of NSE, using r^2 criteria over the existing M_1 model. Figure 3 illustrates the improvement in r^2 as a cumulative percentage distribution in 114 US watershed.

The performance of the proposed model M_2 and M_3 was also investigated using the ranking and grading system. The first, second, and third rank assigned a grade 3, 2, 1, respectively, to the model M_1, M_2, and M_3 as per their NSE obtained in applications to all 114 watershed datasets. The first rank means maximum NSE and given to grade 3. Similarly, other grades (grade 1 assigned for minimum NSE) were given to each model for all watersheds. The assigned grades were added for ranking of all three models in order to assess their overall performance. Figure 4 shows that the M_1 model gained score 1 (less score) for 86 watersheds, but M_2 and M_3 model gained scores 2 and 3 (high score) for 92 (66 + 26) and 108 (71 + 37) watersheds, respectively. Overall, M_2 and M_3 models attained 254 and 282 marks, respectively, while M_1 scored only 148 marks. Based on the overall results obtained, both M_2 and M_3 models performed significantly well in comparison to the M_1 model.

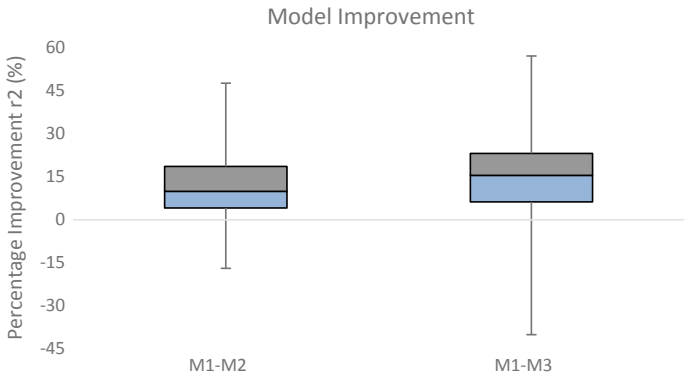

Fig. 2 Percentage improvement of M_2 and M_3 model over M_1 using r^2 criteria

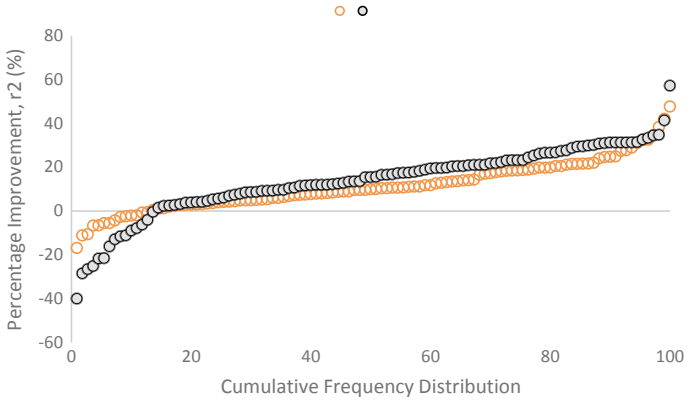

Fig. 3 Improvement as cumulative percentage distribution in 114 US watershed

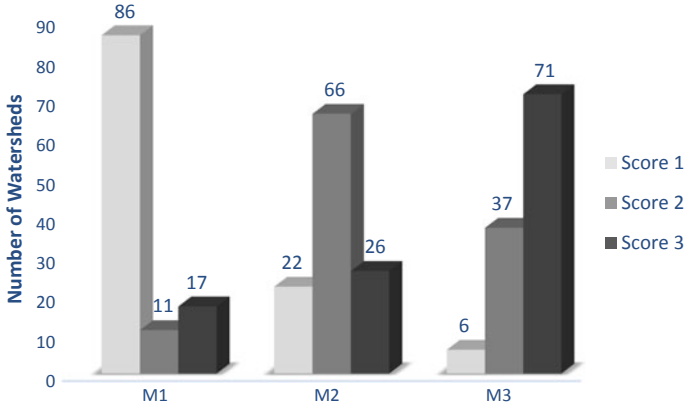

Fig. 4 Number of watersheds having score is 1, 2, or 3 in ranking and grading system

The CN model (M_1) generally underestimated the runoff value. It was evident that the CN model (M_1) predicted runoff approaching zero for events having less amount of rainfall. Due to this fact, S obtained from the CN model does not predict runoff in a well manner. Based on all the above criteria, both M_2 and M_3 models performed slightly well in terms of RMSE and NSE and significantly well in PBIAS values compared to the CN model.

4 Conclusions

In this study, we investigated two simple models that are based on universally used NRCS model (M_1). In the M_2 model which is a refinement of the M_1 model, we

considered the effects of both rainfall variation and maximum potential retention on initial abstraction. To improve the prediction efficiency of estimated runoff and circumvent undesirable sudden jumps on runoff calculation, the M_3 model considered the effect of antecedent 5-days rainfall which could vary with initial moisture condition for that rainfall-runoff event. Compared to CN model (M_1), both formulated modified versions indicate significant improved performance in terms of RMSE, NSE, PBIAS, r^2 statistics, and ranking and grading system criterion. Due to its simplicity (M_2 model) and characteristics to obviate the undesirable sudden jump (M_3 model) in a very simple way, both models may be recommended and endorsed for their application in small US agricultural watersheds.

Acknowledgements The authors would like to acknowledge the infrastructural support provided by the Civil Engineering Department, Indian Institute of Technology, Roorkee, India.

References

1. Ponce VM, Hawkins RH (1996) Runoff curve number: has it reached maturity? J Hydrol Eng 1(1):11–19
2. Ajmal M, Kim TW (2015) Quantifying excess storm water using SCS-CN–based rainfall runoff models and different curve number determination methods. J Irrig Drain Eng 141(3):04014058
3. Hawkins RH (1993) Asymptotic determination of runoff curve numbers from data. J Irrig Drain Eng 119(2):334–345
4. Tedela NH, McCutcheon SC, Rasmussen TC, Hawkins RH, Swank WT, Campbell JL, Adams MB, Jackson CR, Tollner EW (2011) Runoff curve numbers for 10 small forested watersheds in the mountains of the Eastern United States. J Hydrol Eng 17(11):1188–1198
5. Upreti P, Ojha CSP (2021) Comparison of antecedent precipitation based rainfall-runoff models. Water Supply 21(5):2122–2138
6. Woodward DE, Hawkins RH, Jiang R, Hjelmfelt AT, Van Mullem JA, Quan QD (2003) Runoff curve number method: examination of the initial abstraction ratio. World Water Environ Resour Congr 1–10
7. Senbeta DA, Shamseldin AY, O'Connor KM (1999) Modification of the probability-distributed interacting storage capacity model. J Hydrol 224(3–4):149–168
8. Upreti P, Ojha CSP (2022) Development and performance evaluation of SCS-CN based hybrid model. Water Sci Technol 85(9):2479–2502

Development of Short-Term Reservoir Level Forecasting Models: A Case Study of Ajwa-Pratappura Reservoir System of Vishwamitri River Basin of Central Gujarat

Urvish P. Nagar and H. M. Patel

Abstract Flood events in the rivers are increasing across the world due to the possible impact of climate change. In the case of reservoirs, flood routing is becoming very important to reduce the damage to the downstream area. The operation of reservoirs needs reliable information on inflow in real time. In the case of an ungauged catchment, it is difficult to apply rainfall-runoff simulation models. In small catchments, the lag time is also very short, and long-term prediction is very difficult to operate reservoirs in case of flood situations. In this study, a hybrid reservoir inflow forecasting model is developed for the Ajwa-Pratappura twin reservoir system. Ajwa and Pratappura reservoirs are constructed to supply the drinking water to Vadodara City. The combined catchment area is 203 km^2. Aasoj feeder canal diverts the water from Pratappura reservoir to Ajwa Reservoir. Ajwa Reservoir has a storage capacity of 2240 MCFT. During heavy flood events, both the reservoirs release water into the Vishwamitri River which is passing through the Vadodara City. A careful operation of the Ajwa Reservoir is very much required to manage the flood downstream covering the city area of Vadodara. The objective of the present study is to predict the reservoir water level based on a short-term inflow forecast at the Ajwa-Pratappura Reservoir system. A mathematical model based on the SCS curve number is developed to predict the inflows from the catchment of both the reservoirs during storm events. Catchment delineation is done using DEM data from ISRO-BHUVAN using QGIS. Major storm years from 2015 to 2020 are selected to calibrate and validate the model. The model is further coupled to use 3 h of forecast data of Vadodara Station from meteograms generated through the IMD-GFS model. The framework developed for the inflow prediction is found to have high applicability for generating early warnings and for reservoir operation.

Keywords Inflow forecast · Rainfall-runoff model · Flood early warning system

U. P. Nagar (✉) · H. M. Patel
Civil Engineering Department, Faculty of Technology and Engineering, The M.S. University of Baroda, Vadodara 390001, India
e-mail: urvishnagar2797@gmail.com

H. M. Patel
e-mail: hmpatel-ced@msubaroda.ac.in

P. V. Timbadiya et al. (eds.), *Hydrology and Hydrologic Modelling*,
Lecture Notes in Civil Engineering 312,
https://doi.org/10.1007/978-981-19-9147-9_20

1 Introduction

We know that water is necessary for sustainable human development and the healthy functioning of the planet's ecosystem. South Asia is one of the most disaster-prone regions in the world [5]. India is one of the worst flood-affected countries in the world. Building resilience to natural disasters is a pressing challenge for achieving sustainable development in the region. Floods are one of the natural disasters in India having devastating impacts on the vulnerable population, especially the poor, who live along the riverside and are dependent on agriculture for their livelihood.

Flood events in the rivers are increasing across the world due to the possible impact of climate change. In the case of reservoirs, flood routing is becoming very important to reduce the damage to the downstream area [2]. Flood early warning is one of the most effective nonstructural flood disaster damage mitigation methods [10, 11]. In recent years, this approach has gained momentum due to the availability of space-based inputs, high-resolution digital terrain models, advanced modeling software, and high-end computing systems. Many researchers and engineers across the country are working on flood early warning activity in isolation using different methods and models [4, 8, 9]. Hence, there is a need to bring synergy among the modelers and researchers to understand the latest technological developments in flood early warning [1]. Early warning is an important measure for disaster risk reduction. The present study is to predict the reservoir water level based on a short-term inflow forecast at the Ajwa-Pratappura Reservoir system. A mathematical model based on the SCS curve number is developed to predict the inflows from the catchment of both the reservoirs during storm events. By conducting the present study, the water level at Ajwa Reservoir can be determined in advance, and thus flood management can be done.

2 Materials and Methods

2.1 Estimation of Runoff Using SCS-CN Method

A mathematical model based on the SCS curve number is developed to predict the inflows from the catchment of both the reservoirs during storm events. In the early 1950s, the United States Department of Agriculture (USDA) Natural Resources Conservation Service (NRCS) (then named the Soil Conservation Service (SCS)) developed a method for estimating runoff from rainfall [3, 7, 12]. The SCS curve number method is based on the water balance equation and two fundamental hypotheses which are stated as,

(1) Ratio of the actual direct runoff to the potential runoff is equal to the ratio of the actual infiltration to the potential infiltration,

(2) The amount of initial abstraction is some fraction of the potential infiltration (Handbook of hydrology, 1972).

$$Q/(P - \text{Ia}) = F/S \tag{1}$$

$$F = (P - \text{Ia}) - Q \tag{2}$$

Substituting Eq. (2) in Eq. (1) and by solving;

$$Q/(P - \text{Ia})^2/(P - \text{Ia} + S) \tag{3}$$

where Q = Actual runoff (mm), P = rainfall (mm), and Ia = initial abstraction, which represents all the losses before the runoff begins and is given by the empirical equation.

$$\text{Ia} = 0.2\ S \tag{4}$$

Substituting Eq. (4) in Eq. (3), Eq. (3) becomes

$$Q = (P - \text{Ia})^2/(P - \text{Ia} + S) \tag{5}$$

S = the potential infiltration after the runoff begins given by the following equation where CN is curve number.

$$S = 25400/\text{CN} - 254 \tag{6}$$

3 Study Area and Data Source

3.1 Ajwa Dam

The area selected for the study to be conducted is the Ajwa Dam. The dam is located on the Surya River, in the Waghodia Taluka of the Vadodara district. The dam is an earthen dam constructed with the main aim to meet the water requirements of the people of Vadodara city. The dam was constructed in the year 1891 and was designed by Mr. Jagannath Sadashiv [6]. The reservoir created by the construction of the dam is named Sayaji Sarovar and has a total catchment area of 132 km^2. The topography of the city is generally flat with a gentle slope from the Northeast to the Southwest, following the basin of the Vishwamitri River [13].

The dam supplies water from the Pratappura dam via the Aasoj feeder canal and the Narmada canal in addition to the water coming from the catchment. The reservoir water is supplied to the Nimeta water treatment plant for purification from the intake structure provided to withdraw the water. The dam is provided with 62 numbers of spillways with gates that are operated as and when required.

3.2 Data Used

The daily rainfall data for nine rain gauge stations were collected from Vadodara Municipal Corporation (VMC), and the water level data for Ajwa and Pratappura Reservoir were obtained from VMC Office, to understand catchment characteristics like geology, soil, land use, and drainage digital elevation models (DEMs) of the study area are prepared using QGIS 3.12. For the development of the model, various features of the actual dam and its connected structures are studied (Fig. 1).

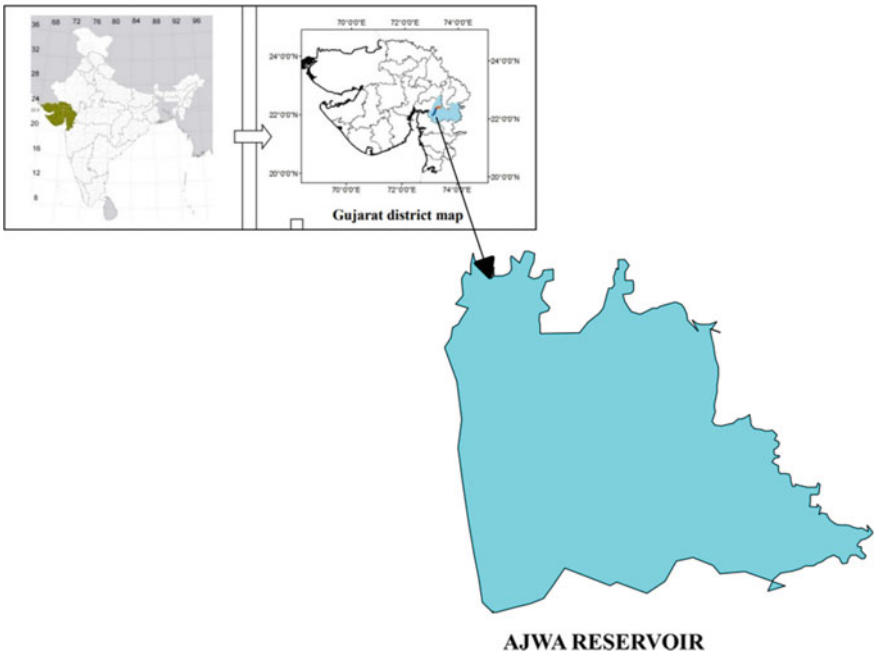

Fig. 1 Location of study area—Ajwa Reservoir

3.3 Rainfall and Reservoir Water Level Data

Daily rainfall data for five years starting from July 2015 to October 2020 have been collected, and storm events are identified as having rainfall greater than 100 mm in a day. These storms are found to be resulting in a rise in reservoir level. The area under each rain gauge station is identified. The Thiessen polygon method is used to calculate the spatial distribution of rainfall storms; events with $P \geq 100$ mm have been considered to determine CN values, and runoff is derived from SCS-CN model. After that total inflow is found, and from it, the water level is predicted by following the VMC chart of storage vs water level.

3.4 Model Development

A mathematical model based on the SCS curve number is developed to predict the inflows from the catchment of both the reservoirs during storm events. The runoff contribution from all rain gauge stations found then total runoff and runoff depth is calculated by considering the total combined catchment area of the Ajwa-Pratappura Reservoir system as 132 km^2. After that total inflow is found, and from it, the water level is predicted by following the VMC chart of storage vs water level. In the modeling work, forecasted rainfall data are taken from the IMD Web site, and real-time rainfall data are taken from the VMC Water Works department. In this project, total 3 types of the hybrid model framework are done:

1) Daily water-level prediction model
2) Hourly water-level prediction model
3) 3-hourly water-level prediction model.

The 3-hourly model is further developed to use 3 h forecast data of Vadodara station from meteograms generated through the IMD-GFS model. The framework developed for the inflow prediction is found to have high applicability for generating early warnings and for reservoir operation.

Daily rainfall data from the meteorological station in Vishwamitri Basin are analyzed for the years from 2015 to 2020. Basic statistical analyses were conducted on the seasonal rainfall data. From the process of identification of independent storms, various storm events are selected for the study. The Thiessen polygon method is used to calculate the spatial distribution of rainfall and % area of influence for rainfall over different sub-basins is obtained, and runoff is derived from SCS-CN model. For the present study, a mathematical model based on the SCS curve number is developed to predict the inflow in the Ajwa Reservoir.

4 Results and Discussions

Major storm years from 2015 to 2020 are selected to calibrate the model. The model is further coupled to use forecast data of Vadodara Station from meteograms generated through the IMD-GFS model. The framework developed for the inflow prediction is found to have high applicability for generating early warnings and for reservoir operation.

4.1 2019 Storm

The simulation is carried out on 31st July 2019 rainstorm. On this day, catchment recorded 360 mm of rainfall in a day. Ajwa Reservoir reaches at rule level on this day. It is assumed that the rainfall occurring in Ajwa and internal catchments is considered accumulating into Ajwa Reservoir, whereas rainfall occurring in Pratappura catchment is only considered if the Vishwamitri gates are closed, and all the runoff is diverted into Ajwa Reservoir through the feeder channel. The calculated value of weighted CN is 86 for the study area. From the entered rainfall data, this mathematical hybrid model based on SCS curve number is analyzed, and modified CN is obtained. From the present research, predicted water level and the actual observed water level are compared, and a graph of water level vs time is plotted. Inflow forecast calculation is also obtained by the model which is shown in Fig. 3.

Figure 2 shows the water level variation with time. The graph of water level versus time indicates the reservoir level increases with time from 209.05 ft to 212.5 ft. The comparison between observed and predicted water levels is shown. Water level is continuously rising due to the presence of inflow. Figure 3 shows that inflow is increasing with time, and after some time, it is reducing concerning the storm. Predicted inflow from forecasted rainfall and actual inflow with real-time rainfall is compared and shown in the graph.

In this case, the previous 5 days' rainfall is 44.8 mm, so AMC-II condition is considered, and obtained CN is 72.92. The predicted level and the observed levels are matching with the observed level.

The sum squared error for observed and computed values is minimised by calibrating the CN. Using calibrated value of CN (65.36), the water levels are predicted for 31 July 2019 event and compared with observed values as shown in Figs. 4 and 5.

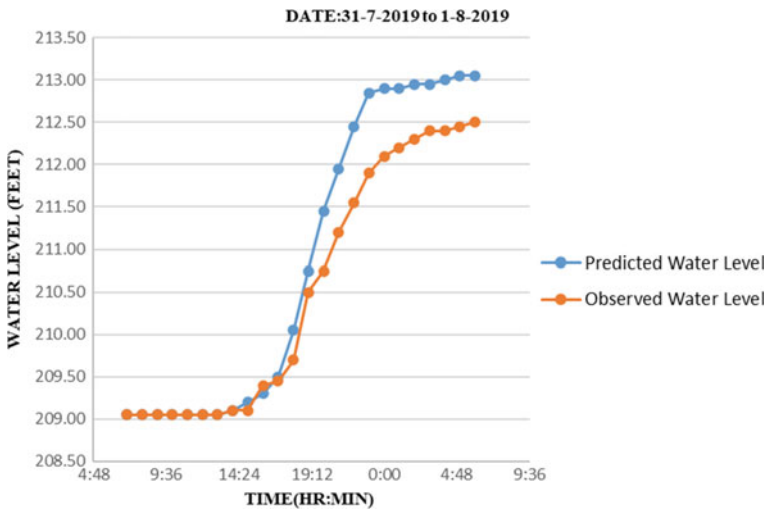

Fig. 2 Observed and predicted water level for 2019 storm

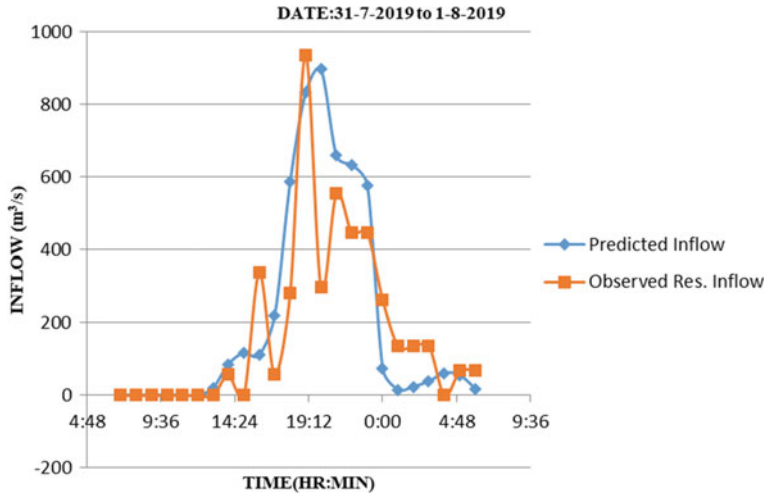

Fig. 3 Observed and predicted inflow for 2019 storm

5 Conclusions

The following conclusions are derived from the foregoing study:

- The present study reveals the nature of the rainfall-runoff process in the Ajwa Reservoir catchment. The Ajwa Reservoir receives water from 95 km^2 catchment area directly and 27 km^2 of intermediate catchment area between Ajwa and Pratappura.

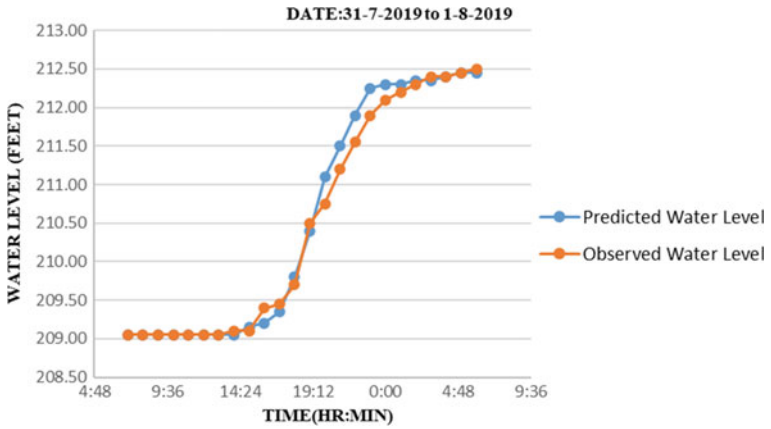

Fig. 4 Water level after calibration for 2019 storm

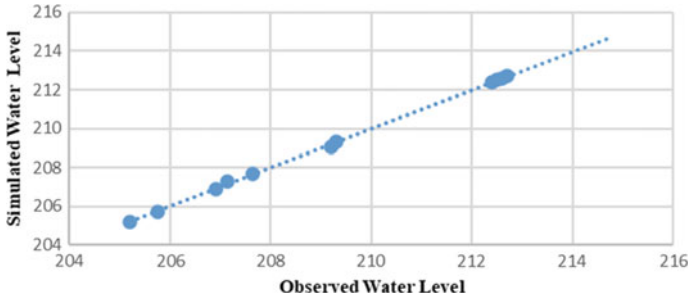

Fig. 5 Correlation performance of calibration

- The catchment is ungauged, and the natural flow is found to be affected by the SSP Main canal, Vadodara-Halol toll road, and Aasoj feeder canal. In absence of a clear channel network and gauging data, HEC-HMS or other sophisticated models are not feasible to predict storm runoff.
- SCS-CN-based model is developed to predict the reservoir water level. The model is calibrated using the past 11 major storm events, and the curve number for the catchment is found to be varying from 60 to 90 for AMC Type-II.
- The model is further developed to predict the water level in the Ajwa Reservoir using IMD-GFS model short-term forecast data. In the event of a heavy flood, the developed model can provide a very useful prediction of the reservoir elevation under the short-term forecast, particularly when the reservoir water level is near the rule level or FRL.
- Short duration runoff estimation model is very much helpful to the authority for the management of reservoirs during heavy storm events.

Acknowledgements The authors are thankful to Vadodara Municipal Corporation for providing such necessary data to carry out the present work. The authors are also thankful to India Meteorological Department (IMD) for providing the necessary data to conduct the present study.

References

1. Ahmad I, Vivek V, Verma MK (2014) Estimation of runoff potential using SCS-CN method with remote sensing and GIS. In: 19th international conference on hydraulics, water resources, coastal and environmental engineering (HYDRO 2014)
2. Durga Rao KHV, Amanpreet S, Sindhu K, Shraddha M (2019) Spatial flood early warning system for the Godavari and Mahanadi Rivers—using space inputs challenges in India. In: Proceedings of national conference on flood early warning for disaster risk reduction 30–31 May 2019, Hyderabad Jointly organized by NRSC, NHP & CWC, Delhi
3. Geetha K, Mishra SK, Eldho TI, Rastogi AK, Pandey RP (2016) Development of SCS-CN-based modified model for hydrologic forecasting. J Hydraul Eng Am Soc Civ Eng
4. Jha R, Sharma KD, Neupane B (2009) Technique for supporting the identification and remediation of water scarcity issues and global change impact on water resources in India. Int J Hydrol Environ (IHES) Korea 2009:1–11
5. Manual of National Conference on Flood Early Warning System (FLEWS) for disaster risk protection (2019)
6. Manual on Monsoon Action Plan, Vadodara Municipal Corporation, (2020–2021)
7. Mishra SK, Jain MK, Pandey RP, Singh VP (2005) Catchment area-based evaluation of the AMC-dependent SCS-CN-based rainfall-runoff models. Hydrol Process 19(14)
8. Neha M, Kurian C, Sudheer KP (2016) Development of a flood forecasting model using HEC-HMS. In: National conference on water resources & flood management
9. Nithin PP, Janga R (2017) Flood modeling in the upper Krishna River basin using HEC-HMS and GIS tools. In: Proceedings of international conference on hydraulics, water resources & coastal engineering 21–23 December 2017
10. Kumar Bales R, Jubach R, Kane MD (2006) Flash flood warning system for upper Sutlej River Basin Northern India. J Hydraul Eng Am Soc Civ Eng
11. Pani RK, Mishra SK, Singh RD (2019) Flood forecasting and inundation mapping of a river basin in South–East India. J Indian Water Resour Soc (IWRS)
12. Subramanya K (2013) Engineering hydrology, 4th edn. McGraw Hill Publishing Company Limited, New Delhi, India
13. Suvarna S, Patel JN (2010) Development of flood forecasting model on Vishwamitri river basin. Indian J Flood Eng

Performance Assessment of Modest Event-Based Rainfall-Runoff Model

Pankaj Upreti and C. S. P. Ojha

Abstract A very simple and widely used SCS-CN method is a time-independent method that is used to calculate accumulated runoff corresponding to a single rainfall event. The method requires only two parameters initial abstraction coefficient (λ) and the potential maximum retention (S) expressed in terms of curve number (CN). The CN value incorporates many factors in its own and can be adopted for different climatic conditions. In the present study, a modest and easy to use non-linear event-based rainfall-runoff model is used which consist a single parameter α without taking into consideration of initial abstraction coefficient (λ) and curve number (CN). The quantitative model performance was assessed and compared based on RMSE, NSE and PBIAS (per cent bias) value. Based on the statistical criterion, the proposed model without CN concept reveals more statistically significant results (low RMSE, high NSE and statistically significant PBIAS values) and depicted improved performance than the conventional CN model.

Keywords SCS-CN model · Antecedent moisture condition · Initial abstraction · Event-based non-linear model

1 Introduction

SCS-CN model is globally used and most reliable empirical-based lumped rainfall-runoff model for calculating runoff from a rainfall event. Based on watershed and rainfall characteristics, this method estimates peak rate and volume of runoff from ungauged watersheds. Due to its simplicity, less data requirement, modesty in use and clearly stated assumptions, this methodology is used in various complex hydrological and ecological models. Therefore, this method has been used in design of various

P. Upreti (✉) · C. S. P. Ojha
Department of Civil Engineering, IIT Roorkee, Roorkee 247667, India
e-mail: pupreti@ce.iitr.ac.in

P. Upreti
Department of Agricultural Engineering, GMV Rampur Maniharan, Saharanpur 247451, India

P. V. Timbadiya et al. (eds.), *Hydrology and Hydrologic Modelling*,
Lecture Notes in Civil Engineering 312,
https://doi.org/10.1007/978-981-19-9147-9_21

types of hydraulic and water harvesting structures, storm water modelling, watershed development and management, flood forecasting, river bank filtration, evapotranspiration modelling, problem to identify non-point source pollution, etc. Since its development, model evolved numerous refinements beyond original one. Verma et al. [1] integrated this model with RS and GIS techniques for runoff estimation of spatially and temporally varied gauged and ungauged watersheds. Since SCS-CN model produced inconsistent results, hydrologist of modern era cross examine the SCS-CN methodology with more field data.

According to Hawkins and Ward [2], SCS-CN model require a key element as an input parameter called Curve Number (CN) which is basically a land condition coefficient, vary seasonally and its variation is depends on physiographic and climatic characteristics of watershed. It means variation in CN value is a function of rainfall amount and its duration, soil type, land cover condition and most importantly on antecedent moisture condition. The accurate and reliable estimation of curve number (CN) is required under different soil and land use condition for better result and overall acceptance of this model. The SCS consider curve number as a constant value for each watersheds with long term unchanged land use-land cover and hydrologic condition. Hawkins et al. [3] found in his study that due to change in moisture condition of a watershed as rainfall progressed, curve number value which is a scale of maximum potential retention S, can also varies between storms. Upreti and Ojha [4] formulated a model that incorporated 5-days antecedent rainfall in the SCS-CN model and improve model efficiency. Jain et al. [5] assess and compared the performance of various curve number-based methods by employing National Engineering Handbook (NEH-4) procedure for US watersheds. Ali and Sharda [6] compared five CN estimation methods, i.e., NEH-4, rank order, storm event, lognormal frequency and S-probability methods, and predicted runoff with lognormal frequency method found better than other method for small catchments in the semi-arid regions of India. Overall, to predict somewhat correct value of curve number, a critical study is needed under different watersheds. The curve number value obtained from NEH-4 table shows poorer prediction of runoff than CN value calculated from measured rainfall-runoff data. Kim et al. [7] suggest CN value should be calibrated before its use since tabulated CN value overestimate the hydrologic system. Upreti and Ojha [8] proposed a SCS-CN-based hybrid model and improve the prediction efficiency. Soulis and Valiantzas [9] suggested curve number value should be obtained from measured storm events.

Due to ambiguity in the selection of best possible curve number (CN) value, present study suggest a modest and easy to use non-linear event based and single parameter required rainfall-runoff model without taking into consideration of curve number (CN). This model performance were checked over existing NRCS-CN model and a relationship was developed between CN and constant parameter of proposed model.

1.1 NRCS-CN Model

When partial amount of water from an event rainfall (P) flow over land surface in form of direct surface runoff (Q) after satisfying initial abstraction and infiltration of water into soil, the water balance equation can be expressed as:

$$P = I_a + F + Q \tag{1}$$

The two fundamental hypothesis of a Soil Conservation Services-Curve Number (SCS-CN) method can be written as:

$$\frac{Q}{P - I_a} = \frac{F}{S} \text{ or } \frac{(P - I_a - Q)}{S} \tag{2}$$

$$I_a = \lambda S \tag{3}$$

where I_a = initial abstraction, F = total infiltration, S = maximum potential retention and λ is initial abstraction coefficient. After combining Eq. (2) and Eq. (3), makes the popular and universally used SCS-CN equation as:

$$Q = \frac{(P - I_a)^2}{P - I_a + S} \text{for} \quad P > I_{a,} \text{ otherwise } Q = 0 \tag{4}$$

Considering $I_a = \lambda S$ and assuming λ value as 0.2, Eq. (4) becomes:

$$Q = \frac{(P - 0.2\mathrm{S})^2}{(P + 0.8S)} \tag{5}$$

Equation (5) is popularly known as NRCS-CN model equation. The value of S can be obtained using CN value with following equation

$$S = \frac{25400}{\mathrm{CN}} - 254 \tag{6}$$

For measured values of event rainfall (P) and its corresponding runoff (Q) for gauged watershed, the value of S can be obtained by below given Eq. (7)

$$S = 5\left[(P + 2Q) - \sqrt{\left(4Q^2 + 5PQ\right)}\right] \tag{7}$$

This S value obtained from Eq. (7), can be transformed into curve number using Eq. (6).

1.2 Proposed Model

Instead of using most commonly event-based rainfall-runoff NRCS-CN model, a modest and easy to use non-linear event-based rainfall-runoff model was proposed in this study without taking into consideration of both curve number (CN) and initial abstraction coefficient (λ), using least square Marquarted algorithm after randomized configuration. The general form of this model was expressed as:

$$Q = \frac{\alpha P^2}{(\alpha P + 1)} \tag{8}$$

where P and α are rainfall and model constant, respectively, and both are greater than zero. If this condition is not satisfied then Q becomes zero. In order to find optimized value of α, least square fitting technique is used in this study. The detailed procedure is given in the methodology section.

2 Materials and Methods

2.1 Study Area

To study the performance of both models, data is taken from the United State Department of Agriculture-Agricultural Research Service (USDA-ARS) water database. A total 114 watersheds have been selected for this study with areas varying from 0.17 ha to 30,351.45 ha. Both models were applied to this event-based dataset for their comparative evaluation.

2.2 Data Selection

In this study only larger events for which rainfall amount is greater than 25.4 mm have been selected. In this way we can avoid the biasing effects of small storm towards high CN value (lower S value). A total 7314 events were sorted which rainfall value is greater than 25.4 mm.

2.3 Parameter Estimation

In order to compute optimized value of curve number (CN) for NRCS-CN model and α value of proposed model, least square fitting technique was used to minimize the sum of squared difference between predicted and observed runoff amount employing

Microsoft Excel (Solver) [9].

$$\sum_{i}^{n}(Q_{oi} - Q_{ci})^2 = \sum\left[Q_o - \left\{\frac{(P - \lambda S)^2}{P + (1 - \lambda S)}\right\}\right]^2 \Rightarrow \text{Minimum} \tag{9}$$

In NRCS-CN model, initial value of CN considered as 50 and allowed to vary in between 0 and 100, however in proposed model, starting value of α is taken as 0.01 and acceptable range to vary in between 0 and 1. The optimized values of CN and α, resulting from both models are presented in Table 1.

2.4 Performance Evaluation

For evaluating model performance, root mean square error (RMSE), Nash–Sutcliffe efficiency (NSE) and PBIAS criterion were used as indices of agreement between observed and predicted runoff. These are given in Eqs. (8), (9) and (10), respectively, as follows:

$$\text{RMSE} = \left[\frac{1}{n}\sum_{i=1}^{n}(Q_o - Q_c)_i^2\right]^{1/2} \tag{10}$$

$$\text{NSE} = 1 - \left[\frac{\sum_{i=1}^{n}(Q_o - Q_c)_i^2}{\sum_{i=1}^{n}\left(Q_o - \overline{Q_O}\right)_i^2}\right] \tag{11}$$

$$\text{PBIAS} = \left[\frac{\sum_{i=1}^{n}(Q_o - Q_c)_i}{\sum_{i=1}^{n}(Q_o)_i}\right] \tag{12}$$

where Q_O is the observed runoff in mm, Q_c is the computed or calculated runoff in mm, $\overline{Q_O}$ is the mean runoff value calculated from n number of events from that particular watershed and i is an integer varying from 1 to n.

2.5 Methodology

The following steps were taken to perform this study:

i. Selected those events for which rainfall amount is greater than 25.4 mm.
ii. Calculate curve number of each such events using Eq. (7) for rainfall and its corresponding runoff dataset for a particular watershed.
iii. Calculate average (CN_{ave}) and median curve number (CN_{median}) of a watershed using all event CN values. This work have been done for all 114 watersheds (mean, median, standard deviation and confidence interval at 10% value of CN_{ave} and CN_{median} is given in Table 1).

Table 1 Mean, Median, SD and CI at 10% under different area range of all watersheds

	Statistics	CN_{ave} *(i)*	CN_{med} *(ii)*	**NRCS-CN model**				**Proposed model**			
				CN_{opti} *(iii)*	*RMSE (iv)*	*NSE (v)*	*PBIAS (vi)*	*α (vii)*	*RMSE (viii)*	*NSE (ix)*	*PBIAS (x)*
< 1 ha (15 WS)	*Mean*	79.94	80.75	74.91	9.09	0.41	7.74	0.0104	8.86	0.45	−1.12
	Median	80.58	82.40	82.27	8.60	0.46	5.43	0.0107	8.56	0.49	0.05
	SD	5.71	6.84	17.25	1.76	0.28	9.25	0.0061	1.72	0.23	12.03
	CI(10%)	2.43	2.90	7.33	0.75	0.12	3.93	0.0026	0.73	0.10	5.11
1–2 ha (36 WS)	*Mean*	80.87	82.37	76.10	9.24	0.44	5.81	0.0110	8.86	0.55	−2.63
	Median	81.81	84.26	82.85	9.17	0.57	3.77	0.0110	8.94	0.61	−1.64
	SD	4.21	5.35	16.91	1.76	0.40	8.18	0.0038	1.83	0.17	8.73
	CI(10%)	1.15	1.47	4.64	0.48	0.11	2.24	0.0011	0.50	0.05	2.39
2–10 ha (20 WS)	*Mean*	78.81	80.40	73.63	10.74	0.48	9.93	0.0097	10.42	0.52	2.83
	Median	78.21	80.05	78.75	11.44	0.54	7.23	0.0080	10.97	0.56	0.17
	SD	5.32	5.99	16.46	3.98	0.35	11.20	0.0059	3.88	0.31	8.86
	CI(10%)	1.96	2.20	6.05	1.46	0.13	4.12	0.0022	1.43	0.11	3.26

(continued)

Table 1 (continued)

	Statistics	CN_{ave} (i)	CN_{med} (ii)	NRCS-CN model				Proposed model			
				CN_{opti} (iii)	*RMSE* (iv)	*NSE* (v)	*PBIAS* (vi)	α (vii)	*RMSE* (viii)	*NSE* (ix)	*PBIAS* (x)
10–100 ha (19 WS)	*Mean*	79.07	79.95	71.43	9.10	0.32	12.32	0.0093	8.89	0.33	2.44
	Median	79.23	80.02	76.12	9.06	0.48	5.55	0.0091	8.22	0.49	0.80
	SD	6.12	6.61	17.23	3.77	0.35	13.30	0.0057	3.77	0.45	7.68
	CI(10%)	2.31	2.49	6.50	1.42	0.13	5.02	0.0021	1.42	0.17	2.90
100–1000 ha (17 WS)	*Mean*	77.07	78.09	71.16	7.19	0.51	16.46	0.0067	6.92	0.57	0.74
	Median	77.04	78.91	76.44	7.27	0.65	10.34	0.0061	6.68	0.65	−1.31
	SD	4.34	4.79	13.60	2.06	0.38	16.03	0.0039	2.03	0.29	12.53
	CI(10%)	1.73	1.91	5.42	0.82	0.15	6.39	0.0016	0.81	0.11	5.00
> 1000 ha (7 WS)	*Mean*	78.09	80.16	75.07	10.13	0.40	18.70	0.0064	9.25	0.51	7.03
	Median	79.12	81.25	77.36	11.25	0.43	18.73	0.0064	10.24	0.54	6.65
	SD	2.76	2.97	6.39	2.35	0.28	13.55	0.0023	2.24	0.18	9.88
	CI(10%)	1.71	1.85	3.98	1.46	0.17	8.42	0.0014	1.39	0.11	6.14
All (114 WS)	*Mean*	79.35	80.63	73.93	9.21	0.43	10.25	0.0095	8.87	0.50	0.47
	Median	79.99	81.65	79.75	9.01	0.53	6.01	0.0088	8.81	0.55	0.08
	SD	5.01	5.78	15.83	2.87	0.36	12.03	0.0050	2.84	0.29	9.96
	CI(10%)	0.77	0.89	2.44	0.44	0.05	1.85	0.0008	0.44	0.04	1.53

iv. Using Eqs. (5) and (6), optimized and a constant value of curve number (applying criteria given in Eq. (9)) for NRCS-CN model was calculated for all watersheds. Similarly, a constant and optimized value of α was calculated using Eq. (8) for proposed model for all the watersheds.
v. A scatter plot was constructed which shows the relationship between curve number value of NRCS-CN model and α (model constant) value of proposed model.
vi. The RMSE, NSE and PBIAS values were determined for both models using Eqs. (10), (11) and (12).
vii. All these data were characterize according to different watersheds sizes and a comparable table were made to assess proposed model performance over existing NRCS-CN model.

3 Results and Discussion

Due to simplicity and one parameter requirement in the proposed non-linear event-based rainfall-runoff model, it is necessary to check its performance using three most commonly statistical criterion, i.e. RMSE, NSE and PBIAS in order to find the degree of agreement between the observed and predicted direct runoff and compared the results with most generally used existing NRCS-CN model. The comparison of data for both models is shown in Table 1. The average and median value of CN were obtained (using step ii and iii in methodology section) and presented in column (i) and (ii) of Table 1. The optimized value of CN and α after applying step (iv) of methodology section, also presented in column (iii) and (vii) of Table 1. The range of optimized constant parameter 'α' for proposed model after minimizing the sum of squared difference between predicted and observed runoff amount were found in between 0.001 to 0.0289 with a mean and median value of 0.0095 and 0.0088, respectively. When we grouped value of 'α' in a certain range, i.e., 0–0.005, 0.005–0.01, 0.01–0.015, 0.015–0.02, 0.02–0.025 and 0.025–0.03, out of 114 watersheds maximum 46 watersheds (40.35%) lies their value in between 0.005–0.01 (Fig. 1) with a mean and median value as 0.0075 and 0.0078, respectively.

Since 'α' of proposed model depicted CN characteristics of NRCS-CN model. It means 'α' inherently shows the dependency of rainfall-runoff behaviour on soil-moisture interaction with maximum potential retention. To show the relationship between α and CN, a scatter plot was draw. This graph (Fig. 2) with α and CN values shows a polynomial equation of second order with R^2 value of 0.88. It also revealed that α value decreases with increased CN up to its value as 58 and then increases. The second order polynomial equation can be represented as:

$$\alpha = 2{*}10^{-5}\mathrm{CN}^2 - 0.0022CN + 0.0637 \tag{13}$$

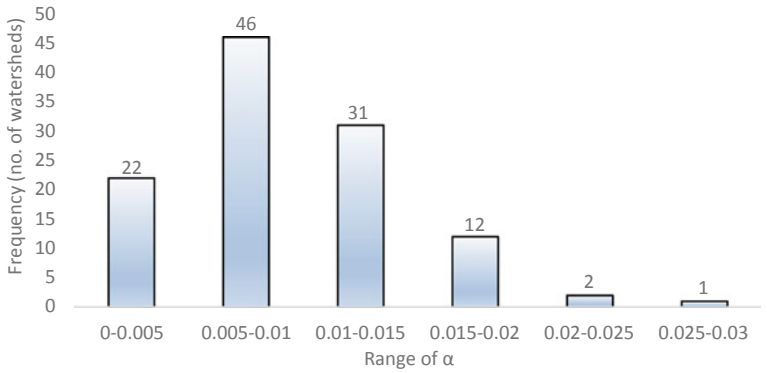

Fig. 1 Frequency distribution of optimized α value for all watersheds

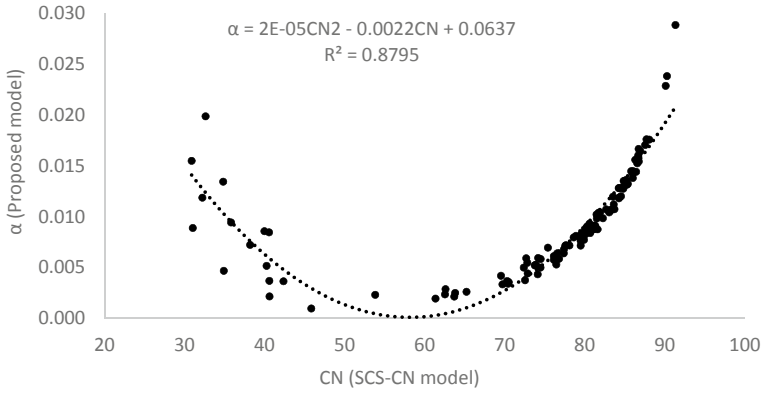

Fig. 2 Scatter plot between optimized CN of NRCS-CN model and α of proposed model

Using Eq. (13), we can directly convert CN value obtained from rainfall-runoff dataset (using Eqs. (6) and (7)) into α (model constant) of proposed model. This generated α value, put into proposed non-linear Eq. (8) will calculate runoff for any rainfall value.

The values of RMSE, NSE and PBIAS of all 114 watersheds for both models have been shown in Figs. 3, 4 and 5. These figures and Table 1 revealed the significant improvement of proposed model over NRCS-CN model for all three statistical criterion. All 114 watersheds are classified into six categories according to watersheds area. These are less than 1 ha area (15WS), in between 1–2 ha (36WS), 2–10 ha (20WS), 10–100 ha (19WS) and 100–1000 ha (17WS) area and more than 1000 ha (7WS) size.

The mean value of RMSE is decreased from 9.21 to 8.87 and out of 114 watersheds, 84 watersheds have less RMSE value (Fig. 3). It shows that mean and median RMSE value is less for proposed model than NRCS-CN model for all 114 watersheds. If

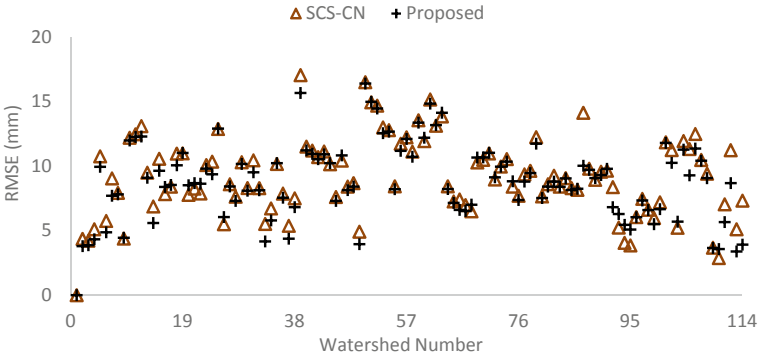

Fig. 3 Comparison of RMSE values of NRCS-CN and proposed model

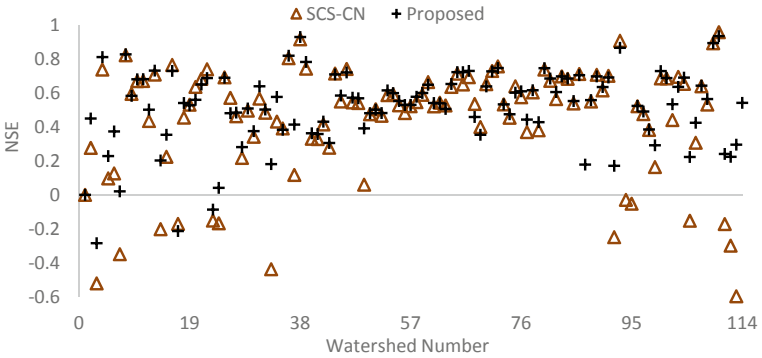

Fig. 4 Comparison of NSE values of NRCS-CN and proposed model

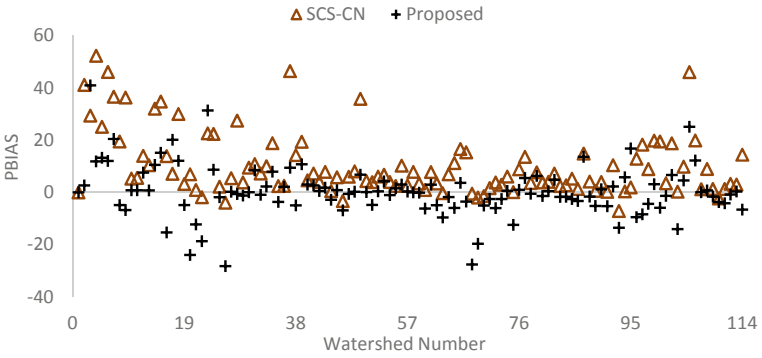

Fig. 5 Comparison of PBIAS values of NRCS-CN and proposed model

we classify the watersheds based on its area, RMSE value still less for all sizes of watershed with proposed model. The NSE values of proposed model are higher than the existing NRCS-CN model. The mean NSE value shows improvement with a value from 0.43 for NRCS-CN model to 0.50 for proposed model (Fig. 4).

Overall, 84 watersheds shows improvement with proposed model. The value of PBIAS which revealed the over prediction or under prediction behaviour of a model, significantly towards zero for proposed model (Fig. 5). The mean PBIAS value declined from + 10.25 to just + 0.47. Its value near to zero is a good assessment of model. The range of watershed area in between 100 and 1000 ha, predicted significant better runoff result for proposed model in term of mean value of RMSE, NSE and PBIAS.

4 Conclusions

In this study, we proposed a very simple and easy to use non-linear model to predict runoff from an event rainfall. The CN value of NRCS-CN model, incorporates many factors in its own and can be adopted for different climatic conditions. Due to uncertainty in curve number value, this study suggest a model without curve number concept and incorporating a new constant parameter α, to calculate effective runoff. This model performance were checked over existing NRCS-CN model. The quantitative model performance was assessed and compared based on the root mean square error (RMSE), Nash–Sutcliffe efficiency (NSE) and per cent bias (PBIAS). Based on the statistical criterion, proposed model without CN concept reveals more statistically significant results (low RMSE, high NSE and statistically significant PBIAS values) and depicted improved performance than the conventional CN model. A relationship was proposed between CN of NRCS-CN model and constant parameter α of proposed model to directly convert curve number value into α value. Due to simplicity of this model, α value can be determine for another biomes and check model efficacy and suitability for other regions.

Acknowledgements The authors are grateful to Prof. R.H. Hawkins, Emeritus Professor, University of Arizona, for providing edited data available on USDA-ARS website and also acknowledge the infrastructural support provided by the Civil Engineering Department, Indian Institute of Technology, Roorkee, India.

References

1. Verma S, Verma RK, Mishra SK, Singh A, Jayaraj GK (2017) A revisit of NRCS-CN methodology and application of RS and GIS for surface runoff estimation. Hydrol Sci 62(12):1891–1930
2. Hawkins RH, Ward TJ (2012) Expected value of event runoff with curve number theory. In: World environmental and water resources congress 2012: crossing boundaries, 3844–3853

3. Hawkins RH, Ward T, Woodward DE, Van Mullem J (2009) Curve number hydrology: state of the practice Reston. ASCE, Virginia, p 106
4. Upreti P, Ojha CSP (2021) Comparison of antecedent precipitation based rainfall-runoff models. Water Supply 21(5):2122–2138
5. Jain MK, Mishra SK, Singh VP (2006) Evaluation of AMC-dependent SCS-CN-based models using watershed characteristics. Water Resour Manage 20(4):531–552
6. Ali S, Sharda VN (2008) A comparison of curve number based methods for runoff estimation from small watersheds in a semi-arid region of India. Hydrol Res 39(3):191–200
7. Kim NW, Lee JW, Lee J, Lee JE (2010) SWAT application to estimate design runoff curve number for South Korean conditions. Hydrol Process 24(15):2156–2170
8. Upreti P, Ojha CSP (2022) Development and performance evaluation of SCS-CN based hybrid model. Water Sci Technol 85(9):2479–2502
9. Soulis KX, Valiantzas JD (2012) SCS-CN parameter determination using rainfall-runoff data in heterogeneous watersheds–the two-CN system approach. Hydrol Earth Syst Sci 16(3):1001–1015

Performance Evaluation of Lumped Conceptual Rainfall-Runoff Genie Rural (GR) Hydrological Models for Streamflow Simulation

Akash Singh Raghuvanshi, Siddik Ahmed Barbhuiya, and H. L. Tiwari

Abstract Hydrological modeling is essential for water resources management, impact assessment and risk evaluation. From the point of view of water resources planning, estimation of runoff from a watershed is of great importance in most hydrological analysis. Due to the model's complex structure and huge data requirement in semi-distributed or distributed models, nowadays lumped conceptual models are frequently used for operational applications because they represent and transform catchment scale rainfall-runoff in a simplified way. As a result, these models usually require less data and can be readily implemented. The present study uses package *airGR* which facilitate the daily versions of the GR lumped hydrological models, namely GR4J, GR5J and GR6J and compares their performance for streamflow simulation within RStudio interface. The Bharathapuzha river's sub-basin in Kerala is selected for this study. The models are calibrated and validated using observed data of daily rainfall, and daily discharge and estimates of daily potential evapotranspiration for a period of 27 years (1987–2013). Daily potential evapotranspiration is estimated using FAO ET0 calculator (version 3.2). The performance of the model streamflow predictions is evaluated based on various statistical measures. Results of the analysis are presented and discussed.

Keywords Rainfall-Runoff modeling · GR4J model · GR5J model · GR6J model · Model complexity · ET_0 calculator (version 3.2)

A. S. Raghuvanshi (✉) · S. A. Barbhuiya
Department of Hydrology, Indian Institute of Technology Roorkee, Roorkee 247667, Uttarakhand, India
e-mail: akash_sr@hy.iitr.ac.in

S. A. Barbhuiya · H. L. Tiwari
Department of Civil Engineering, Maulana Azad National Institute of Technology, Bhopal 462003, Madhya Pradesh, India

P. V. Timbadiya et al. (eds.), *Hydrology and Hydrologic Modelling*,
Lecture Notes in Civil Engineering 312,
https://doi.org/10.1007/978-981-19-9147-9_22

1 Introduction

The hydrological models have been used widely to examine the influence of climate and land-use change on water budgets, as well as to forecast severe occurrences such as floods and droughts [6]. Many scientific fields employ hydrological models to simplify the description of hydrological systems and to forecast the behavior of hydrological systems [14]. Among various hydrological models, lumped models are being commonly used for various applications because they represent catchment scale rainfall-runoff in a simplified way. As a result, these models require less input data (primarily climatic inputs and streamflow) and are simple to apply. For these reasons, such models are frequently used in hydrological science training and teaching [3]. CEMAGREF, a French national applied research agency, has created a collection of lumped hydrological models known as the Genie Rural (GR) hydrological models [14]. These are conceptual hydrological models that may be implemented at different time scales ranging from daily to yearly. This is the goal of the airGR package given in this paper, which makes GR models open-source in R [2, 3]. This study evaluates the performance of three daily version of GR models in estimating streamflow in Bharathapuzha river sub-basin in Kerala.

2 Study Area and Data Source

2.1 Bharathapuzha River Sub-Basin

The study area is a part of the Bharathapuzha river basin in Kerala extending from 10° 45′ to 11° 30′ N and 75° 45′ to 76° 45′ E. Bharathapuzha River is the second longest river of Kerala. The main tributary in the study area is Thuthapuzha. This tributary starts from the Silent Valley hills. The geographical extent of the sub-basin considered in this study is approximately 913 km^2 and its boundary covers a perimeter of 226 km.

2.2 Data Used

Lumped conceptual models incorporates rainfall and potential evapotranspiration (PET) information. The daily Meteorological data (rainfall, maximum & minimum temperature, wind speed, relative humidity and no. of sunshine hours) were collected from Regional Agriculture Research Station, Pattambi for the period of 27 years (1987–2013). It is assumed to be uniform throughout the catchment. The daily discharge data for stream gaging site at Pulamanthole was obtained from Central Water Commission (CWC) for the period of 27 years (1987–2013). Daily potential evapotranspiration is estimated using FAO ET_o calculator (version 3.2). PET

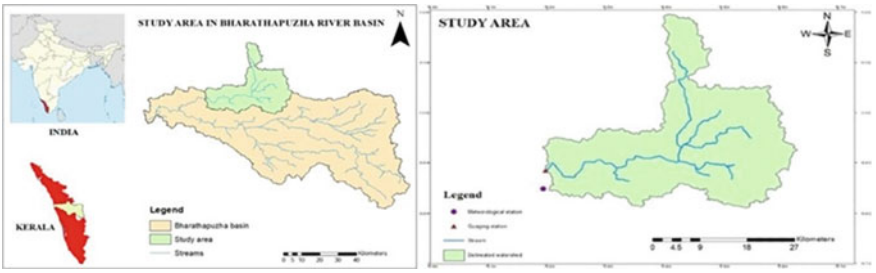

Fig. 1 Index map of the study area

was computed based on FAO Penman–Monteith equation from meteorological data using the ETo calculator software [1]. In this study, it was assumed that the reference crop evapotranspiration is equal to the potential evapotranspiration due to lack of readily available detailed information on the crops, plantations, forests, their aerial spread, etc.

3 Materials and Methods

3.1 Rainfall-Runoff Models

The hydrological models evaluated in this study are; GR4J, GR5J and GR6J (Fig. 1). The conceptual models are set up in RStudio interface using an R-package, *airGR* [2, 3]. These models work at daily scale, are parsimonious in data and are easy to calibrate and validate thus making them very popular among hydrologist [14]. The description of parameters involved in every model are in the following section (Fig. 2).

3.2 GR4J Model

The GR4J model is a lumped conceptual model used for rainfall-runoff modeling [11]. The GR4J conceptual model comprises four parameters: production store maximum capacity (mm) [$x1$], the groundwater exchange coefficient (mm) [$x2$], routing store maximum capacity one day ahead (mm) [$x3$] and the time span of the unit hydrograph (day) [$x4$] [11]. This model was run using the airGR package [2, 3] in R software [13] (Fig. 3).

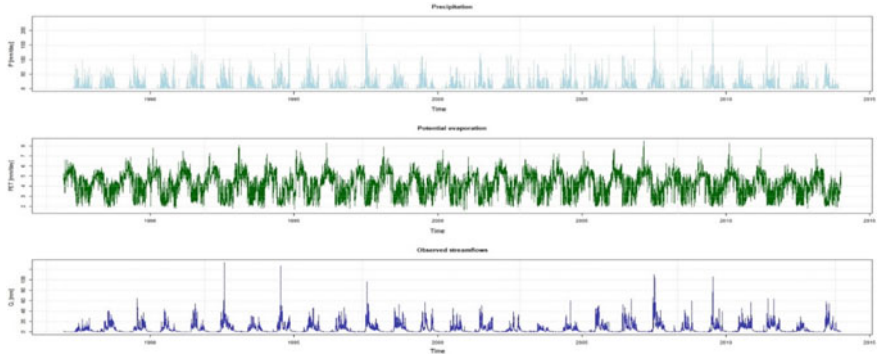

Fig. 2 Daily precipitation, potential evapotranspiration and streamflows data for the study area (1987–2013)

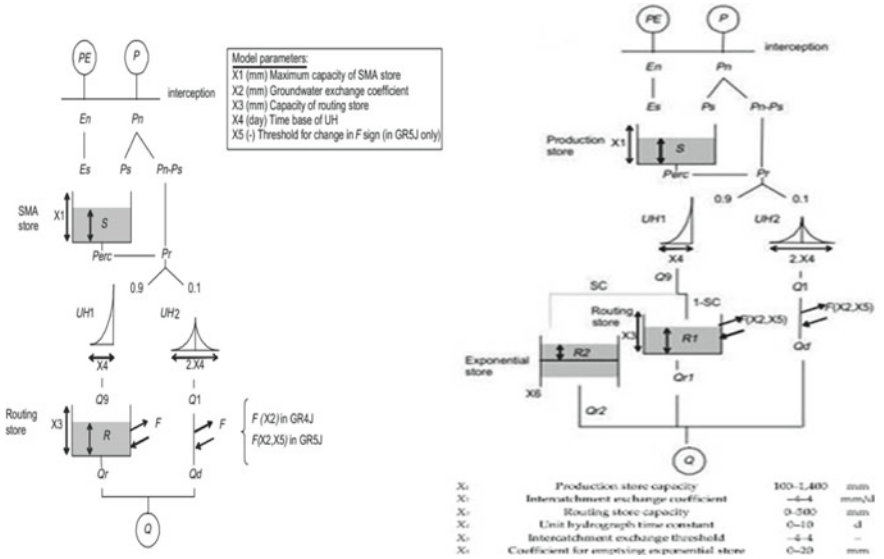

Fig. 3 Schematic representation of the GR4J, GR5J (Left) and GR6J (Right) hydrological model [12]

3.3 GR5J Model

The GR5J model is a five-parameter enhanced daily lumped conceptual model ($x1$, $x2$, $x3$, $x4$ and $x5$). The first four parameters are identical to those of the GR4J model. The extra parameter $x5$ represents the change in the sign of the F (ground water exchange term) [8]. Le Moine [8] developed the GR5J model to increase the

low flow simulation performance over the GR4J model. The GR5J daily rainfall-runoff modeling in this work was also carried out in R software using the airGR package [2, 3, 13].

3.4 GR6J Model

The GR6J model is a six-parameter enhanced daily lumped conceptual model ($x1$, $x2$, $x3$, $x4$, $x5$ and $x6$). Apart from initial four parameters which are the same as those of the GR4J model. The additional parameters ($x5$ and $x6$) denote the change in the F (ground water exchange term) sign threshold and the new routing storage, respectively [11, 12]. The GR6J model was developed to improve the low flow simulation performance [12]. In this investigation, the GR6J rainfall-runoff modeling was also carried out using the airGR package [2, 3] in R software [13].

3.5 Calibration and Validation Procedure

The GR4J, GR5J and GR6J models' parameters are calibrated using Michel algorithm [9] which optimizes the error criterion selected as objective function. The algorithm combines a global and a local approach. First, a screening is performed using either a rough predefined grid or a list of parameter sets. Then a steepest descent local search algorithm is performed, starting from the result of the screening procedure. In this study, calibration was carried out using Nash–Sutcliffe efficiency (NSE) as the objective function. The calibration period was considered as 1988–2006 and the validation period as 2008–2013. The one-year warm up period was considered for all three models while performing calibration (1987) and validation (2007).

3.6 Assessment of Model Performance

Model performance evaluation is essential in order to provide an estimate of its ability to replicate historic and future watershed response, it is a means for evaluating improvements to the modeling approach by adjusting the model parameter values, model structural modifications, the inclusion of additional observational information and representation of important spatial and temporal characteristics representation of the watershed as well as to compare current modeling efforts with previous study results [5]. In the present study, Nash–Sutcliffe Efficiency (NSE), coefficient of correlation (R) and percentage bias (PBIAS) are used as mathematical measures to assess how well the results of model simulation is close to the available observations. NSE (Eq. 1) is a measure to evaluate the predictive power of hydrological model. An efficiency of 1 indicates a perfect fit between observed and predicted value.

Coefficient of correlation (Eq. 2) is a measure of the linear relation between two variables. A correlation of 1 indicates perfect linear relation between the observed and the predicted values. Percentage bias (Eq. 3) is a measure to evaluate whether the model is under-predicting or over-predicting with respect to observed value. A value of PBIAS > 0 and PBIAS < 0 indicates that the model is under-predicting and over-predicting, respectively. Moriasi et al. [10] specified model performance guidelines for evaluations performed with monthly time step. According to the guidelines, model simulation can be defined satisfactorily if NSE > 0.5 and PBIAS = ± 25% for streamflow.

$$\mathrm{NSE} = 1 - \frac{\sum_i^N \left[Q_{\mathrm{obs},i} - Q_{\mathrm{sim},i}\right]}{\sum_i^N \left[Q_{\mathrm{obs},i} - \overline{Q}_{\mathrm{obs}}\right]} \tag{1}$$

$$R = \frac{\sum_i^N (Q_{\mathrm{sim},i} - \overline{Q}_{\mathrm{sim}})(Q_{\mathrm{obs},i} - \overline{Q}_{\mathrm{obs}})}{\sqrt{\sum_i^N (Q_{\mathrm{sim},i} - \overline{Q}_{\mathrm{sim}})^2 \sum_i^N (Q_{\mathrm{obs},i} - \overline{Q}_{\mathrm{obs}})^2}} \tag{2}$$

$$\mathrm{PBIAS} = \frac{\sum_i^N \left[Q_{\mathrm{obs},i} - Q_{\mathrm{sim},i}\right] \times 100}{\sum_i^N Q_{\mathrm{obs},i}} \tag{3}$$

where $Q_{\mathrm{obs},i}$ and $Q_{\mathrm{sim},i}$ are observed discharge at time i and simulated discharge at time I, respectively, $\overline{Q}_{\mathrm{obs}}$ and $\overline{Q}_{\mathrm{sim}}$ are mean observed discharge and mean simulated discharge, respectively.

4 Results and Discussion

For the present study, calibration is performed using data of 19 years starting from January 1st 1988 and ending on December 31st 2006. A total of four parameters related to GR4J, five parameters related to GR5J and six parameters related to GR6J are estimated through the calibration algorithm described by C. Michel (1991). The values of these parameters are presented in Table 1.

The values of the GR model parameters have been fixed such that a reasonably good agreement is obtained between the observed and computed streamflow. The

Table 1 Calibrated parameters

Parameters	GR4J	GR5J	GR6J
$x1$	742.483	523.182	559.584
$x2$	3.665	− 0.767	1.661
$x3$	159.174	159.539	65.560
$x4$	1.632	1.424	1.739
$x5$	–	1.000	0.361
$x6$	–	–	23.405

observed and computed values of streamflow are presented in Figs. 4, 5 and 6. Overall, there is reasonably good agreement between the observed and computed streamflow. It can be seen that the all three models slightly underestimate peak flows in few years, and overestimates low flows. The values of the statistical measures for the model performance during calibration and validation periods are given in Table 2.

Validation of the three GR models is performed using streamflow data for 6 years from January 1st 2008 to December 31st 2013. Figures 7, 8 & 9 illustrates the plot of observed and simulated streamflow for the validation period for GR4J, GR5J and GR6J model, respectively.

The efficacy of GR4J, GR5J and GR6J model is compared by calculating the statistical measures of performance, i.e., NSE, PBIAS and coefficient of correlation (R). NSE for GR4J, GR5J and GR6J varies between 0.65 and 0.71. The best performance is obtained by the GR4J model in terms of NSE, PBIAS and R. NSE and R values during validation period are better than calibration period for all three GR

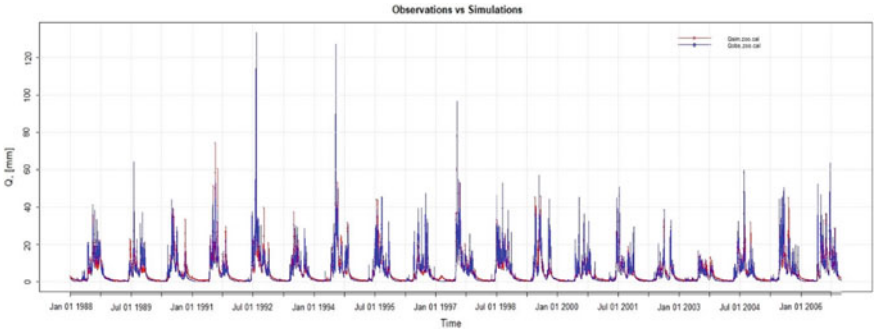

Fig. 4 Results of calibration of GR4J—observed and computed streamflow—period (1988–2006)

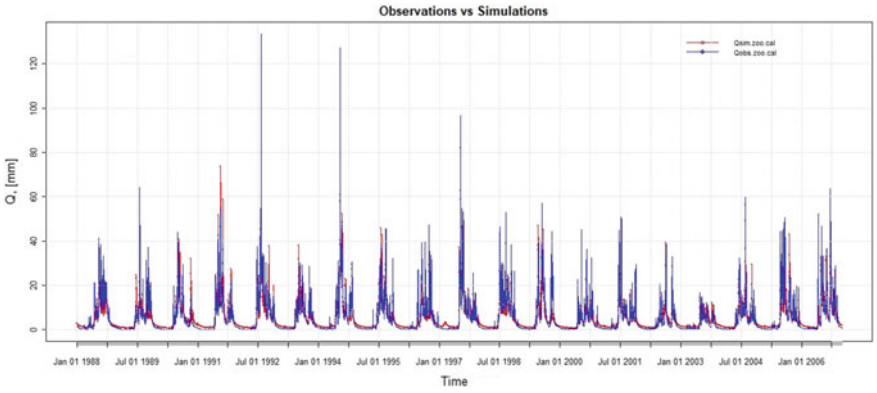

Fig. 5 Results of calibration of GR5J—observed and computed streamflow—period (1988–2006)

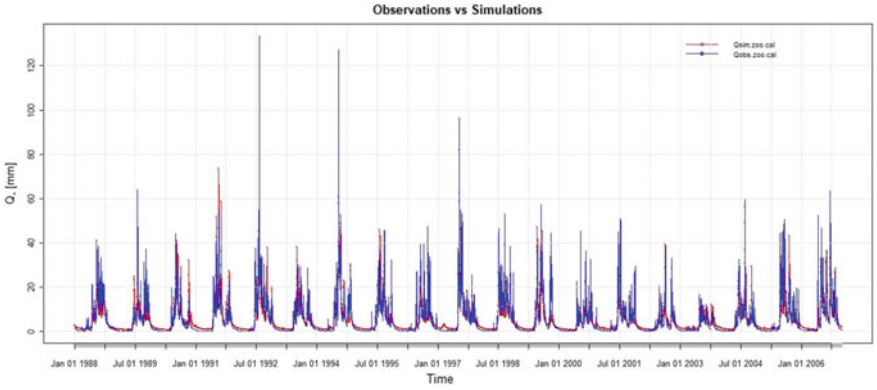

Fig. 6 Results of calibration of GR6J—observed and computed streamflow—period (1988–2006)

Table 2 Summary statistics of model performance

Performance criteria	Calibration (1988–2006)			Validation (2008–2013)		
	GR4J	GR5J	GR6J	GR4J	GR5J	GR6J
PBIAS	− 0.4	− 3.7	− 1.1	− 10.6	− 13	− 11.2
NSE	0.67	0.65	0.67	0.72	0.71	0.71
R	0.83	0.81	0.83	0.85	0.85	0.85

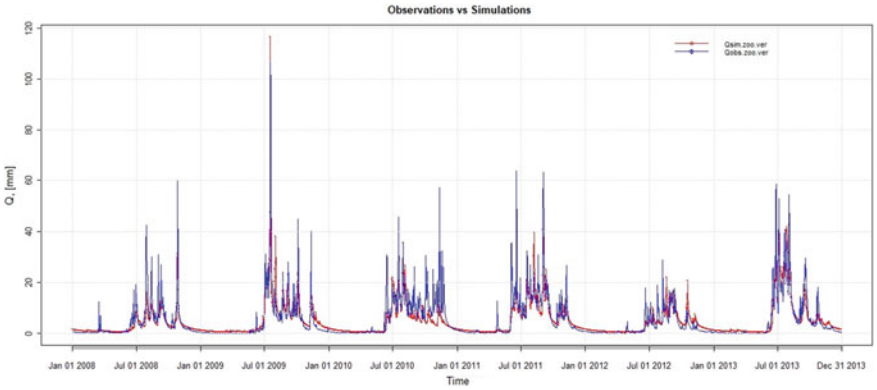

Fig. 7 Results of validation of GR4J—observed and computed streamflow—period (2008–2013)

models. PBIAS values during calibration period are better than validation period for all three GR models. Negative values of PBIAS indicate the overestimation in simulated runoff by the models. Among all the three models, GR4J model overestimated streamflow least. GR4J and GR6J model performed better than the GR5J in terms of NSE, PBIAS and R.

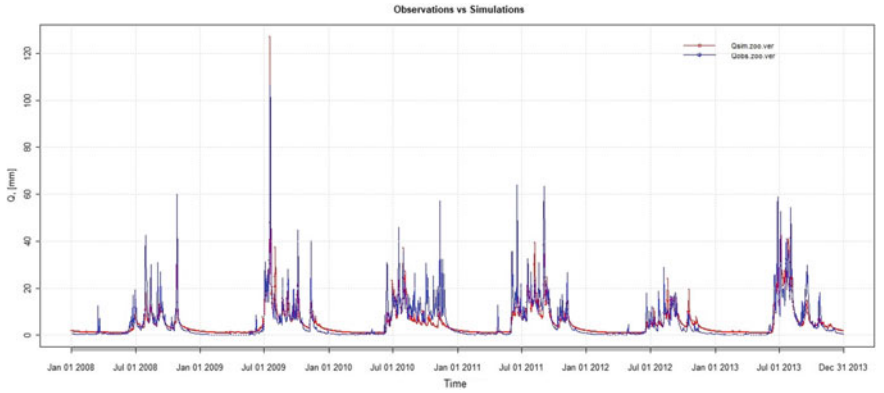

Fig. 8 Results of validation of GR5J—observed and computed streamflow—period (2008–2013)

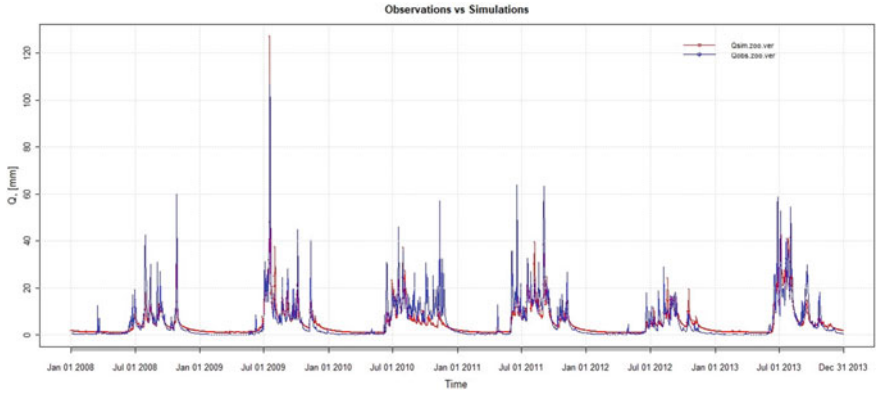

Fig. 9 Results of validation of GR6J—observed and computed streamflow—period (2008–2013)

5 Conclusions

This study compared GR4J, GR5J and GR6J lumped conceptual rainfall-runoff models in estimating the runoff in a sub-basin of the Bharathapuzha river basin in Kerala. The following conclusions are derived from the foregoing study:

- The performance of GR4J model in estimating streamflow was better than GR5J and GR6J model.
- NSE and R values during validation period were better than calibration period for all three GR models.
- PBIAS values during calibration period were better than validation period for all three GR models. All three GR model overestimated the streamflow.
- Among all the three models, GR4J model overestimated streamflow least.

- GR4J and GR6J model performed better than GR5J model in terms of NSE, PBIAS and R values.
- From the statistical indices evaluated, it can be concluded that all the three GR models have given a satisfactory result.

References

1. Allen R, Pereira LS, Raes D, Smith M (1998) Crop evapotranspiration—guidelines for computing crop water requirements. FAO Irrigation and Drainage Paper N° 56. Rome, Italy
2. Coron L, Delaigue O, Thirel G, Dorchies D, Perrin C, Michel C (2021) airGR: suite of GR hydrological models for precipitation-runoff modelling. R package version 1.6.12. https://CRAN.R-project.org/package=airGR
3. Coron L, Thirel G, Delaigue O, Perrin C, Andréassian V (2017) The suite of lumped GR hydrological models in an R package. Environ Model Softw 94:166–171
4. FAO (2009) ETo calculator. Land and Water Digital Media Series, N° 36. FAO, Rome, Italy
5. Krause P, Boyle DP, Bäse F, Comparison of different efficiency criteria for hydrological model assessment. Adv Geosci 5:89–97
6. Kunnath-Poovakka A, Eldho T (2019) A comparative study of conceptual rainfall- runoff models GR4J, AWBM and Sacramento at catchments in the upper Godavari River basin, India. J Earth Syst Sci 128(2)
7. Lavtar K, Bezak N, Šraj M (2019) Rainfall-runoff modeling of the nested non-homogeneous Sava river sub-catchments in Slovenia. Water 12(1):128
8. Le Moine N (2008) Le bassin versant de surface vu par le souterrain: une voie d'amélioration des performance et du réalisme des modéles pluie-débit? Ph.D. thesis. Université Pierre et Marie Curie (Paris), Cemagref (Antony), 324 pp
9. Michel C (1991) Hydrologie appliquée aux petits bassins ruraux. Hydrology handbook (in French), Cemagref, Antony, France
10. Moriasi DN, Arnold JG, Van Liew MW, Bingner RL, Harmel RD, Veith TL (2007) Model evaluation guidelines for systematic quantification of accuracy in watershed simulations. Trans ASABE 50:885–900
11. Perrin C, Michel C, Andréassian V (2003) Improvement of a parsimonious model for streamflow simulation. J Hydrol 279(1–4):275–289
12. Pushpalatha R, Perrin C, Le Moine N, Mathevet T, Andréassian V (2011) A dowward structural sensitivity analysis of hydrological models to improve low-flow simulation. J Hydrol 411(1–2):66–76
13. R Development Core Team (2015) R: a language and environment for statistical computing; R foundation for statistical computing: Vienna, Austria. http://www.R-project.org/
14. Traore VB, Sambou S, Fall STS, Diaw AT, Cisse MT (2014) Calibrating the rainfall-runoff model GR4J and GR2M on the Koulountou River basin, a tributary of the Gambia River. Am J Environ Prot 3(1):36–44

Spatio-Temporal Variability Analysis of Snow Cover in Sutlej Basin Using MODIS Snow Cover Data

V. Madhavi Supriya, B. Simhadri Rao, Ch. Sai Krishna, P. Venkat Raju, and V. Venkateshwar Rao

Abstract Snow is a crucial component of the cryosphere and is an Essential Climate Variable (ECV), an indicator of climate change. Large number of studies suggests climate change is affecting the snow cover and the resulting snowmelt runoff in Himalaya mountainous region. Monitoring the snow cover area dynamics becomes very essential amidst the growing importance of the snow and glaciers in Indian Himalayan region and its efficient utilization of water resources. The present study examines the spatial and temporal variations of Snow Cover Area (SCA) in the Sutlej basin, using eight-day snow cover products derived from Moderate Resolution Imaging Spectroradiometer (MODIS) aboard Terra (MOD10A2) and Aqua (MYD10A2) with a spatial resolution of 500 m (version-6) for the period 2002–2020 (18 years). The cloud cover quantity is minimized by means of taking the combination of Terra and Aqua MODIS snow cover products. The analysis is done on a monthly, seasonal and annual time scale along with the elevation, slope and aspect SCA variation in the basin. The average SCA in Sutlej basin is 41.03% of the total basin area (52,553 km^2). It is observed that the minimum annual average SCA is 33.26% in 2015–2016 and the maximum annual average SCA is 49.95% in 2014–2015. The trend analysis was performed for elevation, slope, aspect and the result doesn't indicate any significant trend for the period 2002–2020 (18 years).

V. Madhavi Supriya (✉) · B. Simhadri Rao · Ch. Sai Krishna · P. Venkat Raju · V. Venkateshwar Rao
Water Resources Group, National Remote Sensing Centre (NRSC), ISRO, DOS, Balanagar, Hyderabad 500037, India
e-mail: venigallasupriya@gmail.com

B. Simhadri Rao
e-mail: simhadrirao_b@nrsc.gov.in

Ch. Sai Krishna
e-mail: saikrishna_c@nrsc.gov.in

P. Venkat Raju
e-mail: raju_pv@nrsc.gov.in

V. Venkateshwar Rao
e-mail: vvrao@nrsc.gov.in

P. V. Timbadiya et al. (eds.), *Hydrology and Hydrologic Modelling*,
Lecture Notes in Civil Engineering 312,
https://doi.org/10.1007/978-981-19-9147-9_23

The average inter-annual seasonal variability over the decade (2002–2011) is more as compared to other decade (2011–2020).

Keywords Snow Cover · MODIS · Elevation · Slope · Trend

1 Introduction

Snow cover is a vital water resource for agricultural crops and fresh water resources in the mid and high latitude areas [1] making the snow cover monitoring essential for its proper utilization. Global Climate Observation System (GCOS) has recognized snow as an Essential Climate Variable (ECV) due to its crucial function in energy exchange and weather change. The snow cover is characterized by high reflectance in visible bands and low reflectance in shortwave infrared band. The primary factor of the earth's atmospheric circulation system is the spatial and temporal variability of seasonal snow cover upon land that plays a key role in governing the earth's global radiation balance. The high albedo of snow cover influences land surface temperature by using reflecting incoming short wave solar radiation. The snowmelt, snow distribution and snow cover depletion are inter related according to Liston [2]. In snowmelt hydrology models the timing and magnitude of snowmelt runoff and the end of winter snow distribution which is determined by the snow distribution [3]. It is important to monitor the seasonal snow cover to assess the distribution of water in north Indian rivers [4] such as Indus, Ganga and Brahmaputra as these originate in the high altitude regions such as Himalayas. The analysis of spatial and temporal variability of snow cover is used to forecast snowmelt runoff in spring period [5] to evaluate changes in flood regime. Because of extreme weather conditions in the Himalayan region the ground measurements of snow are very limited due to which satellite-based remote sensing takes the advantage. The present study was taken up with the principal objectives to study the Inter-Annual and Intra-Annual snow cover area variability in Sutlej basin at different temporal scales (monthly, seasonal and annual) and also with respect to different zones of elevation, slope and aspect.

2 Study Area and Data Source

2.1 Sutlej River Basin

The Sutlej is one of the longest rivers among the five rivers of Punjab state and one of the most important eastern tributary of the river Indus. Sutlej along with its tributaries is known as the "Power House of Himalayas". Its origin is near the Mansarovar Lake which enters Zaskar range and flows through the Tibetan Plateau at an elevation about 4500 m (mean sea level—msl) before entering India in Himachal Pradesh and flows generally from west and south-west.

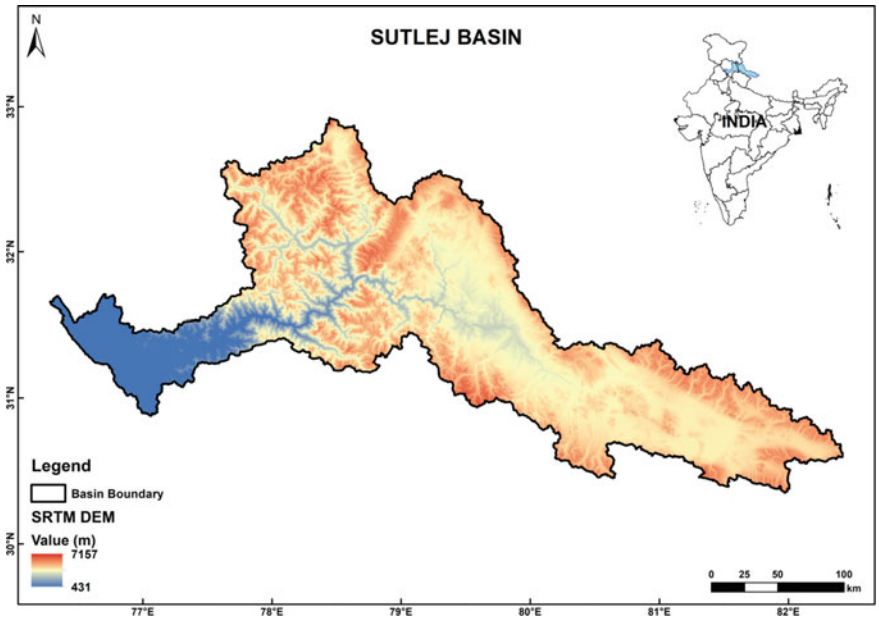

Fig. 1 Location of the study area

The Tibetan plateau is characterized by a cold desert winter climate except for the Spiti (major tributary) in Himachal Pradesh. The major snowfall contribution is due to westerly weather disturbances mostly happening in spring season [6]. The study area is extending from 30° 22′ N to 32° 42′ N and 76° 57′ E to 82° 51′ E and covers an area of 52,553 km^2 explained in Fig. 1. The hypsometry of the basin area along with the glaciers shows that maximum area lies between 4000 and 5000 m.

3 Data Used

3.1 Satellite Snow Cover Product

The National Aeronautics and Space Administration (NASA) launched a Moderate Resolution Imaging Spectroradiometer (MODIS) sensor onboard the Terra and Aqua satellites viewing the earth every one to two days with swath width of 2330 km and acquiring data in 36 spectral bands ranging between 0.405 and 14.385 μm (visible to thermal infrared sensor). Aqua sensor crosses the equator from south to north (ascending node) at approximately 1.30 P.M. local time whereas Terra sensor crosses the equator from north to south (descending node) at approximately 10.30 A.M. local time. The MODIS Terra and Aqua data specifications are explained in Table 1.

Table 1 MODIS Terra and Aqua data specifications

Satellite	Product	Nominal data Array dimensions	Spatial resolution	Temporal resolution	Starting period of acquisition
Terra	MOD10A2	1200 km × 1200 km	500 m	Eight-day	February 24th 2000
Aqua	MYD10A2	1200 km × 1200 km	500 m	Eight-day	July 4th 2002

Table 2 Pixel values categorized in MODIS snow cover product [7]

Pixel value	0	1	11	25	37	39	50	100	200	254	255
Category	Missing data	No decision	Night	No snow	Lake	Ocean	Cloud	Lake Ice	Snow	Detector saturated	Fill

MODIS provides a composite 8-day (MOD10A2/MYD10A2) global snow cover datasets as two layer namely as maximum snow extent and chronology of snow/no snow occurrence observations during an eight-day period. In our study the algorithm maps a pixel value as snow, if any one of the days during the entire 8-day period is mapped as snow. The pixel is mapped as cloud, if observed as a cloud on all the days during the entire 8-day period. The pixels are categorized as snow, no snow, cloud, ocean, snow covered lake, lake ice or other state [7] as described in Table 2.

The 8-day SCP of MODIS Terra (MOD10A2) and Aqua (MYD10A2) from September 2002 to August 2020 (18 years) data are only used for the analysis. There are 46 scenes available in a one particular year. Therefore a total of 3308 scenes are obtained for our study area covered in two scenes (h24v05 & h25v05) from both Aqua and Terra. MODIS SCP datasets are missing on two days, i.e., February 18th 2016 and August 21st 2020.

3.2 Digital Elevation Model (DEM)

The elevation information is derived from the Shuttle Radar Topography Mission (SRTM) global data coverage with 90 m resolution (3 Arc—second) in C-band wavelength (5.6 cm). The Geo—TIFF files are used to delineate basin boundaries for the study area at its original resolution of 90 m. The DEM is re-sampled from 90 to 500 m resolution (using Nearest Neighborhood) which corresponds to the grid size of MODIS snow cover product for the preparation of elevation, slope and aspect classified images as explained in Fig. 2.

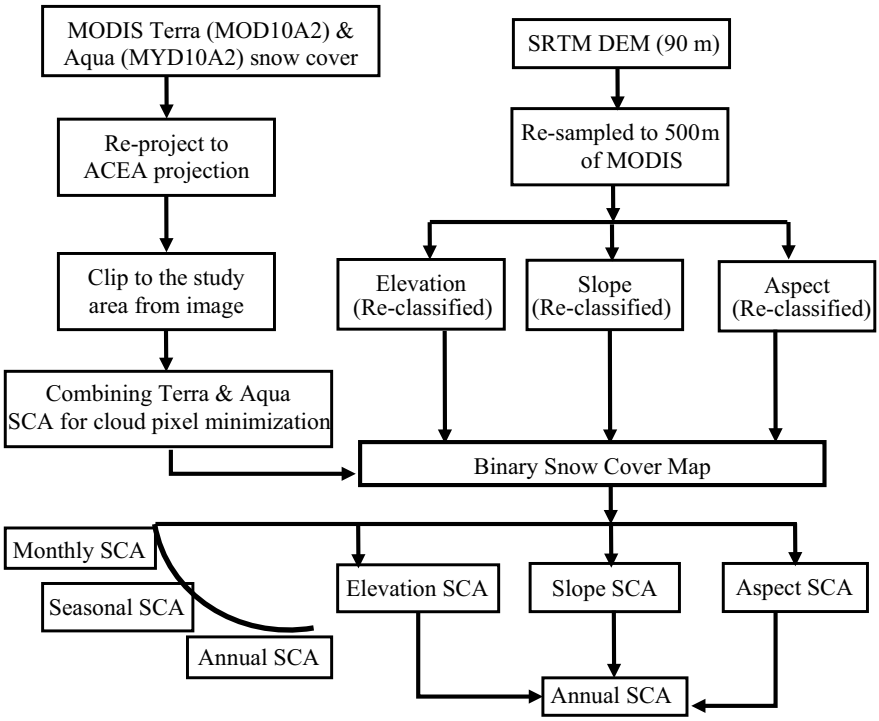

Fig. 2 Flowchart of methodology

4 Methodology

The preprocessing of the MODIS data includes projection transformation from sinusoidal to the Albers Conical Equal Area (ACEA) and clipping to the study area extent using ERDAS Imagine software. The detailed methodology is explained in Fig. 2.

4.1 Terra and Aqua Combination for Minimizing Cloud Pixels

A frequently used approach in different literatures to minimize the cloud cover is combining Terra and Aqua SCP [8–11]. The approach can be illustrated as follows if a pixel in MOD10A2 is classified as cloud and the same pixel is cloud-free (i.e., either snow or land) in MYD10A2, the cloud-free observation is assumed [12]. Since MYD10A2 uses band 7 instead of band 6 in deriving the NDSI index it suffers from inaccuracies. Thereby better input is provided by MOD10A2 compared to MOD10A1 [13–15] through cloud suppression by minimizing the cloud cover and

Table 3 Classification of seasons

Season	Months
Winter	October to March
Spring	April to June
Summer	July to September

maximizing snow cover resulting in higher classification accuracy for snow. Yang et al. [16] also demonstrates the higher accurate retrievals than the MYD10A2. Hence, the methodology gives priority to MOD10A2 observations due to the previous validation studies [12].

4.2 Generation of Binary Snow Cover Map

There are only two classes namely snow covered area with snow pixels and non-snow covered area (cloud pixels) in the binary snow cover map [17]. Binary snow cover is generated by retaining only snow class as '1' and non-snow cover pixels as '0'.

The snow hydrological year is considered from September to August as the snow cover is lowest in September. The annual Snow Cover Area (SCA) is taken as the average of the snow hydrological year. Monthly SCA are derived from the 8-day snow cover maps taking average from 8-days spanned period in each month from 2002–2020. Table 3 explains the seasonal analysis of the months in a year categorized into the three seasons as winter, spring and summer using the previous studies [18, 19].

4.3 Elevation, Slope and Aspect Zonation

A decisive role is played by Elevation during snow accumulation [18]. The elevation map is classified into the class interval of 1000 m of each into seven zones. Slope is measured in degrees with the convention of 0° for horizontal plane. The slope zones are generated at 11.25° intervals to analyze the slope-based snow distribution and depletion analysis. The aspect is defined as the orientation of the slope representing the compass eight directions, i.e., North (N), North-East (NE), East (E), South-East (SE), South (S), South-West (SW), West (W), North-West (NW) that a slope faces. Zone classes used for SCA analysis in elevation, slope, and aspect are explained in detail in Table 4.

Table 4 Zone classes used for SCA analysis

Zone	Elevation range (km)	Slope range (degrees)	Aspect
1	< 1	0.3–11.25	N
2	1–2	11.25–22.5	NE
3	2–3	22.5–33.75	E
4	3–4	33.75–45	SE
5	4–5	45–56.25	S
6	5–6	56.25–67.5	SW
7	> 6	67.5–78.75	W
8	–	78.75–90	NW

4.4 Mann–Kendall Test

A broadly used long term non-parametric trend analysis is Mann–Kendall test [20]. It is used for SCA trend analysis during the period 2002–2020 (18 years). The relative importance of the sample data magnitude instead of the information values itself. This statistically assess if there is a monotonically increasing or decreasing trend.

5 Results and Discussion

5.1 Intra-Annual Variations of Snow Cover Area

The maximum 8-day SCA is observed on Feb 11th 2015 to Feb 18th 2015 with area of 46.41 × 103 km^2 reaching upto 88.32% of the total Sutlej basin area and minimum 8-day SCA is 4.14 × 103 km^2 during July 13th 2004 to 20th July 2004 reaching upto 7.88%. Figure 3 represents the SCA from September 2002 to August 2020.

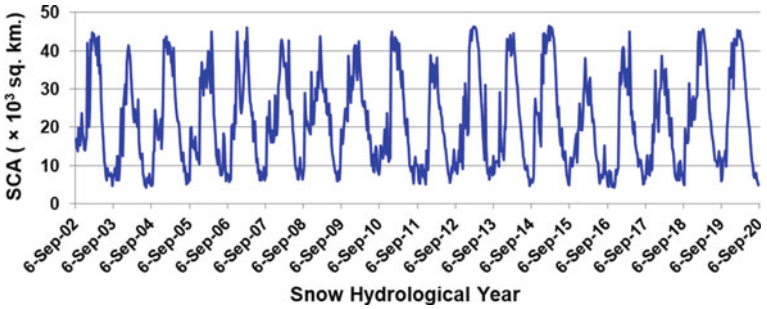

Fig. 3 The intra-annual 8-day SCA variations from September 2002 to August 2020

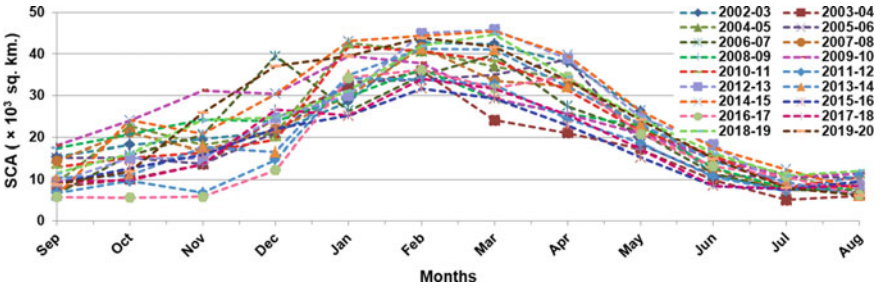

Fig. 4 The monthly mean SCA variations from September to August

5.2 *Monthly Variations of Snow Cover Area*

The monthly estimates in Fig. 4 show that maximum SCA in February and least SCA in August. The monthly SCA variations showed that from September to February the SCA increases due to the fresh snowfalls. From March the SCA decreases as the melting period commences and melting continues till June. The SCA reaches minimum in July and August.

5.3 *Inter-Annual Variations of Snow Cover Area*

Inter-Annual SCA variation was analyzed for the years 2002 to 2020 using average annual values. The maximum SCA is in 2014–15 with an area of 26.25 × 103 km^2 (49.95%) and minimum SCA is in 2003–04 with area of 17.42 × 103 km^2 (33.14%). The Mean SCA from 2002 to 2020 is 21.57 × 103 km^2 (41.03%). This shows that SCA is higher in the 2002–2011 decade when compared to the decade of 2011–2020 as shown in Fig. 5.

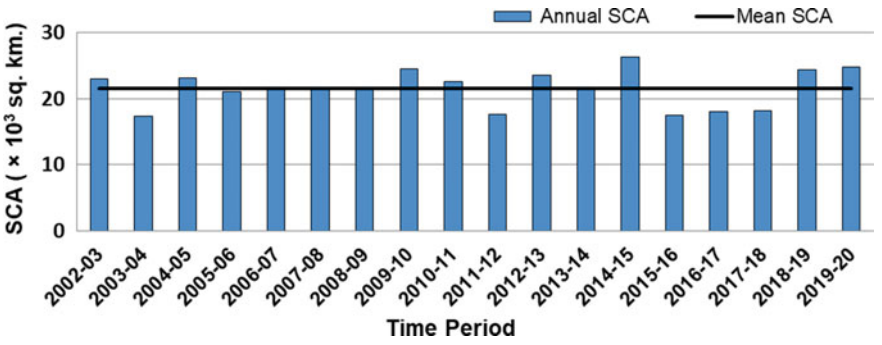

Fig. 5 Inter-annual mean SCA variations from 2002 to 2020

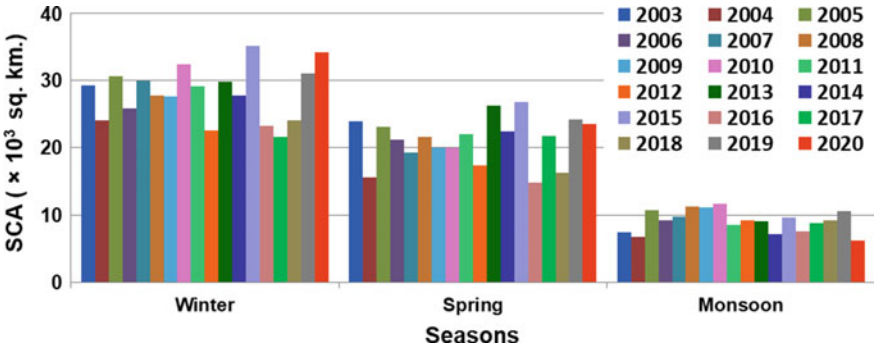

Fig. 6 The seasonal SCA variations from 2003 to 2020

5.4 Seasonal Variations of Snow Cover Area

Further SCA was analyzed for different seasons. The fresh snowfall during winter is the main controlling factor for the more seasonal variations of snow when compared to the other seasons. Figure 6 represents that the maximum SCA is observed during the winter, followed by spring and monsoon. During spring the SCA decreases because of the melting of snow.

5.5 Elevation Variations of Snow Cover Area

A significant role is played in snow accumulation during winter months by elevation. The Inter-annual variation of the snow cover was analyzed for the seven elevation zones is shown in Fig. 7. The higher elevation ranges such as above 4000 m have more favorable conditions for the formation and persistence of snow cover due to lower air temperature and higher precipitation [21]. During the accumulation period because of higher temperatures there is less snow in lower elevations and latitudes. The hypsometric curve reveals that basin area is more in 4–5 km and followed by 5–6 km. We observe that there is a higher SCA in 5–6 km due to the presence of glacier area.

5.6 Slope Variations of Snow Cover Area

The slope of 0.32°–11.25° SCA has the maximum SCA when compared to the other slope classes in Fig. 8. The quantitative variation is almost similar in 11.25°–22.5°and 22.5°–33.75° classes. The SCA in greater than 33.75° class is smaller SCA compared to other classes.

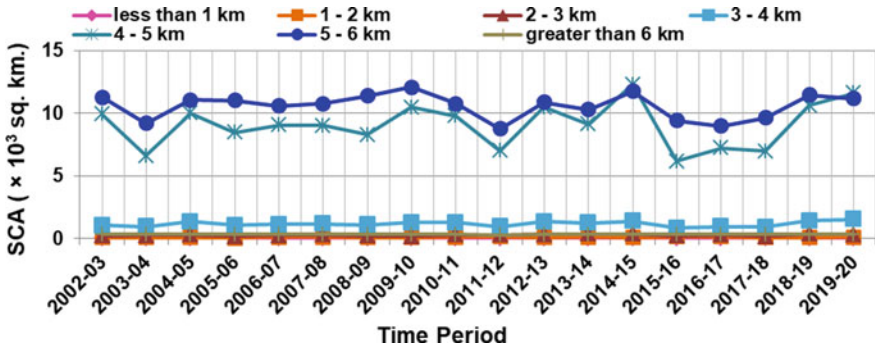

Fig. 7 Inter—annual SCA variations in each elevation zone of 1 km

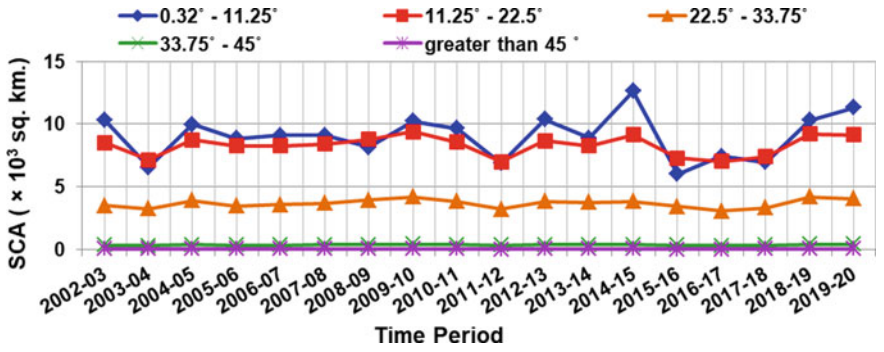

Fig. 8 Inter—annual SCA variations in different slopes

5.7 Aspect Variations of Snow Cover Area

The NE and E have higher SCA. SE, S, W, N and NW have less SCA compared to NE & E. The Fig. 9 shows that the years 2003–04, 2011–12, 2013–14, 2015–16 have decreasing SCA whereas 2005–09 and 2015–18 SCA is consistent. We observe that the quantitative changes in the SCA are following a similar pattern in all the aspects.

6 Conclusions

The present study is analyzed over Sutlej basin during 2002–2020 (18 years) using MODIS Terra and Aqua data combination for cloud reduction. There are no significant trends in Inter-annual, seasonal, monthly SCA with respect to elevation, slope and aspect with the Mann–Kendall test. The SCA in the lower elevations have less SCA as compared to the higher elevations. Though 2014–2015 showed the highest annual, winter and spring SCA whereas monsoon showed a less SCA. It was

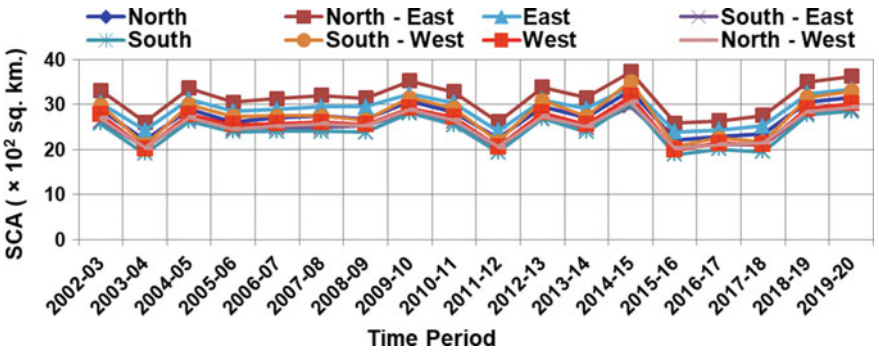

Fig. 9 Inter-annual SCA variations in different aspects

observed that aspect has major impact on snow accumulation. According to Jain et al. [19] the highest SCA is in NE due to the reason that north facing slopes are less exposed to insolation and warm wind, which provides favorable conditions for snow accumulation even though the highest basin area exists in the SW.

Acknowledgements The authors acknowledge the National Snow and Ice Data Center (NSIDC) for providing free data for conducting this study. This study is being supported by and implemented at the National Remote Sensing Centre, ISRO, Dept. of Space, Govt. of India, Hyderabad, under the World Bank funded "National Hydrology Project" (NHP), which is being taken up by the Dept. of Water Resources, RD and GR, Ministry of Jal Shakti, Govt. of India. The authors acknowledge the abundant support and encouragement received from the Director, NRSC-ISRO, to the Deputy Director (RSAA) NRSC-ISRO and the Project Director (NHP), for their profound guidance and direction.

References

1. Che T, Li X (2005) Spatial distribution and temporal variation of snow water resources in China during 1993–2002. J Glaciol Geocryology 27(1):64–67
2. Liston GE (1986) Seasonal snow cover of the foothills region of Alaska's Arctic slope: a survey of properties and processes. University of Alaska, Fairbanks, p 123
3. Gray DM, Male DH (1981) Handbook of snow, principles, processes, management and use—snow cover ablation and runoff. Pergamon Press, pp 360–436
4. Kulkarni AV, Rathore BP, Singh SK, Ajai (2010) Distribution of seasonal snow cover in central and western Himalaya. Ann Glaciol 51(54):123–128
5. Nester T, Kirnbauer R, Parajka J, Bloschl G (2012) Evaluating the snow component of a flood forecasting model. Hydrol Res 43(6):762–779
6. Singh P, Jain SK (2003) Modelling of stream flow and its components for a large Himalayan basin with predominant snowmelt yields. Hydrol Sci J 48(2):257–276
7. Hall DK, Riggs GA, Salomonson VV, DiGirolamo NE, Bayr KJ (2002) MODIS snow-cover products. Remote Sens Environ 83(1–2):181–194
8. Parajka J, Bloschl G (2008) Spatio-temporal combination of MODIS images—potential for snow cover mapping. Water Resour Res 44(3):1–13

9. Gafurov A, Bardossy A (2009) Cloud removal methodology from MODIS snow cover product. Hydrol Earth Syst Sci 13(7):1361–1373
10. Lopez-Burgos V, Gupta HV, Clark M (2013) Reducing cloud obscuration of MODIS snow cover area products by combining spatio-temporal techniques with a probability of snow approach. Hydrol Earth Syst Sci 17(5):1809–1823
11. Da Ronco P, De Michele C (2014) Cloud obstruction and snow cover in Alpine areas from MODIS products. Hydrol Earth Syst Sci 18(11):4579–4600
12. Dariane AB, Khoramian A, Santi E (2017) Investigating spatiotemporal snow cover variability via cloud-free MODIS snow cover product in Central Alborz Region. Remote Sens Environ
13. Zhou X, Xie H, Hendrickx JMH (2005) Statistical evaluation of remotely sensed snow-cover products with constraints from streamflow and SNOTEL measurements. Remote Sens Environ 94(2):214–231
14. Ault TW, Czajkowski KP, Benko T, Coss J, Struble J, Spongberg A, Templin M, Gross C (2006) Validation of the MODIS snow product and cloud mask using student and NWS cooperative station observations in the Lower Great Lakes Region. Remote Sens Environ 105(4):341–353
15. Wang X, Xie H, Liang T (2008) Evaluation of MODIS snow cover and cloud mask and its application in Northern Xinjiang China. Remote Sens Environ 112(4):1497–1513
16. Yang G, Ning L, TanDong Y (2011) Evaluation of a cloud-gap-filled MODIS daily snow cover product over the Pacific Northwest USA. J Hydrol 404(3–4):157–165
17. Shafiq MU, Ahmed P, Islam ZU, Joshi PK, Bhat WA (2019) Snow cover area change and its relations with climatic variability in Kashmir Himalayas, India. Geocarto Int 34(6):688–702
18. Immerzeel WW, Droogers P, de Jong SM, Bierkens MFP (2009) Large-scale monitoring of snow cover and runoff simulation in Himalayan river basins using remote sensing. Remote Sens Environ 113(1):40–49
19. Jain S, Goswami A, Saraf A (2009) Role of elevation and aspect in snow distribution in Western Himalaya. Water Resour Manage 23(1):71–83
20. Mann HB (1945) Nonparametric tests against trend. Econometrica 13(3):245–259
21. Duo C, Xie H, Wang P, Guo J, La J, Qiu Y, Zheng Z (2014) Snow cover variation over the Tibetan Plateau from MODIS and comparison with 6 ground observations. J Appl Remote Sens 8(1):1–13

River and Inlets Cross-Sections Extraction Using Stereo Pair Images for Hydraulic Modeling

Mark Prabhakar Vuppati, Shubham Dixit, Rajani B. Deogade, and Prabhat Chandra

Abstract In order to conduct a hydraulic model simulation for gage and discharge, a very essential part is the bathymetry data of river channel. Ground survey of these rivers for their cross-sections is a very tedious and expensive task and continuous availability of these cross-sections data for longer river stretch is sometimes hard to find. This paper presents an approach to extract the cross-sections with the help of Cartosat-1 Stereo pair images procured from NRSC. This approach was used to extract the portions of missing cross-sections for the main river and its inlet channels for the 127 km stretch of Mula-Mutha river flowing through Pune city and suburbs starting from Khadakwasla dam up to Daund, located in upper Bhima Basin. This study is a part of Purpose Driven Study (PDS), under National Hydrology Project (NHP). Freely available DEMs like ASTER DEM and SRTM DEM does not give satisfactory results when it comes to extracting the cross-sections for small inlets, therefore, Cartosat-1 stereo pair images were used to generate DEM of 5 m resolution using ERDAS IMAGINE 2014. Further, to extract the cross sections, QGIS2RAS (A Plugin for Q-GIS) was used. Out of the total reach length of 127 km, a good quality surveyed data was available for 77 km in parts, this data was used for the required corrections and verification of extracted data. With a few modifications for fine tuning, the cross-sections produced were of satisfactory quality.

Keywords River cross-sections · Stereo pair images · DEM generation · Mula-Mutha River

M. P. Vuppati (✉) · S. Dixit · R. B. Deogade
River Rejuvenation Division, Central Water and Power Research Station, Pune 411024, India
e-mail: vmprabhakar@gmail.com

S. Dixit
e-mail: shubamdixit95@gmail.com

R. B. Deogade
e-mail: deogade_rb@cwprs.gov.in

P. Chandra
PH-I Division, Central Water and Power Research Station, Pune 411024, India

P. V. Timbadiya et al. (eds.), *Hydrology and Hydrologic Modelling*,
Lecture Notes in Civil Engineering 312,
https://doi.org/10.1007/978-981-19-9147-9_24

1 Introduction

To successfully simulate the river flow processes onto a mathematical model, one of the very basic yet crucial requirement to precisely predict the depth of water corresponding to the flow magnitude and vice versa, is a good quality Geometry data. The best source for this geometry data is always the physically surveyed data, but such surveys tend to be very expensive and difficult to execute. To overcome this, a few GIS tools are developed to extract geometrical features from various remotely sensed datasets [1]. Many studies are done that try to extract the missing datasets using such tools. The main products mostly used for this purpose are Digital Elevation Model incorporated with GIS. [1–4]. A digital elevation model is spatial representation of elevations of ground surface, it is a raster image whose pixels store the value of elevation, of corresponding point on ground. Freely available DEMs in public domain have poor resolution for the purpose of cross-sections extraction, these free DEMs can be used for very wide channels, but for better accuracy and for cross sections of narrow lateral inlets, DEMs with high resolution is required. NRSC publically provides CartoDEM of 30 m resolution, and stereo pair images of 2.5 m resolution. These stereo pair images can be used to produce high resolution DEM, however vertical elevation correction will further be required [5].

This paper presents a part of study which was carried out under a purpose driven study for NHP titled "River Rejuvenation of Mula-Mutha river flowing through Pune city and suburbs", The said study is to be conducted on a 127 km river stretch from Khadawasla dam to Daund. For preparation of hydrodynamic model, a good quality surveyed cross-sections data was available from Khadakwasla dam to Mundhwa (27 km) and from Loni to Pargaon (50 km) and for rest of the river stretch, cross-section data was missing. To extract the cross-section data where it is missing, the present study was carried out with the following objectives.

a. To prepare high resolution DEM using stereo pair images,
b. To extract the cross-sections for missing portions of river and small lateral inlets,
c. To identify the required elevation correction for extracted cross-sections,
d. To apply correction and smoothen cross-sections for irregularities (if any).

2 Materials and Methods

2.1 Study Area and Data Source

2.1.1 Mula-Mutha River

Mula-Mutha river flows through Pune city and suburbs and acts as the major source of water for Pune city for various activities. Mula river originates from Mulshi dam and flows for around 64 km to meet Mutha river at Sangamwadi. Mutha river originates from Khadawasla Dam and after flowing for around 15 km through Pune city, it meets

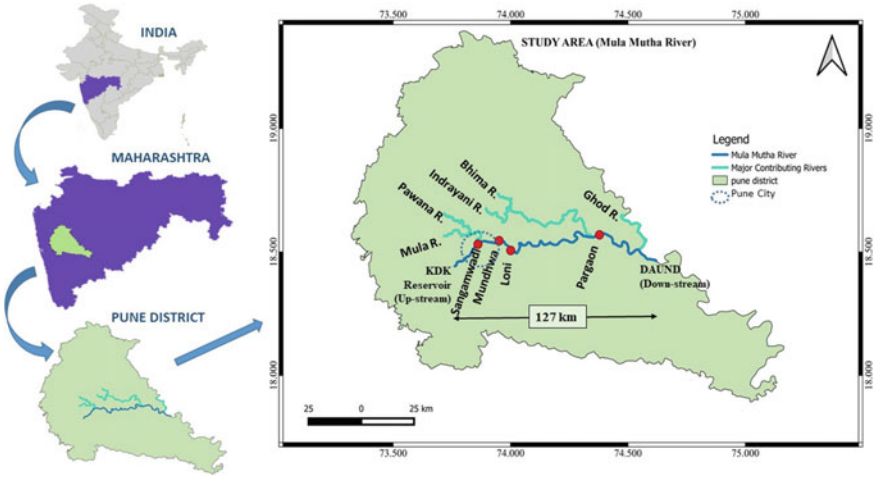

Fig. 1 Index map of study area

with Mula river. After the confluence point at Sangamwadi the river now called as Mula-Mutha river, which travels 50 km to meet Bhima river at a point near Pargaon. The scope of our study ends at Daund where the river completes a total reach of 127 km, for this river stretch, the delineated watershed area is around 11,340 km^2 (Fig. 1).

2.1.2 Data Collection

The high quality surveyed cross-section data for the river was sourced from Irrigation Department, Pune. The various software and datasets used in the study are listed in Tables 1 and 2.

Table 1 Software used and their applications

Software	Application
Erdas Imagine 2014 (Imagine photogrammetry toolbox)	To process stereo pair images and prepare DEM
Q-GIS and Q-SWAT	Q-SWAT model was used for creation of all streams and delineation of watershed using the prepared DEM With the help of vector file of streams, Q-GIS software was used to prepare, input files required for QGIS2RAS
QGIS2RAS (GIS plugin)	To extract cross-sections from DEM
HEC-RAS	To process the extracted cross-sections

Table 2 Data used for the study

Surveyed cross section data		
From	To	Distance and interval
Khadakwasla Dam	Mundhwa	885 cross-sections across 27 km at 30 m interval
Loni	Pargaon	500 cross-sections across 50 km at 100 m interval
Satellite data		
	Band A	Band F
Satellite ID	P5	P5
Sensor	PAA	PAF
Date of imageries	Jan 2nd 2018–Jan 21st 2019	Jan 2nd 2018–Jan 21st 2019
Path-Row	517—308, 309, 310, 311 518—307, 308,309, 310, 311, 312 519—307, 308, 309, 310, 311 520—308, 309, 310, 311 521—308, 309, 310, 311 522—309, 310, 311 523—309, 310, 311	517—308, 309, 310, 311 518—307, 308, 309, 310, 311, 312 519—307, 308, 309, 310, 311 520—308, 309, 310, 311 521—308, 309, 310, 311 522—309, 310, 311 523—309, 310, 311

2.2 Methodology

The whole study can broadly be divided into two parts:

1. The first step consists of DEM generation and
2. The second step consists extraction of cross-sections from generated DEM.

The methodology adopted in this study is shown in Fig. 2:

2.2.1 DEM Generation

For generation of DEM using Cartosat-I stereo pair images (Fig. 3), Imagine photogrammetry toolbox of Erdas Imagine 2014 [6] was used.

DEM can be generated by performing the following steps in Imagine photogrammetry:

1. Create a new block (.blk) file.
2. Add a new frame to input images.
3. Provide Rational Polynomial Coefficients (RPC) file.
4. Calculation of Pyramid Layers and generate automatic tie points.
5. Triangulation and Generate DEM.

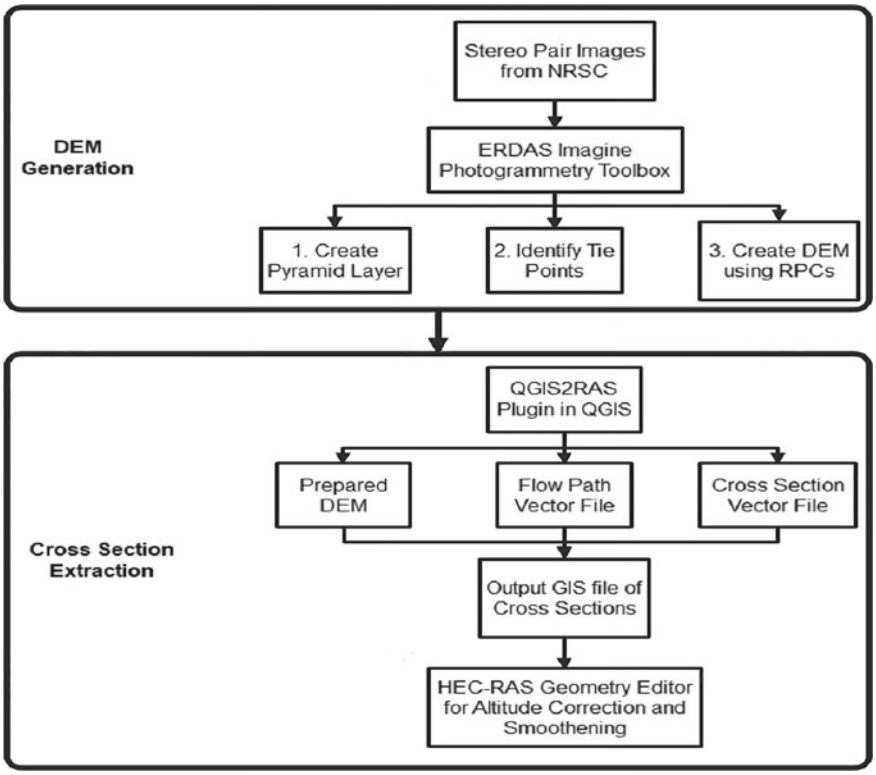

Fig. 2 Methodology flow chart

To start the DEM generation procedure, a block file was created, with geometric model category set to 'rational functions', because sensors in Cartosat-I are based on rational functions. The stereo pair images were given as input via adding a new frame. Since, the geometry model was set to rational functions, the software asks for a rational polynomial coefficients (RPC) files, which were provided with the stereo pair images.

These RPC files contains coefficients that relate the image pixels (rows and columns) with the latitude, longitude and elevation on the ground. These coefficients are the ratios of cubic polynomial expressions, which represents the image and actual objects parameters [7].

After providing the RPC file, automatic Tie points were generated by software, these are the points responsible for tying together the two images of stereo pair. More the number of tie points higher will be the accuracy of DEM generated. Software generates these tie points by identifying similar points on the two images, which

represent the same point on ground. DEM generation cannot proceed if no tie points are found in stereo pair. Tie points can also be given manually with the help of some additional field data for better accuracy.

These tie points are then used by software to start block triangulation process, where a mathematical relation is established between the image captured and ground. The error is reported by software in the form of root mean square error (RMSE). This RMSE value should be less than one to prepare a DEM with good accuracy. After completing the block triangulation process, DEM can be generated.

2.2.2 Cross-Section Extraction

For extraction of cross-sections, A GIS plugin named "QGIS2RAS" was used, the input required for this plugin is:

1. DEM for the concerned area.
2. A vector file marking centerline of flow path for which cross-sections are to be extracted.
3. A vector file of the cross-sections, each cross-section marked as individual attributes on the above-mentioned centerline.

The output of QGIS2RAS was obtained in GIS format as a geometry file (.sdf) which can be accessed in HEC-RAS using the import function.

2.2.3 Cross-Section Comparison

Cross-sections that were generated using imagine photogrammetry toolbox on Erdas imagine 2014 were checked for accuracy, by comparing the geometry and elevation values with that of existing high quality surveyed cross-sections. 25 cross-sections were checked and in each cross-section, elevations of lowest point, left bank and right bank were used to compare with that of extracted cross-section. After the comparison, a weighted average value of vertical elevation correction was adopted and applied in all extracted cross-sections using the HEC-RAS geometry editor. The cross-sections after the applied correction and additional smoothening were ready to use for further modeling purposes.

3 Results and Discussion

3.1 DEM Generation

The tie points were generated automatically by Imagine photogrammetry tool and using these tie points, triangulation was performed, for a DEM with good accuracy

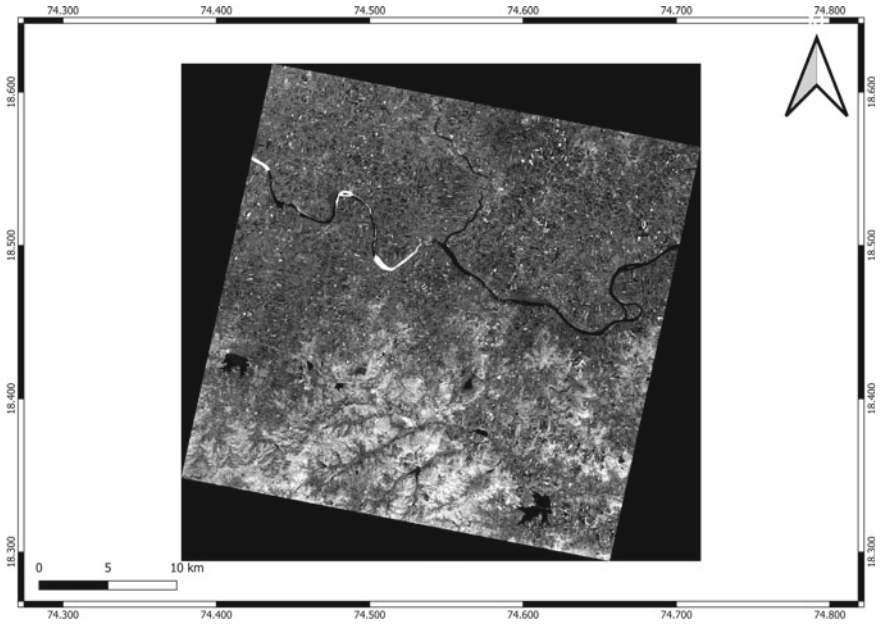

Fig. 3 Stereo pair image obtained

the RMSE for triangulation process is suggested to be less than 1. In this study, for a total of 29 pair of images, the RMSE values obtained were ranged between 0.246 and 0.769. After successful triangulation DEM was generated as shown in Fig. 4.

3.2 Cross-Section Extraction

The generated DEM was used to extract cross-section using GIS plugin QGIS2RAS, for this purpose vector files of centerline of flow path and cross-sections as shown in Fig. 5, were used. The extracted cross-section from QGIS2RAS without vertical elevation correction and smoothening is shown in Fig. 6.

3.3 Cross-Section Comparison

A total of 25 cross-sections were compared for geometry and were found to be having nearly same width and shape of section, the elevation difference observed in these

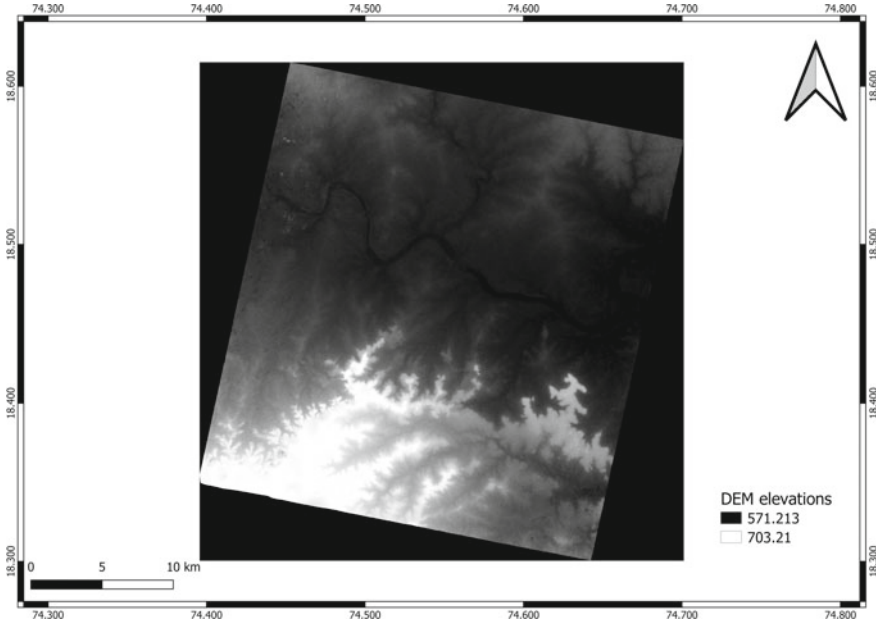

Fig. 4 DEM generated from stereo pair using Erdas Photogrammetry tool

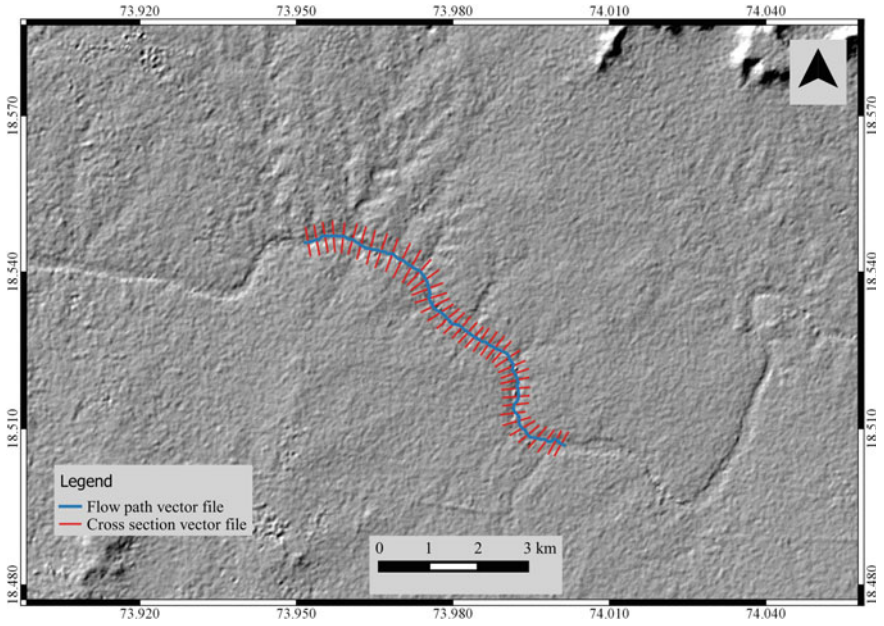

Fig. 5 Input vector files for Q-RAS

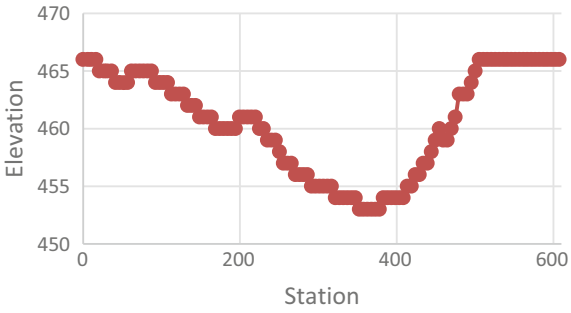

Fig. 6 Raw extracted cross-section

sections was such that the extracted cross-sections were having elevation lower that the surveyed sections. The difference in elevations of station points came out to be in range of 59–64 m, so a weighted average value of + 62.01 m was adopted as vertical elevation correction for all the extracted cross-section. Few cross-sections before and after application of correction and smoothening are shown in Fig. 7

4 Conclusion

The present study showcased an economical and efficient approach that can be used when dealing with the case of missing cross sections data. Since the requirement of the study was to obtain high quality cross-sections for river reach as well as the narrow inlets, a DEM of 5 m resolution was generated using the Cartosat-I stereo pair images, with the help of Imagine Photogrammetry toolbox. The RMSE value for the generated DEMs was found to be between 0.246 and 0.769, which is in the desirable limits. This DEM is used to extract the cross-sections of river and its inlets using the GIS plugin named QGIS2RAS, the cross-sections obtained, were found to be at lower elevation than the actual surveyed cross-sections, so with the help of the data from existing cross-sections, a suitable vertical elevation correction of + 62.01 m was adopted as an average value and applied to all extracted cross-sections, and the smoothening of corrected sections was carried out in HEC-RAS geometry editor. The final prepared cross-sections were found to be satisfactory for use. For wider river channels, the publically available DEM can also be used, where the distance between points of elevation in a cross-section will be equal to the resolution of DEM, so more number of station points along the width of river will be available for wider sections.

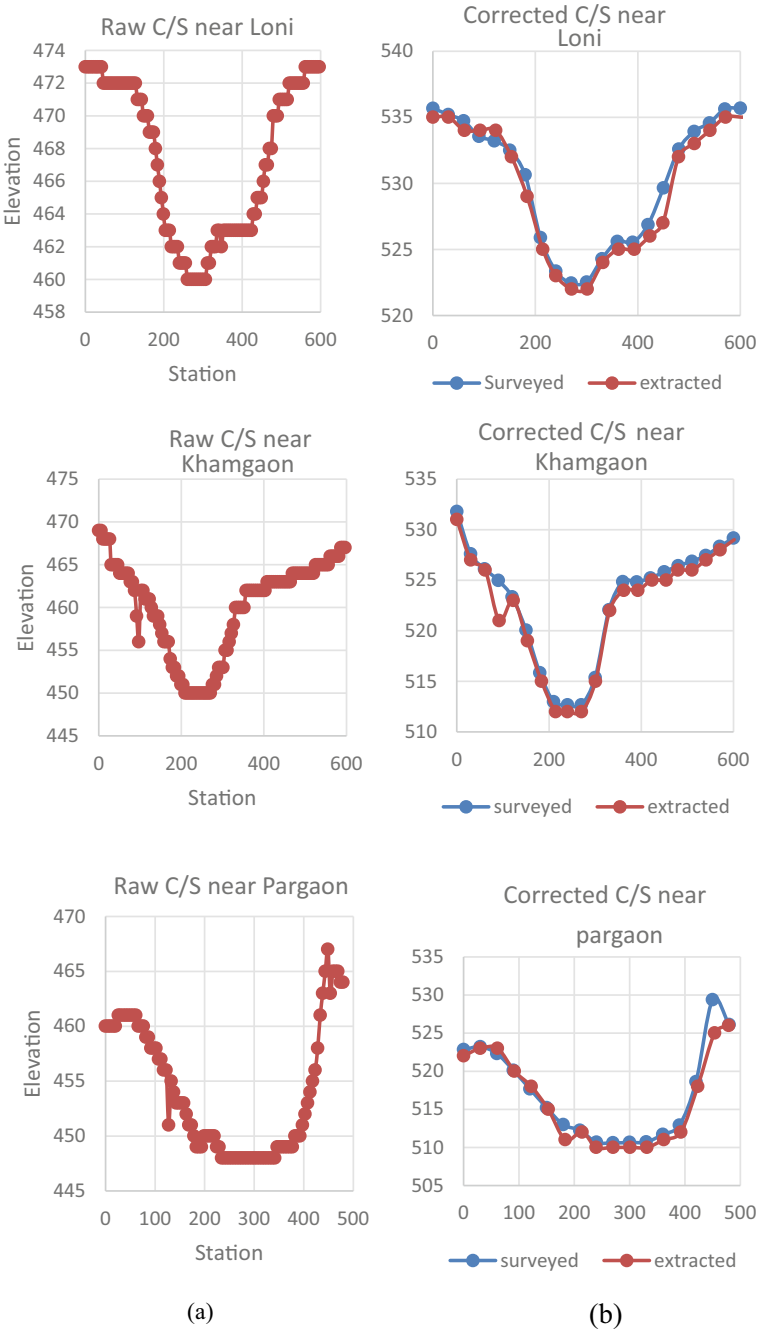

Fig. 7 Showing **a** the raw extracted cross-section and **b** corrected extracted cross-sections v/s surveyed cross-section at some major locations

Acknowledgements The authors humbly acknowledge to National Hydrology Project (NHP) for providing financial assistance for this study. Authors also acknowledges the Director of Central Water and Power Research Station (CW and PRS) for support. A sincere gratitude is extended to the laboratory staff and research colleagues of River Rejuvenation Division, CW and PRS.

References

1. Merwade V, Cook A, Coonrod J et al (2008) GIS techniques for creating river terrain models for hydrodynamic modelling and flood inundation mapping. Environ Model Softw 23:1300–1311
2. Asante K, Arlan G, Pervez S, Rowland J (2008) A linear geospatial streamflow modeling system for data sparse environments. Int J River Basin Manage 6(3):233–241
3. Herath S, Dutta D, Wijesekera S (2003) A coupled river and inundation modeling scheme for efficient flood forecasting. Geoinformatics 14(1):37e41
4. Sanders B (2007) Evaluation of on-line DEMs for flood inundation modeling. Adv Water Resour 30(8):1831e1843
5. Gichamo TZ, Popescu I, Jonoski A, Solomatine D (2012) River cross-section extraction from the ASTER global DEM for flood modelling. Environ Model Software 31, Elsevier:37–46
6. ERDAS Field Guide (2003), Integraph, October
7. Saha K (2014) DTM extraction and evaluation from Cartosat-I stereo data for Bhopal city, Madhya Pradesh. Int J Sci Res Publ 4(5):1–5

Flood Routing Using Numerical Methods: A Review

Ekant Sarkar, Biswajit Pradhan, and Kishanjit Kumar Khatua

Abstract Many water resource management problems require river flow projections. For river flow analysis, the partial differential equations of continuity and momentum, defining free surface flow in open channels were presented by French engineer Saint–Venant. Because these equations are quite nonlinear, they have no analytical solutions. These equations can be solved for flood routing by numerical methods which consist of wave models and numerical models. The numerical model consists of two methods: the finite difference method and the characteristic method. This paper aims on comparative study of the various numerical models based on the works done previously on the flood routing numerical modelling. The numerical methods available to solve these equations for river discharge calculations are reviewed in this literature. The findings from various literatures show that the finite difference method is more accurate than the characteristic method, and larger mesh size can be handled more efficiently by the finite difference models. On further investigation of the finite difference models, the explicit simplified dynamic model yields similar outflow hydrograph characteristics as the other models under the same conditions. Furthermore, it is found that the simplified dynamic model is easier to formulate and simpler to calculate than the other ones. Newer numerical models were also studied, and the lack of use of artificial intelligence in flood routing was a critical review of this study.

Keywords Flood routing · Numerical models · Simplified dynamic model · Wave models

1 Introduction

Urban, commercial, and agricultural regions may sustain harm as a result of flooding near rivers. Along the major rivers, a number of buildings are built to reduce flood

E. Sarkar (✉) · B. Pradhan · K. K. Khatua
Department of Civil Engineering, National Institute of Technology Rourkela, Rourkela 769008, India
e-mail: ekant1234@gmail.com

P. V. Timbadiya et al. (eds.), *Hydrology and Hydrologic Modelling*,
Lecture Notes in Civil Engineering 312,
https://doi.org/10.1007/978-981-19-9147-9_25

damage. The design of these structures depends heavily on the estimation of floods as well as the impact of stream channels on floods. The fluctuation of discharge with time at a place on a stream channel can be calculated by taking into account comparable data from a point upstream. Flood routing is the mechanism by which storage in the reach between any two places changes the shape of the flood as it proceeds downstream through river reaches. In hydrology and hydraulics, it's crucial to understand flood wave routing theory and solve the governing equations correctly. The velocity and water depth change with time and longitudinal position in unsteady open channel flows. The relevant flow parameters, like the depth of flow and velocity of flow, for one-dimensional applications are functions of time and longitudinal distance. The Saint–Venant equations, which consist of a continuity equation that conserves the mass of the flow and a momentum equation that conserves the flow momentum, are the basic equations that describe gradually varied unsteady flow in open channel for flood routing problems.

Various approximations to the Saint–Venant equations have been proposed given the complex nature of the Saint–Venant equations. Mathematical models must properly represent physical processes and offer a numerical solution to a system of differential equations, which must be solved using appropriate boundary conditions and empirical connections to characterise flow and turbulence resistance. River mechanical issues are usually described by partial differential equations with two independent variables, which are simplified versions of the conservation of mass and momentum equations (time and space or 2D space variables).

Wave models that solve various approximations of the St. Venant equations and numerical models that solve the St. Venant equations for gradually varied, unsteady flow are the two types of mathematical models that are now practical for resolving gradually varied, unsteady flow problems. Two wave models are the diffusion wave method and the kinematic wave approach. The solutions of the consolidated Saint–Venant equations are used in the kinematic wave and diffusion wave techniques. While the diffusion wave technique disregards variations in velocity as a function of time and place, the kinematic wave approach ignores all differential components in the momentum equation. The Saint–Venant equations were solved by Greco and Panatoni [6] using an implicit framework. The kinematic and diffusion wave models were employed by Akan et al. [1] for their research. In order to determine runoff, Akan et al. [2] employed the kinematic wave method. Both the diffusion approximation and kinematic wave routing [3], which utilise simplifications to the full momentum equation, are prevalent techniques (Akan and Yen et al. [1]). The validity of these approximations to the momentum effects in flood routing is covered in a number of publications, including Ponce et al. [12] and Chagas et al. [13].

The Saint–Venant equations, on the other hand, have been solved using a variety of numerical methods without any simplification. The numerical model mainly consists of Finite Difference method and the Method of Characteristics. Previous research has focused on comparing two or three different schemes. The accuracy and stability of the method of characteristics were improved by Kibler [7] using the technique of lines solution along the method of characteristics (MOLAC). To predict flood wave propagation, Greco and Panatoni [6] and Lee et al. [8] used an implicit method and

compared the results to laboratory data from a physical model. They demonstrated that the implicit method of solution could accurately predict the depth hydrograph.

2 Materials and Methods

Flood routing in terms of channel length and duration is entirely defined by the Saint–Venant equations, which model one-dimensional unsteady flow in an open channel. As illustrated in the diagram below, these equations, sometimes referred to as dynamic wave equations (Cunge et al. [5]), can be expressed as continuity Eq. (1) and momentum Eq. (2).

Continuity equation

$$\frac{\partial A}{\partial t} + \frac{\partial Q}{\partial x} = 0 \tag{1}$$

Momentum equation

$$\frac{\partial Q}{\partial t} + \frac{\left(\beta \frac{Q^2}{A}\right)}{\partial x} + gA\left[\frac{\partial y}{\partial x} - S_0 + S_f\right] - q\beta V_x = 0 \tag{2}$$

where

Q Flow discharge
S_f Friction slope
x Longitudinal coordinate
g Acceleration dur to gravity
S_0 Bed slope
A The cross-section area

The mathematical models that are currently available to treat problems involving gradually varying, unsteady flow can be broadly categorised into two groups: (a) numerical models, which solve the St. Venant equations for progressively varying, unsteady flow; and (b) wave models, which solve various approximations of the St. Venant equations.

2.1 Wave Models

2.1.1 Kinematic Wave Model

Equation (2) may be expressed as Eq. (1) when the pressure and acceleration parts of the momentum equation are eliminated and the slope of the energy line matches

the slope of the beds (3) (Soleymani et al. [13]).

$$S_0 = S_f \tag{3}$$

Solving Eqs. (2) and (3) gives Eq. (4),

$$\frac{\partial Q}{\partial x} + \alpha\beta Q^{\beta-1}\frac{\partial Q}{\partial t} = 0 \tag{4}$$

The explicit discretisation of (4) gives Eq. (5),

$$Q_{i+1}^{j+1} = \frac{\frac{\Delta t}{\Delta x} Q_i^{j+1} + \alpha\beta Q_{i+1}^{j}\left(\frac{Q_{i+1}^{j}+Q_i^{j}+1}{2}\right)^{\beta-1}}{\frac{\Delta t}{\Delta x} + \alpha\beta\left(\frac{Q_{i+1}^{j}+Q_i^{j+1}}{2}\right)^{\beta-1}} \tag{5}$$

α and β are constant coefficient and their values can be given by Eq. (6).

$$\alpha = \left[\frac{np^{2/3}}{\sqrt{s_0}}\right] \text{and } \beta = 0.6 \tag{6}$$

The downstream boundary condition is not required for the kinematic wave method. This model can be used in a river basin with a steep inclination.

Figure 1 shows the hydrographs plotted by the kinematic wave method where some assumptions are taken in the Saint–Venant's Equation, and the dynamic wave method where all the terms in the momentum equation are taken into consideration. From the above hydrograph, it can be easily seen that the attenuation provided by the dynamic wave method is more than that of the kinematic wave method. Hence, the dynamic wave approach is more practical for real-life application and hence is widely used as compared to any other method for flood routing applications.

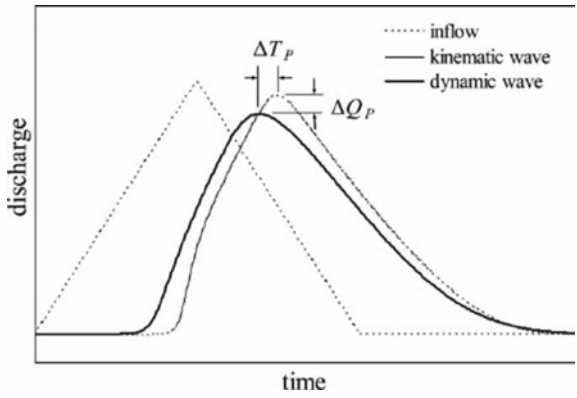

Fig. 1 Comparision hydrographs by kinematic and dynamic wave method Solmeyani et al. [13]

2.1.2 Diffusion Wave Model

The first two terms in Eq. (2) left hand side are assumed to be zero. As the dynamic equation for the diffusive model, we get the following Eq. (7) (Majumdar et al. [9]).

$$s_f = s_0 - \frac{\partial y}{\partial x} \tag{7}$$

Equations (1) and (7) can be resulted in the following equation

$$\frac{\partial Q}{\partial t} + C\frac{\partial Q}{\partial x} = M\frac{\partial^2 Q}{\partial x^2} \tag{8}$$

M and C in Eq. (8) change as the flood time progresses. Equation (9) could be used to calculate M and C.where

$$M = \frac{Q}{2BS_0} \text{ and } C = \frac{5}{3}\frac{R^{2/3}}{n}s^{1/2} \tag{9}$$

Final model of diffusive scheme is given by Eq. (10).

$$Q_i^{j+1} = \left[1 - \frac{\Delta t}{\Delta x}C_i^j - 2M_i^j\frac{\Delta t}{\Delta x^2}\right]Q_i^j + \left[\frac{\Delta t}{\Delta x}C_i^j + M_i^j\frac{\Delta t}{\Delta x^2}\right]Q_{i-1}^j + M_i^j\frac{\Delta t}{\Delta x}Q_{i-1}^j \tag{10}$$

In Fig. 2, the four-point implicit scheme for diffusive wave model is shown. The space co-ordinates are shown in the x-axis with spatial nodal notation as 'i' and the spatial interval is given as Δx. The vertical axis shows the temporal components with notation as 'j' and temporal interval as Δt. The given grid formation is called as the implicit scheme because of the unknown internal nodal value of discharge at $(j + 1)$ time step. All the internal node values at the jth time step are known. For calculating the discharge value at the next time step and next spatial node which is given as Q_{i+1}^{j+1}, , which means that the discharge value at the internal node at $(i + 1)$th spatial step and $(j + 1)$th temporal step. From the previous known time and spatial step values, the next time step value of discharge can be calculated using simultaneous equations involving variables from jth and $(j + 1)$th time step which will give the required discharge values at desired nodes of the grids. The diffusive model scheme using four-point implicit formula is given in Eq. (10).

In Fig. 3, the flowchart showing the diffusion wave model scheme is shown. After the collection of required input data, the model is started. The initial conditions for the ith spatial step and the jth temporal steps are defined as the inflow hydrograph. The Courant stability condition is applied for the discretised numerical equation of the diffusive wave model and is checked for stability of the hyperbolic Saint-Venants equation. After the satisfaction of the model stability conditions, the internal nodal

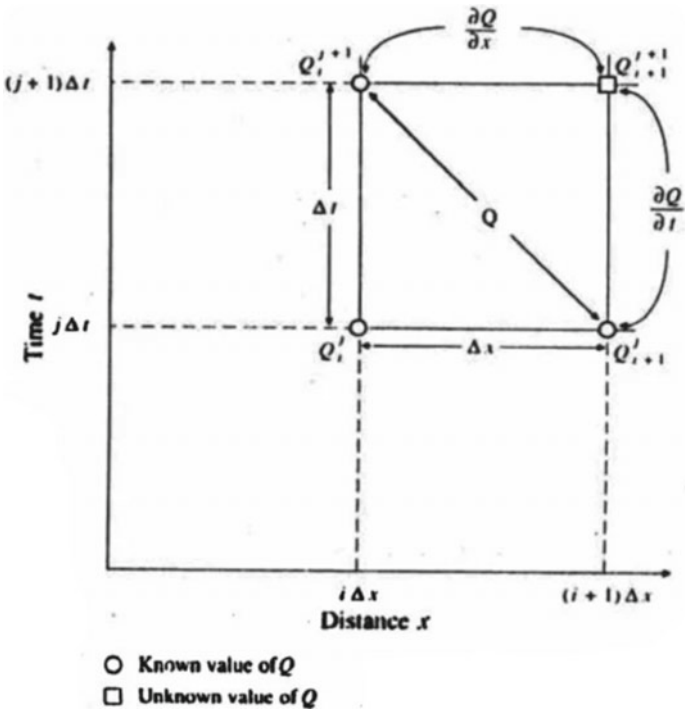

Fig. 2 Grids and nodes for four-point implicit scheme for diffusive wave model (Applied hydrology by Ven Te Chow, 1988)

values of unknown discharges at various spatial and temporal nodes are calculated using the simultaneous discretised equations obtained for the diffusive wave model. Subsequently, the process is repeated until all the discharges values are known for all the designated nodal points on the generated mesh grid. After the completion of the model run, the data are checked for the convergence and hence the downstream discharge values are henceforth calculated. After reaching the last time step for a particular spatial node, the model run is stop for that spatial node and hence a hydrograph is generated at the desired location downstream by the diffusive wave model.

2.2 Numerical Models

The numerical models are classified as follows which are given in the subsequent sections (Ostad et. al. [11]).

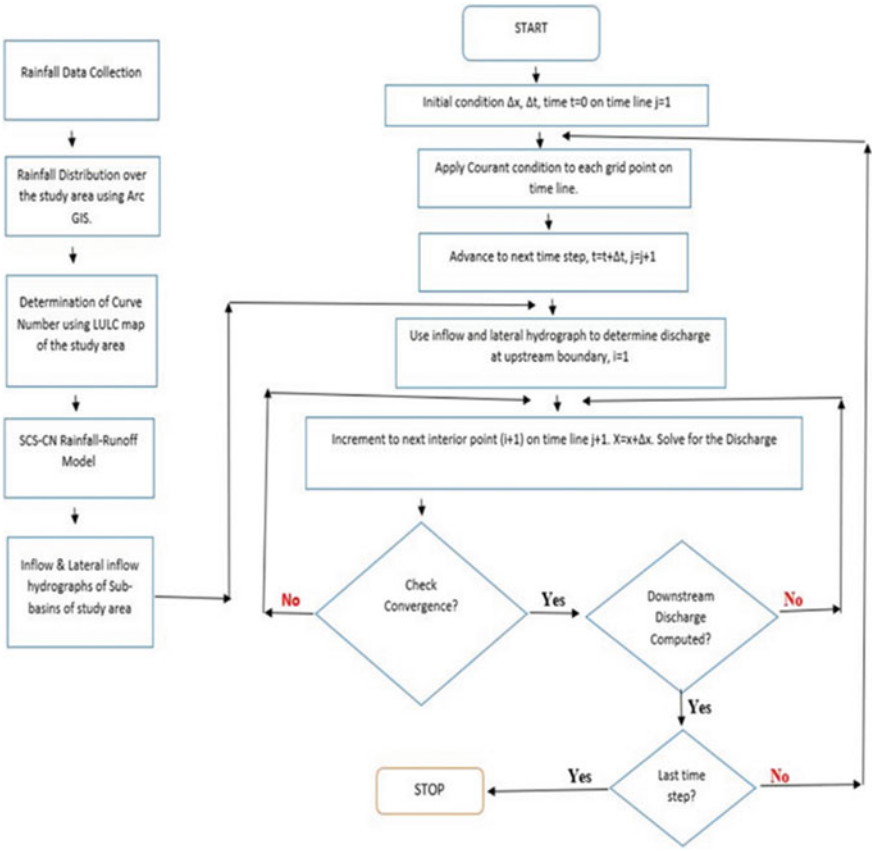

Fig. 3 Flowchart showing the process of Diffusive Wave Model (Majumdar [9])

2.2.1 Finite Difference Method

The finite difference model is mainly classified as classical dynamic model and the simplified dynamic model. The detailed review of both the models under the finite difference numerical model is given in the subsequent sections.

2.2.2 Classical Dynamic Model

The governing equations are derived using the subsequent assumptions:

(i) Hydrostatic pressure distribution
(ii) Uniform velocity distribution over a channel section
(iii) Small average channel bed slope
(iv) Homogeneous and incompressible flow
(v) No lateral flow.

Equations (1) and (2) can have numerical solutions if the proper beginning and boundary conditions are given. In the numerical study of one-dimensional unsteady flow in rivers with a free surface, implicit finite difference techniques are demonstrated to be more effective than explicit and characteristic methods (Cunge et al. [5], Nyogen [10], Chagas et al. [4]) Since finite difference equations have a high degree of numerical stability, the implicit technique, for instance, theoretically has no restrictions on the size of the time step. Because the time steps are bigger, the implicit technique is more computationally effective than other methods, especially for long-duration floods. The weighted four-point system approximates the time and spatial derivative and non-derivative terms of the Saint–Venant equations as Eq. (11) and (12).

$$\frac{\partial D}{\partial t} = \frac{\left(D_i^{j+1} + D_{i+1}^{j+1}\right) - \left(D_i^j + D_{i+1}^j\right)}{2\Delta t} \tag{11}$$

$$\frac{\partial D}{\partial x} = \frac{\theta\left(D_{i+1}^{j+1} + D_i^{j+1}\right) + (1-\theta)\left(D_{i+1}^j - D_i^j\right)}{\Delta x} \tag{12}$$

where t is the time step, x denotes the spatial step, I denotes the spatial index, D denotes a general parameter that represents the dependent variables, j denotes the temporal index, and θ denotes the weighting factor, which has a range of 0 to 1.0. A completely implicit system is produced when $\theta = 1$. A highly clear scheme is created when $\theta = 0$, whereas a box scheme is produced when $\theta = 0.5$ (Barati et al. [2]). The four-point implicit approach is unconditionally stable when θ is between 0.5 and 1.0 (Akan et. al [1]). A set of nonlinear algebraic equations is produced by including the aforementioned finite difference approximations and coefficients into the equations of gradually changing unsteady flow and specifying the beginning and boundary conditions. These equations can be resolved by an iterative functional approach, such as the Newton–Raphson method.

2.2.3 Simplified Dynamic Model

Another form of the momentum equation is created to estimate flood routing for a rectangular channel with constant width, and then the resulting momentum equation and the continuity equation are solved using an explicit finite difference technique. To construct this model from the classical dynamic equation, the derivative of friction slope is considered to be small in comparison to other parts of the equation. A dynamic cascade is a simplified dynamic model that is built as a series of discrete channel segments with flood routing explained using dynamic wave equations. In the solution, a simple numerical cascade approach similar to the kinematic one (Kibler [7]) is utilised.

In the simplified dynamic model, momentum equation is revised as given in Eq. (13)

$$\frac{\partial Q}{\partial t} + \alpha \frac{\partial Q}{\partial x} + \beta = 0 \tag{13}$$

where,

$$\alpha = 2\frac{Q}{A} + \frac{\frac{gA}{b}\left(\frac{Q}{A}\right)^2}{\frac{Q}{A}\left(\frac{5}{3} - \frac{4R}{3b}\right)} \tag{14}$$

$$\beta = gA\left(S_f - S_0\right) \tag{15}$$

The governing equations are solved numerically using an explicit finite difference approach. The discretisation for the space derivative in explicit form is given as Eq. (16).

$$\frac{\partial f(x,t)}{\partial x} = \frac{f_i^j - f_{i-1}^j}{\Delta t} \tag{16}$$

The discretisation for the time derivative in explicit form is given as Eq. (17).

$$\frac{\partial f(x,t)}{\partial t} = \frac{f_i^{j+1} - f_{\mathrm{i}}^{j-1}}{\Delta t} \tag{17}$$

in which, Δx and Δt are space and time increments, respectively. Substitution of Eqs. (17) and (18) into modified momentum equation, Eq. (14), and into continuity equation, Eq. (1), one obtains Eqs. (18) and (19).

$$Q_i^{j+1} = Q_i^j - \frac{\Delta t}{\Delta x}\alpha_i^j\left(Q_i^j - Q_{\mathrm{i}-1}^j\right) + \beta_i^j \Delta t \tag{18}$$

$$A_i^{j+1} = A_i^j - \frac{\Delta t}{\Delta x}\left(Q_i^{j+1} - Q_{i-1}^{j+1}\right) \tag{19}$$

It is clear that α and β are obtained from Eqs. (14) and (15). Using the given initial and boundary conditions at the start of (i, j), Q_i^{j+1} from Eq. (18) is obtained. From $Q_i^{(j+1)}$, $A_i^{(j+1)}$ will be calculated from Eq. (19). This system is repeated for each value of (i, j). Within the suggested simplified dynamic model, the discharge from the downstream boundary reaches the upstream boundary of the adjacent segment, providing the upstream condition for flow on that segment.

2.2.4 Method of Characteristics

In this method, using the $C = \sqrt{gy}$, Saint–Venant equations are changed into two complete differential equations given by Eqs. (20) and (21).

$$\frac{\mathrm{d}x}{\mathrm{d}t} = V \pm C \tag{20}$$

$$\frac{\mathrm{d}(V \pm 2C)}{\mathrm{d}t} = g\left(s_0 - s_f\right) \tag{21}$$

where C is velocity of wave transfer (m/s).

If the flow characteristics at the S and R points at time t_1 are known in Fig. 4, the flow characteristics at the point P at time t_2 may be estimated. The lines illustrated in Fig. 4 are the distinctive lines. The line crossing from P to R has a positive characteristic, and its significant equations are used with the positive sign, whereas the line crossing from S to P has a negative characteristic, and its significant equations are used with the negative sign. The separation of Eqs. (20) and (21) yields four algebraic equations, the solutions to which yield the values of the four unknowns v_P, c_P, x_P, and t_P.

After obtaining C_p, the value of y_P can be also obtained from the Eq. (22).

$$y_P = \frac{C_P^2}{g} \tag{22}$$

Finally, the flow rate can be calculated. This is done for all points at the time t_2 and flows characteristic being known at the time t_2, it can be also computed at the time t_3 and this can be continued. Therefore, at each time, the water surface profile and hydrograph of the flow can be drawn (Ponce et al. [12]).

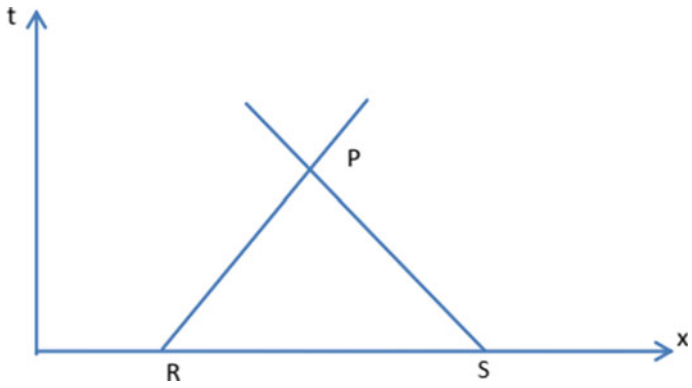

Fig. 4 Characteristics Curve K. Ostad-Ali-Askari [11]

2.3 Muskingum Method Hybridised with Improved Bat Algorithm

Chagas et al. [4] developed a model by hybridising Muskingum method with improved bat algorithm. The Bat Algorithm (BA) is based on the replication and reflection of bat sounds. The bat can distinguish the barrier from food based on the difference in loudness from the surrounding surroundings. Bats create very loud sound pulses and listen for them to return from the things in their environment. Each pulse lasts barely a fraction of a second. The chaos is a strategy for developing various algorithms in which the core concept is based on the exchange of members in the range of (1, 1). The algorithms are modulated using the logic mapping function. Individuals are then added to the chaotic sequence to ensure that it satisfies the chaos variable space. The members are then returned to their original positions using linear transformation. The sole usage of the aforementioned algorithm is to select appropriate coefficient values numerically which are associated with the conventional Muskingum method of flood routing.

2.4 Two-Dimensional Flood Routing by McCormack Scheme

Nyugen et al. [10] developed a model to demonstrate two-dimensional flood routing. In the study, the model simulated flood routing in two dimensions. The model was based on the shallow water equations which were solved using the finite difference method. It employed the explicit McCormack scheme which proved to have a substantial amount of stability in the calculation procedure. The McCormack scheme was modified in this study by accommodating artificial viscosity as an additional parameter through a diffusion factor so as to remove the oscillations which were one of the main concerns of the previous researches. In order to identify the wet and dry cells of the computational domain, a water depth threshold was also implemented. The model could provide maps of the area of inundation, water depths, and depth-averaged water velocities. Finally, the research showed rigorous testing of the model in real-world flood simulation studies by comparing it to analytical solutions and experimental data.

2.5 Flood Routing Using Artificial Intelligence

Greco et al. [6] developed an artificial neural network (ANN) using genetic algorithm (GA) which was combined with conventionally available numerical models to develop the flood hydrograph. The goal of this research was to offer an integrated technique for flood modelling that includes an optimization model and a hydrodynamic numerical model to calculate the upstream hydrograph using the downstream

hydrograph observed along a river. The goal of this research was to offer an integrated technique for flood modelling that included an optimization model and a hydrodynamic numerical model to calculate the upstream hydrograph using the downstream hydrograph observed along a river. The flood routing procedure was broken down into three steps: (1) generating a hypothetical upstream hydrograph using the genetic algorithm method; (2) hydrodynamic modelling using a numerical simulation model for flood routing based on the hypothetical hydrograph generated in the first step; and (3) comparing the calculated and observed hydrograph in the downstream using a fitness function. The reverse flood routing method (RFRM) was called after this proposed approach, which was later used on the Karun River, Iran's greatest river. The great accuracy of the proposed model in the research was demonstrated by a comparison of the final generated upstream hydrograph using the RFRM model with the corresponding measured hydrograph at the upstream boundary.

3 Research Gaps

In this literature review, many literatures were studied for flood routing models. There are many conventional mathematical models available which linearly relates the inflow hydrograph to obtain the output hydrograph. Since the hydro-climatic parameters shoes complex nonlinear relationships, these linear mathematical models can falter for predicting the actual discharge. To overcome the issue of non-linear relationship of the hydro-climatic parameters which is affecting the discharge, hybridised artificial intelligence models can be used. Such a hybridised intelligence model is the Adaptive Neuro-Fuzzy Inference System (ANFIS) which can accurately study the nonlinear and complex relationship between the input and the target parameter with very high accuracy. Fuzzy logic can accurately study the uncertainties in the hydro-climatic parameters which is an essential part of any natural process. Flood routing models using such algorithms are lacking. Hence, attempts can be made to incorporate ANFIS for flood routing studies to enhance the predictive capabilities of the models.

4 Conclusions

This literature is an attempt to study the various methods of computational flood routing by reviewing the various works performed by the researchers over the years. The method of flood routing is broadly classified as wave models and numerical models. From the literature review, it was found that:

- The attenuation of the wave model is very small, and is due to numerical error) when compared to the numerical models. Among the numerical models, the findings were that both the models, i.e., the finite difference method and the characteristic curve method can determine and plot the water surface profile as well as

the flow hydrograph, but finite difference method being the more accurate as finer mesh size can be handled by the finite difference models when compared to the characteristic curve method.

- On further investigation of the finite difference models, the simplified dynamic model yields similar outflow hydrograph characteristics as the classical dynamic model under the same initial and boundary conditions, but it is found that the simplified dynamic model is easier to formulate and is simpler to calculate than the former.
- Hence, to conclude the literature review of the various researchers that this study dealt with, it can be said that the simplified dynamic model is the most accurate computational model which gives realistic results with higher computational stability.
- Also, among the new models, to calculate the Muskingum coefficients, an improved bat algorithm has been introduced which eases the randomness in the conventional bat algorithm.
- It was also seen that various efforts have been put into two-dimensional flood routing which is a complex phenomenon to deal with. McCormack Explicit solution using the finite difference solution has shown the best results as compared to the other methods available for two-dimensional flood routing.
- The gap in the literatures was found to be the lack of use of ANFIS model for flood routing.

References

1. Akan AO, Yen CY (1981) Diffusion-wave flood routing in channel networks. J Hydrol Eng Div ASCE 107 (HY6 June):719–732
2. Barati R, Badfar M, Azizyan G, Akbari GH (2018) Parameter estimation of extended nonlinear muskingum models with the weed optimization algorithm J Irrig Drain Eng:144–150
3. Bharali B, Misra UK (2021) Development of a diffusive wave flood routing model for an ungauged basin: a case study in Kulsi River Basin India. Model Earth Syst Environ 7:1053–1069
4. Chagas P, Souza R (2005) Development of a numerical model, with explicit solution, to study flood wave propagation. Federal University of Ceara, Department Environmental and Hydraulics Engineering
5. Cunge J, Holly FM, Verwey A (1980) Practical aspects of computational river hydraulics. Pitman, London
6. Greco F, Panatoni L (1975) An implicit method to solve Saint-Venant equations. J Hydrol 24(1):171–185
7. Kibler DF, Woolhiser DA (1970) The kinematic cascade as a hydrologic model, Colorado State University, Hydrol Pap, pp 39, 27
8. Lee K, Huang PC (2012) Evaluating the adequateness of kinematic-wave routing for flood forecasting in midstream channel reaches of Taiwan. J Hydroinformatics 14:1075. https://doi.org/10.2166/hydro.2012.093
9. Mujumdar PP (2001) Flood wave propagation the Saint-Venant equations, Department of Civil Engineering, Indian Institute of Science
10. Nguyen QK, Kawano H (1995) Simultaneous solution for flood routing in channel networks. J Hydrol Eng, ASCE 121(10):744–750

11. Ostad-Ali-Askari K, Shayannejad M, Eslamian S, Navabpour B (2018) Comparison of solutions of Saint-Venant equations by characteristics and finite difference methods for unsteady flow analysis in open channel. Int J Hydrol Sci Technol 8(3):229–243
12. Ponce VM, Simons DB, Li R-M (1978) Applicability of kinematic and diffusion models. J Hydrol Eng Div Am Soc Civ Eng 104(12):1663–1667
13. Soleymani M (2012) Comparison of flood routing models (case study: Maroon River, Iran). World Appl Sci J 16(5):769–775

Application of the HEC-RAS Model for the Floodplain Delineation in a Flat Semi-Arid River Basin

Mohamedmaroof P. Shaikh, Sanjaykumar M. Yadav, and Vivek L. Manekar

Abstract Floods in a semi-arid region with flat terrain have been examined in this study. The Rel River is a river that runs through Dhanera town and vanishes in the little desert of Kutch (which is almost flat). There was a lot of rain in July of 2017, and huge damages were noted in the Dhanera town and surrounding areas. The floodwater covers many square kilometres in the Rel River Basin. The current study has been used two-dimensional (2D) hydraulic modelling to simulate the flood of 2017. For this event, the Hydraulic Engineering Centre-River Analysis System (HEC-RAS) model has been utilised to simulate 2D overland flow. The Shuttle Radar Topography Mission (SRTM) digital elevation model (DEM), which has been acquired from the earth explorer, has been utilised for this study. Upstream boundary conditions are based on flow hydrograph of Dhanera highway bridge gauge station, whereas downstream boundary condition is based on normal depth. The HEC-RAS model has been calibrated and validated using field survey data collection. During the flood in the year 2017, the Dhanera town was 75–77% submerged. Due to the villagers' encroachment on the floodplains to conduct farming, the observed flood depths in rural areas were high. Streams and nullahs in urban areas had been blocked, resulting in greater flood depth and a longer flood recession time. To deal with severe flooding scenarios, it is believed that significant mitigating measures are necessary. The findings of this 2D hydraulic model may be used to recommend flood mitigation techniques.

Keywords 2-Dimensional hydraulic modelling · HEC-RAS · RAS mapper · Rel River Basin · SRTM DEM

M. P. Shaikh (✉) · S. M. Yadav · V. L. Manekar
Department of Civil Engineering, Sardar Vallabhbhai National Institute of Technology Surat, Surat 395007, India
e-mail: shaikhmaroof034@gmail.com

P. V. Timbadiya et al. (eds.), *Hydrology and Hydrologic Modelling*,
Lecture Notes in Civil Engineering 312,
https://doi.org/10.1007/978-981-19-9147-9_26

1 Introduction

Worldwide, flooding has become one of the most frequent, recurrent, and widespread hazards. The flood is one of the most destructive natural disasters in the world, affecting both developing and developed countries [1]. Thousands of human lives are lost every year due to floods, which damage and destroy a great deal of property. Flood maps enable communities to learn about flood hazards consistent with the area they live in. By doing so, losses and hazards can be minimised [2]. With one-fifth of the world's flood-related deaths occurring in India, it is one of the most flood-affected countries after Bangladesh. The area of the country that is subject to flooding is approximately 0.4 million km^2 [3]. The main causes of floods in urban areas are extreme precipitation and human intervention [4]. In addition to the acceleration and intensification of the hydrological system, climate change also increases the frequency and magnitude of floods [5].

Hydrodynamic models such as HEC-RAS 2D are widely used in flood analyses. A big advantage of the HEC-RAS tool is that it is open source. In 2D models, the water flow is allowed to move in a longitudinal and transverse direction. The velocity along the longitudinal and transverse directions is simulated, and the vertical velocity is expected to be negligible. 2D models represent the topography as a continuous surface through a finite mesh component. 2D models can solve the lateral interface of the water flow between the main river or channel and the floodplain due to the continuous representation of the terrain. Flow can be simulated in two-dimensions with RAS Mapper by using a continuous surface. The terrain data or mesh resolution in the 2D model have a major influence on the inundation result [6]. Flood maps are a very important tool for analysing urban growth, municipal planning, flood insurance, emergency action plans, and environmental research [7]; however, developing flood maps is a difficult task due to data scarcity [8]. Several studies about 2D hydraulic modelling have been conducted in recent years [9–13].

The objective of this study was to develop a 2D hydraulic model of a data-scarce semi-arid region. The developed models are proposed to calibrate and validate by the collection of field data because no data is available for the basin.

2 Study Area and Data Collection

2.1 Rel River Basin

The Rel River originates near the village of Keshua, Rajasthan (Fig. 1). The area of the catchment of the river is 570 km^2 around. The average annual rainfall of the Rel River Basin is 600 mm. Flooding in this river is due to rainfall as well as lower and undefined banks where overtopping of floodwater takes place and generates sheet flow by joining with an adjacent river. One small irrigation scheme, namely the Jetpura weir, is situated on this river near village Jetpura. The Dhanera gauge

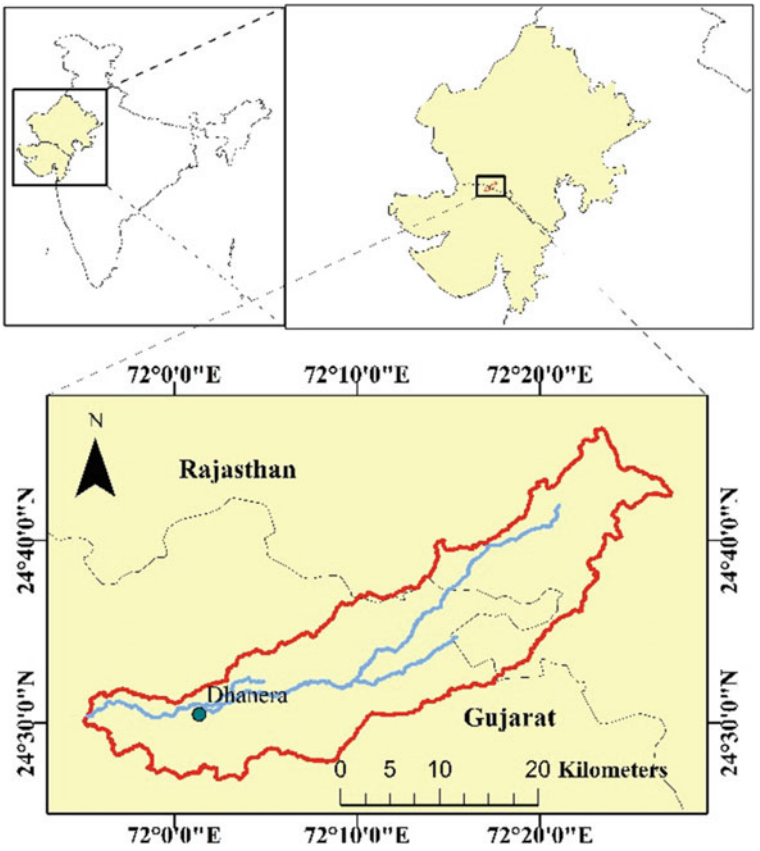

Fig. 1 Index map of study area [15]

discharge station is the sole gauge discharge station across the Rel River. This river is passing through the Dhanera town meeting little run of Kutch [14].

2.2 Data Collection

The discharge data of site Dhanera Stage-Discharge Station has been collected from the river gauging section in Palanpur for the flood event 2017. The SRTM DEM with a resolution of 30 × 30 m^2 has been downloaded from the website earthexplorer.usgs.gov.

3 Methodology

The theory of continuity and momentum is used to derive the governing formula for unsteady open-channel flow in a 2D model. The HEC-RAS is fully resolved using the 2D Saint–Venant formula [10]:

$$\frac{\partial \xi}{\partial t} + \frac{\partial p}{\partial x} + \frac{\partial q}{\partial x} = 0 \tag{1}$$

$$\frac{\partial p}{\partial t} + \frac{\partial}{\partial x}\left(\frac{p^2}{h}\right) + \frac{\partial}{\partial y}\left(\frac{pq}{h}\right) = -\frac{n^2 pg\sqrt{p^2+q^2}}{h^2} - gh\frac{\partial \xi}{\partial x} + pf + \frac{\partial}{\rho \partial x}(h\tau_{xx}) + \frac{\partial}{\rho \partial y}(h\tau_{xy}) \tag{2}$$

$$\frac{\partial q}{\partial t} + \frac{\partial}{\partial y}\left(\frac{q^2}{h}\right) + \frac{\partial}{\partial y}\left(\frac{pq}{h}\right) = -\frac{n^2 qg\sqrt{p^2+q^2}}{h^2} - gh\frac{\partial \xi}{\partial y} + qf + \frac{\partial}{\rho \partial y}(h\tau_{yy}) + \frac{\partial}{\rho \partial y}(h\tau_{xy}) \tag{3}$$

where h = depth of water (m); p = specific flow in the x-direction (m/s); q = specific flow in the y-direction (m/s); ξ = surface elevation (m); g = gravitational acceleration (m/s2); n = Manning roughness; ρ = density of water (kg/m3); and τ_{xx}, τ_{yy}, and τ_{xy} = components of effective shear stress.

The detail methodology used in this study is shown in Fig. 2. The DEM is the main input of 2D hydraulic modelling (Fig. 3). A computation mesh was first developed for the Rel basin. Closed polygon and computing cells were constrained in the downloaded SRTM DEM. The computational mesh can be combined from a minimum of three to a maximum of eight sides of the cells. Thousands of grid cells were generated for the 30 × 30-m^2 DEM of the Rel river basin by computing the point spacing. An implicit finite-volume algorithm was used to solve such equations. A finite-volume solution approximates the average integral to the reference volume, which extends the application of an unstructured mesh [11]. For each cell, the hydraulic property tables were calculated. The relationships between the elevation and volume properties and between the elevation and hydraulic properties were determined for computational cell sides. In the next step, the options of storage area and 2D flow area connection (SA/2D Area Conn) were used to pinpoint the bank and retaining wall inside the 2D flow areas. The Rel River does not include any levees or retaining walls. Thus, the results of the aforementioned step were not considered in this study. A 2D flow area was created, and thousands of cells were generated for the 30 × 30-m^2 DEM grid. Equations (1)–(3) were then solved using the iteration scheme. In the iteration scheme, 20 iterations were generated using 1 h as the initial time step. In the initial condition, the fraction was assumed to increase by 0.5 for the 2D simulation of Mevada to Dhanera. The flow hydrograph of Dhanera highway bridge gauge station was considered as an upstream boundary condition, and the normal

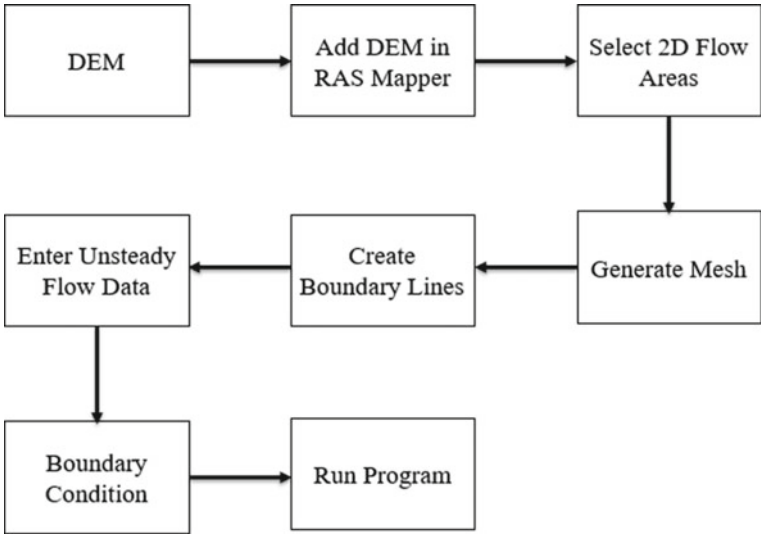

Fig. 2 Methodology

depth was considered as the downstream boundary condition. Boundary conditions permit hydraulic modelling software to start doing calculations; therefore, they're an important element of the process. The flow hydrograph is a graph that shows the relationship between time and discharge. In this case, a flow hydrograph was used to determine the flood extent. The most widely used boundary condition is normal depth. For normal depth, only the river slope is necessary. The HEC-RAS will utilise Manning's formula to calculate depth by using these boundary conditions. The unsteady flow condition was implemented, and the models were simulated. The water surface elevation (WSE), flood inundation depth, and flood velocity were measured for each hour.

4 Results and Discussions

The major flood of July 2017 was simulated for the Rel basin. The period of this flood was from 23 to 30 July 2017 [16]. The WSE, flood inundation (depth), and flood velocity were simulated. The simulated results were validated with the observed flood depth in Dhanera for 2D hydraulic modelling.

The flood of July 2017 was simulated under the 2D unsteady flow condition for Mevada to Dhanera. The depth of water was simulated by deducting the bottom level from the corresponding WSE. The area near the highway bridge and some of the surrounding villages were the initial areas affected by the flood. These areas exhibited a rapid rise in water levels. Dhanera is located 40 km downstream of the Jetpura weir, and the water released from the Jetpura weir requires approximately

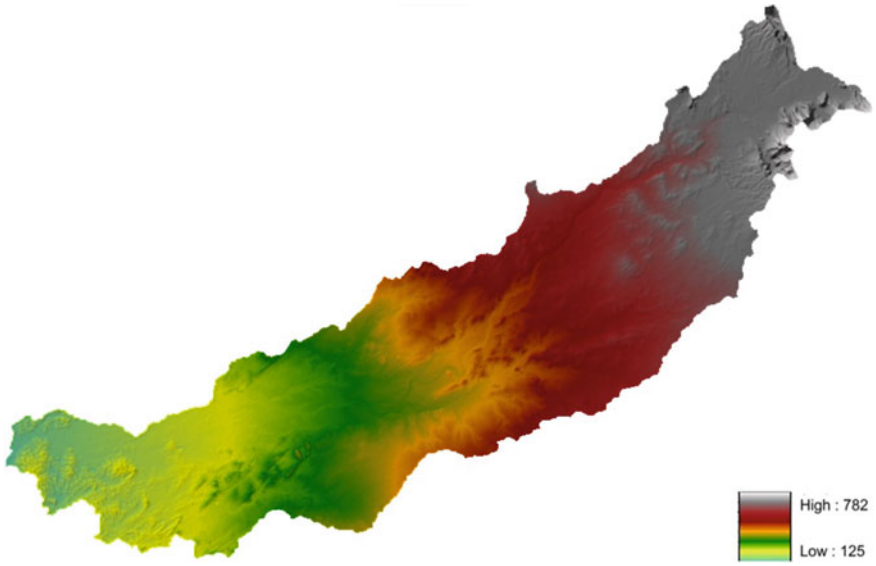

Fig. 3 Digital elevation model of study area

3–4 h to reach Dhanera. An extreme flow of 3355 m^3/s passed over the Jetpura weir. The water flowed with an average velocity of 3.5 m/s in the Rel River and 0.5 m/s in the floodplain to reach Dhanera and flood the town. The flood inundation, WSE, and velocity maps are illustrated in Figs. 4, 5 and 6, respectively.

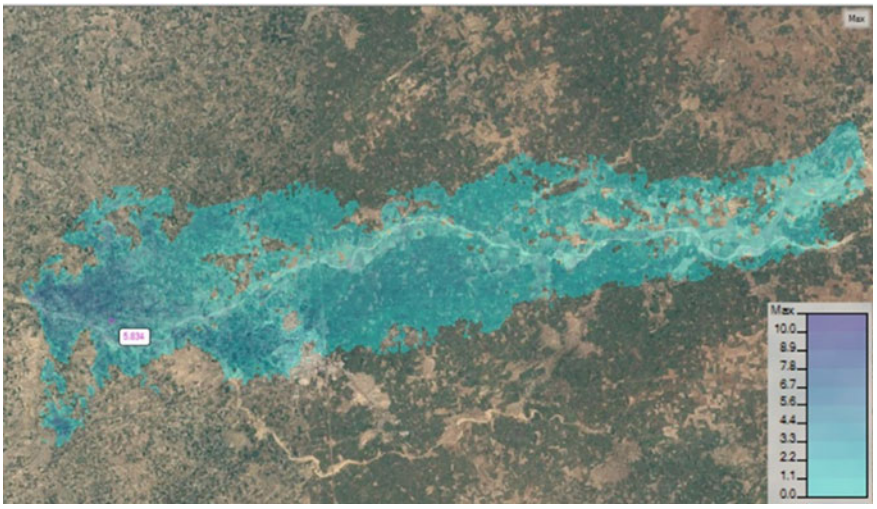

Fig. 4 Inundation depth (m) map

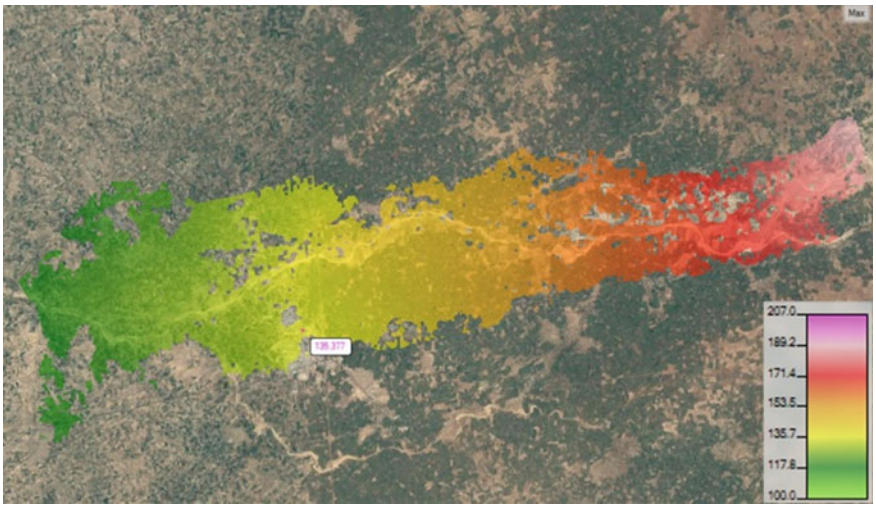

Fig. 5 Water surface elevation (m) map

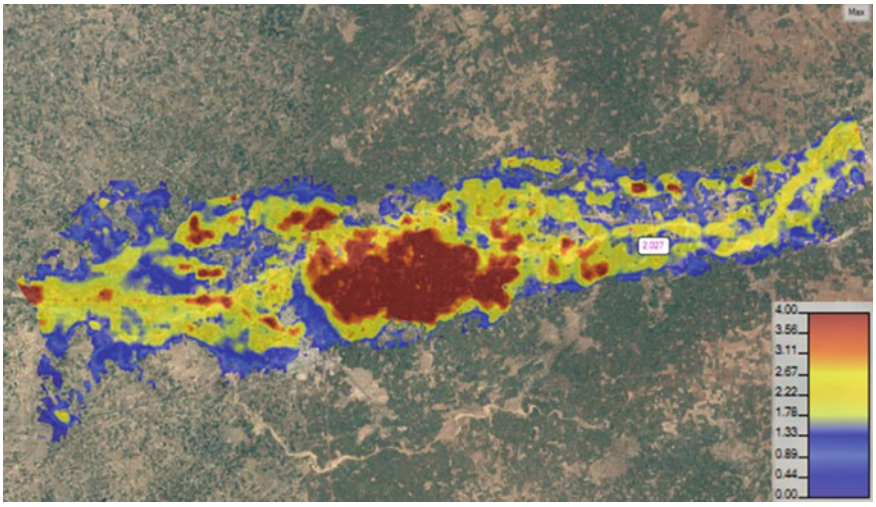

Fig. 6 Velocity (m/s) magnitude map

Good agreement (Correlation Coefficient (R^2) and root mean square error (RMSE)) was observed between the simulated and observed water depths (Fig. 7). The R^2 has been calculated for the model performance. As an alternative, R^2 can be expressed as a squared ratio of covariance to standard deviation multiplied together. Usually, the range is 0–1 for R^2. When a R^2 is zero, it indicates no correlation at all, and when a R^2 is one, it means perfect correlation. The R^2 for this modelling was 0.8361. The RMSE has been also calculated for the model performance. A common

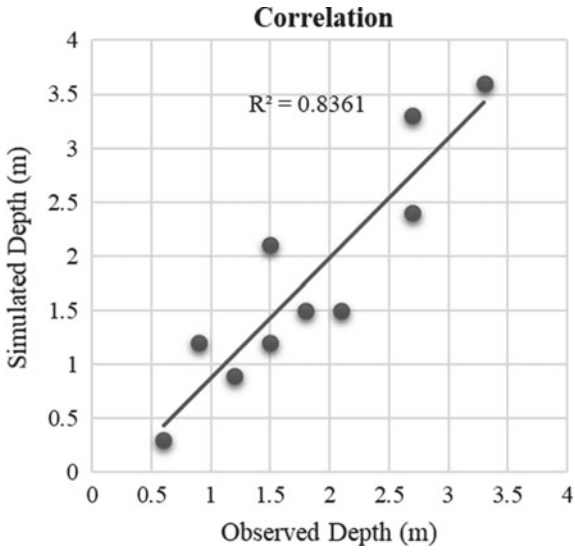

Fig. 7 Correlation between observed and simulated depth

metric used to compare simulated values to observed values is the RMSE. Individual differences are also called residuals, and by using RMSE, they are aggregated to yield a single predictive power measure. We can measure the error level between two sets of data with the RMSE, and ranges from 0 to ∞. Observational values and predicted values are perfectly matched when the RMSE value is zero. The RMSE for this modelling was 0.42 m. The main reason behind this difference between observed and simulated, is low resolution (30 m) of DEM. If high resolution DEM will used for this study, might be these differences could be minimised. The other reason is less number of observed data. Here, only ten values have been surveyed for model calibration and model validation. If more observation will consider for this study, then model can be performed excellent and might be get more better result.

5 Conclusions

The Rel River at Dhanera would have very limited carrying capacity. Due to this, floods occur in many low-lying areas of the river basin when a high discharge occurs. Both the observed and simulated depths are in good agreement with each other. Levees constructed at low-lying cross-sections are essential for increasing the flood capacity of rivers experiencing high-magnitude discharges. 2D modelling indicates that 32 villages on either side of the Rel River can be inundated. Therefore, emphasis must be placed on building levees on either bank of the river. The flood damage was assessed using a synthetic method. This synthetic approach involves using data obtained from real field scenarios and secondary sources. Integrated flood management (economic, technological, and social) was suitable for assessing the

flood damage in this study. The flood area was identified using a GIS and the HEC-RAS. In addition, the total damage caused to the affected people by the 2017 flood in the Rel River was determined. The results of this study can be used to develop plans and policies for rapidly evacuating people during flood and reducing losses due to floods. The analysis method used in this study is novel in the sense that it can be applied to a data-scarce river basin. The developed model accurately provided the breach of the river as well as the depth of floods in a number of villages in the Rel River Basin.

Acknowledgements Authors would like to thank Shri S. J. Makwana (D.E.E., Deesa irrigation department), Shri H. M. Joshi (A.E., Dantiwada dam), Shri Bhavani Singh Rathod (Incharge, River gauging section office, Palanpur), and State Water Data Centre (SWDC) for providing the necessary data required for the study.

References

1. Demir V, Kisi O (2016) Flood hazard mapping by using geographic information system and hydraulic model: Mert River, Samsun, Turkey. Adv Meteorol 2016:1–9
2. Shaikh MP, Yadav SM, Manekar VL (2022) Assessment of the empirical methods for the development of the synthetic unit hydrograph: a case study of a semi-arid river basin. Water Pract Technol 17(1):139–156
3. Patel DP, Dholakia MB (2010) Feasible structural and non-structural measures to minimize effect of flood in lower tapi basin. WSEAS Trans Fluid Mech 5(3):104–121
4. Patel DP, Srivastava PK (2013) Flood hazards mitigation analysis using remote sensing and GIS: correspondence with town planning scheme. Water Resour Manag 27(7):2353–2368
5. Kvočka D, Falconer RA, Bray M (2015) Appropriate model use for predicting elevations and inundation extent for extreme flood events. Nat Hazards 79(3):1791–1808
6. Shaikh MP, Yadav SM, Manekar VL, Samtani BK (2022) Flood modelling for a data-scarce semi-arid region by using a synthetic unit hydrograph and 1D or 2D hydrodynamic model. Int J Hydrol Sci Technol 13(4):373–402
7. Goodell C, Warren C (2006) Flood inundation mapping using HEC-RAS. *Obras y Proy.*, pp 18–23
8. Bajabaa S, Masoud M, Al-Amri N (2014) Flash flood hazard mapping based on quantitative hydrology, geomorphology and GIS techniques (case study of Wadi Al Lith, Saudi Arabia). Arab J Geosci 7(6):2469–2481
9. Gharbi M, Soualmia A, Dartus D, Masbernat L (2016) Comparison of 1D and 2D hydraulic models for floods simulation on the medjerda riverin tunisia. J Mater Environ Sci 7(8):3017–3026
10. Brunner GW, Piper SS, Jensen MR, Chacon B (2015) Combined 1D and 2D Hydraulic Modeling within HEC-RAS. World Environ Water Resour Congr 2015:1432–1443
11. Patel DP, Ramirez JA, Srivastava PK, Bray M, Han D (2017) Assessment of flood inundation mapping of Surat city by coupled 1D/2D hydrodynamic modeling: a case application of the new HEC-RAS 5. Nat Hazards 89(1):93–130
12. Tarekegn TH, Haile AT, Rientjes T, Reggiani P, Alkema D (2010) Assessment of an ASTER-generated DEM for 2D hydrodynamic flood modeling. Int J Appl Earth Obs Geoinf 12(6):457–465
13. Alzahrani AS (2017) Application of two-dimensional hydraulic modeling in riverine systems using HEC-RAS. University of Dayton, Dayton, OH, USA

14. Shaikh MP, Yadav VG, Yadav SM (2018) Simulation of rainfall-runoff event using HEC-HMS model for Rel Sub-Basin, Gujarat, India. J Emerg Technol Innov Res 5(4):402–407
15. Shaikh M, Yadav S, Manekar V (2022) Application of the compound factor for runoff potential in sub-watersheds prioritisation based on quantitative morphometric analysis. J Geol Soc India
16. Shaikh MP, Yadav SM, Manekar VL (2021) Hydraulic modelling of extreme flood event of semi-arid river basin. In: EGU General Assembly 2021, pp EGU21–10218

Assessment of Drought Using Drought Indices and Analysing the Relationship Between Groundwater Levels and Drought Indices: A Case Study of Ahmedabad District

Viraj V. Bhuva, B. R. Andharia, and T. M. V. Suryanarayana

Abstract Drought is a natural and frequently occurring phenomenon in many parts of the country. Drought also affects a lot to the economy, environment, agriculture, industries, and the community. Also, a great part of the country depends a lot on the groundwater for their water requirement, be it agriculture, industrial, or municipal. Groundwater levels change with the number of parameters like rainfall, temperature, streamflow, etc. Very little work has been done on the effect of drought on groundwater fluctuations. Hence, it becomes important to assess the co-relationship between groundwater levels and drought severity. Viramgam and Dhandhuka talukas of Ahmedabad district in Gujarat state are selected for the present study. In the first part, the quantification of the drought using various drought indices, i.e., Standard Precipitation Index (SPI), Reconnaissance Drought Index (RDI) and drought assessment using their respective values is done. The second part deals with analysing the relationship of drought indices with groundwater levels in the Viramgam and Dhandhuka regions. Rainfall and temperature data from 1981 to 2020 were used for the calculation of SPI and RDI using "DrinC" software. In Viramgam, extreme drought was recorded in 1986–87 and 2017–18, according to both SPI and RDI. In Dhandhuka, extreme drought was recorded in 1981–82 and 1986–87 according to SPI, whereas according to RDI in Dhandhuka extreme drought was recorded in 1986–87. In this paper, a total of eight regression models were developed for the relationship between SPI, RDI, and groundwater (GW) levels for Viramgam and Dhandhuka talukas (two models each for SPI and RDI for both talukas). In Viramgam, correlation coefficients were found to be 0.63, 0.6 and 0.65, 0.63, respectively, for SPI and

V. V. Bhuva · B. R. Andharia (✉)
SMC Division, CSIR—Central Salt and Marine Chemicals Research Institute, Bhavnagar, Gujarat 364002, India
e-mail: brandharia@csmcri.res.in

T. M. V. Suryanarayana
Water Resources Engineering and Management Institute, The M. S. University of Baroda, Samiala, Vadodara, Gujarat 391410, India
e-mail: drsurya-wremi@msubaroda.ac.in

P. V. Timbadiya et al. (eds.), *Hydrology and Hydrologic Modelling*,
Lecture Notes in Civil Engineering 312,
https://doi.org/10.1007/978-981-19-9147-9_27

RDI models. In Dhandhuka, correlation coefficients were found to be 0.64, 0.62 and 0.75, 0.73, respectively, for SPI and RDI models.

Keywords Drought · SPI · RDI · GW levels · RMSE

1 Introduction

India is a groundwater economy. India is the leading country in using groundwater globally ahead of the US and China. India uses 260 cubic km per year of groundwater which is around 25% of total groundwater extracted globally. The water from the precipitation infiltrates into the ground because of which groundwater levels ultimately depends upon the amount of precipitation. So, when drought occurs, it can cause depletion of groundwater levels. Drought is a recurring phenomenon that can last for years months or even days. In India, most of the country is prone to the drought of different degrees (around 68%). 35% of the total area in the country which gets precipitation between 750 and 1125 mm is considered drought-prone while 33% which gets precipitation between less than 750 mm is considered chronically drought-prone. To understand the severity of the drought, it becomes important to calculate its severity. Drought is water deficiency compared to demand and drought severity is nothing but reduction of water availability from its normal condition [9, 16]. Indices are used to predict drought severity. Drought indices that are developed to give a succinct overall idea of droughts are mainly derived from hydroclimatic data and are used for making decisions on water resources management and water allocations for mitigating the impact of droughts [14].

Different drought indices have their strengths and weaknesses. Selection of the drought index depends on factors, i.e., available data, region of interest, the purpose of the drought assessment, etc. Researchers have found ut that as RDI uses PET data, it can represent drought more accurately [4, 13]. In most cases, RDI and SPI show similar behaviour but as RDI includes PET, it is very sensitive to climate variability and shows more critical results for "extremely dry" classes [8]. However, it was found that affinity between SPI and RDI decreases from hyper-arid zones to humid zones [2]. Other than this, many researchers have worked on assessing drought severity using different indices [1, 3, 5–7, 11, 12, 15, 17].

In the present study, two indices, namely SPI and RDI were calculated using rainfall and temperature data collected from State Water Data Centre (SWDC), Gandhinagar for Viramgam and Dhandhuka talukas of Ahmedabad district. The collected indices were used for the purpose of assessing drought severity in the area. Later on, the relationship between these calculated indices and the groundwater levels were developed using regression models. About 70% of the data of drought indices and groundwater levels were used for model development, and 30% of data were used for testing of developed regression models. The evaluation of the developed regression models for the Dhandhuka and Viramgam region was carried out using RMSE and correlation coefficient.

2 Study Area and Data Source

2.1 Study Area

Ahmedabad district is chosen considering the low average annual rainfall of 795 mm and because it is the drought-prone area for the study of drought assessment and its relationship with groundwater fluctuations. It is the most populated city in the Gujarat state in India.

Ahmedabad is located at 23.03° N 72.58° E in the western part of India (Fig. 1). It is located 53 m above sea level. Two talukas, namely Viramgam and Dhandhuka were selected for the purpose of this study Ahmedabad is the district that has faced depletion in the groundwater level over the years. Also, it has seen irregularities in rainfall; therefore, it was chosen for the present study.

2.2 Data Collection

This study is classified into two aspects, one is the assessment of drought, and the second is its relationship with groundwater fluctuation. The data of precipitation, temperature (for PET) and groundwater levels were collected for the study. Timespan from 1981–82 to 2019–20 is selected for the calculation of SPI and RDI. SPI requires monthly rainfall data, whereas RDI requires monthly rainfall and potential evapotranspiration data for its calculation.

Rainfall data for the Viramgam and Dhandhuka was collected from State Water Data Centre, Gandhinagar. The temperature data was acquired from the NASA power portal. Central Ground Water Board (CGWB) monitors 15,640 groundwater observation wells in the country (four times a year—January, April/May, August, November), which were used to develop the model with calculated indices.

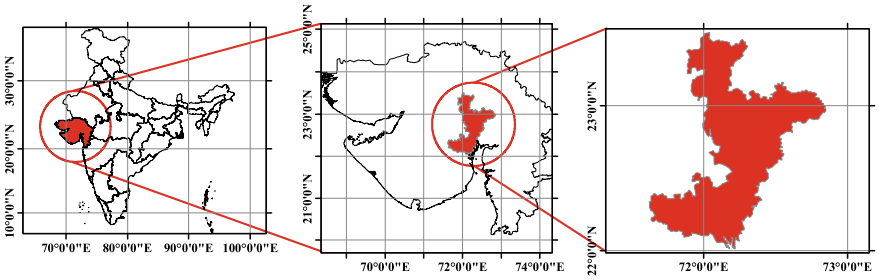

Fig. 1 Geographic location of the present study area of Ahmedabad district

3 Methodology

The principal objective of this study is to assess the severity of drought using drought indices and test the relationship between drought in terms of drought indices and groundwater levels. For this, the steps involved are listed in chronological order in Fig. 2.

3.1 Procedure

Step 1: Calculation of drought indices
The software for the calculation of drought indices, DrinC, was used for the deriving values of SPI and RDI utilising the input data of monthly rainfall and Temperature data (from the years 1981 to 2020) for the Viramgam and Dhndhuka talukas.

Step 2: Assessing the drought severity
From the calculated values of the drought indices, drought severity can be assessed. Different values of the indices suggest different dryness of the season, month and year, from which drought classification has been carried out. Origin 2019 software has been used for plotting the graphs.

Step 3: Development of regression models for the prediction of drought severity by formulating correlation between calculated drought indices and GW levels
The eight regression models have been developed using 70% of data from 1996 to 2012 using calculated SPI and RDI values and GW levels for the Viramgam and Dhandhuka talukas. The relationship has been developed between GW levels and drought indices using nonlinear regression models, i.e., polynomial regression model, truncated fourier series, and rational model.

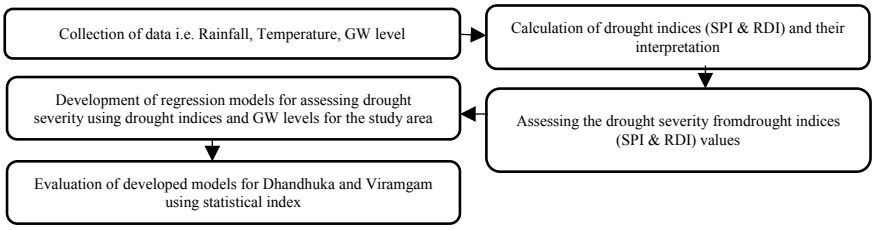

Fig. 2 Methodology applied for the present study

Step 4 Validation of developed regression models for the prediction of drought severity
The developed eight regression models were validated and tested using 30% of data from 2013 to 2020 for calculated SPI, RDI, and GW levels. The performance of the developed models has been assessed using statistical indices for the recommendation for the best-performing model.

Step 5: Evaluation and performance assessment of the developed models
The statistical indices, root mean squared error (RMSE) and correlation coefficient (r) have been calculated and compared during the model development and validation for all eight regression models.

4 Results and Analysis

4.1 Drought Assessment

For classification of the drought in the Viramgam and Dhandhuka talukas of Ahmedabad district from 1981 to 2020 values of the drought indices are used.

1. *Standard Precipitation Index (SPI)*

SPI 12 annual values have been calculated from the DrinC for Viramgam and Dhandhuka talukas of Ahmedabad district for the timespan 1981–82 to 2019–20, as per Figs. 3a and 4a.

The trend observed for the given values of SPI for the Viramgam and Dhandhuka is shown in Figs. 3b and 4b. The trend for the Viramgam shows a slightly downward slope which means the drought situation in the Viramgam has increased over the years. While the trend for Dhandhuka shows an upward slope with reference to increasing years which means the drought severity decreases from the years 1981–82 to 2019–2020.

For the classification of the drought pre-defined classification is used. Drought is classified as mild for the values of SPI between − 0.99 to 0, moderate for values of SPI between − 1.49 and − 1, severe for values of SPI between − 1.99 and − 1.5 and extreme for values of SPI less than − 2 [10].

From the results, it is observed that there were dry periods in both Viramgam and Dhandhuka. Viramgam reported severe drought in the year 2001–02, and extreme drought was reported in the year 1986–87 and 2017–18. Dhandhuka reported severe drought in the year 1984–85 and 2017–18, and extreme droughts were recorded in the year 1981–82 and 1986–87. Full details of all the droughts, i.e., mild, moderate, severe, and extreme as per SPI are as per Table 1,

It is observed from Fig. 5 that when the SPI-12 values suggest drought period, the groundwater levels are lower and vise versa, i.e., in the drought period, the groundwater levels are lowering and vise versa.

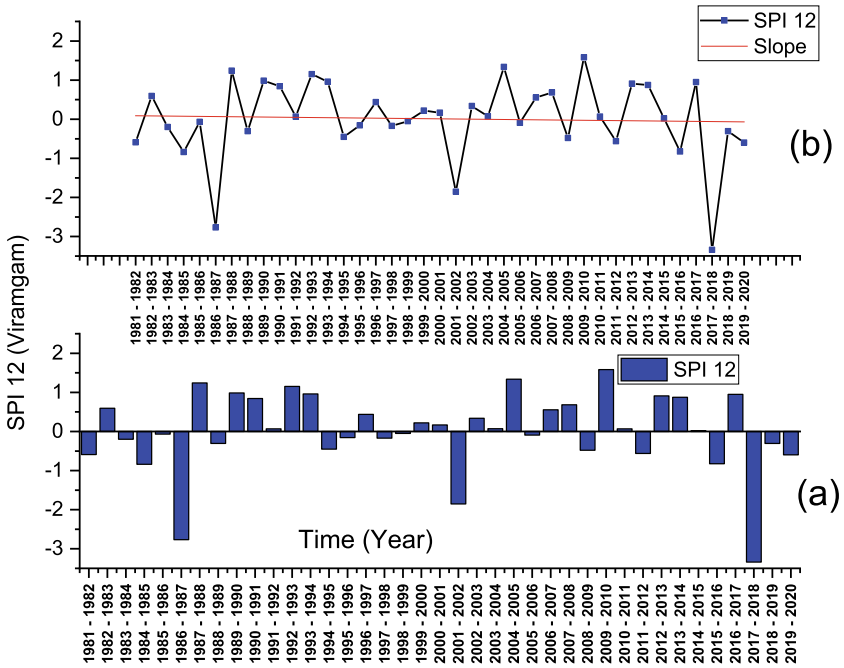

Fig. 3 **a** SPI 12 values and **b** their trend analysis for Viramgam taluka

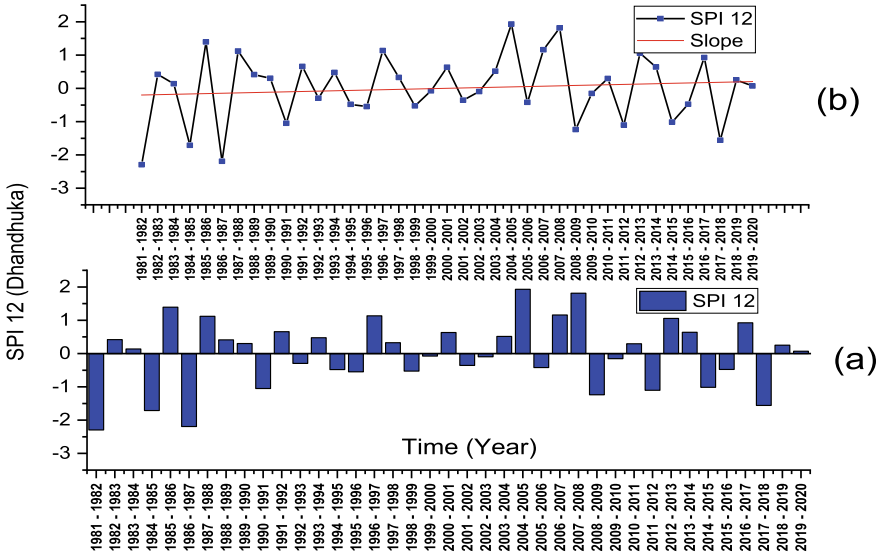

Fig. 4 **a** SPI 12 values and **b** their trend analysis for Dhandhuka taluka

Table 1 Drought categorisation based on SPI for Viramgam and Dhandhuka

Classification	Viramgam	Dhandhuka
Mild	1981–82, 1983–84, 1984–85, 1985–86, 1988–89, 1994–95, 1995–96, 1997–98, 1998–99, 2005–06, 2008–09, 2011–12, 2015–16, 2018–19, 2019–20	1992–93, 1994–95, 1995–96, 1998–99, 1999–00, 2001–02, 2002–03, 2005–06, 2009–10, 2015–16
Moderate		1990–91, 2008–09, 2011–12, 2014–15
Severe	2001–02	1984–85, 2017–18
Extreme	1986–87, 2017–18	1981–82, 1986–87

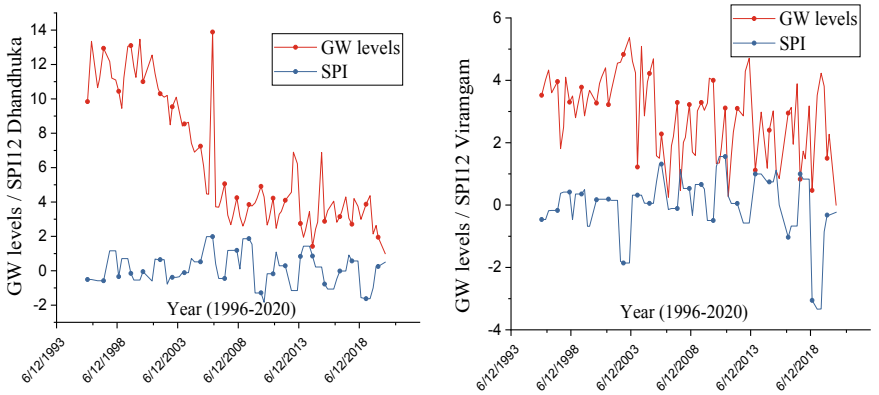

Fig. 5 Comparision of values of SPI-12 and GW levels for Dhandhuka and Viramgam

2. *Reconnaissance Drought Index (RDI)*

RDI 12 annual values have been calculated from the DrinC for Viramgam and Dhandhuka taluka of Ahmedabad district for the period of 1981–82 to 2019–20, as shown in Figs. 6a and 7a.

The trend observed for the given values of RDI for the Viramgam and Dhandhuka can be drawn as Figs. 6b and 7b. The trend for Viramgam shows an almost zero slope which means that the drought situation in the Viramgam has almost remained the same over the years. While the trend for Dhandhuka shows an upward slope (the drought severity decreases from 1981–82 to 2019–20).

For the classification of the drought pre-defined table is used. Drought is classified as mild for the values of RDI between − 0.5 and − 1, moderate for values of RDI between − 1 and − 1.5, severe for values of RDI between − 1.5 and − 2 and extreme for values of SPI less than − 2 [16].

From the results, it is observed that there were dry periods in both Viramgam and Dhandhuka. Viramgam reported severe drought in the year 2001–02, and extreme drought was reported in the year 1986–87 and 2017–18. Dhandhuka reported severe droughts in the year 1981–82, 1984–85, and 2017–18 and extreme drought was

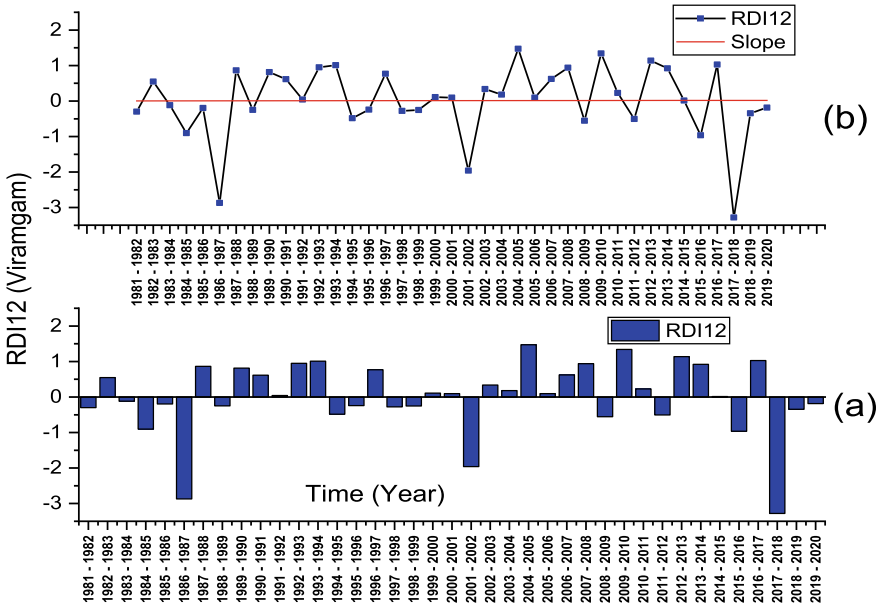

Fig. 6 **a** RDI 12 values and **b** their trend analysis for Viramgam taluka

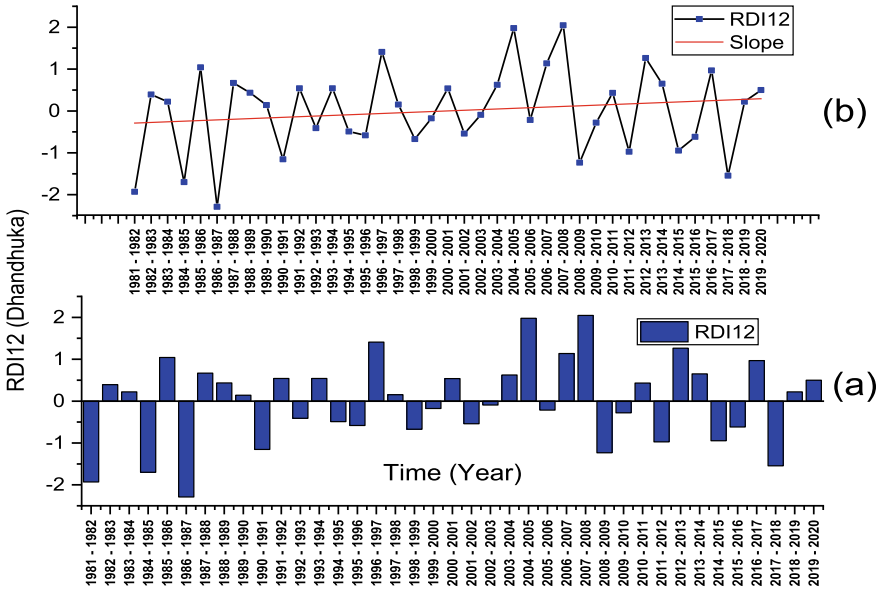

Fig. 7 **a** RDI 12 values and **b** their trend analysis for Dhandhuka taluka

Table 2 Drought categorisation based on RDI

Classification	Viramgam	Dhandhuka
Mild	1984–85, 2008–09, 2011–12, 2015–16	1995–96, 1998–99, 2001–02, 2011–12, 2014–15, 2015–16
Moderate		1990–91, 2008–09
Severe	2001–02	1981–82, 1984–85, 2017–18
Extreme	1986–87, 2017–18	1986–87

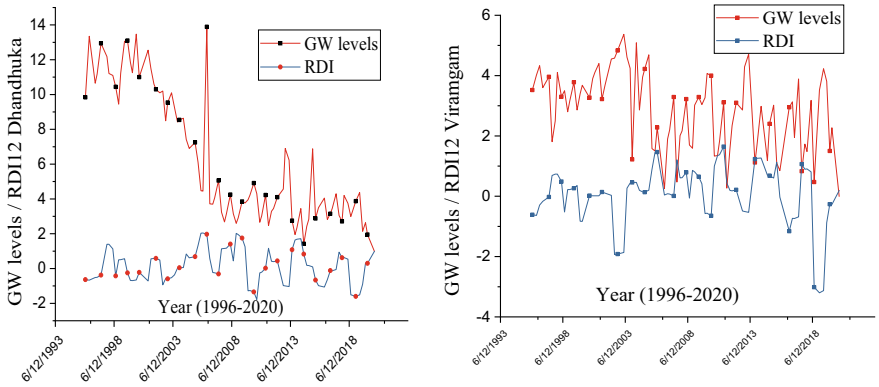

Fig. 8 Comparision of values of RDI-12 and GW levels for Dhandhuka and Viramgam

reported in the year 1986–87. Full details of all the droughts, i.e., mild, moderate, severe, and extreme as per RDI is as per Table 2,

It is observed from Fig. 8 that when the RDI-12 values suggest drought period, the groundwater levels are lower and vise versa, i.e., in the drought period, the groundwater levels are lowering and vise versa.

4.2 Analysing Relationship of Drought Indices and GW Levels

Total eight nonlinear regression models have been developed using calculated values of RDI and SPI values and groundwater levels using 70% of the data from the year 1996 to 2012, and their performance has been evaluated using 30% data from the year 2013 to 2020 for Viramgam and Dhandhuka talukas.

Model 1 and 2 have been developed for calculated values of RDI and SPI of both talukas in the study area using CurveExpert Professional 2.6.5 software. For Viramgam, model 1 is the truncated fourier series, and model 2 is the polynomial regression of degree 4, whereas, for Dhandhuka, model 1 is the polynomial regression of degree 5, and model 2 is the rational model.

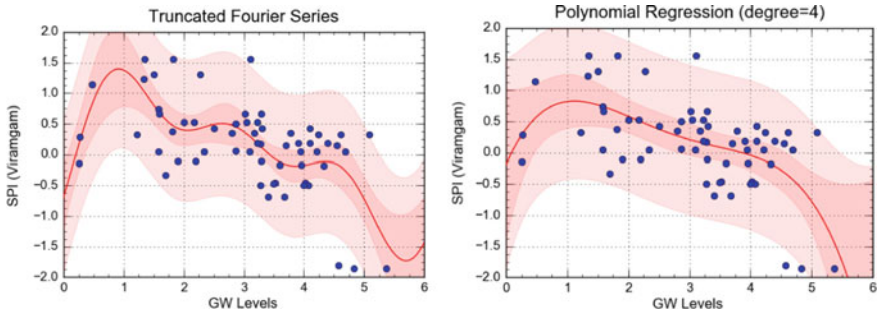

Fig. 9 Model 1 and Model 2 for SPI vs GW levels of Viramgam

1. *SPI versus GW models for Viramgam*

The regression models developed using calculated SPI values and GW levels for Viramgam taluka are shown in Eqs. (1–2) and Fig. 9.

$$\begin{aligned}\text{SPI} = &-0.9429\cos(GW + 1.2155) - 0.6176\cos(2GW + 1.2155) \\ &- 0.412\cos(3GW + 1.2155)\end{aligned} \tag{1}$$

$$\begin{aligned}\text{SPI} = &-0.1833 + 2.2155\,GW - 1.5723\,GW^2 + 0.3999\,GW^3 \\ &- 0.03574\,GW^4\end{aligned} \tag{2}$$

2. *SPI versus GW models for Dhandhuka*

The regression models developed using calculated SPI values and GW levels for Dhandhuka taluka are shown in Eqs. (3–4) and Fig. 10.

$$\begin{aligned}\text{SPI} = &12.7741 - 10.4958\,GW + 3.3802\,GW^2 - 0.4994\,GW^3 \\ &+ 0.03392\,GW^4 - 0.00086\,GW^5\end{aligned} \tag{3}$$

$$\text{SPI} = \frac{0.475 - 0.0573\,GW}{1 - 0.2438\,GW + 0.01699\,GW^2} \tag{4}$$

3. *RDI versus GW models for Viramgam*

The regression models developed using calculated RDI values and GW levels for Viramgam taluka are shown in Eqs. (5–6) and Fig. 11.

$$\begin{aligned}\text{RDI} = &-1.0059\cos(GW + 1.2314) - 0.5928(2GW + 1.2314) \\ &- 0.4117\cos(3GW + 1.2314)\end{aligned} \tag{5}$$

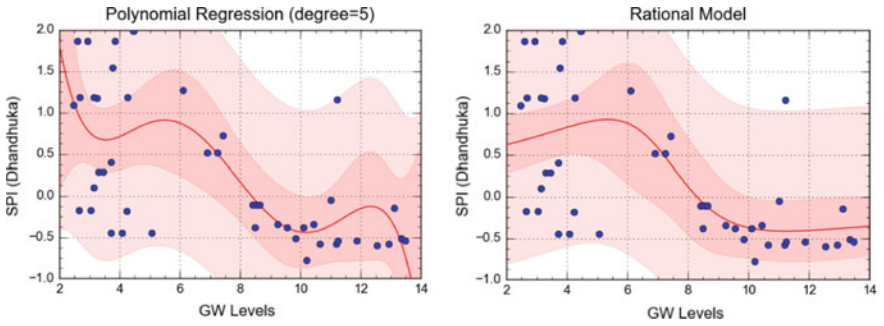

Fig. 10 Model 1 and Model 2 for SPI vs GW levels of Dhandhuka

$$\text{RDI} = -0.02573 + 2.0372\,GW - 1.4145\,GW^2 + 0.3448GW^3 - 0.02986\,GW^4 \tag{6}$$

4. *RDI versus GW models for Dhandhuka*

The regression models developed using calculated RDI values and GW levels for Dhandhuka taluka are shown in Eqs. (7–8) and Fig. 12.

$$\text{RDI} = 14.046 - 11.494\,GW + 3.6589\,GW^2 - 0.5311\,GW^3 + 0.03528\,GW^4 - 0.00087\,GW^5 \tag{7}$$

$$\text{RDI} = \frac{0.5248 - 0.06267\,GW}{1 - 0.2318\,GW + 0.01503\,GW^2} \tag{8}$$

The performance of the developed eight regression models have been assessed using statistical indices, i.e., root mean squared error (RMSE) and coefficient of correlation (r) (refer Table 3). RMSE has been calculated for both development

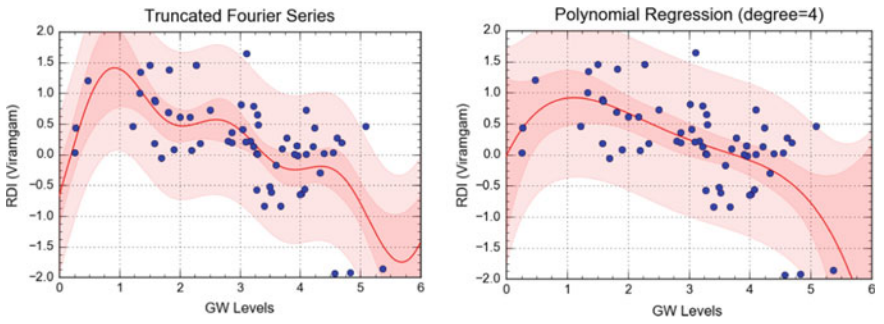

Fig. 11 Model 1 and 2 for RDI versus GW levels for Viramgam

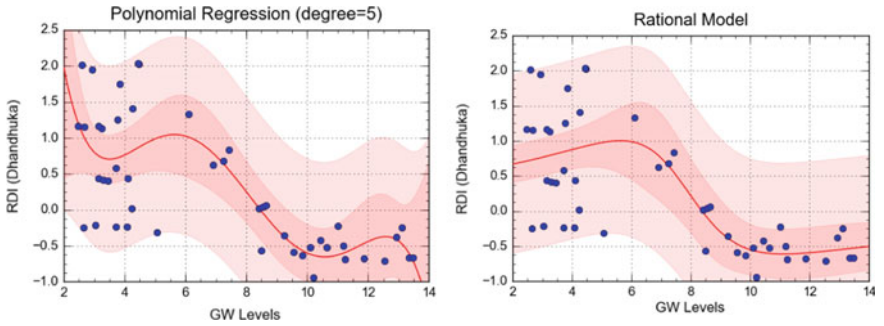

Fig. 12 Model 1 and 2 for RDI versus GW levels for Dhandhuka

Table 3 Performance of developed models using statistical indices

Statistical index	Viramgam		Dhandhuka		Viramgam		Dhandhuka	
	SPI				RDI			
	Model 1	Model 2	Model 1	Model 2	Model 1	Model 2	Model 1	Model 2
r	0.63	0.60	0.65	0.63	0.64	0.62	0.75	0.73
$RMSE_d$	0.54	0.56	0.65	0.66	0.57	0.58	0.82	0.59
$RMSE_v$	0.72	0.67	1.06	0.66	0.77	0.71	1.22	0.81
Diff	0.17	0.11	0.41	0.002	0.20	0.13	0.40	0.22

($RMSE_d$) and validation ($RMSE_v$) of the models, and the difference between both of them have been shown in Table 3. RMSE and r can be calculated using Eq. (9) and (10), respectively.

$$\text{RMSE} = \frac{\sum_{i=1}^{N} (C_i - A_i)^2}{N} \tag{9}$$

where $(C_i - A_i)^2$ = Squared difference between the calculated and actual value

N = Size of data set

$$r = \frac{\sum[(x_i - \overline{x})(y_i - \overline{y})]}{\sqrt{\sum(x_i - \overline{x})^2 * \sum(y_i - \overline{y})^2}} \tag{10}$$

where

x_i values of x variables
y values of y variables
$\overline{x}$ mean of values of x variables
$\overline{y}$ mean of values of y variables.

Figures 13, 14, 15 and 16 shows accuracy of various developed models.

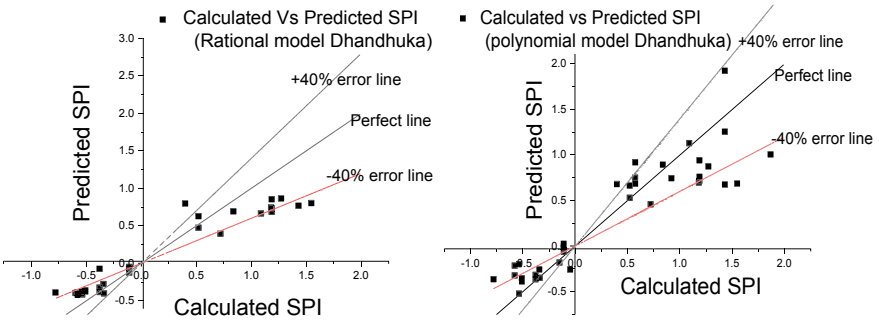

Fig. 13 Calculated versus predicted SPI for rational model and Polynomial model in Dhandhuka

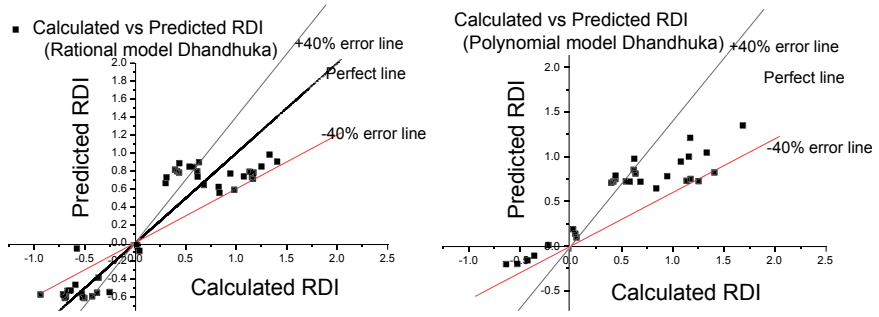

Fig. 14 Calculated versus predicted RDI for rational model and polynomial model in Dhandhuka

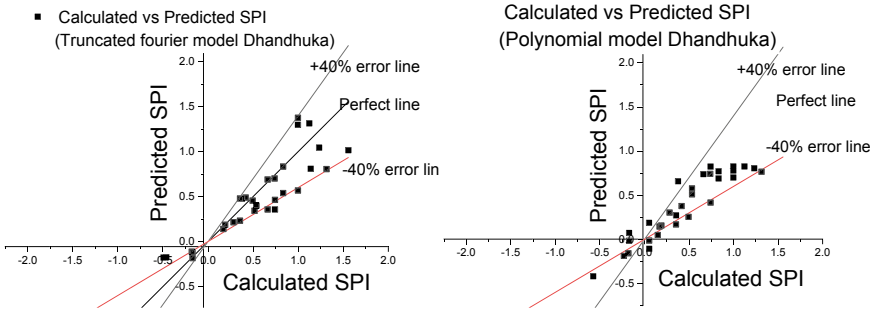

Fig. 15 Calculated versus predicted SPI for truncated fourier and polynomial model in Dhandhuka

5 Conclusions

(a) The drought indices SPI and RDI have been calculated using monthly rainfall and temperature data of Viramgam and Dhandhuka talukas of Ahmedabad district.

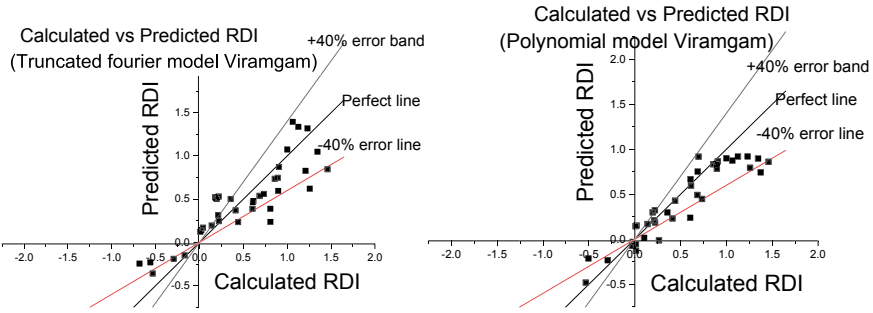

Fig. 16 Calculated versus predicted RDI for truncated fourier and polynomial model in Viramgam

(b) The classification of the drought severity from mild to extreme was derived for the specific region of the Viramgam and Dhandhuka talukas.
(c) As RDI incorporates temperature data along with rainfall data, it gives better prediction of drought severity as compared to SPI.
(d) From the results, it can be concluded that when the values of drought indices indicate dry periods, the values of groundwater levels decrease, which shows the close relationship between drought indices and groundwater levels.
(e) The eight nonlinear regression models have been developed to assess the drought severity using drought indices (SPI and RDI) and groundwater fluctuations for the Viramgam and Dhundhuka talukas of Ahmedabad district. The RMSE and r values for the developed models show the satisfactory performance of the developed models.
(f) Polynomial regression models of degree four and degree five have been found to be the best fitting curve for the prediction of drought severity for the Viramgam and Dhandhuka, respectively.
(g) It has been concluded from the analysis of the results of drought indices that there is a close interdependency and co-relation between drought occurrence and groundwater fluctuations for the Ahemdabad district.

Acknowledgements The authors are thankful to State Water Data Centre (SWDC), Gujarat, Central Ground Water Board (CGWB) and freely available data website from NASA, the USA for providing the necessary data to conduct the present study. This work is carried out under the funding of the CSIR-FTT project no. MLP0050.

References

1. Ahmad L, Parvaze S, Majid M, Kanth RH (2016) Analysis of historical rainfall data for drought investigation using standard precipitation index (SPI) under temperate conditions of Srinagar Kashmir. Pakistan J Meteorol 13(25):29–38

2. Asadi Zarch MA, Sivakumar B, Sharma A (2014) Droughts in a warming climate: a global assessment of standardized precipitation index (SPI) and Reconnaissance drought index (RDI). J Hydrol 526:183–195
3. Ganapati H (2018) Assessment of drought severity using standard precipitation index in Ahmednagar District, India. Int Res J Eng Technol 5(5):1777–1780
4. Haied N, Foufou A, Chaab S, Azlaoui M, Khadri S, Benzahia K, Benzahia I (2017) Drought assessment and monitoring using meteorological indices in a semi-arid region. Energy Procedia 119:518–529
5. Jacobi J, Perrone D, Duncan LL, Hornberger G (2013) A tool for calculating the Palmer drought indices. Water Resour Res 49(9):6086–6089
6. Jain VK, Pandey RP, Jain MK, Byun H (2015) Comparison of drought indices for appraisal of drought characteristics in the Ken River Basin. Weather Clim Extremes 8:1–11
7. Khade M, Morgenschweis G, Schlenkhoff A (2009) Analysis of meteorological drought in the Ruhr basin by using the standardized precipitation index. Int J Environ Ecol Eng 3(9):291–300
8. Khalili D, Farnoud T, Jamshidi H, Kamgar-Haghighi AA, Zand-Parsa S (2011) Comparability analyses of the SPI and RDI meteorological drought indices in different climatic zones. Water Resour Manage 25:1737–1757
9. Leelaruban N, Padmanabhan G, Odour P (2017) Examining the relationship between drought indices and groundwater levels. Water 9(82):1–16
10. McKee TB, Doesken NJ, Kleist J (1993) The relationship of drought frequency and duration of time scales. In: Proceedings of 8th conference on applied climatology, American Meteorological society, Anaheim, 17–23 Jan, 1993
11. Mahmoudi P, Rigi A, Miri Kamak M (2019) A comparative study of precipitation-based drought indices with the aim of selecting the best index for drought monitoring in Iran. Theoret Appl Climatol 137:3123–3138
12. Morid S, Smakhtin V, Moghaddasi M (2005) Comparison of seven meteorological indices for drought monitoring in Iran. Int J Climatol 26(7):971–985
13. Malakiya AD, Suryanarayana TMV (2016) Assessment of drought using standardised precipitation index (SPI) and reconnaissance drought index (RDI): a case study of Amreli District. Int J Sci Res 5(8):1995–2002
14. Ntale HK, Gan TY (2003) Drought indices and their application to East Africa. Int J Climatol 23(11):1335–1357
15. Szalai S, Szinell C (2000) Comparison of two drought indices for drought monitoring in Hungary—a case study. Drought and Drought Mitig Europe 14:161–166
16. Tsakiris G, Vangelis H (2005) Establishing a drought index incorporating evapotranspiration. European Water 9(10):3–11
17. Uddin MJ, Hu J, Islam ARMT, Eibek KU, Nasrin ZM (2020) A comprehensive statistical assessment of drought indices to monitor drought status in Bangladesh. Arab J Geosci 13(323):1–10

Meteorological Drought Analysis of Sabarmati Basin, India

Jakka Sai Priya, Madhu Priya Aedla, Theertha Ravi, P. L. Patel, and Alka Sharma

Abstract Drought intensity and severity are significant in agriculture, especially in predicting irrigation needs. In the present study, the meteorological drought is analyzed district-wise by using the Standardized Precipitation Index (SPI) at various time scales for the semi-arid Sabarmati basin, India. Daily gridded precipitation information of spatial resolution 0.25° × 0.25° is collected from the Indian Meteorological Department (IMD), Pune. Monthly rainfall values of 14 districts of the basin for the years 1980–2019 are used to compute SPI-6 (June-Nov) and SPI-12 (June-May) using Drought Indices Calculator (DrinC) software for the analysis of meteorological drought. SPI values are classified as dry or wet, according to McKee et al. (Proceedings of the 8th Conference on Applied Climatology, pp. 179–183, 1993) classification. The observed drought years are 1983–84, 1985–86, 1986–87, 1987–88, 2000–01, 2002–03, and 2009–10. According to SPI results, the severely dry and extreme dry periods are reported in 1983–84, 1986–87, and 1987–88. The drought severity and drought intensity are extreme for most of the districts during the drought years 1987–1988 for SPI-6 and SPI-12. Such research would be useful for water resource management in the semi-arid river basins.

Keywords Meteorological drought · Standardized precipitation index (SPI) · Sabarmati basin · Drought indices calculator (DrinC)

J. S. Priya (✉) · M. P. Aedla (✉) · T. Ravi · P. L. Patel · A. Sharma
Department of Civil Engineering, Sardar Vallabhbhai National Institute of Technology Surat, Surat 395007, India
e-mail: saipriya32542@gmail.com

M. P. Aedla
e-mail: priyamadhu460@gmail.com

T. Ravi
e-mail: theertha.ravi@gmail.com

P. L. Patel
e-mail: premlalpatel1966@ced.svnit.ac.in

P. V. Timbadiya et al. (eds.), *Hydrology and Hydrologic Modelling*,
Lecture Notes in Civil Engineering 312,
https://doi.org/10.1007/978-981-19-9147-9_28

1 Introduction

Drought is a natural catastrophic with significant economic and human consequences [2–4]. Extreme heat, strong winds, minimum relative humidity, rainfall frequency, climate change, and population expansion are all factors that contribute to drought. Droughts are common in several places of the world [5]. Droughts affect an estimated 55 million people worldwide each year, and it pose a threat to animals and crops in almost every country. According to World Health Organization, drought might force 700 million people to flee their homes by 2030, affecting 40% of the world's population. Droughts have an influence on both surface and groundwater resources, resulting in minimizing water availability, degraded quality of the water, crop deterioration, low production, limited power generation, disturbed ecosystems, and plenty of other socio-economic impacts [6].

Based on the American Meteorological Society, drought is classified into four classifications: meteorological, agricultural, hydrological, and socio-economic [7]. The Indian Meteorological Department (IMD) defined meteorological drought as when seasonal rainfall falls below 75% of its long-term mean value over a given area. It also stated that if the rainfall deficit is between 26 and 50%, the drought is classified as 'moderate', and if the deficit exceeds 50%, the drought is classified as 'severe'.

The drought characteristics include severity, intensity and duration which can be determined using drought indices. The mathematical formula for calculating the amount of water irregularity in a hydrometeorological variable is a drought index [5]. Among the meteorological indices, the Standardized Precipitation Index (SPI) is the most often used which was developed by McKee et al. [1] to assess the inadequacy of rainfall over various intervals of time. Both short-term droughts, like the agricultural drought, and long-term droughts, like the hydrological drought, are examined using SPI [8].

Livada and Assimakopoulos [9] applied SPI to identify the drought periods in Greece, based on drought intensity and duration and found that on 3, 6 and 12 month time scale, the frequency of mild, moderate, and severe droughts was observed, respectively. For the drought assessment, 35 years of rainfall data of Amreli station was used to compute SPI in DrinC software, and concluded that Amreli had a mild drought situation, but its duration and intensity were above average [10]. Over the Krishna basin in Maharashtra, Mahajan and Dodamani [11], employed SPI to detect the spatio-temporal evaluation of drought events at several time steps and the analysis led to the preparation of layouts of drought to identify the drought severity across the basin. For 3, 6 and 9 month time series SPI was calculated using DrinC software for Madurai district, Tamil Nadu, and found that 20 years out of 100 years were drought affected and periodic in nature and happened for nearly every 3−7 years [12]. Daily precipitation data (1971–2011) for 14 districts were used to calculate the SPI in the Gomti basin, Uttar Pradesh, India at the spatial and temporal scales and the results revealed that severe drought was in upper regions during (1971–2000) and frequency of drought was maximum in central and lower parts of the basin during

(2001–2011) [13]. From past studies, it is clear that SPI is a powerful and flexible index for analyzing the meteorological drought.

The Sabarmati River basin is one of the foremost seriously water stressed river basins in India, because the need for water has steadily increased as a result of the population rise, agricultural, energy, and industrial sectors expansion, and in part due to climate impacts and tainting of water sources [14]. Therefore, it is important to understand the drought and its characteristics for better water resource planning and management. The key objectives of the present study are (i) Analyzing the meteorological drought, district wise by employing Standardized Precipitation Index (SPI) at 6-month and 12-month scale of time over a period of 1980–2019 for Sabarmati basin and (ii) Characterizing drought severity, duration, and intensity at spatial–temporal scales across the basin.

2 Study Area and Data Source

2.1 Sabarmati River Basin

Sabarmati River Basin is one among the 20 significant river basins in India. It is an inter-state river basin. Sabarmati stream originates within the Aravalli hills in Mount Abu area, and flows in a southwesterly direction. Sabarmati basin stretches between 70.97° to 73.85° east longitudes and 22.25° to 24.78° north latitudes. Sabarmati basin is situated in the semi-arid zone of western part of India that extends over states of Gujarat and Rajasthan. In the Rajasthan part, the basin covers Dungarpur, Sirohi, and Udaipur districts and in the part of Gujarat, the basin covers Sabarkantha, Banaskantha, Mahesana, Surendranagar, Gandhinagar, Ahmedabad, Kheda, Bhavnagar, Rajkot, Anand, and Panchmahal.

The catchment area of the Sabarmati basin is 31,674 km^2. Sabarmati basin receives a high to moderate rainfall with mean annual rainfall of 787.5 mm. The basin is divided into three sub-basins: Dharoi, Hathmati, and Watrak. The average annual rainfall for the Watrak, Dharoi, and Hathmati sub-basins was 794 mm, 729 mm, and 692 mm, respectively. Vital part of the Sabarmati basin is balanced with agricultural land with an area of 16,186.38 km^2 (74.68% of total area). Forest cover in the basin is 2595.69 km^2 (11.98% of total area). Wasteland covers an area of 1549.13 km^2 (7.15% of total area). There are 50 Dams in the Sabarmati basin among which 17 dams fall in Sabarmati lower sub-basin and 33 dams, 10 weirs, 2 barrages fall in the Sabarmati upper sub-basin. Around 91.67% dams are used for the purpose of irrigation. The longest dam in the basin is Sabarmati (Dharoi) dam located in Gujarat with a total length of 1207 m and 908.6 MCM total capacity. The index map of the Sabarmati basin is depicted in Fig. 1.

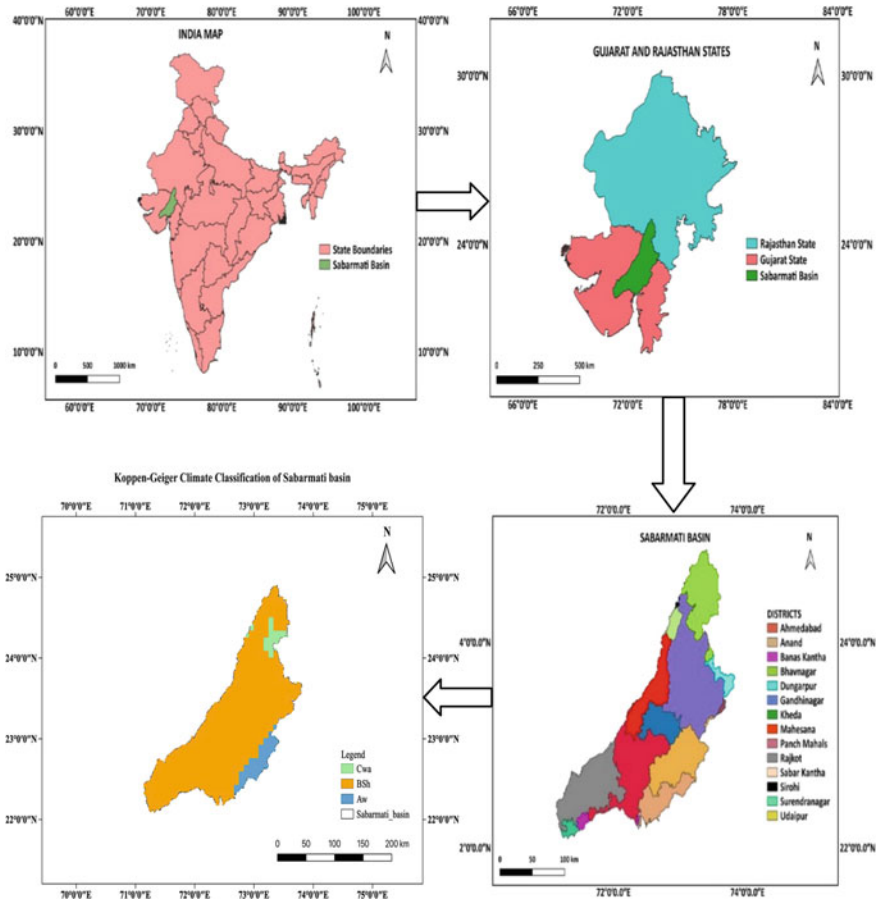

Fig. 1 Index map of study area and Köppen–Geiger climate classification of Sabarmati basin

2.2 Köppen–Geiger Climate Classification

The Köppen–Geiger climate classification system, which was classified using monthly averages of mean temperature and precipitation from 1951–1980 and 1981–2010, is the most extensively used climatic classification system. The Köppen climate classification separates the world's climate into five major categories. A: tropical climate, B: dry climate, C: temperate climate, D: continental climate, and E: polar climate are indicated by the first letter of the KG classification. For a total of 30 classes, the system was divided into five subclasses and identified with a second and third letter. The second letter denotes the type of seasonal precipitation, while the third denotes the degree of heat. Summers are defined as the six months between April and September and/or October and March that are warmer, while winters are defined as the six months between October and March that are cooler. This classification

is useful for describing climatic conditions that are determined by temperature and precipitation. This classification system has been widely used to map the worldwide distribution of long-term climate and ecosystem conditions [15].

In this study, Sabarmati basin climate falls in 3 classes of KG climate classification. Major part of the basin has Hot Semi-Arid Climate (B_{sh}), and other part of the basin has Tropical Wet Climate (A_w) and Monsoon influenced Humid Subtropical Climate (C_{wa}) (Fig. 1).

2.3 Data Source

The 0.25° × 0.25° daily gridded data of precipitation was collected from India Meteorological Department (IMD), Pune and used to develop monthly rainfall data for 14 districts of Sabarmati basin during the period of 1980–2019 for SPI calculation in analyzing drought conditions in Sabarmati basin.

3 Methodology

3.1 DrinC

Drought Indices Calculator (DrinC) is a user-friendly software system for calculating a variety of drought indices. The broadest potential applicability for various forms of drought (meteorological, hydrological, and agricultural) is the key objective in its design. This software requires relatively little data, and their results are simple to understand and can be used in planning and operational implementations. Hence, it can be used to carry out the drought studies even in the arid and semi-arid areas, where information is often scarce [16]. In this research, DrinC software is utilized to find the SPI for semi-arid, Sabarmati Basin.

3.2 Standardized Precipitation Index (SPI)

Generally, SPI can be computed from the following equations:

$$\mathrm{SPI} = \begin{Bmatrix} -\left(t - \frac{C_O + C_1 t + C_2 t^2}{1 + d_1 t + d_2 t^2 + d_3 t^3}\right) & \text{if } 0 < p \leq 0.5 \\ +\left(t - \frac{C_O + C_1 t + C_2 t^2}{1 + d_1 t + d_2 t^2 + d_3 t^3}\right) & \text{if } 0.5 < p \leq 0 \end{Bmatrix} \quad (1)$$

$$t = \left\{ \sqrt{ln \frac{1}{H(x)^2}} \right\} \quad (2)$$

$$G(x) = \frac{1}{\beta^{\gamma}\Gamma(\gamma)_0}\int_0^x x^{\gamma-1}\mathrm{e}^{-x/\beta}\mathrm{d}x \tag{3}$$

$$x > 0,\ \Gamma(\gamma) = \int_0^{\infty} x^{\gamma-1}\mathrm{e}^{-x}\mathrm{d}x \tag{4}$$

where x denotes rainfall values, β and γ are the scale and shape parameters of the Γ function, respectively. $C_0 = 2.515517$, $C_1 = 0.802853$, $C_2 = 0.010328$, $d_1 = 1.432788$, $d_2 = 0.189269$, and $d_3 = 0.001308$. $G(x)$ is the cumulative probability of precipitation distribution. $S = 1$ when $G(x) > 0.5$, $H(x) = 1-G(x)$ and $S = -1$ when $G(x) \leq 0.5$, $H(x) = G(x)$. According to McKee et al. [1] drought starts when the SPI value approaches -1 or less and ends when it becomes positive.

In the present study, DrinC software was used to find the SPI. The daily gridded rainfall data of $0.25° \times 0.25°$ of Sabarmati basin obtained from IMD, Pune is converted to monthly district-wise rainfall data of 1980–2019 using thiessen weights and used as input in DrinC software. SPI has been calculated for each district during the period 1980–2019 for 6-month and 12-month time scales in DrinC software and classified as dry or wet according to McKee et al. [1] classification (Fig. 2).

The drought analysis can be performed using spatial and temporal analysis. Spatio-temporal analysis is the integration of the series of time events into aggregated drought regions, and computation of the percentage of area of drought in every timestep [17]. SPI has positive and negative values, whereas the positive values indicate wetness and the negative values indicates dry events [18]. Maps showing drought severity are produced to analyze the severity of the drought for various drought years spatially using QGIS software. The number of months during which SPI remains under the threshold value is the drought duration (D). In this study, the threshold value was taken as -1.00 [17]. The duration of the drought event lasts till the SPI value will be positive. The ratio of drought severity to drought duration is known as drought intensity.

4 Results and Discussion

4.1 Temporal Analysis of Drought

For the Sabarmati basin, the drought severity values were determined using DrinC software for 6 and 12-month temporal scales for each and every individual year with respect to the classification recommended by Mc Kee et al. [1]. The drought severity values of SPI-6 and SPI-12 were plotted against the time series graph. A dry year happens if SPI value ≤ -1.00. The periods whose drought severity values below

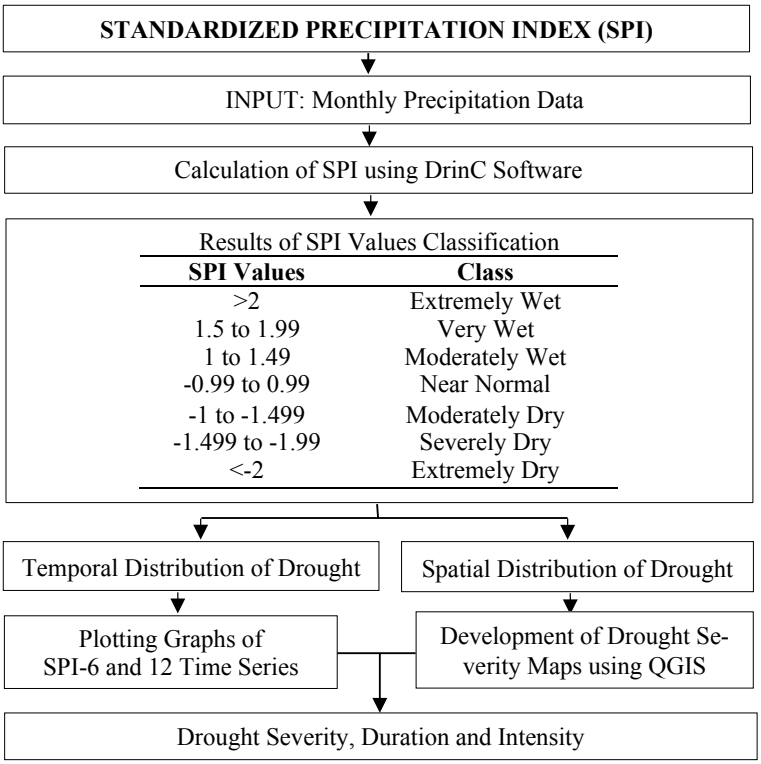

Fig. 2 Flowchart of methodology

threshold value of −1.00 for SPI-6 and SPI-12 time series (Figs. 3, 4 and 5) are classified into three classes of drought periods as, moderately dry year, severely dry year and extremely dry year.

From Fig. 3, 1987–1988 is an extremely dry year with a drought severity value of −2.281, 1986–87 is the severely dry year with a drought severity value of −1.541, and 2002–03 is observed as a moderately dry year with a drought severity value of −1.369 using SPI-6 (June-Nov).

From the Fig. 4, 1983–84 is the severely dry year with a drought severity value of −1.564 and 2001–02 is observed as moderately dry year with a drought severity value of −1.093 using SPI-6 (Dec-May).

For SPI-12 (June-May) (Fig. 5), it can be inferred that 2002–03, 2009–10, and 1985–86 are observed as moderately dry years with a drought severity value of −1.369, −1.008, −1.001, respectively, whereas 1986–87 is the severely dry year with a drought severity value of −1.672 and 1987–1988 is an extremely dry year with a drought severity value of −2.202.

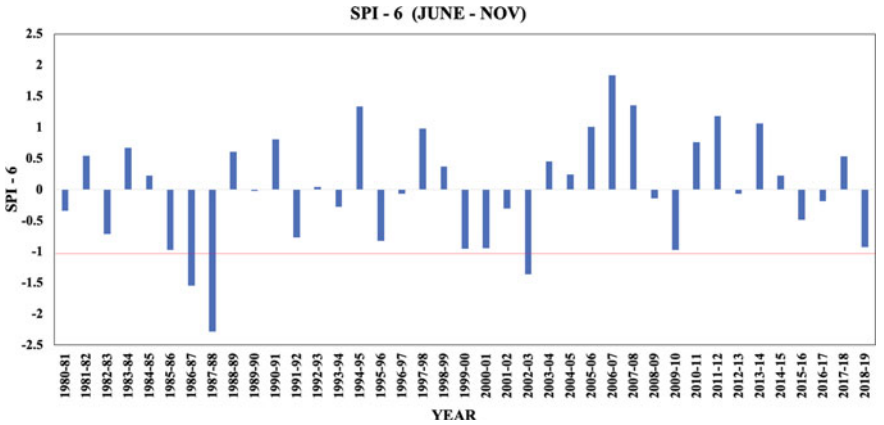

Fig. 3 Drought severity for the years 1980–2019 using SPI-6 (June–Nov)

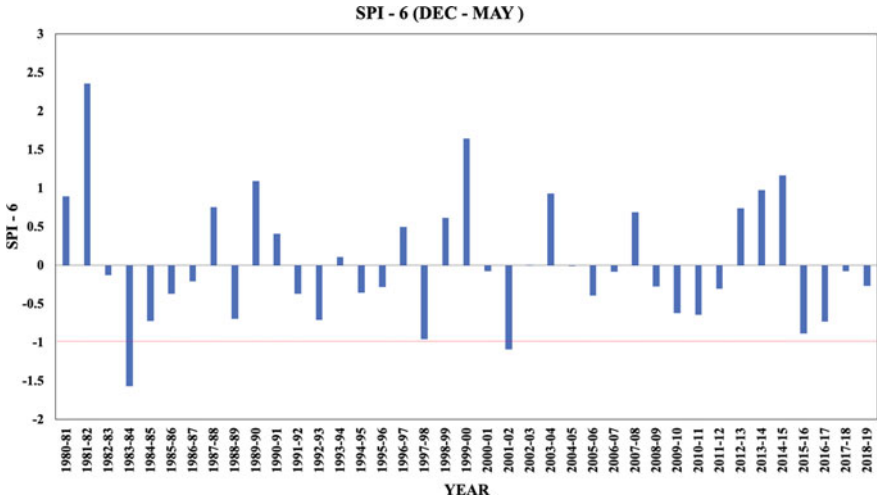

Fig. 4 Drought severity for the years 1980–2019 using SPI-6 (Dec–May)

4.2 Spatial Analysis of Drought

The maps of drought severity representing the spatial variation of drought for the whole Sabarmati basin are prepared using QGIS for the drought years obtained from 12 and 6-month SPI values during the interval 1980–2019 as shown in the Fig. 6.

From Fig. 6, it was observed that all the districts except Anand, Bhavnagar, Dungarpur, Panch Mahal and Rajkot experienced extremely dry situation during 1987–88 period with respect to 6-month SPI (June-Nov). Whereas, all the districts except Anand, Dungarpur, Panch Mahal, Rajkot, and Sabar Kantha faced extremely dry conditions during 1987–88 with respect to 12-month SPI (June-May).

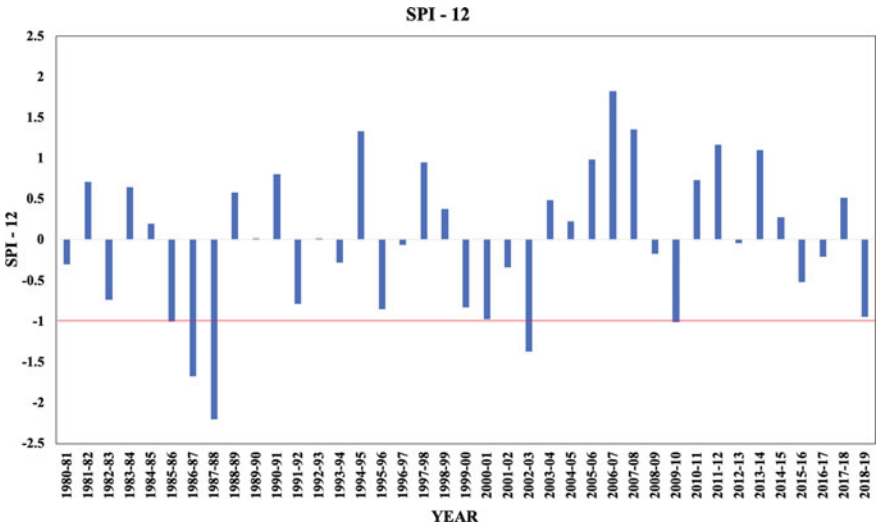

Fig. 5 Drought severity for the years 1980–2019 using SPI-12 (June–May)

5 Conclusions

The following conclusions are derived from the foregoing research:

- The spatial and temporal variability of drought is considered for the Sabarmati basin.
- According to SPI-6 (June-Nov and Dec-May) values, observed drought years are 1983–84, 1986–87, 1987–88, 2001–02, and 2002–03 for drought event of 6 months.
- According to SPI-12 (June-Nov) values, observed drought years are 1985–86, 1986–87, 1987–88, 2002–03, and 2009–10 for drought event of 12 months.
- From SPI-6 (Dec-May), hydrological years of 1983–84 and 2001–02 are observed as seasonal drought years.
- Drought severity of -2.202 and drought intensity of -0.366 occurred during the extreme dry year 1987–88 using SPI-12 (June-May).
- Maximum drought severity of -2.281 and maximum drought intensity of -0.380 occurred during extreme dry year 1987–1988 using SPI-6 (June-Nov) in Sabarmati basin.
- From the drought severity maps, it can be concluded that nine districts except Anand, Bhavnagar, Dungarpur, Panch Mahals and Rajkot faced extreme dry situation during 1987–88 period with respect to 6-month SPI (June-Nov).
- From the drought severity maps, it can also be concluded that 9 districts except Anand, Dungarpur, Panch Mahals, Rajkot, and Sabar Kantha faced extreme dry conditions during 1987–88 with respect to 12-month SPI (June-May).

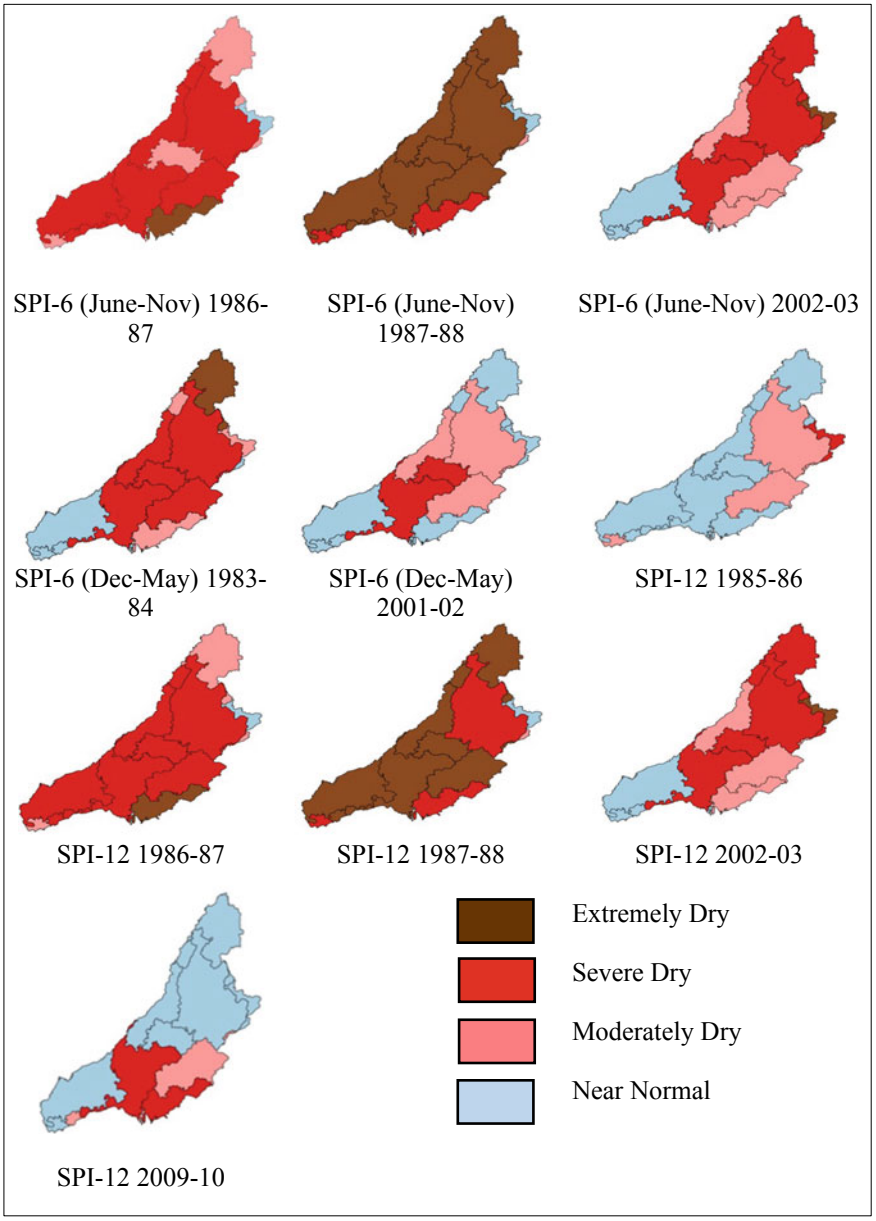

Fig. 6 Drought severity maps based on 12 and 6-month SPI (June-November and December-May) for observed drought years

- Understanding drought severity and intensity is critical in agriculture, particularly in determining irrigation needs.
- It is possible to evaluate the accessibility of soil dampness at the border of the hydrological year. Thus, drought investigation can have additional influence in controlling the productivity of summer crops.

Acknowledgements The authors are grateful to the Directorate, Indian National Committee on Climate Change (INCCC), Ministry of Jal Shakti, Government of India (GoI) for funding the research project titled "Impact of Climate Change on Water Resources of Sabarmati Basin". The authors appreciate the financial assistance and computational resources provided by the Centre of Excellence (CoE) on Water Resources and Flood Management under TEQIP-II, Sardar Vallabhbhai National Institute of Technology. The authors gratefully acknowledge the India Meteorological Department (IMD), Pune for providing the information needed to carry out the current study.

References

1. McKee TB, Doesken NJ, Kleist J (1993) The relationship of drought frequency and duration to time scales. In: Proceedings of the 8th conference on applied climatology, vol 17(22). pp 179–183
2. Tallaksen LM, Madsen H, Hisdal H (2004) Frequency analysis hydrological drought-processes and estimation methods for streamflow and groundwater. In: Tallaksen LM, van Lanen HAJ (eds) Development Water Science, vol 48. pp 199–271
3. Below R, Grover-Kopec E, Dilley M (2007) Documenting drought-related disasters: a global reassessment. The J Environ Developm 16(3):328–344
4. Sheffield J, Wood EF, Roderick ML (2012) Little change in global drought over the past 60 years. Nature 491(7424):435–438
5. Mishra AK, Singh VP (2010) A review of drought concepts. J Hydrol 14;391(1–2):202–16
6. Riebsame WE, Changnon SA, Karl TR (2019) Drought and natural resources management in the United States: impacts and implications of the 1987–89 drought. Routledge
7. Heim RR Jr (2002) A review of twentieth-century drought indices used in the United States. Bull Am Meteor Soc 83(8):1149–1166
8. Zhong F, Cheng Q, Wang P (2020) Meteorological drought, hydrological drought, and NDVI in the Heihe River basin, Northwest China: evolution and propagation. Advances in Meteorology
9. Livada I, Assimakopoulos VD (2007) Spatial and temporal analysis of drought in Greece using the standardized precipitation index (SPI). Theoret Appl Climatol 89(3):143–153
10. Malakiya AD, Suryanarayana TM (2016) Assessment of drought using standardized precipitation index (SPI) and reconnaissance drought index (RDI): a case study of Amreli District. Int J Sci Res 5(8):1995–2002
11. Mahajan DR, Dodamani BM (2016) Spatial and temporal drought analysis in the Krishna river basin of Maharashtra India. Cogent Eng 3(1):1185926
12. Surendran U, Kumar V, Ramasubramoniam S, Raja P (2017) Development of drought indices for semi-arid region using drought indices calculator (DrinC)–a case study from Madurai District, a semi-arid region in India. Water Resour Manage 11:3593–3605
13. Sarma R, Singh DK (2019) Spatio-temporal analysis of drought and aridity in Gomti basin. Current Sci (00113891):116(6)
14. Mishra V, Patel PL (2015) Impacts of climate variability and climate change on water resources in the Sabarmati River basin. Ministry of Water Resources, GoI
15. Beck HE, Zimmermann NE, McVicar TR, Vergopolan N, Berg A, Wood EF (2018) Present and future Köppen-Geiger climate classification maps at 1 km resolution. Scientif Data 5(1):1–2

16. Tigkas D, Vangelis H, Tsakiris G (2015) DrinC: a software for drought analysis based on drought indices. Earth Sci Inf 8(3):697–709
17. Diaz V, Corzo G, Van Lanen HA, Solomatine DP (2019) Spatiotemporal drought analysis at country scale through the application of the STAND toolbox. In: Spatiotemporal analysis of extreme hydrological events, Elsevier, pp 77–93
18. Edwards DC (1997) Characteristics of 20th century drought in the United States at multiple time scales. Air Force Inst of Tech Wright-Patterson Afb Oh

Drought Analysis for the Region in and Around of Mizoram State, India

Vanlalhmuaka Ralte and Briti Sundar Sil

Abstract Drought is a climatic condition characterized by a lack of precipitation. In the last few years, it is found that some areas of the state of Mizoram and its vicinity is facing scarcity of water. A study is conducted to see the present drought condition using simple techniques. The present study shows the frequency of drought by analyzing standardized precipitation index (SPI) of the Mizoram state. The rainfall data were taken from twenty-two rain gauge stations for almost thirty years (1986–2015). The study helps in understanding the importance of SPI and rainfall regarding climate change impacts and droughts which helps in the assessment and management aspects for the society.

Keywords Rainfall analysis · Drought · Standardized precipitation index (SPI) · DrinC · Mizoram

1 Introduction

Drought can be defined as a natural disaster which leads to food, fodder, and water shortages along with destruction of vital ecological system. It is a natural hazard having negative effect on society and environment which is intensified by increasing water demand [1]. In simple words, we can say that it is a situation when there is scarcity of water and insufficiency in quantity to meet the demand [2].

V. Ralte (✉) · B. S. Sil
Department of Civil Engineering, National Institute of Technology Silchar, Silchar 788010, India
e-mail: gunner.tea@gmail.com

B. S. Sil
e-mail: britisil@gmail.com

P. V. Timbadiya et al. (eds.), *Hydrology and Hydrologic Modelling*,
Lecture Notes in Civil Engineering 312,
https://doi.org/10.1007/978-981-19-9147-9_29

Especially nowadays due to climate change issues droughts are occurring very frequently worldwide and have become a severe hazard in many areas. In India, around 68% area is drought susceptible. If a region receives rainfall less than 750 mm in a year, then it is chronically drought-prone area, and the worst drought years in India happened in the years 1877, 1899, 1918, 1972, 1987, 2002, 2009 [3].

The economy of Mizoram depends largely on agriculture. Based on the economic classification of workers—2011 census, more than 60% of the total workers are engaged in agriculture and allied sector [4]. Therefore, abundance of water in the areas are necessary and a lots of problems may arise if the water demand is not met.

In this paper, SPI method is used to determine the drought index over the entire Mizoram state, and a software called DrinC is used for the study.

2 Materials and Methodology

2.1 Standardized Precipitation Index (SPI)

The SPI and its characteristics are explained by McKee et al. [5] for drought monitoring and analysis. SPI can be characterized in multiple time scales (1, 3, 6, 12, 24, 48 months, etc.). For example, the SPI of October time scale represents the standard deviation of precipitation for October. The SPI of 3 month time scale in October represents the standard deviation of precipitation in October-December. The October 12-month time scale SPI represents the standard deviation of October-September precipitation. This paper mainly analyzes the 1-month and 12-month time scale SPI. The larger time scale, i.e., the 9-month and 12-month time scale SPI can give a clearer reflect of the stage changes of drought and flood, and shorter time scale like the 1-month and 3-month time scale SPI can reflect the seasonal drought, which is closely related to agricultural drought [6].

Drought index calculator (DrinC) software is used for calculating the SPI. The structure details and calculation steps of the software can be referred from Tigkas et al. [7]. DrinC is a straightforward software which can calculate the drought indices by considering all the variables through the adaptable interface and giving a simple and justifiable output. However, for better output, it is preferable to have input of long-term datasets [8]. DrinC can be used to calculate the indices in terms of deciles, Standardized Precipitation Index (SPI), Streamflow Drought Index (SDI), and Reconnaissance Drought Index (RDI), based on which the intensity of drought can be assessed and the trend of drought occurrence can be predicted, which can then be used further for drought monitoring, drought spatial distribution assessment, investigation of climatic and drought scenarios and declaration of drought for subsidy related issues.

2.2 Study Area and Data Source

2.3 Mizoram State

The study area is Mizoram (area ≈ 21,087 km^2) and its location range at Latitude 21° 58′ and 24° 35′ N Longitude 92° 15′ and 93° 29′ E and is one of the seven states of the Northeast India. The index map of the Mizoram is shown in Fig. 1.

Fig. 1 Index map of Mizoram

2.4 Data Collection

The monthly rainfall data for twenty two rain gauge stations were collected from meteorological data of Mizoram compiled by the State Meteorological Centre, Directorate of Science and Technology. The data were taken for a period of almost thirty years (1986–2015), except for the data for the district of Mamit which is taken for only 16 years (1999–2015). Details of rain gauge stations and their district headquarters are given in Table 1.

Table 1 Rain gauge stations with their respective district headquarters

Sl. no.	Name of rain gauge station	Name of district	Area of district	District headquarters coordinates
1	2	3	4	5
1	Reiek	Mamit	2967 km^2	23.9294°N, 92.4906°E
2	Mamit	Mamit		
3	Zawlnuam	Mamit		
4	W. Phaileng	Mamit		
5	Bilkhawthlir	Kolasib	1386 km^2	24.2246°N, 92.6760°E
6	Kolasib	Kolasib		
7	Bukpui	Kolasib		
8	Aibawk	Aizawl	3577 km^2	23.8789°N, 92.8976°E
9	Darlawn	Aizawl		
10	Thingsulthliah	Aizawl		
11	Aizawl	Aizawl		
12	Khawzawl	Champhai	3168 km^2	23.4566°N, 93.3282°E
13	Champhai	Champhai		
14	Vaphai	Champhai		
15	Ngopa	Champhai		
16	Serchhip	Serchhip	1424 km^2	23.3417°N, 92.8502°E
17	Lunglei	Lunglei	4572 km^2	22.8671°N, 92.7655°E
18	Hnahthial	Lunglei		
19	Lungsen	Lunglei		
20	Lawngtlai	Lawngtlai	2519 km^2	22.5284°N, 92.8926°E
21	Sangau	Lawngtlai		
22	Siaha	Siaha	1414 km^2	22.4897°N, 92.9793°E

Table 2 Weather classification based on SPI

SPI values	Class
> 2	Extremely wet
1.5−1.99	Very wet
1.0−1.49	Moderately wet
− 0.99−0.99	Near normal
− 1 to −1.49	Moderately dry
− 1.5 to −1.99	Severely dry
< −2	Extremely dry

2.5 Selection of Input Parameters

A specified recurrence distribution of rainfall totals at a climate station was used to fit a gamma probability density function to calculate SPI [9]. SPI is normalized by keeping mean value 0 and standard deviation value unity that is beneficial to identify wet and dry periods equally. For any observed precipitation data, probability is calculated from the gamma function and this is used to estimate the precipitation deviation by SPI normalized. Positive values of SPI shows greater precipitation and negative values shows lesser precipitation than average precipitation [10]. The ranges of SPI values for different classification of drought conditions are given in Table 2 [5].

3 Results and Discussions

The detailed analysis has been carried out for the state of Mizoram using DrinC software, and the results are described in following paragraphs.

From Fig. 2 SPI-1 for the 1-month time scale shows that extremely dry and severely dry conditions occurs only in one occasion in the year 1997–98 and 1994–95, respectively. However, moderate dry conditions occurs in four occasionsin the years 1990–91, 2002–03, 2004–05, and 2006–07 (Fig. 3).

From Figure SPI-3 for the 3-month time scale shows that severely dry conditions occurs in two occasions in the year 2004-05 and 2006–07. However, moderate dry conditions occurs in five occasions in the year 1994–95, 1997–98, 1998–99, 2011–12, and 2014–15.

From Fig. 4, SPI-9 for the 9-month time scale shows that severely dry conditions occurs in two occasions in the year 2006–07 and 2014–15 and moderately dry conditions occurs in five occasions in the year 1994–95, 1998–99, 2008–09, 2011–12, and 2013–14 (Fig. 5).

From Fig. 3, SPI-12 for the 12-month time scale shows that extremely dry conditions occurs only in one occasion in the year 2008–09 and severely dry conditions

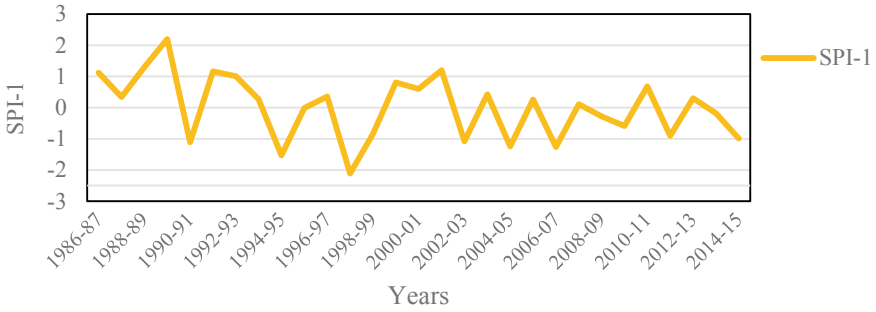

Fig. 2 1-month SPI value for Mizoram

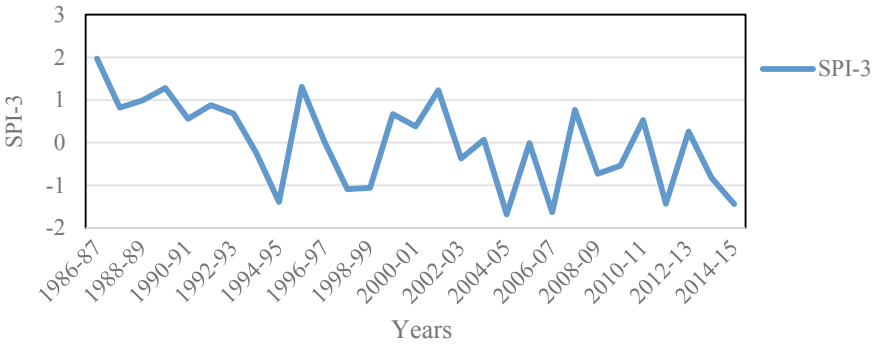

Fig. 3 3-month SPI value for Mizoram

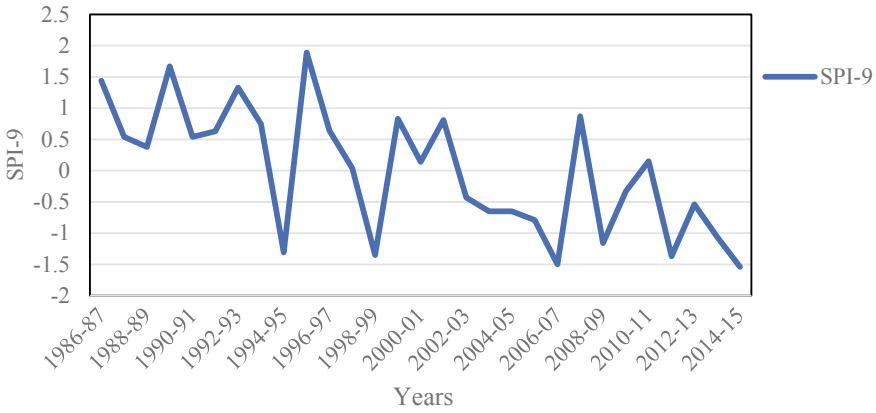

Fig. 4 9-month SPI value for Mizoram

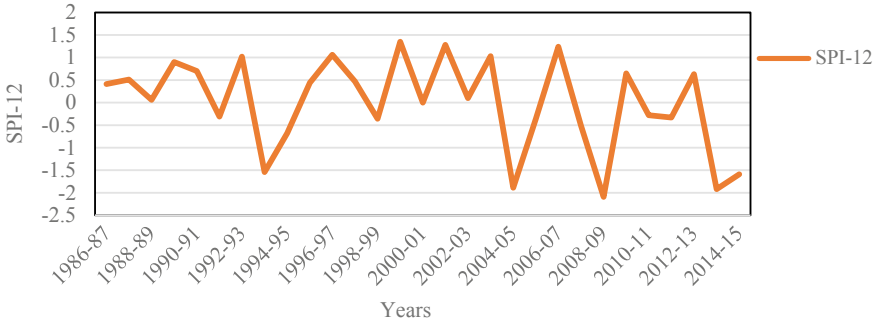

Fig. 5 12-month SPI value for Mizoram

occurs in four occasion in the year 1993–94, 2004–05, 2013–14, and 2014–15. However, no moderate dry conditions occurs.

From the SPI-1, SPI-3, SPI-6, SPI-9, and SPI-12 value for each district based on the 16 years (1999–2015) data, the rank for the most drought-prone area is determined.

The following are the discussions made based on the above results of the study:

(i) From the shorter time scale assessment, the SPI-1 in Fig. 2 shows a more positive skew; it shows an extremely dry condition during the year 1997–1998. However, conditions remain normal but on the drier side every 2 years after that. We can say that the area is on the safer side against short term or seasonal drought. However, looking at the fluctuations that may occur it is advised that further assessment and analysis for the upcoming years is advisable.

(ii) The SPI-12 in Fig. 3 shows a more negatively skewed graph, and it shows that severe dry condition occurs during the period of 1993–1994 and conditions remain favorable for the next 9 years; however, from the 10th year, it shows severe to extreme dry conditions every 4 to 5 years.

(iii) From the shorter time scale assessment (SPI-1 and SPI-3) from the period between 1999 and 2015 Champhai and Kolasib have observed eight seasonal drought years which is more than the other districts, and from the longer time scale assessment (SPI-9 and SPI-12) Kolasib, Lunglei, and Aizawl faced the most drought years of 8 years each.

4 Conclusions

Taking our analysis into consideration it is recommended that the state authorities take certain measures such as giving awareness to the local communities and farmers concerning water management and providing necessary infrastructures for irrigation purposes. The rankings in Table 3 show the most drought prone areas which can be used for administrators and water managers for allocation of funds and to decide for further drought mitigation works.

Table 3 Ranking of rain gauge stations as per Local droughts at multiple time scales

District	SPI-1	SPI-3	SPI-6	SPI-9	SPI-12	Total	Rank
Aizawl	2	4	5	4	4	19	2
Lunglei	1	4	3	4	4	16	4
Champhai	4	4	3	2	4	17	3
Kolasib	3	5	6	4	4	22	1
Lawngtlai	2	2	0	3	3	10	7
Siaha	4	3	1	4	3	15	5
Mamit	2	3	3	3	2	13	6

Acknowledgements The authors are thankful to the SVNIT, Surat and to all the organisers who are involved in the event Hydro 2021 International through which the presentation of this paper is possible and to the State Meteorological Centre, Directorate of Science and Technology for providing necessary data to conduct the present study.

References

1. Mishra AK, Singh VP (2010) A review of drought concepts. J Hydrol 391:202–216
2. Mahajan DR, Dodamani BM (2016) Spatial and temporal drought analysis in the Krishna river basin of Maharashtra, India. Cogent Eng 3:1. https://doi.org/10.1080/23311916.2016.1185926
3. Poorest Areas Civil Society (PACS) Programme (2008) Drought in India. New Delhi, India
4. Planning and Programme Implementation Department (2013) Economic survey Mizoram, 2012-13. Government of Mizoram, India
5. McKee TB, Doesken NJ, Kleist J (1993) The relationship of drought frequency and duration to time scales. In: The 8th conference on applied climatology. 1993 Jan 17. Boston, MA, vol 17(22). American Meteorological Society, pp 179–183
6. Liu DH, You JF, Xie QJ, Huang YY, Tong HJ (2018) Spatial and temporal characteristics of drought and flood in quanzhou based on standardized precipitation index (SPI) in recent 55 years. J Geosci Environ Protect 6:25–37
7. Tigkas D, Vangelis H, Tsakiris G (2015) (2015) DrinC: software for drought analysis based on drought indices. Earth Sci Inf 1:697–709
8. Surendran U, Kumar V, Ramasubramoniam S, Raja P (2017) Development of drought indices for semi-arid region using drought indices calculator (DrinC)—a case study from Madurai District, a Semi-Arid Region in India. Water Resour Manage 31:3593–3605. https://doi.org/10.1007/s11269-017-1687-5
9. Meshram SG, Gautam R, Kahya E (2018) Drought analysis in the Tons River Basin, India during 1969–2008. Theor Appl Climatol 132:939–951. https://doi.org/10.1007/s00704-017-2129-2
10. Verma MK, Verma MK, Yadu LK, Murmu M (2016) Drought analysis in the Seonath River Basin using reconnaissance drought index and standardised precipitation index. Int J Civil Eng Technol 7(6):714–719

Implementation of Rainfall-Based Drought Indices for Regional Drought Assessment

Shradhanjalee Pradhan and Bibhuti Bhusan Sahoo

Abstract Regional drought monitoring is a vital constituent of drought risk management. The effects of drought on the environment and ecosystem may cause disasters and result in socio-economic problems. Drought indices are an extremely useful tool for regional drought assessment. In this study, various rainfall-based drought indices are used for drought assessment of its four districts of the state of Odisha India. The six indices Standardized Precipitation" Index (SPI), Percent of Normal Index (PN), China-Z index (CZI), modified CZI (MCZI), Z- Score Index (ZSI), and deciles index (DI)"differ in their exposure and classification of drought procedures in the study area. Further, a comparative analysis has been done among all the rainfall-based indices. The differences mention among the drought indices in noticing drought in the events in the study area can be reduced by using numerous drought indices in computation to the use of SPI, in drought taxations. It is observed that SPI captured the historical extreme and severe drought periods successfully, and can be suggested to be applied to this district as drought assessment tools.

Keywords Drought · SPI · EDI · DI

1 Introduction

Droughts are usually periods that rainfall is below typical, leading to extended stages of water storage. It is every so often generally defined as a brief meteorological event that branches from the lack of rush over an extended historical compared with some continuing average condition of precipitation. However, drought develops slowly, is difficult to determine, and has many facets in any single area. The victory of drought

S. Pradhan (✉)
Department of Civil Engineering, Veer Surendra Sai University and Technology, Burla, Odisha, India
e-mail: shradha4972@gmail.com

B. B. Sahoo
Department of Agricultural Engineering, Centurion University of Technology and Management, Paralakhemundi, Odisha, India

P. V. Timbadiya et al. (eds.), *Hydrology and Hydrologic Modelling*,
Lecture Notes in Civil Engineering 312,
https://doi.org/10.1007/978-981-19-9147-9_30

preparedness and reduction depends, largely, based on current information on the commencement, progress, and region affected by the drought. Drought monitoring can provide you with this piece of communication. Drought indices are commonly used for monitoring. Drought indices provide information on the severity of drought to decision-makers and, if accessible, can be used to trigger drought eventuality measures. To date, many drought indexes have been established.

The Palmer Drought Severity Index (PDSI) [13] is a frequently used drought severity index in the U. S.. The decile index [4], that is, used in Australia, the Surface Water Supply Index (SWSI), Shafer and Dezman [16], which was adopted by many states in the U.S., as well as the standardized precipitation index (SPI) [9], which has achieved worldwide acclaim, the China-Z index (CZI), which is castoff by the National Meteorological Center of China (Wu The majority of these indicators are dependent on weather information (temperature and rainfall). There is no such thing as an ideal or all-encompassing index. The index's ability to consistently discern regional and temporal variations during a drought, as well as the volume of weather data available in the event should ultimately guide the selection of indices for drought nursing in a specific area.

Drought is one of the devastating expected disaster in India affecting various dimensions of society. It has major impacts on the environment, agriculture, the economy, and society as a whole. In recent decades, the severity and the frequency of droughts have increased due to erratic rainfall [10, 18]. To know the spatiotemporal behavior of drought over India, multiple drought indices have been used in the past" [1, 6, 8, 19]. SPI is one of the most commonly used drought index for assessment of drought [3, 12, 14, 15]. Some of the other studies on drought assessment in India context include the use of various drought indices for example PDSI, Integrated Drought Index (IDI), Standard Precipitation Evapotranspiration (SPEI), Effective Drought Index ('EDI), and many more [7, 17, 22]. Nevertheless, a drought index is appropriate for one region may not be applicable for other region or basin [20, 22]. Therefore, numerous researchers across the globe have compared different drought indices with an aim of discovery suitable drought index for a certain region or basin [2, 11, 21]. Morid et al. [11] used EDI, SPI, Percent Departure from Normal, Deciles Index, Z-index, modified CZI (MCZI), and China Z index (CZI) for six locations in Iran. They found that the EDI outperformed other indices. Barua et al. [2] compared Percent Departure from Normal, Deciles Index. Used for the Yarra River Catchment in Australia, Aggregated Drought Index (ADI), SPI, and the SWSI were used. They accomplish that the ADI performed better in sensing fraud based on decision criteria of historic droughts.

This drought assessment in the four selected districts of Odisha has never been the subject of a serious scientific study. In addition, nothing is known about the features of drought in the observed area. Therefore, the objective of this observed is to evaluate the drought situation in the four selected district as shown in Fig. 1. As there is no universal index for drought assessment it's more preferred to do a regional assessment and check which index fits the best for that area.

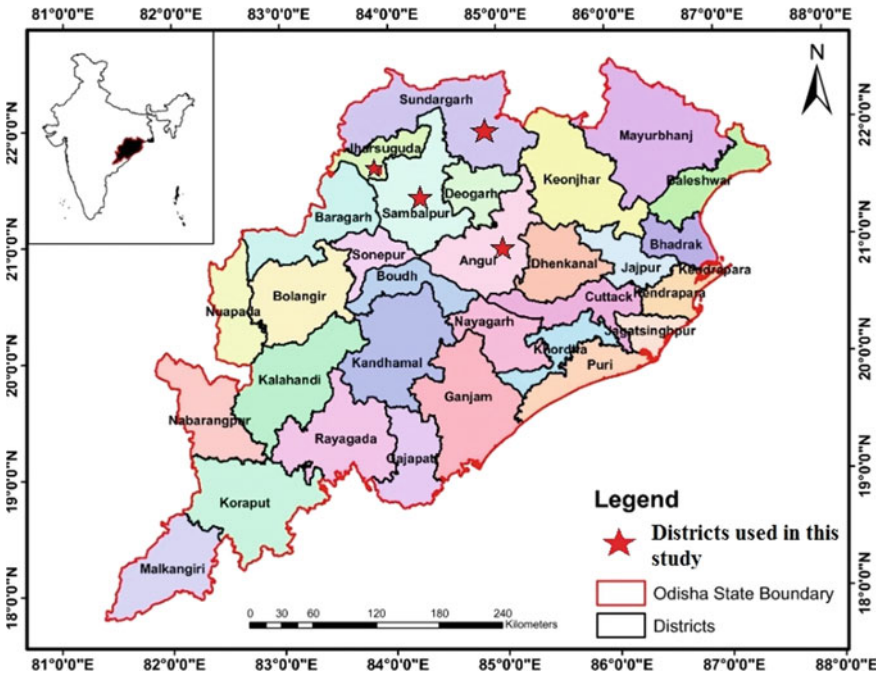

Fig. 1 Study area map

2 Study Area and Data Collection

An attempt was finished to perform drought susceptibility analysis in four districts of Odisha as shown in Fig. 1. The study area Long monsoon breaks (dry spells) in the course of the crop increasing in rich, as well as huge variations in rainfall quantity from year to year, outcome in crop failure on a regular basis, making the entire area drought prone. However, there is a need to analyze the spatial and secular distinction of drought in this area so that water users can frame drought alleviation plans and make decisions based on the future skyline to decrease the harmful footprint of drought. The rainfall data were collected from the Indian meteorological department.

3 Drought Indices

The goal of this study was to evaluate whether six indices "Standardized Precipitation Index (SPI), deciles index (DI), Percent of Normal Index (PN), China-Z index (CZI), "modified CZI (MCZI), Z-Score Index (ZSI)" detect and arrange droughts occurrences. One aspect that all of the carefully chosen indices have in mind is that they really rely only on precipitation data. Every one of the indexes examined have

indeed been applied to the study's different measurement variables. Each monthly has a separate time scale. The drought's point-by-point and spatial scope were determined correspondingly. The resulting text includes a summary of a indices of these values.

3.1 The Percent of Normal (PN)

The percent of normal index is one of the most simple ways to determine how far rainfall has deviated from its long-term average rainfall. 'Normal' is commonly set to a location's long-term mean rush value. The value of 'normal' is 100% and can be determined for a month, a season, or a period. Because the same PN might have various specific implications in different places, it's a bit of a crude metric of precipitation shortfall. In addition, what is normal may be perceived differently in divergent regions.

3.2 The Decile Index (DI)

Gibbs and Maher [4] proposed the Decile Index approach, which is widely used in Australia. Seasonal rainfall totals from a long track record are first ranked from highest to lowest to construct a cumulative probability dispensation. After then, the dispensation is divided into eleven pieces (tenths of distribution or deciles). The first decile is the quantity of precipitation that is not exceeded by the lowest 10% of all precipitation readings in a period. The second decile, which varies from 10% in terms to 20%, is situated between both the lowest and highest deciles. When evaluating the amount of precipitation in a month (or over several months) with the long-term cumulative dispersal of precipitation quantities in that period, the severity of drought can be determined.

There are five classes of deciles, each with two deciles. If precipitation falls into the lowest 20 percentage points of year, it is considered significantly below normal (deciles 1 and 2). Below-normal rainfall is noted by deciles three to four (20–40%), close precipitation is noted by deciles 5–6 (40–60 percent), above-normal precipitation is indicated by deciles 7 and 8 (60–80 percent), and substantially above-normal rush is indicated by deciles 9 and 10 (80–100%).

3.3 The Standard Precipitation Index (SPI)

A long-term rush record at the selected station is first fitted to a probability distribution, which will then be transformed into a normal distribution with mean zero SPI [9]. A variety of time periods could be used to determine the SPI (e.g., 1 month,

3 months, and 24 months). Also with long-term sets of data, Guttman [5] showed that employing SPI at extra duration increments is not recommended so because sample size diminishes. Different timeframes can be used to examine the effects of a precipitation shortage on different water resource elements (groundwater, soil moisture, reservoir storage, and streamflow). The dryness section of the SPI scale is classified at random into 'very dry' (SPI2.0), 'severely dry' (1.5 > SPI > 1.99), 'moderately dry' (1.0 > SPI > 1.49), and 'near normal' (0.99 > SPI > 0.99) conditions.

Positive SPI values show more precipitation than average, while negative results suggest less precipitation.

3.4 China-Z Index (CZI), Modified CZI (MCZI) and Z-Score

The CZI is constructed on the Wilson-Hilferty cube-root transformation. Undertake that haste data follow the Pearson Type III dissemination, the index is calculated as:

$$\mathrm{CZI}_i = \frac{6}{S_c}\left(\frac{S_c}{2}\Phi i + 1\right)^{1/3} - \frac{6}{S_c} + \frac{S_c}{6} \tag{1}$$

$$S_c = \frac{\sum_{i=1}^{n} (xi - \overline{x})^3}{n \times \sigma^3} \tag{2}$$

$$\Phi i = \frac{xi - \overline{x}}{\sigma} \tag{3}$$

where i is the present month, S_c" is coefficient of unevenness, n is the total number of months in the data, Φ_i is standard variate, also called the Z-Score and x_i is precipitation of i month." Instead of using the mean of precipitation in the CZI calculation, the median of precipitation is used to calculate the MCZI (i.e., Med is substituted for x in Eqs. 2 and 3). Wu et al. [23] attempted to lessen the discrepancies between the SPI and the MCZI by doing so. They determined, however, that the gaps between these two indexes did not narrow as much as the discrepancies between the CZI and the SPI.

4 Result and Discussion

The values obtained of the MCZI, CZI, Z-Score, and SPI all are almost identical (Table 1). As a consequence, they are all on the same page in this respect. The DI and PN, on the other side, have broad variations than the SPI, as previously established. To make the DI and PN values comparable to the SPI classes, they have indeed been organized into similar classes (Table 1). DI classes of 60–70% (slightly

Table 1 Different classes of various drought indices based on the index value

SPI	CZI	MCZI	Z score	DI (%)	PN (%)	Classes
≥ 2	≥ 2	≥ 2	≥ 2	≥ 90		Extremely wet
1.5–1.99	1.5–1.99	1.5–1.99	1.5–1.99	80–90		Severely wet
1–1.49	1–1.49	1–1.49	1–1.49	70–80	≥ 110[a]	Moderately wet
− 0.99–0.99	− 0.99–0.99	− 0.99–0.99	− 0.99–0.99	30–70	80–110	Normal
− 1–1.49	− 1–1.49	− 1–1.49	− 1–1.49	20–30	55–80	Moderately dry
− 1.5–1.99	− 1.5–1.99	− 1.5–1.99	− 1.5–1.99	10–20	40–55	Very dry
≤ -2	≤ -2	≤ -2	≤ -2	≤ 10	≤ 40	Extremely dry

[a] ≥ 110 considered as WET

above normal), 50–60% (normal), and 30–40% (slightly below normal) have been combined to form a broader 'normal' DI class of 30–70% (which correlates to the 'normal' SPI range). High PN values were not classified for this investigation, and all value higher than 110% were considered 'wet' circumstances (Table 1).

In all of the four districts SPI out performed in the year 1995, 2000, 2005, 2010, 2015 among all indices considered in this study. The SPI shows close resemblance with the actual percentage of drought affected in all the four districts. In most of the districts the CZI, MCZI and Z score overestimated than the actual area affected by drought. For example, in case of Sundargarh district the actual drought affected is 35% in the year 1995, while the SPI estimation shows 38% of the drought-affected area. Meanwhile CZI, MCZI and Z shows 41, 44 and 47%, that is, quite higher than the actual data. Which can be easily interpreted from the Fig. 2 and for other districts and for other years. Figure 2 shows a comparison between the actual drought percentage and various drought indices used in this study. All four districts rainfall-based drought indices (SPI, DI, PN, MCZI, CZI, and Z SCORE) are shown in Fig. 3.

5 Conclusions

- In this study, six drought indice" Standardized Precipitation Index (SPI), deciles index (DI), Percent" of Normal Index (PN), China-Z index (CZI), modified CZI (MCZI), and Z-Score Index (ZSI) were evaluated for monitoring and detecting drought periods, four districts of Odisha. The SPI method gives the superior result as compared to other rainfall-based results.
- Results derived by the SPI method are more similar to actual drought in the study districts. Therefore, SPI can be a suitable drought index for the four districts.

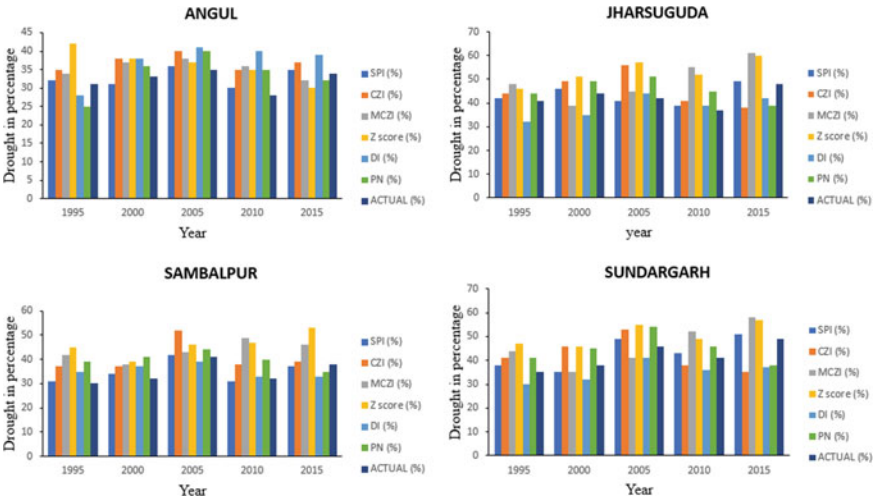

Fig. 2 Comparison between actual drought and rainfall-based drought indices for all the fore districts

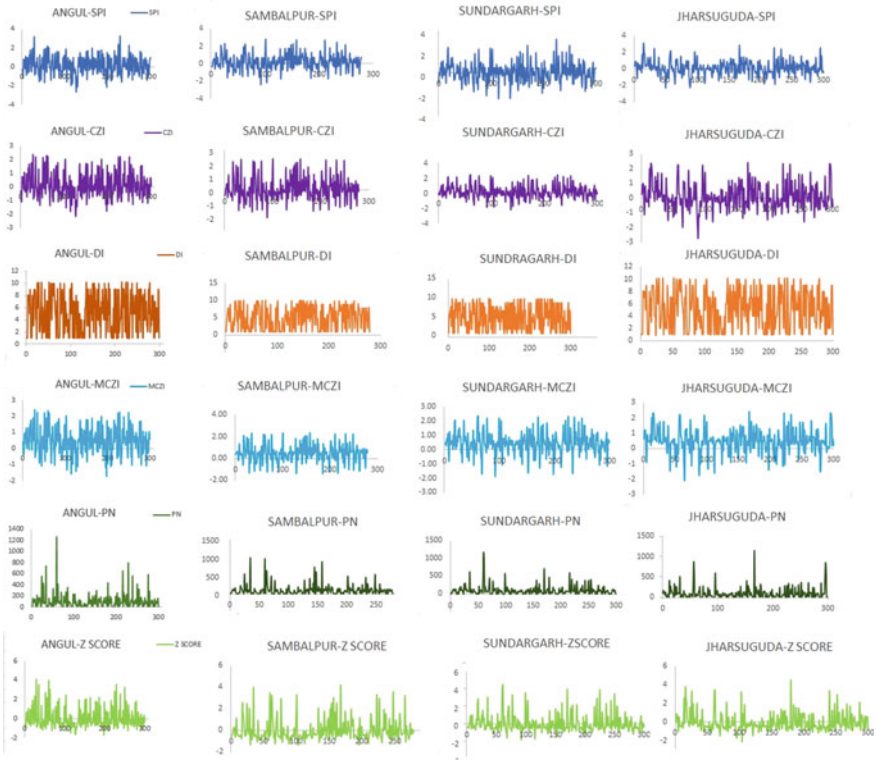

Fig. 3 All four districts rainfall-based drought indices (SPI, DI, PN, MCZI, CZI, Z SCORE)

The SPI index is capable drought nursing and describing attribute of drought circumstances.

- Having concerns to the effects of weather change, deficiency of comforting about various drought condition or span in various parts of the world is connected with climate change of climatical factors and requires estimation in a longer period. Totally, the occurrence of droughts is unavoidable, but observe and forecast of drought can be give rise to improve adversarial impressions of drought.

Acknowledgements I gratefully acknowledge the resourceful guidance, active supervision and constant encouragement of **Associate Prof. Bibhuti Bhusan Sahoo**, Department of Civil Engineering, MVR College of Engineering and Technology Vijayawada Andhra Pradesh, India who despite their other commitment and could make time to help me in completing my research work. I do my sincere thanks to them.

I would also like to thanks my family and friends for their cooperation directly or indirectly for the completion of the report.

References

1. Aadhar S, Mishra V (2017) High-resolution near real-time drought monitoring in South Asia. Scient Data 4:170145
2. Barua S, Ng A, Perera B (2011) Comparative evaluation of drought indexes: case studyon the Yarra River catchment in Australia. J Water Resour Plan Manag 137(2):215–226
3. Bhunia P, Das P, Maiti R (2020) Meteorological drought study through SPI in three drought prone districts of West Bengal India. Earth Syst and Environ 4(1):43–55
4. Gibbs WJ, Maher JV (1967) Rainfall deciles drought inddicators
5. Guttman NB (1998) Comparing the palmer drought index and the standardized precipitation index 1. JAWRA J Amer Water Resour Assoc 34(1):113–121
6. Kumar KN, Rajeevan M, Pai D, Srivastava A, Preethi B (2013) On the observed variability of monsoon droughts over India. Weather and Climate Extremes 1:42–50
7. Malik A et al (2020) Analysis of dry and wet climate characteristics at Uttarakhand (India) using effective drought index. Natural Hazards 1–20
8. Mallya G, Mishra V, Niyogi D, Tripathi S, Govindaraju RS (2016) Trends and variability of droughts over the Indian monsoon region. Weather and Climate Extremes 12:43–68
9. McKee TB, Doesken NJ, Kleist J (1993) The relationship of drought frequency and duration to time scales. In: Proceedings of the 8th conference on applied climatology. Boston, pp 179–183
10. Mishra V et al (2019) Drought and famine in India, 1870–2016. Geophys Res Lett 46(4):2075–2083
11. Morid S, Smakhtin V, Moghaddasi M (2006) Comparison of seven meteorological indices for drought monitoring in Iran. Int J Climatol: A J Royal Meteorol Soc 26(7):971–985
12. Naresh Kumar M, Murthy C, Sesha Sai M, Roy P (2009) On the use of standardized precipitation index (SPI) for drought intensity assessment. Meteorol Appl0: A J Forecasting Pract Appl Training Techniques and Model 16(3):381−389
13. Palmer WC (1965) Meteorological drought, 30. US Department of Commerce, Weather Bureau
14. Patel N, Chopra P, Dadhwal V (2007) Analyzing spatial patterns of meteorological drought using standardized precipitation index. Meteorol Appl: A J Forecasting Practical Appl Training Techniques and Model 14(4):329–336
15. Rawat KS, Tripathi VK (2016) Standardized precipitation index based approach for development of regional drought monitoring system. J Remote Sens Technol 4:48–57

16. Shafer B, Dezman L (1982) Development of surface water supply index (swsi) to assess the severity of drought condition in snowpack runoff areas. In: Proceeding of the western snow conference
17. Shah D, Mishra V (2020) Integrated drought index (IDI) for drought monitoring and assessment in India. Water Resour Res 56(2):e2019WR026284
18. Shah R, Mishra V (2014) Evaluation of the reanalysis products for the monsoon season droughts in India. J Hydrometeorol 15(4):1575–1591
19. Singh C (2001) Probabilities and distribution of monsoon rainfall in normal, flood and drought years over India. Meteorol Atmos Phys 78(3–4):205–214
20. Smakhtin VU, Hughes DA (2007) Automated estimation and analyses of meteorological drought characteristics from monthly rainfall data. Environ Model Softw 22(6):880–890
21. Vicente-Serrano SM et al (2012) Performance of drought indices for ecological, agricultural, and hydrological applications. Earth Interact 16(10):1–27
22. Wable PS, Jha MK, Shekhar A (2019) Comparison of drought indices in a semi-Arid River Basin of India. Water Resour Manage 33(1):75–102
23. Wu H, Hayes MJ, Weiss A, Hu Q (2001) An evaluation of the standardized precipitation index, the China-Z index and the statistical Z-Score. Int J Climatol: A J Royal Meteorol Soc 21(6):745–758

Investigation of Crop Evapotranspiration and Irrigation Water Requirement in the Ukai-Kakrapar Command Area, India

K. B. Baladaniya, P. L. Patel, and P. V. Timbadiya

Abstract Water shortage and competing demand of water need judicious usage of water in the agriculture sector. The present study includes crop water estimate and irrigation water requirements for Ukai left bank command area (ULBCA), Ukai right bank command area (URBCA), Kakrapar left bank command area (KLBCA), and Kakrapar right bank command area (KRBCA) using meteorological data for period from 2010 to 2019. Using daily climatic data, the FAO Penman–Monteith technique has been used to determine reference evapotranspiration (ET_0). The crop coefficient is used to determine the crop evapotranspiration (ETc) of various types of crop types. The effective rainfall is calculated using the Soil Conservation Service (SCS) method. Then, net irrigation requirement (*NIR*) has been calculated using effective rainfall and estimated crop water requirements. The maximum gross irrigation water requirement (*GIWR*) in ULBCA, URBCA, KLBCA, and KRBCA has been estimated to be 149.31 MCM, 103.72 MCM, 269.43 MCM, and 205.42 MCM, respectively, by considering the water conveyance efficiency of 70% and water application efficiency of 60% (flood irrigation). Crop water requirement (*CWR*) estimated in lakh mm Ha. Such irrigation water demand would be useful for optimization of reservoir releases in optimal growth of crops in the command area.

Keywords Crop evapotranspiration · Crop water requirement · Gross irrigation requirement · Ukai-Kakrapar command area · FAO Penman–Monteith

K. B. Baladaniya (✉) · P. L. Patel · P. V. Timbadiya
Department of Civil Engineering, Sardar Vallabhbhai National Institute of Technology Surat, Surat 395007, India
e-mail: kalpeshb1701@gmail.com

P. L. Patel
e-mail: plpatel@ced.svnit.ac.in

P. V. Timbadiya
e-mail: pvtimbadiya@ced.svnit.ac.in

P. V. Timbadiya et al. (eds.), *Hydrology and Hydrologic Modelling*,
Lecture Notes in Civil Engineering 312,
https://doi.org/10.1007/978-981-19-9147-9_31

1 Introduction

The developing and underdeveloped countries across the globe are experiencing severe water shortages, particularly, in agricultural sectors. The requirement water is increasingly becoming limited due to rising water demands in various sectors [10]. Irrigation is an essential component of inland river basin water resource management, and it is crucial to agricultural policy formations. Water security in arid places is very vulnerable to climate change and increased human activity [11]. Agriculture consumes major share of water in India (approximately 81%) and thus forms a major focus for effective water usage in agriculture in coming years [9]. Crop production in the agricultural industry can be increased by making better use of current land and water resources. Furthermore, determining the water demand for the crops and supplying them, accordingly, can help in minimizing large-scale wastage of water in crop watering [2, 7]. Evapotranspiration is one of the greatest indicators for quantifying the consequences of climate change and estimating the agricultural water usage [4, 5].

Accurate information on crop water needs, irrigation withdrawal based on crop, soil type, and meteorological conditions is required for successful water resource planning. Rainfall and evapotranspiration eventually affect the region's water balance and irrigation water requirements for various crops. Such climate parameter studies are therefore useful in establishing degrees of risk in arable agriculture. The FAO Penman–Monteith [3] is used in this work to determine ET0, since it has been shown to produce values that are extremely consistent with real crop water consumption across the world [1, 6]. The objectives of the present study are to explore the spatiotemporal variations in crop evapotranspiration (ETc) with special water needs for leaching for the primary crops in Ukai-Kakrapar canal command area. The ETc of sugarcane, plantain, groundnut, paddy, cotton, wheat, juwar/bajari, vegetables, and other perennial crop; other crop net irrigation requirement (NIR); and gross irrigation water requirement (GIWR) were assessed throughout the growing seasons from 2010 to 2019. Such irrigation water demand would be beneficial for optimizing reservoir releases for maximizing crop yield from the command area.

2 Study Area and Data Collection

2.1 Description of Study Reach

After the Narmada, the Tapi River is India's second biggest west-flowing river. Tapti and Surya Putri are other names for the Tapi River. From the Multai forest in Betul district, the Tapi River flows into Madhya Pradesh, Maharashtra, and Gujarat. The elevation at the start is approximately 752 m above mean sea level. The Tapi River flows 724 km from its sources to its mouth in the ocean. It runs 282 km through M.P., 228 km through Maharashtra, and 214 km through Gujarat before joining the

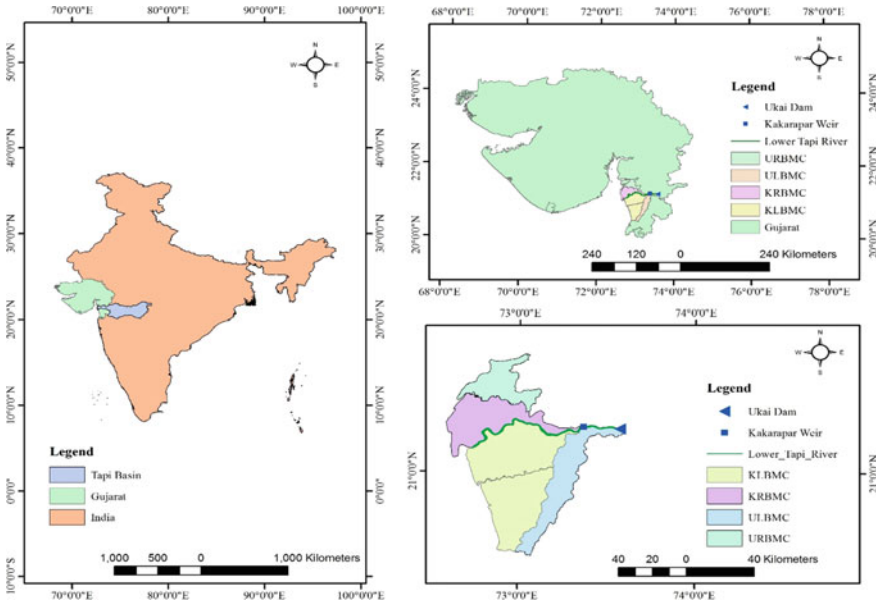

Fig. 1 Index map of study area

Arabian Sea near Dumas. The Tapi basin is having a total catchment area of 65,145 km^2, out of which 79.1% of the area is in Maharashtra, 15% of the area is in Madhya Pradesh, and 5.9% of the area is in Gujarat. Gujarat's second largest multipurpose project is the Ukai-Kakrapar Irrigation Project on the Tapi River. The Kakrapar weir (latitude 21°16′9.72″N and longitude 73°21′54.66″E) lies 24 km downstream of the Ukai Dam (latitude 21°15′12.21″N and longitude 73°35′35.49″E), which served as multipurposes, like irrigation, hydropower, domestic and industrial sectors, and hydropower.

The current study considers the ULBCA, URBCA, KLBCA, and KRBCA as shown in Fig. 1. The gross command area (GCA) of ULBCA, URBCA, KLBCA, and KRBCA is 1,21,458 ha, 84,686 ha, 2,47,000 ha, and 1,18,838 ha, respectively, and culturable command area (CCA) of ULBCA, URBCA, KLBCA, and KRBCA is 66,168 ha, 48,117 ha, 1,45,335 ha, and 71,937 ha, respectively.

2.2 Data Source and Collection of Data

The data required for present research work were collected from different agencies/institutions in India. The data required for present study and their sources are described in Table 1.

Table 1 Data sources for the present study

Data type	Data source
• *Crop-wise irrigation area in various command areas for Rabi, Kharif, and hot seasons*: • KLBMC command area • KRBMC command area • ULBMC command area • URBMC command area	• Surat canal division, Surat, Gujarat • Ambica division, Navsari, Gujarat • Kakrapar right bank canal division, Surat, Gujarat • Ukai left bank canal division, Valod, Gujarat • Ukai right bank canal division, Ankleshwar, Gujarat
• *Meteorological data* • RH_{min} and RH_{max}(relative humidity) • T_{max} and T_{min} (temperature) • AW (average wind speed) • Daily sunshine hours • Rainfall	• Navsari Agricultural University, Navsari, Gujarat • State Water Data Center, Hydrology Project, Gandhinagar, Gujarat
• *Crop coefficient*	• Navsari Agricultural University, Navsari, Gujarat

3 Methodology

3.1 Reference Evapotranspiration (ET0)

When the reference surface is not depleted of water, the rate of evapotranspiration is called reference evapotranspiration. A hypothetical grass reference crop that is constantly rising and entirely shading the ground is used as the reference surface, with parameters such as 0.12 m crop height, surface resistance is set at 70 s/m, and albedo is 0.23. The 'FAO Irrigation and Drainage Paper No. 56 for Crop Evapotranspiration' recommends the Penman–Monteith method for calculating ETo. The FAO Penman–Monteith approach was used to determine *ETo* Eq. (1) for the daily time scale.

$$ETo = \frac{0.408*\Delta*(R_n - G) + \gamma*(\frac{900}{T+273})*u_2*(e_s - e_a)}{\Delta + \gamma*(1 + 0.34*u_2)} \tag{1}$$

ETo is an abbreviation for reference evapotranspiration [mm day-1], T denotes mean daily air temperature at 2 m elevation [°C], u_2 denotes wind speed at 2 m elevation [m s−1], R_n is an abbreviation for net radiation at the crop surface [MJ m-2 day-1], e_s denotes saturation vapor pressure [kPa], G is an abbreviation for soil heat flux density [MJ m-2 day-1], and e_a denotes actual vapor pressure [kPa], and Eqs. (2 and 3) are used to compute the mean saturation vapor pressure (e_s).

$$e^{\circ}(T) = 0.6108*\exp\left(\frac{17.27*T}{T + 237.3}\right) \tag{2}$$

$$e_s = \frac{e*(T_{max}) + e*(T_{min})}{2} \tag{3}$$

where $T_{\max}$ denotes the highest temperature (°C), $T_{\min}$ denotes the minimum temperature (°C), and e_s denotes the saturation vapor pressure [kPa]. The computed real vapor pressure (e_a) is derived using Eq. (4).

$$e_a = \frac{e^o(T_{\min})\frac{\mathrm{RH}_{\max}}{100} + e^o(T_{\max})\frac{\mathrm{RH}_{\min}}{100}}{2} \tag{4}$$

where $\mathrm{RH}_{\max}$ is the highest relative humidity (%), $\mathrm{RH}_{\min}$ is the minimum relative humidity (%), and e_a is the actual vapor pressure (kPa). Equation (5) is used to compute the slope of the saturation vapor pressure curve.

$$\Delta = \frac{4098^*0.6108^* \exp\left(\frac{17.27\mathrm{T}}{T+237.3}\right)}{(T+237.3)^2} \tag{5}$$

where Δ is the slope of the saturation vapor pressure curve at air temperature T [kPa °C−1], and T is the air temperature in °C.

The rate of longwave energy emission is proportional to the surface's absolute temperature raised to the fourth power; this connection is defined by the Stefan–Boltzmann equation, which is represented as Eq. (6).

$$R_{nl} = \sigma * \frac{(T_{\max}+273.3)^4 + (T_{\min}+273.3)^4}{2} * \left(0.34 - 0.14\sqrt{\mathrm{e}_a}\right) * \left(1.35\frac{R_s}{R_{so}} - 0.35\right) \tag{6}$$

where $R_n = R_{\mathrm{ns}} - R_{\mathrm{nl}}$; $R_{\mathrm{ns}} = 0.77 \times R_s$; $R_s = 0.75 \times \mathrm{Ra}$; R_{ns} is the net shortwave radiation (MJ/(m2.d)); R_{nl} denotes net longwave radiation (MJ/(m2.d)), whereas R_s denotes incoming solar radiation (MJ/(m2.d)). The Stefan–Boltzmann constant (4.90310–9 MJ/(m2.d)); $T_{\max}$ and $T_{\min}$ are the maximum and lowest temperatures (°C), respectively; and R_{so} is the solar radiation from the clear sky (MJ/m2. d).

3.2 Crop Water Requirement (CWR)

Crop water demand is the quantity of water lost from a crop owing to evapotranspiration (ET_c), which may be determined using Eq. (7):

$$\mathrm{CWR} = ET_c = K_c \times ET_o \tag{7}$$

ET_c denotes crop evapotranspiration (mm), K_c denotes crop coefficient at a certain development stage (dimensionless), and ETo denotes reference evapotranspiration (mm).

3.3 Effective Precipitation (P_{eff})

The Soil Conservation Service (SCS) method, as defined in Eq. (8) below, was used to determine effective rainfall.

$$P_{\text{eff}_t} = \frac{P_t}{125} * (125 - 0.2 * P_t) \quad P_t \leq 250\,\text{mm}$$
$$P_{\text{eff}_t} = 125 + 0.1 * P_t \quad P_t > 250\,\text{mm} \tag{8}$$

where P_{eff_t} = effective rainfall in t_{th} month, and P_t = rainfall in t_{th} month.

3.4 Net Irrigation Requirement (NIR)

Net irrigation need is the amount of irrigation water required to fulfill a crop's evapotranspiration demand as well as additional needs such as leaching (special needs), as expressed in Eq. (9).

$$\text{NIR} = \text{CWR} - P_{\text{eff}} + \text{Special needs} \tag{9}$$

Filed irrigation requirement (FIR) and gross irrigation water requirement are calculated as per Eqs. (10) and (11).

$$\text{FIR} = \frac{\text{NIR}}{n_a} \tag{10}$$

$$\text{GIWR} = \frac{\text{FIR}}{n_c} \tag{11}$$

where NIR = net irrigation requirement; FIR = field irrigation requirement; GIWR = gross irrigation water requirement; n_a = application efficiency (60% for flood irrigation); and n_c = conveyance efficiency (70% considered for the present study).

4 Data Analysis, Results, and Discussions

4.1 Estimation of ET0

The potential evapotranspiration was calculated using 10 years' (2010 to 2019) climate data by FAO 56. The weighted average potential evapotranspiration for each canal command area was estimated using Thiessen polygon approach (Subramanya K., 1991). The weighted area was calculated using ArcGIS 10.5. On daily time

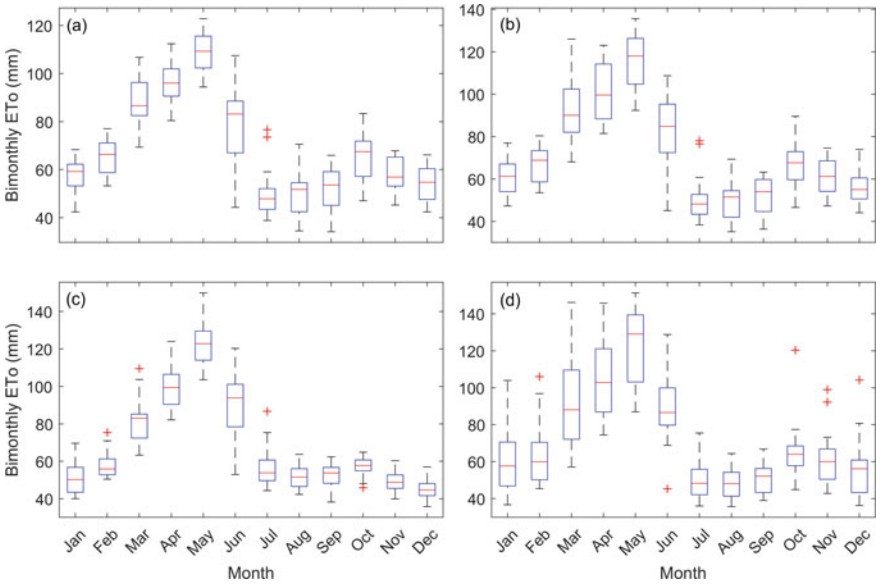

Fig. 2 Bimonthly ETo in **a** KLBCA, **b** KRBCA, **c** ULBCA, and **d** URBCA. The box and whisker plots show the median, first (lower) quartile, third (upper) quartile, minimum score, and maximum score

scale, the ETo values were calculated and converted to bimonthly (shown in Fig. 2). The maximum value of ETo in May, KLBCA, KRBCA, ULBCA, and URBCA is 122.80 mm, 135.72 mm, 149.5 mm, and 150.99 mm respectively, and the corresponding minimum value is 34.20 mm (September), 35.11 mm (August), 35.85 mm (December), and 35.67 mm (August), respectively.

4.2 Estimation of Monthly Effective Rainfall (Peff) and Gross Irrigation Water Requirement (GIWR)

i. Monthly effective rainfall was calculated using SCS method (CROPWAT software), the maximum effective rainfall in KLBCA, KRBCA, ULBCA, and URBCA has been calculated as 206.90 mm (July), 182.44 mm (August), 214.53 mm (July), and 176.99 mm (August), respectively, which are shown in Fig. 3. The maximum monthly gross irrigation water requirement in KLBCA, KRBCA, ULBCA, and URBCA has been found to be 269.43 MCM (April), 205.42 MCM (May), 149.31 MCM (May), and 103.72 MCM (March), respectively, which are shown in Fig. 4.

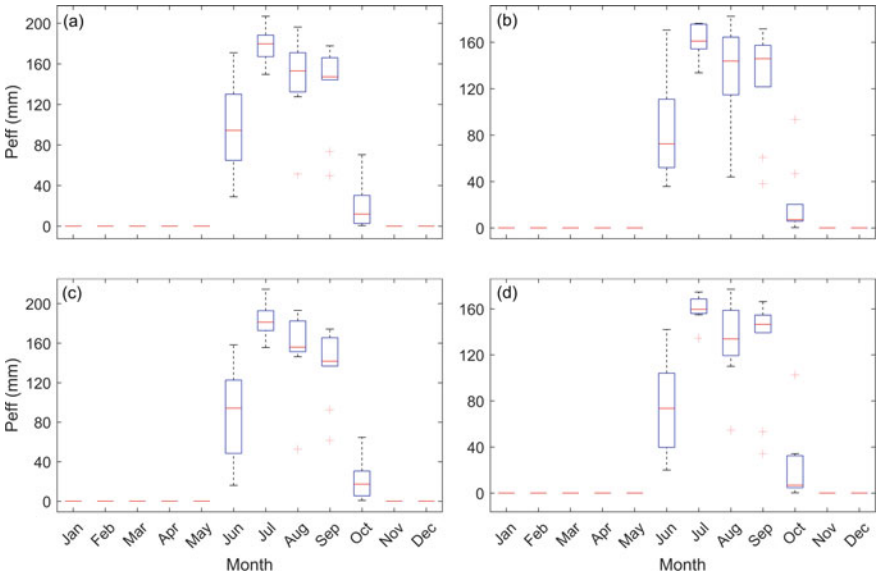

Fig. 3 Effective rainfall (Peff) in **a** KLBCA, **b** KRBCA, **c** ULBCA, and **d** URBCA

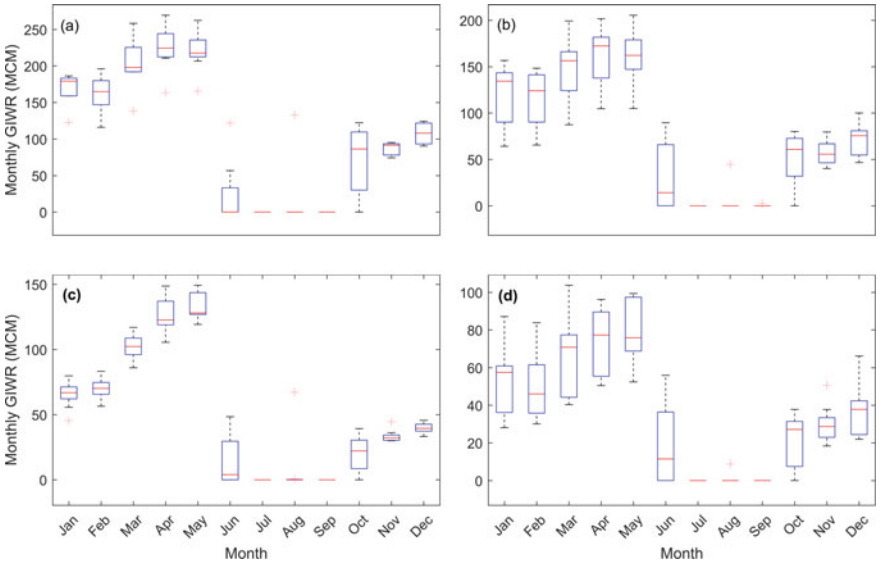

Fig. 4 Monthly GIWR in **a** KLBCA, **b** KRBCA, **c** ULBCA, and **d** URBCA

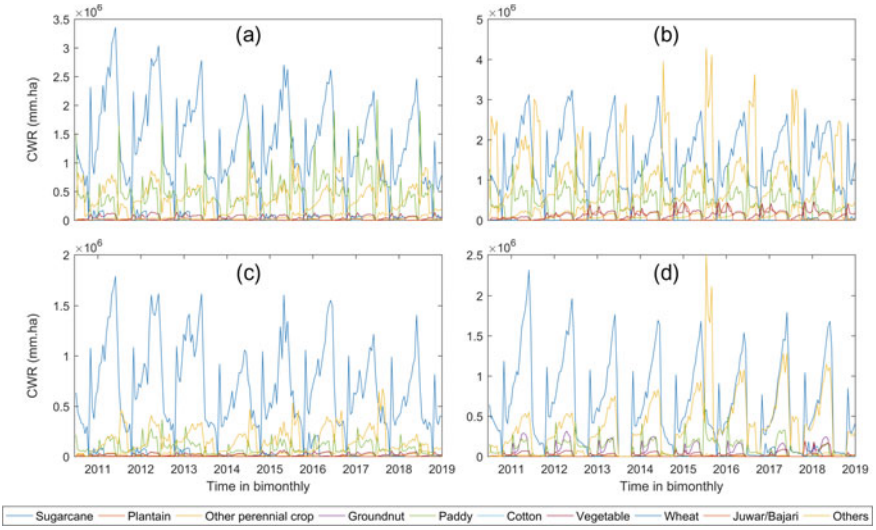

Fig. 5 Bimonthly CWR in **a** KLBCA, **b** KRBCA, **c** ULBCA, and **d** URBCA

4.3 Estimation of Crop Water Requirement (CWR)

CWR values for several crop kinds were estimated independently for the Ukai-Kakrapar command region from 2010 to 2019. Maximum bimonthly major crop (sugarcane) in KLBCA, KRBCA, ULBCA, and URBCA has been estimated to be 3.24 million mm Ha, 3.36 million mm Ha, 2.31 million mm Ha, and 1.79 million mm Ha, respectively, and other crop CWR is shown in Fig. 5.

5 Conclusions

The following are the important findings of the preceding study:

i. The maximum effective rainfall in KLBCA, KRBCA, ULBCA, and URBCA has been estimated to be 206.90 mm (July), 182.44 mm (August), 214.53 mm (July), and 176.99 mm (August), respectively.
ii. The maximum monthly gross irrigation water requirement in KLBCA, KRBCA, ULBCA, and URBCA has been found to be 269.43 MCM (April), 205.42 MCM (May), 149.31 MCM (May), and 103.72 MCM (March), respectively.
iii. The sugarcane has been found to have maximum CWR values in the command area, and its bimonthly CWR values in KLBCA, KRBCA, ULBCA, and URBCA have been estimated to be 3.24 million mm Ha, 3.36 million mm Ha, 2.31 million mm Ha, and 1.79 million mm Ha, respectively, for sugarcane crop.

iv. Such estimated crop water requirement would be useful for development of optimal irrigation planning in the command area.

Acknowledgements The authors would like to acknowledge the Indian National Committee on Climate Change, Ministry of Jal Shakti, Department of Water Resources, River Development and Ganga Rejuvenation, Government of India (GoI), for providing funding for this research. The authors would also appreciate the infrastructural support provided by the Center of Excellence on 'Water Resources and Flood Management', TEQIP-II, Ministry of Education, GoI. All data disseminating agencies, i.e., India Meteorological Department, Pune, Ukai Civil Circle, Central Water Commission, Surat Division and Navsari Agricultural University, Gujarat, are duly acknowledged.

References

1. Allen RG, Pereira LS, Raes D, Smith M (1998) Crop evapotranspiration-guidelines for computing crop water requirements-FAO irrigation and drainage paper 56. Fao, Rome 300(9):D05109
2. Duchemin B, Hadria R, Erraki S, Boulet G, Maisongrande P, Chehbouni A, Simonneaux V (2006) Monitoring wheat phenology and irrigation in Central Morocco: on the use of relationships between evapotranspiration, crops coefficients, leaf area index and remotely sensed vegetation indices. Agric Water Manag 79(1):1–27
3. FAO (Food and Agriculture Organization) Land and Water Division (2021) CROPWAT Software, Available online: http://www.fao.org/landwater/databases-and-software/cropwat/en/
4. Herath IK, Ye X, Wang J, Bouraima AK (2018) Spatial and temporal variability of reference evapotranspiration and influenced meteorological factors in the Jialing River Basin China. Theoret Appl Climatol 131(3):1417–1428
5. Huang X, Luo G, Ye F, Han Q (2018) Effects of grazing on net primary productivity, evapotranspiration and water use efficiency in the grasslands of Xinjiang China. J Arid Land 10(4):588–600
6. López-Urrea R, Montoro A, Mañas F, López-Fuster P, Fereres E (2012) Evapotranspiration and crop coefficients from lysimeter measurements of mature 'Tempranillo' wine grapes. Agric Water Manag 112:13–20
7. Stancalie G, Marica A, Toulios L (2010) Using earth observation data and CROPWAT model to estimate the actual crop evapotranspiration. Phys Chem Earth, Parts A/B/C 35(1–2):25–30
8. Subramanya K (1991) Engineering hydrology. Tata McGraw-Hill, New Delhi
9. Surendran U, Sandeep O, George M, Joseph EJ (2013) A Novel technique of magnetic treatment of saline and hard water for irrigation and its impact on cow pea growth and water properties. J Agri Envt and Biotech 6(1):85–92
10. Taron A, Drechsel P, Gebrezgabher S (2021) Gender dimensions of solid and liquid waste management for reuse in agriculture in Asia and Africa. Colombo, Sri Lanka: International Water Management Institute (IWMI). CGIAR Research Program on Water, Land and Ecosystems (WLE), pp 33
11. Waseem M, Ahmad I, Mujtaba A, Tayyab M, Si C, Lü H, Dong X (2020) Spatiotemporal dynamics of precipitation in southwest arid-agriculture zones of Pakistan 12(6):2305

Estimation of Crop Evapotranspiration and Irrigation Water Requirement for Dharoi Command Area, India

Payal B. Bhujbal, K. B. Baladaniya, P. L. Patel, and P. V. Timbadiya

Abstract The Sabarmati River basin is one of India's most water-scarce delicate basins as far as water availability is concerned. The major source of water in Dharoi command area is storage of water in Dharoi reservoir. The mean rainfall in the Dharoi command area is 633 mm. Optimal water allocation plays a crucial role in irrigation water management. In this study, crop water requirement and irrigation water requirement of different crops are estimated for Dharoi left bank main canal (LBMC) and Dharoi right bank main canal (RBMC) of the command area using the data of period 2001–2016. FAO Penman–Monteith method is used for estimating reference crop evapotranspiration (ET_o) in the command area. The estimated values of reference evapotranspiration (ET_o) have been multiplied with crop coefficient (K_c) of respective crops to obtain their crop evapotranspiration (ET_c) or consumptive use on daily time scale. Further, effective rainfall is estimated using SCS method on monthly time scale. It is subtracted with ET_c of same time scale to obtain the net irrigation requirement (NIR) of the crops in the command area. The results showed that lower ET_o values were found in month of August, while maximum values were reported for May month. Maximum monthly NIR of Dharoi LBMC and RBMC command area is found to be 7.63 MCM and 39.34 MCM, respectively.

Keywords Crop water requirement · Irrigation water requirement · Effective rainfall

P. B. Bhujbal (✉) · K. B. Baladaniya · P. L. Patel · P. V. Timbadiya
Department of Civil Engineering, Sardar Vallabhbhai National Institute of Technology Surat, Surat 395007, India
e-mail: payalbhujbal2911@gmail.com

P. L. Patel
e-mail: plpatel@ced.svnit.ac.in

P. V. Timbadiya
e-mail: pvtimbadiya@ced.svnit.ac.in

P. V. Timbadiya et al. (eds.), *Hydrology and Hydrologic Modelling*,
Lecture Notes in Civil Engineering 312,
https://doi.org/10.1007/978-981-19-9147-9_32

1 Introduction

The water is one of the precious resources and became vulnerable due to changing climatic condition and anthropogenic changes across the globe. Nature has limited amount of water accessible for our usage. Spatiotemporal availability of water has become another challenge for the water user. As water consumption is rising day by day due to overgrowing population, there is a need to have proper water planning to cater the increasing demands of water. Agriculture activity consumes major part of the water in India up to 81 percent, and hence, efficient water management in agriculture sector should be the top focus [13]. Due to urbanization, climate variability, and overgrowing population, water competition has increased significantly in India. For an agricultural field to grow the crops effectively along with rainfall, some supplementary water is required which is supplied through irrigation. Some soils have low water holding capacity which requires frequent irrigation. The command areas having hot weather with low rainfall require significant irrigation. Rabi crops which are mostly cultivated in dry and winter seasons need irrigation. Proper irrigation scheduling increases crop productivity, and fallow land may be converted to cultivable land. Canal irrigation in one of the prevalent irrigation systems in India. It is most popular irrigation system in India after well irrigation [7]. Irrigation water management is a challenging task which includes optimal water allocation to the various crops grown in the command area.

The optimal irrigation planning of a command area can be formulated using the metaheuristics approaches. The availability of water for the irrigation is one of the prerequisites for development of optimal irrigation planning of a command area. The present study aims to obtain the net irrigation requirement of the Dharoi command area using the availability of data on cropping pattern, rainfall, and weather data of the same command area. The results will be useful for optimal water allocation and increasing the efficiency of the irrigation system.

2 Study Area and Data Collection

2.1 Study Area

The Sabarmati River, one of India's major west-flowing rivers, rises from the Aravalli Mountains at an elevation of 762 m near Tepur in Rajasthan's Udaipur district. The Sabarmati basin spans the states of Rajasthan and Gujarat, covering 21674 km^2 with maximum length and width of 300 and 150 km, respectively. Sabarmati basin lies between 70°58′ to 73°51′ east and 22°15′ to 24°47′ north, and the total length of river from origin to outfall into the Arabian Sea is 371 km. The Sabarmati (Dharoi) irrigation project is located on the Sabarmati River near village Dharoi in Kheralu taluka of Mehsana district, which is 103 km from the river's source. The project comprised a composite dam across Sabarmati River having ogee-type spillway of

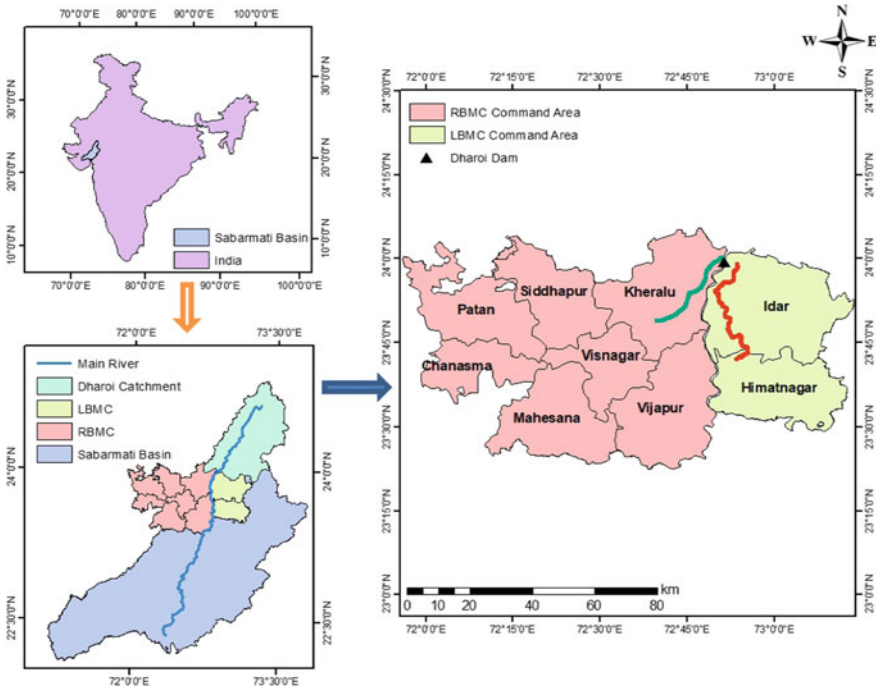

Fig. 1 Index map of study area

length 219 m. The length at the top of dam is 1207 m, and maximum height above the lowest point of foundation is 46 m. The catchment area of this project is 5539.98 square kilometers with live storage capacity of the reservoir which is 776.5 MCM and gross storage capacity which is 908.6 MCM. The estimated cost of the project is Rs. 125.74 crores. Total CCA of the project is 57.99*103 ha with ultimate irrigation potential of 64.75*103 ha. The index map of the Dharoi catchment is shown in Fig. 1.

Despite significant surface water supply difference, the cropping pattern in the Dharoi Irrigation Project is fairly similar; groundwater is exploited to make up for the deficiency in surface water supplies. Major crops present in Dharoi command area are castor, wheat, cotton, mustered, fennel, fodder, sesame. Cropping patterns and area allocated to various crops are estimated to remain relatively unchanged, although increasing surface water availability combined with agricultural support will result into increase in yields.

2.2 Data Collection

2.3 Meteorological Data

The daily meteorological data from 2001 to 2016 of Dharoi catchment are collected from State Water Data Center (SWDC), Gandhinagar. The data included rainfall data of various stations and other weather data. Badoli, Dharoi (Sabarmati Dam), Himatnagar, Kabola, Khandiol, Khedbrahma, Kundla campo, Lalpur, Mankadi, Prantij, Ransipur, Red Laxmi, Sabli, Vajepur, Virpur are the rain gauging stations contributed to Dharoi LBMC. Ambaliyasan, Dharoi (Sabarmati Dam), Dhinoj, Gadh, Kanodar, Katosan (Dhanpura), Khandosan, Lalpur, Mansa, Patan, Prantij, Ransipur, Ranuj, Red Laxmi, Sitapur, Umbari, Vadgam are the rain gauging stations contributed to Dharoi RBMC as shown in Fig. 2.

Daily maximum temperature, daily minimum temperature, average wind speed, daily sunshine hours, daily maximum relative humidity, daily minimum relative humidity are included in weather data. Dharoi (Sabarmati Dam), Kabola, Khandiol, Khedbrahma, Mankadi, Prantij, Red Laxmi, Vajepur are the weather stations contributed to Dharoi LBMC, and Dharoi (Sabarmati Dam), Gandhinagar, Khandiol, Prantij, Red Laxmi, Sanand are the weather stations contributed to Dharoi RBMC as shown in Fig. 3.

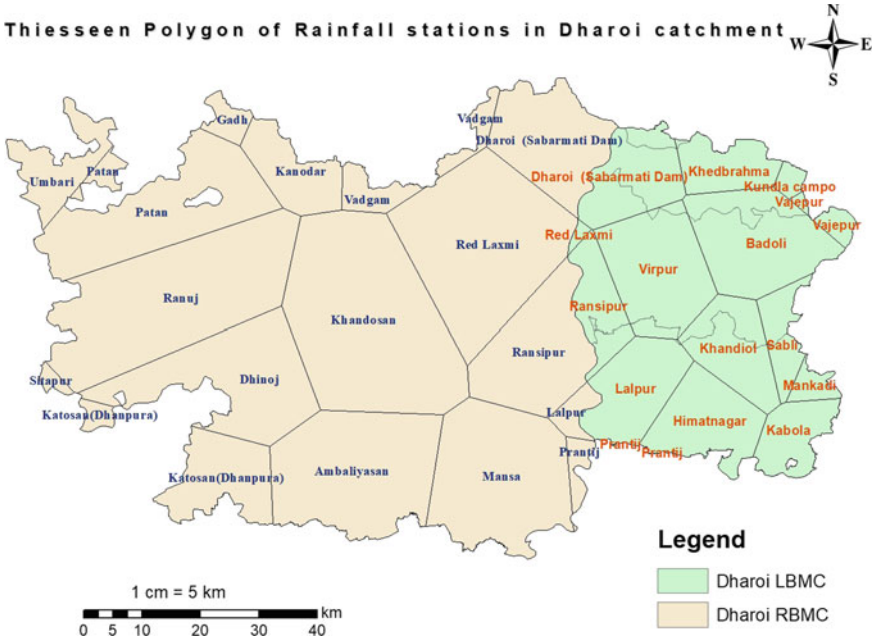

Fig. 2 Rainfall stations in study area

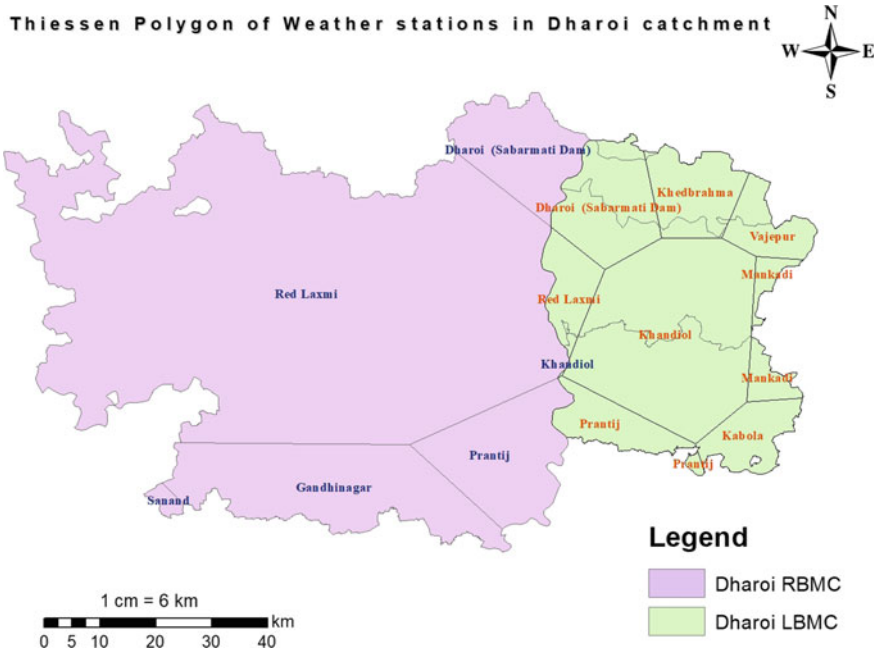

Fig. 3 Weather stations in study area

2.4 Crop Data

The crop data included crop coefficients and present cropping pattern in Dharoi command area. These data are collected from Dharoi irrigation office, Visnagar.

2.5 Weighted Average Data

The station rainfall data are converted to areal rainfall using Thiessen polygon method. Thiessen polygon is created using rainfall stations to determine the area that is contributed to each station. The weightages are given to the stations according to the area contributed to the rainfall as per Thiessen polygon. Weighted average rainfall is calculated on daily basis. In similar manner, weighted average reference evapotranspiration is calculated.

3 Methodology

3.1 Reference Evapotranspiration (ET_o)

ET_o is estimated for daily time scale using Eq. (1). The data required for calculations are daily maximum and minimum temperatures, relative humidity, actual duration of sunshine and average wind speed [5].

$$ET_o = \frac{0.408\Delta(R_n - G) + \gamma \frac{900}{T+273} u_2 (e_s - e_a)}{\Delta + \gamma(1 + 0.34u_2)} \tag{1}$$

where ET_o is reference evapotranspiration [mm/day], R_n is net radiation at the crop surface [MJ/m^2/day], G is soil heat flux density [MJ/m^2/day], T is mean daily air temperature at 2 m height [°C], u_2 is wind speed at 2 m height [m/s], e_s is saturation vapor pressure [kPa], e_a is actual vapor pressure [kPa], $(e_s - e_a)$ is saturation vapor pressure deficit [kPa], Δ is slope vapor pressure curve [kPa/°C], and γ is psychrometric constant [kPa/°C].

e_s is calculated using maximum and minimum temperatures as per Eq. (2) and Eq. (3), and e_a is given by Eq. (4).

$$e^o(T) = 0.6108 \exp\left(\frac{17.27T}{T + 237.3}\right) \tag{2}$$

$$e_s = \frac{e(T_{\max}) + e(T_{\min})}{2} \tag{3}$$

where $T_{\max}$ is the maximum temperature (°C), $T_{\min}$ is the minimum temperature (°C), and e_s is saturation vapor pressure [kPa].

$$e_a = \frac{e(T_{\min}) \frac{RH_{\max}}{100} + e(T_{\max}) \frac{RH_{\min}}{100}}{2} \tag{4}$$

where $RH_{\max}$ is maximum relative humidity [%], $RH_{\min}$ is minimum relative humidity [%], and e_a is actual vapor pressure [kPa].

$$\Delta = \frac{4098(0.6108 \exp\left(\frac{17.27T}{T+237.3}\right)}{(T + 237.3)^2} \tag{5}$$

where Δ is slope of saturation vapor pressure curve at air temperature T [kPa/°C], and T is air temperature [°C] in Eq. (5). Net radiation, net shortwave radiation, incoming solar radiation, and net longwave radiation are calculated using Eqs. (6), (7), (8) and (9), respectively.

$$R_n = R_{ns} - R_{nl} \tag{6}$$

$$R_{ns} = 0.77 \times R_s \tag{7}$$

$$R_s = 0.75 \times R_a \tag{8}$$

$$R_{nl} = \sigma \frac{(T_{\max} + 273.3)^4 + (T_{\min} + 273.3)^4}{2} \times \left(0.34 - 0.14\sqrt{e_a}\right) \times \left(1.35\frac{R_s}{R_{so}} - 0.35\right) \tag{9}$$

where R_{ns} is the net shortwave radiation [MJ/m^2/day]; R_{nl} is the net longwave radiation [MJ/m^2/day]; R_s is the incoming solar radiation [MJ/m^2/day]; Ra is the extraterrestrial solar radiation [MJ/m^2/day], σ is the Stefan–Boltzmann constant [4.903 × 10^{-9} MJ/m^2/day]; $T_{\max}$ and $T_{\min}$ are the maximum and minimum temperatures, respectively [°C]; and R_{so} is the clear sky solar radiation [MJ/m^2/day].

3.2 Crop Water Requirement

It is the amount of water lost from a crop during evapotranspiration (ET_c) and given by Eq. (10) [5].

$$\text{CWR} = ET_c = K_c \times ET_o \tag{10}$$

where ET_c is the crop evapotranspiration [mm]; K_c is the crop coefficient at a particular growing stage (dimensionless); and ET_o is the reference evapotranspiration [mm].

3.3 Effective Precipitation (P_{eff})

Effective precipitation (P_{eff}) is calculated for daily scale using Soil Conservation Service (SCS) method [3] in Eqs. (11) and (12).

$$P_{\text{eff}} = \frac{P \times (125 - 0.2P)}{125} \quad P \leq 250\,\text{mm} \tag{11}$$

$$P_{\text{eff}} = 125 + 0.1 \times P \quad P > 250\,\text{mm} \tag{12}$$

where P_{eff} is monthly average effective rainfall, and P is total monthly rainfall.

3.4 Net Irrigation Requirement (NIR)

NIR is IWR to meet evapotranspiration need of a crop as well as other needs such as leaching (special needs) as Eq. (13) [5].

$$\text{NIR} = \text{CWR} - P_{\text{eff}} + \text{Special needs} \tag{13}$$

where NIR is net irrigation requirement [mm], CWR is crop water requirement [mm], and P_{eff} is effective rainfall [mm].

4 Results and Discussions

4.1 Estimation of ET_o

On daily time scale, the ET_o values are calculated and later converted to monthly scale. The maximum value of ET_o is found in May (i.e., 481.85 mm) and the minimum value is observed in August (i.e., 78.88 mm) for Dharoi LBMC command area. The maximum value of ET_o is found in May (i.e., 471.62 mm) and the minimum value is observed in August (i.e., 78.28 mm) for Dharoi RBMC command area as per Fig. 4. X-axis is plotted as per calendar year (January to December).

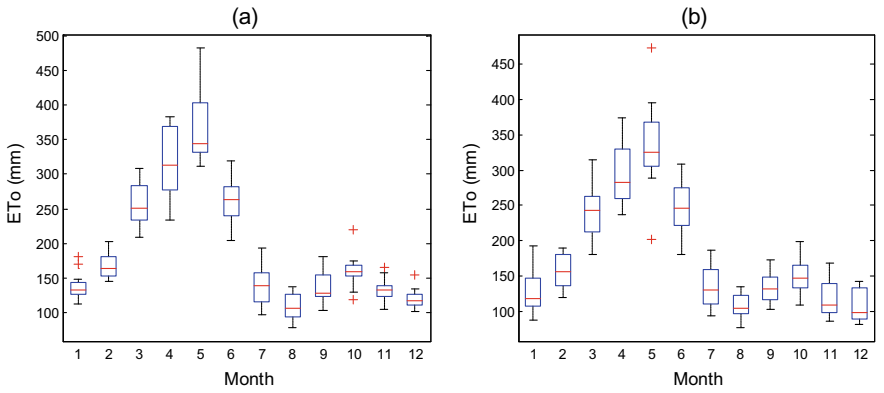

Fig. 4 ET_o of Dharoi **a** LBMC **b** RBMC command area

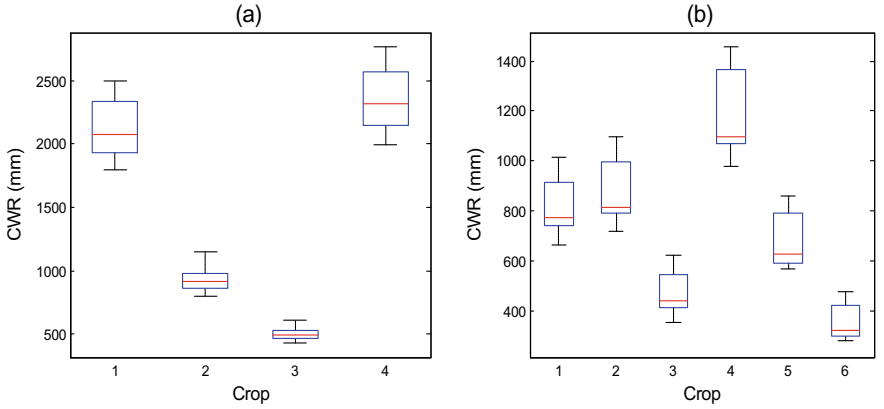

Fig. 5 CWR of Dharoi **a** LBMC **b** RBMC command area. (where 1 = cotton/tobacco; 2 = castor/raido; 3 = wheat; 4 = other; 5 = variyali/vegetable; 6 = juwar/bajari)

4.2 Estimation of CWR

CWR value for Dharoi LBMC and Dharoi RBMC command areas is computed separately for each crop from 2001 to 2016. Maximum yearly CWR values for cotton/tobacco (kharif + rabi), castor/raido (kharif + rabi), wheat, and other (kharif + rabi) present in LBMC command area are 2494.3, 1146.8, 614.7, and 2763.2 mm, respectively, and minimum value observed is 436.7 for wheat. Maximum yearly CWR values for cotton/tobacco (kharif + rabi), castor/raido (kharif + rabi), variyali/vegetable, juwar/bajari, mustered/ rajko, wheat, and other (kharif + rabi) present in RBMC command area are 1015.9, 1097.5, 862.6, 477.2, 563.3, 624.6, and 1455.5 mm, respectively, and minimum value observed is 282.6 mm for juwar/ bajari as shown in Fig. 5.

4.3 Estimation of the $\mathbf{P}_{eff}$ *and NIR*

Irrigation water requirement is decided by effective rainfall. Lower the effective rainfall, higher the water required for irrigation. Maximum monthly NIR of Dharoi LBMC and RBMC command areas is 7.63 MCM and 39.34 MCM, respectively, as per Fig. 6. The X-axis is plotted as per calendar year (January to December).

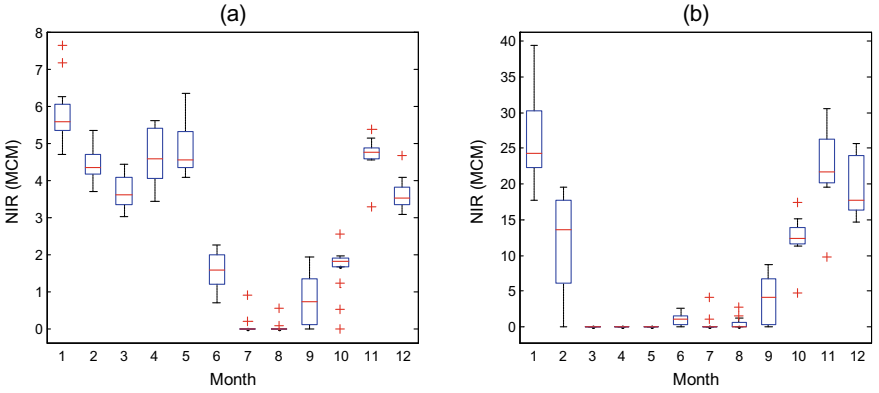

Fig. 6 NIR of Dharoi **a** LBMC **b** RBMC command area

5 Conclusions

In the present study, crop water requirement and irrigation water requirements of Dharoi LBMC and RBMC command areas are computed. The following are the key findings of the present study:

- The Dharoi LBMC and RBMC command areas have higher reference evapotranspiration (ET_o) in month of May (481.85 mm and 471.62 mm for LBMC and RBMC command areas, respectively) and lower ET_o in August (78.88 and 78.28 mm for LBMC and RBMC command areas, respectively).
- From June month onward, ET_o values are found to decrease consistently till December month.
- Maximum monthly NIR of Dharoi LBMC and RBMC command areas is 7.63 and 39.34 MCM, respectively, during January month.

Acknowledgements The authors are thankful to State Water Data Center (SWDC) and Dharoi irrigation office, Visnagar, for providing necessary daily meteorological data and crop data, respectively, to conduct the present study.

References

1. Allen RG, Pereira LS, Smith M, Raes D, Wright JL (2005) FAO-56 dual crop coefficient method for estimating evaporation from soil and application extensions. J Irrig Drain Eng 131(1):2–13
2. Allen RG (2006) FAO irrigation and drainage paper crop by 56
3. Ashofteh PS, Haddad OB, A Mariño M (2013) Climate change impact on reservoir performance Indexesin agricultural water supply. J Irrigation and Drainage Eng 139(2):85–97
4. Beshir S (2017) Review on estimation of crop water requirement, irrigation frequency and water use efficiency of cabbage production. J Geosci Environ Protect 05(07):59–69

5. FAO (1998) Crop evapotranspiration: guidelines for computing crop water requirements. FAO irrigation and drainage paper 56. Rome, Italy
6. FAO (2009) Cropwat 8.0 for windows user guide. Rome, Italy
7. Garg SK (2005) Irrigation engineering and hydraulic structure
8. Khaydar D, Chen X, Huang Y, Ilkhom M, Liu T, Friday O, Farkhod A, Khusen G, Gulkaiyr O (2021) Investigation of crop evapotranspiration and irrigation water requirement in the lower Amu Darya River Basin Central Asia. J Arid Land 13(1):23–39
9. López-Urrea R, Montoro A, Mañas F, López-Fuster P, Fereres E (2012) Evapotranspiration and crop coefficients from lysimeter measurements of mature 'Tempranillo' wine grapes. Agric Water Manag 112:13–20
10. Mehta R, Pandey V (2016) Crop water requirement (ETc) of different crops of middle Gujarat. J Agrometeorol 18(1):83–87
11. Moratiel R, Martínez-Cob A, Tarquis AM, Snyder RL (2016) Soil water balance correction due to light rainfall, dew and fog in Ebro river basin (Spain). Agric Water Manag 170:61–67
12. Srivastava RK, Panda RK, Chakraborty A, Halder D (2018) Comparison of actual evapotranspiration of irrigated maize in a sub-humid region using four different canopy resistance based approaches. Agric Water Manag 202:156–165
13. Surendran U, Sushanth CM, Mammen G, Joseph E J (2015) Modelling the crop water requirement using FAO-CROPWAT and assessment of water resources for sustainable water resource management: a case study in Palakkad District of Humid Tropical Kerala, India. Aquatic Proc 4(Icwrcoe):1211–1219
14. Tan M, Zheng L (2019) Increase in economic efficiency of water use caused by crop structure adjustment in arid areas. J Environ Manage 230:386–391

Spatiotemporal Variation of Interception in an Agriculture Watershed—Tadepalligudem, West Godavari, India

Rajkumar Tammisetti, Reshma Talari, and Savitha Chirasmayee

Abstract Interception refers to the quantity of rainfall prevented by vegetation from reaching the soil surface, which is one of the significant and integral parts of the hydrological cycle. Most hydrological models depend on the water balance components, where the rainfall intercepted by vegetation is considered a loss. It is an essential and controlling parameter in hydrological modeling studies and flood forecasting analysis, thus establishing that its impacts at local, regional, and global scales are imminent. Remote sensing is one of the advanced techniques that helps generate a spatiotemporal variation of interception by vegetation canopy. The present study aimed to generate spatiotemporal variation interception maps for an agricultural watershed covering 53.75 km^2 of the area near Tadepalligudem, West Godavari district, Andhra Pradesh. The study area is covered with vegetation cover that constitutes about 40–55% of the total catchment; thus, interception is a critical component in hydrological modeling studies in this watershed. Landsat 8 datasets acquired from USGS EarthExplorer during different months of 2020 are used in this study. Leaf area index (LAI) and canopy storage capacity (S_{max}) are the influential parameters in estimating canopy rainfall interception. The interception maps at varying spatial and temporal scales are generated using MATLAB programming platform. The result obtained gives a better understanding of the spatiotemporal variation of interception and its importance at a regional scale. The canopy rainfall interception model derived can be applied to various agriculture watersheds. Further, results obtained from the analysis can be used in rainfall–runoff modeling and water resource management studies.

Keywords Interception · Remote sensing · Leaf area index · Canopy storage capacity

R. Tammisetti (✉) · R. Talari · S. Chirasmayee
Department of Civil Engineering, National Institute of Technology, Tadepalligudem, Andhra Pradesh 543101, India
e-mail: rajkumar.sclr@nitandhra.ac.in

R. Talari
e-mail: reshma@nitandhra.ac.in

P. V. Timbadiya et al. (eds.), *Hydrology and Hydrologic Modelling*,
Lecture Notes in Civil Engineering 312,
https://doi.org/10.1007/978-981-19-9147-9_33

1 Introduction

Interception is one of the critical parameters of the hydrological process, which indicates the amount of precipitation lost due to vegetation interception. Interception is a crucial process because it influences other hydrological processes like an infiltration, evapotranspiration, runoff generation, and flood generation [1, 2]. Considering interception by vegetation as an essential parameter of the hydrological processes in the water balance cycle helps achieve accurate runoff estimation analysis [3]. Interception also plays a vital role in water resource management and climate change. The appraisal of vegetation canopy interception is remarkably significant for describing and interpreting water cycling and has possible suggestions for land use–land cover planning and water and soil conservation [4].

The interception by vegetation cannot be determined directly. Interception is usually estimated as the difference between total rainfall and the sum of stem flow and through fall [5, 6] which is generally determined by studying an individual plant or group of plantations. Although collecting data from individual plants or groups of plantations gives high estimation accuracy, it is an expensive and time-consuming process and also interpolating it to a large study area becomes a difficult task. Modeling provides an excellent solution to generate a spatiotemporal variation of interception to a large study area in a short time [7, 8]. Canopy storage capacity ($S_{\max}$) is one of the critical parameters mentioned in best existing models like the Rutter model [9, 10] and Gash model [11], which indicated that excess rainfall would most likely result in water overflow through the canopy and toward the canopy ground surface [3, 5]. So, canopy storage capacity controls the rainfall interception by vegetation cover [12–14]. Studies showed that canopy storage capacity could be derived using leaf area index (LAI), which is generated using remote sensing data [15, 16]. Remote sensing is emerging as an effective tool for studying spatial and temporal variations of the land surface, which covers a wide range of vegetation indices used in this study. The study area (Tadepalligudem region) falls tropical part of India and is also close to Godavari delta regions with very fertile soil. The study area is covered a quality amount of vegetation throughout the year, so rainfall interception by the canopy plays a significant part in runoff analysis.

Most studies have been focused on estimating interception using a Geographic Information System (ArcGIS), which requires you to give the numerical equations as input in using a Raster Calculator tool each time to perform the analysis. The present study is aimed to develop a canopy rainfall interception model using a programming language for the estimation of rainfall loss due to vegetation in the form of interception. Landsat 8 satellite data with 30 m resolution is used as an input in the model. Maps are generated for different periods in 2019, 2020 and 2021, using the canopy rainfall interception model for three different precipitation scenarios. This model gives a better understanding of the relation between canopy storage capacity ($S_{\max}$), canopy rainfall interception (S_v), and precipitation. This estimated interception by vegetation could be further used in assessing the water balance cycle and hydrological analysis within this study region.

2 Materials and Methods

2.1 Study Area

The study area falls between 81° 28′ and 81° 32′ 30″ east longitude and 16°48′ 30″ and 16° 54′ 30″ north latitude. Figure 1 shows the location of the study area in the Tadepalligudem region of West Godavari district (Andhra Pradesh). The total area covered under the study region is about 53.75 km^2. It experiences tropical climate conditions with summer temperatures ranging from 38° to 45°C and winter temperatures ranging from 15° to 28°C.

The soil distribution in the region mainly falls under the clay soil's (black cotton soils) category with a mix of silt. The grounds are very fertile, which produce about two to three harvests in a year. Rice is the major crop in this region. Though there are enough rainfalls in the area, most agriculture depends on groundwater due to the lack of proper rainfall water storage, watershed management practices, and distribution network.

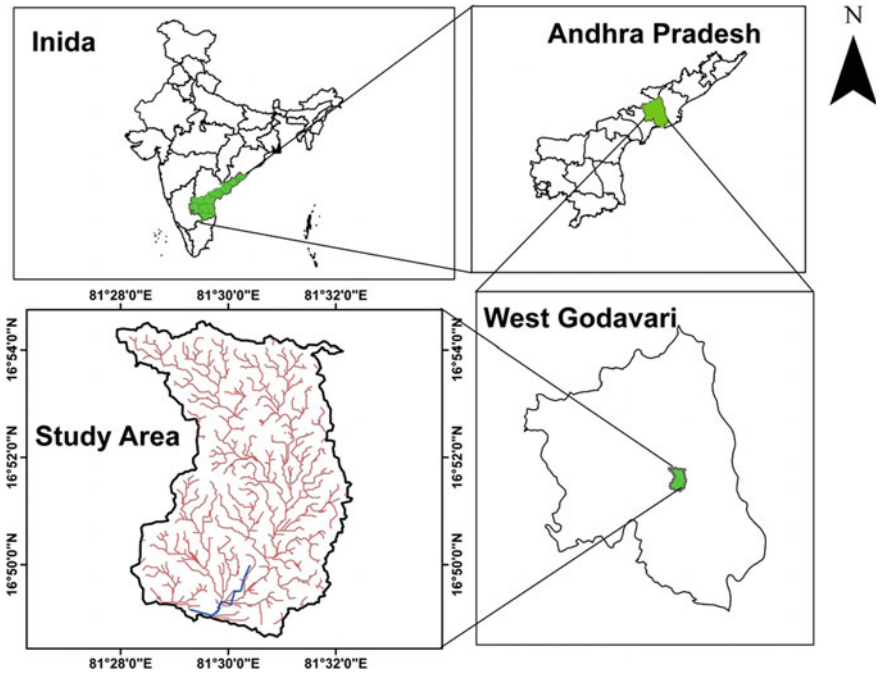

Fig. 1 Location map of study area

Table 1 Details of data used

Type	Details	Source
Toposheets	Nos. 65 H/9 SW and 65 H/5 SE at 1:25,000 scale	Survey of India (SOI)
Satellite data	Landsat 8 band data for the years 2019, 2020 and 2021 at 30 m resolution	USGS EarthExplorer
Rainfall data	Rainfall in mm	Automatic Weather Station at NIT Andhra Pradesh, Tadepalligudem

2.2 Data Collection

Table 1 shows the details of the data used and its sources. Toposheets of no's 65 H/9 SW and 65 H/5 SE, which are of 1:25,000 scale, were purchased from the Survey of India (SOI).

These toposheets are used in delineating watershed boundary as shown in Fig. 1. USGS EarthExplorer, an open-source (https://earthexplorer.usgs.gov/), is used to acquire the Landsat 8 satellite data. Downloaded Landsat 8 cloud-free band datasets are covering the study area during November 2019, October 2020, and March 2021 which are used in the study. Rainfall data used in the study are collected from Automatic Weather Station which located at $16^{O}50'02.7''$ north latitude and $81^{O}29'09''$ east longitude covering the study region.

2.3 Methodology

Figure 2 shows the flowchart representation of the methodology followed in this study. Watershed boundary is delineated using the toposheets purchased. The boundary delineated is further used on Landsat 8 band data to clip the datasets to the boundary scale. Landsat 8 datasets are used in the generation of Normalized Difference Vegetation Index (NDVI) and Soil-Adjusted Vegetation Index (SAVI) maps. SAVI is used in the generation of LAI maps; this LAI is further used in the generation of canopy storage capacity (S_{max}). LAI, canopy storage capacity, and rainfall data are used in the interception model to generate spatiotemporal variation maps of canopy rainfall interception.

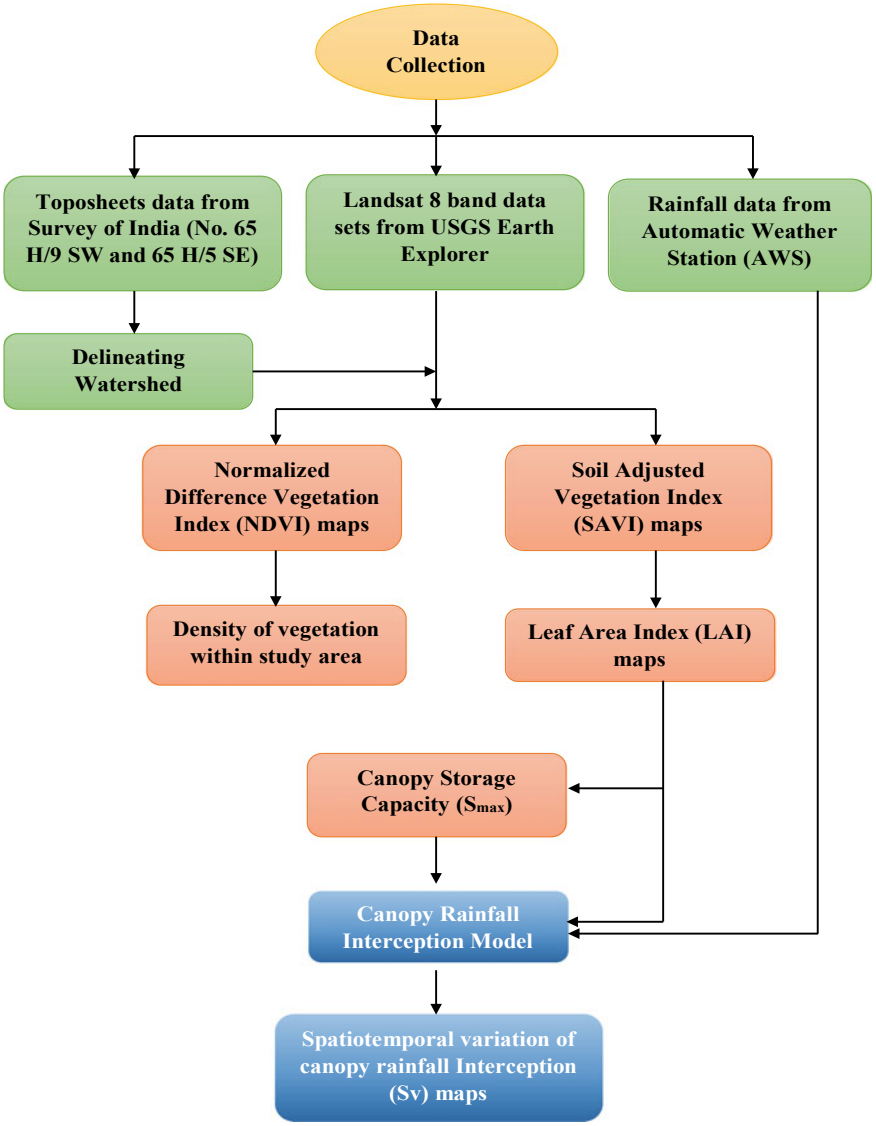

Fig.2 Flow chart of methodology

2.4 Selection of Input parameters

2.5 Normalized Difference Vegetation Index (NDVI)

Normalized Difference Vegetation Index (NDVI) is one of the indexes derived using remote sensing data. It is a dimensionless parameter that ranges from −1 to + 1. It is used as an indicator to understand the density of vegetation cover. The higher value of NDVI indicates healthy vegetation cover. The NDVI map for Landsat 8 satellite is generated using Eq. (1).

$$\text{NDVI} = \frac{\text{Band 5} - \text{Band 4}}{\text{Band 5} + \text{Band 4}} \tag{1}$$

Band 5 indicated near-infrared (NIR) band, and Band 4 indicated red band.

2.6 Soil-Adjusted Vegetation Index (SAVI)

Soil-Adjusted Vegetation Index (SAVI) is another vegetation index derived using remote sensing data. It is used as a correction to NDVI to minimize the impact of soil brightness in low vegetation cover regions by using the soil brightness correction factor. SAVI is given by Delegido et al. [17], as shown in Eq. (2).

$$\text{SAVI} = \frac{(\text{Band 5} - \text{Band 4})}{(\text{Band 5} + \text{Band 4} + L)} \times (1 + L) \tag{2}$$

Band 5 indicated the near-infrared (NIR) band, Band 4 indicated the red band, and L is the soil brightness correction factor. L is taken as 1 in case of no vegetation, 0.5 in moderate vegetation conditions, and 0 in high dense vegetation scenarios [17]. In this study area, L is taken as 0.5.

2.7 Leaf Area Index (LAI)

Leaf area index (LAI) is used to indicate the rate of vegetation growth in an area. It is defined as the total one-sided leaf area per unit ground surface area [18, 19]. LAI from the METRIC method is given by De Wasseige et al. [20], as shown in Eq. (3).

$$\text{LAI} = -\frac{\ln\left(\frac{0.69 - \text{SAVI}}{0.59}\right)}{0.91} \tag{3}$$

where SAVI is the Soil-Adjusted Vegetation Index.

2.8 Canopy Rainfall Interception Model

The primary factor in estimation interception by vegetation is the canopy storage capacity ($S_{\max}$). Canopy storage capacity, also known as the maximum interception storage capacity, is given by [21], as shown in Eq. (4).

$$S_{\max} = 0.935 + (0.498 \times \text{LAI}) - \left(0.00575 \times \text{LAI}^2\right) \tag{4}$$

where LAI is the leaf area index.

Canopy cumulative interception during a rainfall event is given by Aston [22] which is modified from [23] as shown in Eq. (5).

$$S_v = S_{\max} \times \left[1 - \mathrm{e}^{-\eta \frac{P_{\text{cum}}}{S_{\max}}}\right] \tag{5}$$

where S_v represents canopy rainfall interception in mm, P_{cum} shows the value of cumulative precipitation in mm for a rainfall event, and η is the correction factor ($\eta = 0.046 \times$ LAI).

The assumption made by Aston [22] for Eq. (5) is: if cumulative rainfall is equal to zero, then canopy rainfall interception is also zero. But, in the case of cumulative rainfall approaching infinity, then canopy rainfall interception is equal to canopy storage capacity.

3 Results and Discussions

3.1 Spatiotemporal Variation Patterns of NDVI

NDVI maps are generated using Eq. (1). The maps are generated for the years 2019, 2020, and 2021 as shown in Fig. 3. It is observed that the value of NDVI is within the range of −1 to + 1. The maximum value of NDVI is 0.548, 0.39, and 0.45 in the year 2019, 2020, and 2021, respectively. There is a decrease in NDVI value in the year 2020, because it is crop harvesting and sowing period. The study area contains fertile soil with good agricultural conditions, and it is observed that vegetation coverage is seen at almost 75% (considering three months as the gap between harvesting and sowing for each crop season) of the year. It is noted that the maximum NDVI value ranges from 0.4 to 0.55 in the study area, indicating a good density of vegetation cover in the study area.

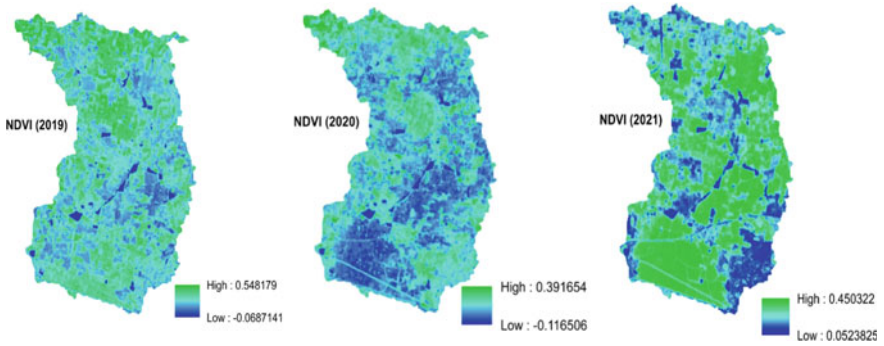

Fig. 3 Spatial patterns of NDVI in study area

3.2 Spatiotemporal Variation Patterns of LAI

LAI maps are generated using Eqs. (3) and (4). LAI maps for the years 2019, 2020 and 2021 are shown in Fig. 4. The LAI indicates the growth rate of vegetation, so the high value indicates a reasonable growth rate. It can be observed that for the year 2019, though the maximum LAI value is 9.55, the area under that category of high LAI value is very low; most of the study area is in the range of −0.325 to 4.612, so the average LAI is approximately 2.143. For 2020, it can be spotted that most of the study area is under the LAI value of 0.75 or below. But, for 2021, the maximum LAI value of 4.07 is observed in 50% of the study area. The average LAI value decreased from 2.143 in 2019 to 0.75 in 2020, mainly because the data collected for 2020 are in October, during which seasonal crop change occurs. The average value of LAI in 2021 increased to 2.01. LAI values generated can support the study area which has good fertile soil, which can harvest two or three crop seasons in a year.

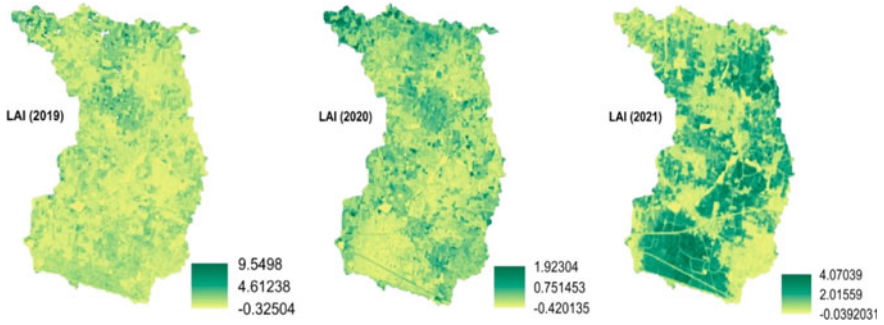

Fig. 4 Spatial patterns of LAI in study area

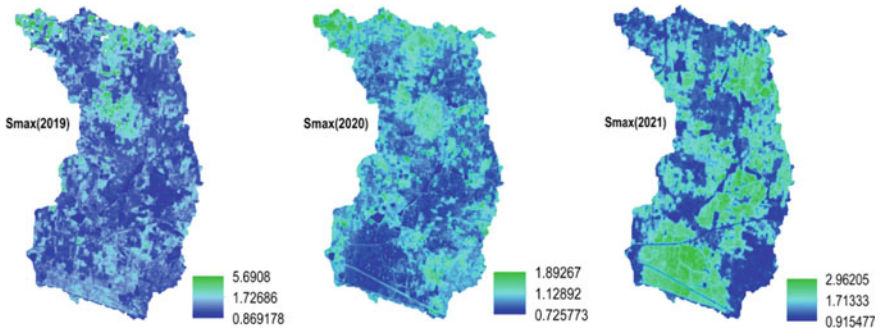

Fig. 5 Spatial patterns of canopy storage capacity ($S_{\max}$) in study area

3.3 Spatiotemporal Variation Patterns of Canopy Storage Capacity (S_{max})

Canopy storage capacity ($S_{\max}$) is the maximum quantity of interception that the canopy can store. Canopy storage capacity maps are generated using Eq. (4) of canopy rainfall interception model. Canopy storage capacity maps for the years 2019, 2020, and 2021 are shown in Fig. 5. Similar to the LAI maps, though the maximum canopy storage capacity value was high in 2019, the area covered under that increased value is minimal. So, it is better to consider average values for all the years. The average canopy storage capacity value for 2019, 2020, and 2021 is 1.726, 1.28, and 1.71, respectively. It is a good indicator that interception plays a crucial role in the hydrological cycle. So, interception cannot be neglected in the hydrological studies for this region.

3.4 Spatiotemporal Variation Patterns of Canopy Rainfall Interception (S_v)

Canopy rainfall interception (S_v) maps are generated using Eq. (5) of canopy rainfall interception model. The value ranges in the maps indicate the canopy rainfall interception with the unit of mm. One of the components in canopy rainfall interception estimation is cumulative rainfall (mm). The study is conducted for three rainfall events to understand the variation in canopy rainfall interception with changes in precipitation. The rainfall events over the years 2019, 2020 and 2020 are categorized as maximum cumulative rainfall event, moderate cumulative rainfall event, and low cumulative rainfall event. The cumulative rainfall amounts considered in the study are:

(i) Maximum cumulative rainfall = 165.25 mm
(ii) Moderate cumulative rainfall = 40 mm
(iii) Low cumulative rainfall = 15 mm

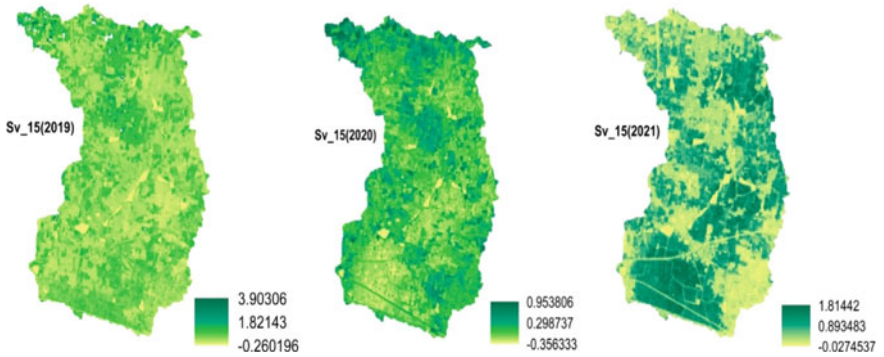

Fig. 6 Spatial patterns of canopy rainfall interception (S_v) for 15 mm rainfall event in study area

The maximum rainfall of 165.25 mm in the study area occurred during the 12th and 13th of October 2020. The maps are generated for each rainfall event. A total of nine maps are developed for different periods and with varying amounts of precipitation.

Canopy rainfall interception (S_v) maps during 15 mm of precipitation for the years 2019, 2020, and 2021 are shown in Fig. 6. From the generated maps, it is observed that a significant portion of the surface area is contributing to interception. The canopy rainfall interception values for 15 mm rainfall event are 1.83, 0.95 and 1.81 mm during 2019, 2020, and 2021, respectively. It indicates that for the 15 mm quantity of rainfall received, on average, 1.53 mm of rainfall received is lost in the form of interception.

Canopy rainfall interception (S_v) maps during 40 mm of precipitation for the years 2019, 2020, and 2021 are shown in Fig. 7. From the generated maps, it is observed that a significant portion of the surface area is contributing to interception. The canopy rainfall interception values for 40 mm rainfall events are 2.26, 1.6 and 2.72 mm during 2019, 2020, and 2021, respectively. It indicates that for the 40 mm quantity of rainfall received, on average, 2.2 mm of rainfall received is lost in the form of interception.

Canopy rainfall interception (S_v) maps during 165 mm of precipitation for the years 2019, 2020, and 2021 are shown in Fig. 8. From the generated maps, it is observed that the maps of the canopy rainfall interception values for 165 mm rainfall events are 5.69, 1.89 and 2.96 mm during 2019, 2020, and 2021, respectively. It indicates that for the 165 mm quantity of rainfall received, on average, 3.5 mm of rainfall is lost in the form of interception.

If you observe Figs. 5 and 8, the maximum values for both canopy storage capacity ($S_{\max}$) and canopy rainfall interception (S_v) for 165 mm rainfall events are the same proving the assumption made by [22]. In the study area, it is recognized that the maximum storage capacity of vegetation is reached when the cumulative rainfall is above 40 mm and under 165 mm.

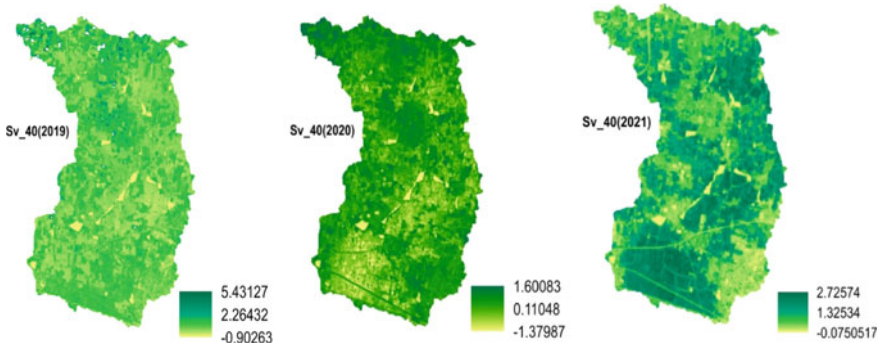

Fig. 7 Spatial patterns of canopy rainfall interception (S_v) for 40 mm rainfall event in study area

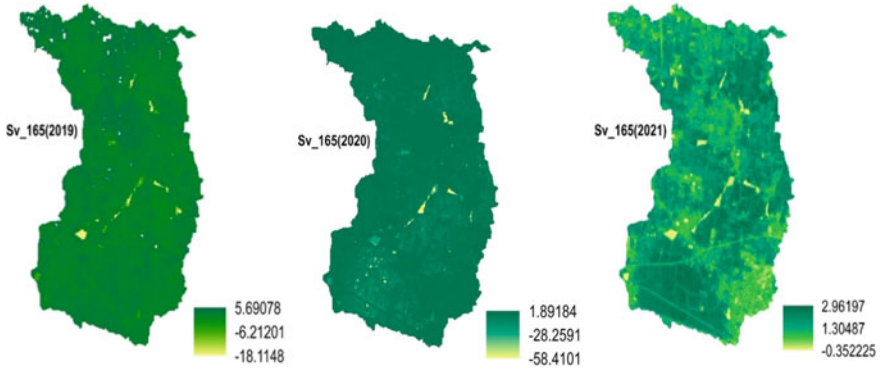

Fig. 8 Spatial patterns of canopy rainfall interception (S_v) for 165 mm rainfall event in study area

4 Conclusions

The canopy rainfall interception is being effectively assessed with the combination of remote sensing and interception model. The outcomes offer insight into the variation of canopy rainfall interception at both spatial and temporal scales within the study area. Depending on the rainfall event, nearly 1–5.7 mm of rainfall received is being lost due to the interception by vegetation over the years 2019–2021; it is apparent that a significant quantity of precipitation is lost in the form of interception in areas covered with vegetation and crops. Hence, it can be acknowledged that interception plays a significant role in the hydrological processes even at a regional scale. The present methodology applies to micro to medium level watersheds in different geographical regions. The interception results obtained from this study will be helpful for rainfall and runoff studies within the study area.

Acknowledgements This research is funded by the Department of Science and Technology-Science and Engineering Research Board (DST-SERB) sponsored project bearing the sanction

number EEQ/2019/000463 undertaken in the Department of the Civil Engineering, NIT Andhra Pradesh, titled Monitoring and Analysis Nonpoint Source Pollutants in Agricultural Watershed using Soil Water Assessment Tool (SWAT) under Principal Investigation of Dr T. Reshma Assistant Professor.

References

1. Murakami S (2006) A proposal for a new forest canopy interception mechanism: splash droplet evaporation. J Hydrol 319:72–82. https://doi.org/10.1016/j.jhydrol.2005.07.002
2. Tsiko CT, Makurira H, Gerrits AMJ, Savenije HHG (2012) Measuring forest floor and canopy interception in a savannah ecosystem. Phys Chem Earth Parts ABC 47–48:122–127. https://doi.org/10.1016/j.pce.2011.06.009
3. Zhang Y, Li XY, Li W, et al (2017) Modeling rainfall interception loss by two xerophytic shrubs in the Loess Plateau
4. Wu J, Liu L, Sun C et al (2019) Estimating rainfall interception of vegetation canopy from MODIS imageries in Southern China. Remote Sens 11:1–19. https://doi.org/10.3390/rs11212468
5. Dunkerley D (2000) Measuring interception loss and canopy storage in dryland vegetation: a brief review and evaluation of available research strategies. Hydrol Process 14:669–678. https://doi.org/10.1002/(SICI)1099-1085(200003)14:4%3c669::AID-HYP965%3e3.0.CO;2-I
6. Carlyle-Moses DE, Laureano JSF, Price AG (2004) Throughfall and throughfall spatial variability in Madrean oak forest communities of northeastern Mexico. J Hydrol 297:124–135. https://doi.org/10.1016/j.jhydrol.2004.04.007
7. Peng H, Zhao C, Shen W et al (2009) Modeling canopy interception of Piceacrassifolia forest in Qilian Mountains using quickbird satellite data. Int Geosci Remote Sens Symp IGARSS 4:370–373. https://doi.org/10.1109/IGARSS.2009.5417390
8. Cui Y, Zhao P, Yan B et al (2017) Developing the remote sensing-gash analytical model for estimating vegetation rainfall interception at very high resolution: a case study in the Heihe River Basin. Remote Sens 9:1–12. https://doi.org/10.3390/rs9070661
9. Rutter AJ, Morton AJ, Robins PC (1975) A predictive model of rainfall interception in forests. II. Generalization of the model and comparison with observations in some coniferous and hardwood stands. J Appl Ecol 12:367. https://doi.org/10.2307/2401739
10. Rutter AJ, Morton AJ (1977) A predictive model of rainfall interception in forests. III. sensitivity of the model to stand parameters and meteorological variables. J Appl Ecol 14:567. https://doi.org/10.2307/2402568
11. Gash JHC, Lloyd CR, Lachaud G (1995) Estimating sparse forest rainfall interception with an analytical model. J Hydrol 170:79–86. https://doi.org/10.1016/0022-1694(95)02697-N
12. Dunkerley DL (2008) Intra-storm evaporation as a component of canopy interception loss in dryland shrubs: observations from Fowlers Gap, Australia. Hydrol Process 22:1985–1995. https://doi.org/10.1002/hyp
13. Jr DFL, Frost EE (2003) A review and evaluation of stemflow literature in the hydrologic and biogeochemical cycles of forested and agricultural ecosystems. J Hydrol 274:1–29
14. Wang XP, Zhang YF, Wang ZN et al (2013) Influence of shrub canopy morphology and rainfall characteristics on stemflow within a revegetated sand dune in the Tengger Desert, NW China. Hydrol Process 27:1501–1509. https://doi.org/10.1002/hyp.9767
15. de Jong SM, Jetten VG (2007) Estimating spatial patterns of rainfall interception from remotely sensed vegetation indices and spectral mixture analysis. Int J Geogr Inf Sci 21:529–545. https://doi.org/10.1080/13658810601064884
16. Delegido J, Fernandez G, Gandia S, Moreno J (2008) Retrieval of chlorophyll content and LAI of crops using hyperspectral techniques: application to PROBA/CHRIS data. Int J Remote Sens 29:7107–7127. https://doi.org/10.1080/01431160802238401

17. Huete AR (1988) A soil-adjusted vegetation index (SAVI). Remote Sens Environ 25:295–309
18. Bréda NJJ (2003) Ground-based measurements of leaf area index: a review of methods, instruments and current controversies. J Exp Bot 54:2403–2417. https://doi.org/10.1093/jxb/erg263
19. De Wasseige C, Bastin D, Defourny P (2003) Seasonal variation of tropical forest LAI based on field measurements in Central African Republic. Agric For Meteorol 119:181–194. https://doi.org/10.1016/S0168-1923(03)00138-2
20. Allen RG, Tasumi M, Morse A et al (2007) Satellite-based energy balance for mapping evapotranspiration with internalized calibration (METRIC)—applications. J Irrig Drain Eng 133:395–406. https://doi.org/10.1061/(asce)0733-9437(2007)133:4(395)
21. De Roo APJ, Wesseling CG, Ritsema CJ (1996) Lisem: a single-event physically based hydrological and soil erosion model for drainage basins. I: theory, input and output. Hydrol Process 10:1107–1117. https://doi.org/10.1002/(sici)1099-1085(199608)10:8%3c1107::aid-hyp415%3e3.0.co;2-4
22. Aston AR (1979) Rainfall interception by eight small trees. J Hydrol 42:383–396. https://doi.org/10.1016/0022-1694(79)90057-X
23. Merriam RA (1960) A note on the interception loss equation. J Geophys Res 65:3850–3851. https://doi.org/10.1029/jz065i011p03850

A Dual Porosity Lumped Parameter Model of Hillslope Hydrological Processes—A Case Study

S. Raazia and R. Khosa

Abstract The components of hydrological cycle remain more or less the same in almost all kinds of terrains. However, the redistribution of precipitation over hillslopes differs from that over moderate terrains in a number of ways. On hillslopes, non-horizontal water table and non-uniform soil saturation levels over the length of slope lead to simultaneous occurrence of infiltration and overland flow over different parts of the slope. Flow paths of a hillslope differ greatly in length, direction and response time, and the path taken by precipitation depends on the soil cover, the slope and the underlying geological setup. Moreover, the existence of preferential flow paths also modifies the hydrological response. In the present study, an attempt was carried out to model runoff generation processes on hillslopes. The model was applied to simulate the hydrology of Zabarwan hillslope, a part of the catchment of the Dal Lake in India. The model could successfully capture the physically observed hydrological phenomena in the study area.

Keywords Hillslope hydrology · Hillslope runoff · Dual porosity model · Dal Lake catchment · Lumped hydrological model

1 Introduction

Hydrology is mainly concerned with the transformation and redistribution of precipitation as it approaches the ground surface. Water reaching the ground surface redistributes by means of interception, infiltration, surface detention and runoff, evapotranspiration, deep percolation and base flow. Hydrological modeling aims at understanding the behavior of a catchment in generating a hydrological response in terms of these components of a hydrological cycle. Of all the hydrological components,

S. Raazia (✉)
Department of Civil Engineering, National Institute of Technology Srinagar, Srinagar 190006, India
e-mail: syeedahraazia.sr@gmail.com

R. Khosa
Department of Civil Engineering, Indian Institute of Technology Delhi, New Delhi 110016, India

P. V. Timbadiya et al. (eds.), *Hydrology and Hydrologic Modelling*,
Lecture Notes in Civil Engineering 312,
https://doi.org/10.1007/978-981-19-9147-9_34

infiltration is considered to be the most important since it is responsible for distribution of precipitation into portions flowing above and below the ground surface and hence for determining runoff. Thus, most hydrological models rely on quantifying runoff by Horton's [1] infiltration excess mechanism. However, on hillslopes, in addition to infiltration excess overland flow, other processes may significantly contribute to the production of runoff.

Hydrological response of hillslopes differs from that of plain to moderate terrains for the following reasons. 1. The water table on hillslopes is not horizontal. Moreover, the lower end of the slope receives water flowing down the slope in addition to the precipitation infiltrating directly into the ground. Thus, the entire depth at this end may get saturated allowing no more infiltration and generating runoff, known as saturation excess overland flow, while the higher parts are still experiencing infiltration. This leads to variable response simultaneously in different parts of the hillslope unlike plain to moderate terrains where only one process occurs at one time. 2. Precipitation approaching the higher end of the hillslope may take different flow paths [2] that differ in length, medium and hence response time. Precipitation (or melting snow) in excess of the absorbing capacity of the ground flows over the ground surface within the shortest time to the outlet/lower end of the slope. The portion that percolates down the soil moves vertically or takes a curved path till it joins the water table wherefrom it moves with the longest response time to the outlet, known as base flow. However, if the percolating water encounters an impediment such as a shallow rocky layer, it moves nearly parallel to the ground slope causing the water table at the lower end of the slope to rise and even intercept the slope. This portion of flow that contributes to runoff at the lower end of the slope is known as the return flow. This phenomenon is responsible for the formation of springs. 3. Presence of preferential flow paths such as cracks/fissures in the rocks, burrow holes, decayed root holes referred to as macropores significantly affects the response time of subsurface flow since water moves rapidly through these pores without mixing with the water in the pores of the soil matrix [3–5]. Bypassing of flow through these macropores leads to a high perceivable permeability of the soil medium.

2 Hillslope Runoff Model

Catchments may be thought of a series of moisture stores, wherein water passes from one domain to another by ways of surface detention and runoff, infiltration, unsaturated vertical percolation, saturated downslope flow and channel flow [6]. However, the hydrological response of the catchment may be dominated by the stores with the longest response time. Hence, hydrology of small catchments may be efficiently modeled by taking infiltration, percolation and downslope flow into account.

Runoff generation processes on hillslopes include infiltration excess overland flow, saturation excess overland flow, lateral subsurface flow and return flow. In the present study, a physically based lumped parameter model was developed that

calculates each of these components of runoff separately to give the total runoff from the catchment.

2.1 Conceptualization of a Hillslope

Where hillslope runoff processes are significant, a convenient and efficient method of catchment modeling is to discretize the catchment into a set of parallel flow strips [7] assumed to have negligible hydrological interactions with each other. The overall hillslope response is then derived by integrating the outputs of the individual hillslopes, assuming homogeneous response.

A unit width of hillslope has been considered as a prismatic storage element of length *L*, a constant slope angle α and a constant depth *D* to the impervious layer over the entire length of the slope (Fig. 1). Two cases arise: (i) water table is below the ground surface for the entire slope, and its height above the impervious layer varies from 0 at the top to H at the bottom. (ii) Water table intersects the slope at a distance L_s known as the saturated slope length, from the lower end of the slope.

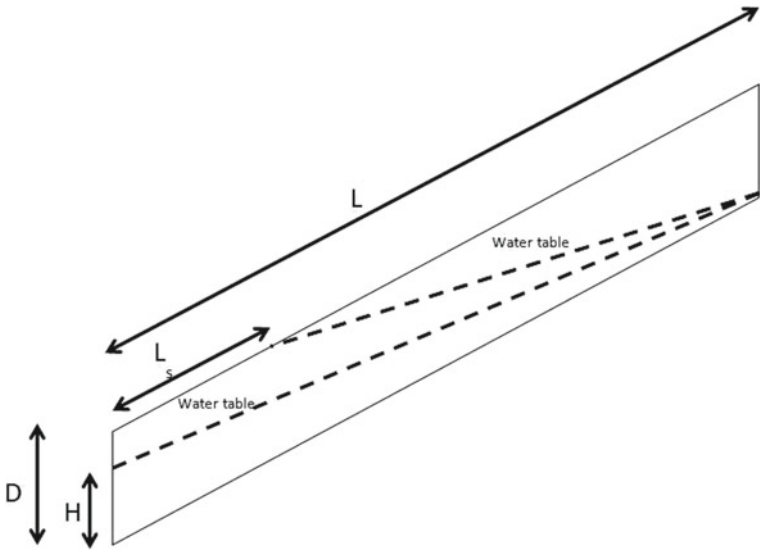

Fig. 1 Prismatic element of hillslope

2.2 Net Precipitation Input

The precipitation volumes, $P_{v,s}$ and $P_{v,u}$ (m^3/m) received by the saturated and the unsaturated portions of the slope length, respectively, in a unit time step Δt are given by Eqs. (1) and (2).

$$P_{v,s} = P L_s \cos\alpha \tag{1}$$

$$P_{v,u} = P(L - L_s) \cos\alpha \tag{2}$$

2.3 Redistribution Over the Unsaturated Slope Length

On the unsaturated ground surface, precipitation is partitioned into surface runoff and the amount that moves into the soil medium through its primary and secondary porosities (micropores and macropores, respectively). Where macropores are significant as is the case with hillslopes, Shakya and Chander [8] and Jain et al. [9] suggest to model micropores and macropores separately as two domains, as has been done in the present study.

The capacity of the micropore domain depends on the infiltration capacity of the soil as well as the conductivity of the soil medium beneath the surface. The Horton's [1] model is the most common approach to model infiltration. However, this model is valid only when precipitation occurs at a rate greater than the infiltration capacity of the soil such that infiltration occurs at potential rate. Moreover, the model is based on a decreasing infiltration capacity which is a valid assumption in case of single storm events. However, in the time gap between storms, the soil regains its infiltration capacity as the water drains down. Thus, the Horton's infiltration model was modified to account for infiltration occurring at a rate less than or equal to the potential rate as well as for the regain of infiltration capacity of soil. Moisture movement in the unsaturated zone is largely regulated by the conducting capacity of the soil matrix. Hydraulic conductivity of unsaturated soil, which is less than the saturated hydraulic conductivity, is a function of soil matric potential. The present model uses Van Genuchten [10] soil constitutive relationships for unsaturated hydraulic conductivity of the soil.

Water in the macropore domain partly moves down the pores and is partly absorbed by the walls of the macropores into the primary pores of the soil matrix. To quantify the water moving down the macropores, the macropore domain is assumed to constitute of only two sized pores [8]. Flow through each minimum size pore is estimated by the Poisecille's equation, whereas that through each maximum size pore is estimated using Manning's equation. Then, the total flow through the macropores, $Q_{m,}$ is estimated to be equal to the average of the flows that would occur when either only the minimum size pores or the maximum size pores would exist (Eq. 3).

$$Q_m = \frac{1}{2}\left(\frac{g r_{\min}^2}{8\nu} + \frac{1}{n}\left(\frac{r_{\max}}{2}\right)^{\frac{2}{3}}\right) A_m \tag{3}$$

where A_{m} is the area of the unsaturated part of the prismatic slope element of unit width covered with macropores and depends on the macroporosity η_{mac} of the soil as given by Eq. (4).

$$A_m = \eta_{\mathrm{mac}}(L - L_s)\cos\alpha \tag{4}$$

$r_{\min}$ is the radius of each minimum size macropore, and $r_{\max}$ is the radius of each maximum size macropore.

The lateral transactional flow through the walls of the macropores into the soil matrix, $Q_{\mathrm{trans}}^{\mathrm{mac-mic,}}$ depends on the sorption capacity of the soil matrix and the net effective area of the macropore walls and is estimated using Eq. 5, with the above assumptions of minimum and maximum size pores.

$$Q_{\mathrm{trans}}^{\mathrm{mac-mic}} = i_h\left(\frac{1}{r_{\min}} + \frac{1}{r_{\max}}\right) A_m D_{\mathrm{eff}} \tag{5}$$

Here, the rate of absorption, $\mathrm{i_{h,}}$ which depends on sorptivity, Sr, is given by Philip's [11] equation (Eq. 6).

$$i_h = \frac{1}{2}\frac{\mathrm{Sr}}{t^{\frac{1}{2}}} \tag{6}$$

where t is the time elapsed since the beginning of absorption process. Sorptivity is a function of soil moisture deficit and is estimated using Eq. 7 given by Youngs and Price [12].

$$\mathrm{Sr} = 6.3(\theta_s - \theta_u)^{0.5} K_{sh}^{0.25} \tag{7}$$

For both the two cases of water table intersecting or not intersecting the hillslope, the effective depth, $D_{\mathrm{eff,}}$ in Eq. 5 is taken as the average depth of the unsaturated zone in each case. Also, in Eq. 7, θ_s and θ_u represent the saturated and the actual soil water content and K_{sh} represents the saturated hydraulic conductivity of the soil.

The maximum capacity of the macroporedomain, $Q_{m,in}^{\max}$, would be the total of the quantity of water that can flow through the macropores and the amount of water that is absorbed by the soil matrix from the macropore wall (Eq. 8).

$$Q_{m,in}^{\max} = Q_m + Q_{\mathrm{trans}}^{\mathrm{mac-mic}} \tag{8}$$

2.4 Flow Situations Over the Unsaturated Zone

For non-zero precipitation, four types of flow situations as identified by Shakya and Chander [8] may exist over the unsaturated length of the hillslope, depending on the amount of precipitation and the capacity of the micropore and the macropore domains. We define F as the cumulative infiltration depth obtained from the modified Horton's model that can infiltrate into the soil in time interval Δt, $V_{m,in}^{\max} = Q_{m,in}^{\max} \cdot \Delta t$ as the maximum volume of water that can flow into the macropore domain per unit width of the hillslope in time interval Δt and K_h as the unsaturated hydraulic conductivity of the soil matrix.

1. When the net precipitation volume received in a time interval exceeds the combined maximum capacities of the soil matrix and the macropores, that is,

$$P_{v,u} > F(L - L_s)\cos\alpha + V_{m,in}^{\max},$$

   it leads to infiltration excess overland flow.
2. If this capacity is not exceeded, but the soil matrix has low conducting capacity such that

$$K_h(L - L_s)\cos\alpha\Delta t + V_{m,in}^{\max} < P_{v,u} < F(L - L_s) + V_{m,in}^{\max},$$

   then most of the flow is bypassed through the macropores leading to their saturation or near-saturation condition.
3. If the soil matrix has significant conducting capacity but cannot alone handle the entire precipitation volume, that is,

$$K_h(L - L_s)\cos\alpha\Delta t < P_{v,u} < K_h(L - L_s)\cos\alpha\Delta t + V_{m,in}^{\max},$$

   then the soil matrix carries flow to the maximum of its capacity, while the remaining flow occurs through the macropores. Flow is dominated by transaction between the macropores and the soil matrix. In this case, all macropores are not involved in carrying the flow.
4. Lastly, if the soil matrix can alone conduct the entire precipitation volume, that is,

   $P_{v,u} < K_h(L - L_s)\cos\alpha\Delta t$,

   this situation is characterized by empty macropores.

2.5 Redistribution Beneath the Ground Surface

For flow situations (1) and (2) discussed above, flow into the macropore domain during a given time interval equals its maximum capacity. Inflow into the soil matrix for situation (1) equals its potential infiltration, and for situation (2), it equals the

input precipitation less by the maximum capacity of the macropore domain. For flow situation (3), flow into the soil matrix equals its conducting capacity and that into the macropore domain equals precipitation less by the amount flowing into the soil matrix. In this case, the area of macropore domain involved carrying the flow is assumed to be proportional to the flow into the macropore domain, and the transactional flow between the macropores and the soil matrix is calculated accordingly. For flow situation (4), flow into the soil matrix equals the net precipitation while the inflow and outflow of the macropore domain are both zero. The outflow from the soil matrix is taken equal to the vertical gravity drainage above the field capacity of the soil, which is a valid assumption if shallow water table is present. The outflow from the macropore domain for all cases except (4) equals the inflow less by an amount that is absorbed by the soil matrix through macropore walls. The net outflow from the unsaturated zone recharges the saturated zone and causes the water table to rise.

Return flow through seepage face for both the cases of the water table fully below the slope and the water table intersecting the slope is computed using the kinematic storage model of Sloan and Moore [5]. Fluctuation in water table and change in the saturated slope length are calculated by applying continuity equation and geometrical concepts.

2.6 Runoff

The net overland flow is calculated as the sum of infiltration excess overland flow and saturation excess overland flow which equals the precipitation approaching saturated slope length. The model includes a nonlinear reservoir routing equation of the form given in Eq. 9 to incorporate the storage effect of the catchment on the overland flow that causes attenuation, smoothening and delay of the outflow hydrograph.

$$S_{nlr} = k_{nlr} Q^{n_{nlr}} \tag{9}$$

S_{nlr} is the stored volume, that is, the overland flow volume, and Q is the outflow rate. k_{nlr} and n_{nlr} are the adjustable parameters for calibration.

Total runoff per unit width of the hillslope is obtained by adding the return flow component to the overland flow. Total catchment runoff is obtained by multiplying the runoff per unit width by the effective width of the hillslope, which equals the catchment area divided by the average slope length.

The model was programmed and executed using Fortran 90.

3 Study Area

The Zabarwan mountain range is situated in the central part of the Kashmir Valley in the state of Jammu and Kashmir. It is a sub-mountain range of the Zanskar

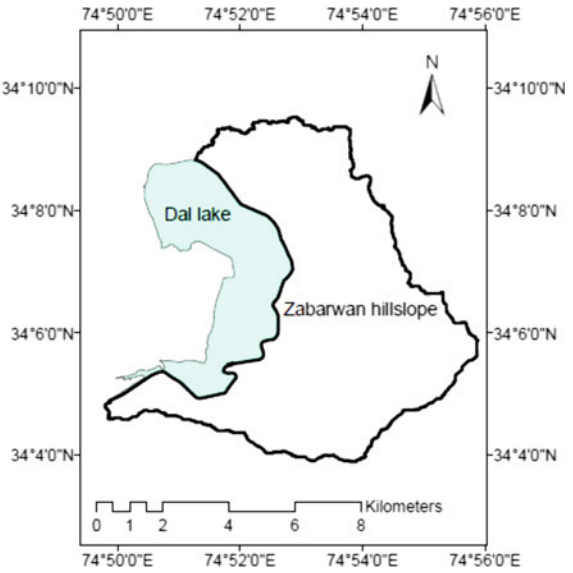

Fig. 2 Location of the study area

Range. The Zabarwan borders the world famous Dal Lake along its eastern shore and hosts a number of gardens including Asia's largest tulip garden. The region has a rocky geology with a very shallow soil cover. Dominant land covers on the slopes include forest cover and bare exposed rock devoid of any vegetation. The foothills are mostly used for cultivation of vegetable. Residential setups too exist in lower reaches constrained by the highly mountainous terrain. The climate is of sub-mediterranean type with two dry spells from April to June and September to November. Annual average rainfall in this region is 870 mm. The west-facing slope of this range drains directly into the Dal Lake with the average flow direction from east toward west and has been considered for hydrological modeling. The region is situated between 74° 49′ 47.68″ and 74° 55′ 53.1″ E longitudes and 34° 3′ 53.79″ and 34° 9′ 31.95″ N latitudes (Fig. 2).

3.1 Regional Hydrology

This region is devoid of a prominent drainage network resulting in a diffused runoff flowing toward the lake. Slopes vary from gentle to very steep with mild slopes occurring in the region in close vicinity of the Dal Lake having a backdrop of highly steep mountains further from the lake (Fig. 3). Forested peaks have a spatial network of large connected soil pores formed as a result of activities of soil fauna, decay of plant roots and soil cracking, which provide preferential flow paths conducting appreciable amounts of flow to the saturated zone. Presence of a rocky bed at a very shallow depth results in a shallow water table. Water percolating downward and

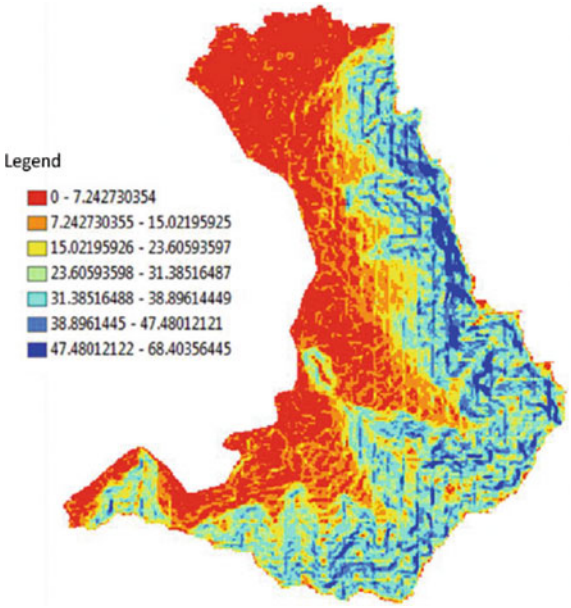

Fig. 3 Variation of slope in the study area

impeded by the shallow rocky layers flows toward the lower reaches nearly parallel to the hillslope with a very short response time. This lateral subsurface flow from upper reaches together with the water added into the groundwater regime from vertical percolation saturates the soil profile up to the surface level in the lower reaches. As a result, the soil appears mostly wet in the foothill region of the Zabarwan hillslope. The saturated soil profile behaves as an impervious surface obstructing infiltration and generating runoff by saturation overland flow.

Water can also be seen impounded in regions of profile concavities near the foothills. A large number of very small streams of not more than 1 m width are seen flowing through the vegetated gardens in the foothills. Fed mostly by the return flow seeping in from below the land surface, these streams form as a result of local undulations.

The hillslope is ungauged, and also for the fact that the runoff is diffused, it is impractical to directly measure the hillslope runoff. However, some important observed physical phenomena are a significant aid in developing and evaluating a hydrological model for this hillslope.

3.2 Hydrological Modeling

The Zabarwan hillslope can be topographically divided into two regions: the gently sloping foothills and the steep mountains [13]. These two regions were modeled separately using the hillslope runoff model developed in the present study. The steep

region was first considered for evaluation of precipitation redistribution, and the surface and subsurface outflows from this region were suitably routed through the various domains of the lower region in addition to the precipitation received by that region. Higher macroporosity was considered for the first region due to the presence of vegetated surface. Soil parameters of dominant soil groups were used to run the model. Average values of slope and slope length used in the model were calculated using the geographical mapping software ArcGIS. Moreover, a number of initial conditions including both water table intersecting the slope surface and otherwise were tested. Simulation was carried out using daily precipitation data from January 1990 to December 2010. However, the period up to December 2000 was considered to be the warm-up period for the model as indicated in the next section. Only the model results from January 2001 onward were considered to be representative of the hydrology for the study area.

The model was used to identify the dominant flow situation as well as the dominant runoff generation process in each of the two regions of the study domain.

4 Results and Discussions

4.1 Steep Region Hydrology

The model results indicated that infiltration excess overland flow rarely occurred on the steep region, which is true to the observation. Similar observation has been reported by Dunne and Black [14] in Sleepers River watershed. Absence of surface drainage channels also indicates that Hortonian overland flow is a rare process here. During wet days, most of the flow is conducted through the primary porosity of the soil while the macropores either remain empty or conduct the flow partially.

For all the tested initial conditions of water table, the model stabilized around 125 m of saturated slope length after a warm-up period (Fig. 4), the total average length of slope is being 2000 m. Thus, a value of 100 m saturated slope length was finalized to be used as initial condition. The presence of springs in this region including the famous spring Chesma Shahi is indicative of the fact that the water table intersects the slope and hence confirms that the model is capable of simulating the actual hillslope behavior.

Figures 5, 6 and 7 show the total overland flow, which in this case is the saturation excess overland flow, return flow and total outflow from the steep region. Results have been presented for different time scales so as to reflect the response of various moisture storages to precipitation fluctuations. Surface processes are more sensitive to precipitation fluctuations and have very short response time as is evident from Fig. 5. On the other hand, subsurface processes are less sensitive to precipitation fluctuation and have a longer response time as indicated by Fig. 6.

Figure 7 indicates that the return flow contributes a significant proportion of the total catchment outflow with the overland flow contributing only a small portion. This

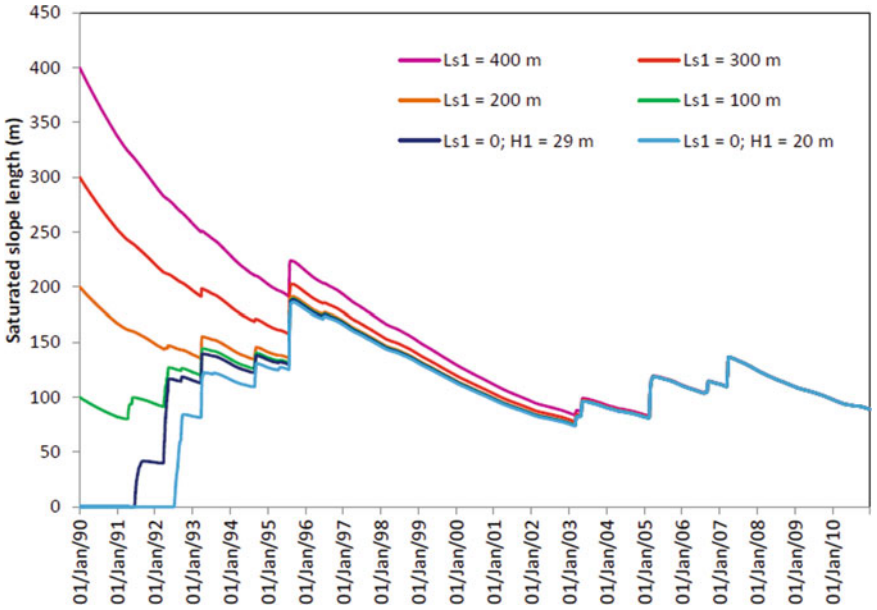

Fig. 4 Saturated slope length in steep region for different initial conditions

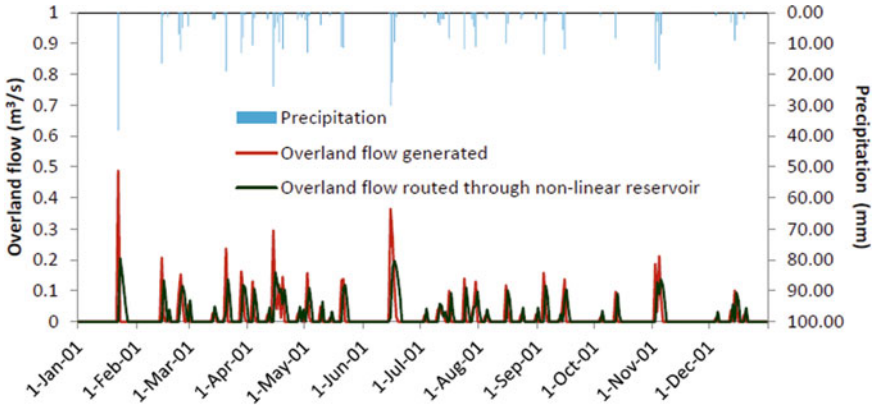

Fig. 5 Overland flow from the steep region

is because most of the precipitation infiltrates into the ground over the unsaturated part of the hillslope and moves down as subsurface flow. This return flow feeds the perennial springs in this region.

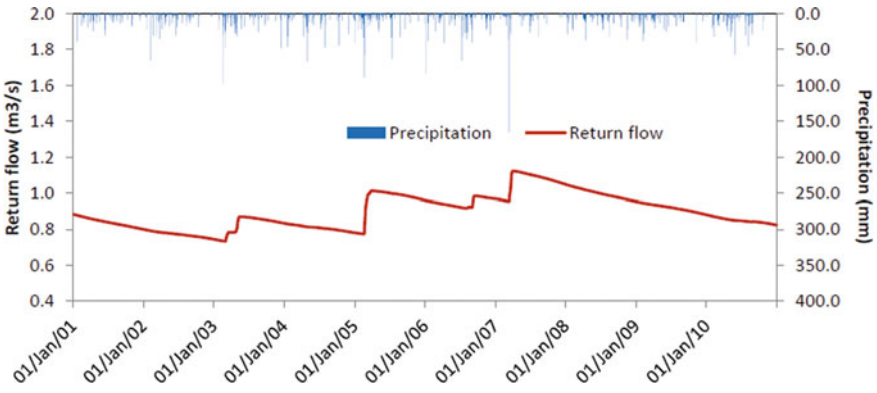

Fig. 6 Return flow from the steep region

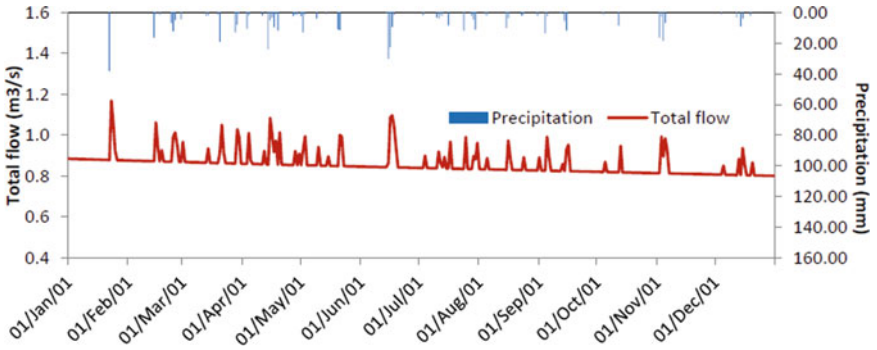

Fig. 7 Total outflow from the steep region

4.2 Foothill Hydrology and the Net Hillslope Runoff

Figure 8 shows that the entire slope length of the foothill, which is 1200 m, is saturated up to the ground surface throughout the modeled period. This is also evident from the presence of near-surface water table and perennial streams fed by return flow.

Figures 9 and 10, respectively, show the total overland flow and total outflow of the entire hillslope. A non-zero overland flow on days without precipitation occurs from the part of the return flow from the steep region that seeps out of the ground and flows as overland flow in the foothill region. In the net response of the hillslope, the overland flow contributes a significant proportion to the outflow hydrograph because of the saturation excess overland flow occurring over the entire slope length of the foothill region.

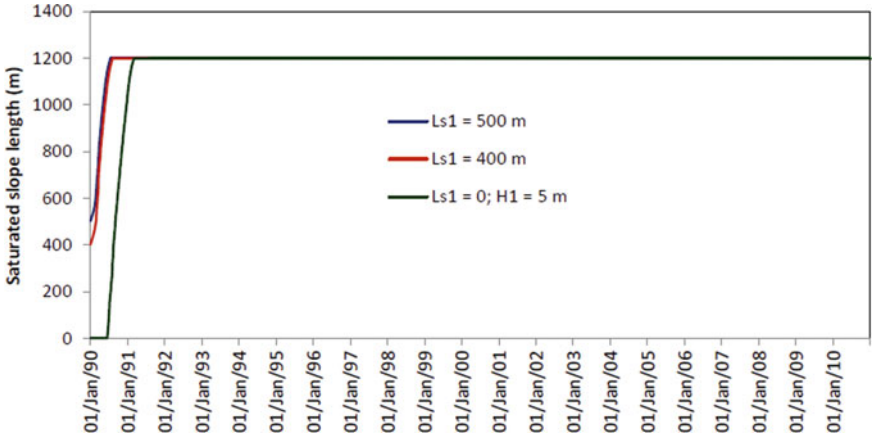

Fig. 8 Saturated slope length in the foothills

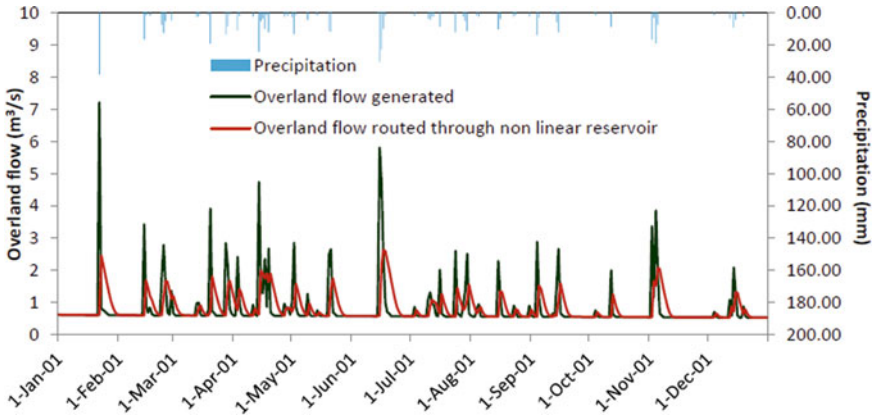

Fig. 9 Net overland flow from the hillslope

5 Conclusions

A hillslope hydrological model has been developed to predict the average hydrological behavior of an ungauged hillslope. The model is based on average topographical, geological and soil conditions, thus having lesser number of parameters compared to the commonly used distributed hydrological models. Moreover, the model considers only the most significant processes affecting redistribution of precipitation over a hillslope. The model considers flow in two domains within the soil, one due to the primary porosity of the soil and the other due to the preferential flow paths which are a characteristic of hillslopes, formed as a result of faunal activities, decayed vegetative matter in the vadose zone and cracking of rocks.

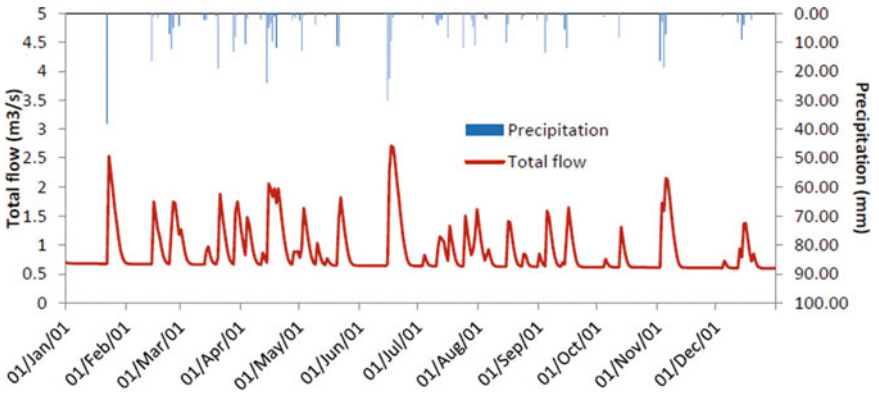

Fig. 10 Net runoff from the hillslope

The model was used to identify runoff generating processes and the total outflow of the Zabarwan hillslope that feeds the world famous Dal Lake on its eastern side. Two regions of the hillslope with significant topographical difference were modeled separately. Though the results of the model could not be objectively validated, the observed phenomena were well simulated, and hence, the model can be considered to be an effective tool to depict the hydrological behavior of this hillslope.

References

1. Horton RE (1933) The role of infiltration in the hydrologic cycle. Eos Trans Am Geophy Union 14(1):446–460. https://doi.org/10.1029/TR014i001p00446
2. Dunne T (1978) Field studies of hillsope flow processes. In: Hillslope hydrology, pp 227–293
3. Mosley MP (1979) Streamflow generation in a forested watershed, New Zealand. Water Resour Res 15(4):795–806
4. Beven K, Germann P (1982) Macropores and water flow in soils. Water Resour Res 18(5):1311–1325
5. Sloan PG, Moore ID (1984) Modeling subsurface stormflow on steeply sloping forested watersheds. Water Resour Res 20(12):1815–1822
6. Kirkby M (1988) Hillslope runoff processes and models. J Hydrol 100(1–3):315–339
7. Yang D, Herath S, Musiake K (2002) A hillslope-based hydrological model using catchment area and width functions. Hydrol Sci J 47(1):49–65
8. Shakya NM, Chander S (1998) Modelling of hillslope runoff processes. Environ Geol 35(2):115–123
9. Jain L, Haldar R, Khosa R (2014) Hillslope runoff processes and modelling. Int J Earth Sci Eng 7(1):193–201
10. Van Genuchten MT (1980) A closed-form equation for predicting the hydraulic conductivity of unsaturated soils. Soil Sci Soc Am J 44(5):892–898
11. Philip JR (1957) The theory of infiltration: 4. Sorptivity and algebraic infiltration equations. Soil Sci 84(3):257–264
12. Raazia S, Khosa R (2014) Approaches to hydrological Modeling of the Heterogeneous Catchment of the Dal Lake. Int J Eng Res 7–11

13. Youngs EG, Price RI (1981) Scaling of infiltration behavior in dissimilar porous materials. Water Resour Res 17(4):1065–1070
14. Dunne T, Black RD (1970) An experimental investigation of runoff production. Water Resour Res 6:478–490

Investigations on Hydraulic Conductivity Assessment of Porous Media Treated with Fly Ash

Abhishish Chandel, Vijay Shankar, and M. A. Alam

Abstract Hydraulic conductivity (K) is important in many tasks involving the flow of fluids through porous media, including dissolved contaminant transport and groundwater investigations. Experimental investigations concerning fly ash mixed porous media result in decreasing the K value and can be used as a barrier to different compaction characteristics. The investigation focuses on the compaction properties and K of porous media with varying quantities of fly ash content. The standard Proctor compaction test (SPCT) was performed on two different porous media with varying fly ash contents ranging from 10 to 50%. According to the SPCT, when the fly ash content increases, the maximum dry density declines, and the associated optimum moisture content increases. The optimum content of fly ash in soil samples 1 and 2 was found to be 30% and 40%, respectively, because the K value reduces uniformly. Further increases in fly ash content result in a minimal fall in K value. The obtained K values of soil–fly ash mix at optimum content lie within the domains of silt, which substantiate its use for constructing impervious embankments or groynes.

Keywords Compaction · Hydraulic conductivity · Groundwater

1 Introduction

The term hydraulic conductivity (K) describes flow-through porous media and is considered an important metric in the building of water-retaining and drainage structures, stability and settlement assessments of embankment dams, and groundwater management [1]. Henry Darcy originally proposed flow via the porous media in 1856 [2]. Flow velocity is proportional to the tangent of the hydraulic gradient, and the proportionality constant in that equation is referred to as K [3, 4]. Furthermore, the

A. Chandel (✉) · V. Shankar
Department of Civil Engineering, National Institute of Technology, Hamirpur, India
e-mail: abhishishchandel@gmail.com

M. A. Alam
Department of Civil Engineering, PEC University of Technology, Chandigarh, India

P. V. Timbadiya et al. (eds.), *Hydrology and Hydrologic Modelling*,
Lecture Notes in Civil Engineering 312,
https://doi.org/10.1007/978-981-19-9147-9_35

flow regime is governed by the computation of the friction factor and the Reynolds number of porous sediments [5].

A waste by-product, i.e., fly ash is obtained from the explosion of naturally cementitious coal and is collected in the smoke vessels via electrostatic precipitators to minimize its influence on the environmental ecosystem [6]. Increasing demand for electrical energy and coal is being the main source of energy consequences in the establishment of many thermal power plants [7]. Generally, in India, a large quantity of fly ash is produced per year, and as per estimates, this generation of fly ash is expected to increase to about 190MT per year by the year 2022. Numerous studies and analyses have been conducted to utilize this waste product in building sectors, but basically, it is most commonly used in cement concrete works and manufacturing of lightweight bricks industries [8]. In the present scenario, only 15% of fly ash is used in various engineering sectors. Hence, it is important to investigate new ideas and approaches so that this waste product can be effectively used [9]. Landfilling is the primary disposal method for fly ash, but due to higher treatment costs and limited space, alternate fly ash usage is encouraged [10]. The most important limitation governing the acceptability of employing the soil–fly ash mix at the optimal fly ash content in various water retention structures and for constructing impermeable embankments is the K [11, 12].

Various studies related to the utilization of fly ash in water-retaining structures and impermeable embankment construction have been carried out. Gupta and Alam [7] studied the seepage and hydraulic analyses of fly ash treated with various cement and lime proportions. The K of fly ash decreases with the addition of lime and cement up to certain content. Lime and cement proportions of 40% and 15% were found to be optimum content in this study. Muhunthan et al. [9] studied the influence of various proportions of bottom ash on the K of fly ash. The K of fly ash at 40% bottom ash content was found to be the least and is relatively equivalent to that of silt. Fly ash's hydraulic properties were studied by Sivapllaiah and Lakshmikantha [6], who also examined how the bentonite affected these characteristics. Marto et al. [13] examined the K and compaction behavior of ash blends (fly ash and bottom ash). It was revealed that the K of compacted ash blends decreases as the fly ash content increases. Ige and Ajamu [14] studied the K and strength properties of sand treated with various proportions of fly ash. The K value of sand was found to be lowest at 40% fly ash content and had the greatest influence on sand strength increase. Wasil [15] examined the effect of varied bentonite contents on the K of fly ash ranging from 0 to 15%.

According to the literature study, several researchers investigate the potential application of fly ash, such as mixing fly ash with cement, bentonite, and lime to reduce the K value. Furthermore, the effect of different quantities of fly ash by weight, followed by typical compaction conditions, on the K of porous media must be investigated. The objectives of this investigation are to (1) study the compaction characteristics of porous media with different proportions of fly ash content and (2) determine the optimum content of fly ash in the porous media, at which the K values reduce to a significant value.

2 Porous Material and Experimental Methodology

2.1 Porous Material

Two different porous media were acquired from two different riverbanks in Himachal Pradesh, India, for this study. The first sand sample was collected from the Sutlej River in Bilaspur district and the second sample from the Beas River in Mandi district of Himachal Pradesh, respectively. The obtained sand samples were tested in the laboratory for analysis of the fundamental engineering properties. The fly ash was gathered from the Guru Har Gobind Thermal Plant in the Punjab region of Bhatinda. The fly ash particles are generally finer than the sand particles. Initially, the dry sieve analysis was carried out on the sand samples to determine the various particle sizes, i.e., d_{10}, d_{30}, and d_{60}. Also, based on the computed values of particle size, the uniformity and curvature coefficients (C_u and C_c) were determined as per standard procedure [16]. The standard expressions to compute the value of C_u and C_c are given:

$$C_u = \frac{d_{60}}{d_{10}} \tag{1}$$

$$C_c = \frac{d_{30}^2}{d_{60} * d_{10}} \tag{2}$$

where d_{10}, d_{30}, and d_{60} are the particle sizes equivalent to 10%, 30%, and 60% finer by weight. Table 1 represents the basic engineering properties of the collected sand samples and fly ash.

2.2 Experimental Methodology

Initially, various proportions of sand samples with the fly ash content were prepared, i.e., in increments of 5% from 10 to 50% by weight, and then, the standard Proctor compaction test (SPCT) was performed on each sand–fly ash mix. The SPCT test is useful for identifying the optimum moisture content (OMC) and maximum dry density (MDD) for a mix. For SPCT, an oven-dried sample of 3 kg has been mixed with water to reach the water content of 6%. The sample was then placed for 24 h in a sealed container for maturing. Further, the sample was packed in the mold uniformly with 25 blows for every three layers. The weight of the mixture was determined. To determine the moisture content of the mix, two samples were collected from the top and bottom of the mold and placed in an oven for 24 h, with the mean value of the sample corresponding to the moisture content of the mix. For each mix, four to five readings were recorded at different moisture contents. To determine the OMC and

Table 1 Basic engineering properties of collected sand samples and fly ash

S. No.	Properties	Sample 1	Sample 2	Fly ash
1	Maximum dry density (kN/m^3)	14.79	15.46	8.63
2	Minimum dry density (kN/m^3)	12.83	13.58	6.76
3	Optimum moisture content (%)	9.73	11.58	35.85
4	Sand (%)	97.58	78.73	48.85
5	Silt (%)	2.42	15.84	47.73
6	Clay (%)	0.00	5.43	3.42
7	d_{10} (mm)	0.09	0.06	0.03
8	d_{30} (mm)	0.19	0.08	0.06
9	d_{60} (mm)	0.25	0.18	0.11
10	Uniformity coefficient[a] (C_u)	2.78	3.00	3.67
11	Curvature coefficient[a] (C_c)	1.60	0.59	1.09
12	Specific Gravity[a]	2.64	2.67	1.97

([a] represents the dimensionless properties)

MDD value of the mix, a plot between water content and dry weight was plotted [17].

Further, the hydraulic conductivity of each mix was determined using the constant head permeameter test. The diameter and test height of the permeameter column are 15.3 and 46.5 cm, respectively, as shown in Fig. 1. The sand–fly ash mixtures were compacted in the permeameter to get the MDD value, which was obtained during the SPCT test. Further, the compacted specimen was saturated initially to maintain the steady conditions of flow, and then, the discharge value was measured at different constant heads. The mean value of discharge helps to compute the value of K for each mix. The K of each mix was calculated using the general methodology as explained by Chandel and Shankar [18] and ASTM [19]. The standard equation to compute the K is defined as:

$$K = \frac{q * L}{a * h} \tag{3}$$

where q = volume of discharge, L = test height, h = pressure taps head difference, and a = cross-sectional area of sample.

3 Results and Discussion

Grain-size analyses of soil samples and fly ash are among the experimental experiments. The flow regime was determined by examining the variation between Fr and Re. Further, the SPCT and the hydraulic conductivity tests were performed on the

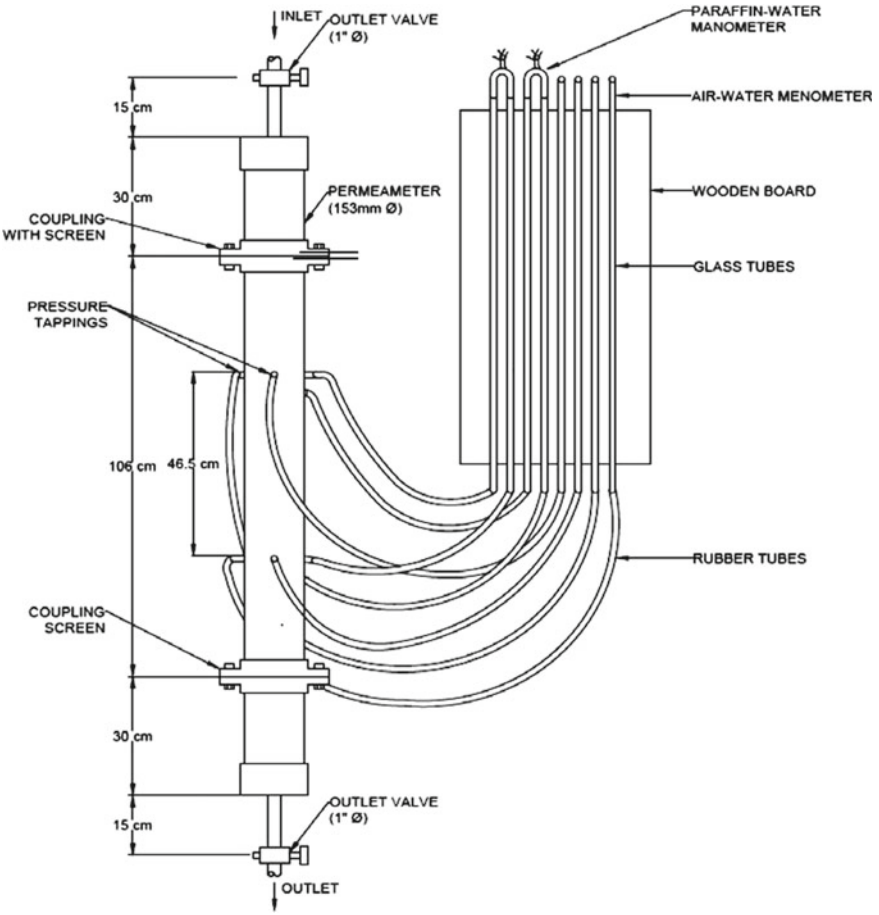

Fig. 1 Line diagram of K measuring setup

various proportions of the sand–fly ash mixes. The primary purpose of this study is to establish the optimal fly ash quantity at which K declines significantly.

3.1 Grain-Size Analysis

The obtained soil samples were first examined using a mechanical shaker, and a sieve with bigger openings on the top and smaller ones below was arranged. The curve shows that roughly 48% of fly ash is retained on a 75-micron sieve opening. The various particle sizes, i.e., d_{10}, d_{30}, and d_{60} for fly ash, and samples 1 and 2 have been computed as mentioned in Table 1. By using the values of particle size, the C_u and C_c were determined. The C_u and C_c values help to govern the soil samples to be

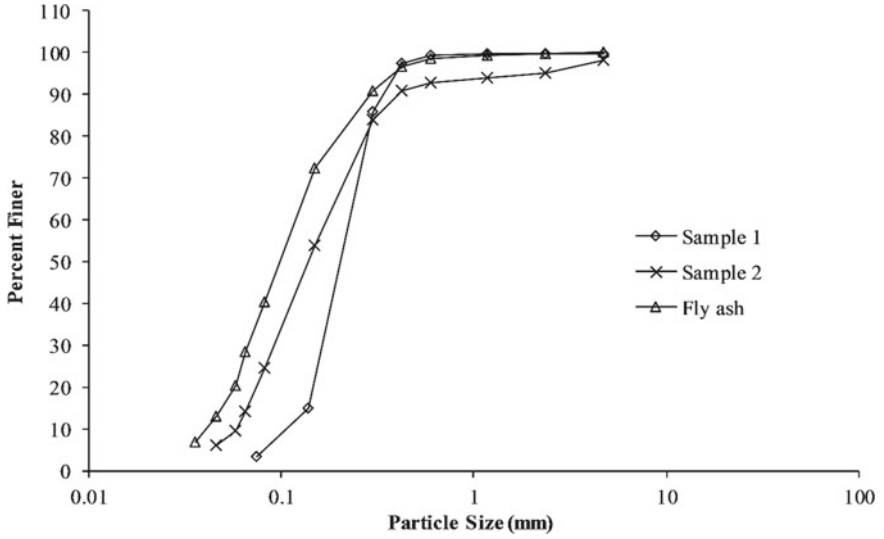

Fig. 2 Grain-size distribution of soil samples and fly ash

well or poorly graded. For a well-graded sample, the uniformity coefficient value is greater than 6, and the C_c value ranges from 1 to 3. For samples 1 and 2, the C_u and C_c values are 2.78 and 1.60 and 3.00 and 0.59, respectively. The computed values of C_u and C_c show that the collected soil samples are poorly graded. Figure 2 depicts the grain-size curve for soil samples and fly ash.

3.2 Compaction Characteristics Analysis

Various mixes of sand–fly ash were prepared by varying the proportions of fly ash in increments of 5% from 10 to 50% by weight. Then, the SPCT has been conducted on these mixes to determine the OMC and the MDD of each mix. Table 2 represents the MDD and OMC values for the various mixes. The curve between the dry density and water content indicates that the MDD value increases initially with the addition of a small quantity of water, and then, the curve reaches a maximum value that corresponds to the MDD and OMC value of the mix. Further, as demonstrated in Fig. 3, increasing the water content results in a drop in the dry density value. For samples 1 and 2, with the increases in the fly ash content from 10 to 50% in the increments of 5%, the MDD value decreases from 13.60 to 11.50 kN/m^3 and 14.78 to 10.46 kN/m^3 and the associated OMC increases from 9.10 to 15.20% and 13.20 to 17.40%, respectively, as shown in Table 2.

Because fly ash is a lighter material than sand, the MDD value decreases as the content of fly ash increases, whereas an increase in the OMC value was observed which is linked with the notion that the fly ash has dust-like sediments having more

Table 2 MDD and OMC for various sand–fly ash mixes

S. No	Fly ash content (%)	Sample 1		Sample 2	
		OMC (%)	MDD (kN/m^3)	OMC (%)	MDD (kN/m^3)
1	10	9.10	13.60	13.20	14.78
2	15	9.80	13.40	13.60	14.18
3	20	10.90	13.00	14.20	13.62
4	25	11.43	12.70	14.66	13.05
5	30	12.00	12.39	15.10	12.44
6	35	12.60	12.15	15.50	11.93
7	40	13.20	11.94	16.10	11.38
8	45	14.30	11.69	16.76	10.94
9	50	15.20	11.50	17.40	10.46

contact area to be enclosed by fluid particles. Notably, the fly ash particles absorb more fluid, which increases the water content of the mix [9].

3.3 Flow-Regime Investigation

To determine the flow regime, F_{r} and R_e values were computed. Figure 4 depicts a logarithmic plot of these quantities to govern the flow regime. The general expression for calculating Fr and Re is as follows:

$$F_{\mathrm{r}} = \frac{h_i * g * d_{50} * 2}{U^2} \tag{4}$$

$$R_e = \frac{U d_{50}}{\varphi} \tag{5}$$

where h_i = hydraulic gradient, d_{50} = mean size, g = constant of gravity, U = velocity of flow, and φ = kinematic viscosity.

Figure 4 shows that the variation between F_{r} and R_{e} indicates a straight-line behavior with a Reynolds number less than one, implying that the flow regime is Darcy's or laminar regime [20].

3.4 Hydraulic Conductivity Determination

The hydraulic conductivity of both the samples was determined with the different proportions of fly ash by compacting the sand–fly ash mixture in the permeameter at the obtained values of OMC and MDD during SPCT. The K of samples 1 and 2 was

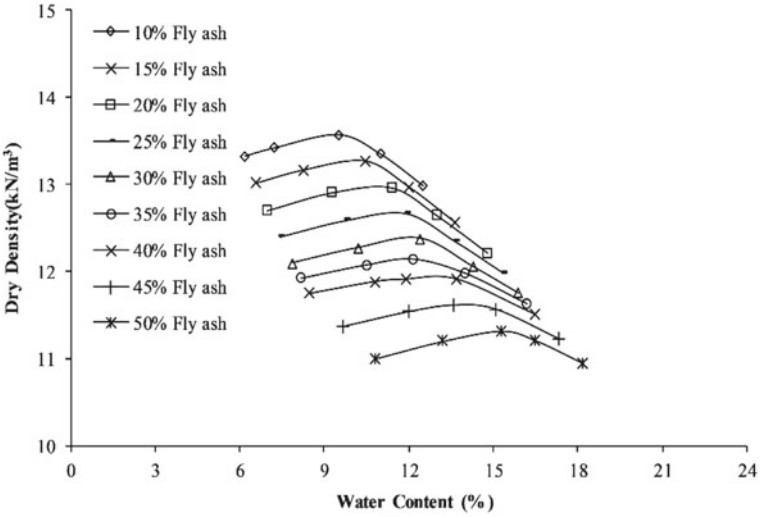

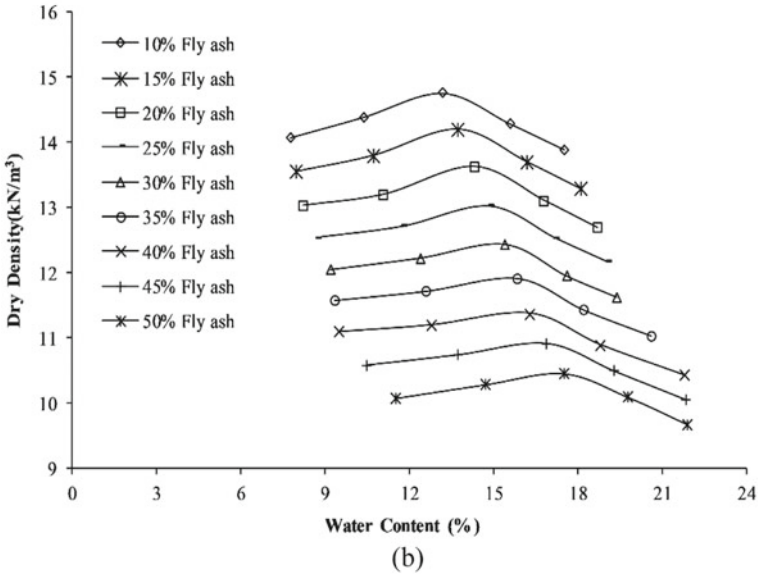

Fig. 3 Compaction curves of sand–fly ash mixes **a** sample 1 **b** sample 2

observed to be 7.32×10^{-3} cm/s and 4.51×10^{-3} cm/s as given in Table 3. In samples 1 and 2, with the addition of fly ash in the increments of 5% up to 30% and 40%, the K value reduces uniformly to 2.13×10^{-3} cm/s and 1.31×10^{-3} cm/s, respectively, whereas further increases in the fly ash content result in a negligible change in the

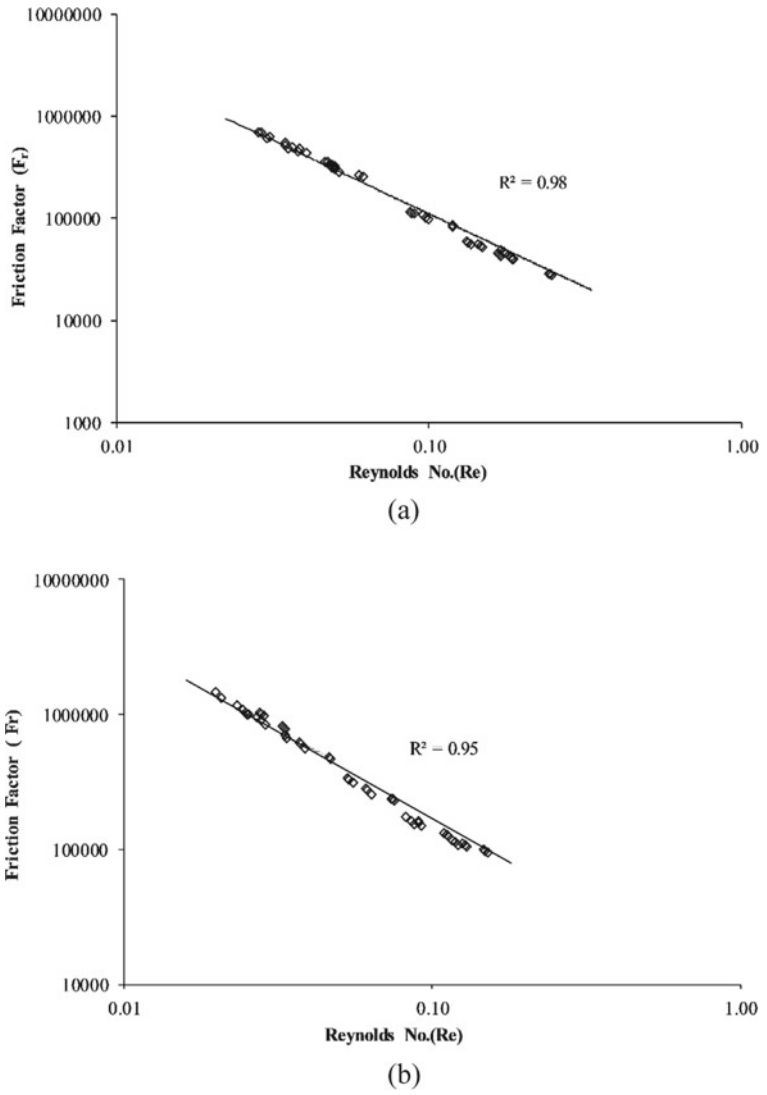

Fig. 4 Plot between Fr and Re for **a** sample 1 and **b** sample 2

K value as shown in Fig. 5. The optimum content of the fly ash in samples 1 and 2 was found to be 30% and 40%, respectively.

For samples 1 and 2, the MDD and OMC values at the optimum content of fly ash were obtained as 12.39 kN/m^3 and 12% and 11.38 kN/m^3 and 16.10%, respectively. The obtained values from the compaction analysis at the optimum content postulated that the observed weight is much lower than those of silt and clays. The *K* value drops with the addition of fly ash up to the optimum level in both soil samples because the

Table 3 Hydraulic conductivity values for various sand–fly ash mixes

S. No	Fly ash content (%)	K (cm/s) ($1*10^{-3}$)	
		Sample 1	Sample 2
1	0	7.32	4.51
2	10	5.88	3.49
3	15	4.96	2.95
4	20	4.07	2.57
5	25	3.06	2.10
6	30	2.13	1.70
7	35	2.09	1.52
8	40	2.07	1.31
9	45	2.06	1.28
10	50	2.05	1.27

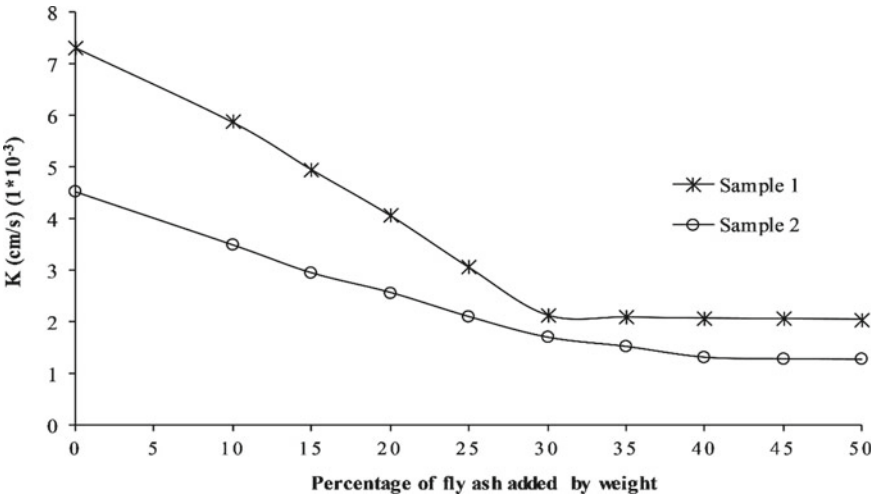

Fig. 5 K variations of samples 1 and 2 with different fly ash contents

specific contact area of the sand particle increases with the addition of tiny fly ash particles, giving more hindrance to fluid particles moving through the interconnected pores [8].

4 Conclusions

The purpose of this research is to determine how adding fly ash to sand changes its K and compaction properties. In addition, the study found the following results:

- Addition of fly ash in sand results in decreases in the MDD value, whereas the corresponding OMC value increases in various mixes.
- Friction factor and Reynolds number suggest laminar flow because Reynolds number is smaller than 1 for all mixes.
- The K of sand samples 1 and 2 reduces gradually with the addition of fly ash up to a particular point, i.e., 30% and 40%, respectively, which is referred to as the optimum fly ash content. The addition of more fly ash results in a minimal decrease in the K value.
- In samples 1 and 2, the MDD, OMC, and K value at the optimum content of fly ash are observed to be 12.39 kN/m^3, 12%, and 2.13×10^{-3} cm/s and 11.38 kN/m^3, 16.10%, and 1.31×10^{-3} cm/s, respectively.
- The acquired K values at the optimal content fall inside the domain of silts, indicating that it can be used to build impermeable embankments and fills.

Acknowledgements The authors acknowledge the Department of Civil Engineering, National Institute of Technology Hamirpur (India), for providing experimental facilities related to the study.

References

1. Boadu FK (2000) Hydraulic conductivity of soils from grain-size distribution: new models. J Geotech Geoenvironmental Eng 126(8):739–746
2. Toumpanou IC, Pantazopoulos IA, Markou IN, Atmatzidis DK (2021) Predicted and measured hydraulic conductivity of sand-sized crushed limestone. Bull Eng Geol Env 80(2):1875–1890
3. Alabi OO (2011) Validity of Darcy's law in laminar regime. Electron J Geotech Eng 16:27–40
4. Chandel A, Sharma S, Shankar V (2022) Prediction of hydraulic conductivity of porous media using a statistical grain-size model. Water Supply 22(4):4176–4192
5. Li Z, Wan J, Zhan H, Cheng X, Chang W, Huang K (2019) Particle size distribution on Forchheimer flow and transition of flow regimes in porous media. J Hydrol 574:1–11
6. Sivapullaiah PV, Lakshmikantha H (2004) Properties of fly ash as hydraulic barrier. Soil Sediment Contam 13(5):391–406
7. Gupta RD, Alam J (2004) An experimental study of the seepage and strength characteristics of Dadri fly-ash mixed with cement and lime. ISH J Hydraul Eng 10(2):49–57
8. Galupino J, Dungca J (2015) Permeability characteristics of soil-fly ash mix. ARPN J Eng Appl Sci 15:6440–6447
9. Muhunthan B, Taha R, Said J (2004) Geotechnical engineering properties of incinerator ash mixes. J Air Waste Manag Assoc 54(8):985–991
10. Sreekantan PG, Sinha AK, Havangi VG (2019) Red mud-fly ash mix as an embankment fill material. In: Geotechnics for transportation infrastructure, vol 29, pp 247–258
11. Samanta M (2018) Investigation on geomechanical behaviour and microstructure of cement-stabilized fly ash. Int J Geotech Eng 12(5):449–461
12. Chandel A, Shankar V, Alam MA (2021) Experimental investigations for assessing the influence of fly ash on the flow through porous media in Darcy regime. Water Sci Technol 83(5):1028–1038
13. Marto A, Awang AR, Makhtar AM (2011) Compaction characteristics and permeability of Tanjung Bin Coal Ash Mixtures. In: IPCBEE in proceeding of the international conference on environment science and engineering: selected papers, vol 8. Ed. By IACSIT Press, Singapore, pp 134–137

14. Ige JA, Ajamu SO (2015) Unconfined compressive strength test of a fly ash stabilized sandy soil. Int J Latest Res Eng Technol 1(3):1–11
15. Wasil M (2020) Effect of bentonite addition on the properties of fly ash as a material for landfill sealing layers. Appl Sci 10(4):1–13
16. ASTM (2007) Standard D422—Particle-size analysis of soils. West Conshohocken, PA, USA
17. ASTM (2012) Standard D698—Laboratory compaction characteristics of soil using standard effort. West Conshohocken, PA, USA.
18. Chandel A, Shankar V (2022) Assessment of hydraulic conductivity of porous media using empirical relationships. In: Pasquali D (ed) Sediment transport, IntechOpen. London. https://doi.org/10.5772/intechopen.103127
19. ASTM (2006) Standard D2434—Permeability of granular soils (Constant head). West Conshohocken, PA, USA
20. Chandel A, Shankar V (2021) Evaluation of empirical relationships to estimate the hydraulic conductivity of borehole soil samples. ISH J Hydraul Eng 1–10

Permeability of Sloping Soil Layer: An Experimental Study

M. Kafi, J. Alam, M. Muzzammil, and M. U. Haque

Abstract Permeability is an important property influencing flow-through porous media. Seepage of water through earth dams, stability of slopes and ground water recharge are some of the problems related to permeability of soil. The accurate determination of permeability is a cause of concern to the hydraulic engineers. As the stratification of earth crust exists in any direction, the study of permeability of soil is imminent in multiple directions. Although ample work has been reported regarding the permeability of soil in horizontal and vertical directions, the work on inclined layer seems to be sparse in the literature. Therefore, permeability of sloping soil layer has been investigated in this paper. Four samples of fine sand were selected from different sites for the experimentation. Permeability has been determined for horizontal layer, for positively as well as negatively sloped layer. Inclination of layer was varied from 0° to ± 20°. With the increase in inclination with respect to horizontal, the permeability of positively sloped layer was found to increase, whereas for the negatively sloped layer, it was found to decrease. When the slope was increased from 0° to + 20°, the maximum deviation of − 27% was observed between the observed permeabilities of horizontal and positively sloped layer, whereas for the opposite slope, i.e., from 0° to − 20°, the maximum deviation found was 34%. For a constant slope, the permeability of the said layers was found to increase with the particle size.

Keywords Observed permeability · Horizontal layer · Sloping layer · Porous media

M. Kafi · M. Muzzammil
University Polytechnic, Aligarh Muslim University, Aligarh 202002, India

J. Alam · M. U. Haque (✉)
Department of Civil Engineering, Aligarh Muslim University, Aligarh 202002, India
e-mail: misbahnnc@gmail.com

P. V. Timbadiya et al. (eds.), *Hydrology and Hydrologic Modelling*,
Lecture Notes in Civil Engineering 312,
https://doi.org/10.1007/978-981-19-9147-9_36

1 Introduction

Permeability is an intrinsic soil property. This property plays a major role in seepage of water through the earth dams, foundations, soil erosion, soil pollution, settlement of buildings, stability of roads and even yield of crop. Its importance has further been increased due to its pivotal role in presenting a solution to the problems of environmental control, dewatering and filtration process. The drainage through soil and thus the permeability assume a matter of high significance to hydraulic engineers, hydrologist and geologists.

The flow of water in earth crust takes place in vertical and horizontal directions and at any inclination. Determination of permeability thus becomes imminent in all the directions. A number of investigators have worked for the de6termination of permeability in vertical directions as Kenney [1], Shepherd [2], Okagbue [3], Sridharan and Prakash [4], Gupta et al. [5], Koomishi and Azarhoosh [6]. Alam et al. [7] carried out experiments to find out the horizontal permeability of some materials along with CFD simulation. Alam et al. [8] carried out the experimental work on stratified soils to determine the permeability in horizontal as well as in vertical directions with CFD simulation. Many investigators have determined the permeability both in vertical and horizontal directions, notable among them are Aronvici and Donman [9], Evans [10], Chan and Kenney [11], Dungca and Galpino [12], Shedid [13]. But, the work on permeability for sloping soil layers seems scarce in the literature. Thus, the present study was undertaken to investigate the pattern of permeability of sloping layers. Experiments have been conducted on the positively sloped layers as well as negatively sloped layers.

2 Methodology and Experimental Setup

The material selected for the study was fine sand as this material is frequently found in the water bearing strata. Thus, the study of movement of water through fine sand will be more useful as compared to other soil types. The material was collected from four different sites. Sieve analysis of the selected material was carried out as per IS: 2720 Part-IV 1985. The gradation curve for the said materials was plotted to ascertain the particle size range, as shown in Fig. 1.

The samples have been named as FS-1, FS-2, FS-3 and FS-4 on the basis of range of particle size. FS-1 is being the sample having finest particle size and FS-4 was having the coarser particles as evident from the figure. For the determination of permeability for the sloping layer, as no standard equipment was available, the horizontal permeameter fabricated at the Department of Civil Engineering, Aligarh Muslim University, was used for the purpose with slight modification. A layer of clay was laid at a slope of 10° and 20° to the horizontal, respectively, and the sample of fine sand layer with 15 cm thickness was placed over clay layer. Thereafter, another clay layer was placed above the sample. So, the fine sand layer was sandwiched

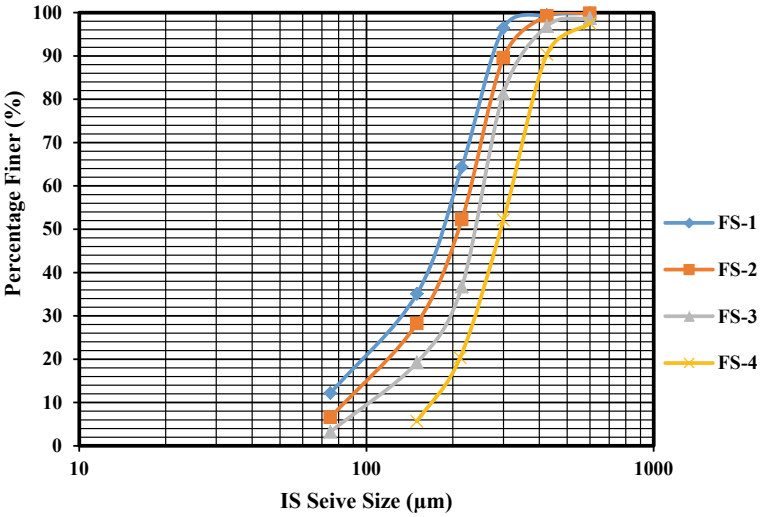

Fig. 1 Grain-size distribution curves for four samples of fine sand

between the clay layers. Water was allowed to flow through the sand layer to make it completely saturated. Sufficient time was allowed to stabilize the water level in inlet as well as outlet tube to get the accurate head loss occurring through the sample. For the accurate measurement of discharge, the measurement of time interval and the volume of water collected were done with utmost care. The arrangement is shown in Fig. 2.

Fig. 2 Permeability determination for inclined fine sand layer

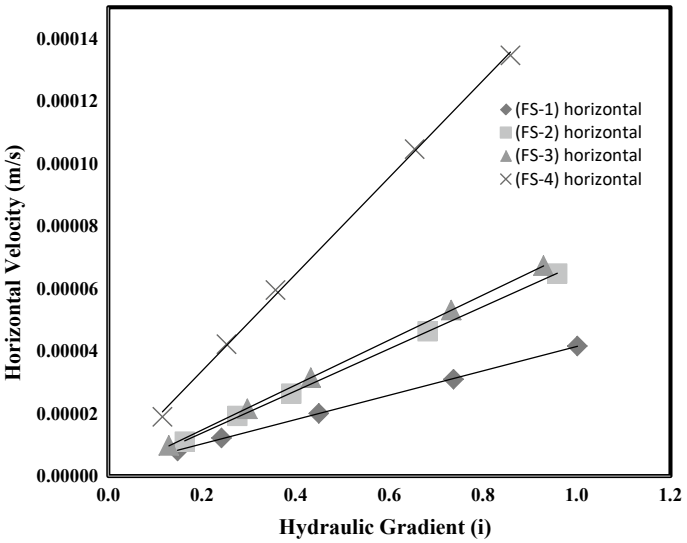

Fig. 3 Variation of horizontal velocity with hydraulic gradient for materials at 0º slope

The permeability of sand layer was initially determined keeping the layers in horizontal direction or 0° slope. For the determination of permeability, the variation of velocity was plotted against the hydraulic gradient of the sample at 0° slope. This variation is shown in Fig. 3. The slope of the curve gives the average permeability of the sample. Similarly, the variation of velocity with hydraulic gradient for +10° slope and −10° slope is shown in Figs. 4 and 5, respectively, and for the slope of + 20° and −20° is shown in Figs. 6 and 7, respectively.

Initially, the layer of fine sand was placed at a slope of +10° and then −10° with respect to horizontal. Thereafter, the slope of the layers was increased to +20° and − 20°. The observations were recorded and permeability was determined for the above four cases for all the samples with the help of above figures.

3 Results and Discussion

The analysis of the experimental data of permeability of sloping layers on designated inclination and the obtained inferences are presented below.

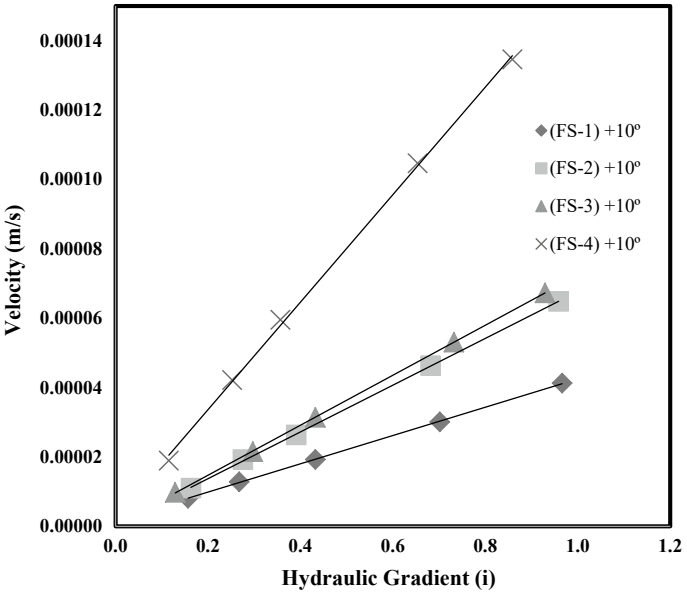

Fig. 4 Variation of velocity with hydraulic gradient for 10º negative slope

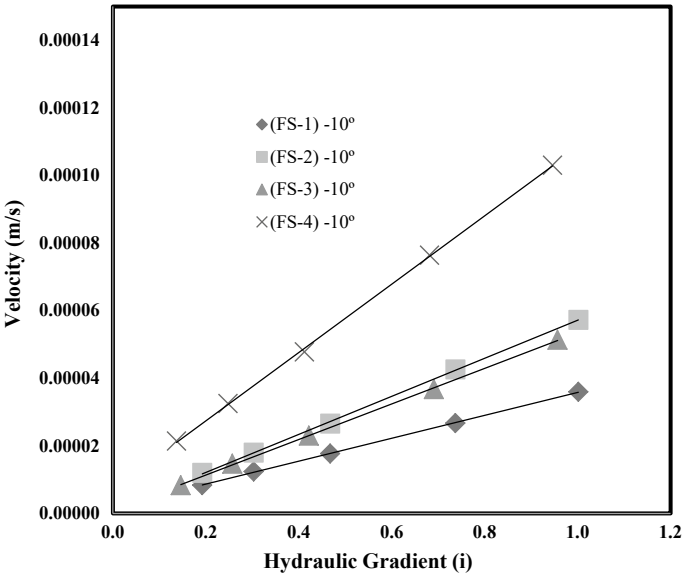

Fig. 5 Variation of velocity with hydraulic gradient for 10º positive slope

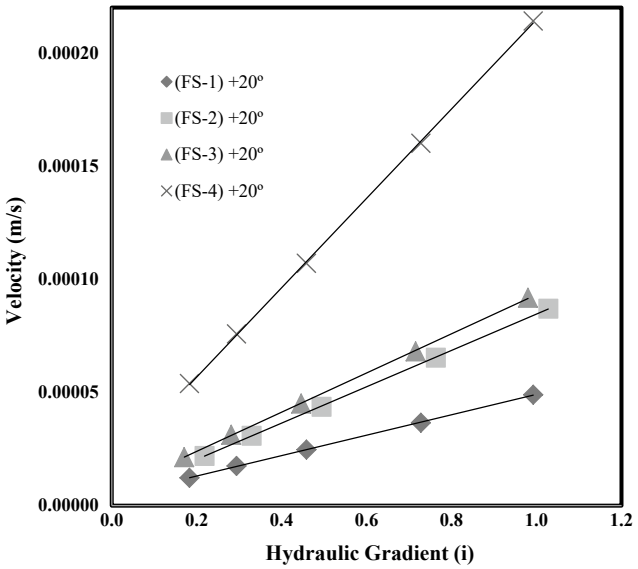

Fig. 6 Variation of velocity with hydraulic gradient for 20º positive slope

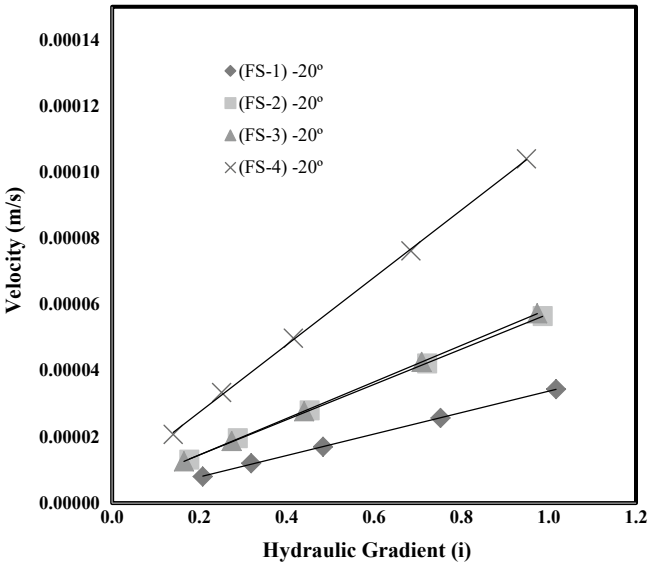

Fig. 7 Variation of velocity with hydraulic gradient for 20º negative slope

Table 1 Permeability of fine sand inclined at 0º and at 10º

S. No.	Soil combinations	Observed permeability (m/s)		Percent deviation
		0° slope	*10° positive slope*	
1	Fine sand-1 (FS-1)	3.90E−05	4.07E−05	− 4.36
2	Fine sand-2 (FS-2)	6.74E−05	7.73E−05	− 14.7
3	Fine sand-3 (FS-3)	7.20E−05	8.37E−05	− 16.3
4	Fine sand-4 (FS-4)	1.55E−04	1.89E−04	− 21.9

Table 2 Permeability of fine sand inclined at 0º and at − 10º

S. No.	Soil combinations	Observed permeability (m/s)		Percent deviation
		0º slope	*10º negative slope*	
1	Fine sand-1 (FS-1)	3.90E−05	3.39E−05	13.1
2	Fine sand-2 (FS-2)	6.74E−05	5.63E−05	16.5
3	Fine sand-3 (FS-3)	7.20E−05	5.26E−05	26.9
4	Fine sand-4 (FS-4)	1.55E−04	1.01E−04	34.8

3.1 Permeability at 10° Slope

The permeability of fine sand layer in horizontal direction and at +10° slope is presented in Table 1. It can be seen from Table 1 that permeability of positively sloped layer has increased with respect to the permeability in horizontal direction. Moreover, the permeability of the samples can be seen on a rising trend with increase in particle size. The deviation between horizontal permeability and positively sloped layer is thus found to have negative values.

Thereafter, the slope was reversed, i.e., fine sand layer was placed at −10° slope. The values of permeability obtained for this case are presented in Table 2 along with the values of permeability of same material in horizontal direction.

The permeability of negatively sloped layer was found to decrease as compared with the horizontal permeability. The percentage deviation was thus positive. However, with the increase in particle size, a rise in permeability was noticed for negative slope case. The maximum deviation observed in case of negative slope of 10° was obtained as 34.8%, whereas for the case of positive slope, the maximum deviation was found as −21.9%.

3.2 Permeability at 20° Slope

The slope of the fine sand layer was increased to 20°. In this case also, the permeability of positively sloped layer was found to increase when compared with corresponding horizontal permeability values. Thus, the percent deviation was negative as shown in

Table 3 Permeability of fine sand inclined at 0º and at 20º

S. No.	Soil combinations	Observed permeability (m/s)		Percent deviation
		0º slope	*20º positive slope*	
1	Fine sand-1 (FS-1)	3.90E−05	4.52E−05	− 15.9
2	Fine sand-2 (FS-2)	6.74E−05	8.03E−05	− 19.1
3	Fine sand-3 (FS-3)	7.20E−05	8.65E−05	− 20.1
4	Fine sand-4 (FS-4)	1.55E−04	1.97E−04	− 27.1

Table 4 Permeability of fine sand inclined at 0º and at − 20º

S. No.	Soil combinations	Observed permeability (m/s)		Percent deviation
		0º slope	*20º negative slope*	
1	Fine sand-1 (FS-1)	3.90E −05	3.24E−05	16.9
2	Fine sand-2 (FS-2)	6.74E−05	5.32E−05	21.1
3	Fine sand-3 (FS-3)	7.20E−05	5.51E−05	23.5
4	Fine sand-4 (FS-4)	1.55E−04	1.02E−04	34.2

Table 3. But, the deviation in values of permeability horizontal layers and the permeability of sloping layer at 20° slope was found to be higher than the corresponding values of deviation at 10°. In the former case, the maximum deviation was −21.9%, while for latter case, it was −27.1% (Tables 1 and 3).

After the experiment on positive slope of fine sand layer, the slope was changed to −20°. The values of permeability obtained for negative slope case is presented in Table 4 along with the values of permeability of same material in horizontal direction.

In general, the values of permeability for negatively sloped layer were found to be lesser than the corresponding values of horizontal permeability of the same layers. For −20° slope, the deviation between horizontal permeability and the permeability of sloped layer was found to be higher than the corresponding layers at −10° slope but only for the finer particle fragment. For coarser particle fragment, the corresponding deviation for −20° slope was slightly lesser as compared to −10° slope (Tables 2 and 4).

Comparison of deviation of permeability of layers inclined at +10° and − 10° with the deviation of permeability of layers in horizontal direction is shown in Table 5 and for the layers at slope of +20° with − 20° with horizontal layers is shown in Table 6.

With increase in slope from 10° to 20°, an increase in values of percent deviation was noticed for positively sloped layers. But for negatively sloped layers, the increase in percent deviation was noticed only for finer fraction of sand, while for coarser fraction, a slight decrease was observed. The minimum percent deviation was obtained for the finest sand (FS-1), and an increase in percent deviation was observed with the increase in particle size. Maximum percent deviation was obtained for the coarser sand (FS-4). When the permeability of +10° sloped layer and −10° sloped layer was

Table 5 Deviation of permeability of fine sand inclined at 10º and − 10º with horizontal

S. No.	Soil combinations	Deviation of permeability (%)	
		10º positive slope	*10º negative slope*
1	Fine sand-1 (FS-1)	− 4.36	13.1
2	Fine sand-2 (FS-2)	− 14.7	16.5
3	Fine sand-3 (FS-3)	− 16.3	26.9
4	Fine sand-4 (FS-4)	− 21.9	34.8

Table 6 Deviation of permeability of fine sand inclined at 20º and − 20º with horizontal

S. No.	Soil combinations	Deviation of permeability (%)	
		20º positive slope	*20º negative slope*
1	Fine sand-1 (FS-1)	− 15.9	16.9
2	Fine sand-2 (FS-2)	− 19.1	21.1
3	Fine sand-3 (FS-3)	− 20.1	23.5
4	Fine sand-4 (FS-4)	− 27.1	34.2

compared with respective permeability of horizontal layer (Table 5), it was found that the magnitude of the deviation of negatively sloped layer was more as compared to the deviation of positively sloped layer. Similar trend can be observed in Table 6, where the deviation of positive 20° sloped layer is lesser than the deviation of negative 20° sloped layer. It indicates that for positively sloped layer, the percentage increase in permeability is less than the percentage decrease in permeability for negatively sloped layer when compared with respective horizontal permeabilities. If the slope is kept constant, the difference between deviation of permeability of positive and negative sloping layers increases with increase in particle size.

4 Conclusion

From the present study, the following conclusions may be drawn:

- Permeability of positively sloped layer was found to increase, whereas for negatively sloped layer the permeability was found to decrease with respect to horizontal permeability of same layers.

- For positively sloped layer, at the same slope, the percentage increase in permeability is less than the percentage decrease in permeability for negatively sloped layer when compared with respective horizontal permeabilities.
- At constant slope, the deviation of permeability between positively and negatively sloped layers was found to increase with increase in particle size.

Acknowledgements The present study has been undertaken as part of a UPCST Project entitled "An experimental study on permeability of layered soils parallel to the bedding plane". We would like to give special thanks to Uttar Pradesh Council of Science and Technology for funding the project.

References

1. Kenney TC et al (1984) Permeability of compacted granular materials. Can Geotech J 21(4)
2. Shepherd RG (1989) Correlations of permeability and grain size. National Ground Water Assoc 27(5):633–638
3. Okagbue CO (1995) Permeability of stratified sands. Geotech Geolog Eng 13:157–168
4. Sridharan A, Prakash K (2002) Permeability of two layered soils. Geotech Testing J 25(4):443–448
5. Gupta P et al (2020) A simulation and experimental approach for flow through stratified porous media perpendicular to bedding plane. Water Energy Int 63(1):59–72
6. Koomishi M, Azarhoosh A (2021) Assessment of permeability of granular drainage layer considering particle size and air void distribution. Constru Build Mater
7. Alam J et al (2020) An experimental study with CFD simulation of horizontal flow through porous media. Water Energy Int 63(3):48–55
8. Alam J et al (2020) An experimental and simulation study of flow through stratified soils. Water Energy Int 63(9):60–72
9. Aronovici VA, Donnan WW (1946) Soil-permeability as a criterion for drainage-design. Am Geophys Union 27(1):95–101
10. Evans HE (1962) A note on the average coefficients of permeability for a stratified soil mass. Ph.D. Thesis
11. Chan HT, Kenney TC (1973) Field investigation of permeability ratio of New Liskeard varved soil. Can Geotech J 10(3)
12. Dungca JR, Galupino JG (2016) Artificial neural network permeability modeling of soil blended with Flyash. Int J GEOMATE, 12(31):77–82
13. Shedid SA (2019) Vertical-horizontal permeability correlations using coring data. Egypt J Pet 28(1):97–101

Groundwater Flow Modeling for Evaluating Specific Yield Sensitivity of a Sandstone Aquifer System in Gunderu Sub-basin

S. V. Vijaya Kumar, A. Vara Prasada Rao, N. Srinivas, and D. Srija

Abstract Gunderu is an important minor stream in West Godavari district and drains through upland region. It finally joins the Kolleru Lake, a freshwater lake sandwiched between Krishna and Godavari deltas. Gunderu sub-basin considered has an aerial extent of 297 km^2 with stream length 35 km. Intensive irrigation with ground water is prevailing in the study area, and the long term water levels are in depleting nature. The overall rates and magnitude of groundwater depletion in most of the aquifers are not well characterized. To understand the groundwater flow in the study area, modeling is carried using FREEWAT based on QGIS and MODFLOW to simulate the effect of different stress conditions of pumping and recharge. In this paper, an attempt is made to determine the sensitivity of specific yield of the model in satisfying continuity of groundwater flow for variation of pumping to simulate the different groundwater developments in the aquifer. The analysis helped to understand the existing behavior of ground water flow, and various scenarios are performed to observe the sensitivity of model by taking different specific yield conditions such as 3, 4, 5, 10, and 15% to determine its influence under various stress conditions such as wells, river, recharge due to rainfall, and tanks. Any change in volume of water in the aquifer due to pumping and recharge is associated with the specific yield of the aquifer. From the model same is analyzed for different specific yield values. Thus, with pumping, for different specific yield of aquifer formation, the change in aquifer volume and hydraulic heads changes differently in the aquifer system. The sensitivity of aquifer system to spatial variation in specific yield and thus variation in piezometric heads in the study area is presented in the paper.

Keywords Groundwater model · FREEWAT · Water balance theory · Specific yield

S. V. Vijaya Kumar (✉) · D. Srija
Deltaic Regional Centre, National Institute of Hydrology, Kakinada 533003, India
e-mail: vijayakumar.nihr@gov.in

A. Vara Prasada Rao · N. Srinivas
A.P. State Groundwater and Water Audit Department, Vijayawada 520011, India

P. V. Timbadiya et al. (eds.), *Hydrology and Hydrologic Modelling*,
Lecture Notes in Civil Engineering 312,
https://doi.org/10.1007/978-981-19-9147-9_37

1 Introduction

In any aquifer system, the natural consequence of recharge results in addition of groundwater storage. Similarly, the natural consequence of groundwater withdrawal is the removal of water from subsurface storage. Knowledge of geologic structure is very important to understand aquifer characteristics and its groundwater flow and its water level fluctuation. The scenario is complex in multi-aquifer systems. Groundwater flow is mainly controlled by the continuity and interconnectedness of the aquifers, particularly in the vertical direction, rather than the hydraulic conductivity. Variation of specific yield also makes it more complex.

A groundwater flow model can simulate hydraulic heads (and water table elevations in the case of unconfined aquifers) and groundwater flow rates within and across the boundaries of the system under consideration. It can provide estimates of water balance and travel times along flow paths [7]. Groundwater models, however, even as approximations are a useful investigation tool that groundwater hydrologists may use for a number of applications [6].

1.1 FREEWAT Model

The FREEWAT (Free and open source software tools for water resource management) platform integrates a hydrological model in the QGIS GIS interface, where data are managed through a SpatiaLite Data Base Management System (DBMS), enabling the assessment of water balances and the availability of water resources in space and time, in order to support the management and planning processes [2]. Input and output data are managed through the SpatiaLite Data Base Management System [3]. Koltsida and Kallioras [5] demonstrated using the FREEWAT plug-in directly in the QGIS environment, to easily archive, pre-process, and analyzes large datasets, build a set of models, and post-process results.

2 Study Area and Data Source

Gunderu is an important minor stream in West Godavari district and drains through upland region. It finally joins the Kolleru Lake, a freshwater lake sandwiched between Krishna and Godavari deltas. Gunderu sub-basin considered has an aerial extent of 297 km^2 with stream length 35 km (Fig. 1). Groundwater is the main irrigation source in this area, and utilization of groundwater is very high with more than 70% stage development. The overall rates and magnitude of groundwater depletion in most of the aquifers are not well characterized [1]. Hence, it is necessary to model the pattern of the groundwater flow in multi-aquifer systems of Gunderu sub-basin for sustainable development of groundwater resources.

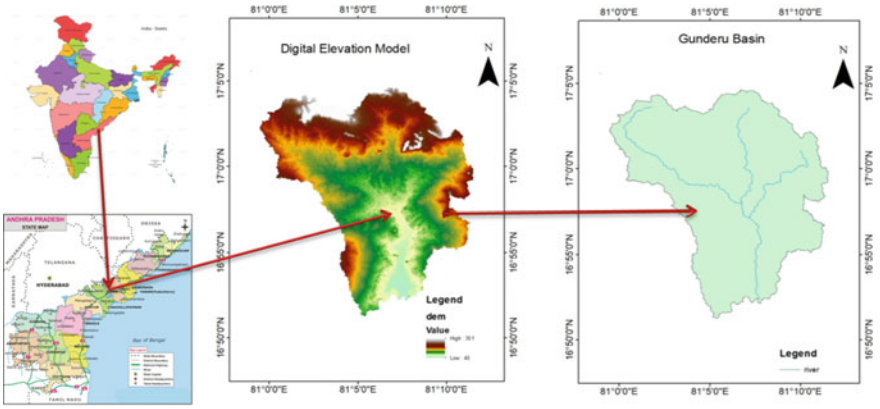

Fig. 1 Location map of the study area

The SRTM DEM (Shuttle radar topography mission digital elevation model) of 30 m resolution is used for hydrological processing of the Gunderu river basin. Using HEC-Geo HMS software, DEM is processed to obtain boundary and river line. The maximum area in which river streams outcropped from the hilly areas is extracted based on Survey of India (SOI) toposheets and DEM. The catchment extracted has an area of 297.16 km^2 and the length of the river is 35 km. A slope map is also prepared using DEM.

In the study area, the piezometer readings are observed at Kamavarapukota, K. Gokavaram, Kallacheruvu, and Munduru. These readings represent piezometric head with respect to m.s.l. To get the piezometric head, the depth of groundwater level is subtracted from an elevation of measuring point or ground level. Using piezometers data, contours are generated for the post-monsoon period (Dec 2019), pre-monsoon (May 2020), and groundwater slope maps are prepared (Fig. 2). Piezometric head variation of 90 m at upland sandstone aquifers to 20 m at the downstream of the basin in December 2019 and 85 m to 15 m in May 2020 is observed in the study area.

Well density is a crucial factor from the supply as well as the demand side. Well density is defined as the number of wells present per square kilometer area. The well density for each village in the study area is considered for modeling. A variation of well density from 71 to 5 wells/km^2 is observed at different locations in the study area. Landsat 8 satellite image of 30 m resolution dated 06/05/2019 is used for the preparation of land use/land cover maps using supervised classification in an image processing software after field visits for ground truth verification for each classification.

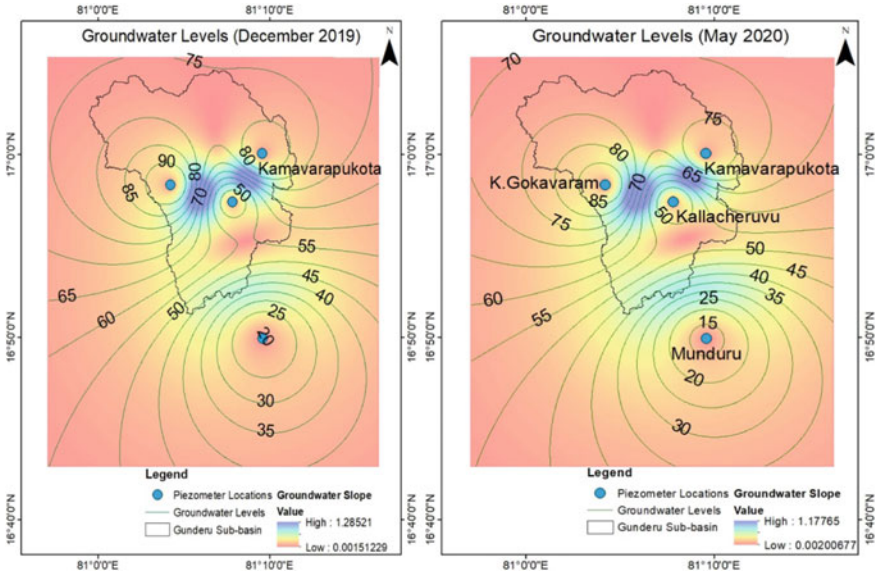

Fig. 2 Groundwater level contours on slope map in December 2019 and May 2020

3 Methodology

The SRTM DEM (Shuttle Radar Topography Mission Digital Elevation Model) of 30 m resolution is used for hydrological processing of the Gunderu river basin. Using HEC-Geo HMS software, DEM is processed to obtain boundary and river lines. The maximum area in which river streams are outcropped from the hilly areas is extracted based on SOI toposheets and DEM. The catchment extracted has an area of 297.16 km^2, and the length of the river is 35 km. According to GEC-2015, Hilly areas having slopes > 20% contribute to direct runoff rather to groundwater recharge. So the areas having a slope > 20% are identified from the slope map and taken as the inactive zone for model simulation.

Other thematic layers (Fig. 3) such as tanks and wells are prepared based on observed data and land use/land cover map. According to GEC-2015 norms, seepage from tanks and ponds can be taken as 1.4 mm/day [8]. The return flow factor considered for recharge is 33% in non-monsoon. According to GEC-2015, the specific yield for sandstone formations in Gunderu basin is taken as 3% or 0.03. Various scenarios are performed by taking different specific yield conditions such as 3, 4, 5, 10 and 15% to determine its sensitivity under various stress conditions such as wells, river, recharge due to rainfall, and tanks using FREEWAT model. The influence of wells, river, and tanks is determined for a one-year simulation consisting of six stress periods (SP's). The impact due to river recharge (SP3-SP2), impact due to no pumping (SP5-SP4), and impact due to tank recharge (SP6-SP5) are determined by performing raster analysis.

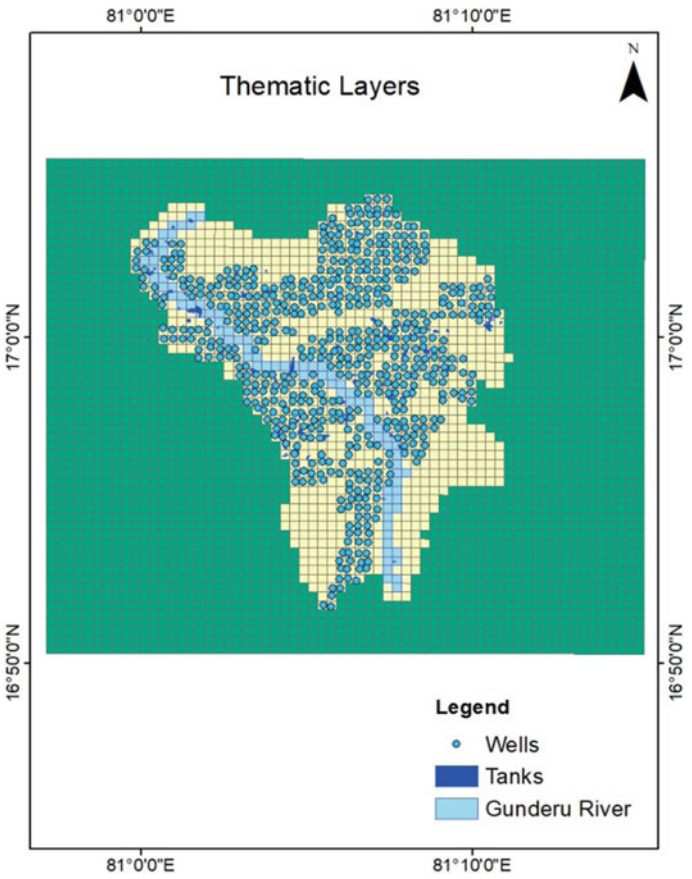

Fig. 3 Thematic layers used as input in model

4 Groundwater Modeling

FREEWAT software through the application of MODFLOW-2005 [4] is used for the analysis. The grid cell size taken for modeling is 500 m * 500 m. The two model layers considered for modeling are the upper aquifer and lower aquifer, respectively. The initial surface elevation of the upper aquifer and lower aquifers is 90 m and 70 m above the m.s.l, respectively (Table 1). To represent the real conditions of aquifer geometry, the surface elevation of the upper aquifer is varied 120 m at the upstream to 80 m at downstream, and similarly surface elevation of the lower aquifer is varied 100 m at the upstream to 60 m at the downstream. Aquifer parameters considered are hydraulic conductivity in x, y, and z directions, i.e., K_x, K_Y, and K_z, initial head, specific yield and taken accordingly with the field observed data. Specific yield is taken as 0.03 and hydraulic conductivity is taken as 1 km/year or 2.74 m/d. Initial head is considered as 75 m above m.s.l (according to observed piezometric data).

Table 1 Modeled aquifer layers (initial values)

S. No.	Layer name	Top w.r.t m.s.l	Bottom w.r.t m.s.l	Thickness
1	Upper_Aquifer	90	70	20
2	Lower_Aquifer	70	0	70

To match with the real conditions of the aquifer, the actual pumping rate of the well is not considered directly. Instead, the pumping rate from each well for simulation is taken as 12.5% of what has been pumped from the observed well and gradually increased the pumping stage up to 100% to represent the past and present situations and thus evaluating groundwater development changes in the aquifer.

Time discretization in MODFLOW is based on stress periods (SP), namely time intervals during which boundary conditions and sink/source terms are constant. Each SP can be further subdivided into time steps (TS's), namely shorter time intervals which allow evaluating the time evolution of the solution. The length of duration for initial stress conditions referred as SP1 and followed by SP2, SP3, SP4, SP5, and SP6. In this study, SP1 is defined for 10 days consisting of 2 time steps with evapotranspiration, rainfall recharge, recharge due to tanks, and well pumping as stress conditions. SP2 is defined for 60 days consisting of 8 time steps with evapotranspiration, rainfall recharge, and recharge due to tanks and well pumping as stress conditions. SP3 is defined for 10 days consisting of 2 time steps with river flow having stage of 1 m, evapotranspiration, rainfall recharge, and recharge due to tanks and well pumping as stress conditions. SP4 is defined for 60 days consisting of 8 time steps with evapotranspiration, rainfall recharge, and recharge due to tanks and well pumping as stress conditions. SP5 is defined for 114 days consisting of 15 time steps with evapotranspiration, recharge due to tank, and recharge due to return flow from groundwater irrigation as stress conditions. SP6 is defined for 110 days consisting 15 time steps with evapotranspiration, and recharge due to tanks, recharge due to return flow from groundwater irrigation, and well pumping as stress conditions (Tables 2 and 3).

Table 2 Initial stress condition

Initial stress conditions considered for one-year simulation						
SP	State	Length	Time steps	Stress conditions		
				RIVER in terms of stage w.r.t bed level in m	EVTR m/d	WELL in terms of % draft considered from each well
1	Transient	10	2	0	0.003	12.5
2	Transient	60	8	0	0.003	12.5
3	Transient	10	2	1	0.003	12.5
4	Transient	60	8	0	0.003	12.5
5	Transient	114	15	0	0.003	0
6	Transient	110	15	0	0.003	12.5

Table 3 Recharge conditions

Recharge conditions: initial values			
SP	Recharge due to rainfall in m/d	Recharge due to tanks in m/d	Recharge due to return flow from ground water irrigation in m/d
1	0.002	0.0014	0
2	0.002	0.0014	0
3	0.002	0.0014	0
4	0.002	0.0014	0
5	0	0.0014	0.00066
6	0	0	0.00066

Here, Rch is the rainfall recharge in m/d and EVTR is the evapotranspiration rate from upper aquifer in m/d. WELL is Pumping Rate or Recharge Rate in m^3/d. For pumping negative sign is considered and for recharge positive sign is considered.

To determine the impact due to river recharge, raster analysis is performed by subtracting the head calculated for the lower aquifer layer at the end of SP 3 and the head calculated for each model layer at the end of SP 2, i.e., SP3-SP2. To determine the impact due to no pumping, raster analysis is performed by subtracting the head calculated for the lower aquifer layer at the end of SP 5 and the head calculated for each model layer at the end of SP 4, i.e., SP5-SP4. Similarly, to determine the impact due to tank recharge, raster analysis is performed by subtracting the head calculated for the lower aquifer layer at the end of SP 6 and the head calculated for each model layer at the end of SP 5, i.e., SP6-SP5. The same procedure is repeated for specific yields 0.04, 0.05, 0.10, and 0.15 with well-pumping rates 12.5%, 25%, 37.5%, 50%, 75% and 100%, respectively.

5 Results and Discussions

The impact due to river recharge (SP3-SP2), impact due to no pumping (SP5-SP4), and impact due to tank recharge (SP6-SP5) are determined by performing raster analysis between various stress periods. Volumetric changes at the end of one-year simulation when wells pumping rate taken from 12.5 to 100.0% for specific yield values 3, 4, 5, 10 and 15% are given in Table 4.

5.1 The Pattern of Hydraulic Heads

Hydraulic heads obtained from the model under various stress conditions with pumping rates 12.5, 25, 37.5, 50, 75 and 100% when specific yield values 3, 4, 5, 10 and 15% are considered to determine the behavior flow (Table 5).

Table 4 Quantitative aspects in lower aquifer at the end of one-year simulation

(a) Change in aquifer volume in MCM due to impact of river recharge (SP3-SP2)						
Sy/pumping stage	12.50%	25%	37.50%	50%	75%	100%
0.15	3.9639	−3.0515	−10.055	−17.19	−31.623	−45.999
0.1	3.5102	−6.915	−17.507	−28.381	−49.859	−72.166
0.05	1.7233	−19.499	−41.442	−63.164	−106.7	−151.45
0.04	−0.5257	−25.422	−52.418	−79.885	−133.62	−187.55
0.03	−6.2276	−41.81	−80.212	−117.71	−193.37	−270.22
(b) Change in aquifer volume in MCM due to impact of no pumping (SP5-SP4)						
Sy/pumping stage (%)	12.50	25	37.50	50	75	100
0.15	38.5505	40.5745	41.6949	43.374	46.7742	50.5039
0.1	43.9003	48.7675	52.4403	53.2051	58.1634	64.0073
0.05	46.7754	59.9112	72.8779	77.8556	97.8867	114.736
0.04	54.0506	65.2637	82.1243	91.2791	119.442	140.548
0.03	69.7271	77.5003	100.408	122.753	167.022	202.469
(c) Change in aquifer volume in MCM due to impact of tank recharge (SP6-SP5)						
Sy/pumping stage (%)	12.50	25	37.50	50	75	100
0.15	−57.77	−141.18	−225.03	−312.2	−491.99	−669.4
0.1	−94.656	−218.9	−345.57	−474.31	−741.7	−1005.9
0.05	−187.28	−446.44	−699.97	−963.65	−1483.4	−2018.6
0.04	−228.29	−549.33	−859.12	−1182.9	−1824.7	−2493.8
0.03	−328.49	−779.99	−1216.6	−1677.8	−2601.1	−3556.6

5.2 Normalization of Results

Normalization basically means bringing all the values to one scale. In this analysis, normalization is used for determining the impact of change in the average head with an increase in specific yield and pumping stage (Fig. 4). The change in the average hydraulic head is scaled from 0 to 1 with corresponding to an increase in specific yield and well pumping. Normalized value (Y') is given as follows:

$$Y' = \frac{Y - Y_{\min}}{Y_{\max} - Y_{\min}}$$

For any normalized factor between 1 and 0, the change in the average head in meters and specific yield (S_y) corresponding to that factor can be determined at a particular pumping rate using this analysis. For example at 12.5% pumping for a normalized head factor 0.3 (Y'), the corresponding change in the average head (Y) due to impact of river recharge can be determined by substituting $Y_{\max} = 0.0133$ and $Y_{\min} = -0.0210$ from Table 5(a) in the above equation. The change in the average head due to impact of river recharge corresponding to normalized head factor 0.3 is −0.0107,

Table 5 Change in the average head of lower aquifer at the end of one-year simulation

(a) Change in average head in m due to impact of river recharge (SP3-SP2)						
Sy/pumping stage	0.125	0.25	0.375	0.5	0.75	1
0.15	0.0133	−0.0103	−0.0338	−0.0578	−0.1064	−0.1548
0.1	0.0118	−0.0233	−0.0589	−0.0955	−0.1678	−0.2428
0.05	0.0058	−0.0656	−0.1395	−0.2126	−0.3591	−0.5096
0.04	−0.0018	−0.0855	−0.1764	−0.2688	−0.4497	−0.6311
0.03	−0.021	−0.1407	−0.2699	−0.3961	−0.6507	−0.9093
(b) Change in average head in m due to impact of no pumping (SP5-SP4)						
Sy/pumping stage	0.125	0.25	0.375	0.5	0.75	1
0.15	0.1297	0.1365	0.1403	0.146	0.1574	0.17
0.1	0.1477	0.1641	0.1765	0.179	0.1957	0.2154
0.05	0.1574	0.2016	0.2452	0.262	0.3294	0.3861
0.04	0.1819	0.2196	0.2764	0.3072	0.4019	0.473
0.03	0.2346	0.2608	0.3379	0.4131	0.5621	0.6813
(c) Change in average head in m due to impact of tank recharge (SP6-SP5)						
Sy/pumping stage	0.125	0.25	0.375	0.5	0.75	1
0.15	−0.1944	−0.4751	−0.7573	−1.0506	−1.6556	−2.2526
0.1	−0.3185	−0.7366	−1.1629	−1.5961	−2.4959	−3.3851
0.05	−0.6302	−1.5023	−2.3555	−3.2428	−4.9918	−6.7928
0.04	−0.7682	−1.8486	−2.8911	−3.9806	−6.1403	−8.3921
0.03	−1.1054	−2.6248	−4.0939	−5.6459	−8.753	−11.9686

and the corresponding specific yield by interpolating the adjacent values is 0.035, i.e., 3.5%. Similarly, the change in the average head (Y) due to the impact of no pumping can be determined by substituting $Y_{\max} = 0.2346$ and $Y_{\min} = 0.1297$ from Table 5(b) in the above equation. The change in the average head due to impact of no pumping corresponding to normalized head factor 0.3 is 0.1612, and corresponding specific yield by interpolating the adjacent values is 0.042, i.e., 4.2%. Similarly, the change in the average head (Y) due to impact of tank recharge can be determined by substituting $Y_{\max} = -0.1944$ and $Y_{\min} = -1.1054$ from Table 5(c) in the above equation. The change in the average head due to impact of tank recharge corresponding to normalized head factor 0.3 is −0.8321 corresponding specific yield by interpolating the adjacent values is 0.038, i.e., 3.8%.

5.3 Depth to Water Level

The patterns of depth to water level (DWL) with respect to the piezometric surface when there is no pumping are evaluated from modeling to observe the change in

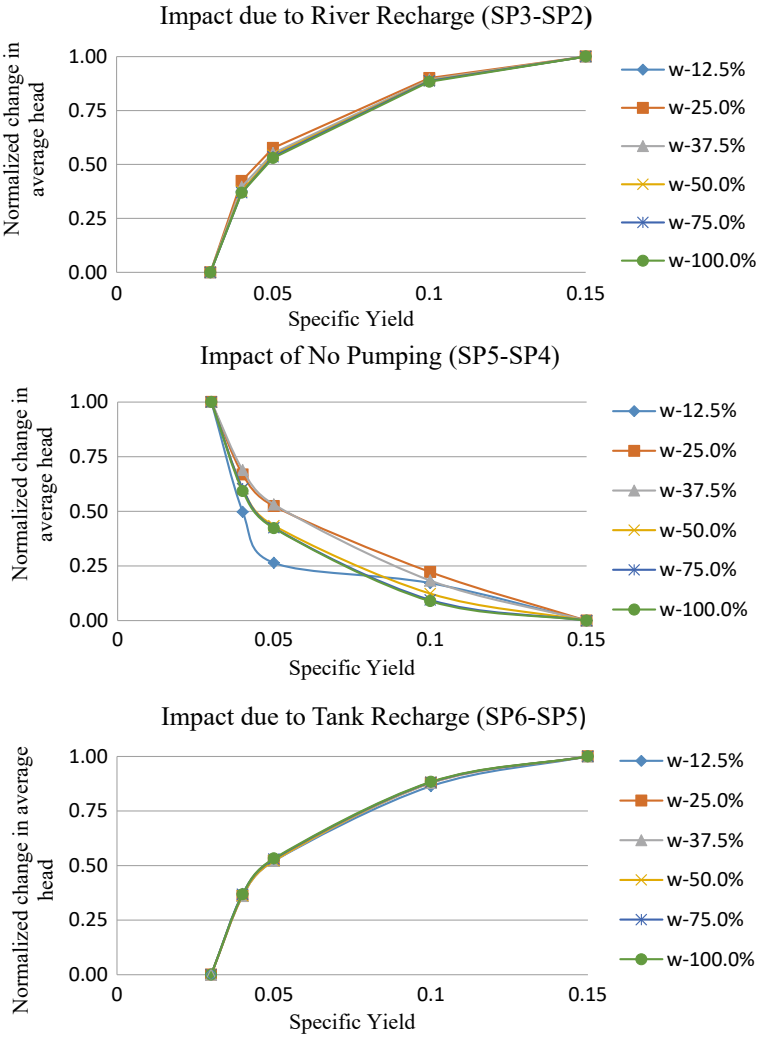

Fig. 4 Normalized change in the average head with specific yield and stages of pumping

ground water elevation. The DWL is changed from 20 m at the downstream sub-basin to 15 m at upland aquifers is observed when pumping is stopped at the stage of 12.5% which has shown a significant variation of 25 m to 15 m over the study area when pumping is stopped at the stage of 100% (Fig. 5).

Further, the variation of maximum depth to piezometric head with specific yield is analyzed (Fig. 6) at each pumping stage. The maximum depth to water level varies from 30 m at 3% specific yield to 25 m at 15% specific yield is observed when pumping stopped at the stage 100%. These details helped to evaluate the storage of the aquifer in terms of the head and sensitivity of the specific yield of the aquifer.

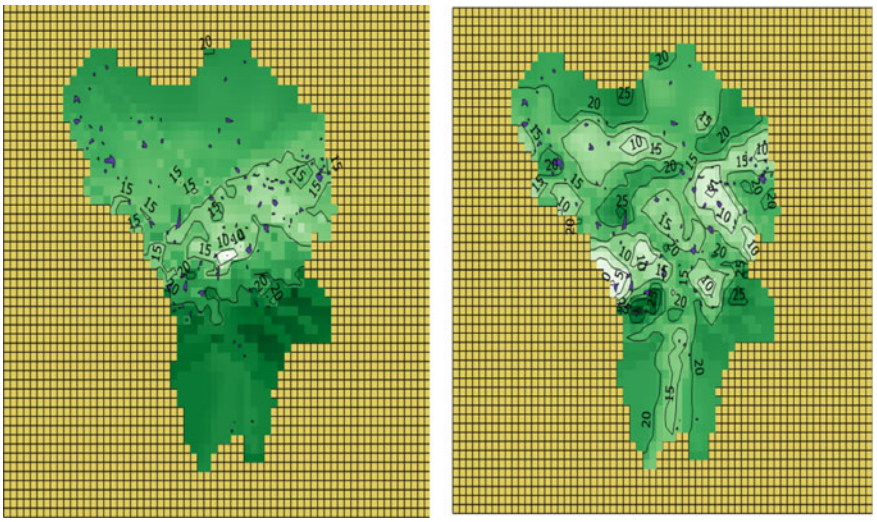

At 12.5% pumping stage *At 100% pumping stage*

Fig. 5 Depth to water level w.r.t piezometric surface resulted from 12.5% pumping and 100% pumping, respectively, when pumping stopped at 3% specific yield (SP5-SP4)

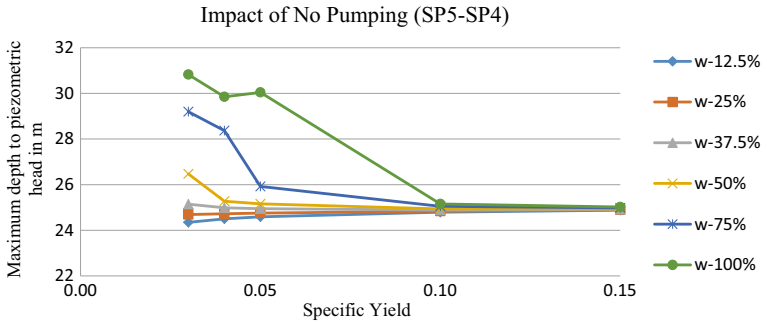

Fig. 6 Depth to water level w.r.t piezometric surface resulted from different pumping stages respectively when pumping stopped (SP5-SP4)

6 Conclusions

In this paper, an attempt is made to understand the sensitivity of the model in satisfying continuity of groundwater flow for variation of pumping from past 12.5% to present 100% at an incremental pumping of 25, 37.5, 50 and 75% to simulate the different groundwater developments in the aquifer. Various scenarios are performed by taking different specific yield conditions such as 3, 4, 5, 10 and 15% to determine its influence under various stress conditions such as wells, river, recharge due to rainfall, and tanks using FREEWAT model. The minimum depth to the piezometric surface

when pumping stopped at 100% pumping rate and 3% specific yield is nearly −0.7 m, i.e., the water level is raised to 0.7 m above the ground surface at that region which is actually 15 m below the earth surface, whereas the minimum depth to the piezometric surface when pumping stopped at 12.5% pumping rate and 3% specific yield is nearly 5 m, i.e., this resulted in 10 m rise of the head at that region. The minimum depth to the piezometric surface when pumping stopped at 100% pumping rate and 15% specific yield is nearly 11 m, i.e., this resulted in 4 m rise of the head at that region, whereas the minimum depth to the piezometric surface when pumping stopped at 12.5% pumping rate and 15% specific yield is nearly 11 m, i.e., this resulted in 5 m rise of the head at that region. It is observed from the analysis that the amount of water pumped is constant as it is to meet the crop water requirement and is irrespective of the specific yield of the aquifer. The change in aquifer volume and the average head keeps on increasing as specific yield increases at a certain pumping rate. The change in water volume keeps on decreasing as specific yield increases at a certain pumping rate. With an increase in well-pumping rate and specific yield, there is a reduction in change in aquifer volume and hydraulic heads and the relationship is presented.

Acknowledgements The authors thank Director, NIH, Roorkee and Director, APSGW & WA Dept., Vijayawada and NHP, MoJS, New Delhi for funding the study.

References

1. CGWB (2017) Aquifer mapping and management of ground water resources sandstone area of East Godavari, West Godavari and Krishna Districts, Andhra Pradesh, CGWB Report (2016–2017), CGWB, Faridabad
2. Dadaser-Celik F, Celik M (2017) Modelling surface water-groundwater interactions at the Palas Basin (Turkey) using FREEWAT. AcqueSotterranee—Italian J Groundwater 6(3/149):53–60. https://doi.org/10.7343/as-2017-288
3. De Filippis G, Borsi I, Foglia L, Cannata M, Velasco Mansilla V, Vasquez-Sune E, Ghetta M, Rossetto R (2017) Software tools for sustainable water resources management: the GIS-integrated FREEWAT platform. Rendiconti Online SocietàGeologicaItaliana 42:59–61. https://doi.org/10.3301/ROL.2017.14
4. Harbaugh AW (2005) MODFLOW-2005. The US Geological Survey Modular Ground-Water Model—the Ground-Water Flow Process. U.S. Geological Survey, Techniques and Methods, 6-A16, p 253
5. Koltsida E, Kallioras A (2019) Groundwater flow simulation through the application of the FREEWAT modeling platform. J Hydroinf 21(5):812–833. https://doi.org/10.2166/hydro.2019.040
6. Kumar CP (2003) Conceptualization in groundwater modelling. J Appl Hydrol Assoc Hydrol India XVI(1):17–28
7. Kumar CP (2015) Modelling of groundwater flow and data requirements. Int J Mod Sci Eng Technol (IJMSET) 2(2):18–27
8. MoWR (2017) Ground water resource estimation committee report. GEC-2015. MoWR, New Delhi

Groundwater Flow Modeling in a Heterogeneous Porous Medium Using Meshless Method

Tinesh Pathania and T. I. Eldho

Abstract Groundwater flow modeling plays an important role in managing the groundwater resources. Several numerical models have been used to model the groundwater flow in hypothetical and field aquifers. These models can predict future groundwater level in an aquifer system using the available groundwater information and incoming/outgoing water into it for the selected time period. In most of the past studies, finite difference (FDM) and finite element methods (FEM) have been used to solve the variety of groundwater problems. In the last two decades, meshless methods have been successfully used to model the groundwater flow in porous media. These methods represent the problem domain with scattered and unconnected nodes in contrast to the mesh/grids in FDM/FEM. In the present study, meshless element-free Galerkin method (EFGM) is used to model the groundwater flow in a hypothetical heterogeneous porous medium. The considered flow domain is assumed to consist of zones of different hydraulic conductivities and also has a few pumping and recharge wells. In this study, both finer and coarser nodes are also used to represent the computational domain and compare their EFGM solution. The results of the EFGM flow model are checked against those with MODFLOW model, and it showed a good agreement, showing the applicability of EFGM.

Keywords Element-free Galerkin method · Groundwater flow · Heterogeneous aquifer · Meshless method

T. Pathania (✉)
Department of Environmental Science and Engineering, Indian Institute of Technology (Indian School of Mines), Dhanbad, Jharkhand 826004, India
e-mail: tineshpathania@iitism.ac.in

T. I. Eldho
Department of Civil Engineering, Indian Institute of Technology Bombay, Mumbai 400076, India
e-mail: eldho@civil.iitb.ac.in

P. V. Timbadiya et al. (eds.), *Hydrology and Hydrologic Modelling*,
Lecture Notes in Civil Engineering 312,
https://doi.org/10.1007/978-981-19-9147-9_38

1 Introduction

Groundwater resources store the fresh water and hence, extensively used to meet the daily water needs of large population of the world. These resources also play a crucial role in the industrial and agricultural sectors. Worldwide increasing dependency on the groundwater resources demands for proper management of these resources. To manage these resources, numerical models are effective in simulating the response of precipitation and groundwater withdrawals in real aquifer systems. The mesh-based finite difference method (FDM) and finite element method (FEM) have been used to model the groundwater flow in many studies [1–4]. The other type of numerical methods known as meshless methods have shown significant potential to solve the variety of groundwater problems in the last two decades. These methods solve the governing groundwater flow equation using a set of scattered field nodes in the computational domain. They do not require computational mesh unlike FDM/FEM, and it makes them more flexible to represent complex aquifer shapes.

Meshless methods have been applied to develop the several meshless groundwater models in the recent years. A variety of meshless methods such as meshless element-free Galerkin method (EFGM), point collocation method (PCM), meshless local Petrov–Galerkin method (MLPGM), radial point collocation method (RPCM) have been used to develop these models. Park and Leap [5] used the meshless EFGM to model the confined groundwater flow for a hypothetical problem. Praveen Kumar and Dodagoudar [6] used the meshless EFGM to analyze the contaminant transport in an unsaturated porous media. Meenal and Eldho [7] used the meshless PCM to solve the groundwater flow problems. They solved the hypothetical as well as real case studies. Meenal and Eldho [8] extended the application of PCM to solve the coupled groundwater flow and contaminant transport equations and successfully tested it over the real field problem. Mategaonkar and Eldho [9] designed the optimized in-situ bioremediation system using the PCM simulations and particle swarm optimization (PSO). Swathi and Eldho [10] estimated the groundwater levels with the MLPGM. They also used it for the real aquifer simulations. Guneshwor Singh et al. [11] presented the coupled flow and transport simulations of meshless RPCM in different problems. Boddula and Eldho [12] successfully applied the MLPG to different types of contaminant transport problems. Pathania et al. [13] modeled the unconfined flow using the EFGM and also applied it to a real field sloping aquifer. Seyedpour et al. [14] combined the RPCM simulations of flow and transport models with the genetic algorithm (GA) for optimal groundwater remediation. Pathania and Eldho [15] coupled the EFGM simulations of flow and transport models and applied it to both hypothetical and real aquifers. Anshuman and Eldho [16] integrated the RPCM simulations of flow and multispecies reactive transport models. Pathania et al. [17] solved the coupled flow and reactive transport equations by EFGM. Pathania et al. [18] developed a BIOEFGM model for aerobic biodegradation of petroleum

hydrocarbons in groundwater and integrated it with PSO to estimate the optimized cost of in-situ bioremediation operation.

In the above studies, meshless EFGM has been tested over several types of flow and transport problems. In the present study, EFGM is selected to demonstrate its potential to model the groundwater flow in a heterogeneous porous medium. For verification purpose, EFGM results are tested against those with MODFLOW results. EFGM performance with both finer and coarser nodal distribution in the heterogeneous aquifer is also tested in this study.

2 Governing Equation

The steady state groundwater flow equation for the unconfined aquifer is expressed as [19]

$$\frac{\partial}{\partial x}\left(K_x h \frac{\partial h}{\partial x}\right) + \frac{\partial}{\partial y}\left(K_y h \frac{\partial h}{\partial y}\right) = Q_w \tag{1}$$

The Dirichlet and Neumann types of boundaries for Eq. (1) are, respectively, expressed as

$$h(x, y) = h_1(x, y) \quad x, y \epsilon \partial\Omega_1 \tag{2a}$$

$$Kh\frac{\partial h}{\partial n} = q_1(x, y) \quad x, y \epsilon \partial\Omega_2 \tag{2b}$$

where $h(x, y)$ is the groundwater head (m), K_x and K_y denote the hydraulic conductivity in the x- and y-axis, respectively, (m/d), Q_w represents the pumping (negative) or recharge (positive) rate per unit area of the well ($m^3/d/m^2$), h_1 is the given head at the Dirichlet boundaries (m), and $q_1(x, y)$ represents the inflow/outflow at the Neumann boundaries ($m^3/d/m^2$).

3 EFGM Flow Model

The meshless EFGM uses the Galerkin weak integral form and shape functions computed by the moving least approximation (MLS) method [20]. The resultant system thus obtained is finally solved for unknown variable [21]. EFGM formulation of Eq. (1) is given by

$$\int_{\Omega}\left(\frac{\partial}{\partial x}\left(K_x h \frac{\partial h}{\partial x}\right) + \frac{\partial}{\partial y}\left(K_y h \frac{\partial h}{\partial y}\right) - Q_w\right)\Phi \mathrm{d}\Omega = 0 \tag{3}$$

In this study, cubic spline weight functions are used to derive the EFGM shape functions (Φ) in the MLS method [5]. The groundwater flow model formulated through Eq. (3) is available in Pathania et al. [13], and its resultant expression is given below

$$\left(\left[K^{(1)}\right] + \left[K^{(2)}\right]\right)\{h_J\} = \{f_J\} \tag{4}$$

In Eq. (4), components of two global matrices, i.e., $\left[K^{(1)}\right]$ and $\left[K^{(2)}\right]$ for x and y directions, respectively, and a global flux vector $\{f\}$ are evaluated as

$$K_{IJ}^{(1)} = \int_{\Omega} \left(K_x b \frac{\partial \phi_I(x, y)}{\partial x} \frac{\partial \phi_J(x, y)}{\partial x} \right) \mathrm{d}\Omega \tag{5a}$$

$$K_{IJ}^{(2)} = \int_{\Omega} \left(K_y b \frac{\partial \phi_I(x, y)}{\partial y} \frac{\partial \phi_J(x, y)}{\partial y} \right) \mathrm{d}\Omega \tag{5b}$$

$$f_J = q_1 \int_{\partial\Omega_2} \phi_J(x, y) d\Omega - \int_{\Omega} Q_w \phi_I(x, y) \phi_J(x, y) \mathrm{d}\Omega \tag{5c}$$

where I and J vary from 1 to N, i.e., total nodes (N) in the computational domain. Here, b denotes the saturated thickness of the unconfined aquifer (m). The integrals terms are evaluated using the Gauss quadrature method in the EFGM model. The Dirichlet boundaries are included in Eq. (4) with the help of penalty method. In EFGM model, solution of Eq. (4) represents the groundwater head (h_J) at N nodes for steady state condition.

4 Numerical Problem

Here, a heterogeneous and unconfined aquifer (1000 m × 500 m) as shown in Fig. 1 is selected to model the groundwater flow using the meshless EFGM. This aquifer is divided into ten zones of different hydraulic conductivity, and it varies from 7 m/d to 25 m/d as shown in Fig. 1. Here, the saturated thickness of this aquifer is taken as 20 m. This problem assumes the steady state flow condition and groundwater movement toward the eastern side of the aquifer. Therefore, western and eastern aquifer boundaries are assumed to have the constant head values of 40 m and 32 m, respectively, and the other two boundaries are satisfying the no-flow condition. Here, three pumping and two recharge wells are also assumed in the flow domain and their locations are also shown in Fig. 1. The pumping rate of all pumping/extraction wells

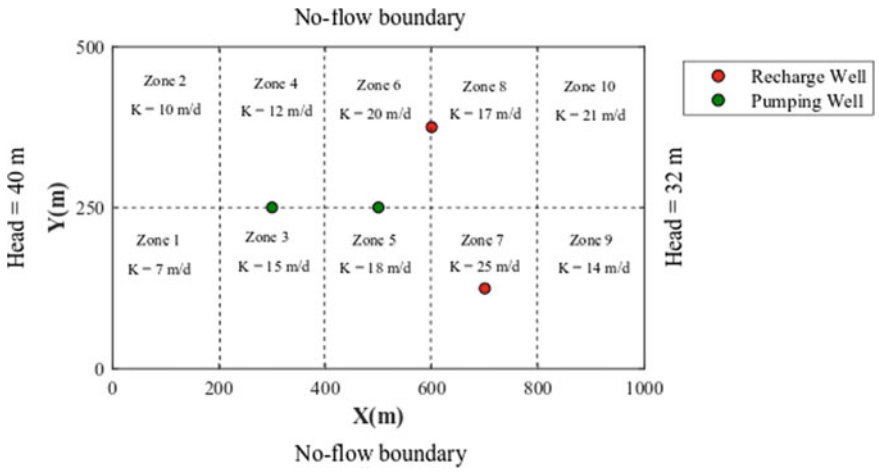

Fig. 1 Aquifer of size 1000 m × 500 m with ten zones of different hydraulic conductivity

is considered as 450 m^3/d and that of both injection wells is taken as 350 m^3/d. To apply the EFGM, the flow domain is represented with uniformly distributed nodes in such a way that internodal spacing is 25 m in both longitudinal (x-axis) and transverse (y-axis) directions (Fig. 2). This arrangement uses 861 nodes in the flow domain. The contours of groundwater head at steady state by the EFGM flow model are shown in Fig. 3. These are verified with those obtained with MODFLOW model [22] and shown in Fig. 4. Both EFGM and MODFLOW estimated the similar groundwater distribution. It indicates the ability of EFGM to successfully model the groundwater flow in heterogeneous aquifers. The head values given by the EFGM and MODFLOW at six observation points are also shown in Table 1, and these are very close to each other. A coarser nodal distribution with internodal spacing of 50 m in longitudinal direction (x-axis) and 25 m in transverse (y-axis) direction is also tested in the EFGM model. It can be seen in Fig. 5 that groundwater head profiles at three different sections using both finer and coarser nodes in EFGM are also closely matching to those with MODFLOW.

5 Conclusions

In the current study, the application of the meshless EFGM model is presented to model the steady state groundwater flow in a heterogeneous porous medium. For the studied problem on an unconfined aquifer, the simulated groundwater distribution

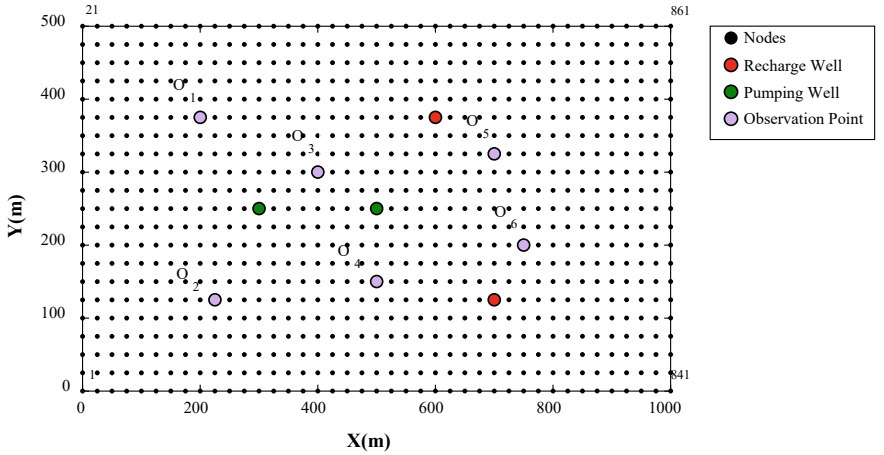

Fig. 2 Representation of aquifer with 861 scattered field nodes ($\Delta x = \Delta y = 25$ m)

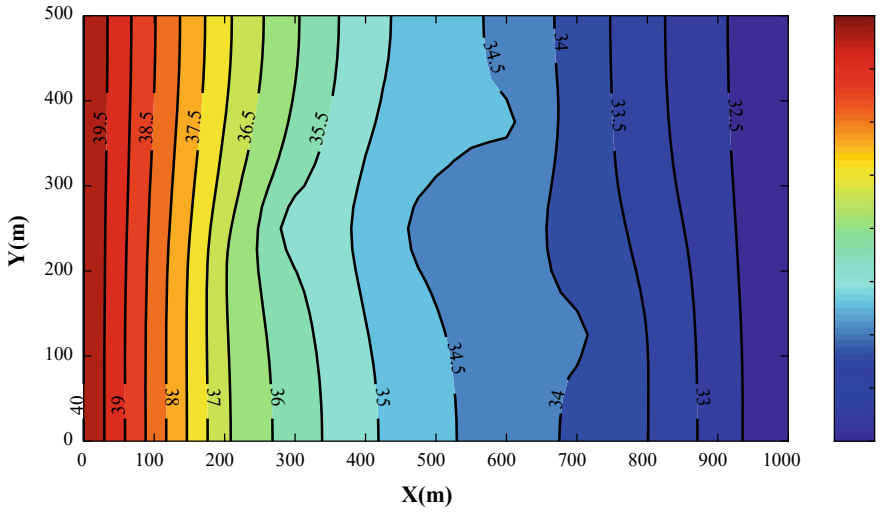

Fig. 3 EFGM-based steady state groundwater head in heterogeneous aquifer

with the EFGM model is found to be closer to that of the MODFLOW model. The pumping and recharge wells are also assumed in the aquifer, and results show that the presented model is capable of successfully including the groundwater source and sink terms. EFGM solutions with both finer and coarser nodal arrangements are also found almost same. It indicates that suitable coarse nodes can also be used in EFGM model to solve similar aquifer problems, and it will reduce the computational time of the model. This study thus shows that EFGM flow model can be applied to estimate the groundwater distribution in a highly heterogeneous porous media.

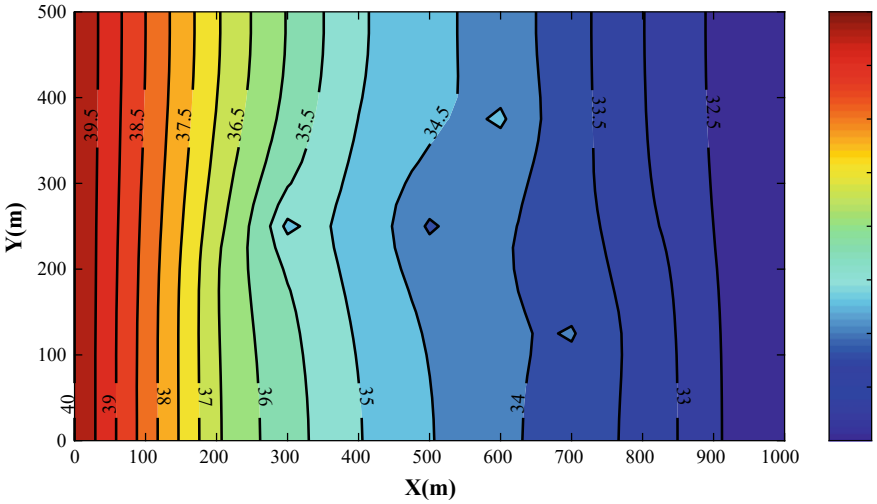

Fig. 4 MODFLOW-based steady state groundwater head in heterogeneous aquifer

Table 1 Head (in m) at six observation points by EFGM and MODFLOW models

Observation point	EFGM	MODFLOW
O_1	37.00	36.97
O_2	36.28	36.23
O_3	34.93	34.84
O_4	34.52	34.42
O_5	33.82	33.69
O_6	33.66	33.51

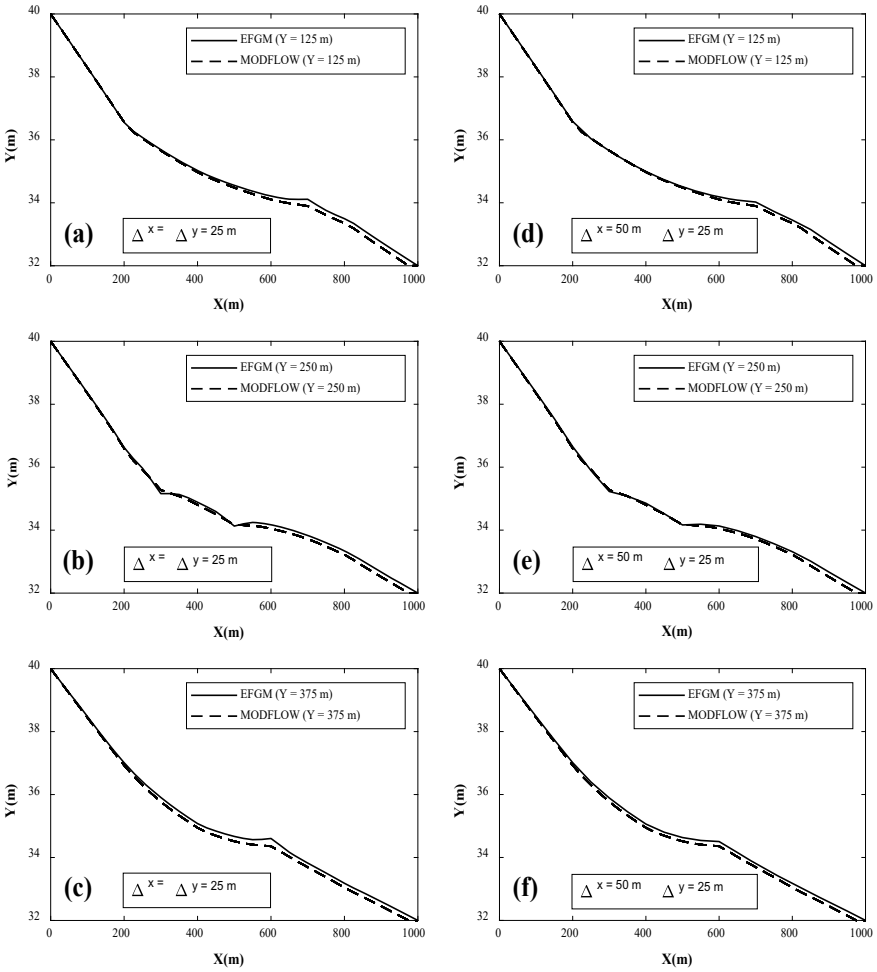

Fig. 5 EFGM-based groundwater head profiles along three different longitudinal axis for finer and coarser nodes, and their comparison with MODFLOW solution

References

1. Rastogi AK (1989) Optimal pumping policy and groundwater balance for the Blue Lake aquifer, California, involving nonlinear groundwater hydraulics. J Hydrol 111(1–4):177–194
2. Hu L, Chen C, Chen X (2011) Simulation of groundwater flow within observation boreholes for confined aquifers. J Hydrol 398(1–2):101–108
3. Zhu Y, Shi L, Lin L, Yang J, Ye M (2012) A fully coupled numerical modeling for regional unsaturated–saturated water flow. J Hydrol 475:188–203
4. Kim JM (2005) Three-dimensional numerical simulation of fully coupled groundwater flow and land deformation in unsaturated true anisotropic aquifers due to groundwater pumping. Water Resour Res 41(1)

5. Park YC, Leap DI (2000) Modeling groundwater flow by the element-free Galerkin (EFG) method. Geosci J 4(3):231–241
6. Praveen Kumar R, Dodagoudar GR (2010) Meshfree analysis of two-dimensional contaminant transport through unsaturated porous media using EFGM. Int J Numer Methods Biomed Eng 26(12):1797–1816
7. Meenal M, Eldho TI (2011) Simulation of groundwater flow in unconfined aquifer using meshfree point collocation method. Eng Anal Boundary Elem 35(4):700–707
8. Meenal M, Eldho TI (2012) Two-dimensional contaminant transport modeling using meshfree point collocation method (PCM). Eng Anal Boundary Elem 36(4):551–561
9. Mategaonkar M, Eldho TI (2012) Simulation-optimization model for in situ bioremediation of groundwater contamination using mesh-free PCM and PSO. J Hazar Toxic Radioact Waste 16(3):207–218
10. Swathi B, Eldho TI (2014) Groundwater flow simulation in unconfined aquifers using meshless local Petrov-Galerkin method. Eng Anal Boundary Elem 48:43–52
11. Guneshwor Singh L, Eldho TI, Kumar AV (2016) Coupled groundwater flow and contaminant transport simulation in a confined aquifer using meshfree radial point collocation method (RPCM). Eng Anal Boundary Elem 66:20–33
12. Boddula S, Eldho TI (2017) A moving least squares based meshless local Petrov-Galerkin method for the simulation of contaminant transport in porous media. Eng Anal Boundary Elem 78:8–19
13. Pathania T, Bottacin-Busolin A, Rastogi AK, Eldho TI (2019) Simulation of groundwater flow in an unconfined sloping aquifer using the element-free Galerkin method. Water Resour Manage 33(8):2827–2845
14. Seyedpour SM, Kirmizakis P, Brennan P, Doherty R, Ricken T (2019) Optimal remediation design and simulation of groundwater flow coupled to contaminant transport using genetic algorithm and radial point collocation method (RPCM). Sci Total Environ 669:389–399
15. Pathania T, Eldho TI (2020) A moving least squares based meshless element-free Galerkin method for the coupled simulation of groundwater flow and contaminant transport in an aquifer. Water Resour Manage 34(15):4773–4794
16. Anshuman A, Eldho TI (2020) Meshfree radial point collocation-based coupled flow and transport model for simulation of multispecies linked first order reactions. J Contam Hydrol 229:103582
17. Pathania T, Eldho TI, Bottacin-Busolin A (2020) Coupled simulation of groundwater flow and multispecies reactive transport in an unconfined aquifer using the element-free Galerkin method. Eng Anal Boundary Elem 121:31–49
18. Pathania T, Eldho TI, Bottacin-Busolin A (2020) Optimal design of in-situ bioremediation system using the meshless element-free Galerkin method and particle swarm optimization. Adv Water Resour 144:103707
19. Bear J (1979) Hydraulics of groundwater. McGraw Hill Publishing, New York
20. Belytschko T, Lu YY, Gu L (1994) Element-free Galerkin methods. Int J Numer Meth Eng 37(2):229–256
21. Liu GR, Gu YT (2005) An introduction to meshfree methods and their programming. Springer, The Netherlands
22. Harbaugh AW (2005) MODFLOW-2005, The U.S. Geological Survey modular ground-water mode—The ground-water flow process. U.S. Geological Survey Techniques and Methods 6-A16, Reston, Virginia

Characteristics and Frequency Analysis of Annual Daily Maximum Rainfall at Surat, Gujarat, India

K. B. Bobade and S. G. Manjunatha

Abstract The technical and engineering suitability of infrastructure projects such as nuclear/hydro/thermal power plants, dams, bridges, storm water drains and flood control measures need to be carried out during the planning and formulation stages of such projects. In a hydrological point of view, it is well recognised that whatever extreme the design loading, more sever conditions are likely to be encountered in nature. For the reason, frequency analysis of recorded hydro meteorological data such as flood discharge, rainfall, wind speed and temperature relating to the geographical region where the project is located, is a basic requirement for assessing such phenomena and arriving at structural and other design parameters for the project. The annual daily maximum rainfall data recorded at Surat for a period of 38 years (1969–2006) were used in this study. The statistical parameters viz. mean, standard deviation, coefficient of skewness, coefficient of kurtosis and correlation coefficient of original and log transformed rainfall series have been computed. The annual rainfall series has been checked for randomness and homogeneity by parametric and nonparametric test viz. median crossing tests, turning point test, rank difference test, run test, Wald-Wolfowitz test, runs above and below median test, Van Neuman ratio test, auto correlation test, Man Kendall test, Spearman's Rho test, Kendall's rank correlation test, etc. For long persistence evolution, Hurst coefficient test has been used. To explore the forms of relationships between time and rainfall, linear regression test has been used. The magnitudes of daily maximum rainfall corresponding to 10, 20, 25, 50 and 100 years return period were estimated using various distributions viz. Gumbel, Frechit, normal, log normal, GEV, Wakeby, logistic, G. logistic, G. Pareto, etc. Analytical procedures such as order statistics, probability weighted moments, L-moments and method of least square are applied for determination of estimators of the distribution. The adequacy of fitting of probability distribution to the recorded rainfall data is assessed by D-index goodness-of-fit test. Based on the identified frequency distribution rainfall amounts for different return periods

K. B. Bobade · S. G. Manjunatha (✉)
Central Water and Power Research Station, Khadakwasla, Pune 411024, India
e-mail: sg_manjunatha1998@rediffmail.com

K. B. Bobade
e-mail: keshavbobade@gmail.com; bobde.kb@cwprs.gov.in

P. V. Timbadiya et al. (eds.), *Hydrology and Hydrologic Modelling*,
Lecture Notes in Civil Engineering 312,
https://doi.org/10.1007/978-981-19-9147-9_39

were estimated. The analysis of annual daily maximum rainfall data and results are discussed in detail in this paper. The results of this study could be beneficial for design engineers and hydrologists for planning and design of small and medium hydrologic structures at Surat, Gujarat, India.

Keywords Probability · Hydrology · Return period · Parametric test · D-index test

1 Introduction

Meteorological parameters like wind speed, rainfall intensity as well as total rainfall, storms, cyclones, maximum and minimum temperature play a major role in the design of the various hydraulic structures from the safety point of view. Structural safety requires that structures shall be designed to withstand the extreme values of these parameters likely to occur during the life of generation of revenue of the project. The plans of hydraulic structures are to be intended in such a way that they can withstand the occurrence of extreme values of the above parameters during their lifetime. It is, therefore, essential that safety of design of hydraulic structure is assessed for flooding.

Most of the hydrological events occurring as natural wonders are observed only once. One of the important problems in hydrology deals with understanding past records of hydrological events for the future probabilities of occurrences. Flood frequency analysis refers to approximation of floods of various return periods. The primary objective of frequency analysis is to relate the magnitude of extreme events to their frequency of incidence through the use of probability distributions. Frequency distribution is fitting observed data series into a theoretical frequency distribution. The applicability of the theoretical distribution lies in the fact that it can be generalised for obtaining values of future events. Annual daily maximum rainfall corresponding to return period varying from 10, 20, 25, 50 and 100 years is used by project engineers and hydrologists for the economic planning, design of small and medium hydrologic structures and determination of drainage coefficient for agricultural fields. Statistical frequency analysis assumes that the record to be analysed is a reliable set of sizes of independent random events from a stationary population. The validity of this assumption can be verified using various statistical tests of short and long-term independence.

The study was taken up with the objective of estimation of rainfall quantities for different return periods for Surat city, Gujarat, India. The study also includes identifying features of the data used in this study and suitable probability distribution function for frequency analysis.

Foster [1] gave the theoretic frequency analysis. Hazen [2] discovered that if the logarithms representing the annual floods are used instead of the number themselves, the contract with the normal mistake is closer. This is true because the frequency distributions of annual floods are usually slanted and the distribution can be suitably represented by such frequency distribution law as the log normal probability law.

Also, he proposed the use of log normal probability paper for graphical fitting of the data. In 1941, Gumbel [3] published the first of a countless number of papers on the application of a Fisher Tippett theory of extreme values of flood frequency analysis. Both the logarithmic (lognormal) probability law and extreme value law have been used extensively in recent years. From a theoretic point of view, Chow [4] had revealed that the extreme value probability law is practically a special case of the lognormal probability law. Jenkinson [5] gave concept of general extreme value distribution and applied the same to annual maximum and minimum values of meteorological elements. Nash and Shaw [6] made estimates of the accuracy of the prediction of floods at a high return period using extreme value distribution with prosecutions from finite to large samples and arrived at the conclusion that extrapolation of frequency estimate is not hazardous even with finite sample if the assumed distribution is correctly chosen. Benson [7] explained that no regional statistical criteria exist on which a comparison of distribution can be based and therefore, the choice of log Pearson type III was to some extent particular. Houghton [8] introduced a five-parameter distribution known as Wakeby distribution for modelling of flood flows. This is becoming popular among investigators because of its capabilities to model both the extremity ends of the flood series separately. The large numbers of parameters in the Wakeby distribution permit better fitting of data than by fewer parameters. It can house a variety of flows ranging from low flows to floods. Landwehr et al. [9] used probability weighted moments (PWMs) which avoid using higher order conventional moments to estimate Wakeby parameters. Rao [10] used method of mixed moments to estimate parameters of log Pearson type III distribution. This method attempts to avoid effect of regional variation of skewness coefficient by intermixing the first two moments of data which is mean and variance, with the mean of logarithmically transformed data to estimate indirectly coefficient of skewness of the log transformed series. Such estimate is not subject to distortion due to transformation for the five-parameter Wakeby distribution. Rossi et al. [11] introduced two component extreme value distributions for flood frequency analysis for the rivers where floods are caused by two distinct physical mechanisms. Ahmad et al. [12] introduced a new distribution named log-logistic distribution and compared it with GEV, LN III and PT III distribution. They further recommended the use of this distribution for flood frequency analysis. Hosking [13] first introduced the L-moments. L-moments are linear mixtures of probability weighted moments (PWMs). It can be seen that the L-moments can be estimated directly from the PWMs. However, the L-moments are more suitable, as they are directly interpretable as measures of the scale and shape of probability distributions. L-moments can be used to estimate parameters when fitting a distribution to a sample, by equating the first p-sample L-moments to corresponding population L-moments. Parameter estimation with L-moments has been found more precise than maximum likelihood estimate, in case of small sample. Rao and Hamed [14] mention that the data observed over an extended period of time in a river system or hydro meteorologically standardised region are analysed in frequency analysis. The data are assumed to be independent and identically distributed. The flood data are considered to be stochastic and space and time dependent. Further, it is assumed that the floods have not been affected by natural or manmade changes

in the hydrological regime in the system. The authors' further mention that in practice, the true probability distribution of the data at a site or a region is unknown. The assumption that data in a given system arise from a single-parent distribution may be questionable when data from large watershed are analysed. In such cases, more than one type of rainfall or flow may contribute to extreme events in a region. However, for the analysis to be of practical use, simpler distributions are frequently used to describe the relation between flood magnitudes and their frequencies. The performance of distributions is evaluated by using different statistical test.

2 Study Area Data Availability

Surat located approximately at latitude 21°17′ N and longitude 72°83′ E. The height above mean sea level is 13 m. Figure 1 shows the location map of the study area. The climate of Surat is characterised by a hot summer and general dryness except during the southwest monsoon season. The period from June to September is the southwest season. About 96% of the annual rainfall in the district is received during the southwest monsoon months June to September, July being the rainiest month. The average annual rainfall in the district is 1384.3 mm. The heaviest rainfall in 24 h recorded at Surat was 467.7 mm on 7 September 1970 from 1901 to 2006 [15].

The daily rainfall data for Surat meteorological station for a period of 38 years (1969–2006) was procured from India Meteorological Data (IMD), Pune and were used in this study [16].

3 Methodology

The frequency analysis of annual daily maximum rainfall for Surat involves fitting of probability distribution to the recorded data. Briefly, the methodology adopted is given below.

1. Processing of data for missing value.
2. Preparation of data series of maximum from the processed data.
3. Data validation using statistical tests for randomness, homogeneity, etc.
4. Fitting of probability distribution using order statistic approach, present worth moments, least square and L-moments, etc.
5. Assessing the suitability of fitting of probability distribution using goodness-of-fit (GoF tests)
6. Selection of probability distribution.

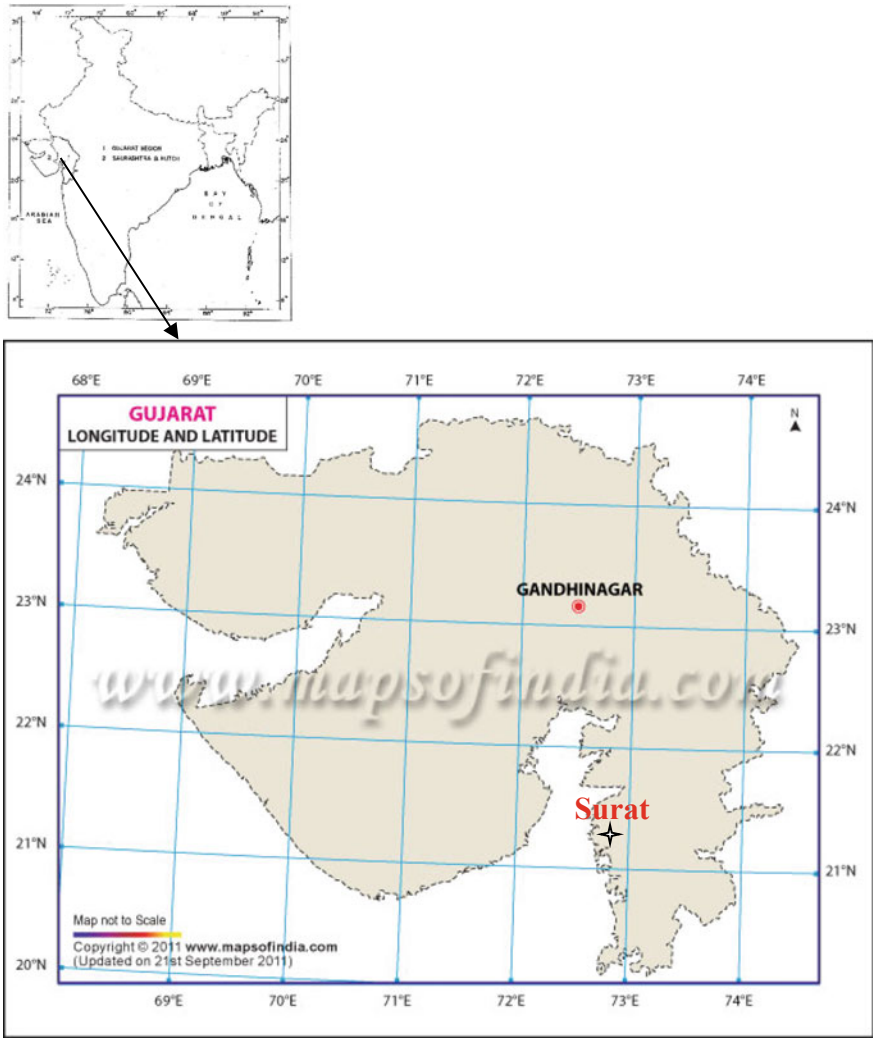

Fig. 1 Location map of study area. *Source* www.mapsofindia.com

3.1 Missing Data

The data set has been studied for determination of annual daily maximum rainfall values and assessment of its quality from the reliability and completeness point of view. Some data for interim periods in the overall time span were not available. For conservation, it has been assumed that the missing values of the rainfall were the highest observed during the entire period of data set in case of maximum extreme and lowest for minimum of the extreme.

3.2 Statistical Parameters

The statistical parameters viz. mean, standard deviation, coefficient of skewness, coefficient of kurtosis and correlation coefficient of original and log transformed series were computed [17].

3.3 Short-Term and Long-Term Dependence Tests

The parametric and nonparametric tests were used for checking the randomness and homogeneity of the data series. Following tests were applied to annual daily maximum rainfall series to test short-term and long-term dependence. The first ten tests are nonparametric, and the last two tests are parametric to test short-term dependence. The last test is used to test long-term dependence.

3.3.1 Median Crossing Test

X is replaced by zero if $x_i < x$ (median), and X is replaced by one if $x_i > x$. If the original sequence of X_s has been generated by a purely random process, then m, the number of times zero is followed by one or one is followed by zero, is approximately normally distributed, i.e.

$$m \approx N\left[\frac{n-1}{2}, \left(\frac{n-1}{4}\right)^{1/2}\right] \tag{1}$$

3.3.2 Turning Point Test

Kendall's test is based on binary series. If $x_i - 1 < x_i > x_i + 1$ or $x_i - 1 > x_i < x_i + 1$, then x_i is assigned the value one, otherwise it is assumed to be zero. The number of ones, m, is approximately normally distributed, i.e.

$$m \approx N\left\{\frac{2(n-2)}{3}, \frac{(16n-29)}{90}^{1/2}\right\} \tag{2}$$

3.3.3 Length of Runs Test

A run length s is defined by a set of s consecutive flows either above or below the median. If ms denotes the total number of runs above and below the median length s, then for a random process

$$E(ms) = \frac{(n+3-s)}{2^{s+1}} \tag{3}$$

$$\sum_{s=1}^{s} [ms - E(ms)]^2 / E(ms) \approx X^2(\overline{s} - 1) \tag{4}$$

3.3.4 Rank Difference Test

Flows are replaced by their relative ranks R_i with the lowest being denoted by Rank 1. The U statistic is calculated by

$$U = \sum_{i=2}^{n} |R_i - R_i - 1| \tag{5}$$

For large n,

$$N\left\{\frac{(n+1)(n-1)}{3}, \left[\frac{(n-2)(n+1)(4n-7)}{90}\right]^{1/2}\right\} \tag{6}$$

3.3.5 Wald-Wolfowitz Test

For a sample of size n,

$$R = \sum_{i=1}^{n-1} X_i * X_i - 1 + x_i * x_n \tag{7}$$

If the elements of the sample are independent,

$$R \approx N\left\{\frac{S_1^2 - S_2}{n-1}, \left[\frac{S_2^2 - S_4}{n-1} - \left(\frac{S_1^2 - S_2}{n-1}\right) + \frac{S_1^4 - 4S_1^2 S_2 + 4S_1 S_1 + S_2^2 - 2S_4}{(n-1)(n-2)}\right]^{1/2}\right\} \tag{8}$$

where $S_1 = X_1^r + X_2^r + \cdots + X_n^r$

3.3.6 Runs Above and Below the Median Test for General Randomness

Data are ranked in chronological order. An A or B is assigned according to whether the corresponding data is above or below or equal to the median. The number of

runs, RUNAB, is determined. For n_1 A and for n_2 B with n_1 and n_2 both greater than 20, the sampling distribution of RUNAB tends to normally distribute with

$$Z = \frac{|\text{RUNAB} - |(2n_1n_2)/(n_1 + n_2) + 1||}{2n_1n_2(2n_1n_2 - n_1 - n_2)/\left[(n_1 + n_2)^2(n_1 + n_2 - 1)\right]^{1/2}} \tag{9}$$

Z is an N (0, 1) variate and as used in this programme the region of rejection is $z > 1.96$ for $\alpha = 0.05$, $z > 1.645$ for $\alpha = 0.10$.

3.3.7 Rank Von Neuman Ratio Test

Let $r_1 \ldots r_n$ denote the ranks associated with the x_i values. The rank Van Neumann ratio is given by

$$v = \frac{\sum_{i=2}^{n} (r_i - r_{i-1})^2}{n(n^2 - 1)/12} \tag{10}$$

Critical values of $c = (n\ (n^2 - 1)/12)\ v$ and approximate critical values of v were given by Madansky (1988). For large n, v is approximately distributed as N (2, 4/n), although Bartels recommended $20/(5n + 7)$ as a better approximation to the variance of v.

3.3.8 Mann Kendall Test

The MK test is based on the test statistic. S defined as follows

$$S = \sum_{i=1}^{n-1} \sum_{j=i+1}^{n} \text{sgn}(x_j - x_i) \tag{11}$$

where the x_j are the sequential data values, n is the length of the data set, and $\text{sgn}(\theta) = \{1 \text{ if } \theta > 0, 0 \text{ if } \theta = 0, -1 \text{ if } \theta < 0\}$ Mann (1945) and Kendall (1975) have documented that when n $\geq$ 8, the statistic S is approximately normally distributed with the man and the variance as follows: $E(S) = 0$

$$V(S) = \frac{n(n-1)(2n+5) - \sum_{i=1}^{n} \text{ti}_i(i-1)(2i+5)}{18} \tag{12}$$

where ti is the number of ties of extent i. The standardised test statistic Z is computed by

$$\text{ZMK} = \left\{ \frac{S-1}{\sqrt{\text{Var}(S)}} \text{ if } S > 0, 0 \text{ if } S = 0, \frac{S+1}{\sqrt{\text{Var}(S)}} S < 0 \right\} \tag{13}$$

The standardised MK statistic Z follows the standard normal distribution with mean zero and variance of one.

3.3.9 Spearman's Rho test

SR test is another nonparametric rank order test. Given a sample data set (X_i, $i = 1, 2, n$) the null hypothesis H_0 of the SR test against trend test is that all the X_i, are independent and identically distributed. The alternative hypothesis is that X_i increase or decrease with i, that is, trend exists. The test statistic is given by

$$D = 1 - \frac{6\sum_{i=1}^{n}[R(X_i) - i]^2}{n(n^2 - 1)} \tag{14}$$

where $R(X_i)$ is the rank of the ith observation X_i in the sample size n. Under the null hypothesis, the distribution of D is asymptotically normal with the mean and variance as follows, $E(D) = 0$ and $V(D) = 1/(n - 1)$.

3.3.10 Kendall's Rank Correlation Test

Kendall's rank correlation test is applied to check trend of time series

$$\tau = \frac{4p}{n(n-1)} - 1 \tag{15}$$

where p is the number of times exceeding x_i in the time series.

$$\mathrm{Var}\,\tau = \frac{2(2n+5)}{9n(n-1)}, \tag{16}$$

$$Z = \frac{\tau}{\sqrt{\mathrm{Var}\,\tau}} \tag{17}$$

Test criteria: If, $-1.96 \leq Z \leq 1.96$, no trend exists, the time series is stationary. If, $Z \leq -1.96$, the trend is falling and if $Z \geq +1.96$, the trend is rising in the time series.

3.3.11 Auto Correlation Test

Short-term dependence is usually measured by the magnitude of the low order autocorrelation coefficient (r_k).

$$r_k = \left[\sum_{i=1}^{n-k}(x_i - \overline{x})(x_i + k - \overline{x}\right] \Big/ \left[\sum_{i=1}^{n}(x_i - \overline{x)}(x_i - \overline{x})\right] \tag{18}$$

where k is lag, x_i is annual flow at time i, n is sample size, and

$$\overline{x} = 1/n \sum_{i=1}^{n} x_i \tag{19}$$

The lag-one autocorrelation, r_1, is calculated from Eq. 3.15 and is normally distributed.

$$r1 = N\left\{-\frac{1}{n}, \left[\frac{n^3 - 3n^2 + 4}{n^2(n^2 - 1)}\right]^{1/2}\right\} \tag{20}$$

r_k is checked whether or not it is significantly different from the expected value.

3.3.12 Von Neumann Ratio Test

Let,

$$V = \frac{\sum_{i=2}^{n}(x_i - x_{i-1})^2}{\sum_{i=1}^{n}(x_i - \hat{x})^2} \tag{21}$$

If data are independent, V is approximately normally distributed with $E(V) = 2$ and $\mathrm{Var}(V) = 4(n-2)/(n^2-1)$, i.e.

$$Z = \frac{V - 2}{\left[4(n-2)/\left(n^2 - 1\right)\right]^{(1/2)}} \tag{22}$$

These tests are used by Lye and Lin (1994) for analysis of peak flow series of 90 Canadian rivers for short-term dependence. The Mann Kendall test and Spearman's Rho test are used for detection of monotonic trends in hydrological series (Sheng Yue, 2002).

3.3.13 Hurst Coefficient

Long-term dependence is measured by the magnitude of Hurst coefficient (K).

$$K = \frac{\log(R/s)}{\log(n/2)} \tag{23}$$

where R is the range of cumulative departures from the mean, s is the standard deviation and n is the sample length. K is theoretically 0.5 for series of independent data; it increases when there is greater degree of dependence and cannot exceed 1.0. The Hurst coefficient is at present the only measurement available for long-term dependence. These tests are used by Lye and Lin (1994) for analysis of peak flow series of 90 Canadian rivers for short-term dependence. The details of long-term dependence tests are given in the literatures. To explore the forms of relationships between time and rainfall, linear regression test has been used.

3.4 Frequency Analysis

The following distributions are used for estimation of quantities for different return periods [17–19].

3.4.1 Gumbel or Extreme Value Type I or Fisher Tippet Type I Distribution

The estimates of meteorological parameters for different periods of T (years) of 2, 5, 10, 20, 25, 50 and 100 were obtained using Eqs. 24 and 25.

$$\text{Gumbal}(\text{max}ima): XT = u + \alpha\left\{-\ln\left[-\ln\left(1-\frac{1}{T}\right)\right]\right\} \tag{24}$$

$$\text{Gumbal}(\text{min}ima): XT = u - \alpha\left\{-\ln\left[-\ln\left(1-\frac{1}{T}\right)\right]\right\} \tag{25}$$

3.4.2 Frechet or Extreme Value Type II or Fisher Tippet Type II Distribution

The estimates of meteorological parameters for different periods of T (years) of 2, 5, 10, 20, 25, 50 and 100 were obtained by using Eqs. 26 and 27.

$$\text{Frechet}(\text{max}ima): X_T = \beta * e^{\frac{-\ln\left[-\ln\left(1-\frac{1}{T}\right)\right]}{k}} \tag{26}$$

$$\text{Frechet}(\text{min}ima): X_T = u - \beta * e^{\frac{-\ln\left[-\ln\left(1-\frac{1}{T}\right)\right]}{k}} \tag{27}$$

3.4.3 The Five-Parameter Wakeby Distribution (WAK 5)

The estimates of meteorological parameters for different periods of T (years) of 2, 5, 10, 20, 25, 50 and 100 were obtained using Eq. 28.

$$X_T = m + a\left[1 - T^{-b}\right] - c\left[1 - T^{d}\right] \tag{28}$$

3.4.4 The Four-Parameter Wakeby Distribution (WAK 4)

The estimates of meteorological parameters for different periods of T (years) of 2, 5, 10, 20, 25, 50 and 100 were obtained using Eq. 29.

$$X_T = a\left[1 - T^{-b}\right] - c\left[1 - T^{d}\right] \tag{29}$$

3.4.5 Generalised Extreme Value Distribution (GEV)

The estimates of meteorological parameters for different periods of T (years) of 2, 5, 10, 20, 25, 50 and 100 were obtained using Eq. 30.

$$X_T = u + \alpha * (1 - (-\ln(1 - 1/T))^{-k})/k \tag{30}$$

where u, α and k are the location, scale and shape parameters of the distribution.

3.4.6 Normal Distribution

The estimates of meteorological parameters for different periods of T (years) of 2, 5, 10, 20, 25, 50 and 100 were obtained using Eq. 31.

$$X_T = \alpha 1 + u\alpha 2 \tag{31}$$

3.4.7 Log Normal Distribution

The estimates of meteorological parameters for different periods of T (years) of 2, 5, 10, 20, 25, 50 and 100 were obtained using Eq. 32.

$$X_{\mathrm{p}} = u + \exp(\mu y + \sigma y\, \Phi^{-1}(p)) \tag{32}$$

3.4.8 Generalised Pareto Distribution

The estimates of meteorological parameters for different periods of T (years) of 2, 5, 10, 20, 25, 50 and 100 were obtained using Eq. 33.

$$X_{\mathrm{p}} = u + \frac{\alpha}{k}\left[1 - (1-p)^{k}\right] \tag{33}$$

3.4.9 Logistic Distribution

The estimates of meteorological parameters for different periods of T (years) of 2, 5, 10, 20, 25, 50 and 100 were obtained using Eq. 34.

$$X_T = m + a\log(T-1) \tag{34}$$

3.4.10 Generalised Logistic Distribution

The estimates of meteorological parameters for different periods of T (years) of 2, 5, 10, 20, 25, 50 and 100 were obtained using Eq. 34.

$$XT = \varepsilon + \frac{\alpha}{k}\left[1 - (T-1)^{-k}\right] \tag{35}$$

3.5 Parameter Estimation Methods

The following methods are used for estimation various parameters of the distribution. The procedures in detail are given in the literatures.

1. Order statistics alternatively known as Lieblein technique: It is used to estimate the parameters of Gumbel and Frechet distributions.
2. Method of Moment: It is used to estimate the parameters of Gumbel distributions.
3. Least Square: It is used to estimate the parameters of Gumbel distributions.
4. Probability Weighted Moments: It is used to estimate the parameters of Gumbel, generalised extreme value, Wakbay (4) and Wakbay (5) distributions.
5. L-moments: It is used to estimate the parameters of Gumbel alternatively known as extreme value I, generalised extreme value, logistic, generalised logistic, generalised Pareto, normal and log normal distributions.

3.6 Goodness-of-Fit Test

The validity of a probability distribution function proposed to fit the empirical frequency distribution of a given sample may be tested graphical and analytical methods. A number of analytical tests have been proposed for testing the goodness-of-fit of proposed distribution. Some of the commonly used tests are (1) chi-square test and (2) Kolmogorov–Smirnov tests. These tests are not very powerful in the sense that the probability of accepting the hypothesis when it is in fact false is very high when these tests are used. In this light, D-index test is bit better. Hence, it is used in this paper. The D-index for the comparison of the fit of various distributions in upper tail is given as

$$\text{D-insdex} = \left(1/\overline{X}\right) \sum_{i=1}^{6} \text{Abs}\left(X_i - \widehat{X_i}\right) \tag{36}$$

where X_i and $\widehat{X}_i$ are the ith highest observed and computed values for the distribution. The distribution giving the least D-index is considered to be the best fit distribution.

4 Results and Discussions

The annual daily maximum rainfall data recorded at Surat for a period of 38 years (1969–2006) were used in this study. The data was missing for the years 1992–95. The missing data has been filled by extreme value of daily rainfall for the period. The daily rainfall data for the period from 1969 to 2006 of Surat meteorological station were analysed, and annual daily maximum rainfall is given in Table 1. Figure 2 shows the series of observed annual daily maximum rainfall at Surat.

4.1 The Statistical Parameters

The statistical parameters viz., mean, standard deviation, coefficient of skewness, coefficient of kurtosis and correlation coefficient of original and log transformed series are computed for the rainfall data recorded at Surat and given in Table 2.

4.2 Short-Term and Long-Term Dependence Tests

These tests were applied to rainfall series of Surat station. The results obtained thereof are given in Table 3. Table 3 indicates that rainfall series is random and trend free. Regarding long-term persistence, it shows no long-term persistence in rainfall series of stations. Randomness indicates that data is original, not manipulated and

Table 1 Annual daily maximum rainfall (mm/day) at Surat

Year	Annual daily maximum rainfall (mm)	Year	Annual daily maximum rainfall (mm)
1969	140.8	1988	326.4
1970	247.5	1989	63.2
1971	88.8	1990	110.4
1972	155.6	1991	130.5
1973	202.6	1992	326.4[a]
1974	109.0	1993	326.4[a]
1975	192.8	1994	326.4[a]
1976	240.8	1995	326.4[a]
1977	133.0	1996	90.4
1978	191.4	1997	82.6
1979	129.2	1998	208.6
1980	105.8	1999	187.8
1981	154.3	2000	96.4
1982	221.4	2001	82.0
1983	183.2	2002	146.6
1984	186.8	2003	261.5
1985	59.6	2004	245.0
1986	115.8	2005	224.0
1987	164.4	2006	144.1

[a] Missing data

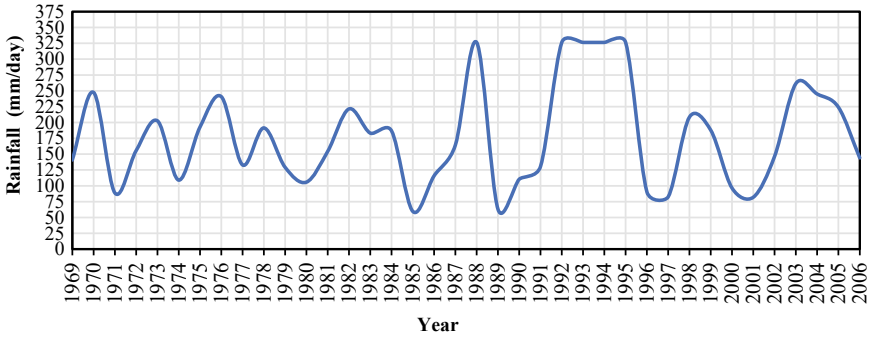

Fig. 2 Annual daily maximum rainfall (mm/day)

homogeneous. Trend free indicates that data has no trend. Correlation indicates, does data has any relation with each other. Persistence indicates weather data has indepedent or not.

Table 2 Statistics of annual daily maximum rainfall

Statistical parameters	Mean	Standard deviation	Coefficient of skewness	Coefficient of kurtosis	Coefficient of correlation
	(α)	(δ)	(Cs)	(Ck)	(r)
Original series	159.5	63.8	0.5	3.1	0.0
Log transformed series	5.0	0.4	–0.3	2.7	0.0

Table 3 Tests results on rainfall series at Surat, Gujarat

S. No.	Tests	Result	Remark
1	Median crossing test	−0.1741	Random
2	Turning point test	−0.9754	Random
3	Rank difference test	−0.2995	Random
4	Kendall's rank correlation test	−0.22237	Trend free
5	Linear regression test	0.0081	Positive correlation
6	Run test	−0.6966	Random
7	Wald-Wolfowitz test	0.378	Random
8	Runs above and below median test	−0.0012	Random
9	Rank Van Neuman ratio test	−0.4828	Random
10	Van Neuman ratio test	−0.1967	Random
11	Auto correlation test	0.366	Random
12	Mann Kendall test	−0.2075	Random
13	Spearman's Rho test	−0.0781	Random
14	Hurst coefficient	0.6498	No persistence

4.3 Frequency Analysis

The frequency analysis of daily rainfall recorded at Surat has been carried out by using Gumbel, Frechet, Wakbay (4), Wakbay (5), Generalised extreme value (GEV), logistic, generalised logistic (G. logistic), generalised Pareto, normal and log normal probability model. The distribution parameters were estimated using order statistics alternatively known as Lieblein technique, least square, probability weighted moments (PWM) and L-moments (LM) techniques. Table 4 gives the rainfall estimates for different return periods of 10, 20, 25, 50 and 100 years. Figure 3 shows the probability plot of estimated annual daily rainfall at Surat by using logistic and normal distributions. From Table 4, it may be noted that the rainfall estimates using Frechet distribution are on the higher side.

Table 4 Estimated daily maximum rainfall (mm)

Distribution	Parameter estimation method	Return period (year)				
		10	20	25	50	100
Gumbel	Order statistic approach	298.0	349.5	365.8	416.1	465.9
	Least square	292.7	341.5	356.9	404.5	451.8
	Present worth method	248.6	287.0	299.1	336.6	373.8
	L-moments	248.6	287.0	299.1	336.6	373.8
Frechet	Order statistic approach	369.3	524.0	585.5	824.2	1157.3
Wakbay (4)	Present worth method	254.0	282.0	289.48	308.6	323.1
Wakbay (5)	Present worth method	247.4	279.0	288.6	317.2	343.7
GEV	Present worth method	248.2	281.0	291.0	320.4	347.8
	L-moments	248.2	281.0	291.0	320.4	347.8
Logistic	L-moments	240.6	268.2	276.8	303.2	329.2
G. logistic	L-moments	242.8	279.1	291.0	329.7	370.9
G. Pareto	L-moments	255.3	277.5	283.0	295.9	304.5
Normal	L-moments	243.3	267.1	274.1	293.9	311.7
Log normal	L-moments	247.5	280.2	290.3	320.5	349.6

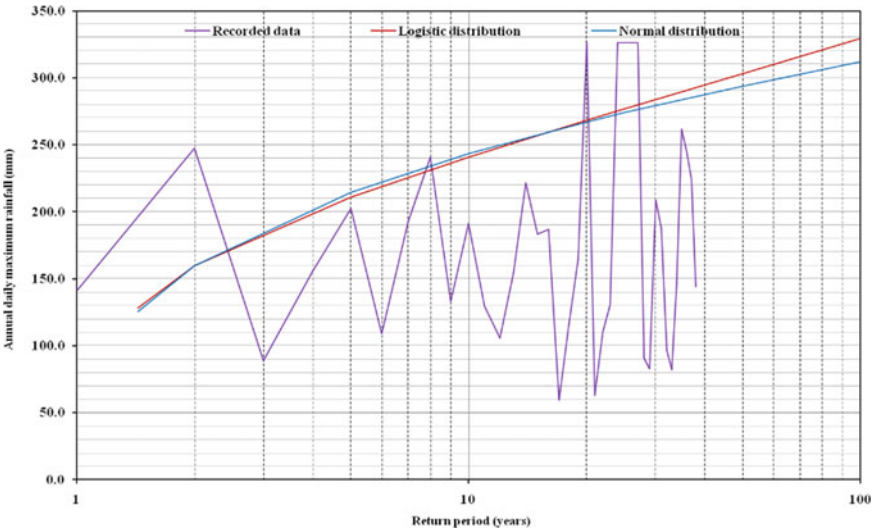

Fig. 3 Logistic and normal probability plot

Table 5 D-index goodness-of-fit test results

Distribution	Test results	Distribution	Test results
Wakbay (4) distribution—PW M	0.46	Generalised extreme value—LM	0.53
Wakbay (5)—PWM	0.47	Logistic—LM	0.31
Extreme value I/Gumbel-PWM	0.79	Generalised logistic—LM	0.72
Generalised extreme value—PWM	0.53	Generalised Pareto—LM	0.60
Extreme value I/Gumbel—LM	0.79	Normal—LM	0.31
Log normal—LM	0.53		

4.4 Goodness-of-Fit Test

Goodness-of-fit of distributions is tested using D-index test. The results are presented in Table 5. Table indicates that logistic and normal distribution are suitable for frequency analysis of rainfall at Surat, Gujarat.

5 Conclusions

This paper details the methodology used for determination of characteristics of rainfall prevailing at Surat by using short-term and long-term parametric and nonparametric tests and frequency analysis. The results of parametric and nonparametric tests were showed that the data were random and homogeneous. From the results of D-index test, it is found that logistic and normal distribution are better suited for frequency analysis in this region. A daily maximum rainfall of 240.6, 268.2, 276.8, 303.2 and 329.2 mm is predicted to occur at Surat for a return period of 10, 20, 25, 50 and 100 years, respectively.

The results of this study could be beneficial for design engineers and hydrologists for planning and design of small and medium hydrologic structures at Surat, Gujarat, India.

Acknowledgements The authors are thankful to Shri. A. K. Agrawal, Ex-Director, CWPRS for his kind permission to publish this paper. The authors are like to express deep sense of gratitude and sincere regards to Dr. N. K. Goel, Professor, Department of Hydrology, Indian Institute of Technology, Roorkee for their keen personal interest, excellent guidance and constant encouragement throughout the course of the study M. Tech (Hydrology). The authors are also thankful to India Meteorological Department (IMD), Pune for providing necessary meteorological data for the study.

References

1. Foster HA (1924) Theoretical frequency curves and their application to engineering problems. Trans Am Soc Civil Eng 87:142–173
2. Hazen A (2932) Flood flows'. Wiley, New York, 199 pp
3. Gumbel EJ (1941) Probability interpretation of the observed return periods of floods. Trans Am Geophys Union 21:836–850
4. Chow VT (1954) The log probability law and its engineering applications. In: Proceedings of American Society for civil engineers, November, vol 80 paper no. 536, pp 1–25
5. Jenkison AF (1955) The frequency distribution of the annual maximum or minimum of meteorological elements. Quar J Royal Meteor Soc 81:158–171
6. Nash JE, Shaw BL (1965) Flood frequency as a function of catchment characteristic. In: Proceedings of symposium on river flood hydrology. Institution of Civil Engineers, London, pp 115–136
7. Benson MA (1962) Evolution of methods for evaluation the occurrence of floods. In: United States geology survey. Water-supply paper: 1550-A
8. Houghton JC (1978) Birth of a parent: "The Wakeby distribution for modelling flood flows." Water Resour Res 14(6):1105–1109
9. Landwehr JM, Matalas NC, Wallis JR (1979) Probability weighted moments compared with some traditional techniques of estimating Gumbel parameters and quantiles. Water Resour Res 15(6):1361
10. Rao DV (1980) Log Pearson type 3 distribution: evaluation. J Hydraul Div 853–872 (ASCE)
11. Rossi F, Fiorentino M, Versace P (1984) Two-component extreme value distribution for flood frequency analysis. Water Resour Res 20(7):847–856
12. Ahmad MI, Sinclair CD Werritty A (1988) Log-logistic flood frequency analysis. J Hydraul 98:205–224
13. Hosking JRM, Wallis JR (1997) Regional frequency analysis—An approach based on L-moments. Cambridge University Press, New York
14. Rao AR, Hamed KH (2000) Flood frequency analysis. CRC Press, United States of America
15. India Meteorological Department (1980) Climate of Gujarat
16. Bobade KB (2012) Hydrological analysis for a Coastal Power Project. M. Tech (Hydrology) thesis, Department of Hydrology, Indian Institute of Technology, Roorkee, Uttarakhand, India
17. Chow VT (1964) Handbook of applied hydrology. Mcgraw Hill Book Company
18. Mutreja KN (1986) Applied hydrology. Tata McGraw- Hill, New Delhi
19. Singh VP (1994) Elementary hydrology. Prentice-Hall of India Private Limited, New Delhi

Groundwater Flow Simulation in an Unconfined Aquifer Using Local Radial Point Interpolation Meshless Method (LRPIM)

K. Swetha, T. I. Eldho, L. Guneshwor Singh, and A. Vinod Kumar

Abstract To tackle the groundwater flow issues, numerical approaches like the finite difference method and the finite element method are frequently utilized. The pre-processing portion of these traditional methods involves the usage of elements or a grid to solve the issue. Pre-processing or re-meshing process consumes more time and computationally complex. In order to avoid these difficulties, meshless techniques are evolved. Based on the formulation procedure, meshless methods were classified into strong form and weak form. In this paper, one of the weak form method known as local radial point interpolation method (LRPIM) is used to simulate the groundwater flow in an unconfined aquifer. The LRPIM flow model is developed using the MATLAB® platform and applied to a hypothetical unconfined aquifer problem. The results obtained from the model is compared with finite difference method (FDM) and found to be satisfactory. The LRPIM model takes the advantage of having shape functions with weaker consistency because of the reduced order of the governing equation in the weak form formulation. Background cells are not needed for interpolation and integration in LRPIM. Implementation of both essential and Neumann boundary condition is easier because of Kronecker delta property and weak form formulation. In LRPIM, multi-quadratics radial basis function (MQ-RBF) is used for calculating the shape function and the approach provided high accuracy.

Keywords Local radial point interpolation method · Meshless method · Numerical methods · Unconfined aquifer · Groundwater flow simulation

K. Swetha (✉) · A. Vinod Kumar
Homi Bhabha National Institute (HBNI), Mumbai 400094, India
e-mail: swetha.kamarajj@gmail.com

A. Vinod Kumar
e-mail: avkumar@barc.gov.in

T. I. Eldho
Department of Civil Engineering, Indian Institute of Technology Bombay, Mumbai 400076, India
e-mail: eldho@civil.iitb.ac.in

L. Guneshwor Singh
Health Physics Division, Bhabha Atomic Research Centre, Mumbai 400085, India
e-mail: gune@barc.gov.in

P. V. Timbadiya et al. (eds.), *Hydrology and Hydrologic Modelling*,
Lecture Notes in Civil Engineering 312,
https://doi.org/10.1007/978-981-19-9147-9_40

1 Introduction

Natural resources like groundwater are mostly used in agriculture and irrigation. Wells and springs are the main sources of groundwater. When the rainfall occurs, part of the water drains as run off whereas the part of the water penetrates or infiltrated through the various layers of sand, stones, and rocks. This infiltrated water is collected and stored in a hydro geological formation called aquifers. In recent decades, because of over extraction of groundwater, the quality and quantity of water in the aquifer are not maintained. Hence, there is a need for groundwater models to solve these problems.

Groundwater models are developed using various techniques such as the finite difference method (FDM), finite element method (FEM), meshless methods, etc. Groundwater modeling is used to simulate the exact aquifer condition and for predicting the changes in the aquifer. Finite difference and finite element method involve computational complexities, and it leads to the usage of the meshless method. Meshless method involves generation of nodes and establishing the relation between the nodes in terms of shape function using support domain. It does not require any mesh or grid formation.

Several types of meshless methods are available as given by Liu and Gu [1]. Most commonly used meshless methods in groundwater are the radial point collocation method (RPCM), meshless local Petrov–Galerkin method (MLPG), and element free Galerkin methods (EFG). Based on the local weak forms, the local radial point interpolation method (LRPIM) is described in Liu and Gu [1]. The implementation procedure of LRPIM is easier and gives higher accuracy as other strong form methods [1].

LRPIM has been effectively applied to solid mechanics by Liu and Gu [2], fluid mechanics by Wu and Liu [3], and soil mechanics by Wang et al. [4]. Wang et al. [4] analyzed the dissipation process of excess pore water pressure in porous media using the local radial point interpolation method and found that the LRPIM is having advantage over collocation methods. It requires lower order derivatives, easier in handling the boundary conditions and is a true meshless method. Saeedpanah et al. [5] studied the influence of leakage on tidal response in the coastal leaky aquifer system with LRPIM. The results are discussed with numerical solution. Saeedpanah and Jabbari [6] used LRPIM with the local Heaviside weight function to conduct numerical tests in groundwater and fluid flows. The results obtained are compared with finite element method. In order to determine the effects of the sizes of the local sub-domain and interpolation domain, authors have also performed a sensitivity study.

This paper develops the local radial point interpolation approach for two-dimensional unconfined aquifer flow problems. The generated model is then used to simulate groundwater flow in an imaginary unconfined aquifer problem, and the results are compared with those of a conventional FDM model.

2 Governing Equations and Boundary Conditions

It is derived using the continuity equation and Darcy's law. The governing equation for an unconfined aquifer is stated as [7]

$$\frac{\partial}{\partial x}\left[K_x h \frac{\partial h}{\partial x}\right] + \frac{\partial}{\partial y}\left[K_y h \frac{\partial h}{\partial y}\right] = S_y \frac{\partial h}{\partial t} + \sum_{w=1}^{n} Q_w \delta(r - r_w) - f \tag{1}$$

The boundary conditions for unconfined aquifer problems are

$$h(x, y, t) = h_1(x, y, t) \text{ where } x, y \in \partial\Omega_1 (\text{Dirichlet boundary}) \tag{2}$$

$$Kh \frac{\partial h}{\partial n} = q(x, y, t) \text{ where } x, y \in \partial\Omega_2 (\text{Neumann boundary}) \tag{3}$$

where K_x, K_y are the hydraulic conductivities in x and y directions; $h(x, y, t)$ is the piezometric head (m) which is the state variable; Q_w is the source or sink term ($m^3/d/m^2$); $\frac{\partial}{\partial n}$ denotes the normal derivative to the boundary; S_y is the specific yield; $h_1(x, y, t)$ is the known head value at the boundary head (m); $q(x, y, t)$ is the known inflow rate ($m^3/d/m$). The boundary is denoted by $\partial\Omega$ and the flow region is represented by Ω.

3 LRPIM Formulation for an Unconfined Aquifer

There are two types of approximation functions to find out shape functions. They are polynomial point interpolation functions and radial point interpolation function. Among these two, radial point interpolation function can be used for both strong and weak form meshless methods. Because of the radial basis function (RBF) used in radial point interpolation function, and it overcomes the singularity problem [1]. The approximation function of a variable $h(x)$ inside a local support domain can be constructed as a linear combination of n RBF and m polynomial basis functions.

$$h(x) = \sum_{i=1}^{n} a_i R_i(x) + \sum_{j=1}^{m} b_j P_j(x) = R^T(x)a + P^T(x)b \tag{4}$$

where $R_i(x)$ is a RBF such as a multi-quadrics, exponential or Gaussian function, thin plate spline, and logarithmic RBF [8–11]; n is the number of points in the support domain; a_i and b_j are the unknown coefficients and can be determined by enforcing the interpolation function to pass through all the n nodes within the support domain [1]; $P_j(x)$ are polynomial basis functions; m is the number of polynomial basis function [1]. The variable $r_i(x)$ in RBF (for 2D) is the distance between the point of

interest x (data site) and a node at x_i (center point)

$$r_i = \sqrt{(x - x_i)^2 + (y - y_i)^2} \tag{5}$$

The expression for multi-quadratics (MQ) is given as

$$R_i(x, y) = \left[r_i^2 + C_s^2\right]^q = \left[(x - x_i)^2 + (y - y_i)^2 + C_s^2\right]^q \tag{6}$$

The shape parameters of the RBF are q and C_s. In this study, the parameter q has been kept as 1.03 as in [1]. The shape parameter of the MQ-RBF, C_s is usually given as a characteristic length (d_c), i.e.,

$$C_s = \alpha_c d_c \tag{7}$$

The characteristic length (d_c) is the nodal spacing in the local support domain. The accuracy of the solution depends upon the shape parameter value. The best value for the shape parameter must therefore be determined via sensitivity or parametric studies. Rippa [12], Schaback and Wendland [13–14] explain how to choose the shape parameter.

It is stated that the interpolation expression is

$$h(x) = \Phi^T(x) h_i \tag{8}$$

where the shape functions, denoted by $\Phi(x)$, is as follows:

$$\Phi^T(x) = \left\{ \Phi_1(x, y)\ \Phi_2(x, y)\ \ldots\ \Phi_n(x, y) \right\} \tag{9}$$

The function's nodal values at the support domain nodes are represented by $h_i = \{h_1, h_2, \ldots h_n\}^T$. The derivatives of $h(x, y)$ at any point $x(x_I, y_I)$ are given as below

$$h(x_I) = \Phi^T(x) h_s = \sum_{i=1}^{n} \Phi_i h_i \tag{10}$$

$$\frac{\partial h_I}{\partial x} = \frac{\partial \Phi^T}{\partial x} h_i = \sum_{i=1}^{n} \frac{\partial \Phi_i}{\partial x} h_i\ ;\ \frac{\partial^2 h_I}{\partial x^2} = \frac{\partial^2 \Phi^T}{\partial x^2} h_i = \sum_{i=1}^{n} \frac{\partial^2 \Phi_i}{\partial x^2} h_i \tag{11}$$

$$\frac{\partial h_I}{\partial y} = \frac{\partial \Phi^T}{\partial y} h_i = \sum_{i=1}^{n} \frac{\partial \Phi_i}{\partial y} h_i;\ \frac{\partial^2 h_I}{\partial y^2} = \frac{\partial^2 \Phi^T}{\partial y^2} h_i = \sum_{i=1}^{n} \frac{\partial^2 \Phi_i}{\partial y^2} h_i \tag{12}$$

The weighted residual approach for LRPIM formulation can be used to write Eq. 1 and is given as

$$\int_{\Omega_s} \nabla \cdot (Kh\nabla h) v \mathrm{d}\Omega = \int_{\Omega_s} \sum_{w=1}^{w} Q_w \delta(r - r_w) v \mathrm{d}\Omega - \int_{\Omega_s} f v \mathrm{d}\Omega + \int_{\Omega_s} S_y \frac{\partial h}{\partial t} v \mathrm{d}\Omega \quad (13)$$

where v is the so-called heavy step function, which represents weight. The LHS of Eq. (13) is subjected to the divergence theorem.

$$\int_{\partial\Omega_s} (Kh\nabla h).n v \mathrm{d}\Omega - \int_{\Omega_s} (Kh\nabla h).\nabla v \mathrm{d}\Omega$$
$$= \int_{\Omega_s} \sum_{w=1}^{w} Q_w \delta(r - r_w) v \mathrm{d}\Omega - \int_{\Omega_s} f v \mathrm{d}\Omega + \int_{\Omega_s} S_y \frac{\partial h}{\partial t} v \mathrm{d}\Omega \quad (14)$$

The value of Heaviside step function (v) is taken as 1 for r in Ω_s, zero elsewhere and the LRPIM formulation is made simpler by setting $\nabla v = 0$. Eq. (14), thus becomes

$$\int_{\partial\Omega_s} (Kh\nabla h).n \mathrm{d}\Omega = \int_{\Omega_s} \sum_{w=1}^{w} Q_w \delta(r - r_w) v \mathrm{d}\Omega - \int_{\Omega_s} f \mathrm{d}\Omega + \int_{\Omega_s} S_y \frac{\partial h}{\partial t} \mathrm{d}\Omega \quad (15)$$

where the normal vector n pointing away from the boundary and $\partial\Omega_s$ is the boundary of the sub-domain Ω_s. Within the sub-domain, the parameters K and f are fixed. Thus, Eq. (15) becomes

$$K_j \int_{\partial\Omega_s} \frac{\partial h}{\partial n} h \mathrm{d}\Omega_j = \int_{\Omega_s} \sum_{w=1}^{w} Q_w \delta(r - r_w) v \mathrm{d}\Omega - f_j A_\Omega + \int_{\Omega_s} S_y \frac{\partial h}{\partial t} \mathrm{d}\Omega \quad (16)$$

where A_Ω is the sub-domain area and the node's index is represented by j. The derivative of h with regard to the positive outward-facing normal directions (n_x, n_y) represents the index of the node considered.

$$\frac{\partial h}{\partial n} = (\nabla h) \cdot n = \frac{\partial h}{\partial x} n_x + \frac{\partial h}{\partial y} n_y \quad (17)$$

The suggested dependent variable is written as

$$h(r) = \sum_{i=1}^{n} \varphi_1(r) h_i \quad (18)$$

Using the time–space derivative, we obtain

$$K_j\left(h_i^{t+\Delta t}\int\limits_{\partial\Omega_s}\left(\frac{\partial\varphi(r)}{\partial x}h_i^{t+\Delta t}n_x+\frac{\partial\varphi(r)}{\partial y}h_i^{t+\Delta t}n_y\right)\mathrm{d}\Omega_j\right)\theta$$
$$+K_j\left(h_i^{t}\int\limits_{\partial\Omega_s}\left(\frac{\partial\varphi(r)}{\partial x}h_i^{t}n_x+\frac{\partial\varphi(r)}{\partial y}h_i^{t}n_y\right)\mathrm{d}\Omega_j\right)(1-\theta)$$
$$=\int\limits_{\Omega_s}\sum_{w=1}^{n}Q_w\delta(r-r_w)\mathrm{d}\Omega-f_jA_\Omega+\int\limits_{\Omega_s}S_y\left[\frac{h_i^{t+\Delta t}-h_i^{t}}{\Delta t}\right]\mathrm{d}\Omega \tag{19}$$

Rearranging the terms in Eq. 19, the resulting equation is

$$K_j\left(h_i^{t+\Delta t}\int\limits_{\partial\Omega_s}\left(\frac{\partial\varphi(r)}{\partial x}h_i^{t+\Delta t}n_x+\frac{\partial\varphi(r)}{\partial y}h_i^{t+\Delta t}n_y\right)\mathrm{d}\Omega_j\right)\theta-\int\limits_{\Omega_s}h_i^{t+\Delta t}\left[\frac{S_y}{\Delta t}\right]\mathrm{d}\Omega$$
$$=\int\limits_{\Omega_s}\sum_{w=1}^{n}Q_w\delta(r-r_w)\mathrm{d}\Omega-f_jA_\Omega$$
$$-K_j\left(h_i^{t}\int\limits_{\partial\Omega_s}\left(\frac{\partial\varphi(r)}{\partial x}h_i^{t}n_x+\frac{\partial\varphi(r)}{\partial y}h_i^{t}n_y\right)\mathrm{d}\Omega_j\right)(1-\theta)-\int\limits_{\Omega_s}h_i^{t}\left[\frac{S_y}{\Delta t}\right]\mathrm{d}\Omega \tag{20}$$

The system of equations that result from Eq. 20 is

$$K\left[h^{t+\Delta t}\right]=f \tag{21}$$

$$\text{where } K=K_j\left(\int\limits_{\partial\Omega_s}\left(\frac{\partial\varphi(r)}{\partial x}h_i^{t+\Delta t}n_x+\frac{\partial\varphi(r)}{\partial y}h_i^{t+\Delta t}n_y\right)\mathrm{d}\Omega_j\right)\theta-\int\limits_{\Omega_s}\left[\frac{S_y}{\Delta t}\right]\mathrm{d}\Omega \tag{22}$$

$$f=\int\limits_{\Omega_s}\sum_{w=1}^{n}Q_w\delta(r-r_w)\mathrm{d}\Omega-f_jA_\Omega$$
$$-K_j\left(h_i^{t}\int\limits_{\partial\Omega_s}\left(\frac{\partial\varphi(r)}{\partial x}h_i^{t}n_x+\frac{\partial\varphi(r)}{\partial y}h_i^{t}n_y\right)\mathrm{d}\Omega_j\right)(1-\theta)-\int\limits_{\Omega_s}h_i^{t}\left[\frac{S_y}{\Delta t}\right]\mathrm{d}\Omega \tag{23}$$

4 Model Development

LRPIM model has been developed for an unconfined aquifer based on the formulation given in Sect. 3 using MATLAB® platform. The groundwater flow simulation methodology is shown in Fig. 1. It explains the model development procedure.

1. Data collection is the initial step, during which aquifer and model parameters, including porosity, permeability, aquifer thickness, specific conductivity, stresses, such as recharge and outflow, total simulation period, and time step, were obtained.
2. The next step is to generate the interior and boundary nodes at an interval in the problem domain.
3. Initialization of groundwater head throughout the problem domain has to be done. The size and shape of the support domain are finalized.
4. Using the support domain, the stiffness matrix is calculated for every individual node in the problem domain. There are different shapes for support domain such as square, rectangular, or circular. Here, circular domain is used with a support

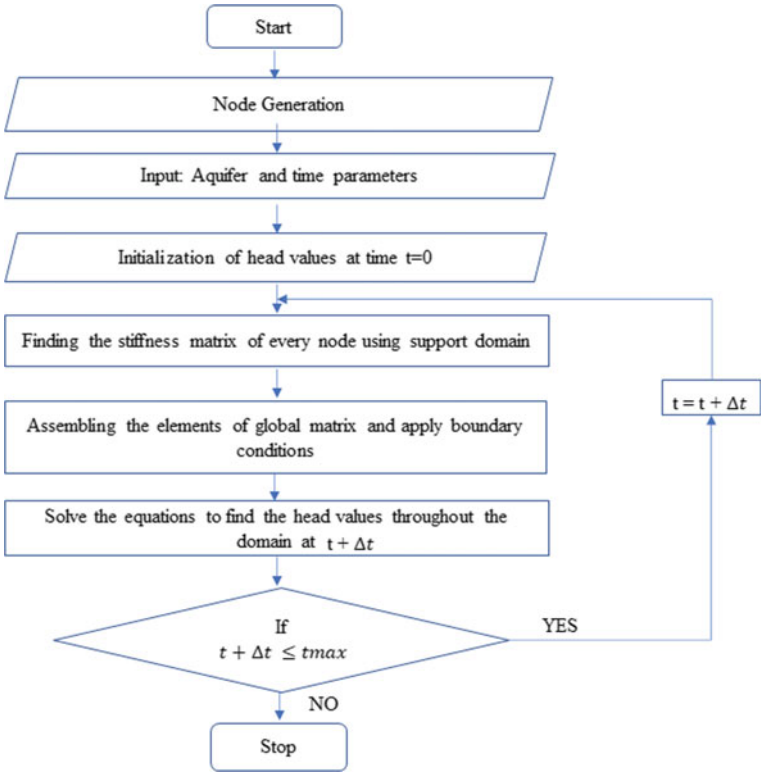

Fig. 1 Flow chart for groundwater flow model

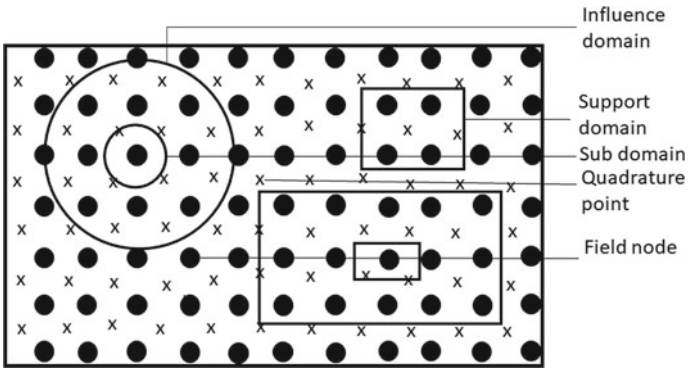

Fig. 2 Problem domain representation for LRPIM

and sub-domain factor as 4 and 0.6, respectively. Figure 2 represents the problem domain for LRPIM method.

5. The essential and Neumann boundary conditions are imposed directly to the boundary nodes. The elements of global matrix are assembled with Eq. 21.
6. The global matrix is solved to give the head values throughout the domain.

The steady state head values were used as a beginning head for unsteady flow.

The method is repeated throughout the whole simulation period using the head values obtained from the previous time step as an initial head for the following time step.

5 Case Study

A heterogeneous irregularly shaped unconfined aquifer of dimensions 1650 m × 1050 m is considered here as a case study. The aquifer configuration is as shown in Fig. 3. The value of specific yield is 0.2. The hydraulic conductivity varies in the range of 5 m/d in zone 1 and zone 3, 10 m/d in zone 2. Porosity values in these zones 1–3 are 0.22, 0.2, and 0.25, respectively. Areal recharge of 0.00013 m/d in zone 1, 0.0002 m/d in zone 2, 0.0003 m/d in Zone 3 are considered. For the LRPIM model, 559 nodes with a uniform nodal interval of 50 m along the x- and y-axes are taken into account. Figure 4 depicts the nodal distribution that was employed. The model is created in MODFLOW similarly, with 532 grids spaced 50 m apart in the x and y directions. The MODFLOW grid configuration is depicted in Fig. 5. The steady state simulation of the groundwater flow model produced the flow contours shown in Fig. 6.

At nodes 172, 247, 436, and 445, respectively, four pumping wells that extract water at rates of 500, 800, 600, and 1000 m^3/day are taken into consideration (Fig. 4). At nodes 241 and 373, two recharge wells with daily recharge rates of 500 and

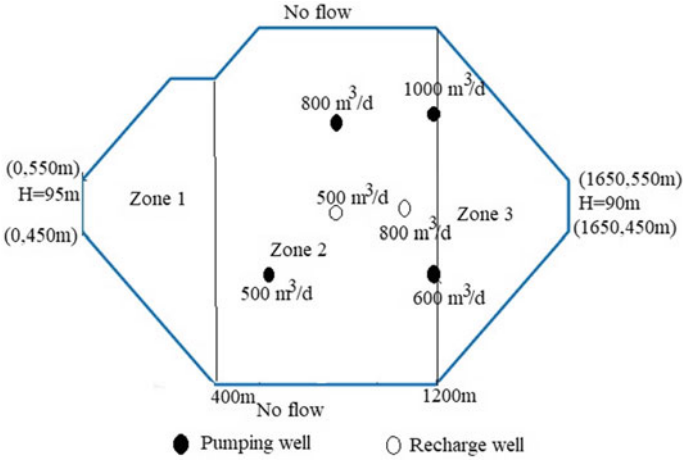

Fig. 3 Aquifer configurations

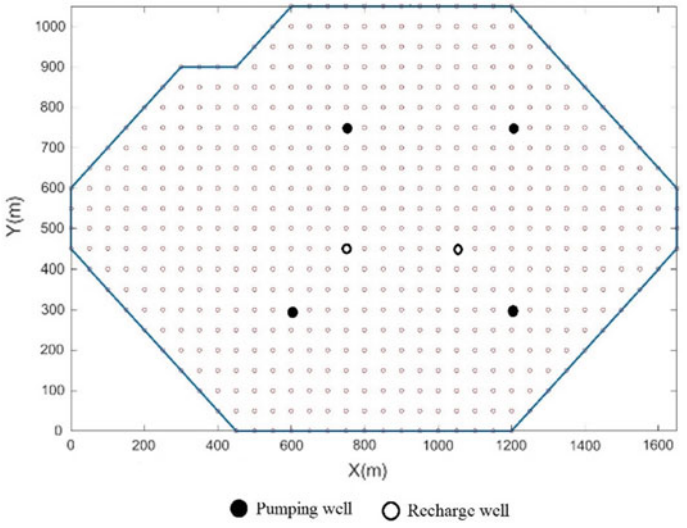

Fig. 4 Nodal distribution

800 m^3/day are located. A time period of 10 days is used for the transient scenario, and the simulation is conducted for 10,000 days. After 10,000 days, the head variation is measured in relation to pumping.

The head variation in the aquifer due to pumping for 10,000 days obtained from LRPIM is shown in Fig. 7. For comparison of the LRPIM model, a model using FDM in MODFLOW [15] is developed (Fig. 5). The head variation obtained after 10,000 days is compared with FDM results as given in Table 1. The application of

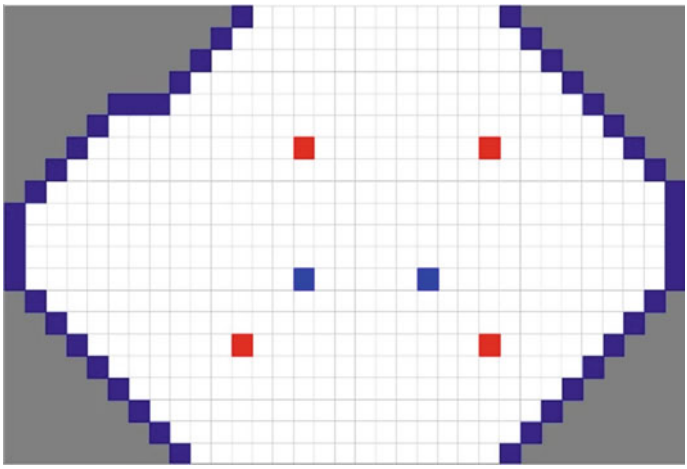

Fig. 5 Grid arrangement for MODFLOW

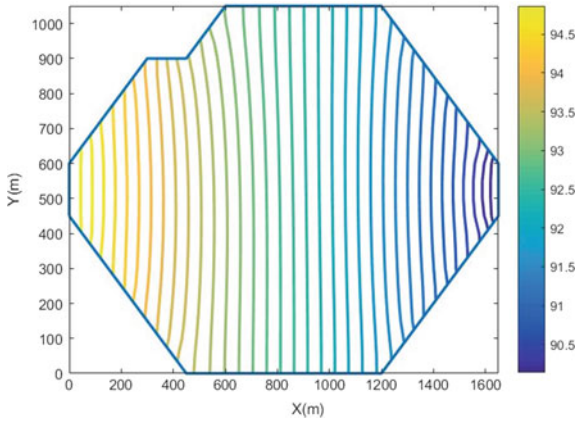

Fig. 6 Steady state head variation

the LRPIM model for simulating groundwater flow has been verified by the findings, as can be seen from the comparison (Fig. 8).

A total of 10,000 days are used to evaluate the transient state groundwater flow model with a different time interval such as 2, 5, and 10 days. The result obtained from the LRPIM model is shown in Table 2. The deviation is found to be very less, which shows the developed model is stable.

By changing the value from 2 to 6, the best shape parameters for multi-quadric RBF are examined. The RMSE error obtained is as shown in Fig. 9. The analysis yields 4 as the ideal value for the form parameter.

By altering the size from 2 to 6, a sensitivity research is conducted to determine the support domain size. The RMSE value obtained is plotted against the support

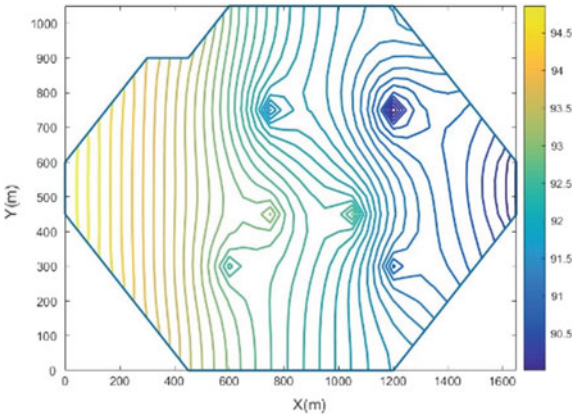

Fig. 7 Head variation in the aquifer after 10,000 days

Table 1 Nodal head variation after 10,000 days

Node No.	FDM (m)	LRPIM (m)	Percentage difference
172	93.15	92.38	0.82
238	92.73	92.60	0.15
301	92.35	92.24	0.12
370	91.91	91.87	0.04
436	91.49	90.69	0.88
493	91.08	90.94	0.15

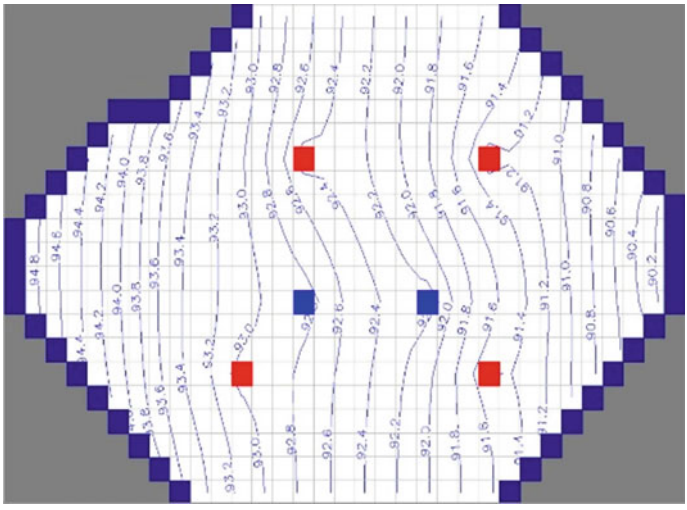

Fig. 8 Head variation in aquifer using MODFLOW

Table 2 Variation in head for different time intervals

Node No.	X Co-ordinate	Y Co-ordinate	$\Delta t = 2$ day	$\Delta t = 5$ days	$\Delta t = 10$ days
172	600	300	92.38	92.38	92.38
238	750	300	92.61	92.61	92.60
301	900	150	92.24	92.24	92.24
370	1050	300	91.87	91.87	91.87
436	1200	300	90.69	90.69	90.69
493	1350	300	90.94	90.94	90.94

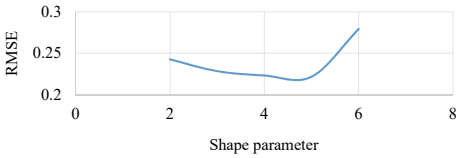

Fig. 9 Shape parameter versus RMSE

Fig. 10 Support domain size versus RMSE

domain size as shown in Fig. 10. The ideal size can be assumed to be 4 when the processing time and RMSE value are taken into account.

6 Discussion

In this study, a MATLAB®-based LRPIM model is created to simulate groundwater flow in an unconfined aquifer. One potential case study was taken into account using the model that was established. With the identical input parameters, the PMWIN MODFLOW software also creates the standard FDM model. As seen, both FDM and LRPIM predict that the head distribution in the domain will be close to the same value.

This studies shown that the LRPIM model can simulate groundwater flow rather than using other numerical techniques. The LRPIM model does not require any grid or element generation. The LRPIM model can solve the problem by simple node generation and there is no need for pre-processing of data, there is no meshing and re-meshing issue, but simply we can add nodes wherever required. The process of implementation is simpler, and accuracy is comparable to other strong form methods. It takes longer to solve the asymmetric matrix and calculate the shape function using

the radial point interpolation technique. The method can be easily used with Neumann type boundary value problems more accurately compared strong form methods. It takes less time for data preparation, which made use of this method for solving large-scale field type groundwater problems.

7 Conclusion

In recent years, LRPIM has been used to tackle several issues in solid mechanics and incompressible fluid flows. In this study, the groundwater flow problem in an unconfined aquifer is solved using LRPIM with multi-quadratics function. The LRPIM formulation is used to create MATLAB® code for a fictitious issue. The FDM result from PMWIN MODFLOW software is compared with the LRPIM results. By adjusting the time interval during the simulation period, the shape parameters, and the support domain size, a sensitivity analysis is conducted. In comparison with other numerical methods, the outcome demonstrates that the LRPIM may be used to tackle the groundwater problem successfully. When the hydraulic parameters are more different, the LRPIM approach is unable to capture the variation in flow contours inside the problem region (such as hydraulic conductivity). The ability of the RBFs to smooth data, which decreases accuracy in some locations. The general asymmetries of the system matrix affect the computation cost efficiency. Alternative interpolation techniques may be the focus of future study to solve the drawbacks outlined above. Further, numerical investigations on the optimal shape parameters for each interpolation method must also be determined.

Acknowledgements The authors are thankful to the Bhabha Atomic Research Centre, Mumbai and Indian Institute of Technology, Bombay for providing the facilities to carry out the work.

References

1. Liu GR, Gu YT (2005) An introduction to meshfree methods and their programming. Springer Science & Business Media
2. Liu GR, Gu YT (2001) A local radial point interpolation method (LRPIM) for free vibration analyses of 2-D solids. J Sound Vib 246(1):29–46
3. Wu YL, Liu GR (2003) A meshfree formulation of local radial point interpolation method (LRPIM) for incompressible flow simulation. Comput Mech 30(5):355–365
4. Wang JG, Yan L, Liu GR (2005) A local radial point interpolation method for dissipation process of excess pore water pressure. Int J Num Methods Heat & Fluid Flow
5. Saeedpanah I, Jabbari E, Shayanfar MA (2011) Numerical simulation of ground water flow via a new approach to the local radial point interpolation meshless method. Int J Comput Fluid Dyn 25(1):17–30
6. Saeedpanah I, Jabbari E (2009) Local Heaviside-weighted LRPIM meshless method and its application to two-dimensional potential flows. Int J Numer Meth Fluids 59(5):475–493
7. Bear J (1979) Hydraulics of groundwater. Mc GrawHill Inc., New York

8. Franke C, Schaback R (1998) Convergence order estimates of meshless collocation methods using radial basis functions. Adv Comput Math 8(4):381–399
9. Franke C, Schaback R (1998) Solving partial differential equations by collocation using radial basis functions. Appl Math Comput 93(1):73–82
10. Kansa EJ (1990) Multiquadrics—a scattered data approximation scheme with applications to computational fluid-dynamics—I surface approximations and partial derivative estimates. Comput Math Appl 19(8–9):127–145
11. Sharan M, Kansa EJ, Gupta S (1997) Application of the multiquadric method for numerical solution of elliptic partial differential equations. Appl Math Comput 84(2–3):275–302
12. Rippa S (1999) An algorithm for selecting a good value for the parameter c in radial basis function interpolation. Adv Comput Math 11(2):193–210
13. Schaback R, Wendland H (2000) Adaptive greedy techniques for approximate solution of large RBF systems. Numer Algorithms 24(3):239–254
14. Schaback R, Wendland H (2000) Numerical techniques based on radial basis functions. Goettingen Univ (Germany) Inst fur Numerische und Angewandte Mathematik
15. Harbaugh AW (2005) MODFLOW-2005, the US Geological Survey modular ground-water model: the ground-water flow process. US Department of the Interior, US Geological Survey, Reston, VA, pp 6–A16

Quality Assessment of Collected Groundwater Samples Around Naregaon Dumping Yard, Aurangabad, Maharashtra, India

Sanju R. Phulpagar and K. A. Patil

Abstract The growth of Municipal Solid Waste (MSW) generation in India has increased due to dominantly increasing population in recent years. The solid waste management is a very important aspect. Improper solid waste management creates many environmental and human health problems. In the present study, assessment of groundwater (GW) contamination due to solid waste dumping site around Naregaon, Aurangabad district of Maharashtra state, India, is carried out. In the present study, GW samples are collected at 15 days interval during June 10, 2016 to May 25, 2017 (i.e., pre as well as post monsoon season). These collected samples are tested by standard methods of testing, and each sample is analyzed for nine parameters: pH, EC, TDS, Cl, SO_4, Ca, NO_3, Pb, and Zn. The variation in contamination levels of corresponding samples with respect to the distance of collected sample from MSW dumping site is also analyzed. The analyses of collected water samples shown that the GW were highly contaminated. Especially during the August to November, wells nearer to the MSW dumping site are highly contaminated, which may cause many waterborne diseases and other environmental problems.

Keywords Leachate · Groundwater pollution · Water quality · Seasonal variation

1 Introduction

The groundwater (GW) is one of the most essential water resources [1]. GW is the prime source for industrial, human consumption, and agriculture purposes [2]. Nowadays the risk of GW pollution has become one of the most vital environmental concerns, particularly in developing countries [1]. The quantity of industrial and

S. R. Phulpagar (✉)
Department of Civil Engineering, Sardar Vallabhbhai National Institute of Technology Surat, Surat 395007, India
e-mail: sanjup1213@gmail.com

K. A. Patil
Civil Engineering, College of Engineering, Pune 411005, India
e-mail: kap.civil@coep.ac.in

P. V. Timbadiya et al. (eds.), *Hydrology and Hydrologic Modelling*,
Lecture Notes in Civil Engineering 312,
https://doi.org/10.1007/978-981-19-9147-9_41

municipal waste originated by society is continuously increasing [3]. The enlargement of Municipal Solid Waste (MSW) generation in India has increased due to dominantly incrementing population in current years [3]. In India, due to fast urbanization and industrialization, more than ninety percent of MSW is produced directly, and its dumping on the land in an unsatisfactory manner poses an environmental risk [4]. As per the Water Quality Status of Maharashtra (WQSM) 2017–18, Maharashtra is the second state in India in terms of population (11.24 crores) [5]. Aurangabad is one of the largest districts in Maharashtra state with a population of around 1.2 million [6]. The Aurangabad city generates around four hundred tons of solid waste [6]. There is no engineered and scientific landfill site in the Aurangabad district, and the capacity of the existing dump site cannot satisfy the future requirement of the produced waste [6]. If the MSW dumping ground site is not properly managed, then it may cause GW and surface water pollution [7]. The landfills and municipal disposal sites have a greater possibility of GW pollution in the area of MSW dumping sites because the leachate originated from the decomposition of the organic wastes is disposed at MSW dumping sites and then infiltrate into the surrounding aquifers [7]. The leachate produced in such a way has a high concentration of pathogenic microorganisms and toxic substances [8]. The concentration of these components and compounds in leachate and the adjacent GW relies on the composition of the dumped waste [8]. This GW contamination causes a sustainable risk to the surrounding environment and local resource users [7]. The assessment of the influence of GW source near to MSW dumps is of considerable significance in the disposal and management of solid waste [9]. Thus, the Aurangabad district of Maharashtra is selected for the current study. Many researchers have carried out studies on the topic of GW quality assessment near MSW dumping ground at various locations in India [1–4, 6–15, etc].

Following research gaps are found from reviewed literature: (1) None of the reviewed studies have studied the effect of MSW dumping site of Naregaon, Aurangabad district, Maharashtra on GW quality of nearby wells, (2) most of the reviewed studies have collected GW samples only twice in a year, i.e., pre-monsoon (PREMON) and post-monsoon seasons, and (3) most of the reviewed studies have not shown variation in contamination levels corresponding to distance of GW sample collection site from the MSW dumping site in PREMON and post-monsoon seasons. Aforesaid research gaps are addressed in the present study by assessing the effect of MSW dumping at Naregaon dumping site on the GW quality of nearby nine wells. The variation in contamination levels of corresponding samples with respect to the distance of collected sample from the MSW dumping site is studied through the analysis of GW samples collected for 15 days interval during June 10, 2016 to May 25, 2017.

2 Study Area

The surrounding area of the Naregaon MSW dumping site of Aurangabad district is selected as the study area for GW quality assessment. Aurangabad is one of the

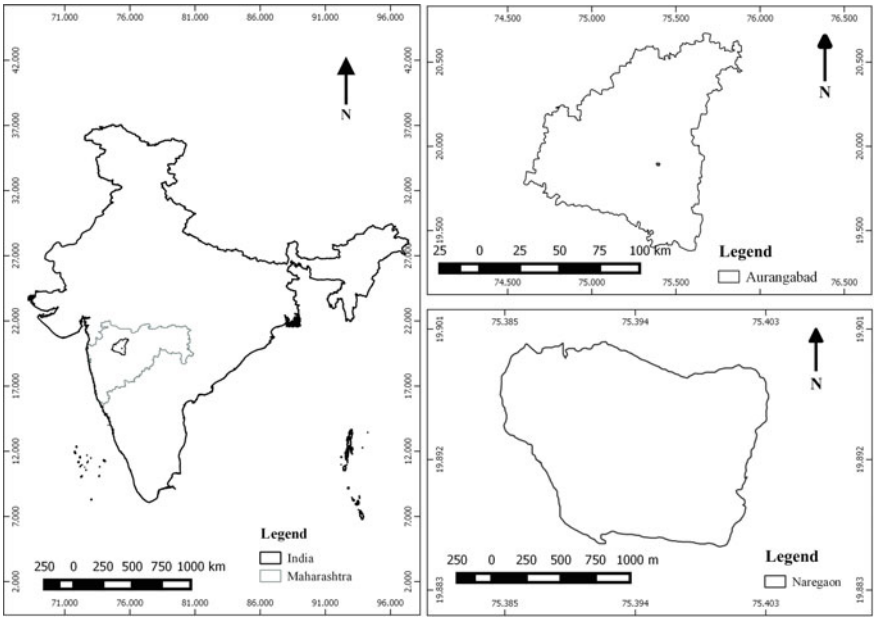

Fig. 1 Location map of study area (not to the scale)

crucial, rapidly growing city of Maharashtra states, India. The waste gathered from Aurangabad city is dumped on the Naregaon MSW dumping ground. The Naregaon is located six kilometers away from the Aurangabad city boundary and having an area of around 46 acres. The study area is located at latitudes 19°53′35″ North and longitude 75°23′55″ East (http://shodhganga.inflibnet.ac.in/bitstream/10603/78863/10/10_chapter%202.pdf [16] assessed on April 17, 2021). The location of the study area is shown in Fig. 1.

3 Methodology

The GW samples are collected at a regular interval of 15 days for the year 2016–2017 (PREMON and post-monsoon). The collection of GW samples are collected from June 10, 2016 and continued up to May 25, 2017. The GW samples are collected for twenty-four times in a year for each well, and analysis of each sample was performed for nine parameters: pH, EC, TDS, Cl, SO_4, calcium (Ca), nitrate (NO_3), lead (Pb), and zinc (Zn). After collection of GW samples, these are transported to the laboratory on the same day for the analysis. The standard methods of testing are used for assessment of GW quality. In this study, GW samples from nine different wells are collected which are located near the MSW dumping site. In this study, the Quantum Geographic Information System (Q-GIS 2.6) software is used to exhibit the

spatial variations of selected parameters and to identify the permissible GW quality zones near the MSW dumping yard, based on the analyzed data.

4 Results and Discussions

The study of GW contamination has become more efficient due to the small-time interval of 15 days. The distance of wells from the boundary of the MSW dumping ground is also very essential for detecting contamination. In the present study, GW samples from nine different wells (i.e., W1, W2, …, W9) are collected which are located near the MSW dumping site at the distances as 1400, 800, 750, 700, 330, 380, 420, 450, 310 m, respectively. Figure 2 shows spatial distribution of seasonal average of pH (a, b), TDS (c, d), and Cl (e, f) for PREMON (a, c, e) and post-monsoon (b, d, f), respectively. Figure 3 shows seasonally average EC (a), TDS (b), NO_3 (c), SO_4 (d), Ca (e), and Cl (f) values for PREMON and post-monsoon season. Figure 4 shows the variation of pH (a), NO_3 (b), and Cl (c) corresponding to 15 days interval. Because of space restriction spatial and seasonal variations are shown for only few parameters.

4.1 pH

The pH value exhibits the balance among basic and acids in water. It is controlled by carbonate, bicarbonate equilibrium, and carbon dioxide (CO_2). The combination of carbon dioxide with water forms carbonic acid, which affects the value of pH parameter of water [8]. As per BIS-10500:2012 [17], the permissible limit of pH value is 6.5–8.5. The pH value of the GW is found to vary from 6.87 to 8.41 (seasonal average value: 7.51–7.87) in PREMON season and 7.26–10.09 (seasonal average value: 7.59–9.01) in the post-monsoon season, respectively. In the PREMON season, the pH value GW is found within the acceptable limit for all nine wells. In the post-monsoon, the pH of GW was found more than the permissible limit at W5, W6, W7, W8, and W9 wells. The spatial distribution of the seasonal average of pH parameter for PREMON and post-monsoon seasons are shown in Fig. 2a, b, respectively.

The variation of pH value corresponding to 15 days interval is shown in Fig. 3a. Noticeable variation in the pH value of the wells is observed for the period July 10, 2016 to January 10, 2017, for all adjacent wells. In this period, precipitation is observed in the study area due to which the contaminated water may be mixed with the GW of the surrounding area, and it may be the reason for higher pH value of the adjacent wells.

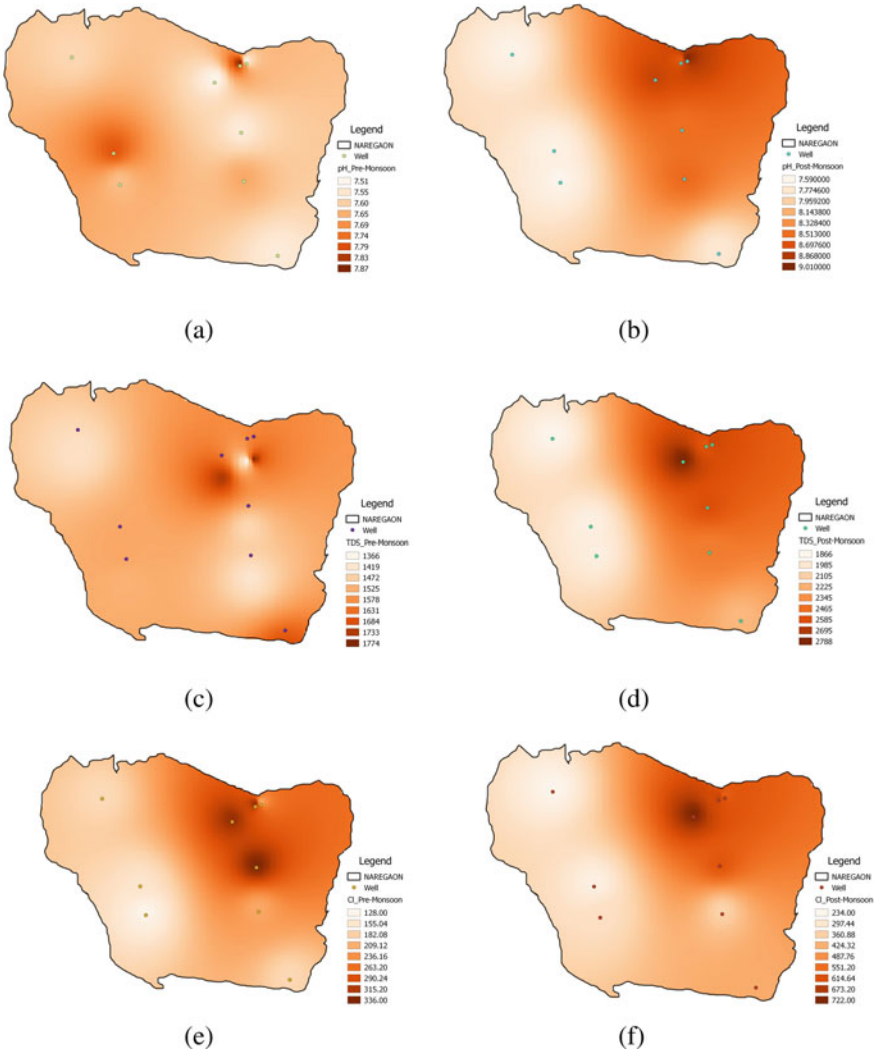

Fig. 2 Spatial distribution of seasonal average of pH (**a**, **b**), TDS (**c**, **d**), and Cl (**e**, **f**) for PREMON (**a**, **c**, **e**) and post-monsoon (**b**, **d**, **f**), respectively

4.2 Electric Conductivity (EC)

The EC is a measure of the capacity of water to convert the electric current and is a function of temperature, the concentration of various ions, and type of ions present in the water. The GW sample having EC values less than 2000 µm hos/cm at 25 °C are usually take into consideration as freshwater [8]. The EC value is found to vary from

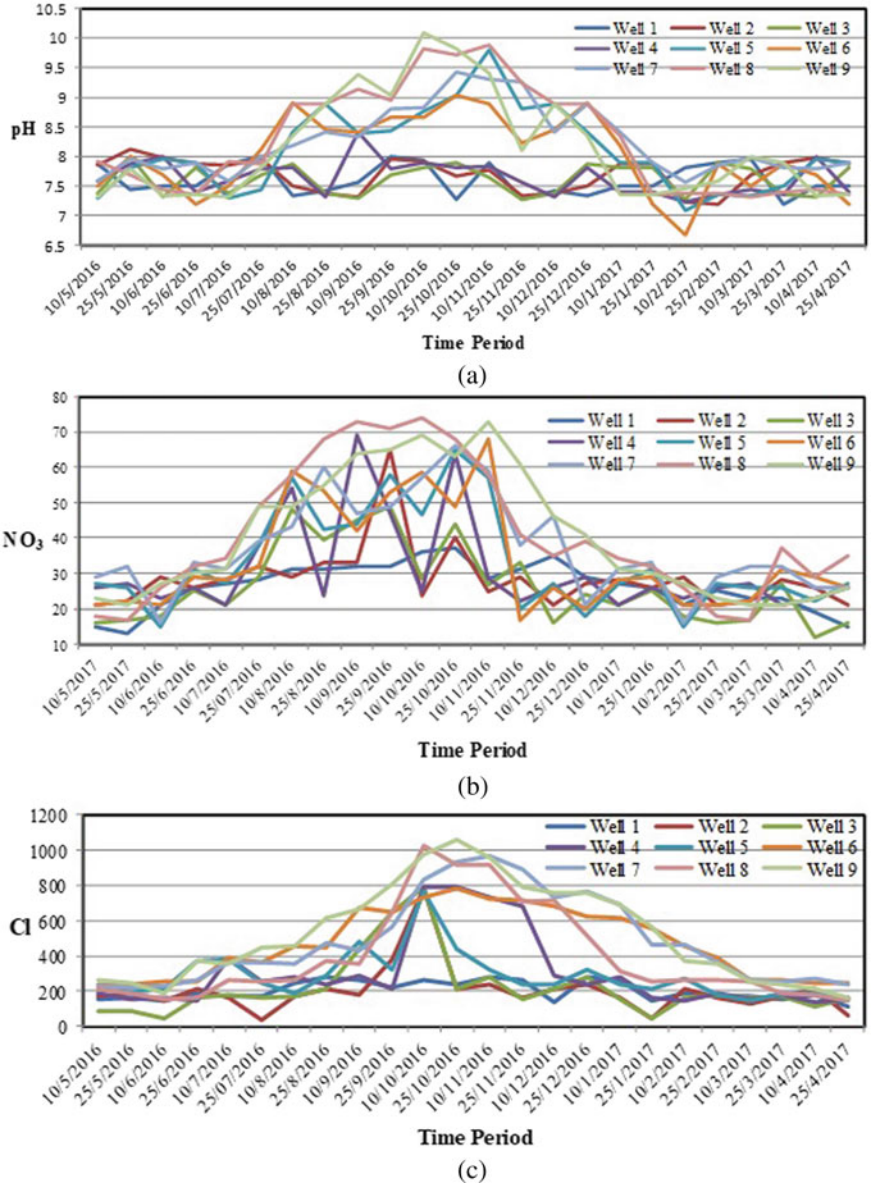

Fig. 3 Variation of pH (**a**), NO_3 (**b**), and Cl (**c**) corresponding to 15 days interval

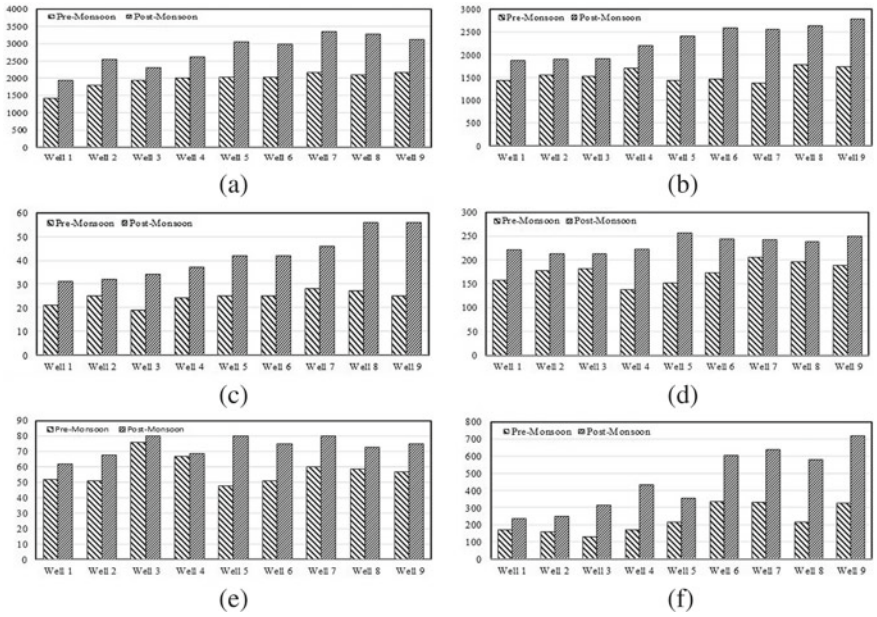

Fig. 4 Seasonally average EC (**a**), TDS (**b**), NO_3 (**c**), SO_4 (**d**), Ca (**e**), and Cl (**f**) values for PREMON and post-monsoon season

1200 to 2980 μm hos/cm (seasonal average value: 1415–2171 μm hos/cm) and 1350–4350 μmhos/cm (seasonal average value: 1944–3341 μmhos/cm) are the PREMON and post-monsoon seasons, respectively. EC in GW was higher at W2, W3, …, W9 wells for post-monsoon season, whereas in PREMON, W4, W5, W6, W7, W8, and W9 wells have shown a higher value of the EC. The variation of a seasonal average of EC in GW for PREMON and post-monsoon season with corresponding to wells is shown in Fig. 4a. It indicates that contamination of EC in GW in post-monsoon is more than the PREMON season.

4.3 Total Dissolved Solids (TDS)

The TDS refers to matter dissolved or suspended in water with high content is inferior and maybe polluted [8]. The TDS in GW varies from 1030 to 2589 mg/l (seasonal average value: 1366–1774 mg/l) in PREMON, whereas it is 1245–4020 mg/l (seasonal average value: 1866–2788 mg/l) in the post-monsoon seasons. The GW at the wells W4, W5, W6, W7, W8, and W9 is found to be contaminated in post-monsoon only. The variation of the seasonal average of TDS in GW for PREMON and post-monsoon season across the corresponding to wells is shown in Fig. 4b. It

indicates the difference between PREMON and post-monsoon contamination corresponding to wells in the aforesaid study area. The spatial distribution of the TDS for PREMON and post-monsoon are shown in Fig. 2c, d, respectively. It indicates that W2 well is less contaminated as compared to the W9 well, which clearly shows that due to contamination TDS in GW changes corresponding to the distance. In the post-monsoon, a number of wells which are adjacent to the MSW dumping ground are found to have TDS beyond the acceptable limit. It may be due to the downward transfer of leachate that impacts the GW quality.

4.4 Nitrate (NO_3)

In subsurface environment, the nitrogen is the most widespread contaminant. It is primarily originating from multipoint and non-point agricultural sources. The excessive concentration of NO_3 in drinking water causes various diseases, like gastric cancer, diabetes, blue baby syndrome (methemoglobinemia), and thyroid disease [8]. The NO_3 value for the PREMON season varies from 12 to 37 mg/l (seasonal average value: 19–28 mg/l), and all wells are found to have NO_3 within the permissible limit, while in post-monsoon season corresponding values are 16–74 mg/l (seasonal average value: 31–56 mg/l). The GW in the wells W7, W8, and W9 is found to be contaminated in post-monsoon only. The variation of the seasonal average of NO_3 in GW for PREMON and post-monsoon season corresponding to wells is shown in Fig. 4c. The figure shows the difference between PREMON and post-monsoon contamination across the wells in the aforesaid study area. The wells which are adjacent to the MSW dumping site (> 450 m) are found to be more affected than that of wells which are having a distance more than 450 m. Figure 3b shows the variation of NO_3 value corresponding to 15 days interval. It is observed that the contamination of GW due to NO_3 is higher during the period July 25, 2016 to November 25, 2016, especially in adjacent wells. Due to the MSW dumping site, the GW quality is slowly deteriorating, especially after the precipitation occurrence in the study area.

4.5 Sulfate (SO_4)

The permissible limit of SO_4 parameter is 200–400 mg/l [17]. The SO_4 value for the in PREMON season varies from 53 to 287 mg/l, whereas in post-monsoon season, it varies between 120 and 641 mg/l. The variation of the seasonal average of SO_4 in GW for PREMON and post-monsoon season corresponding to wells is shown in Fig. 4d. It indicates that the SO_4 value for the post-monsoon season is higher than that of the PREMON season. This indicated that the monsoon precipitation reasonably affects the contamination at the study area.

4.6 Calcium (Ca)

The permissible limit of Ca is 75–200 mg/l for drinking water [17]. The Ca concentration varies from 35 to 192 mg/l for PREMON season and 34–214 mg/l for post-monsoon season. In the PREMON and post-monsoon, the Ca in GW was found nearer to the acceptable limit; however, in post-monsoon season, contamination is found to be more than the PREMON season as shown in Fig. 4e.

4.7 Chloride (Cl)

The results show that Cl concentration in GW varies between 43 and 690 mg/l (seasonal avg. value: 128–336 mg/l) in PREMON season and 32–1059 mg/l (seasonal avg. value: 234–722 mg/l) for post-monsoon. The spatial distribution of the seasonal average of Cl parameter for PREMON and post-monsoon seasons are shown in Fig. 2e, f, respectively. It indicates that adjacent wells are more contaminated as compared to the far distance wells, it clearly shows that the contamination of Cl in GW changes corresponding to distance. In the PREMON and post-monsoon, the Cl in GW is found to be within the acceptable limit, but in post-monsoon the contamination is more than that of the PREMON. The variation of the seasonal average of Cl in GW for PREMON and post-monsoon seasons across the wells is shown in Fig. 4f. The variation of GW contamination corresponding to 15 days interval is shown in Fig. 3c. It indicates that contamination of Cl in GW varies over the period July 25, 2016 to March 10, 2017, especially in adjacent wells contamination is found to be higher. Due to the MSW dumping site, the GW quality is slowly deteriorating, especially after the precipitation occurrence in the study area.

4.8 Zinc (Zn) and Lead (Pb)

Zinc and lead concentrations of the GW are found to be within the permissible limits for both aforesaid seasons. The seasonal averages of each parameter for PREMON and post-monsoon seasons are given in Tables 1 and 2, respectively.

The seasonally averaged GW quality parameters for PREMON and post-monsoon seasons are compared with corresponding permissible limits prescribed by Indian Standard BIS:IS:10500-2012 [17] for drinking purposes. The values of parameters are higher than their corresponding permissible limit, given in BIS. It will create undesirable effects on the human health and environment. The contaminated wells (having contamination more than permissible limits) in the aforesaid study area are given in Table 3.

The analyzed parameter values of GW are found to be higher than acceptable limit, for wells which are situated nearer to the MSW dumping ground site. The analyzed

Table 1 Seasonal averages of GW quality parameters across the wells for PREMON season

Parameter	Well 1	Well 2	Well 3	Well 4	Well 5	Well 6	Well 7	Well 8	Well 9
pH	7.59	7.78	7.63	7.54	7.66	7.54	7.87	7.52	7.51
EC	1415	1791	1947	2015	2026	2032	2163	2094	2171
TDS	1430	1542	1523	1692	1421	1458	1366	1774	1731
NO_3	21	25	19	24	25	25	28	27	25
SO_4	158	177	182	137	152	173	205	196	189
Ca	52	51	76	67	48	51	60	59	57
Cl	170	156	128	172	216	336	329	214	326
Zn	–	–	–	–	–	–	–	–	–
Pb	–	–	–	–	–	–	–	–	–

Note (–) i.e., within the permissible limit

Table 2 Seasonal averages of GW quality parameters across the wells for post-monsoon season

Parameter	Well 1	Well 2	Well 3	Well 4	Well 5	Well 6	Well 7	Well 8	Well 9
pH	7.61	7.62	7.59	7.74	8.54	8.51	8.62	9.01	8.78
EC	1944	2554	2296	2611	3060	2980	3341	3286	3119
TDS	1866	1891	1906	2194	2410	2592	2549	2631	2788
NO_3	31	32	34	37	42	42	46	56	56
SO_4	222	213	213	223	257	244	243	239	249
Ca	62	68	80	69	80	75	80	73	75
Cl	234	249	313	432	353	604	639	582	722
Zn	–	–	–	–	–	–	–	–	–
Pb	–	–	–	–	–	–	–	–	–

Note (–) i.e., within the permissible limit

GW samples are found to be less contaminated in wells which are located far from the MSW dumping ground site. Especially in August to November month maximum leachate is formed in the MSW dumping ground site; therefore, the contamination of wells is found to be high.

5 Conclusions

In the study area, GW is found to be mainly alkaline in nature. The concentrations of parameters such as pH, NO_3, EC, and TDS are found to be exceeded the maximum allowable limits. Thus, water is not suitable for drinking purpose. The concentrations of water quality parameters are found to be reciprocal of distance of well from the

Table 3 Suitability of GW as per IS:10500-2012 [17] code for drinking purposes and contaminated wells in the study area

Parameter	Indian standard (BIS) IS:10500:2012 [17]		Wells exceeding permissible limits		Undesirable effects [18]
	Most probable limit	Maximum allowable limit	PREMON	Post-monsoon	
pH	6.5	8.5	Nil	W5, W6, W7, W8, W9	Taste
EC	–	–	W4, W5, W6, W7, W8, W9	W2, W3, W4, W5, W6, W7, W8, W9	–
TDS	500	2000	Nil	W4, W5, W6, W7, W8, W9	Gastrointestinal irritation
Ca	75	200	Nil	Nil	Scale formation
Cl	250	1000	Nil	Nil	–
SO_4	200	400	Nil	Nil	Laxative effect
NO_3	45	No relaxation	Nil	W7, W8, W9	Blue baby syndrome [8]
Zn	05	15	Nil	Nil	–
Pb	0.01	No relaxation	Nil	Nil	–

MSW dumping site. The contamination of GW is found to be predominant in post-monsoon season as compared to the PREMON season. The study recommends that serious steps for the control of GW pollution by concerned authorities are needed in general, and more attention should be given on controlling GW pollution during August to November months. Also, it is concluded that, for MSW dumping ground site, establishing the suitable site and proper design are important for controlling the leachate.

References

1. Shenbagarani S (2013) Analysis of groundwater quality near the solid waste dumping site. J Environ Sci Toxicol Food Technol 4(2):2319–2399
2. Kamble BS, Saxena PR (2017) Environmental impact of municipal dumpsite leachate on ground-water quality in Jawaharnagar, Rangareddy, Telangana, India. Appl Water Sci 7(6):3333–3343
3. Prasanna K, Annadurai R (2016) Study on ground water quality in and around Perungudi solid waste dumping site in Chennai. Rasayan J Chem 9(2):287–293
4. Mishra S, Tiwary D, Ohri A, Agnihotri AK (2018) Spatial analysis of groundwater quality around MSW landfill site. Nat Environ Pollut Technol 17(3)
5. Water Quality Status of Maharashtra (WQSM) (2017–2018) Compilation of water quality data recorded by 'Maharashtra Pollution Control Board (MPCB). January 2019 Prepared by 'The

energy and resource institute (TERI)'
6. Salve UL, Wankhede P, Pawar H, Baviskar S, Tadvi A, Pawara A (2019) Assessment of solid waste management for Aurangabad city-challenges and solution. Int J Innov Res Sci Eng Technol 8(3):2163–2868
7. Chavan BL, Zambare NS (2014) Ground water quality assessment near municipal solid waste dumping site, Solapur, Maharashtra, India. Impact Int J Res Appl Nat Soc Sci (IMPACT IJRANSS) 2(11):73–78
8. Saini A, Kaur N (2018) Impact of municipal solid waste disposal on groundwater quality near Mathuradaspura-Langadiyawas dumping sites, Jaipur city, India. Int J Environ Rehabil Conserv. https://doi.org/10.31786/09756272.18.9.1.120
9. Agrawal A, Pandey R, Agrawal ML (2013) Water quality surrounding to MSW dumps of Raipur city—a case study. Recent Res Sci Technol 5(5)
10. Chilukuri SK, Chandra DS, Asadi SS (2019) Assessment of ground water quality near municipal dump site and estimation of water quality index by using weighted arithmetic method Tenali, Guntur district, Andhra Pradesh, India. Int J Recent Technol Eng (IJRTE) 7(6):125–129
11. Jebastina N, Arulraj GP (2017) GIS based assessment of groundwater quality in Coimbatore District, India. J Environ Anal Toxicol 7(3):1–9
12. Kamboj N, Choudhary M (2013) Impact of solid waste disposal on ground water quality near Gazipur dumping site, Delhi, India. J Appl Nat Sci 5(2):306–312
13. Mageswari S, Iyappan L, Aravind S, Mohammed SN, Vignesh R, Vinoth KP (2017) Contamination of groundwater quality due to municipal solid waste disposal a GIS based study in Perungudi dump yard. Int Res J Eng Technol 4(5):952–964
14. Pawar K, Rane G (2016) Impact of open solid waste dumping on groundwater quality near dumping site of Jalgaon city, Maharashtra. Int Recogn Multidiscipl Res J 6(2):1–11
15. Pawari MJ, Gavande SM (2015) Underground water quality assessment around Hadapsar region in Pune, Maharashtra. Int J Sci Res 4(7):1102–1105
16. http://shodhganga.inflibnet.ac.in/bitstream/10603/78863/10/10_chapter%202.pdf
17. BIS I (2012) 10500 Indian standard drinking water–specification, second revision. Bureau of Indian Standards, New Delhi
18. Eshanthini P, Padmini TK (2015) Impact of leachate on ground water quality near Kodungaiyur dumping site, Chennai, Tamil Nadu, India. Int J Pharm Tech Res 8(10):171–179

Appraisal of Soil Salinity in Haryana State by Using Electromagnetic Induction Tool

Hemant Raheja, Arun Goel, Mahesh Pal, and D. S. Bundela

Abstract This paper aimed to analyze the soil salinity of the Siwanamal village subsurface drainage site in the Jind district of Haryana. Also, a spatial salinity diagram was applied to observe soil characteristics and controlling constituents of the underground aqua region. In Haryana, more than 50,000 ha area is a waterlogged saline area having a shallow water table at a depth 1.5 m; due to this fact, the natural drainage system is not sufficient for controlling the salinity trouble. Therefore, subsurface drainage (SSD) technology, a synthetic drainage method, is wanted to reclaim waterlogged saline lands in the Haryana region for enhancing crop productivity and controlling the soil salinity. A SSD system is designed to control soil salinity and waterlogging in an affected area. In Haryana, about 10,584 ha waterlogged saline area in nine districts of the state has been reclaimed by SSD technology. In this study, one SSD site (i.e., Siwanamal in Jind district) is selected and measured the soil salinity from Electromagnetic Induction Tool (EM-38) along with the GPS coordinates from Block 3 and 4. Further, it is used in mapping software to develop maps and analyze the status of the selected site. Largest area 64.51% of Block 4 is under moderately saline soil (Ec = 8–16 dS/m) and largest are of Block 3, i.e., 57.28 is under moderately saline soil (Ec = 8–16 dS/m). The area under Ec > 16 dS/m is 1.08% in Block 4 (full pumping) compared to 26.36% area in Block 3 (partial pumping) at SSD site in Siwanamal.

H. Raheja (✉) · A. Goel · M. Pal
Department of Civil Engineering, National Institute of Technology, Kurukshetra, Haryana 136119, India
e-mail: raheja.hemant788@gmail.com

A. Goel
e-mail: darun_goel@nitkkr.ac.in

M. Pal
e-mail: mahesh.pal@nitkkr.ac.in

D. S. Bundela
Division of Irrigation and Drainage Engineering, ICAR-CSSRI, Karnal 132116, India
e-mail: ds.bundela@icar.gov.in

P. V. Timbadiya et al. (eds.), *Hydrology and Hydrologic Modelling*,
Lecture Notes in Civil Engineering 312,
https://doi.org/10.1007/978-981-19-9147-9_42

Keywords Oil salinity · Waterlogging · Electromagnetic Induction Tool (EM-38) · Subsurface drainage (SSD)

1 Introduction

Soil salinity is one of the huge environmental troubles which influence the crop yield and health, mainly of the farming network [1, 2]. So monitoring the soil salinity (quantitatively) within the command place is critical. The assessment of soil salinity in irrigation commands is primarily based on the quantity of waterlogging. The soil conservation and survey departments found the water table records [3–5]. Assessment of soil salinity troubles primarily based on such a technique could not outline the clean photograph in an irrigation command location. Presently, the measurement of soil salinity relies on outdated visual methods or by evaluating the samples in the laboratory. The laboratory methods are comparatively slow, require skilled labor and capital, which is a severe disadvantage in large scale or periodic monitoring. Therefore, there is a dire need to develop and standardize the techniques, which can be fast, non-destructive, and quantify the soil salinity directly inside the area. EM-38 is one of the methods which, without delay, ascertain the soil salinity from the field. EM-38 uses electromagnetic energy to assess and map spatial and temporal versions in the plain conductivity of soils [6, 7]. Geonics EM-38 was procured from Geonics Limited. It could be very lightweight and calls for only one person to perform. The EM-38 m is reasonably light in weight of 2.5 kg. The EM-38 m operates at a frequency of 14,600 Hz. The spacing between the inner coil is 1 m. The advantage of such techniques over the currently available strategies ought to be their fastness, restricted effect of spatial variability on the measurement, and the opportunity to use underneath dry moist, stone covered, cropped, and uncropped soil conditions [8].

2 Materials and Methods

Electromagnetic Induction Tool (EM-38) probe was used to find out the salinity levels in the selected Blocks from the Siwanamal SSD site. The field was surveyed on approximate 100 m by 100 m grid spacing using EM-38 m along with the GPS coordinates of the location. Horizontal and vertical Ec measured with EM-38 device by placing in horizontal and vertical positions at the soil surface. As a precaution, any metal objects that might come within the field of influence of the electromagnetic device were removed. EM-38 horizontal and vertical readings at ground level were taken at about locations 110 from Block number 3 and 93 from Block number 4.

Surfer 13 software was used for the pictorial representation of spatial salinity levels in given Blocks. Spatial salinity maps of Ec value have been developed for different directions with a contour interval of 4 ds/m in Block no. 3 (partial pumping) and 4 (full pumping) of SSD site at Siwanamal in Jind district of Haryana.

3 Study Area and Data Source

Jind is a part of the Indo-Gangetic plain. The district lies between 29.3255° N and 76.2998° E and 226 m above the mean sea level. The area of Jind district is 2702 km^2, and the normal annual rainfall is approximately 515 mm. The soil texture of the Jind district is sandy loam to loam [9]. A subsurface drainage (SSD) site at Siwanamal village in Jind district of Haryana was selected as shown in Fig. 1. The subsurface drainage system consisting of a network of underground corrugated perforated pipes (i.e., laterals and collectors) was installed at a designed drain depth and spacing. The outlet of the SSD system can be pumped outlet type or gravity outlet type. Before the installation of the SSD system, the Siwanamal area had a shallow water table (< 1.5 m). There are seven drainage Blocks, as shown in Fig. 1, and each Block was having three manholes and one sump. Drainage Block no. 3 (area 42.5 ha) and 4 (area 42 ha) in Siwanamal were selected for the study area. The subsurface drainage system has been installed in the year 2012 and covered the 290 ha area. The outlet of Siwanamal site is gravity type Partial water pumping in Block no. 3 and full pumping in Block 4 are being done by some group of farmers. Drained water having salt content, which is collected in sump through a network of laterals and collectors, is lying at a depth below the root zone of crop sown. This water from the sump is then discharged into the nearby surface drain. Thus, the drainage area is reclaimed from waterlogging and salinity by adopting the SSD system. Two Blocks (3 and 4) were selected because in the Block (4), full pumping was done, and while in Block no. 3 partial pumping was done, so that by characterizing salinity levels in these Blocks through EM 38 investigation, we could observe the effect of the SSD system in reducing the salinity levels in different layers of the soil profile.

4 Results and Discussions

The study has been conducted in the area of Siwanamal Jind. At present, approximately 2.96 M ha areas in India are highly affected by the soil salinity problem, and very few organizations have the resources to work upon this practical problem. Jind is the agricultural capital of Haryana in terms of the crops cultivated there since the yield of the area has decreased over the recent years and is greatly affected by the soil salinity problem in the area, and a portentous demand has arisen for research in the area for the agricultural boom in coming years. Table 1 shows the salinity levels in partial pumping (Block 3) and full pumping (Block 4) at SSD site in Siwanamal village. From Table 1, the largest area 64.51% of Block 4 is under moderately saline soil (Ec = 8–16 dS/m) and largest area of Block 3, i.e., 57.28 is under moderately saline soil (Ec = 8–16 dS/m). The area under Ec > 16 dS/m is 1.08% in Block 4 (full pumping) compared to 26.36% area in Block 3 (partial pumping) at SSD site in Siwanamal. Figures 2 and 3 show the spatial maps of soil salinity in Block 3

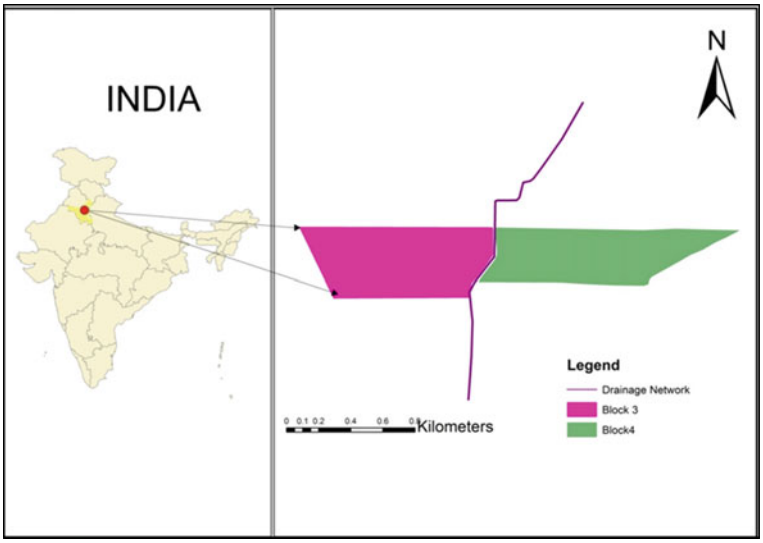

Fig. 1 Location map of the study area (Block 3 and 4)

Table 1 Salinity levels in partial pumping (Block 3) and full pumping (Block 4) at SSD site in Siwanamal village

Location	Normal soil (ECe < 4) (dS/m)	Slightly Saline (ECe = 4–8) (dS/m)	Moderately saline (ECe = 8–16) (dS/m)	Highly saline (ECe > 16) (dS/m)	Total % age of area
Block 3 horizontal	6.36	30.91	54.55	8.18	100
Block 3 vertical	00	16.36	57.28	26.36	100
Block 4 horizontal	5.38	47.31	46.23	1.08	100
Block 4 vertical	2.15	30.11	64.51	3.23	100

horizontal and vertical direction, respectively. Figures 4 and 5 show the spatial maps of soil salinity in Block 4 horizontal and vertical direction, respectively.

5 Conclusions

The study has been conducted in the area of Siwanamal Jind, and the study concludes the following points:

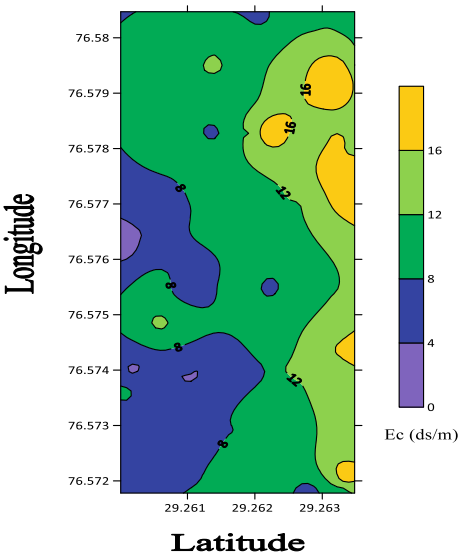

Fig. 2 Spatial map showing improvement in soil salinity in Block 3 horizontal direction

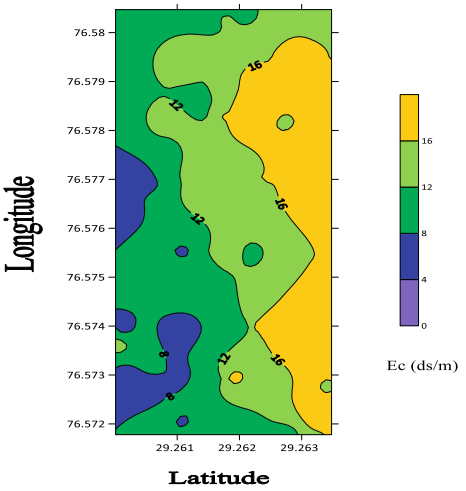

Fig. 3 Spatial map showing improvement in soil salinity in Block 3 vertical direction

- Largest area 64.51% of Block 4 is under moderately saline soil (Ec = 8–16 dS/m) and largest area of Block 3, i.e., 57.28 is under moderately saline soil (Ec = 8–16 dS/m). The area under Ec > 16 dS/m is 1.08% in Block 4 (full pumping) compared to 26.36% area in Block 3 (partial pumping) at SSD site in Siwanamal.
- Soil salinity is an intricate parameter for judging the soil's fitness for different types of crops; hence, a dire need has arisen for soil salinity data that can be referred for macro-level research for the state of Haryana that could benefit the farmer.

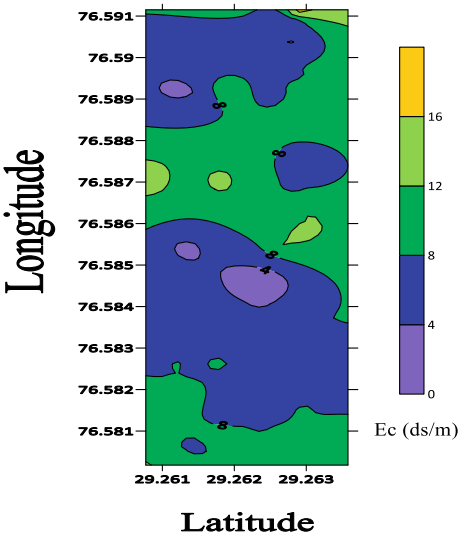

Fig. 4 Spatial map showing improvement in soil salinity in Block 4 horizontal direction

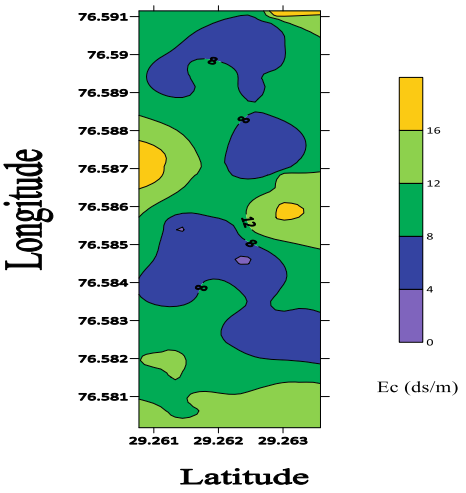

Fig. 5 Spatial map showing improvement in soil salinity in Block 4 vertical direction

- The dataset of the computed electrical conductivity pre-eminence elements can be useful for irrigation purposes. Spatial contour maps are plotted and are color coded for reference of the future researchers to find out the area affected and to further evaluate salinity characteristics of the soil.

Acknowledgements The authors acknowledge the financial support received from Ministry of Human resources and development (MOE), Government of India to carry out present work. The authors would also appreciate the infrastructural support provided by National Institute of Technology, Kurukshetra and ICAR-Central Soil Salinity Research Institute, Karnal (Haryana).

References

1. Ritzema HP (2016) Drain for gain: managing salinity in irrigated lands—a review. Agric Water Manag 176:18–28
2. Raheja H, Goel A, Bundela DS (2019) Reclamation of waterlogged saline lands in Haryana through subsurface drainage technology—a review. Sustain Eng 167–175
3. Sharma DK, Chaudhari SK (2012) Agronomic research in salt affected soils of India: an overview. Indian J Agron 57(3s):175–185
4. Gupta SK (2002) A century of subsurface drainage research in India. Irrig Drain Syst 16(1):69–84
5. Tiwari P, Goel A (2017) An overview of impact of subsurface drainage project studies on salinity management in developing countries. Appl Water Sci 7(2):569–580
6. Sharma DP, Gupta SK (2000) Application of EM38 for soil salinity appraisal: an Indian experience. In: EM38 Workshop, New Delhi, India, pp 23–35
7. Stuyt LCPM, Dierickx W, Beltrán JM (2005) Materials for subsurface land drainage systems, no. 60. Food & Agriculture Org
8. Yu J, Li Y, Han G, Zhou D, Fu Y, Guan B, Wang G, Ning K, Wu H, Wang J (2014) The spatial distribution characteristics of soil salinity in coastal zone of the Yellow River Delta. Environ Earth Sci 72(2):589–599
9. Raheja H, Goel A, Pal M (2022) Prediction of groundwater quality indices using machine learning algorithms. Water Pract Technol 17(1):336–351

Rain-Gauge Network Design and Rainfall Estimation—Case Study of Odisha Basins

Biswajit Choudhury and Anil Kumar Kar

Abstract Rainfall data are important inputs for effective planning, designing and operation of water resources projects. A well-designed optimal rain-gauge network is being difficult task for hydrologist, as comprises rainfall values. Rain-gauge network provides rainfall measurement with high degree of accuracy at specific location, but most cases, the rain-gauge is too sparely distributed to capture accurate high spatial and temporal rainfall data. Therefore, a number of guidelines for setting up rain-gauge network from India Meteorological Department (IMD) and World Meteorological Organization (WMO), still the question is being arisen, where to effectively deploy new or change the current position of RG network. A new rain-gauge network set-up over different part is challenging job for hydrologist and meteorologist. As per the IMD and WMO guidelines, area with high elevation has a greater number of rain-gauge as compared with plain area. Thus, the study demonstrates the designing of the rain-gauge network in different locations and estimating the rainfall with desire accuracy. The results obtained optimal rain-gauge network design through combined use of added and redundant station is equally applicable to any other catchment area. The study represents the guidelines and rainfall estimation utilizing different methods and techniques in a case-to-case basis with respect to basins of Odisha which will help in better flow computation and flood forecasting.

Keywords Torm · Rainfall estimation · Optimum RG · IMD · WMO

1 Introduction

Collection of rainfall data is a continuous process over different basin in Odisha. As rainfall data are very important aspect for hydrologist and hydrometeorologist for prediction of accurate data in spatio-temporal scale. For quantification of rainfall data in an area is very significant for inflow as well as developed a saturated rain-gauge network [1]. As its study define the development of saturated rain-gauge network

B. Choudhury (✉) · A. K. Kar
Department of Civil Engineering, VSSUT, Burla 768017, India
e-mail: biswajit.civil16@gmail.com

P. V. Timbadiya et al. (eds.), *Hydrology and Hydrologic Modelling*,
Lecture Notes in Civil Engineering 312,
https://doi.org/10.1007/978-981-19-9147-9_43

over different basin is key challenges of many hydrologists for place the rain-gauge in accurate places. The objectives to be accomplished were to maximize the estimation accuracy and placing of rain-gauge stations. There are several ways to define the objective of the hydrological network design, but the essential is to take in most of the cases, selection of an optimum, key and saturated number of rain-gauge stations [2]. The rainfall variability depends on the topography, wind, direction of storm movement and type of storm. The location and spacing of gauge depend not only the above factor but also upon the use of that data for that region [3].

In many areas, it may not be feasible to design even an optimum network. So, in case an optimum network may have to be redesigned and the distribution of the available rain-gauges in the various catchments required a good climatological knowledge. In this regards Indian Meteorological Department (IMD) and World Meteorological Organization (WMO) have been given different elevation for putting rain-gauges over different area [4, 5].

WMO recommended for putting rain-gauges densities:

Flat regions 1 station for 600–900 km^2.
Mountainous regions 1 station for 100–250 km^2.
Arid and polar Zones 1 station for 1500–10,000 km^2.

IMD recommended for putting rain-gauges densities:

Flat regions 1 station per 520 km^2.
Regions of average elevation 1 station for 260–390 km^2.
Hilly area 1 station per 130 km^2.

Note: 10% of rain-gauge stations should be equipped with self-recording rain-gauges.

2 Study Area, Data Set and Methodology

2.1 Study Area

The river Baitarani is one of the medium-sized east flowing rivers draining an area of 14,218 km^2. An area of 736 km^2 of Singhbhum district of Jharkhand state lies in the upper part of the basin. The catchment area of the basin is oval shaped. The river Baitarani originates from Guptaganga hills in Keonjhar district Orissa, about 2 km from Gonasika village at an elevation of 900 m at latitude 21°-31′-00″ N and longitude 85°-33′-00″ E (Fig. 1).

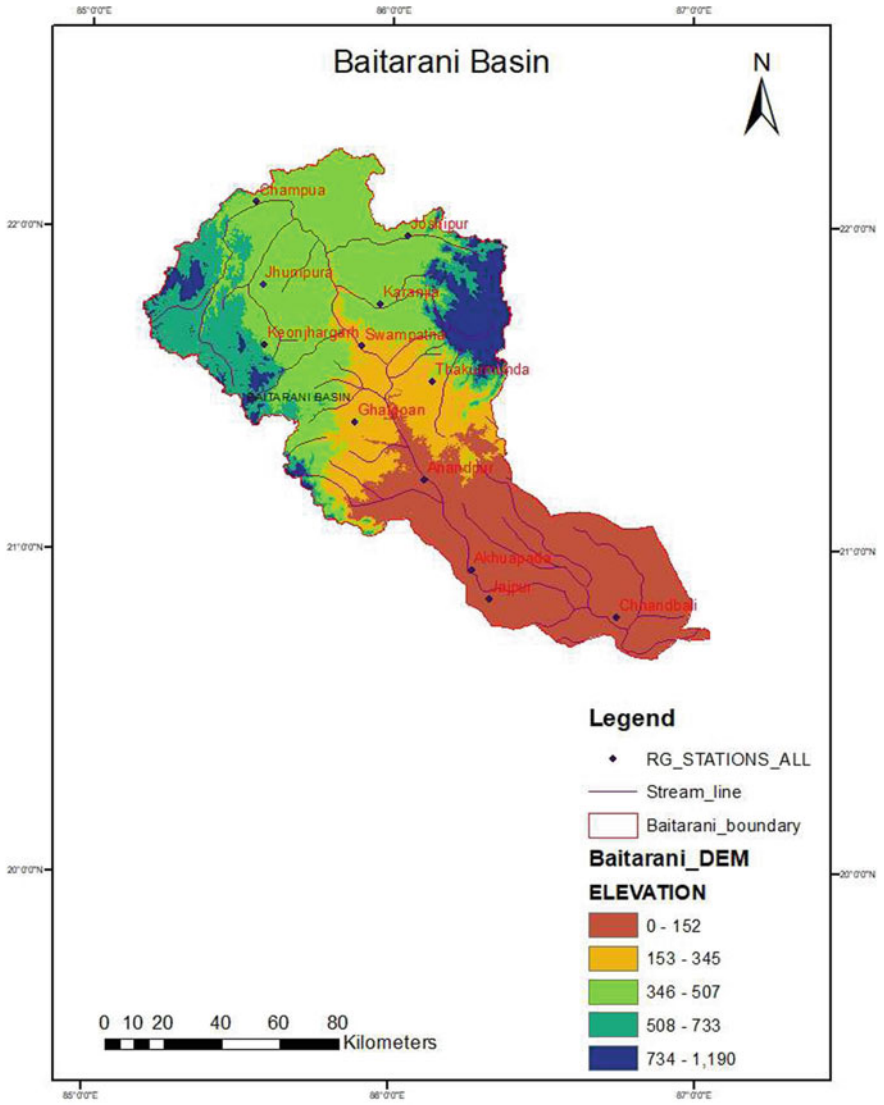

Fig. 1 Showing DEM of Baitarani basin with RG stations

2.2 Data Set

The observed daily rainfall records of the 12 rain-gauges stations located within and neighbouring the Baitarani basin were obtained from Water Resources Department and IMD.

The rain-gauge and their latitude, longitude and elevation are given in Table 1.

Table 1 Rain-gauge site with their elevation

S. No.	RG_SITE	LAT	Long	Elevation (feet)
1	Akhuapada	20.9417	86.2667	54
2	Anandpur	21.2205	86.1095	135
3	Champua	22.0792	85.5483	1375
4	Chnandbali	20.7955	86.7458	7
5	Ghatgoan	21.3998	85.8778	1115
6	Jajpur	20.8524	86.3237	52
7	Jhumpura	21.8222	85.5722	1383
8	Joshipur	21.9763	86.0529	1302
9	Karanjia	21.7649	85.96	1300
10	Keonjhargarh	21.6378	85.5778	1593
11	Swampatna	21.6333	85.9	1044
12	Thakurmunda	21.5257	86.1345	1083

The daily rainfall data of 12 rain-gauges of the study area have been collected for 10 years (2007–2017). The individual RGs have their chosen IDs as fixing by concerned department (Department of Water Resources, Government of Odisha, India).

3 Methodology

A rain-gauge network design methodology was developed in this study using cluster analysis and geostatistical approach which is being used for further analysis. The daily rainfall data of the proposed RG stations are evaluated on the basis of spatial scale and temporal scale. In case of seasonal analysis, evaluated and compared the performance of each RG stations of this area. Considering the topography and sparsely distributed rain-gauge stations, adopted a geo-statistical approach [6], co-kriging for estimation of areal average RG-based rainfall.

A detailed procedure of co-kriging is presented in this paper, i.e. Continuous Evaluation Indices.

3.1 Continuous Evaluation Indices (CEI)

The consistency between storm and elevation profile of RG stations data was quantified by mean error (ME), mean absolute error (MAE), the root mean square error (RMSE), normalized root mean square error (NRMSE) and normalized mean absolute error (NMAE).

3.2 Variogram

The random nature of spatial variation of many natural phenomena can be described by a random filed $Z(x)$, where x represents the spatial location and z is the random phenomenon under investigation. It describes how the data are related with distance.

$$Y(h) = \frac{1}{|2N(h)|} \sum_{N(h)}^{n} (Z_i - Z_j)^2$$

A Variogram is mathematical function of the distance and direction separating two locations used to quantify the spatial autocorrelation in regionalized variables. The theoretical Variogram function $Y^*(h)$ allows the analytical estimation of Variogram values for any distance and provide the unique solution for weights required for kriging interpolation. Spherical Variogram models are mostly used in Hydrology and expressed as

$$Y^*(h) = C_0 + C_1 \left[1.5\left(\frac{h}{a}\right) - 0.5\left(\frac{h^3}{a^3}\right) \right] \ldots \text{Spherical}$$

where $c_0, aand(c_0 + c_1)$ represent nugget, range and sill, respectively, commonly called as Variogram parameters.

Nugget represents measurement error and/or micro-scale variation at spatial scales that are too fine to detect and is seen as a discontinuity at the origin of the Variogram model. Range is a distance beyond which there is little or no autocorrelation among variables. Sill is the constant semi-variance of the regionalized variables.

4 Results and Discussion

4.1 Continuous Evaluation Indices (CEI)

In the first phase of study, co-kriging interpolation was used to interpolate in between elevation profile of each RG stations and storm rainfall for each individual stations. It illustrates co-kriging interpolation; interpolation result of typical scenarios is shown in Fig. 2.

The above CEI graph indicates that elevation (distances) increases with increases in rainfall, where the less rainfall area having a smaller number of rain-gauge stations (Fig. 3).

The predicted error is showing in between measured values and predicted values of different storm and their corresponding elevation. The standard equation/function for co-kriging is 0.695998542457126* × +275.560497991316, Root-Mean-Square

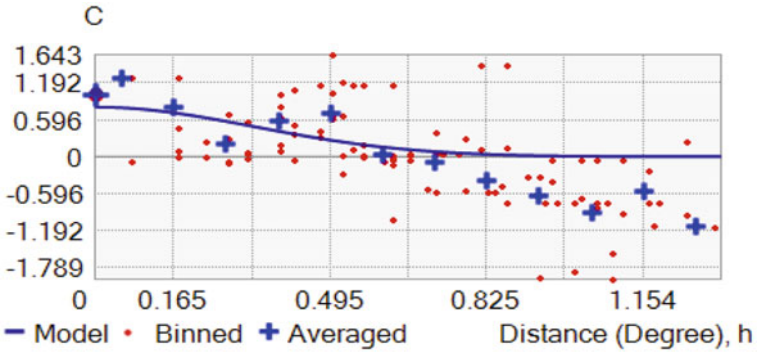

Fig. 2 Graph shows covariance between elevation versus storm rainfall

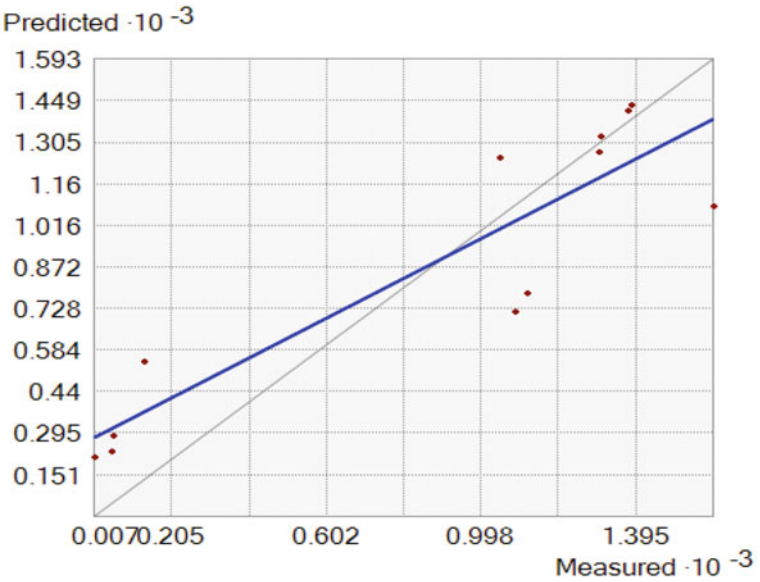

Fig. 3 Graph showing measure values versus predicted values

266.34, Mean Standardized 0.086, Root-Mean-Square Standardized 0.673, Average Standard Error 354.85.

4.2 Variogram

In this study, Variogram is independent of spatial location, i.e. dependents on the distance between two points. From the digital elevation model (DEM) of Baitarani

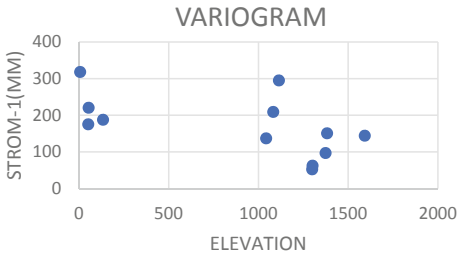

Fig. 4 Graph shows elevation versus strom-1

basin, latitude, longitude and elevation of RG's sites (Table 1) have been extracted. The above data, i.e. latitude and longitude data to get Euclidian distance. The formula is given below:

$$d(x, y) = d(y, x) = \sqrt{(X_1 - X_2)^2 + (Y_1 - Y_2)^2}$$

where

X_1 and X_2 = Longitude between two points.

Y_1 and Y_2= Latitude between two points.

Above, this formula to get Euclidian distance of all the point installed inside the basin boundary. The squared difference was found by the help of this formula is given below:

$$\text{Squared difference} = (E_2 - E_1)^2$$

where E_1 and E_2 are elevation difference.

Above is the Squared difference formula to get the possible difference between all the points. In Variogram method, the average daily rainfall data and elevation data of each rain-gauge station were compared, and it was found that higher elevation has less amount of rainfall and lower elevation has good amount of rainfall shown in below graph, concluded that in Baitarani basin higher elevation RG site has to put more number of rain-gauge stations (Fig. 4).

Figures 3 and 4 are shows that Variogram analysis of different storms occurred in two different years and conclude that higher elevation site has higher number of rain-gauge stations, and lower elevation has a smaller number of rain-gauge stations.

4.3 Kriging Interpolation

Kriging is an optimal surface interpolation technique based on spatially dependent variance. In the help of ARC GIS, It was found that the deep brown color has low

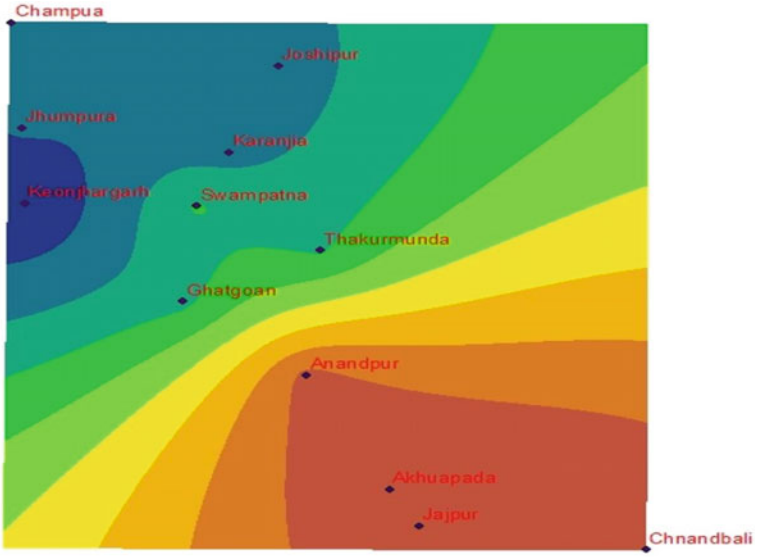

Fig. 5 Kriging interpolation of Baitarani basin

line area shows in Fig. 5. This kriging interpolation technique is used in the form of spherical shape.

4.4 Inverse Distance Weighted (IDW)

IDW is an optimal surface interpolation technique based on spatially dependent variance. In this case green colour area is low line area as compared to the white and pink area as shown in Fig. 6. In pink colour area has more number of RG stations, therefore there is high rainfall intensity area. This IDW interpolation technique is used in the form of spherical shape.

4.5 Adequacy of Raingauge Stations

In this study, the Baitarani basin has already some existing RG stations. The optimal no of stations should be calculated on the basis of percentage error of estimation of mean rainfall.

$$N = \left(\frac{C_v}{E}\right)^2$$

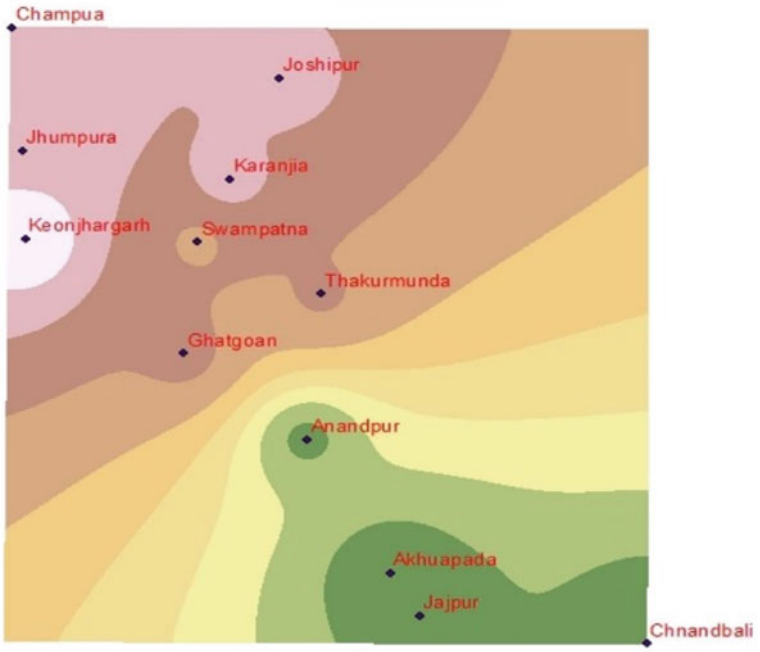

Fig. 6 IDW of Baitarani basin

$$C_V = \frac{100 * \sigma_m}{\overline{P}}$$

From the daily rainfall data to identify the storm analysis of all RG stations and average daily rainfall being calculated from storm rainfall using above formulae. If the degree of allowable error in mean rain fall is 10, 8, 6 and 5%, then the optimal number of rain-gauge is 10, 15, 25 and 36 numbers, respectively.

5 Conclusion

On the basis of results obtained in this study, the following conclusion can be drawn:

- In this study suggests a Co-kriging and entropy-based approach which not only use in the kriging method as an interpolator but also determine rainfall data at ungauged postings with the highest estimation error.
- In Variogram methods used the elevation data compared with storm data, and it is found that the elevation is co-related with distance between two points.
- Adequate number of rain-gauge was calculated and found, if percentage degree of error is high then less number of RG is obtained.

- Thus, this study has established an optimal rainfall network for the Baitarani catchment that consist of more number of rain-gauge stations in higher elevation area.

The recommendation arising from the results obtained in this study is to install and maintain additional RG stations in the Baitarani basin. The concept proposed in this study for optimal design of RG network through combined use of additional and redundant stations together is equally applicable to any other catchment.

References

1. Cheng K-S, Lin Y-C, Liou J-j (2007) Raingauge network evaluation and augmentation using Geostatistics. Hydrol Process 22:2554–2564
2. Adhikary SK, Yilmaz AG, Nitin M (2014) Optimal design of rain gauge network in the middle yarra river catchment, Australia. Hydrol Process 29:2582–2599
3. Xu P, Wang D, Wang Y, Singh VP (2018) A kriging and entropy-based approach to rain-gauge network design. Environ Res 161(2018):61–75
4. Indian Standard Code (2002) Recomendation for establishing network of non-recording type rain-gauge station. IS4986:2002
5. Indian standard code (1994) Recommendation for establishing network of Raingauge stations. IS 4987:1994, p 2
6. Kassim AHM, Kottegoda NT (1991) Rainfall network design through comparative kriging methods. Hydrol Sci J 36:223–224
7. Subramanya K (2013) Engineering hydrology, 3rd edn. Tata Mcgraw-Hill, pp 25–35

Capacity Assessment of Khoupum Reservoir, Manipur, Using Hydrographic Survey—A Case Study

M. S. Bist, Ajay Sonawane, Ajit Singh, Subbarao Murthy, and M. Selva Balan

Abstract The Khoupum Dam is an irrigation project constructed across the Manchen Diu River in Manchen in Tamenglong district of Manipur state in India. The purpose of the dam is to cater the needs of water supplying for irrigation and drinking water to nearby surrounding villages. The dam was built and commissioned by the then Chief Minister, Rishang Keishing, in the year 1982–83. Since after operation of more than 37 years, the dam authority decided to conduct hydrographic survey for evaluation of actual storage capacity and estimation of silt deposited in the reservoir. The purpose of the hydrographic survey was to find out the actual storage capacity of the reservoir so the use of water for irrigation and drinking purpose can be planned optimally. The CWPRS, Pune, carried out hydrographic survey of Khoupum in 2020 by using modern Integrated Bathymetry System (IBS) and collected the survey data. The survey was done by using the bathymetry survey equipment consisting of echo sounder, DGPS, with antenna mounted on a motorized boat and data acquisition system for survey data logging. The survey equipment had accuracy in submeters and in cms for position. The bathymetric survey was done at FRL 724.22 m. The analysis was carried out at CWPRS using software Hypack, Eiva Surfer for volume, area calculation, and graph plotting, whereas Global Mapper, Google earth and imagery were used for plotting reservoir survey area boundary of and plotting grid lines for data collection. After the analysis, it was found that the reservoir gross storage capacity during survey at FRL 724.22 m is 2.725 MCM for water spread area of 0.5320 km^2 and with comparing with the original data, it was concluded that there was a negligible reduction of approximation 2% in the reservoir live storage capacity.

Keywords Hydrography survey · DGPS · Echo sounder · HYPACK · Surfer

M. S. Bist (✉) · A. Sonawane · A. Singh · S. Murthy · M. Selva Balan
Central Water and Power Research Station (CWPRS), Pune 411024, India
e-mail: msbist1974@cwprs.gov.in

P. V. Timbadiya et al. (eds.), *Hydrology and Hydrologic Modelling*,
Lecture Notes in Civil Engineering 312,
https://doi.org/10.1007/978-981-19-9147-9_44

1 Introduction

Sedimentation in reservoirs is a serious problem as it reduces the utility period of the reservoir, which is also termed at its useful life. Dam and storage reservoirs are built-up at enormous cost for augmentation of water resources, and these play a vital role in development of nation. A large quantity of water stored at minimum cost will give rise to maximum output and in turn better return for capital invested on the reservoir project. The life of the reservoir cannot be forecasted precisely as the process of sedimentation is a complex phenomenon which also cannot be so precisely estimated. The rate of sedimentation depends on the various factor including geographical features of the terrain, rain fall, de-forestation, etc. The complexity of various parameters in the process of reservoir such as the space and position occupied by sediment, lack of knowledge regarding contribution of sediment by water from each of the tributaries, the variability of sediment flow from year to year, season to season, the inability to evaluate accurately suspended sediment and bed load, and all prevent the hydraulic engineer from forming definite conclusions regarding useful life of reservoir. It is therefore essential to monitor the actual rate of sediment deposition in the reservoir and redefine the volume–elevation–capacity curves.

Thus the sedimentation survey studies are useful in

1. Ascertaining useful life of reservoir.
2. Revised the capacity curve for more efficient operation of the reservoir.
3. In enforcing better watershed management and understanding climate factors on the rate of sedimentation.
4. Assessing regional silt indices for developing design data for planning of new reservoir.
5. In bringing efficiency and economy in control measures.
6. Forecasting hydropower generating capacity year to year.

The Khoupum Dam construction was completed in the year 1983 and since then dam has been catering the need for providing the water for irrigation and drinking purpose through canal networks to different villages and its nearby area. The Executive Engineer, Water Resources Department, Govt. of Manipur after operational of dam over a period of 37 years, has requested National Project Monitoring Unit (NPMU), of ministry of Jal Shakti Govt. of India, New Delhi, for conducting bathymetry survey of Khoupum dam, Manipur. Subsequently after forwarding the proposal to CWPRS, Pune, and accepted by CWPRS, the CWPRS team carried out hydrographic survey of Khoupum reservoir from January 21 to 22, 2020.

The CWPRS team conducted the hydrographic survey by deploying Integrated Bathymetry System (IBS) consisting of dual frequency echo sounder (210 and 33 kHz) for measuring the water depth and a Global Positioning System (GPS) for finding the accurate location of boat moving on the predefined grid lines loaded on the software in laptop. The survey data (depth and position) collected at reservoir was logged in real time mode in laptop with survey software. Processing and calculations are done later by processing software such as Hypack, surfer Auto CAD [1]. The Khoupum Dam boundary extracted from Google Earth with logged data is shown in Fig. 1.

Fig. 1 Google image of Khoupum Dam boundary with data points

2 Components and Methodology

The hydrographic survey was carried out with a boat equipped with the ultrasonic single beam dual frequency echo sounder [2] Mobile GPS system with beacon correction and a laptop for logging the real time data. The IBS system used during survey consists of the following components:

(i) Single beam dual-frequency echo sounder (210, 33 kHz), Knudsen make
(ii) GPS make Trimble using beacon correction [3]
(iii) Data collection laptop with Hypack software [4] used for real-time data acquisition.

A motorized boat was used for deploying the survey equipment during survey. The echo sounder sensor with special fixture was fitted on one side of the boat, and the GPS antenna was mounted on boat for receiving the satellite signal. The Hypack survey software was used for fixing of grid lines and interfacing of echo sounder and GPS equipment. The software logged the boat position longitude, latitude (x, y) data, and water depth (z) values at grid of 10 m. The depth and position data is logged in real time mode in laptop with survey software. Figure 2 shows GPS equipment with antenna fixed in boat, and Figs. 3 and 4 show echo sounder and recorder and laptop screen showing data logging, respectively.

The echo sounder was calibrated for its accuracy before using it on every day before start of survey. The GPS accuracy for boat location was achieved in submeter with the help of beacon correction from near seashore reference station.

The survey equipment setup consisting of echo sounder, GPS, antenna, battery, invertor, etc., in a survey boat is shown in Fig. 5.

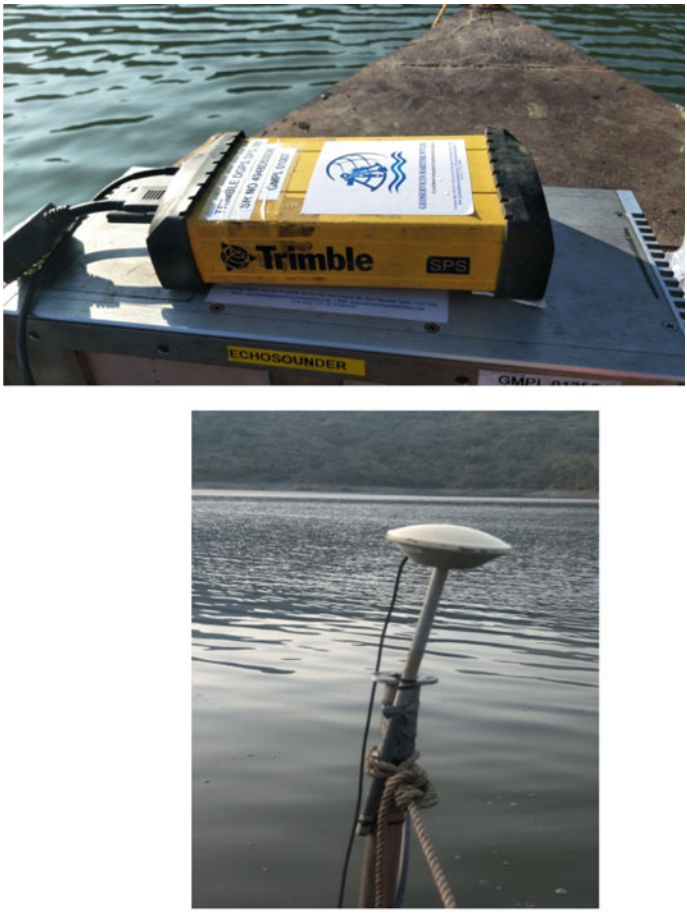

Fig. 2 GPS equipment with antenna

The survey was carried out by running the boat on the predefined straight grid line with the help of software. This included feeding the survey boundary, assigning the proper coordinate system for the Global Positioning System, setting the data logging protocol, zone, coordinate system, etc., in the software. Similarly, the echo sounder needed to be calibrated for the sound velocity before actual depth measurement and data logging. Boat navigation was also controlled by the software, so that boat could track the grid line closely while data logging during survey. The bathymetric survey was carried out during the month of January 2020 at the EL of 724.22 m with a survey grid line of 10 m. The boundary profile was extracted from Google Earth at CWPRS prior to the site visit. The same has been verified by running the boat on the actual cross section at site. After confirmation, the actual survey lines were carried out on the required cross-section, and the bathymetry data collection was completed during survey.

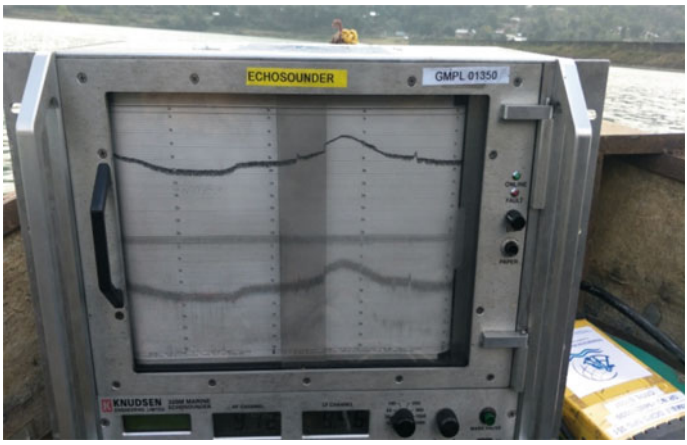

Fig. 3 Echo sounder and recorder

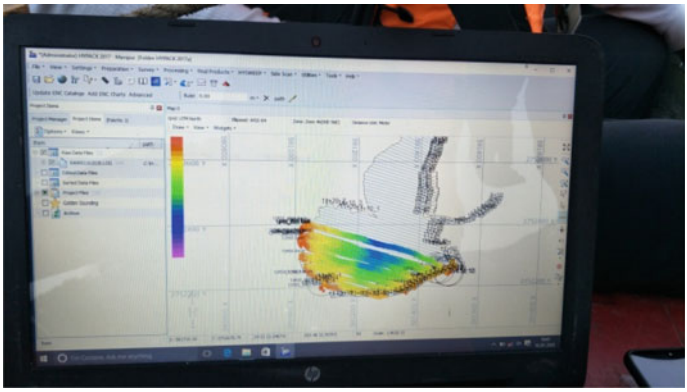

Fig. 4 Laptop screen showing data logging

3 Analysis and Results

After collecting the data at site, the analysis was done at CWPRS. The data filtered and noised were removed using software such as Surfer Auto [5]/Hypack/Eiva. During analyzing the data, the bathymetry raw data were converted in Excel/XYZ format. The grids were made using Kriging method, and volume and corresponding area were calculated at survey EL of 724.22 m using Simpson 1/3 method and Simpson 1/6 method. The different volume value was calculated below survey level with an interval of 1 m up to reservoir bottom. The elevation–volume-capacity, elevation–area curve, Digital Elevation Model (DEM) were plotted. The volumes at survey level and at dead storage level were calculated and compared with original one. Figure 6

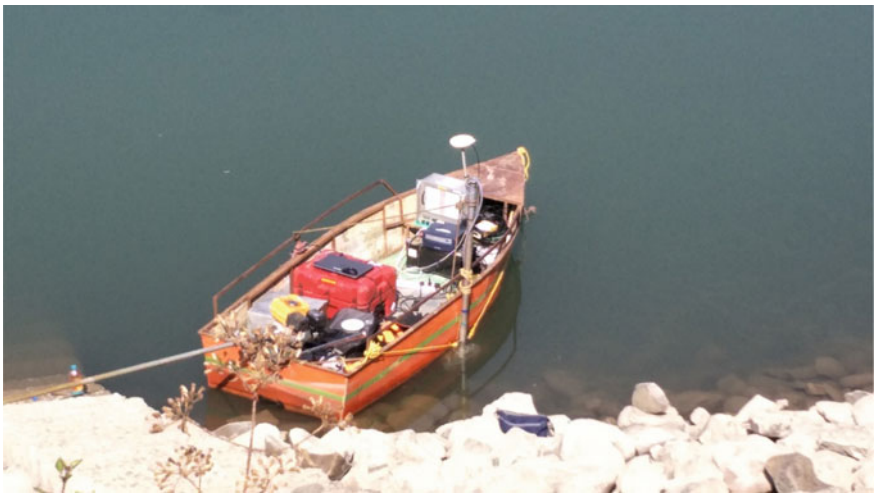

Fig. 5 Hydrographic equipments' setup in boat

shows surface map of Khoupum reservoir. Figures 7 and 8 show elevation–capacity curve and elevation–area–capacity curve [6] of Khoupum reservoir, respectively.

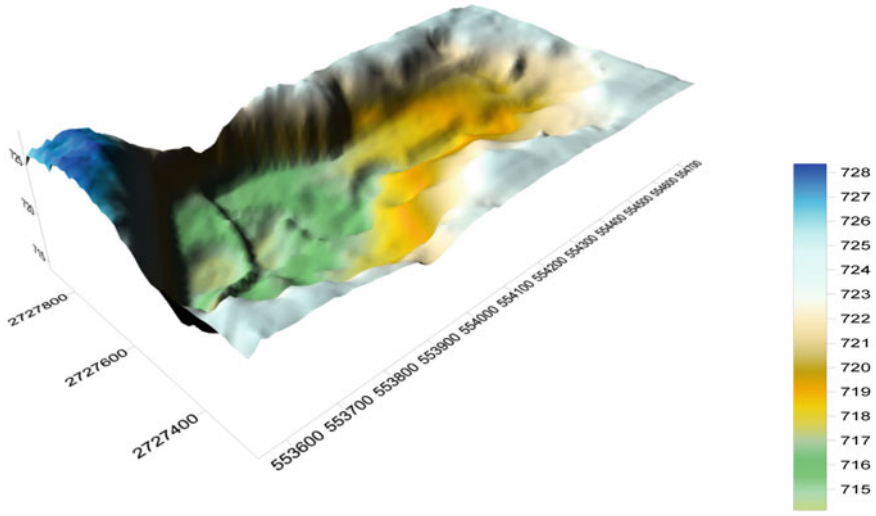

Fig. 6 Surface map of Khoupum reservoir

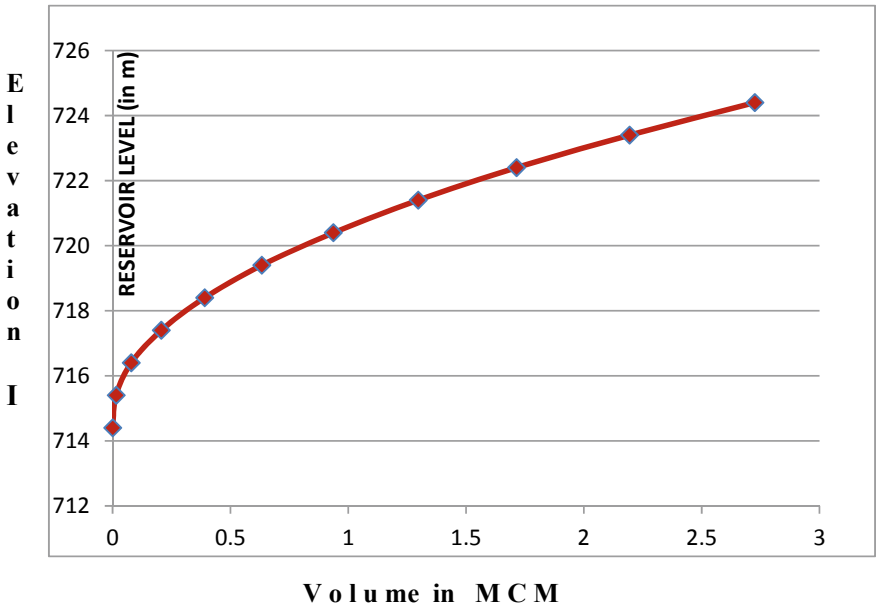

Fig. 7 Elevation–capacity curve of Khoupum reservoir

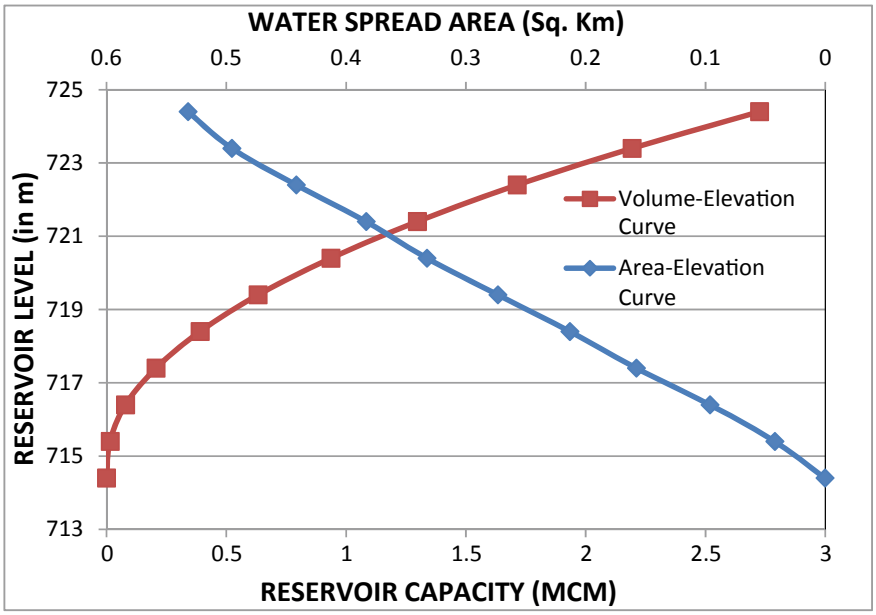

Fig. 8 Elevation–area–capacity curve of Khoupum reservoir

4 Conclusions

The collected data was edited and filtered and analyzed using HYPACK, Surfer. The volume-capacity curves, DEM, surface map, and depth profile were drawn.

- The reservoir gross storage capacity calculated was 2.7252 M.CM for water spread area of 0.5320 km^2 at survey level 724.22 m RL.
- After comparing with the original data, it was found that there is a negligible reduction in volume of 2% compared with the original gross storage capacity.

Acknowledgements The authors are obliged to Shri A. K. Agrawal, Director, CW&PRS for guiding them and giving his consent for publishing this paper. Our sincere thanks to Dr. Prabhat Chandra, Scientist-E and shri S. G. Manjunatha, Scinetist-E and head of TC division who encouraged us during the preparation of this paper. Our sincere thanks due to Shri Rohit Ahanthem, Superintending Engineer, Irrigation Circle-II, WRD, Manipur Shri Irom Royal, Ex. Engineer, Shri Lian Samatee, Executive Engineer, Shri S. Thuamlallian Executive Engineer, Khuga spillway & Intake division (KS&ID) and others officials in Irrigation division of Khuga Dam project, who had extended their support in providing all necessary arrangements required for carrying out the bathymetry survey The service of M/s. Geo Services Maritime Pvt. Ltd, Mumbai, is duly acknowledged for their support in data collection activities.

References

1. AutoCAD Manual. Source: www.autodesk.com
2. Single beam echo sounder manual, Knudsen makes. Source: https://www.knudseneng.co
3. GPS manual, Trimble make. Source: http://www.trimble.com
4. Hypack Manual. Source: https://www.hypack.com
5. Surfer Manual. Source: https://www.goldensoftware.com
6. CWPRS (2020) Pune technical report no. 5853. Bathymetry survey of Khoupum Reservoir in Manipur State under National Hydrology Project (NHP)

Correction to: Assessing the Performance of SWOT Simulator in Estimating River Discharge of a Tropical Basin

Taha Aawar, M. S. Adarsh, and C. T. Dhanya

Correction to:
Chapter "Assessing the Performance of SWOT Simulator in Estimating River Discharge of a Tropical Basin" in: P. V. Timbadiya et al. (eds.), *Hydrology and Hydrologic Modelling*, Lecture Notes in Civil Engineering 312,
https://doi.org/10.1007/978-981-19-9147-9_13

This book was inadvertently published with the incorrect author name in Chapter "Assessing the Performance of SWOT Simulator in Estimating River Discharge of a Tropical Basin". In this chapter the first author name has been corrected as "Taha Aawar". The correction chapter and the book have been updated with the changes.

The updated version of this chapter can be found at
https://doi.org/10.1007/978-981-19-9147-9_13

P. V. Timbadiya et al. (eds.), *Hydrology and Hydrologic Modelling*,
Lecture Notes in Civil Engineering 312,
https://doi.org/10.1007/978-981-19-9147-9_45